GROWTH KINETICS AND MORPHOLOGY OF CRYSTALS IN RELATION TO INTERFACIAL STRUCTURE

Applications to n-Paraffin Crystals

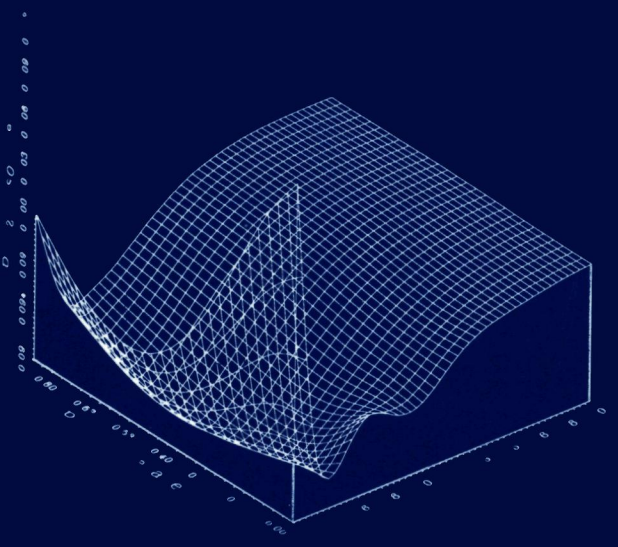

XIANG YANG LIU

GROWTH KINETICS AND MORPHOLOGY OF CRYSTALS IN RELATION TO INTERFACIAL STRUCTURE

Applications to n-Paraffin Crystals

CIP-DATA KONINKLIJKE BIBLIOTHEEK, DAN HAAG

Liu, Xiang-Yang

Growth kinetics and morphology of crystals in relation to interfacial structure: applications to n-paraffin crystals / Xiang-Yang Liu. - [S.l. : s.n.]. - Ill.
Thesis Nijmegen. - With ref. - With summary in Chinese and Dutch.
ISBN 90-9006420-6
Subject headings: growth kinetics / morphology of crystals / solid-fluid interface.

Druk: Quickprint, Nijmegen

GROWTH KINETICS AND MORPHOLOGY OF CRYSTALS IN RELATION TO INTERFACIAL STRUCTURE

Applications to n-Paraffin Crystals

Een wetenschappelijke proeve op het gebied van
de Natuurwetenschappen

Proefschrift

ter verkrijging van de graad van doctor aan
de Katholieke Universiteit Nijmegen
volgens besluit van het College van Decanen
in het openbaar te verdedigen op
maandag 27 September 1993
des namiddags te 1.30 uur precies

door

Xiang-Yang LIU

geboren op 25 November 1960
te Fuzhou (**CHINA**)

Promotor: Professor Dr. P. Bennema

This thesis is based on work carried out by the author, either by him or in conjunction with collaborators Therefore, he is very grateful to the co-authors of the papers presented in this thesis He also wishes to record his appreciation of the help given by the members of the Department of Solid State Chemistry and by Shell Laboratory (Amsterdam) during experiments and discussions The author is deeply indebted to his wife, Mrs Qiu Jie Lin, who patiently and skilfully typed the whole manuscript and is responsible in no small measure for enabling him to undertake a task of this magnitude

This thesis was sponsored by Shell Nederlands BV

Part of this thesis have been published in *Nature* (Macmillan Magazines Ltd), *Physical Review Letters*, *Physical Review* (The American Physics Society), *The Journal of Chemical Physics* (American Institute of Physics), *Surface Science*, *Journal of Crystal Growth* (Elsevier Sci Publ BV) and *Journal of Applied Crystallography* (International Union of Crystallography) The author acknowledges the permission to reprint these

Contents

Chapter 1

INTRODUCTION

1.1. GENERAL

Crystals show a large variety of shapes The shapes which crystals obtain depend on the chemical composition and the growth conditions It has long been realized [1] that the anisotropy of growth rates determines the morphology of crystals A crystallographic orientation with a higher growth rate disappears sooner or later from the crystal form As a consequence, the crystal is bounded by the crystallographic faces having sufficiently low growth rates In this sense, crystal growth kinetics determines the growth rate, and the growth forms of crystals

It is well known that the growth of crystals is a first–order phase transition taking place in the boundary layers between the crystal and the mother phase In this region, growth units are transported from the mother phase to the crystal phase Here two different kinds of processes occur One are the molecular processes at the interface itself The other are transport processes of transporting growth units from the mother phase to the interface, and heat away from the interface Especially the first type of processes are to a large extent determined by the structure of the interface The interfacial structure will significantly influence growth kinetics and therefore affect the growth and the morphology of crystals

At equilibrium or during crystal growth, an interface parameter, the step free energy γkT, plays a key role in growth kinetics and the morphology of the crystal This parameter is the free energy (per unit length) required to form a step on the crystal surface In relation to this parameter, the roughening transition turns out to be a very important physical phenomenon taking place at the crystal surface This is a phase transition occurring at the roughening temperature T^{r} If the temperature T of the system is lower than T^{r}, the step free energy is larger than zero If the temperature T is equal to or higher than T^{r}, the step free energy vanishes The concept of roughening transition plays an essential role in modern theories of crystal growth The growth kinetics depends strongly on the fact whether growth takes place at a temperature above or below T^{r} The relation between the growth rate and supersaturation changes from a nonlinear relation at $T < T^{\mathrm{r}}$ to a linear relation at $T \geq T^{\mathrm{r}}$ Normally rough crystal faces grow faster than faceted crystal faces Faceted faces with a higher step free energy have a higher resistance against growth Therefore, they grow much slower The shape of the growing crystals will be determined by the facets with the highest step free energies

The roughening transition also exerts a significant influence on the equilibrium crystal forms Suppose that at relatively low temperatures, flat faces occur in various orientations It follows from the Gibbs–Wulff theorem that the equilibrium form of a crystal is bounded by flat faces with the lowest surface free energies The step free energy decreases with increasing

temperature Above the roughening temperature, cusps in the Wulff plots become blunt and the associated facets in the equilibrium form become curved When the temperature is above the roughening temperature of the faces of the most morphological importance, all facets disappear and only a smoothly rounded macroscopic morphology remains

Obviously, both in studying growth kinetics and the morphology of crystals, the step free energy or the step energy plays a central role (In case T is much lower than T^r, the step free energy is equal to the step energy since the step entropy does not play a role) The values of these properties depend strongly on both the internal crystal structure and external factors such as properties of the mother phase and growth conditions Therefore, this thesis will concentrate on the description of the interfacial properties, the relevant processes and the controlling factors Moreover, special attention is given to the interfacial structure since any change in this structure will in a subtle way affect the values of the interface parameters

In this thesis, normal alkane or normal paraffin crystals are chosen for our investigations This choice is made for various reasons First, from a practical point of view, normal alkanes are widely distributed in nature, especially in petroleum or heavy oils Studies on the crystallization of n–paraffin will help to solve some problems related to problems of the petroleum industry like the crystallization of heavy fractions of paraffins during the cooling off of gasoline Secondly, in the paraffin series, the size of the molecules changes gradually from a few carbon atoms to a very large number It follows that the physical properties of the molecules will also change gradually with increasing carbon number Henceforth, the studies on the crystal growth of n–paraffins can bridge the gap between the world of normal crystallization (including only relatively small molecules) and of polymer crystallization In addition, the study of the paraffin series is particularly interesting from the standpoint of crystal growth, since the crystals exhibit a large number of phenomena which occur only partially in other materials under normal conditions These phenomena are roughening transitions, kinetic roughening, dendritic growth, polymorphism, different kinds of growth mechanisms, etc It will be shown in this thesis that the paraffin series is an ideal model system for studying such phenomena as mentioned above We note that the study of these phenomena is at present of great interest

The following sections of this introductory chapter are intended to describe the framework of the theories which are relevant for the topic of this thesis This framework serves as a context in which my contributions to experiments and theories can be placed

1.2. TRADITIONAL CELL MODELS FOR CRYSTAL–FLUID SYSTEMS

A crystal is a set of particles (atoms, ions, molecules, etc) which have translational

symmetry in at least three independent space directions This translational symmetry is represented by a lattice The actual crystal corresponds to a particular occupation of this lattice by structural units In investigating crystal growth, all interactions between the occupied lattice points are relevant in addition to the behavior of the structural units, and should therefore be taken into account In fact, the space symmetry of the crystal is also satisfied by those bonds

In order to describe crystal growth, we focus our attention primarily on a suitable formulation of the interface between the crystal and the mother phase From the point of view of statistical mechanics [2], the methods applied to investigate the crystal phase can also be extended to the fluid phase This implies that the first obvious simplification for an interfacial model is to treat assemblies of structural units, which are present in the same form both in the crystal and in the mother phase, as the basic building units In this way, only those bonds which are actually formed during the crystallization process do enter the interface model From this standpoint, Ising models, lattice models or cells models are commonly used for our purpose Since all these models actually belong to the same class, they are collectively referred to as cell models in the present work

The traditional cell models share a number of characteristics, summarized as follows

(i) The whole space of the system, including both the crystal and the fluid phase, is partitioned into cells

(ii) These cells have equal shape and volume

(iii) Each cell is occupied either by a solid unit or a fluid unit

(iv) Cells are connected to each other by bonds, and each cell has in total m bonds connecting it to neighboring cells

In these models, each cell represents a molecule or a building unit, and the internal structure of the unit is irrelevant, in other words, each cell is regarded as a structureless block The symmetry and the bond energies connecting the cells play a crucial role It is implicitly assumed that the the symmetry of the mother phase is the same as that of the crystal It therefore follows that the whole interfacial system is approximated by a network of bonds similar to that of the crystal In different phases, the bond energies of the network are different

Let us restrict ourselves to crystals in which short range interactions are dominant, thus excluding the long range Coulomb interactions from our discussions The network of structural units connected by the strongest bonds (or the crystal graph) was analyzed by Hartman and Perdok [3] In this analysis, the basic concept of periodic bond chain (PBC) is used PBCs are one–dimensional uninterrupted chains of the "strongest bonds", having the translational period $[uvw]$ of the crystal structure According to the PBC theory (or the

Hartman–Perdok theory), crystal faces can be classified into three types. F (flat) faces, S (stepped) faces and K (kinked) faces. F faces are defined as faces $\{hkl\}$ where at least two sets of connected non–parallel PBCs occur within a slice having a thickness of the interplanar distance d_{hkl} (d_{hkl} is corrected for the systematic extinctions of the space group in question) S faces have a slice which contains only one set of parallel PBCs K faces have a slice of (hkl) which contains no PBC Based on the PBC analysis, the theoretical morphology of crystals can be derived from the crystal structure.

We notice that an F face is parallel to a connected net of bonds F faces will undergo a roughening transition at the roughening temperature T_r. Therefore, these faces grow slow below the roughening temperature T_r, due to a two–dimensional nucleation barrier Hence the crystallographic structure of these faces is very important for growth kinetics and morphology Within the framework of the PBC analysis, the nets parallel to S or K faces are not connected in two non–parallel directions by the strongest bonds Therefore the roughening transition temperatures of those faces are "zero" Because of their high growth rates, these faces do not play an important role during the growth process

The theoretical morphologies of n–paraffin crystals with different structures are analyzed in chapter 2 based on PBC analyses. We notice that the PBC analysis is based on traditional cell models Within the framework of these models, the symmetry of the mother phase is assumed to be the same as that of the crystal. In reality, this assumption is only valid when the influence of the mother phase on the morphology is negligible compared with the influence of the crystal phase. If the influence of the mother phase is significant, the results of the PBC analysis can only be considered as the outcome of the morphology for which the crystal structure is responsible

1.3. ROUGHENING TRANSITION

The nature of the roughening transition can be appreciated quite simply with the use of the so–called solid–on–solid (SOS) model [4] (This model is a generalization of the Ising model.) We assume that the crystal surface can be considered as a collection of interacting columns (one for each surface atom) and suppose that introducing a difference in height of one lattice constant between neighboring columns costs a energy J It follows that the Hamiltonian can be taken as

$$\mathcal{H} = J \sum_{<ij>} |h_i - h_j|^2 \qquad (1)$$

(Here the column heights, h_i, are restricted to integer values) Within the framework of this model, no overhangs are permitted and at zero temperature all columns have the same height ($z = 0$), implying that the surface is perfectly flat At finite temperatures, entropy effects should be included At very low temperatures any given facet is microscopically flat with only a few thermally excited surface vacancies or defects However, at higher temperatures more and more energetic fluctuations of the local height of the surface can occur leading to a delocalized interface with long wavelength variations in height The lowest energy excitations are mono steps on the surface that form themselves into plateaus Consequently a loop of length L bounding a plateau has energy JL/a, where a is the lattice constant in directions parallel to the surface The number of possible loops of this length is equivalent to the number of self–avoiding random walks that return to the origin in L/a steps If each column has m nearest neighbor columns, this number is $m^{L/a}$, to within a constant of order unity Thus, the free energy of the system is

$$F = U - TS = L/a\,(J - T \ln m) \tag{2}$$

Below the roughening temperature, T^r, $L = 0$ is favored whereas above this temperature, loops of arbitrarily large length must occur

This roughening transition is but one example of a generic class of two–dimensional phase transformations that were first analyzed systematically by Kosterlitz and Thouless (KT) in the planar XY model [5] This kind of phase transitions is characterized by showing that the required singularity at the transition point is extremely weak,

$$\gamma \sim \exp\left[-A\,|T - T^r\,|^{-1/2}\right], \text{ as } T \to T^r\,(T < T^r) \tag{3}$$

This implies that the roughening transition is of infinite order

This type of roughening transition has been found experimentally for systems consisting of simple building units such as hcp ^{4}He crystals coexisting with its own superfluid [6] Obviously, these systems can be well described by the above mentioned cell models However, when complex molecular systems are under investigation, molecular configurations and other degrees of motional freedom are not negligible This implies that the SOS models simplifying a molecule into a structureless block may not be entirely adequate In this case, the SOS cell models can at best describe the statistical behavior of the center of gravity of the molecules This needs to be coupled with the internal motion of the molecules causing them to attain different molecular configurations This coupling will lead to changes in the interaction energies between the molecules Subsequently, questions arise as to how a

roughening transition occurs in those complex molecular systems, and what character it will have. In order to answer these questions, modified models are needed. For this purpose, a so–called coupled Ising–SOS model (see chapter 3.4) turns out to be a promising alternative model which shows a very rich phase diagram of different kinds of roughening transitions.

The subject matter of chapter 3 is the systematic investigation of the roughening transition of the n–paraffin system. It is shown that the system exhibits some unusual and fascinating critical behavior of the step free energy around the roughening temperature T^r. This critical behavior is associated with the problems discussed above, and may also be valid for other complex molecular systems.

1.4. INTERFACIAL STRUCTURE AND MODELING

It should be emphasized that the cell models discussed above belong to the class of homogeneous cell models, implying that both the crystal and the fluid phase are homogeneous from their bulks up to the dividing surface. Microscopically, the thermodynamic properties of the same type of structural units (such as bond energy, density, etc.) are constant everywhere in the system and do not depend on the positions of those units.

As a matter of fact, we are interested in the interface bond energies ϕ_i. In most cases, however, only the bulk properties are known. Recipes, therefore, are needed to estimate ϕ_i in terms of the bulk properties. For this purpose, Jackson (implicitly) introduced the so–called equivalent wetting condition [7]. This implies that ϕ_i is equal to the bulk bond energy Φ_i, assuming that the solid–fluid interaction energy is equal to the fluid–fluid interaction energy in the same direction of the cells. Obviously, such a condition is satisfied in the homogeneous cell models.

However, the validity of the homogeneous cell models turns out to be questionable because it leads to serious discrepancies between the estimated ϕ_i and the experimental values. From the point of view of modern statistical mechanical models, those discrepancies can be attributed to the following surfaces effects.

(1) Surface reconstruction. When this effect occurs, the bisection of a solid–solid bond at the surface is partially compensated by the strengthening of some bonds parallel to the surface (hkl) or the creation of new bonds.

(2) Surface enrichment. The crystal units close to the surface are rearranged in such a way that less strong bonds and more weak bonds are broken than what would be expected from the bulk structure.

(3) Surface structural phase transition. This effect mainly occurs in complex molecular systems. Due to the influence of fluid molecules, certain degrees of motional freedom of solid

molecules at the surface are released, causing an increase of molecular configurational entropy and a decrease of interfacial bond energies.

(4) Adsorption of impurities or fluid units.

(5) The ordering and the structuring of fluid units near the solid surface. This effect occurs in all solid–fluid interfacial systems. The presence of the solid surface restricts the freedom of molecular motion of the fluid units when they approach the solid surface. This implies that fluid units will lose some configurational, rotational and other entropy in the interfacial regions, resulting in a certain degree of ordering. The interfacial effects (4) and (5) coexist in the fluid part of the interface and the combined effects determine the influence of the interfacial fluid units on the interfacial bond energies.

Obviously, the interfacial effects (1)–(3) can be approximately attributed to the interfacial solid phase, and (4) and (5) to the interfacial fluid phase. Actually, the solid and fluid structures at the interface will influence each other. The degree to which the interface affects the properties of the structural units depends on the distance of these units in the crystal or the ambient phase away from the dividing surface. This subsequently causes the inhomogeneity in the interfacial regions.

In chapter 4, the interfacial regions are examined in detail, both from the points of view of the structure of the interface and statistical thermodynamics. (Special attention is paid to the interfacial bond energies ϕ_i.) In contrast to the traditional homogeneous cell models, a so–called inhomogeneous interfacial cell model is developed, where the thermodynamic properties of the structural units are considered as a function of the distance away from the dividing surface. In context of the modeling, calculations based on self–consistent–field (SCF) theories and experiments are carried out for various systems. (The SCF theories were specially developed to calculate polymer interface systems. The calculation techniques can be to some extent used to supplant Monte Carlo and Molecular Dynamic simulations for the investigation of interfacial systems.) As regards the interfacial structure, the ordering and structuring of fluid interfaces can be investigated in great detail by the SCF techniques.

1.5. MORPHOLOGY OF CRYSTALS AND INTERFACIAL STRUCTURE (IS) ANALYSIS

It can be seen from the discussions in Sec. 1.2 that in the homogeneous cell models, the structure and the symmetry of the crystal extend from the solid side to the fluid side. In reality, the structure and the symmetry of the fluid phase are not the same as that of the crystal phase. Under the conditions that crystals grow from or are in equilibrium with a solution, crystal surfaces correspond to the boundary between the crystal and the ambient

phase (including solute, solvent and impurities) Therefore, the structure of both the crystal and the ambient phase will influence the shape and the size of the crystal surface In other words, the internal factors of the crystals and the external factors determined by the ambient phase will in some way jointly determine the morphology of crystals

Since the influence of the crystal structure on the crystal morphology can be determined by the PBC theory (c f discussions on the relation between the PBC theory and the homogeneous cell models of Sec 1 2), it then follows that the morphology of crystals can be appropriately predicted by coupling the influence of the crystal structure with that of the ambient phase

In order to investigate this coupling quantitatively, in this thesis the concept of so–called Interfacial Structure (IS) analysis is for the first time put forwards (see chapter 5) According to the IS analysis, the "effective" growth units should be identified and their concentration at the surface must be calculated (The "effective" growth units are those growth units at the surface which can be directly incorporated into the crystal without the necessity to pass through a conformational entropy barrier) From an analysis, the surface dependent coupling factor $C^{*}_{\ell(1)}$ can be obtained In association with the PBC analysis, the IS analysis may be applied not only to predict but also to develop recipes for the modification of the morphology of crystals

1.6. SCOPE AND SUMMARY

Since I joined the Laboratory of Solid State Chemistry at the University of Nijmegen in September 1989, a great deal of attention has been devoted to the topic of solid–fluid interfaces Knowledge on solid–fluid interfaces would be of great value for basic surface science, industry, hightech materials and other fields Crystal growth scientists are studying the structure and properties at the interface between the crystal and the mother phase The primary reason is that the structure of the interface is directly related to the central themes of the science of crystal growth the roughening transition, crystal growth mechanisms, crystal growth kinetics and the morphology of crystals Moreover, scientists working in the field of industrial crystallization are interested in tailor–made additives, which are specially designed for modifying the growth habit of crystals, because the morphology of crystals plays an important role in quality control and some industrial processes To understand how the additives affect the morphology of crystals and to carry out molecular design for the additives, the knowledge about the interface is essential These are therefore the motives for me to take the subject of "interfaces" as the central, unifying theme of this thesis

In chapter 2, the morphologies of n–paraffin crystals with three different structures,

triclinic, monoclinic and orthorhombic, have been studied The integrated Hartman–Perdok roughening transition theory and the Bravais–Friedel–Donnay–Harker (BFDH) theory were systematically applied to predict the morphologies of three paraffin structures Simultaneously, crystals of these paraffins have been grown under different conditions of growth in order to compare the predicted and observed morphologies In these studies, special attention has been paid to the influence of the roughening transition on the morphology of crystals Moreover, the dependence of the morphology and the dimensionless roughening temperatures of n–paraffin crystals on the carbon number of n–paraffin molecules have been analyzed taking the crystal structure into account This chapter in a sense reveals the extent of the role of the internal structure on the morphology of crystals

Chapter 3 is devoted to roughening transitions which occur on the {110} faces of odd–paraffin crystals The critical phenomena in relation to the nature of the roughening transition of the n–paraffin systems are the key issues in this chapter In chapter 3 1, a novel type of kinetic transition the so–called "rough–flat–rough" transition occurring in the neighborhood of the roughening transition temperature of n–$C_{21}H_{44}$ crystals in n–hexane solutions is reported This kinetic transition was for the first time observed and identified This phenomenon can be applied to determine the particular critical behavior of the edge free energy in dependence on the temperature T around the roughening temperature T_r In chapter 3 2, a new finding, a first–order roughening transition, is described both experimentally and theoretically This is followed by the description of a novel observation in chapter 3 3 the solvent dependent critical behavior of roughening transition of n–paraffin crystals There it is shown that the roughening transition of the {110} faces of n–paraffin crystals changes from a first–order phase transition to an infinite order phase transition if the solvent of n–hexane is replaced by toluene It was suggested that paraffin–like solvent molecules may promote a surface structural phase transition, which is coupled to the conventional KT type of roughening This surface structural phase transition and the coupling obviously result in an unconventional roughening transition in the n–paraffin system This exceptional surface phenomenon is interpreted in a proper way within the framework of the coupled Ising–SOS model in chapter 3 4 In chapter 3 5, the relation between the step free energy and the critical supersaturation of kinetic roughening is derived for various surface structures To confirm that relation, the step free energies determined from kinetic roughening experiments are compared with the step energies obtained from the roughening experiments The morphology of n–paraffin crystals under the influence of the roughening transition and kinetic roughening is studied experimentally in chapter 3 6

The interfacial structure and interfacial bond energies are the subject of chapter 4 The

so–called inhomogeneous cell model was developed to describe the structure and properties of the interface This model on one hand maintains the main characters of conventional cell models, on the other hand does not have the difficulty in describing the solid–fluid interface, which conventional cell models always encounter with The basic principles and the framework of this model are presented in chapters 4 1 and 4 2 To make a connection between bond energies in the bulk of the crystal and of the mother phase and the corresponding bond energies at the interface, the so–called surface characteristic scaling factor C_l^* is introduced On the basis of this factor, the interfacial properties can be directly related to the wetting conditions of the solid surface A further study of the density distributions and the bond energy distributions at the interface is presented in chapter 4 3 The relation between the interfacial bond energy and the attachment energy of a crystal slice (*hkl*) is also studied qualitatively in chapter 4 3 In chapter 4 4, the surface free energy of crystals consisting of isotropic building units is analyzed according to the principles of thermodynamic statistics and the inhomogeneous cell model The surface free energy is quantitatively expressed as a function of the interfacial factors and the bulk properties To calculate the interfacial properties (such as interfacial bond energies) and to study the structure of the interfacial fluid phase, the self–consistent–field theory (or the Scheutjens–Fleer theory) is for the first time applied to crystal–fluid interfacial systems Using this calculation technique, two different types of systems monomer and polymer are investigated in great detail in chapters 4 5 and 4 6, respectively In particular, the ordering of chain–like fluid molecules near the solid surface is examined in depth, both theoretically and experimentally in chapter 4 7 These results indicate that the modeling and the SCF calculations not only offer a reliable way to calculate the interfacial bond energies ϕ_1, but also greatly improve our knowledge about the interface In chapter 4 8 the structure of odd and even n–paraffin molecules adsorbed on graphite is observed with a scanning tunneling microscopy Chapter 4 9 includes a systematic analysis of the influence of various solvents on the interfacial structure of the n–paraffin crystal system and on the step energy This analysis has substantially improved our knowledge about the basic interfacial structure of the systems of crystals in contact with multi–component solutions According to the calculations, the use of a mixture of two solvents may lead to an increase in the step energy of the system within a certain range of concentrations

The attention in chapter 5 is devoted to the influence of the mother phase on the morphology of crystals Studies on this subject are carried out by the newly developed Interfacial Structure (IS) analysis The principles of the IS analysis are discussed in the prediction of the morphology of n–paraffin crystals In this analysis, the concentration of

"effective" growth units having the proper configuration at the interface plays a central role This analysis can be applied to investigate the effect of tailor–made additives on the growth habit of crystals and the crystallization processes, and may offer a guideline for molecular design of tailor–made additives

The influence of volume transport on the crystal growth rate is another important issue in crystal growth. The volume resistance against mass transport and heat transport during crystal growth reduces the effective driving force at the solid surface. The resistance can be estimated from a relation between "rough growth" and "flat growth". Within this framework, the so–called auxiliary straight line method is introduced in chapter 6. This method is applied to the n–paraffin crystal system.

REFERENCES

1 N. Steno, *De Solido Intra Solidum Naturaliter Contento Dissertationis Prodromus,* (Florence, 1669).

2 S.R Fowler and E.A. Guggenhein, *Statistical Thermodynamic*, (Cambridge University, London, 1960).

3 P. Hartman, in *Morphology of Crystals*, edited by I. Sunagawa, (Terra Sci., Tokyo, 1987) p.271.

4 J.D. Weeks, in *Ordering in Strongly Fluctuating Condensed Matter Systems*, edited by Riste, (Plenum, New York, 1980) p 293

5 J.M. Kosterlitz and D.J. Thouless, J. Phys. C6, 1181 (1973).

6 S.G. Lipson and E. Polturak, in *Progress on Low Temperature Physics*, edited by D.F. Brewer, (Elsevier, Amsterdam, 1987) p.128.

7 K.A. Jackson, in *Liquid Metals and Solidification* (Am. Soc. for Metals, Metal Park, OH, 1958).

Chapter 2

RELATION BETWEEN STRUCTURES AND MORPHOLOGY OF CRYSTALS

Chapter 2.1

On the morphology of crystals of triclinic even normal alkanes: theory and observation

Xiang–Yang Liu and P Bennema

RIM, Laboratory of Solid State Chemistry, Faculty of Science, University of Nijmegen, Toernooiveld 1, 6525 ED Nijmegen, The Netherlands

ABSTRACT–In this paper the morphology of crystals of triclinic even n–alkanes over a range of chain lengths with $10 \leq n \leq 36$ is studied theoretically and experimentally Using the Buckingham potential for C–C, H–H and C–H interatomic interactions between neighboring molecules, the overall interaction energies between n–alkane molecules are calculated Five types of important lateral interactions and three vertical interactions are identified from the structure From these, a crystal graph with primitive cell is obtained Thirteen connected nets corresponding to thirteen F forms, {001}, {010}, {011}, {100}, {101}, {111}, {110}, $\{1\bar{1}1\}$, $\{1\bar{1}\bar{1}\}$, $\{1\bar{1}0\}$, {121}, {122} and {120}, are derived from the crystal graph The dimensionless roughening transition temperatures of the F faces are calculated It follows that a phase diagram of the relative roughening temperature in dependence of n is obtained To predict the theoretical growth forms, several recipes inspired by Ising models, the Hartman–Perdok and the Donnay–Harker theory are applied to the n–paraffins series It turns out that crystals of triclinic even n–paraffins have the shape of long flat needles and are bounded by large faces of the form {001} and the narrow, long side faces of {010}, with the small {100} faces at the top of the needle Some experiments were carried out to study the morphology and the roughening transition of n–C_{24} and n–C_{16} crystals in n–hexane and other systems The predicted and observed results agree quite well

---

J Cryst Growth (to be published)

I. INTRODUCTION

The prediction of the external appearance of crystals from their internal structures is of interest both for scientists working on the fundamentals of crystal growth and scientists working on the problems of industrial crystallization In recent years, new developments in the morphological theories allow us to carry out in depth investigations on the growth morphology of crystals [1-2] Conventionally the relative order of morphological importance MI of face (hkl) is defined as a statistical measure for the relative size or the relative frequency of occurrence of faces of a form $\{hkl\}$ on crystals The faces with the greater MI possess a lower growth rate and dominate external shapes of crystals Previously, some *ad hoc* theories can to some extent be used to describe growth forms of crystals According to the principles of the Bravais–Friedel–Donnay–Harker (or BFDH) theory [3], the interplanar distance of a crystallographic form $\{hkl\}$, d_{nhnknl}, is used to determine the relative MI of faces on crystal forms This geometrical BFDH theory can be justified by assuming that the interactions between growth units are proportional to the mutual distance between the growth units In the Hartman–Perdok theory [4-6], a PBC (Periodic Bond Chain) analysis plays an essential role in search for flat (or F) faces of the crystal structure Based on the theory, the relative MI of F faces is determined by E_{hkl}^{slice} and E_{hkl}^{att} The higher E_{hkl}^{slice} (or the lower E_{hkl}^{att}) of the faces $\{hkl\}$, the higher the relative morphological importance (MI) [7]

Apart from these classical criteria, the developments in statistical mechanical Ising models offer us a powerful tool to judge the relative MI by the calculated Ising temperature θ^c of faces $\{hkl\}$ The so–called dimensionless Ising temperature θ^c is defined as a critical temperature at which the order–disorder transition of a connected net parallel to the $\{hkl\}$ faces occurs [1,2,8-12] The results of computer stimulations reveal that the dimensionless roughening temperature $\theta^F \cong \theta^c$, meaning that θ^c can be used as a reasonable estimation of θ^F [1] This follows that if the dimensionless actual temperature θ is higher than θ^c of $\{hkl\}$ faces, the surface will grow in a rough mode without keeping in the crystallographic orientation (hkl), if θ is lower than θ^c of $\{hkl\}$ faces, the face is flat in a well–defined orientation (hkl), and has to grow by a layer mechanism It is assumed that the higher θ^c the higher the MI Contrary to growth forms, equilibrium forms of crystals can be unambiguously described using the surface free energy of the faces $\{hkl\}$, according to the Gibbs–Wulff theorem For more details, see Ref 13

The reason that we apply the morphological theories to n–alkane crystals is that as one of a basic family of organic crystals, normal alkanes are widely distributed in nature Petroleum or heavy oil consist to a large extent of these compounds Many studies concerning these compounds are carried out in relationship with problems in the petroleum industry and oil

transportation. Moreover, normal alkanes are considered as the first terms of polyethylene series. Therefore, studies on n–paraffins are sometimes regarded as the starting point of the studies on polymers. In this sense, the understanding of morphology of n–paraffins is very important for the industry. From a theoretical point of view, the study of n–paraffin series is particularly interesting since interactions between molecules are of the type of van der Waals interactions. First, interaction energies between paraffin molecules show a high degree of anisotropy. Furthermore, the bond energies between growth units increase with increasing the carbon number. This offers large possibilities for a systematical research on the growth and morphology of paraffin crystals.

n–paraffins crystallize in one of four modifications, depending on the value of the number of C atoms in the n–paraffin chain n and on growth conditions [14]. These four modifications are triclinic, monoclinic, orthorhombic and hexagonal. The last one, which only occurs in the neighborhood of the melting point for the odd numbered n–paraffins from n–C_9 to n–C_{43} and for the even paraffins from n–C_{22} to n–C_{44}, is called α phase or rotational crystalline state (RCS). The other modifications are just known as β phase (β_T, β_M and β_O respectively). In our previous paper [15], we have already presented a study on the morphology of odd orthorhombic n–paraffins. In this paper we will limit ourselves to a study of the morphology and the roughening transition of triclinic even paraffins.

This paper is arranged as follows. After briefly discussing the crystal structure and the bond structure of triclinic even paraffins, we will focus our attention on the roughening transition from the point of view of the Ising models. Later the theoretical growth and equilibrium forms will be derived based on different recipes. Finally, observations on the roughening transition and on observed growth forms of different homologue of even n–paraffin crystals growing under different conditions are presented. The later are compared with those of theories.

II. STRUCTURE, CRYSTAL GRAPH AND NET ANALYSIS

A. Structure of triclinic even n–paraffins

To our knowledge, even n–paraffins starting with n–C_6 to n–C_{26} crystallize in the triclinic structure [14,16-18]. Some investigations show that n–C_{28} can also crystallize in the triclinic modification [19,20]. According to the hypothesis of Nyburg [16], the last member of the series should be n–C_{36}. In our paper, we carry out a morphological study of the triclinic structure of even n–paraffins in the range from n–C_{10} to n–C_{36}.

After analyzing existing paraffin structure data, Nyburg and Potworowski [16] showed how the cell parameters and the crystal structures of all normal paraffins could be predicted on the

basis of a few key structures We will use Nyburg's method to predict all structural data of the triclinic paraffin series needed for this paper. The predictions are based on the key structure of n–C_{18} [21]

The space group of the βr n–paraffins is $P\bar{1}$ Concerning the symmetry of a even paraffin molecule (fulfilling 2/m), a symmetry center occurs in the center of the molecule. This implies that within the triclinic structure the inversion center i coincides with the symmetry center of a molecule. Consequently, only one molecule occurs within one unit cell In Fig 1, the arrangements of n–paraffin molecules in the structure of n–$C_{18}H_{38}$ are presented as the y and the z projection.

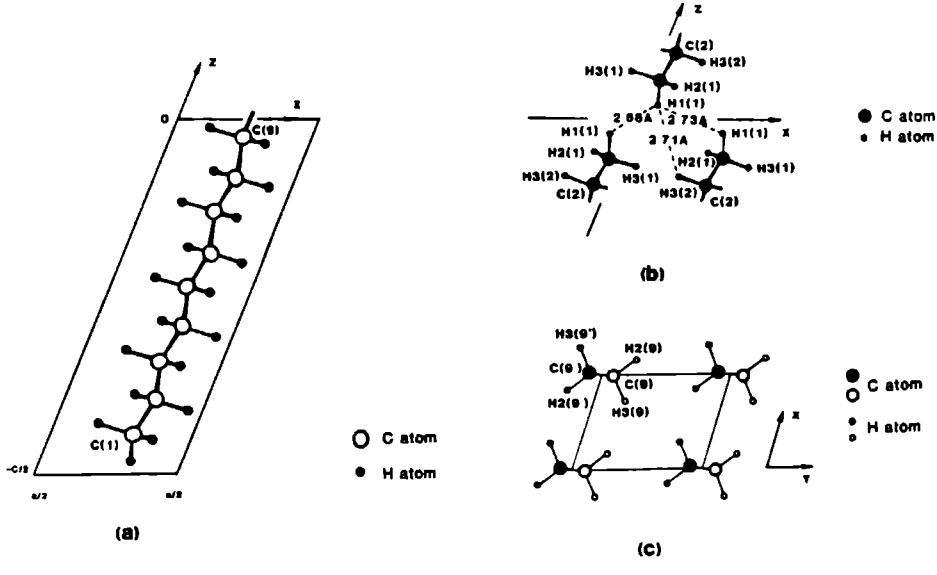

FIG 1 The structure of n–$C_{18}H_{38}$ in different projections (a) Half–molecule in the y projection. (b) Close contacts at ends of molecules (the y projection) (c) Close contacts illustrated for the molecular centers in the z projection

In the series of triclinic even paraffins, the cell parameters a, b and the angle γ change only slightly as a function of n while the c axes and the α and β angle depend strongly on n. The cell parameters from n–C_{10} to n–C_{36} are listed in Table I. They were calculated using Nyburg's method.

TABLE I. Dimensions of the unit cell.

$a = 4.285$ Å	$b = 4.82$ Å		$\gamma = 72.7°$
Carbon number	c(Å)	$\alpha(°)$	$\beta(°)$
n–C_{10}	14.814	81.41	65.20
n–C_{12}	17.326	82.75	66.12
n–C_{14}	19.845	83.76	66.28
n–C_{16}	22.371	84.53	67.37
n–C_{18}	24.900	85.15	67.80
n–C_{20}	27.432	85.66	68.16
n–C_{22}	29.966	86.08	68.45
n–C_{24}	32.502	86.43	68.71
n–C_{26}	35.039	86.73	68.92
n–C_{28}	37.577	87.00	69.11
n–C_{30}	40.116	87.22	69.27
n–C_{32}	42.655	87.43	69.41
n–C_{34}	45.195	87.61	69.54
n–C_{36}	47.736	87.77	69.66

B. Bond structure in triclinic even n–paraffins

In order to identify connected nets from the crystal graph and to calculate Ising temperatures, one has to know the bonds between building units. In the case of growth of n–paraffin crystals from solutions, it is supposed that the growth units are the paraffin molecules themselves. Between n–paraffin molecules, van der Waals interactions are dominant. This in fact simplifies our problems considerably because van der Waals interactions drop drastically with the distance. Then only interactions between neighboring molecules need to be considered. Those between distant molecules are negligible.. To calculate an interaction energy between two molecules, we sum up all C–C, C–H and H–H atom–atom interaction energies between the two molecules. These atom–atom interactions are calculated from the Buckingham potential

$$\phi(r) = -A/r^6 + B\exp(-Cr) \qquad (1)$$

where the empirical potential parameters A, B, and C were taken from Ref 22 for C–C, H–H and C–H interactions, and are the same as parameter set 1b of Ref 15 In this way, interaction energies between any two adjacent molecules can be calculated

To derive the crystal graph of triclinic paraffin crystals, we first reduce the molecules to centers of gravity In our case, we have chosen the inversion centers within molecules as centers of gravity or nodes These nodes fulfill the space group symmetry of the crystal structure A reference node (or molecule) in a reference unit cell is labeled as C[000] All other nodes can be labelled by shifting the reference node over a translation distance t, given by

$$t = ua + vb + wc \tag{2}$$

where u, v, w are integers

The following step is to connect those nodes by the intermolecular bonds calculated above It has to be noted that in our investigations, we will only focus on the strongest bonds in the structure, which play a key role in morphology [1,2,4-6] Different types of bonds identified from the structure are listed in Table IIa

As a consequence, a crystal graph is presented in Fig 2

TABLE IIa. Bonds in the structure of triclinic even n–paraffins

Bonds	Code
C*(0 0 0) – C(1 0 0)	a
C(0 0 0) – C(0 1 0)	b
C(0 0 0) – C(–1 1 0)	c
C(0 0 0) – C(1 1 0)	d
C(0 0 0) – C(0 –1 1)	e
C(0 0 0) – C(0 0 1)	f
C(0 0 0) – C(–1 0 1)	g
C(0 0 0) – C(–2 1 0)	c'

* Here C is the gravity center of a paraffin molecule

TABLE IIb The coefficients of expressions of bond energy in the structure

	ϕ_i^*(kcal/mol)	ϕ_i'(kcal/mol)
ϕ_a	0 787159	–0 93711
ϕ_b	0 552933	–0 83265
ϕ_c	0 344506	–0 38039
ϕ_d	0 0664083	–0 15688
$\phi_{c'}$	0 0365824	–0 09874
ϕ_e	0	0 70743
ϕ_f	0	0 50391
ϕ_g	0	0 95928
E^{cr}	1 787589	–0 23515

Obviously, the whole crystal graph reflects the bond structure of triclinic even n–paraffin crystals and like the system of nodes has the same symmetry as the crystal structure The overall " body–body " bonds a,b,c,d, and c' are the first and the second nearest neighbor lateral interactions between molecules, while the overall head–tail bonds g,e and f are the first

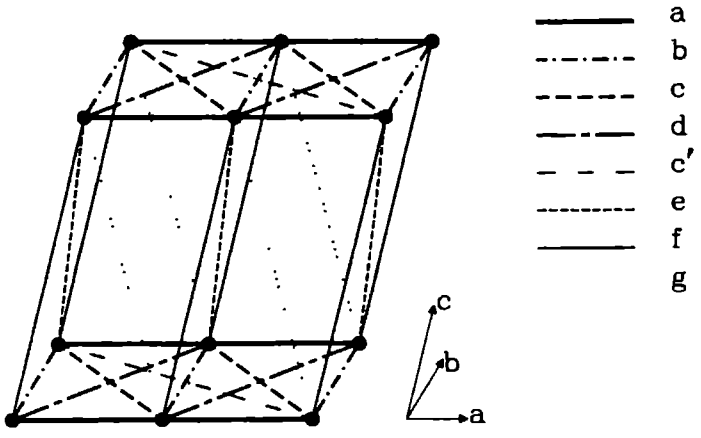

FIG 2. The crystal graph of the triclinic even n–paraffin structure The lateral bonds a, b, c, d and c' and the vertical f, g and h are indicated.

neighbor vertical interactions between molecules. By a least square fitting, we found again as before for orthorhombic paraffin [15] that all the bond energies depend linearly on the carbon number n. The relation can be expressed as

$$\phi_i(n) = \dot{\phi}_i n + \phi_i'. \tag{3}$$

(For the vertical bonds $\dot{\phi}_i = 0$.) The coefficients $\dot{\phi}_i$ and ϕ_i' are listed in Table IIb. the calculated bond energies versus carbon number n are plotted in Fig. 3.

In general, the lateral bonds are much stronger than the vertical bonds due to the high anisotropy of interaction energies. This is the same as orthorhombic odd paraffins [15]. Looking at the lateral bond energies presented in Table II and Fig. 3 in detail, it can be seen that the bond a is the strongest one in the structure, followed by b,c,d, and c'. From bond a to c', intermolecular interactions change from the first nearest neighbor to the second nearest neighbor, and the strength of bonds drops dramatically. As a result, bonds d and c' are as weak as vertical bonds.

Before going further to the next section, we would like to mention two relations. We notice that the bond energies calculated are in fact the solid–solid bond energies ϕ_i^{ss} (i = a,b, ..., g, respectively) referenced to the vacuum. For crystals grown from all kind of solvents these ϕ_i^{ss} bond energies have to be replaced by generalized bond energies ϕ_i [1], given by

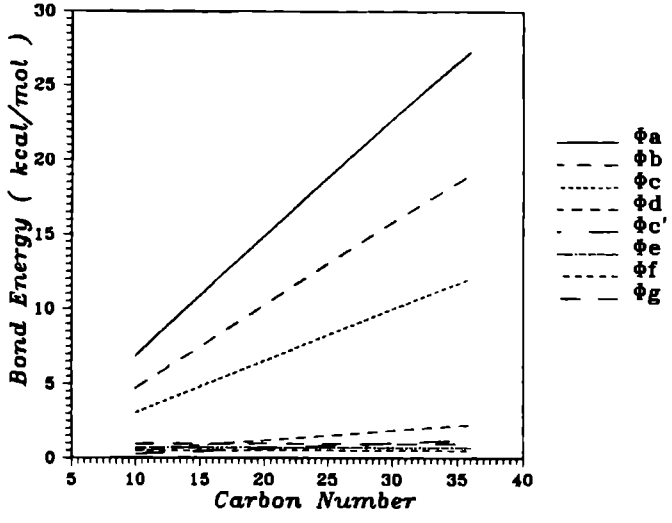

FIG 3. Different bond energies plotted as a function of n, the number of carbon atoms within paraffin chains.

$$\phi_i = \phi_i^{sf} - (\phi_i^{ss} + \phi_i^{ff})/2. \tag{4}$$

Here superscripts sf and ff denote solid–fluid and fluid–fluid bonds, respectively.

Another relation is the so–called proportionality relation [1]. This relation states that

$$\phi_i : \phi_j : \phi_k : \ldots = \phi_i : \phi_j : \phi_k : \ldots \tag{5}$$

This implies that the ratios of bond energies are fixed for a crystal in different situations. This assumption allows us to use the reliable overall ϕ_i^{ss} bond energies to construct the crystal graph, and to carry out a network analysis and to calculate Ising temperatures. It follows from Eq.(5) that for morphological analyses only the ratios of bonds are relevant. Note that in special cases, such as unusual interactions of solid units at crystal surfaces with solvents or impurities, the ratios can be changed for different faces. Nevertheless, in most cases the relative values of bond energies are roughly unchanged, then they are more important than the absolute values. In addition, the relative bond energies are also essential for the calculations of dimensionless Ising temperatures.

To calculate the relative bond energy, we choose as a reference the strongest bond energy

'str and take this equal to unity. It follows for the series of triclinic even n–paraffins that

$$\phi_{str} = \tilde{\phi}_a = 1, \quad (\tilde{\phi}_i = \phi_i/\phi_a). \tag{6}$$

'he values of relative bond energies of triclinic even n–paraffins are listed in Table III.

'ABLE III. The relative values of bond energies.

'araffins	$\tilde{\phi}_i$ (× 10)							
	a	b	c	d	c'	e	f	g
ı–C_{10}	10	6.7729	4.4195	0.7314	0.3852	1.0202	0.7267	1.3834
ı–C_{12}	10	6.8195	4.4115	0.7522	0.3999	0.8314	0.5922	1.1274
ı–C_{14}	10	6.8515	4.4061	0.7665	0.4100	0.7016	0.4998	0.9514
ı–C_{16}	10	6.8748	4.4021	0.7769	0.4174	0.6068	0.4323	0.8229
ı–C_{18}	10	6.8926	4.3991	0.7848	0.4231	0.5346	0.3808	0.7250
ı–C_{20}	10	6.9066	4.3967	0.7911	0.4275	0.4778	0.3403	0.6479
ı–C_{22}	10	6.9180	4.3947	0.7961	0.4310	0.4319	0.3076	0.5856
ı–C_{24}	10	6.9273	4.3931	0.8003	0.4340	0.3940	0.2807	0.5343
ı–C_{26}	10	6.9351	4.3918	0.8038	0.4365	0.3622	0.2580	0.4912
ı–C_{28}	10	6.9418	4.3907	0.8068	0.4386	0.3352	0.2388	0.4546
ı–C_{30}	10	6.9475	4.3897	0.8093	0.4404	0.3119	0.2222	0.4230
ı–C_{32}	10	6.9525	4.3888	0.8116	0.4420	0.2917	0.2078	0.3955
ı–C_{34}	10	6.9569	4.3881	0.8135	0.4434	0.2739	0.1951	0.3714
ı–C_{36}	10	6.9608	4.3874	0.8152	0.4446	0.2582	0.1839	0.3501

Note: the relative bond energies $\tilde{\phi}_i$ (i = a, b, ... , g) = ϕ_i/ϕ_a.

t can be seen directly from Table III that due to the chosen convention, the relative values of 'ertical bond energies drop rapidly with increasing n, while those of lateral bond energies 'emain unchanged or only change slightly. This is understandable as the following. As ıforementioned, all bonds are referenced to ϕ_a, and all lateral bonds (including ϕ_a) depend inearly on n, while all vertical bonds are independent of n. This results in the change of the ınisotropy in bond energies in the given paraffin series. We will come back to this in Sec.III.

3. Network analysis

In order to predict the morphology of paraffin crystals and to calculate Ising temperatures, we have to find connected nets of the structure This can be done by partitioning the crystal graph as presented in Fig 2, in equal parallel nets, having no points in common [1,2] The nets must have an overall thickness of the interplanar distance d_{nhnknl}, corrected by the extinction conditions of the space group of the crystal graph [1,2] Since the space group of the triclinic even n–paraffin structure is the simple space group $P\bar{1}$, having a primitive lattice and no screw axis and glide planes, we do not need to worry about extinction conditions

The other parallel way to identify connected nets is to carry out a PBC analysis According to the Hartman–Perdok theory [4-7], the so–called PBCs are the uninterrupted chains of bonds running through the structure and having a periodicity $[uvw]$ of the lattice If two PBCs occurring in different crystallographic directions intersect each other, a F face is possible A real F face, however, corresponds to a connected net parallel to the face [1,2], consisting of at least two sets of connected PBCs The network analysis will be started with the identification of PBCs.

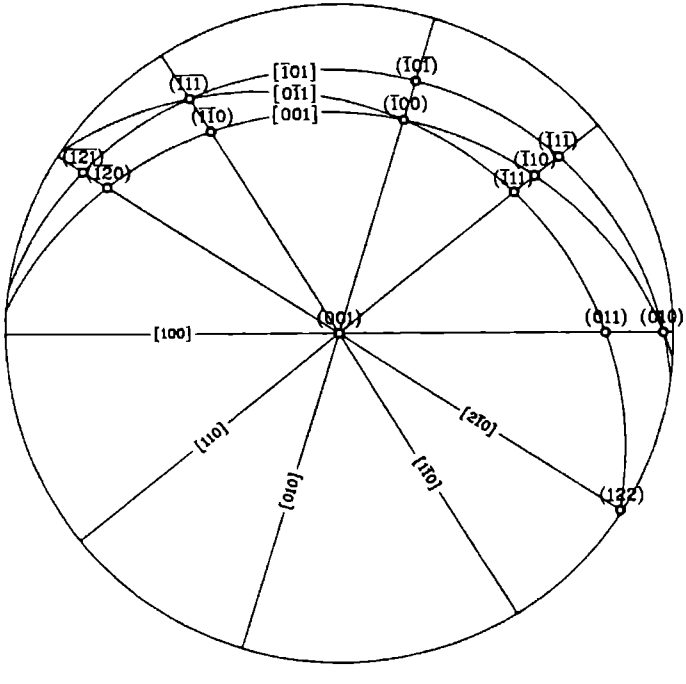

FIG 4 The stereographic projection of PBCs (——) The intersections of these PBCs indicate 13 potential F–forms (o)

It can seen from the crystal graph in Fig 2 that the bond structure with space group of $P\bar{1}$ is very simple Each PBC contains only one bond A total of eight PBC's can be identified in the structure They are listed in Table IV

The next step in the PBC analysis is to search for the real F faces One of the most easy ways to find F faces is to make a stereographic projection of all the PBCs [4-7] This is shown in Fig 4

In Fig 4 each point of intersecting PBCs corresponds to a potential F face Totally 13 potential F forms are then identified (see Fig 4) It is found that all the nets which are parallel to those forms are connected So they are all real F forms The resulting connected nets, the slice thickness of the nets, the involved PBCs and the bonds contained in the PBCs and connected nets are summarized in Table V

TABLE IV Identified PBCs in the triclinic structure of n–paraffins

PBCs	Bonds
[100]	a
[010]	b
$[1\bar{1}0]$ ($[1\bar{1}0]$)	c
[110]	d
$[2\bar{1}0]$ ($[\bar{2}10]$)	c'
$[\bar{1}01]$	g
$[0\bar{1}1]$	e
[001]	f

together with the rectangularized nets

It can be seen from Fig 5 that the (001) connected net is the most complicated one Here bonds d cross bonds c and bonds c' cross both bonds d and bonds b In order to calculate the Ising temperature, the weaker bonds d and c' are omitted, and the remaining hexagonal net is "rectangularized" by splitting nodes into two nodes with a bond of infinite strength (indicated with a wiggled bond) connecting these two nodes [1,8-10] From the obtained rectangular nets the Ising temperatures can be calculated The other three hexagonal nets are the connected

TABLE V. Thirteen connected nets in the structure, along with the contained PBCs, bonds and thickness of the slices.

Connected Nets	Thickness of Slices	PBCs	Bonds
(001)	d_{001}	[100] [110] [$1\bar{1}0$] [010] [$2\bar{1}0$]	a,b,c,d,c'
(010)	d_{010}	[100] [$\bar{1}01$] [001]	a,g,f
(011)	d_{011}	[100] [$0\bar{1}1$]	a,e
(100)	d_{100}	[010] [001] [$0\bar{1}1$]	b,e,f
(101)	d_{101}	[010] [$\bar{1}01$]	b,g
(111)	d_{111}	[$1\bar{1}0$] [$0\bar{1}1$] [$\bar{1}01$]	c,e,g
(110)	d_{110}	[$1\bar{1}0$] [001]	c,f
($1\bar{1}1$)	$d_{1\bar{1}1}$	[110] [$\bar{1}01$]	d,g
($\bar{1}11$)	$d_{\bar{1}11}$	[110] [$0\bar{1}1$]	d,e
($1\bar{1}0$)	$d_{1\bar{1}0}$	[110] [001]	d,f
(120)	d_{120}	[$1\bar{2}0$] [001]	c',f
(122)	d_{122}	[$2\bar{1}0$] [$0\bar{1}1$]	c',e
(121)	d_{121}	[$2\bar{1}0$] [$\bar{1}01$]	c',e

Also, the 13 obtained connected nets are presented in Fig.5,
nets (010), (100) and (111). Similarly, they also need to be rectangularized. The remaining connected nets are already rectangular. (In the theory only relation between points of the crystal graph count and not the angles between the bonds. For the theory, those nets where four bonds originate from all nodes are therefore "rectangular".)

III. ROUGHENING TRANSITION

In order to study under which conditions the crystal faces grow as flat or rough faces, the dimensionless Ising temperatures of the connected nets have to be calculated. The dimensionless Ising temperature of a connected net is defined as a dimensionless temperature [1,2,9-12], by

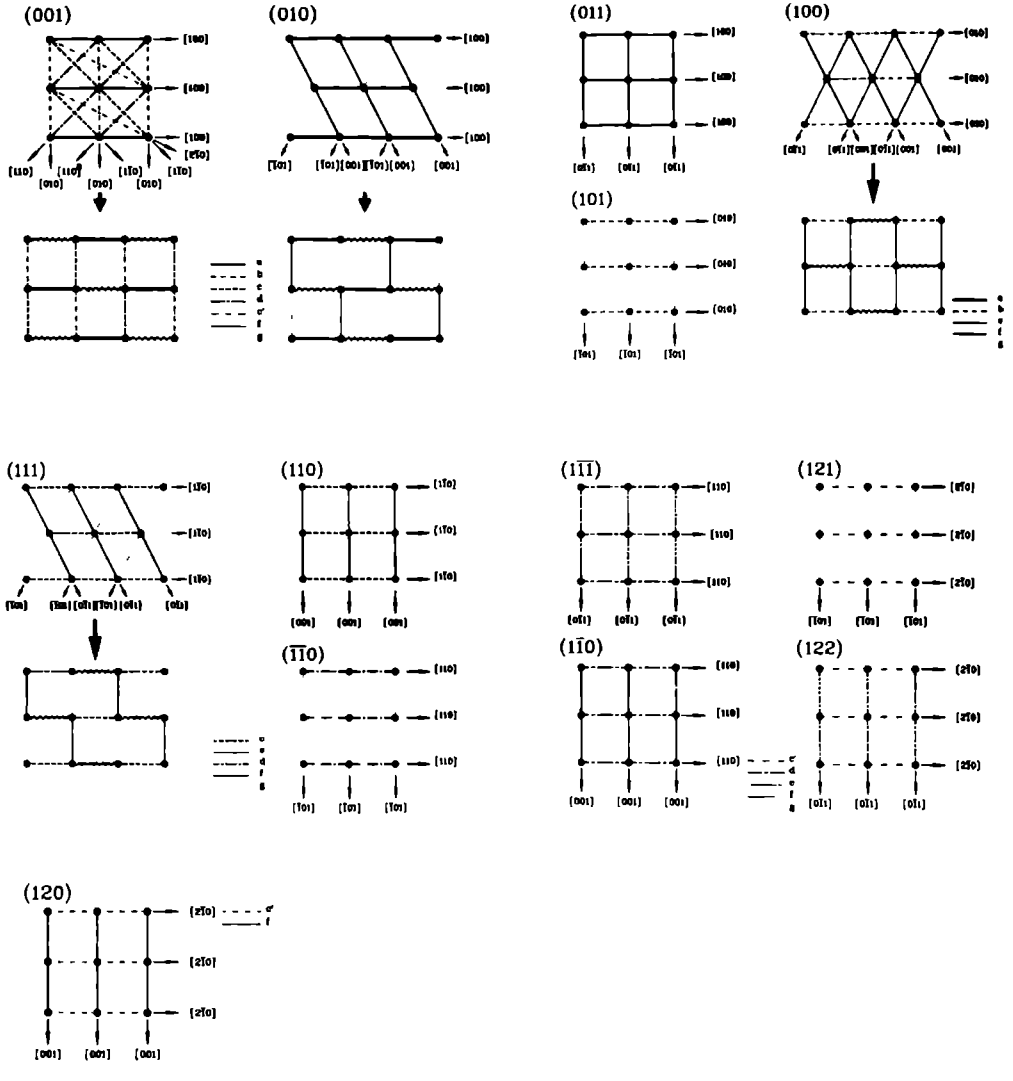

FIG.5. The thirteen connected nets of the triclinic even n–paraffin structure. The rectangularized connected nets (001), (010), (100) and (111) nets are also shown in the figure. The weaker bonds d and c' are omitted in rectangularizing the (001) net.

TABLE VI The dimensionless Ising temperatures of different connected nets

Paraffins	ϕ_{hkl}						
	{001}	{010}	{011}	{100}	{101}	{111}	{110}
n–C_{10}	2 5316	1 1696	0 1116	0 8562	0 7788	0 7698	0 4710
n–C_{12}	2 5381	1 0870	0 8562	0 7949	0 7283	0 6998	0 4390
n–C_{14}	2 5445	1 0246	0 8150	0 7496	0 6897	0 6489	0 4153
n–C_{16}	2 5445	0 9756	0 7819	0 7143	0 6592	0 6101	0 3965
n–C_{18}	2 5445	0 9363	0 7547	0 6854	0 6341	0 5794	0 3814
n–C_{20}	2 5510	0 9042	0 7321	0 6614	0 6135	0 5540	0 3686
n–C_{22}	2 5510	0 8764	0 7128	0 6410	0 5956	0 5328	0 3578
n–C_{24}	2 5510	0 8525	0 6964	0 6234	0 5800	0 5171	0 3486
n–C_{26}	2 5510	0 8313	0 6812	0 6079	0 5666	0 4988	0 3402
n–C_{28}	2 5510	0 8130	0 6680	0 5942	0 5546	0 4850	0 3330
n–C_{30}	2 5510	0 7962	0 6562	0 5821	0 5438	0 4726	0 3265
n–C_{32}	2 5510	0 7813	0 6456	0 5711	0 5339	0 4617	0 3206
n–C_{34}	2 5510	0 7675	0 6357	0 5609	0 5249	0 4517	0 3153
n–C_{36}	2 5510	0 7553	0 6270	0 5519	0 5168	0 4427	0 3104
MI order	1	2	3	4	5	6	7

TABLE VI (continued)

Paraffins	ϕ_{hkl}					
	{1$\bar{1}$1}	{1$\bar{1}\bar{1}$}	{1$\bar{1}$0}	{121}	{122}	{120}
n–C_{10}	0 2326	0 1970	0 1654	0 1786	0 1487	0 1223
n–C_{12}	0 2106	0 1795	0 1519	0 1602	0 1342	0 1112
n–C_{14}	0 1942	0 1665	0 1417	0 1465	0 1234	0 1029
n–C_{16}	0 1815	0 1563	0 1336	0 1358	0 1149	0 0963
n–C_{18}	0 1712	0 1480	0 1271	0 1274	0 1082	0 0911
n–C_{20}	0 1628	0 1412	0 1217	0 1204	0 1026	0 0868
n–C_{22}	0 1556	0 1354	0 1171	0 1145	0 0979	0 0831
n–C_{24}	0 1495	0 1304	0 1132	0 1095	0 0939	0 0799
n–C_{26}	0 1442	0 1261	0 1097	0 1051	0 0904	0 0771
n–C_{28}	0 1396	0 1223	0 1066	0 1013	0 0873	0 0747
n–C_{30}	0 1354	0 1189	0 1039	0 0980	0 0846	0 0726
n–C_{32}	0 1317	0 1159	0 1015	0 0949	0 0821	0 0706
n–C_{34}	0 1284	0 1132	0 0992	0 0922	0 0799	0 0689
n–C_{36}	0 1253	0 1107	0 0972	0 0898	0 0780	0 0673
MI order	8	9	11/10*	10/11*	12	13

* Note the change of the MI order is due to the variation of energies of lateral bonds with the carbon number, especially for $\phi_{r'}$ This bond energy increases gradually from smaller than to larger than those of vertical bonds (See Table III and Fig 3)

$$\Theta^{c}_{hkl} = 2kT^{c}/\phi_{str} \qquad (7)$$

where k is the Boltzmann constant, T^{c} the absolute critical temperature, ϕ_{str} the bond energy of the strongest bond at the crystal surface.

Using the normalized bond energies presented in Table III, the Ising temperatures for the series of triclinic even n–paraffins can be calculated with the formalism and computer program (see Refs.9 & 10). The results from n–C_{10} to n–C_{36} are presented in Table VI. In order to compare with the other data in Sec.IV.A., the order of MI is also presented in Table VI. It can be seen from Table VI that except for the {001} faces the dimensionless Ising temperatures decreases if n increases. This is because the relative values of the vertical bonds decrease (see Table III) and the corresponding nets are getting more anisotropic with increasing n.

Note that in expression (7), the strongest bond in the structure is taken as a reference. Since this bond energy depends on the carbon number of paraffins, for different paraffins the reference is various. In order to compare the Ising temperature for the whole paraffin series we need to have a fixed reference. For this purpose we modify the dimensionless critical temperature as

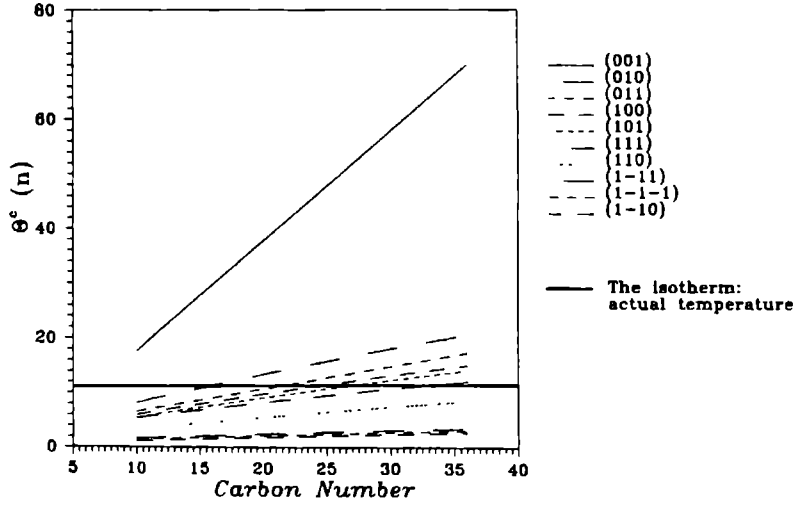

FIG.6. The modified dimensionless roughening temperatures, $\Theta^{c}_{hkl}(n) = \Theta^{c}_{hkl}\phi_{str}(n)/\rho$, plotted as a function of n, the carbon number within paraffin chains; an isotherm corresponding to a horizontal line.

$$\theta^{c}_{hkl}(n) = \theta^{c}_{hkl}\phi_{str}(n)/\rho \tag{8}$$

and define a dimensionless temperature

$$\theta = 2kT/\phi_{str'} \tag{8a}$$

where $\phi_{str}(n)$ is referred to as the strongest molecule–molecule bond at the solid–fluid interface, and $\phi_{str'}$ is the reference value and is fixed for the whole series (Note that the choice of θ will be discussed later in Sec IV A) The factor ρ is introduced to keep $\theta^{c}_{hkl}(n)$ as a dimensionless temperature, and chosen to be equal to 1 kcal/mol In principle, $\phi_{str}(n)$ can be evaluated by the determination of roughening temperature In our case, $\phi_{str}(n)$ is not available for the time being Here we just choose $\phi_{str}(n) \simeq \phi^{ss}_{str}(n)$, which is supposed to be in the vacuum environment, and all results are plotted in Fig 6

In Fig 6 isotherms correspond to horizontal lines and equiv n lines to vertical lines This means that we have a direct relation between $\theta^{c}_{hkl}(n)$ and the carbon number within the whole series If we use a horizontal line to refer to a certain growth condition, the $\theta^{c}_{hkl}(n)$ curves located above the isotherm indicate that the faces grow in a flat mode and below the isotherm the faces grow in a rough mode Obviously, the horizontal line refers to the boundary of flat and rough surfaces This is a kind of presentation of the roughening transition phase diagram This diagram may be used to estimate the roughening transition on surfaces of the triclinic even paraffin crystals

IV CONSTRUCTION OF THEORETICAL GROWTH AND EQUILIBRIUM FORMS

In this section we will predict growth and equilibrium forms of triclinic even n–paraffin crystals according to alternative recipes Contrary to the equilibrium form, which, as mentioned in Sec I, can be logically derived from thermodynamic principles and applied to tiny crystals in thermodynamic equilibrium, for crystal growth forms no unambiguous recipes exist In reality, forms of crystals are unique However, theoretical idealized crystal forms may be constructed using *ad hoc* recipes We notice that the *ad hoc* character of the recipes is due to the fact that qualitative relations between rate of growth and the parameters used are transformed in quantitative relations Nevertheless such constructed growth forms still have an heuristic value From analyses of growth forms obtained from different recipes valuable ideas on growth mechanisms in relation to thermal roughening or kinetic roughening may be obtained [23] As a comparison the following recipes are used

For the growth form

(i) $R_{hkl} \sim E^{att}_{hkl}$ (Hartman–Perdok theory [1,4-6,24])

(ii) $R_{hkl} \sim (E^{slice}_{hkl})^{-1}$ (Hartman–Perdok theory [1,4-6])

(iii) $R_{hkl} \sim (\theta^{c}_{hkl})^{-1}$ (Ising model [1,2])

(iv) $R_{hkl} \sim [\theta^{c}_{hkl}(n) - \theta]^{-1}$ (Ising model)

(v) $R_{hkl} \sim (d_{hkl})^{-1}$ (BFDH theory [3])

where R_{hkl} is the relative growth rate in the orientation of $\{hkl\}$, θ is associated with growth conditions.

For the equilibrium form:

(vi) $D_{hkl} \sim d_{hkl} E^{att}_{hkl}$ (Gibbs–Wulff theorem [13])

where D_{hkl} is the distance of a crystal face with the orientation (hkl) to the center of the crystal.

The recipes (i)–(iii) and (v) are based on the assumptions that the higher E^{slice}_{hkl} and the lower E^{att}_{hkl} (or the larger d_{hkl}, or the higher θ^{c}_{hkl}), the higher resistance against the surface integration, which leads to the lower growth rate. Recipe (1) is the most widely used and can be justified to some extent even quantitatively [24].

We believe that recipe (iv) is the most satisfactory from a general physical point of view. This is because this recipe is associated with the order–disorder phase diagram (see Fig. 6) where the isotherm θ offers a boundary between rough interfaces and the flat interfaces. Flat faces $[\theta^{c}_{hkl}(n) - \theta \geq 0]$ with the roughening temperature close to the actual temperature {i.e. the value of $[\theta^{c}_{hkl}(n) - \theta]$ is small} have a small edge free energy. Then for those faces the resistance against the crystal growth is small, and the faces will grow faster. On the other hand, the flat faces with a large value of $[\theta^{c}_{hkl}(n) - \theta]$ have a larger edge free energy. Henceforth they grow much slower and will be dominant on crystal forms. For those faces with a rough interfacial structure $[\theta^{c}_{hkl}(n) - \theta \leq 0]$, since the edge free energy vanishes, the resistance against the surface integration disappears. The growth is then mainly controlled by the volume diffusion. So they grow much faster than flat faces and will sooner or later disappear from crystal forms. We assume that faces with a negative value of $[\theta^{c}_{hkl}(n) - \theta]$ have such a relatively high growth rate that from a statistical point of view they do not occur on the growth forms if competing faces have a lower growth rate and grow as flat faces. In case other faces are growing as rough faces above their roughening temperatures or are kinetically rough, quite different growth forms are obtained.

A. Calculation of relevant data

In recipes (i) and (ii) the attachment energies E^{att}_{hkl} and E^{slice}_{hkl} are needed for all the thirteen connected nets. According to the Hartman–Perdok theory, E^{att}_{hkl}, E^{slice}_{hkl} and E^{cr}

have the relation

$$E^{cr} = E^{att}_{hkl} + E^{slice}_{hkl} \tag{9}$$

E^{cr} (or ΔH^{ss}) denotes the crystallization energy in reference to vacuum (or vapor) and is equal to the sum of all the bond energies

$$E^{cr} = \tfrac{1}{2}\sum_{total} \phi_i^{ss} = \sum_{a}^{g} \phi_i^{ss} \tag{10}$$

Since ϕ_i^{ss} is a function of the carbon number of paraffins n, E^{cr} depends on n This relation can be expressed in the same way as Eq (3) For the coefficients of the relation, the results of a least square regression are also listed in Table IIb The slice energy E^{slice}_{hkl} can immediately be calculated from the connected nets presented in Fig 5 The expressions of E^{slice}_{hkl} are summarized in Table VII

TABLE VII The expressions of E^{slice}_{hkl} for the thirteen connected nets

E^{slice}_{001}	$= \phi_a + \phi_b + \phi_c + \phi_d + \phi_{c'}$
E^{slice}_{010}	$= \phi_a + \phi_g + \phi_f$
E^{slice}_{011}	$= \phi_a + \phi_e$
E^{slice}_{100}	$= \phi_b + \phi_e + \phi_f$
E^{slice}_{101}	$= \phi_b + \phi_g$
E^{slice}_{111}	$= \phi_c + \phi_e + \phi_g$
E^{slice}_{110}	$= \phi_c + \phi_f$
$E^{slice}_{1\text{-}11}$	$= \phi_d + \phi_g$
$E^{slice}_{\text{-}111}$	$= \phi_d + \phi_e$
$E^{slice}_{\text{-}110}$	$= \phi_d + \phi_f$
E^{slice}_{120}	$= \phi_{c'} + \phi_f$
E^{slice}_{122}	$= \phi_{c'} + \phi_e$
E^{slice}_{121}	$= \phi_{c'} + \phi_g$

It follows that the values of $(E^{slice}_{hkl})^{-1}$ and E^{att}_{hkl} can be easily calculated on the basis of Eqs (9), (10) and the expressions listed in Table VII It shows from the calculated results that the same MI order as given in Table VI is obtained

TABLE VIII. The values of d_{hkl}^{-1} of the thirteen connected nets

Paraffins	d_{hkl}^{-1} (Å $^{-1}$)						
	{001}	{010}	{011}	{100}	{101}	{111}	{110}
n–C_{10}	0 0744	0 2174	0 2278	0 2664	0 2464	0 2771	0 2965
n–C_{12}	0 0631	0 2173	0 2259	0 2652	0 2476	0 2776	0 2937
n–C_{14}	0 0548	0 2173	0 2246	0 2643	0 2487	0 2780	0 2917
n–C_{16}	0 0484	0 2174	0 2237	0 2637	0 2496	0 2783	0 2903
n–C_{18}	0 0434	0 2174	0 2230	0 2632	0 2504	0 2786	0 2891
n–C_{20}	0 0393	0 2175	0 2225	0 2628	0 2510	0 2788	0 2883
n–C_{22}	0 0359	0 2175	0 2221	0 2625	0 2516	0 2790	0 2876
n–C_{24}	0 0331	0 2176	0 2218	0 2622	0 2521	0 2792	0 2870
n–C_{26}	0 0306	0 2176	0 2215	0 2619	0 2526	0 2793	0 2865
n–C_{28}	0 0285	0 2177	0 2213	0 2617	0 2529	0 2794	0 2861
n–C_{30}	0 0267	0 2177	0 2211	0 2616	0 2533	0 2795	0 2858
n–C_{32}	0 0251	0 2178	0 2209	0 2614	0 2536	0 2796	0 2855
n–C_{34}	0 0237	0 2178	0 2207	0 2613	0 2539	0 2797	0 2852
n–C_{36}	0 0224	0 2178	0 2206	0 2612	0 2541	0 2798	0 2850
MI order	1	2	3	5	4	6	7

TABLE VIII. (continued)

Paraffins	d_{hkl}^{-1} (Å $^{-1}$)					
	{1$\bar{1}$1}	{1$\bar{1}\bar{1}$}	{1$\bar{1}$0}	{121}	{122}	{120}
n–C_{10}	0 3731	0 4109	0 3853	0 4328	0 4317	0 4465
n–C_{12}	0 3742	0 4070	0 3858	0 4327	0 4311	0 4434
n–C_{14}	0 3753	0 4042	0 3861	0 4326	0 4308	0 4413
n–C_{16}	0 3763	0 4021	0 3864	0 4326	0 4307	0 4398
n–C_{18}	0 3772	0 4005	0 3866	0 4325	0 4306	0 4387
n–C_{20}	0 3780	0 3992	0 3868	0 4325	0 4306	0 4379
n–C_{22}	0 3787	0 3982	0 3869	0 4325	0 4306	0 4372
n–C_{24}	0 3793	0 3974	0 3870	0 4324	0 4307	0 4367
n–C_{26}	0 3799	0 3966	0 3871	0 4324	0 4307	0 4362
n–C_{28}	0 3804	0 3960	0 3872	0 4323	0 4308	0 4359
n–C_{30}	0 3808	0 3955	0 3873	0 4324	0 4308	0 4356
n–C_{32}	0 3812	0 3951	0 3874	0 4324	0 4308	0 4353
n–C_{34}	0 3815	0 3947	0 3876	0 4323	0 4309	0 4351
n–C_{36}	0 3819	0 3943	0 3875	0 4323	0 4309	0 4349
MI order	8	10	9	12	11	13

TABLE IX The values of $d_{hkl}E_{hkl}^{att}$ of the thirteen connected nets

Paraffins	$d_{hkl}E_{hkl}^{att}$ (kcal · Å · mol^{-1})						
	{001}	{010}	{011}	{100}	{101}	{111}	{110}
n–C_{10}	29 179	42 519	43 902	44 050	48 631	46 586	47 460
n–C_{12}	34 389	51 743	53 123	53 557	58 369	56 898	57 745
n–C_{14}	39 598	60 949	62 331	63 071	68 052	67 198	68 030
n–C_{16}	44 808	70 143	71 528	72 589	77 699	77 490	78 314
n–C_{18}	50 017	79 328	80 716	82 109	87 322	87 776	88 594
n–C_{20}	55 227	88 507	89 898	91 632	96 926	98 058	98 873
n–C_{22}	60 436	97 680	99 074	101 16	106 52	108 34	109 15
n–C_{24}	65 646	106 85	108 25	110 68	116 10	118 61	119 43
n–C_{26}	70 855	116 02	117 42	120 21	125 67	128 89	129 70
n–C_{28}	76 065	125 18	126 58	129 73	135 24	139 16	139 97
n–C_{30}	81 274	134 34	135 74	139 26	144 80	149 43	150 24
n–C_{32}	86 484	143 50	144 91	148 78	154 36	159 70	160 51
n–C_{34}	91 693	152 66	154 07	158 31	163 92	169 97	170 78
n–C_{36}	96 903	161 82	163 23	167 84	173 47	180 24	181 05
MI order	1	6/7/8	9	10	13/11	11/12	12/13

Note for an explanation of the change in the MI order with the carbon number, see Ref 23

TABLE IX (continued)

Paraffins	$d_{hkl}E_{hkl}^{att}$ (kcal · Å · mol^{-1})					
	{1$\bar{1}$1}	{1$\bar{1}\bar{1}$}	{1$\bar{1}$0}	{121}	{122}	{120}
n–C_{10}	43 353	39 976	43 156	37 922	38 605	37 778
n–C_{12}	52 424	48 822	52 029	46 025	46 781	45 943
n–C_{14}	61 443	57 676	60 898	54 129	54 941	54 097
n–C_{16}	70 426	66 534	69 766	62 232	63 098	62 243
n–C_{18}	79 385	75 394	78 632	70 336	71 230	70 381
n–C_{20}	88 325	84 25	87 498	78 440	79 363	78 514
n–C_{22}	97 252	93 117	96 363	86 544	87 492	86 643
n–C_{24}	106 17	101 98	105 22	94 648	95 618	94 769
n–C_{26}	115 08	110 84	114 09	102 75	103 74	102 89
n–C_{28}	123 98	119 70	122 95	110 86	111 86	111 01
n–C_{30}	132 88	128 57	131 82	118 96	119 98	119 13
n–C_{32}	141 77	137 43	140 68	127 06	128 09	127 25
n–C_{34}	150 66	146 29	149 54	135 17	136 21	135 36
n–C_{36}	159 54	155 15	158 41	143 27	144 32	143 48
MI order	8/7	5	7/6	3/2	4	2/3

In Table VIII we have presented the values of $d_{\bar{h}\bar{k}\bar{l}}$ together with the MI order for the triclinic paraffin series, using the dimensions of elementary cells given in Table I. The values of $d_{hkl}E^{c}_{\bar{h}\bar{k}\bar{l}}$ are presented in Table IX. (The values of $\theta^{c}_{\bar{h}\bar{k}\bar{l}}$ have already been presented in Table VI.)

For recipe (iv) the choice of the dimensionless actual temperature θ is a key problem. Conventionally, θ is chosen in the following way

$$\theta = [\theta^{c}_{h_1k_1l_1}(n') + \theta^{c}_{h_2k_2l_2}(n')]/2. \tag{11}$$

TABLE X. The relative values of $[\theta^{c}_{\bar{h}\bar{k}\bar{l}}(n) - \theta]^{-1}$ of the thirteen connected nets.

Paraffins	$[\theta^{c}_{\bar{h}\bar{k}\bar{l}}(n) - \theta]^{-1}$						
	{001}	{010}	{011}	{100}	{101}	{111}	{110}
n–C_{10}	1.0000	–3.9602	–2.0418	–1.8494	–1.6343	–1.6126	–1.1175
n–C_{12}	1.0000	–11.453	–3.8425	–3.2664	–2.8087	–2.6496	–1.7457
n–C_{14}	1.0000	–217.04	–6.9862	–5.3664	–4.4251	–3.9541	–2.4550
n–C_{16}	1.0000	22.494	–13.597	–8.7183	–6.7452	–5.6136	–3.2442
n–C_{18}	1.0000	13.001	–36.595	–14.900	–10.357	–7.8143	–4.1389
n–C_{20}	1.0000	10.045	183.41	–30.122	–16.842	–10.882	–5.1738
n–C_{22}	1.0000	8.6126	33.645	–122.85	–31.132	–15.318	–6.343
n–C_{24}	1.0000	7.7731	20.598	89.839	–89.839	–23.019	–7.699
n–C_{26}	1.0000	7.2356	15.8702	28.049	179.52	–35.193	–9.2729
n–C_{28}	1.0000	6.8474	13.370	25.961	52.386	–66.048	–11.135
n–C_{30}	1.0000	6.5747	11.842	20.557	33.178	–235.04	–13.360
n–C_{32}	1.0000	6.3639	10.808	17.528	25.422	202.429	–16.066
n–C_{34}	1.0000	6.2044	10.079	15.624	21.226	79.012	–19.418
n–C_{36}	1.0000	6.0709	9.5212	14.265	18.592	51.790	–23.678
MI order	1	2	3	4	5	6	–

Note: according to our convention [Eq.(11)], the faces $\{1\bar{1}1\}$, $\{\bar{1}11\}$, $\{1\bar{1}0\}$, {121}, {122} and {120} are always rough under the experimental conditions (the same as {110}). Therefore, they are morphologically irrelevant, and not included in this table.

Here $(h_1k_1l_1)$ corresponds to the weakest flat face whose roughening temperature is slightly above the actual temperature T, and $(h_2k_2l_2)$ is the rough face whose MI order is next to $(h_1k_1l_1)$. In the case of triclinic n–paraffin crystals growing from n–hexane solutions, $(h_1k_1l_1)$ and $(h_2k_2l_2)$ correspond to the (100) and the (101) face of n–$C_{24}H_{50}$ crystals.

Assuming that the strongest bonds in the structure are approximately expressed as $\phi_{str}(n) \cong a'n$ (a' is a constant), the relative values of $(\theta^{f}_{hkl} - \theta)^{-1}$ are obtained and listed in Table X. The faces with negative values correspond to rough faces, which, as mentioned above, are supposed to be absent on growth forms.

In comparison, the Hartman–Perdok theory gives the same MI order of forms $\{hkl\}$ on the crystals as Ising models, while the BFDH theory shows a somewhat different result. In equilibrium forms, the MI order of $\{hkl\}$ faces is quite different from previous ones. Some important crystallographic faces in the growth forms become less important in the equilibrium forms. For an explanation, see Ref.24.

B. Theoretical crystal forms

In Fig. 7a constructed growth and equilibrium forms resulting from recipe (i),(ii),(iii),(v) and (vi) are presented for n–C_{10}, n–C_{22} and n–C_{36} respectively. Since recipe (iv) shows the crystal habits different from others, these habits are presented in Fig.7b independently. Generally speaking, the {001} faces are very dominant for all crystal forms. Moreover the habits of growth forms are flat and somewhat elongated in the direction of the a axis. The habits of crystals resulting from recipe (i) to (v) show a morphology only limited by the faces with higher MI order. So the {010} faces are the most important side faces, followed by the {100}, the {101} and the {111} faces, and in some cases the {011} and the {110} faces have relatively large chance to appear on the crystal growth forms.

As shown in Fig.7 with increasing carbon number of paraffins, triclinic even paraffin crystals become thinner. It is because for those recipes, the anisotropy of bonding plays a key role. An increase in n yields more anisotropic bonding, and thus a more anisotropic growth form.

The crystal habits resulting from recipe (iv) are different from the other recipes. First of all, the flat crystals are bounded by the larger {001} faces and are quite elongated in the [100] direction. This makes the crystal look like a flat needle. Regarding the side faces, the {100} faces are very weak compared to the {010} faces, leading to needle–like crystals. For the faces {100} on n–$C_{16}H_{34}$ crystals growing in normal conditions, $\theta^{f}_{hkl}(16) - \theta < 0$, meaning that for

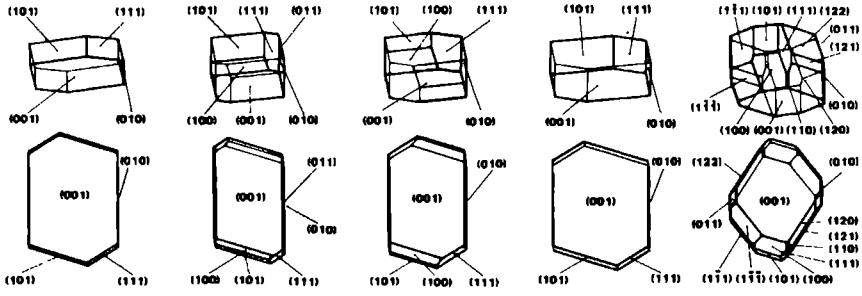
(101) (111) (001) (010)
(101) (111) (011) (100) (001) (010)
(101) (100) (111) (001) (010)
(101) (111) (001) (010)
(001) (010) (101) (111)
(001) (011) (010) (100) (101) (111)
(001) (010) (101) (100) (111)
(001) (010) (101) (111)

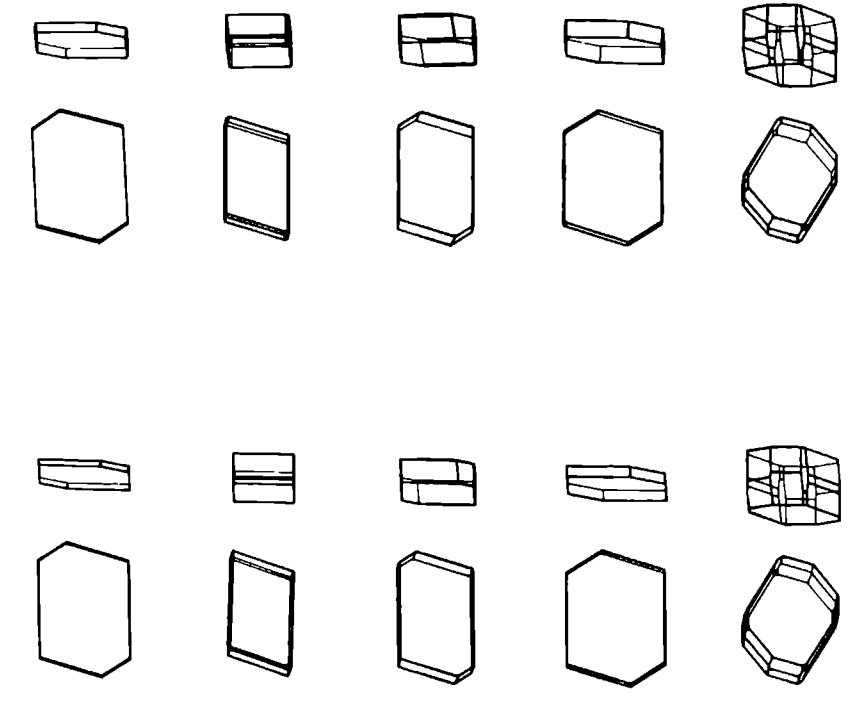

(a)

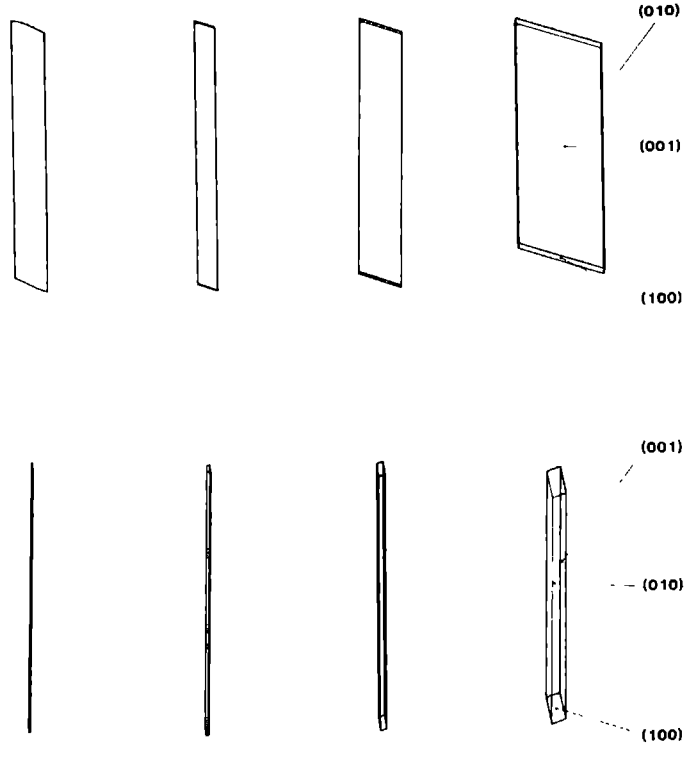

(b)

FIG.7. Gibbs–Wulff constructions of theoretical growth forms and equilibrium forms based on different criteria. (a) From the first to the fifth column, the growth forms and equilibrium forms based on $R_{hkl} \sim E^{att}_{hkl}$, $R_{hkl} \sim (E^{slice}_{hkl})^{-1}$, $R_{hkl} \sim (\theta^{c}_{hkl})^{-1}$, $R_{hkl} \sim (d_{hkl})^{-1}$ and $D_{hkl} \sim d_{hkl}E^{att}_{hkl}$ respectively are presented; the pictures in the first two rows correspond to n–$C_{10}H_{22}$, the second and the third to n–$C_{22}H_{46}$ and to n–$C_{36}H_{74}$ respectively. (b) The growth forms based on $R_{hkl} \sim [\theta^{c}_{hkl}(n) - \theta]^{-1}$; the pictures from the first to fourth column correspond to n–$C_{16}H_{34}$, n–$C_{24}H_{50}$, n–$C_{26}H_{54}$ and n–$C_{36}H_{74}$ respectively; The two rows show the views in different directions.

this face the actual temperature is above its roughening temperature Therefore, as presented in Fig 7b the {100} faces are rounded off Secondly, we can see from Fig 7b that crystals become thicker with increasing the carbon number This is because in the recipe (iv) the roughening transition is taken into account Then it is not the anisotropy of bonding but the absolute bond energy that plays the most important role in the description of growth forms From the foregoing discussions, it is known that absolute bond energies will increase with the carbon number This will enhance the Ising temperature of $\{hkl\}$ faces, resulting in the hyperbolical decrease of the values of $[\theta^c_{hkl}(n) - \theta]^{-1}$ For the {001} faces the value of $[\theta^c_{hkl}(n) - \theta]^{-1}$ doesn't change much This is because $\theta^c_{hkl}(n) >> \theta$, and a change in θ won't influence much the value of $[\theta^c_{hkl}(n) - \theta]^{-1}$ However, for those side faces whose roughening temperatures are close to the actual temperature, the value of $[\theta^c_{hkl}(n) - \theta]^{-1}$ decreases considerably with n Consequently, the relative difference of $[\theta^c_{hkl}(n) - \theta]^{-1}$ between the side faces and the {001} faces becomes smaller as increasing n, and habits of crystals become somewhat thicker

The equilibrium forms resulting from recipe (vi) show a very rich morphology All F forms, except the $\{1\bar{1}0\}$ form, show up on crystals In addition, from n–C_{10} to n–C_{36}, crystals are always thick and the F faces of high index get quite large chance to appear on crystal forms

From the general point of view, the following relation exists between the thicknesses of the crystals D_x [x represents the recipes from (i) to (vi)] $D_{vi} > D_{ii} > D_{iii} > D_v > D_i \geq D_{iv}$ For an explanation, see Ref 23

V COMPARISON WITH EXPERIMENTS

Similar to the situation in orthorhombic odd n–paraffin crystals grown from hexane solutions, we concentrate on the cases of crystals of triclinic even paraffins grown from n–hexane and i–octane solutions and from the melt around the roughening temperature of the side faces This is because from the observed roughening temperature we can estimate the dimensionless actual temperature θ We also expect drastic changes in the morphology of crystals around the roughening temperature Here we just limit ourselves to the accessible temperature which is close to the roughening temperature of {100} faces of n–C_{24} and {010} faces of n–C_{16} The observations of crystal growth and growth forms were carried out in a thermostated double–cell system using polarizing microscopy For all details of experiments we refer to Refs 25 & 26

A. Observed morphology

1. Observations on crystals of $n-C_{24}H_{50}$

Crystals of n–$C_{24}H_{50}$ grown from a n–hexane solution saturated at 8.55° C are illustrated in Fig. 8. At a moderate and a high relative supersaturation σ (Fig.8a), crystals are long flat needle like, bounded by the large faceted {001} faces and the long narrow straight {010} faces, along with the rounded {100} faces at the tops of crystals. At a low supersaturation (Fig. 8b) the faceted {001} faces are still dominant, the {010} faces become less developed, and crystals are bounded by relatively large rounded side faces.

Crystals of n–$C_{24}H_{50}$ grown from i–octane solutions have the same growth habits as the crystals growing from n–hexane solutions. Crystals are also long flat needle like, limited by the faceted {001} faces and the {010} faces. If crystals grow in the solutions with

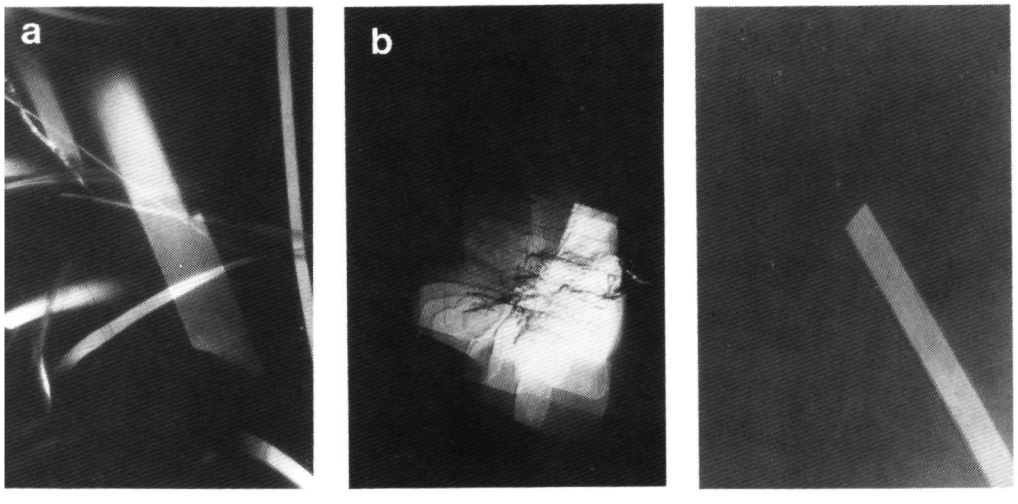

FIG.8. Crystals of n–$C_{24}H_{50}$ grown from n–hexane solutions; $T_s = 8.55°$ C, $X = 0.01489$, $\theta^r_{100}(24) < \theta < \theta^r_{010}(24)$. (a) $\sigma = 3.279$ %, the long flat needle like crystals with rough {100} faces on the top. (b) $\sigma = 0.1213$ %, the faceted {010} faces, but less developed.

FIG.9. A crystal of n–$C_{24}H_{50}$ grown from i–octane solutions; $\theta^r_{111}(24) < \theta < \theta^r_{100}(24)$, the long flat needle like crystals with faceted {100} faces on the top. $T_s = -6.87°$ C, $\sigma = 2.5\%$.

$T_s \leq -2.68°$ C, the {100} faces are faceted at relatively low supersaturations. The morphology with the faceted {100} faces are shown in Fig. 9. For the time being, we assume that the roughening temperature T^r_{hkl} of {100} faces for crystals grown from i–octane solutions: $T^r_{100}(24) > -3.0°$ C. This is the reason that in the last section we took $\theta^r_{100}(24)$ as the lowest

accessible dimensionless actual temperature in our theoretical analysis.

2. Observation on crystals of n–$C_{16}H_{34}$

For n–$C_{16}H_{34}$, special attention is paid to the morphological variation of the {010} faces on the crystals, whose roughening transition is expected to be observed under the experimental conditions. Crystals of n–$C_{16}H_{34}$ grown from the melt is shown in Fig.10a. Similarly, the crystals grown from n–hexane solutions are indicated in Figs.10b, c & d. Considering the melt to be a special case of solutions, it can be seen from Fig. 10 that if $T_s \geq 12.12^\circ$ C the crystals are above the roughening temperature of the {010} faces. At a very low supersaturation ($< 0.1\%$), all side faces roughen, and only the {001} faces remain flat. The

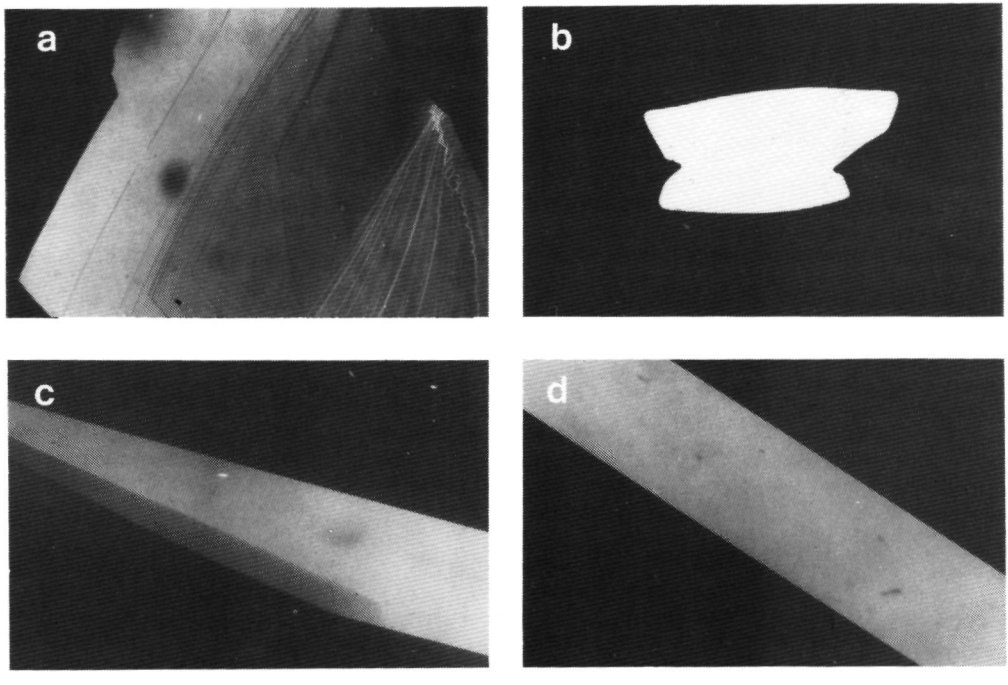

FIG.10. (a) Crystals of n–$C_{16}H_{34}$ (> 99 %) grown from the melt, the {010} and the {100} faces are rounded, but remain anisotropic. $\theta^r_{010}(16) < \theta < \theta^r_{001}(16)$, $T_s = 17.87^\circ$ C, $\Delta T \cong 0$. (b) Crystals of n–$C_{16}H_{34}$ grown from the n–hexane solutions; the roughened {010} and {100} faces. $\theta^r_{010}(16) < \theta < \theta^r_{001}(16)$. $T_s = 12.22^\circ$ C, $\sigma = 0.0759$ %. (c) and (d) The crystals of n–$C_{16}H_{34}$ grown from n–hexane solutions; the long flat needle like crystals with the rough {100} faces on the top, $\theta^r_{100}(16) < \theta < \theta^r_{010}(16)$, $T_s = 9.69^\circ$ C, $\sigma = 0.6185$ %.

shape of crystals can be seen in Figs 10a, b Fig 10a shows a crystal grown from the melt It can be seen from Figs 10a,b that although the {010} faces roughen, crystals are still elongated in the [100] direction Obviously, the faces remain strongly anisotropic If $T_s \leq 10\ 09^\circ C$, the crystals grow below the roughening temperature of {010} faces Similarly to crystals of n–$C_{24}H_{50}$, crystals of n–$C_{16}H_{34}$ are long flat needle like and limited by the faceted {001} and the {010} faces, and the rounded {100} faces This can be seen from Figs 10c, d According to our measurements the roughening temperature of {010} faces of n–$C_{16}H_{34}$ crystals in n–hexane solutions $T^r_{010}(16)$ is $11\ 50 \pm 0\ 25^\circ C$

B. Discussion

Concerning the MI for both n–$C_{16}H_{34}$ and n–$C_{24}H_{50}$ crystals, in practice the order is given by

$$\mathbf{MI}(001) >> \mathbf{MI}(010) > \mathbf{MI}(100) \tag{12}$$

which is in very good agreement with our predications based on criteria (i)–(iv) In comparison of observed growth forms with our theoretical prediction, it can be seen that although all recipes from (i) to (v) predict flat crystals elongated in the [100] direction, recipe (iv) is the most successful one in the prediction of growth forms of crystals It can be seen from Fig 7 that the long flat needle like crystals are obtained only from recipe (iv), which is obviously confirmed by our observations The habits predicted from other recipes are too thick and too short in the [100] direction They yield too many side faces on growth forms The main reason for the success of recipe (iv) is that in this recipe the roughening transition, and experimental conditions are explicitly considered by introducing the dimensionless actual temperature θ

Using expression (9), we expected that the {100} faces of n–$C_{24}H_{50}$ crystals are the last faces for which we can observe the roughening transition under the experimental conditions Using this dimensionless actual temperature θ, it is obtained in Table X that for n–$C_{16}H_{34}$ crystals the {100} faces will roughen {corresponding to the negative value of $[\theta^c_{hkl}(n) - \theta]^{-1}$} and the {010} faces are very close to the roughening temperature {corresponding to a large positive value of $[\theta^c_{hkl}(n) - \theta]^{-1}$} These are all confirmed by our experiments

It can be seen that from previous sections, the {011} faces in the <100> zone are also very important Besides, there is a conflict between the showing up of {010} faces and {011} faces Since crystals are so thin, in the competition the {011} faces have a small chance to show up on the growth form Therefore, as shown in Fig 7b, we do not see the {011} faces in reality

VI SUMMARY AND CONCLUSIONS

Having predicted all structure parameters of triclinic even paraffin series from n–C_{10} to n–C_{36} by Nyburg's method, the overall van der Waals interactions between the molecules are calculated using the Buckingham potential Consequently the crystal graph is derived, where five lateral and three vertical stronger nearest neighbor bonds are identified Based on the crystal graph 13 connected nets are derived Using calculated bond energies quantities such as θ^c_{hkl}, E^{att}_{hkl} and E^{slice}_{hkl} are calculated for triclinic even paraffin crystals with carbon number from 10 to 36, and five types of growth forms and an equilibrium form are constructed We pay much special attention to the roughening transition and a related recipe, and the roughening temperature T^r_{010} for n–$C_{16}H_{34}$ crystals in n–hexane solutions is determined Comparing theoretical growth forms with real growth forms, it is found that the recipe $R_{hkl} \sim [\theta^c_{hkl}(n) - \theta]^{-1}$ yields a very satisfactory prediction of growth habits of n–paraffin crystals The predicted long flat needle like crystals elongated in the [100] direction are limited by large the {001} faces, the long narrow {010} faces and the small {100} faces, in very good agreement with our observations

ACKNOWLEDGEMENTS

The authors wish to thank Shell Netherlands B V for providing a donation to support a research program on the growth and morphology of paraffins They also wish to acknowledge Mr Jan van Kessel for making the drawings of the crystal graph, connected nets and the stereographic projection

REFERENCES

1 P Bennema and J P van der Eerden, in *Morphology of Crystals*, Part A, edited by I Sunagawa (Terra Sci , Tokyo ,1987) p 1

2 P Bennema, in *Morphology and Growth Unit of Crystals*, edited by I Sunagawa, (Terra Sci , Tokyo, 1989) p 219

3 J D H Donnay and D Harker, Am Mineralogist **22**, 446 (1937)

4 P Hartman and W G Perdok, Acta Cryst **8**, 49 (1955a)

5 P Hartman and W G Perdok, Acta Cryst **8**, 521 (1955b)

6 P Hartman and W G Perdok, Acta Cryst **8**, 525 (1955c)

7 P Hartman, in *Morphology of Crystals*, edited by I Sunagawa, (Terra Sci , Tokyo, 1981) p 271

8 P Bennema, E A Giess and J E Weidenborner, J Cryst Growth **62**, 41 (1983)

9 J J M Rijpkema, H J F Knops, P Bennema and J P van der Eerden, J Cryst Growth

61, 295 (1983)

10 R A Terpstra, J J M Rijpkema and P Bennema, J Cryst Growth **76**, 499 (1986)

11 L Onsager, Phys Rev **45**, 117 (1944)

12 W K Butorn, N Cabrera and F C Frank, Phil Trans Royal Soc **A243**, 299 (1951)

13 R Kern, in *Morphology of Crystals*, Part A, edited by I Sunagawa (Terra Sci , Tokyo, 1987) p 79

14 M G Broadhurst, J Res Nat Bur Stand **66A**, 241 (1962)

15 P Bennema, X Y Liu, K Lewtas *et al*, J Cryst Growth **121**, 679 (1992)

16 S C Nyburg and J A Potworowski, Acta Cryst **B29**, 347 (1973)

17 A E Smith, J Chem Phys **21**, 2229 (1953)

18 N Norman and H Mathisen, Acta Cryst **13**, 1043 (1960)

19 A Doussoulin, Ph D Thesis (Univ Aix–Marseilla III, 1975)

20 H E L Madsen and R Roistelle, Acta Cryst **A32**, 868 (1976)

21 S C Nyburg and H Lüth, Acta Cryst **B28**, 2992 (1972)

22 D E Williams, J Chem Phys **47**, 4680 (1967)

23 P Bennema, in *Handbook of Cryst Growth*, edited by D Hurle (Elsevier, Amsterdam, 1993) (in press)

24 P Hartman and P Bennema, J Cryst Growth **49**, 145 (1980)

25 L J P Vogels, Ph D Thesis (Univ Nijmegen, 1991)

26 H J Human, J Cryst Growth **51**, 589 (1981)

J Appl Cryst (1993) **26**, 229–242

On the Morphology of Normal Alkane Crystals with Monoclinic Structures: Theory and Observations

BY XIANG YANG LIU AND P BENNEMA

RIM, Laboratory of Solid State Chemistry, Faculty of Science, University of Nijmegen, Toernooiveld, 6525 ED Nijmegen, The Netherlands

(*Received* 17 *August* 1992, *accepted* 13 *October* 1992)

Abstract

The morphology of crystals of monoclinic even *n*-alkanes over a chain-length range $10 \leq m \leq 40$ is investigated The overall van der Waals interactions between the paraffin molecules are calculated from the structure parameters using the Buckingham potential Subsequently, a crystal graph is obtained, from which 12 connected nets are derived To describe the morphology, the Hartman–Perdok theory, the theory of the roughening transition and the Donnay–Harker theory are applied to the system The results are compared with each other The influence of the chain lengths of paraffin molecules on the Ising temperatures and on the morphology is analysed Experimentally, it can be seen that the predicted growth morphology of the crystals is in good agreement with the observed one In addition, the roughening temperature of the {110} faces, for crystals of n-$C_{32}H_{66}$ and n-$C_{28}H_{58}$ grown from *n*-hexane solutions, are determined They are about 306 (3) and 297 (5) K, respectively Morphological transitions around the roughening temperature are also observed It is found that an unusual morphological phenomenon occurs on long-chain paraffin crystals at low supersaturations This is interpreted as the influence of solvent adsorption at the roughened faces

I. Introduction

Normal alkanes or normal paraffins form a basic series of organic compounds that are widely distributed in nature Investigations of the structure, properties and growth habits of this class of substance are of great interest for various reasons (Nyburg & Potworowski, 1973, Broadhurst, 1962, Boistelle, 1980, Mnyukh, 1963) *n*-Paraffins crystallize in four modifications triclinic, monoclinic, orthohombic and hexagonal, depending on the number of and parity of the number of C atoms in the paraffin molecule, temperature, impurities and other factors (Broadhurst, 1962) Even-numbered *n*-paraffins with $26 \leq m \leq 36$ crystallize mainly in the monoclinic phase β_M, at a temperature which is much lower than the melting temperature if the initial materials are pure enough If the initial materials contain a few per cent ($\geq 2\%$) of neighbouring members of the homologous series, they will crystallize in the orthorhombic phase β_O In this paper, only the morphology of even *n*-paraffin crystals with a monoclinic structure is studied We note that for those even *n*-paraffins ranging from n-C_{10} to n-C_{26} and from n-C_{36} to n-C_{40} the triclinic and the orthorhombic structures are the thermodynamically stable structures, respectively However, in order to allow comparison with other modifications of *n*-paraffins, our theoretical investigations will include carbon numbers from $m = 10$ to $m = 40$

It is known that there are some theories that can be employed to describe the morphological importance (MI) of a crystal face (*hkl*) and the equilibrium and growth forms of a crystal According to the Gibbs–Wulff theorem (Kern, 1987), the equilibrium form can be described in terms of

$$D_{hkl} = K\sigma_{hkl} \tag{1}$$

(a list of symbols and abbreviations is given at the end of the paper) To describe growth forms, some *ad hoc* assumptions, suggested by the Bravais–Friedel–Donnay–Harker (BFDH) theory (Donnay & Harker, 1937) and the Hartman–Perdok theory (Hartman, 1987), are successful to some extent On the basis of the BFDH theory it is suggested that the growth rate of a crystallographic face (*hkl*) may be taken to be inversely proportional to the interplanar distance d_{hkl}, corrected for the extinction conditions of the space group In the Hartman–Perdok theory, the concepts of the periodic bond chain (PBC) and the *F* face play a key role According to the theory, a crystal is bound by *F* faces It is assumed that the relative growth rate of an *F* face (*hkl*) is proportional to its attachment energy E^{att}_{hkl}, which is related to the crystallizing energy E^{cr} and the slice energy E^{slice}_{hkl} by

$$E^{cr} = E^{slice}_{hkl} + E^{att}_{hkl} \tag{2}$$

0021-8898/93/020229-14$06 00

In addition, a statistical mechanical approach based on the concept of the roughening transition can be used to analyse the morphology of crystals. The idea that a crystal surface undergoes the roughening transition at a critical temperature, called the roughening temperature, results from renormalization theories and was inspired by computer simulations on the SOS Kossel model (Weeks & Gilmer, 1979; Gilmer & Jackson, 1977; Bennema & van der Eerden, 1987). With a dimensionless temperature θ to characterize the roughening transition, the dimensionless roughening temperature of face (hkl) can be expressed as (Bennema & van der Eerden, 1987)

$$\theta^{r}_{hkl} = 2kT^{r}\,\varphi_{str} \qquad (3)$$

We notice that the bond energies φ_i have the shape

$$\varphi_i = \varphi_i^{sf} - \tfrac{1}{2}(\varphi_i^{ss} + \varphi_i^{ff}) \qquad (4)$$

Since only φ_i^{ss} can be calculated, the so-called proportionality condition (Bennema & van der Eerden, 1987) is introduced, which implies

$$\varphi_i\ \varphi_j\ \varphi_k\ \ldots = \varphi^{ss}\ \varphi^{ss}\ \varphi^{ss}: \ldots = \ldots \qquad (5)$$

From the concept of the roughening transition and the influence of growth kinetics, it is known that, during growth, rough faces grow much faster than flat faces. Therefore, flat faces with a higher roughening temperature have lower growth rates and dominate on crystal growth forms.

In this paper, we consider several methods, based on the theories mentioned above, of describing the theoretical morphology of monoclinic even paraffin crystals. The results are compared with observed ones. In §2 the bond structure of monoclinic n-paraffins is discussed, the first nearest-neighbour interactions, and to some extent also the second-nearest bonds between the growth units being taken into account. This analysis is followed by a PBC analysis. In §3, the calculated Ising temperature is presented for each connected net, together with the relation of θ^{r}_{hkl} to the carbon number of a paraffin molecule. In §4 both the theoretical growth forms and equilibrium forms are constructed using alternative methods. In §5 the experimentally observed morphology, characterized by crystal forms $\{hkl\}$, is presented. In §6 the results of the theory and of the experiments are compared with each other. Finally, the summary and concluding remarks are also given in this section.

II. Structure and PBC analysis

II.1. *Structure of monoclinic even n-paraffins*

The space group of the monoclinic structure is $P2_1/a$ (Shearer & Vand, 1956). Two molecules occur in each unit cell. In Fig. 1, the arrangement of molecules in the structure is shown in y and z projections. In the series of monoclinic even paraffins, the cell parameters a and b are almost constant on variation of m. In contrast, the c axis and the angle β depend strongly on m. Using Nyburg's method (Nyburg & Potworowski, 1973), the cell parameters from n-C_{10} to n-C_{40} were calculated from the structural data of n-C_{36} (Shearer & Vand, 1956). These values are listed in Table 1.

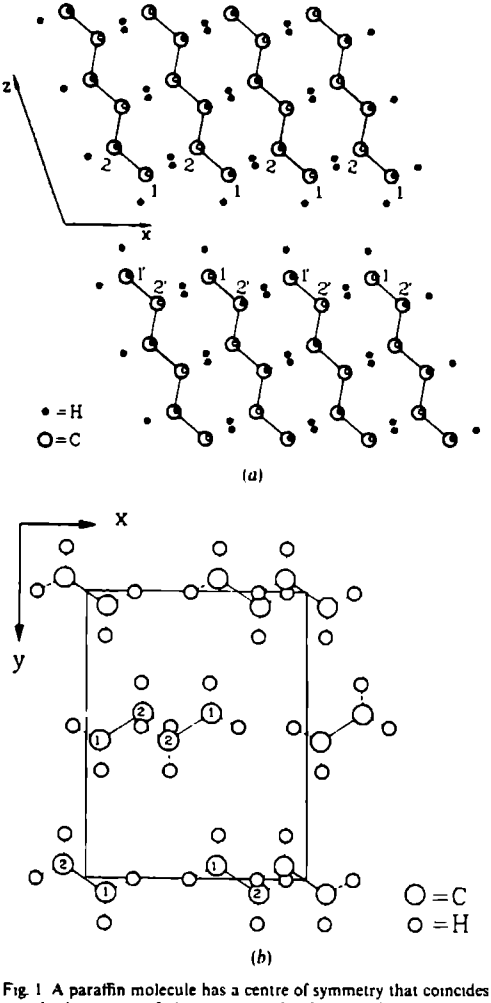

Fig. 1. A paraffin molecule has a centre of symmetry that coincides with the centre of the structure. In the crystal structure the molecules are tilted through a certain angle with respect to the molecular layers so they form an oblique structure. (*a*) Projection along [010] of a monoclinic structure near the (001) interface between two adjacent monomolecular layers. (*b*) Projection normal to (001) of the CH_2 chain end groups in a monoclinic structure; the numbers of C atoms correspond to those of Fig. 1(*a*).

Table 1. *Dimensions of the unit cell*

$a = 5.57$ Å, $b = 7.42$ Å.

Carbon number	c (Å)	β (°)
n-C_{10}	15.328	122.86
n-C_{12}	17.862	122.08
n-C_{14}	20.398	121.49
n-C_{16}	22.935	121.04
n-C_{18}	25.474	120.67
n-C_{20}	28.014	120.37
n-C_{22}	30.554	120.12
n-C_{24}	33.095	119.91
n-C_{26}	35.637	119.73
n-C_{28}	38.178	119.57
n-C_{30}	40.720	119.43
n-C_{32}	43.262	119.31
n-C_{34}	45.804	119.21
n-C_{36}*	48.347	119.11

* This is the key structure used to derive the structure parameters of other paraffins.

Table 2. *Bonds in the structure of monoclinic even n-paraffins*

Bonds	Code
C^* (0 0 0)–C ($\frac{1}{2}$ $\frac{1}{2}$ 0)	a
C (0 0 0)–C (1 0 0)	b
C (0 0 0)–C (0 1 0)	c
C (0 0 0)–C ($\frac{3}{2}$ $\frac{1}{2}$ 0)	d
C (0 0 0)–C ($\frac{1}{2}$ $\frac{1}{2}$ 1)	e
C (0 0 0)–C (1 0 1)	f
C (0 0 0)–C (0 0 1)	g

* Here C is the gravity centre of a paraffin molecule

II.2. *Important bonds and crystal graph*

In order to carry out a PBC analysis and calculate Ising temperatures of connected nets, one should know the important bonds (or the strongest bonds) between growth units. In our case, these units are the n-paraffin molecules themselves. The mutual interactions between the molecules are mainly of the van der Waals type and can be calculated by summing all the C–C, C–H and H–H interaction energies between two molecules, based on the Buckingham potential:

$$\varphi(r) = -A'/r^6 + B' \exp(-C'r) \qquad (6)$$

For the structures of monoclinic paraffins, seven different types of the most important bonds are identified and listed in Table 2. The bond structure can easily be seen from a so-called crystal graph (Bennema & van der Eerden, 1987), an example of which is shown in Fig. 2(*a*). Also, Fig. 2(*b*) shows how the nodes and bonds in different positions of the crystal graph are related to each other by the symmetry elements of the space group.

Among the overall interactions, the interactions *a*, *b*, *c* and *d* are the first- and second-nearest lateral interactions between paraffin molecules, and the bonds *e*, *f* and *g* are the first-nearest-neighbour vertical interactions. In general, the lateral interactions are stronger than the vertical interactions. Using a least-squares regression, a linear relation between φ_i and m is found:

$$\varphi_i(m) = \varphi_i^0 m + \varphi_i'. \qquad (7)$$

Table 3. *The coefficients of expressions of bond energies in the structure*

$\varphi_i(E^{cr}) = \varphi_i^0 n + \varphi_i'$ (kJ mol^{-1})

	φ_i^0 (kJ mol^{-1})	φ_i' (kJ mol^{-1})
φ_a	2.805210	−3.90252
φ_b	1.760135	−4.22071
φ_c	0.220753	−0.44619
φ_d	0.123645	−0.44313
φ_e	0	2.00037
φ_f	0	1.10079
φ_g	0	2.01557
E^{cr}*	7.838598	−6.24118

* $E^{cr} = 2\varphi_a + \varphi_b + \varphi_c + 2\varphi_d + 2\varphi_e + \varphi_f + \varphi_g$.

The coefficients of φ_i^0 and φ_i' according to (7) are listed in Table 3. We notice that, as in the work of Bennema

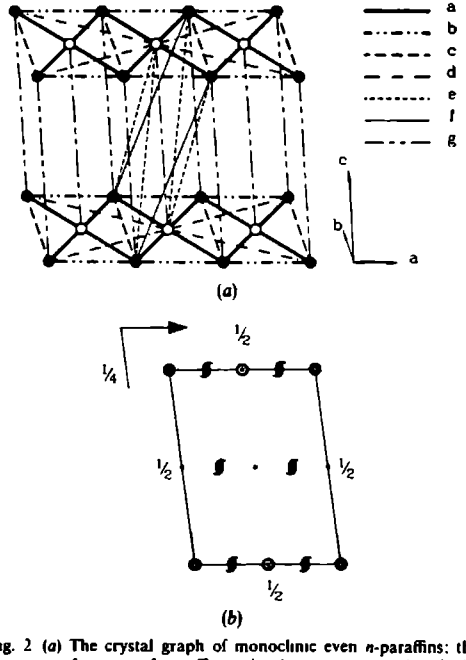

Fig. 2 (*a*) The crystal graph of monoclinic even n-paraffins: the centres of gravity of paraffin molecules are associated with the seven types of bonds identified from the structure (*b*) The nodes and bonds in the crystal graph are related by the symmetrical elements

Table 4. *Identified PBCs in the monoclinic structures of even n-paraffins*

PBCs	Bonds
[110] ([1$\bar{1}$0])	*a, a*
[100]	*b*
[010]	*c*
[310] ([3$\bar{1}$0])	*d, d*
[001]	*g*
[112] ([1$\bar{1}$2])	*e, e*
[101]	*f*

et al. (1992), for the vertical bonds, $\varphi_v^0 = 0$. Consequently, the crystallizing energy of paraffins can also be expressed by (7) and the coefficients are found in Table 3. The calculated bond energies *versus* the carbon numbers of *n*-paraffins are plotted in Fig. 3. In the following, we can see that the large difference in bond strength between the lateral and vertical interactions results in a high degree of anisotropy of *n*-paraffin crystals.

II.3. *PBC analysis*

The main step in the analysis leading to the theoretical morphology of the crystals is the determination of the connected nets of crystals of monoclinic *n*-paraffins. This can be done by partitioning the crystal graph in equal parallel connected nets having no points in common and having an overall thickness of the interplanar distance $d_{nk\,nk\,nl}$, corrected by the extinction conditions of the space group (Hahn, 1983). This can also be obtained from a PBC analysis; first PBCs are identified from the crystal graph, then a stereographic projection of all these PBCs is made in search of potential *F* forms (Hartman, 1987, Bennema & van der Eerden, 1987). Basically, seven different PBCs are found, as summarized in Table 4. The stereographic projection of these PBCs is shown in Fig. 4, taking the structure

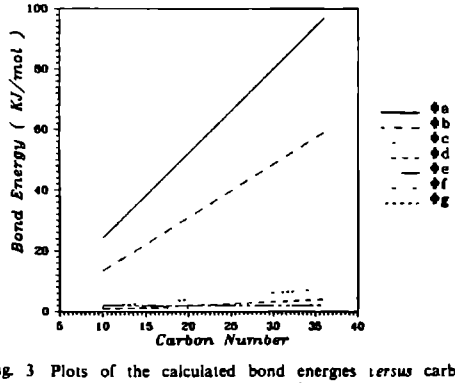

Fig. 3 Plots of the calculated bond energies *versus* carbon numbers of *n*-paraffins

Table 5 12 *connected nets in the structure, together with the contained PBCs, bonds and thicknesses of the slices*

Nets	Thickness	PBCs	Bonds
(001)	d_{001}	[001] [100] [110] [1$\bar{1}$0] [310] [3$\bar{1}$0]	*a, b, c, d*
(110)	d_{110}	[1$\bar{1}$0] [001] [11$\bar{2}$]	*a, e, g*
(11$\bar{1}$)	d_{111}	[101] [1$\bar{1}$0] [112]	*a, e, f*
(010)	d_{020}	[001] [100] [101]	*b, g, f*
(100)	d_{200}	[010] [001]	*c, g*
(10$\bar{1}$)	d_{202}	[010] [101]	*c, f*
(02$\bar{1}$)	d_{021}	[100] [112]	*b, e*
(20$\bar{1}$)	d_{201}	[010] [112] [1$\bar{1}$2]	*c, e*
(130)	d_{130}	[001] [310]	*d, g*
(131)	d_{131}	[310] [112]	*d, e*
(13$\bar{2}$)	d_{132}	[3$\bar{1}$0] [112]	*d, e*
(13$\bar{1}$)	d_{131}	[3$\bar{1}$0] [101]	*d, f*

of n-$C_{26}H_{54}$ as an example. It turns out that 12 *F* forms that occur in the stereographic projection correspond to the 12 nets that are fully connected. Thus, they are all real *F* forms (Bennema & van der Eerden, 1987). The 12 connected nets are shown in Fig. 5. Table 5 summarizes these nets and gives the contained PBCs, bonds and thicknesses of the slices.

III. Ising temperature and roughening transition

One of the most significant steps in an analysis of the morphology of crystals is the determination of the

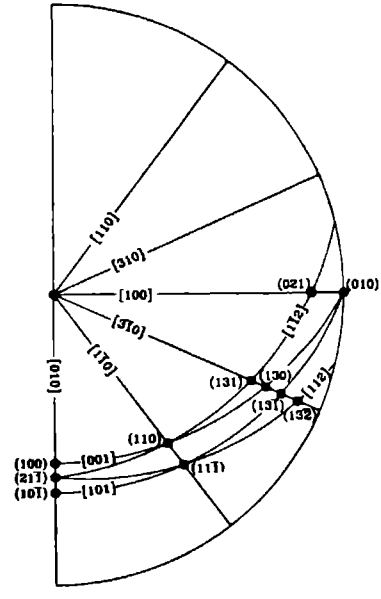

Fig. 4 The stereographic projection of PBCs [uvw]. Intersections (●) of these PBCs (———) indicate potential *F* faces (*hkl*). 12 *F* faces result from the projection

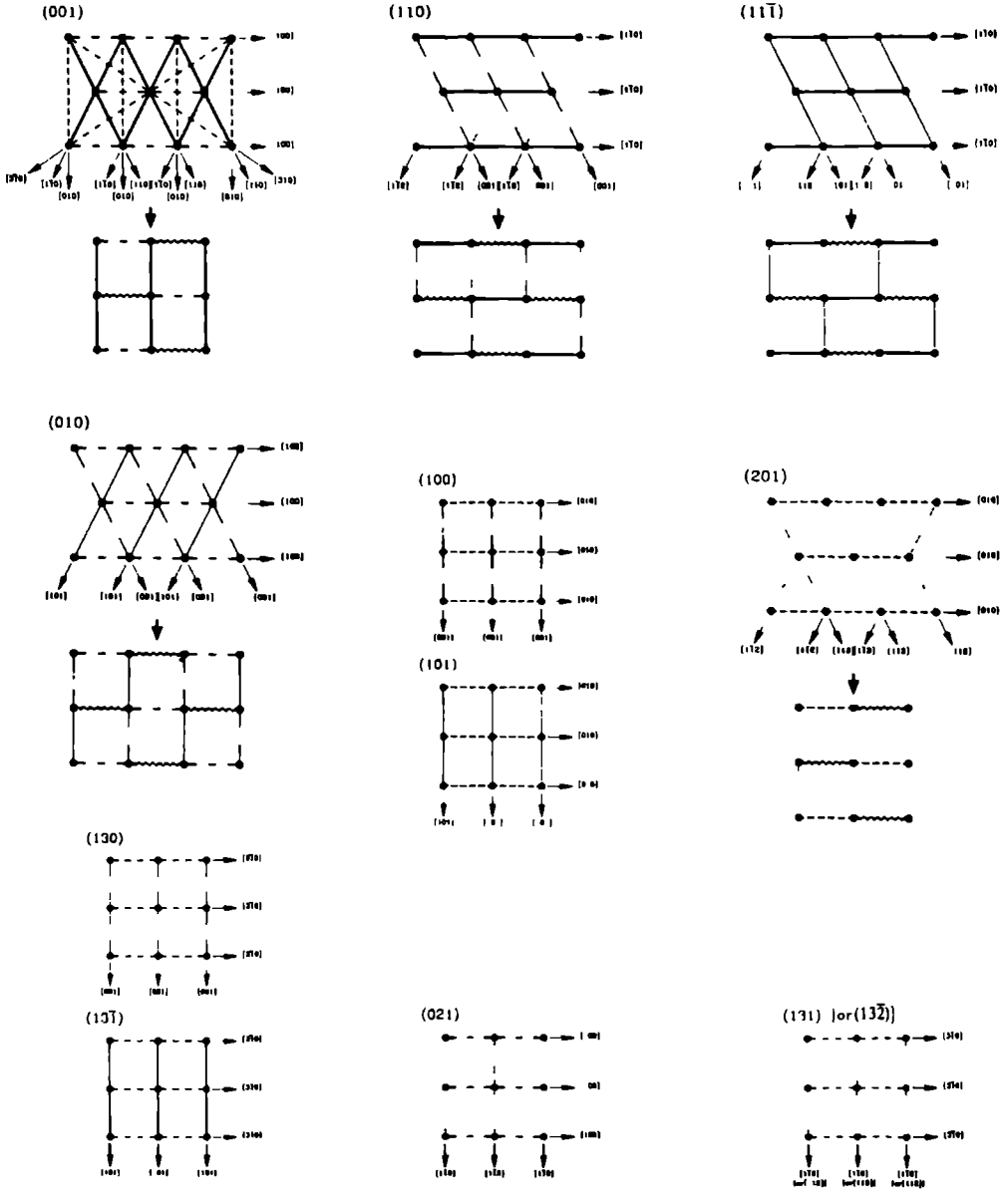

Fig. 5 The 12 connected nets of the 12 *F* slices, together with the 'rectangularized' nets of (001), (110), (111), (010) and (201) To calculate the Ising temperature, the rectangularization' (Bennema & van der Eerden, 1987) must be carried out for some connected nets, such as (001), (110), (11$\bar{1}$), (010) and (201). This can be done by splitting one node into two with a bond of infinite strength (indicated by a wiggly line) connecting these two nodes The rectangularized nets obtained share the same partition function with the original ones and are suitable for calculation of the Ising temperature from a computer program Among those nets, the (001) net is the strongest one Before rectangularizing, the weaker bonds *c* and *d* in the net, which cross with another stronger bond, need to be omitted The crystallographically different faces {132} and {131} have the same connected nets.

Table 6 *The dimensionless Ising temperatures* θ^*_{hkl} *of the* 12 *connected nets*

	{001}	{110}	{111}	{010}	{021}	{201}	{100}	{101}	{130}	{131}	{132}	{13$\bar{1}$}
n-C_{10}	3 0793	1 0736	0 9828	0 6726	0 5716	0 2893	0 1771	0 1321	0 1237	0 1232	0 1232	0 0884
n-C_{12}	3 0933	1 0008	0 9197	0 6329	0 5428	0 2530	0 1594	0 1215	0 1127	0 1122	0 1122	0 0816
n-C_{14}	3 1051	0 9453	0 8715	0 6019	0 5197	0 2274	0 1472	0 1135	0 1043	0 1039	0 1039	0 0765
n-C_{16}	3 1147	0 9018	0 8335	0 5770	0 5010	0 2084	0 1381	0 1072	0 0977	0 0974	0 0974	0 0724
n-C_{18}	3 1225	0 8667	0 8029	0 5565	0 4854	0 1937	0 1311	0 1021	0 0924	0 0920	0 0920	0 0690
n C_{20}	3 1287	0 8378	0 7776	0 5394	0 4721	0 1819	0 1254	0 0980	0 0879	0 0876	0 0876	0 0661
n C_{22}	3 1334	0 8133	0 7561	0 5247	0 4607	0 1723	0 1205	0 0945	0 0842	0 0839	0 0839	0 0637
n C_{24}	3 1369	0 7921	0 7375	0 5120	0 4507	0 1642	0 1162	0 0914	0 0809	0 0806	0 0806	0 0616
n C_{26}	3 1394	0 7735	0 7210	0 5006	0 4417	0 1573	0 1124	0 0888	0 0781	0 0778	0 0778	0 0598
n-C_{28}	3 1412	0 7569	0 7063	0 4904	0 4336	0 1512	0 1089	0 0864	0 0756	0 0753	0 0753	0 0581
n-C_{30}	3 1425	0 7419	0 6930	0 4812	0 4263	0 1459	0 1057	0 0843	0 0734	0 0731	0 0731	0 0566
n-C_{32}	3 1436	0 7283	0 6810	0 4728	0 4196	0 1413	0 1029	0 0824	0 0713	0 0711	0 0711	0 0553
n C_{34}	3 1447	0 7161	0 6702	0 4652	0 4135	0 1371	0 1004	0 0807	0 0695	0 0693	0 0693	0 0541
n C_{36}	3 1460	0 7053	0 6606	0 4584	0 4080	0 1334	0 0985	0 0792	0 0679	0 0677	0 0677	0 0530
n-C_{38}	3 1478	0 6961	0 6524	0 4524	0 4032	0 1301	0 0972	0 0779	0 0665	0 0663	0 0664	0 0521
n-C_{40}	3 1504	0 6885	0 6458	0 4474	0 3990	0 1273	0 0967	0 0768	0 0652	0 0650	0 0650	0 0512
MI order	1	2	3	4	5	6	7	8	9	10	10	11

dimensionless Ising temperature of the connected nets On the one hand, it can be used as an estimate of the roughening temperature θ^*_{hkl} (Bennema & van der Eerden 1987), on the other, it is a key factor in the ranking of all crystallographic faces in MI order As before, we assume that the dimensionless Ising temperature θ^*_{hkl} has the same form as the roughening temperature θ^*_{hkl} [see (3)] Here, θ^*_{hkl} is normalized to the strongest bond energy φ_{str} The effective bond energies correspond to those in interfacial phases and are given by (4) If the proportionality condition, (5), is taken into account, the dimensionless Ising temperature θ^*_{hkl} of all 12 connected nets can be calculated The results are summarized in Table 6

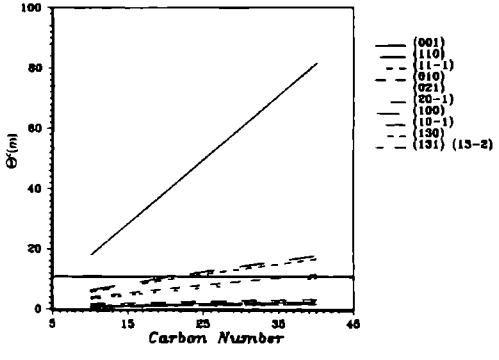

Fig. 6 The modified dimensionless Ising temperatures $\theta^*_{hkl}(m) = \theta^*_{hkl}\varphi_{str}(m)/\rho$ of different F faces plotted as a function of m, the number of carbon atoms in the paraffin chains An isotherm corresponds to a horizontal line and an equal m line to a vertical line The isotherm θ (the horizontal line) corresponding to a certain growth condition offers a boundary between rough and flat faces in the diagram In the case where the $\theta^*_{hkl}(m)$ curves are below the isotherm θ the equilibrium structures of those interfaces are rough If the $\theta^*_{hkl}(m)$ curves are above the isotherm θ, the form are flat

We note that variation of the carbon number of paraffins will influence the ratios of bond energies and hence the Ising temperatures θ^*_{hkl} This influence on θ^*_{hkl} results from variation in the anistropy of interactions It is also worthwhile to see the direct dependence of the Ising temperatures of the faces on the absolute bond energies or on the carbon number So, we modify the dimensionless critical temperature in the following way

$$\theta^*_{hkl}(m) = \theta^*_{hkl}\varphi_{str}(m)/\rho \qquad (8)$$

As $\varphi_{str}(m)$ depends on the medium, and the values are mostly not available, for the time being we choose $\varphi_{str}(m) \simeq \varphi^{ss}_{str}(m)$ This corresponds to the vacuum environment The curves of $\theta^*_{hkl}(m)$ *versus* carbon number m are plotted in Fig 6 It is a presentation of the roughening-transition phase diagram (if we assume $\theta^*_{hkl} \simeq \theta^*_{hkl}$) Moreover, using these conven tions, we can directly compare, qualitatively the roughening temperatures of faces within the n-paraffin series

IV. Theoretical growth and equilibrium forms

Following Bennema *et al* (1992), the following six formulae for growth and equilibrium forms of crystals are used the growth forms (i) $R_{hkl} \simeq E^{att}_{hkl}$, (ii) $R_{hkl} \simeq (E^{slice}_{hkl})^{-1}$, (iii) $R_{hkl} \simeq (\theta^*_{hkl})^{-1}$, (iv) $R_{hkl} \simeq [\theta^*_{hkl}(m) - \theta]^{-1}$ and (v) $R_{hkl} \simeq d^{-1}_{hkl}$, the equilibrium form (vi) $D_{hkl} \simeq d_{hkl}E^{att}_{hkl}$ (this approximation holds for 0 K) The first two formulae are inspired by the Hartman–Perdok theory, the next two by the roughening-transition theory, the fifth by the BFDH theory and the sixth by the equilibrium-form theory

Formulae (iv) is associated with the order–disorder phase diagram (see Fig 6), where the isotherm θ offers a boundary between rough and flat interfaces Those faces with rough interfacial struc- tures [$\theta^*_{hkl}(m) - \theta < 0$] have much higher growth rates

Table 7 *The relative values of* $[\theta^{c}_{hkl}(m) - \theta]^{-1}$ *of the* 12 *connected nets*

	{001}	{110}	{111}	{010}	{021}	{201}	{100}	{101}	{130}	{131}	{13$\bar{2}$}	{13$\bar{1}$}
n-C_{10}	1	−2 218	−1 937	−1 350	−1 229	−0 982	−0 910	−0 884	−0 879	−0 879	−0 879	−0 860
n-C_{12}	1	−4 400	−3 639	−2 257	−2 017	−1 052	−1 388	−1 346	−1 337	−1'336	−1 336	−1 305
n-C_{14}	1	−8 416	−6 367	−3 370	−2 948	−2 038	−1 879	−1 819	−1 804	−1 803	−1 803	−1 758
n-C_{16}	1	−18 037	−11 364	−4 754	−4 054	−2 589	−2,383	−2 302	−2 278	−2 277	−2 277	−2 217
n-C_{18}	1	−70 532	−23 324	−6 509	−5 387	−3 157	−2 899	−2 794	−2 760	−2 759	−2 759	−2 682
n-C_{20}	1	68 271	−88 849	−8 796	−7 011	−3 739	−3 427	−3 294	−3 248	−3 247	−3 247	−3 152
n-C_{22}	1	27 945	83 287	−11 887	−9 029	−4 336	−3 966	−3 803	−3 742	−3 740	−3 740	−3 627
n-C_{24}	1	19 293	33 638	−16 271	−11 594	−4 948	−4 515	−4 320	−4 242	−4 239	−4 239	−4 106
n-C_{26}	1	15 544	22 943	−22 943	−14 951	−5 575	−5 073	−4 844	−4 746	−4 744	−4 744	−4 589
n-C_{28}	1	13 465	18 299	−34 272	−19 521	−6 216	−5 639	−5 376	−5 256	−5 254	−5 254	−5 075
n-C_{30}	1	12 151	15 714	−57 647	−26 089	−6 873	−6 215	−5 915	−5 772	−5 769	−5 769	−5 567
n-C_{32}	1	11 247	14 071	−133 903	−36 319	−7 545	−6 802	−6 463	−6 293	−6 290	−6 290	−6 062
n-C_{34}	1	10 584	12 930	1093 845	−54 478	−8 235	−7 402	−7 021	−6 821	−6 817	−6 817	−6 563
n-C_{36}	1	10 072	12 082	122 722	−95 823	−8 945	−8 022	−7 588	−7 356	−7 351	−7 351	−7 070
n-C_{38}	1	9 653	11 412	68 910	−286 376	−9 678	−8 669	−8 169	−7 899	−7 895	−7 895	−7 584
n-C_{40}	1	9 290	10 852	49 423	369 751	−10 439	−9 355	−8 764	−8 454	−8 448	−8 448	−8 106
MI order	1	2	3	4	5	–	–	–	–	–	–	–

and will disappear from crystal forms Flat faces $[\theta^{c}_{hkl}(m) - \theta > 0]$, having roughening temperatures close to the actual temperature {*i e* the values of $[\theta^{c}_{hkl}(m) - \theta]$ are small} grow much faster than those having roughening temperatures that are much higher than the actual temperature Hence, the flat faces with $\theta^{c}_{hkl}(m)$ closer to θ are less likely to appear on crystals In order to apply formulae (iv) successfully, the value of θ must be chosen properly Conventionally, we take the lower limit of accessible temperature in our growth conditions to scale θ, which is expressed as

$$\theta = [\theta^{c}_{h_1k_1l_1}(m') + \theta^{c}_{h_2k_2l_2}(m')]/2. \qquad (9)$$

Face $(h_1k_1l_1)$ is the face whose roughening temperture is just above the actual temperature, while face $(h_2k_2l_2)$ is the face with a roughening temperature just below the actual temperature For the time being there is no absolute roughening temperature available for the series of monoclinic n-paraffins Therefore we make an estimate from other series of n-paraffins, which shows that the dimensionless actual temperature is somewhere between $\theta^{c}_{11\bar{1}}$ (26) and θ^{c}_{010} (26) If we assume that bond energies have the form $\varphi_i \simeq a(m-1)$ (a is a constant), then the relative values of $[\theta^{c}_{hkl}(m) - \theta]^{-1}$ for the series of n-paraffins with the monoclinic structure are obtained These values are listed in Table 7

Applying formulae (i), (ii) and (vi), we need the data of E^{slice}_{hkl} and E^{att}_{hkl} for the whole paraffin series Each E^{slice}_{hkl} is very easy to calculate from the corresponding connected nets We summarize the expressions of all identified F slices in Table 8 and their values in Table 9 E^{att}_{hkl} can be calculated immediately from (2), on the basis of the data in Table 9 and on E^{cr} [see (7) and Table 3] The results of the calculation of E^{att}_{hkl} are then given in Table 10 Finally, the data for $(d_{hkl})^{-1}$ and $(d_{hkl}E^{att}_{hkl})$ are summarized in Tables 11 and 12, respectively, according to formulae (v) and (vi)

Table 8 *The expressions of* E^{slice}_{hkl} *for the* 12 *connected nets*

E^{slice}_{001}	$= 2\varphi_a + \varphi_h + \varphi_c + 2\varphi_d$
E^{slice}_{110}	$= \varphi_a + \varphi_e + \varphi_g$
E^{slice}_{111}	$= \varphi_a + \varphi_e + \varphi_f$
E^{slice}_{010}	$= \varphi_b + \varphi_g + \varphi_f$
E^{slice}_{100}	$= \varphi_c + \varphi_g$
E^{slice}_{101}	$= \varphi_c + \varphi_f$
E^{slice}_{021}	$= \varphi_b + \varphi_a$
E^{slice}_{201}	$= \varphi_c + 2\varphi_e$
E^{slice}_{130}	$= \varphi_a + \varphi_g$
E^{slice}_{131}	$= \varphi_a + \varphi_e$
E^{slice}_{132}	$= \varphi_d + \varphi_e$
E^{slice}_{131}	$= \varphi_a + \varphi_f$

We can see from the tables that the Hartman–Perdok theory gives the same order of morphological importance of {hkl} forms on crystals as the Ising model, which is somewhat different from the results from the BFDH theory For equilibrium forms, the MI order is changed considerably as compared with the MI order of growth forms Those faces which are very important in the growth forms become less important in the equilibrium forms The reason is given in our previous paper (Bennema *et al*, 1992)

In Fig 7, the growth and equilibrium forms resulting from formulae (i)–(vi) are presented The figures as indicated correspond to the crystals of the monoclinic even n-paraffins with carbon numbers 16, 26 and 36, respectively In general, the following relation holds for the crystal thickness D_x $D_6 > D_2 > D_3 > D_5 > D_1 \sim D_4$ [For an explanation see Bennema *et al* (1992)]

V. Experimental growth forms

A series of observations of the morphology of monoclinic even n-paraffin crystals were carried out

Table 9 *The values of* E_{hkl}^{slice} *for the* 12 *connected nets* (kJ mol^{-1})

	{001}	{110}	{111}	{010}	{021}	{201}	{100}	{10$\bar{1}$}	{130}	{131}	{13$\bar{2}$}	{13$\bar{1}$}
n-C_{10}	65 028	28 166	27 251	16 497	15 381	5 762	3 777	2 862	2 809	2 794	2 794	1 894
n-C_{12}	80 705	33 776	32 861	20 017	18 901	6 204	4 218	3 304	3 056	3 041	3 041	2 141
n-C_{14}	96 380	39 386	38 472	23 538	22 422	6 645	4 660	3 745	3 288	3 288	3 288	2 389
n-C_{16}	112 059	44 997	44 082	27 058	25 942	7 087	5 101	4 187	3 551	3 536	3 536	2 636
n-C_{18}	127 737	50 607	49 692	30 578	29 462	7 528	5 543	4 628	3 798	3 783	3 783	2 883
n-C_{20}	143 414	56 218	55 303	34 098	32 982	7 970	5 984	5 070	4 045	4 030	4 030	3 131
n-C_{22}	159 901	61 828	60 913	37 619	36 503	8 411	6 426	5 511	4 293	4 277	4 277	3 378
n-C_{24}	174 768	67 439	66 524	41 139	40 023	8 853	6 867	5 953	4 540	4 525	4 525	3 625
n-C_{26}	190 445	73 049	72 134	44 659	43 543	9 294	7 309	6 394	4 787	4 772	4 772	3 872
n-C_{28}	206 122	78 659	77 745	48 179	47 063	9 736	7 750	6 836	5 034	5 019	5 019	4 120
n-C_{30}	221 800	84 270	83 355	51 700	50 584	10 177	8 192	7 277	5 282	5 267	5 267	4 367
n-C_{32}	237 477	89 880	88 965	55 220	54 104	10 619	8 633	7 719	5 529	5 514	5 514	4 614
n-C_{34}	253 154	95 491	94 576	58 740	57 624	11 060	9 075	8 160	5 776	5 761	5 761	4 862
n-C_{36}	268 831	101 101	100 186	62 261	61 145	11 502	9 516	8 602	6 024	6 008	6 008	5 109
n-C_{38}	284 508	106 711	105 797	65 781	64 665	11 943	9 958	9 043	6 271	6 256	6 256	5 356
n-C_{40}	300 186	112 322	111 407	69 301	68 185	12 385	10 399	9 485	6 503	6 503	6 503	5 603
MI order	1	2	3	4	5	6	7	8	9	10	10	11

Table 10 *The relative values of* E_{hkl}^{att} *of the* 12 *connected nets* (kJ mol^{-1})

	{001}	{110}	{11$\bar{1}$}	{010}	{021}	{201}	{100}	{101}	{130}	{131}	{13$\bar{2}$}	{13$\bar{1}$}
n-C_{10}	7 117	43 979	44 894	55 648	56 764	66 384	68 368	69 283	69 336	69 351	69 351	70 251
n-C_{12}	7 117	54 046	54 961	67 805	68 921	81 618	83 604	84 518	84 766	84 781	84 781	85 681
n-C_{14}	7 117	64 113	65 028	79 962	81 078	96 854	98 839	99 754	100 196	100 211	100 211	101 111
n-C_{16}	7 117	74 180	75 094	92 119	93 235	112 090	114 075	114 990	115 626	115 641	115 641	116 541
n-C_{18}	7 117	84 246	85 161	104 276	105 392	127 326	129 311	130 226	131 056	131 071	131 071	131 970
n-C_{20}	7 117	94 313	95 228	116 432	117 548	142 561	144 546	145 461	146 486	146 551	146 551	147 400
n-C_{22}	7 117	104 380	105 295	128 589	129 705	157 767	157 782	160 697	161 915	161 931	161 931	162 830
n-C_{24}	7 117	114 447	115 362	140 746	148 862	173 033	175 018	175 933	177 345	177 361	177 361	178 260
n-C_{26}	7 117	124 513	125 428	152 903	154 019	188 268	190 253	191 168	192 775	192 790	192 790	193 690
n-C_{28}	7 117	134 580	135 495	165 060	166 176	203 504	205 489	206 404	208 205	208 220	208 220	209 120
n-C_{30}	7 117	144 647	145 562	177 217	178 333	218 740	220 725	221 640	223 635	223 650	223 650	224 550
n-C_{32}	7 117	154 714	155 629	189 374	190 490	233 975	235 961	236 875	239 065	239 080	239 080	239 980
n-C_{34}	7 117	164 781	165 965	201 531	202 647	249 211	251 196	252 111	254 495	254 510	254 510	255 410
n-C_{36}	7 117	174 847	175 762	213 688	214 804	264 447	266 432	267 347	269 925	269 940	269 940	270 840
n-C_{38}	7 117	184 984	185 829	225 845	226 961	279 683	281 668	282 582	285 370	285 370	285 370	286 269
n-C_{40}	7 117	194 981	195 896	238 002	239 118	294 918	296 903	297 818	300 785	300 800	300 800	301 699
MI order	1	2	3	4	5	6	7	8	9	10	10	11

Table 11. *The values of* d_{hkl}^{-1} *of the* 12 *connected nets* [(10 Å)$^{-1}$]

	{001}	{110}	{11$\bar{1}$}	{010}	{021}	{201}	{100}	{101}	{130}	{131}	{13$\bar{2}$}	{13$\bar{1}$}
n-C_{10}	0 776	2.527	2 277	2 695	2 805	3 908	4 275	3 671	4 573	4 829	4 441	4 441
n-C_{12}	0 661	2 511	2.292	2 696	2 775	3 927	4 238	3 709	4 565	4 771	4 428	4 448
n-C_{14}	0 575	2 500	2.305	2 695	2 756	3 941	4 211	3 741	4 558	4 730	4 424	4 455
n-C_{16}	0 509	2 491	2 316	2 695	2.743	3 952	4 191	3 768	4 554	4 701	4 424	4 461
n-C_{18}	0 456	2 484	2 326	2.695	2.734	3 961	4 175	3 791	4 550	4 678	4 426	4 465
n-C_{20}	0 414	2.479	2 334	2 695	2 727	3 969	4 162	3 811	4 547	4 660	4 430	4 470
n-C_{22}	0 378	2.475	2 341	2.695	2.722	3 975	4 151	3 828	4 545	4 646	4 433	4 473
n-C_{24}	0 349	2.471	2.347	2 695	2.718	3 980	4 142	3 843	4 543	4 634	4 437	4 476
n-C_{26}	0 323	2.468	2.352	2 695	2.715	3 985	4 135	3 855	4 541	4 625	4 440	4 479
n-C_{28}	0 301	2.465	2.357	2 695	2.712	3 988	4 128	3 867	4 540	4 617	4 443	4 482
n-C_{30}	0 282	2 463	2.361	2.695	2 710	3 992	4 123	3 877	4 538	4 609	4 447	4 484
n-C_{32}	0 265	2 461	2.365	2 695	2 708	3 995	4 118	3 886	4 537	4 603	4 450	4 486
n-C_{34}	0 250	2 459	2.368	2 695	2.707	3 998	4 114	3 894	4 536	4 598	4 452	4 488
n-C_{36}	0 237	2 457	2.371	2.695	2 706	4 000	4 110	3 901	4 505	4 593	4 455	4 489
n-C_{38}	0 225	2 456	2.374	2 695	2 705	4 002	4 106	3 908	4 535	4 589	4 457	4 491
n-C_{40}	0 214	2.455	2.376	2 695	2.704	4 004	4 103	3 914	4 534	4 585	4 459	4 492
MI order	1	3	2	4	5	7	8	6	11	12	9	10

Table 12 *The values of* $d_{hkl}E^{att}_{hkl}$ *of the* 12 *connected nets* (kJ Å mol $^{-1}$)

	{001}	{110}	{111}	{010}	{021}	{201}	{100}	{101}	{130}	{131}	{132}	{131}
n-C_{10}	91 636	174 055	197 134	206 453	202 360	169 860	159 938	188 705	151 611	143 613	156 515	158 210
n-C_{12}	107 762	215 223	239 746	251 556	248 323	207 843	197 283	227 877	185 699	177 709	191 439	192 621
n-C_{14}	123 788	256 465	282 658	296 658	294 180	245 748	234 720	266 650	219 800	211 852	226 512	226 967
n-C_{16}	139 865	297 754	324 174	341 760	339 896	283 602	237 216	305 161	253 910	246 014	261 380	261 269
n-C_{18}	155 941	339 074	355 149	386 862	385 515	321 421	309 752	343 493	288 025	280 184	296 110	295 537
n-C_{20}	172 018	380 416	408 022	431 964	431 056	359 214	347 317	381 698	322 144	314 356	330 738	329 782
n-C_{22}	188 094	421 775	449 820	477 067	476 534	396 988	384 902	419 810	356 266	38 528	365 287	364 009
n-C_{24}	204 170	463 146	491 560	522 169	521 962	434 748	422 503	457 850	390 390	382 699	399 774	398 221
n-C_{26}	220 247	504 526	533 255	567 271	567 349	472 496	460 116	495 836	424 516	416 867	434 211	432 423
n-C_{28}	236 323	545 914	574 914	612 373	612 701	510 235	497 739	533 778	458 623	451 034	468 610	466 616
n-C_{30}	252 400	587 308	616 544	657 475	658 245	547 967	535 370	571 686	492 771	485 198	502 975	500 801
n-C_{32}	268 476	628 706	658 150	702 578	703 325	585 693	573 006	609 566	526 899	519 360	537 314	534 981
n-C_{34}	284 554	670 108	699 736	747 680	748 604	623 413	610 648	647 422	561 028	553 520	571 630	569 156
n-C_{36}	300 630	711 515	741 306	792 782	793 866	661 130	648 295	685 259	595 158	587 678	605 927	603 326
n-C_{38}	316 706	752 923	782 862	837 884	839 113	698 843	685 945	723 080	629 288	621 834	640 208	637 493
n-C_{40}	332 782	794 334	824 406	882 986	884 347	736 553	723 598	760 887	663 419	655 989	674 475	671 656
MI order	1	8/9	10	12/11	11 12	7	6	9/8	3	2	4 5	5 4

on crystals of n-$C_{28}H_{58}$ and n-$C_{32}H_{66}$ grown from n-hexane solutions The chemicals used in our experiments are pure enough (n-$C_{28}H_{58}$ and n-$C_{32}H_{66}$ analytically pure, Alfa, >99 0%, n-hexane spectroscopically pure, Merck, >98 0%) The experiments were carried out in a thermostated double-cell system, using polarizing microscopy For more details see Elwenspoek & Boerhof (1987)

In the following we will pay special attention to the morphological variations of crystals of n-paraffins around the roughening temperature of the {110} faces

V 1 *Morphology of crystals of* n-$C_{32}H_{66}$

In agreement with the results of the theories, in all situations, n-paraffin crystals growing from n-hexane solutions are platy Only the side faces are influenced by supersaturations and solvents Owing to these influences, the shapes of the crystals may change drastically

A crystal of n-$C_{32}H_{66}$ growing from an n-hexane solution with the equilibrium temperature of 318 17 K is shown in Fig 8(*a*) Since the side faces of {110} and {010} are rounded at a temperature very close to the equilibrium temperature, we can say that the crystal grows above the roughening temperature of the {110} faces We can see from Fig 8(*a*) that the crystal is platy with an irregular hexagonal shape This kind of growth habit can be observed at the equilibrium temperature above 309 10 K If the equilibrium temperature of the solution is lower than 303 70 K, crystals, in principle, grow below the roughening temperature of the {110} faces In this situation, the crystals reveal quite complex growth patterns At a moderate supersaturation, crystals limited by the large-faceted {001} faces and narrow-faceted {110} faces grow from solutions (see Fig 8*b*) Sometimes the crystals with a rhombic shape are truncated by the rounded {010} faces (Fig 8*c*) At a higher supersaturation, the {110} faces roughen kinetically, and these faces lose their crystallographic orientations in the subsequent growth process An example can be seen in Fig 8(*d*) When the supersaturation of the solution is lowered from the moderate value, the rough {010} faces become larger and larger Simultaneously, the flat {110} faces become smaller and finally disappear from the growth form This morphological variation is shown in Fig 9

More precise experiments for the determination of the roughening temperature have not been carried out yet However, it follows from our morphological observations that we can fix the roughening temperature of the {110} faces of n-$C_{32}H_{66}$ crystals growing from an n-hexane solution in the temperature range $303\ 70 \leq T'_{110}\ (32) \leq 309\ 10$ K

V 2 *Morphology of crystals of* n-$C_{28}H_{58}$

Similarly to n-$C_{32}H_{66}$ crystals, the growth habit of n-$C_{28}H_{58}$ is platy The morphology of crystals growing from n-hexane solutions at a temperature above the roughening temperature of the {110} faces is shown in Fig 10 The crystals are bounded by rounded {010} faces and somewhat curved {110} faces In addition, the step patterns of the {001} faces are asymmetrical (Fig 10*b*) This is caused by the symmetry of the crystals of even n-paraffins with the monoclinic structure This symmetry is different from that of paraffin crystals with the orthorhombic structure (Bennema *et al*, 1992) The growth patterns as shown in Fig 9 have also been observed on n-$C_{28}H_{58}$ crystals growing from a n-hexane solution with $T_s = 292\ 13$ K This temperature is thought to be lower than T'_{110} (28)

The roughening temperature of the {110} faces of n-$C_{28}H_{58}$ crystals growing from a n-hexane solution, based on our observations, occurs in the range $292\ 13 < T'_{110}\ (28) < 301\ 34$ K

VI. Discussion and concluding remarks

Comparing the observed growth form with the theoretical growth forms in Fig. 7, we find that for formulae (iv) and (i) predicted growth forms agree quite well with observed growth forms. Both of them predict thin platy crystals limited by the large {001} faces and the narrow {110} faces. According to formula (i), the flat {010} faces are also expected to emerge on the growth form. But within our experimental conditions, only the roughened {010} faces can be observed. Here a discrepancy with formula (i) occurs. Therefore, it seems that formula (iv) gives a better result than formula (i).

When the temperature is lower than the roughening temperature of the {110} faces, the roughened {010} faces grow slower than the flat {110} faces at a

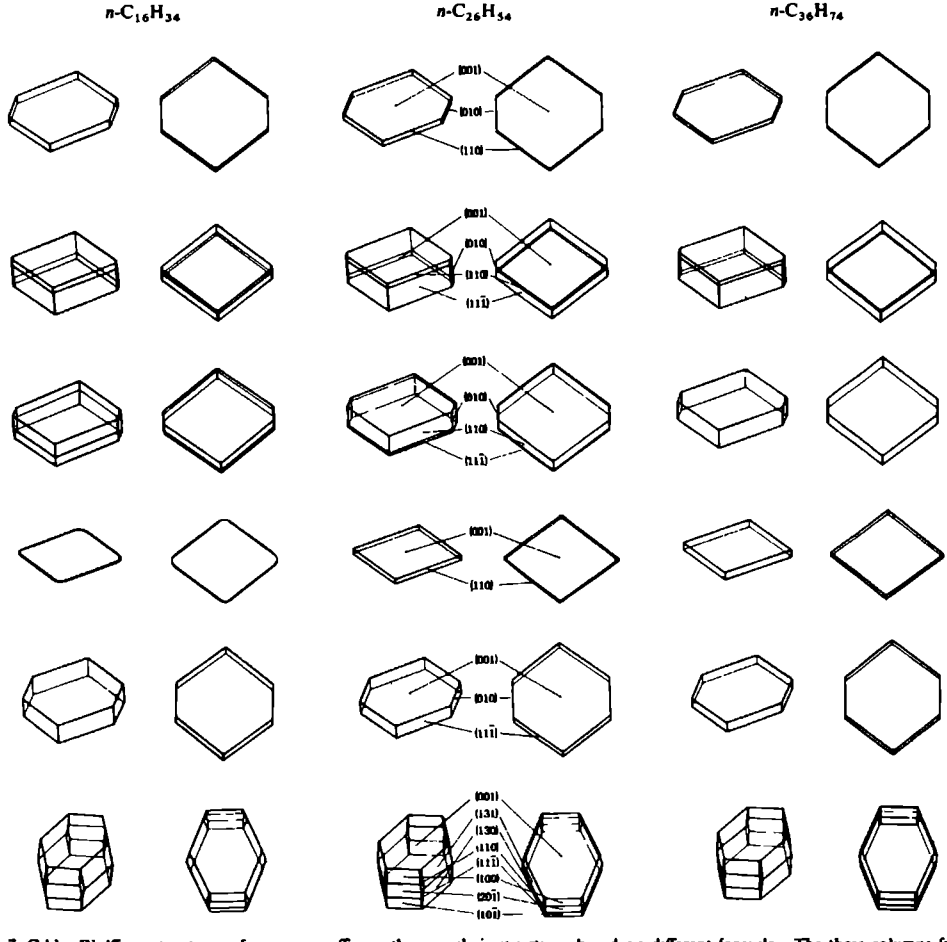

Fig. 7. Gibbs–Wulff constructions of even *n*-paraffins with monoclinic structures based on different formulae. The three columns from the left to the right correspond to n-$C_{16}H_{34}$, n-$C_{26}H_{54}$ and n-$C_{36}H_{74}$ respectively. The six rows are based on the formulae (i)–(vi), respectively. Habits of the growth forms are platy and dominated by the {001} faces, followed by thin side faces of the form {110} and in most cases truncated by the {010} faces. Sometimes the faces of the form of {11$\bar{1}$} have some chance to show up. The increase of carbon number in paraffin chains makes crystals thinner except for formula (iv). Formula (iv) shows a particular figure of growth forms in which the crystals are only limited by the large {001} faces and the narrow {011} faces. The equilibrium forms resulting from formula (vi) show a very rich morphology. All *F* forms, except {13$\bar{2}$}, {13$\bar{1}$}, {010} and {021}, are present on crystal forms. The thickness of different *n*-paraffin crystals remains almost unchanged and *F* faces with high indices are very likely to occur.

lower supersaturation (Figs. 9*a* and *b*). Then the result of formula (iv) deviates from real situations in some cases. A similar deviation can also be seen in the growth of polyethylene single crystals (Toda, 1991; Toda, Miyaji, Ogawa & Takamizawa, 1991). Formula (iv) is based on the hypothesis that the rough faces grow much faster than the flat faces and soon disappear from the growth form. It works extremely well for *n*-paraffins with shorter chain lengths (Bennema *et al.*, 1992). Considering the structure of

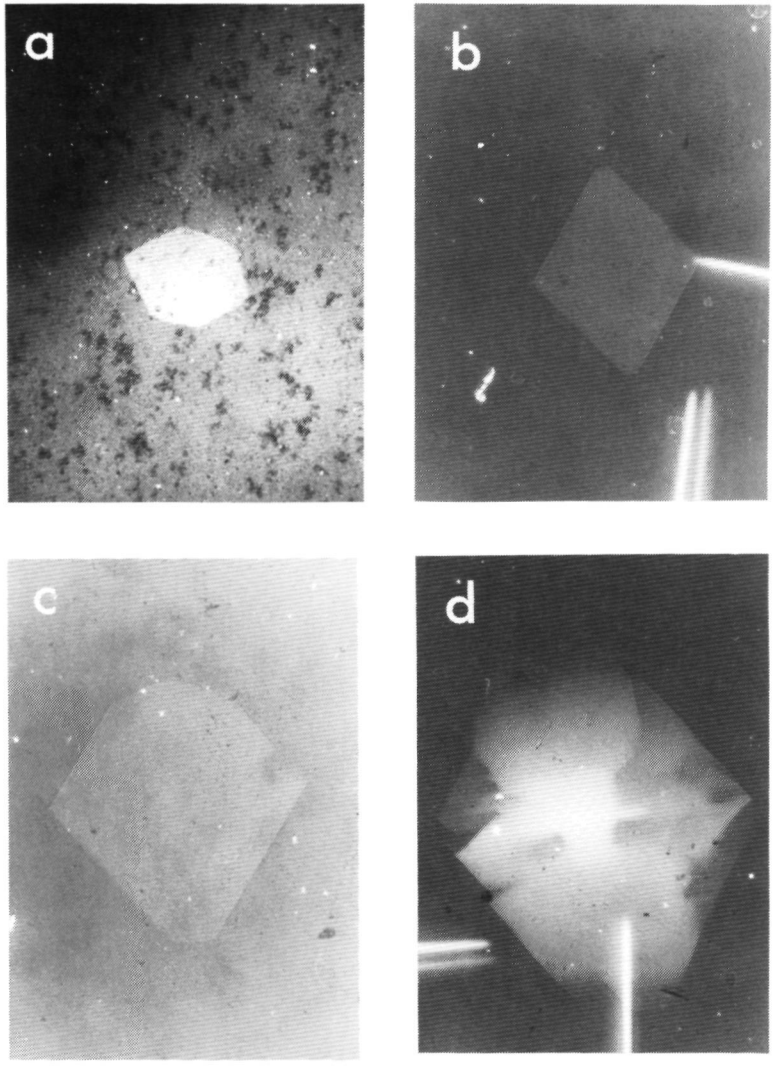

Fig. 8. A crystal of n-$C_{32}H_{66}$ growing at different equilibrium temperatures from *n*-hexane solutions. (*a*) Grown from the temperature above the roughening temperature of the {110} faces, T^r_{110}; $T_s = 318.17$ K, $\beta = 0.122\%$. The roughened {110} and {010} faces maintain some anisotropy and the crystal possesses an irregular hexagonal shape. (*b*) and (*c*) Grown from the temperature below the T^r_{110} at moderate supersaturations; $T_s = 296.08$ K, for (*b*) $\beta = 2.11\%$ and for (*c*) $\beta = 1.41\%$. The crystals are limited by the large faceted {001} and the narrow faceted {110} faces. (*d*) Grown from the temperature below the T^r_{110} at a higher supersaturation ($T_s = 296.08$ K, $\beta = 5.78\%$). The {110} faces roughen kinetically.

interfaces, we can see that it is much easier for *n*-hexane molecules to lie (or be adsorbed) parallel to and in between two solid–solid *n*-paraffin molecules at the rough surfaces (see Fig. 11*a*). This implies that the solvent molecules can be firmly adsorbed on the rough surfaces. Contrary to this, *n*-hexane molecules are not so easily adsorbed firmly onto the flat {110} surfaces (Fig. 11*b*), because at the flat {110} surfaces solid *n*-paraffin molecules pack much more tightly and the steps formed are very straight (Liu & Bennema, 1992). During growth, for all orientations, the adsorbed *n*-hexane molecules should be removed. The

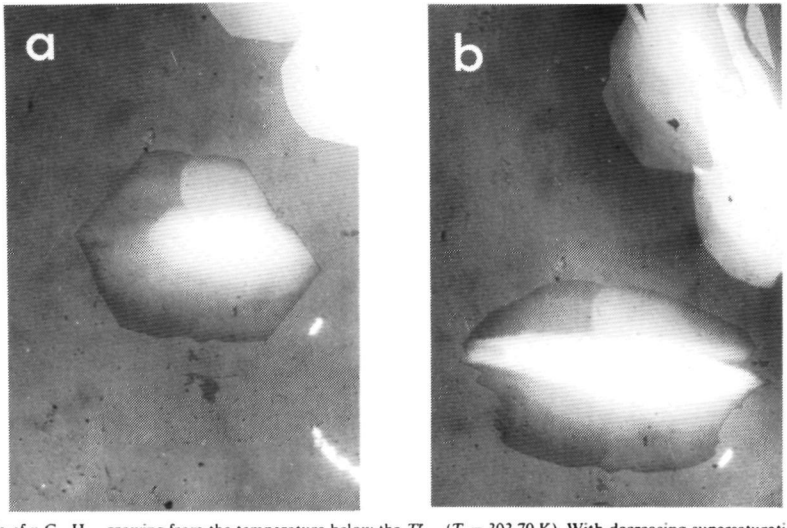

Fig. 9. Crystals of n-$C_{32}H_{66}$ growing from the temperature below the T^r_{110} (T_s = 303.70 K). With decreasing supersaturation, the faceted {110} faces grow faster than other rough side faces and gradually disappear from the growth form. (*a*) β = 2.14%; (*b*) β = 1.31%.

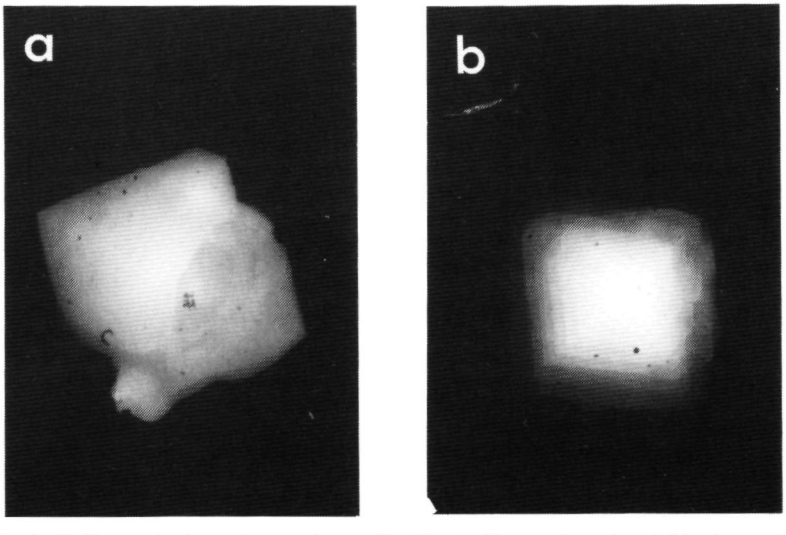

Fig. 10. Crystals of n-$C_{28}H_{58}$ growing from *n*-hexane solutions. $T_s > T^r_{110}$. (*a*) The crystals are bounded by the rounded {010} faces and somewhat rounded {110} faces. T_s = 301.34 K; β = 0.334%. (*b*) The roughened {110} faces still maintain strong anisotropy, and

energy barrier for removing the adsorbed solvent units is higher for rough faces than for flat faces Hence, in any case this process is easy for the flat {110} faces However, for the rough side faces this process becomes difficult when the *n*-paraffin chain is long and the temperature relatively low The reason is that in this case the viscosity of solutions becomes higher and the diffusion of paraffin molecules from the bulk to the interface becomes much more difficult and rate determining The driving force left at surfaces is small and it is very difficult to overwhelm the higher energy barrier at the rough surfaces and to remove the firmly adsorbed solvent molecules from the adsorbing sites As a result, the flat {110} faces grow much faster than the rough {010} faces at a lower supersaturation When the driving force (the supersaturation) is large enough to overcome the resistance of the mass transfer and then to overcome the barrier, it is not difficult to remove the *n*-hexane molecules from the adsorption sites Then, in this case, the rough {010} faces will compete with the {110} faces and may grow faster than the flat {110} faces Thus we see that, as expected from formula (iv), the {110} faces are dominant on the growth form at a moderate supersaturation (Figs 8*b* and *c*) At a temperature higher than the roughening temperature of the {110} faces, all side faces roughen up So the {110} and the {010} faces are in the same situation The growth of these side faces is then controlled by volume diffusion and the anisotropy of the surfaces Since the diffusion condition is similar for the {110} and {010} faces, these faces grow at similar rates This explains why the crystals possess an irregular hexagonal shape

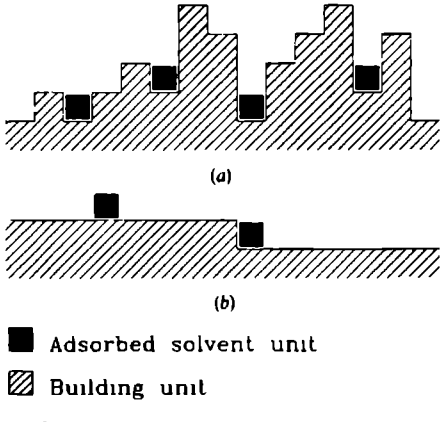

Fig. 11 Schematic illustrations of the adsorption of solvent units at the different types of interfaces (*a*) Solvent units are adsorbed on a rough interface in between two building units They are difficult to remove from the adsorption sites (*b*) Solvent units are adsorbed on a flat interface They are much easier to remove from the adsorption sites

In conclusion, we can see from the foregoing sections that the order of morphological importance (MI) for the *F* faces according to our observations is $MI_{\{001\}} \gg MI_{\{110\}} \geq MI_{\{010\}}$ This is in agreement with the theoretical predictions Apart from this formula (iv), predicting thin platy crystals with a rhombic shape, gives a better description of the growth form of *n*-paraffin crystals than other formulae The deviation of the growth form at a lower supersaturation, when the temperature is lower than the roughening temperature of {110} faces may be due to stronger adsorption of *n*-hexane molecules on the rough side faces When the {110} faces roughen all side faces are rough Then the growth habits of the side faces are determined by the anisotropy of crystal growth and the volume diffusion

Symbols and abbreviations

A, B', C'	The empirical parameters of the Buckingham potential [see (4)], taken from Williams (1967) for C–C, C–H and H–H interactions
C	Carbon atom
d	Interplanar distance
D_{hkl}	The length of the normal to face (hkl) from the origin
D_x	The relative thickness resulting from different recipes, $x = 1$–6 corresponding to recipes (i)–(vi)
E^{att}	Attachment energy defined as the energy per building unit that is released when a new slice is attached to a crystal surface
E^{cr}	Crystallizing energy, defined as the energy per building unit released when a crystal is formed from growth units that are infinitely separated from each other
E^{slice}	Slice energy, corresponding to a two-dimensional crystallizing energy
F face	A crystal face parallel to a connected net containing at least two mutually intersecting PBCs
H	Hydrogen atom
k	Boltzmann constant
K	Constant, defined by (1)
m	The number of carbon atoms in a paraffin chain
PBC	Periodic bond chain, defined as an uninterrupted path of strong bonds running through the whole structure and having a periodicity of $[uvw]$ of the lattice
r	Distance between two atoms in different molecules
T	Temperature
β	Relative supersaturation or the angle between the a and c axes of a unit cell

σ	Specific surface free energy
φ	Interaction energy
θ	Dimensionless temperature
ρ	Factor introduced in (7) to keep $\theta_{hkl}(n)$ dimensionless, here taken equal to 1 J mol^{-1}
Subscripts	
hkl	Crystal face (*hkl*)
i	Referred to different bonds
str	The strongest interaction
Superscripts	
c	Critical point of the order–disorder phase transition
r	Roughening transition
ff	Fluid–fluid interaction
sf	Solid–fluid interaction
ss	Solid–solid interaction

The authors thank Shell Netherlands B V for supporting this work We also acknowledge Dr H Meekes for a critical reading of the manuscript and Mr J van Kessel for help in making some of the drawings

References

Bennema P & van der Eerden, J P (1987) *Morphology of Crystals* edited by I Sunagawa pp 1–75 Tokyo Terra Sci

Bennema P Liu X Y, Lewtas K Tack R D Rijpkema J J M & Roberts, K J (1992) *J Cryst Growth*, **121** 679–696

Boistelle R (1980) *Current Topics in Materials Science* edited by E Kaldis pp 413 480 Amsterdam North-Holland

Broadhurst M G (1962) *J Res Natl Bur Stand* **A66** 241–248

Donnay J D H & Harker, D (1937) *Am Mineral* **22** 446–447

Elwenspoek M & Boerhof W (1987) *Phys Rev B* **36** 5326–5329

Gilmer G H & Jackson, K A (1977) *Crystal Growth and Materials* edited by E Kaldis & H J Scheel, pp 80–114 Amsterdam North-Holland

Hahn T (1983) *International Tables for Crystallography*, Vol A Dordrecht D Reidel

Hartman P (1987) *Morphology of Crystals* edited by I Sunagawa, pp 269–319 Tokyo Terra Sci

Kern R (1987) *Morphology of Crystals* edited by I Sunagawa, pp 79–206 Tokyo Terra Sci

Liu X Y & Bennema P (1992) *J Chem Phys* **97** 3600–3609

Mnyukh Y V J (1963) *Phys Chem Solids* **24** 631–640

Nyburg S C & Potworowski, J A (1973) *Acta Cryst* **B29**, 347–352

Shearer H M M & Vand V (1956) *Acta Cryst* **9** 379–384

Toda A (1991) *Polymer* **32** 771–780

Toda A Miyaji H Ogawa Y & Takamizawa, K (1991) *J Mater Sci* **26** 2793–2796

Weeks J D & Gilmer G H (1979) *Adv Chem Phys* **40** 157–228

Williams D E (1967) *J Chem Phys* **47** 4680–4684

Chapter 2.3

JOURNAL OF CRYSTAL GROWTH

Morphology of orthorhombic long chain normal alkanes: theory and observations

P. Bennema, Xiang Yang Liu

RIM, Laboratory of Solid State Chemistry, University of Nijmegen, Toernooiveld, 6525 ED Nijmegen, Netherlands

K. Lewtas, R.D. Tack

Paramins Esso Chemical Research Centre, Abingdon Oxfordshire OX13 6BB, UK

J.J.M. Rijpkema

Department of Mathematics and Computer Science P O Box 513 5600 MD Eindhoven, Netherlands

and

K.J. Roberts

Department of Pure and Applied Chemistry, University of Strathclyde, 295 Cathedral Street, Glasgow G1 1XL, UK

Received 12 April 1991, manuscript received in final form 23 March 1992

This paper describes a theoretical and experimental investigation of the growth and especially the morphology of paraffin crystals of the odd n-alkanes (C_nH_{2n+2}, $n \neq 2n$) over a range of chain lengths with $15 \leq n \leq 41$, for growth from solution, under pure conditions and under the influence of additives. Three strong and one weak interactions between the bodies of paraffin molecules in a crystal and four weak interactions between the head and the tails of the paraffin molecules are identified and the crystal graph is derived. The elementary cell of this crystal graph is characterized by a pseudo F cell with first nearest neighbour interactions between the points. From this crystal graph ten connected nets giving rise to eight (or nine) different F faces are identified. Using different quantities like $E^{att}_{(hkl)}$, $E^{slice}_{(hkl)}$, Ising temperatures ($\theta^c_{(hkl)}$), interplanar distance, etc. for the connected nets of paraffin crystals, growth and equilibrium forms are constructed. All crystal forms show large {001}, small thin faces {110} and often smallest faces {010}. It is shown that predicted and observed morphologies, agree quite well. In passing the sometimes dramatic change in the expected habit of crystals, caused by tailor made additives is discussed. The theory of roughening transition is applied to paraffin and it is shown how the roughening temperature depends on n, the length of the paraffin chain. An actual roughening temperature of 10.65 ± 0.50°C is measured for faces of the form {110} of paraffin with 23 C atoms, growing from a slightly supersaturated solution of hexane.

1. Introduction

Following Jackson [1] and Burton, Cabrera and Frank [2], who applied the theory of Onsager [3] concerning an order–disorder phase transition in a two-dimensional Ising model to crystal surfaces, in this paper morphology and growth of paraffin crystals will be studied from the point of view of statistical mechanical surface Ising models. The integrated approach: crystallographic morphological Hartman–Perdok theory and statistical mechanical Ising models, described before [4–7] which was applied to inorganic crystals [4,8–12] and organic crystals [13–17], will now be

applied to orthorhombic paraffin crystals of paraffin molecules with an odd number of C atoms In this paper the concept of roughening transition plays an essential role The reasons to choose paraffin as model compound are (i) only first nearest Van der Waals bonds need to be taken into consideration, (ii) crystals are highly anisotropic, this opens new possibilities to test Ising models, (iii) morphology in dependence of chain length can be studied, (iv) results of this study can be compared with previous paraffin studies [18–24], (v) the practical reason to study the morphology of the orthorhombic paraffin crystals is that many of the products derived from crude petroleum contain *n*-alkane paraffins and these waxes can cause severe problems if they are allowed to crystallize Crude oil, heavy fuel, diesel fuel, heating oil, etc all contain significant proportions of higher *n*-alkanes and during cold conditions, such as operating a diesel vehicle during the winter, they can crystallize as thin, flat plates (orthorhombic in nature) which can gel the fuel and block pipes and filters, which are present in every system

Paramins Esso Research Centre at Abingdon has carried out extensive research to develop additives which change the habit of these crystals and significantly decrease their sizes so that they no longer suffer the drawback mentioned above In the constant search to improve the additives and benefits to the customer, it is necessary to fully understand the role of the additives and their relationships to the morphology of the crystal

In this paper, first the paraffin structure with an odd number of C atoms within paraffin molecules is discussed in section 2 Next overall bonds between molecules are calculated using the best available Buckingham potentials for the C–C, H–H and C–H interactions In section 3, bond energies are treated from a thermodynamic point of view In section 4, the crystal graph is introduced and the connected nets are derived In section 5, all kind of theoretical crystal forms are derived In section 6, predicted and observed morphologies are compared and the theory of roughening transition is compared with observed roughening phenomena

2 Structure of orthorhombic systems of bonds

2 1 Crystal structure and identification of bonds

The *n*-alkanes C_nH_{2n+2} ($n \geq 6$) crystallize in one of the four systems, triclinic (n(even) ≤ 26) [25], monoclinic ($26 \leq n$(even) ≤ 36) or orthorhombic if not quite pure and orthorhombic ($11 \leq n$(odd) ≤ 43) [25] For a prediction of unit cells and atomic coordinates of the *n*-alkanes we refer to Nyburg and Potworowski [26], Mnyukh [27] and Kitaigorodski [28 29]

This paper will be based on the structure analysis of Smith [30] of the odd paraffin $C_{23}H_{48}$ Using the approach of Nyburg et al [26], it will be assumed that all odd paraffins are based on this structure In the setting of Smith, the space group is P_{bcm} (P 21/b 21/c 21/m) (In the following we will use the same choice of axes as Smith)

In table 1 the cell dimensions are given a and b are to a high extent independent of the chain length and c is linearly dependent on the chain length In orthorhombic structures, a subcell, called the H subcell, can be distinguished with $a = 4\,97$ Å, $b = 7\,478$ Å and $c_0 = 2\,546$ Å, the length of a C_2H_4 group measured along the c axis (see also refs [26,28,30])

In table 2, the extinction conditions of the space group are given Using these extinction conditions, the effective thicknesses of slices or connected nets to be presented in section 4 are given in the last column of the table

In fig 1a, the structure of paraffin is presented in a schematic way The molecules are reduced to strips seen end-on, and screw axes and glide planes of the real paraffin structures are indicated according to the international crystallographic tables (see ref [31]) A distinction is made between molecules lying on a high layer

Table 1
Basic vectors a b and c of the elementary cell it is indicated how c depends on the chain length n c_0 and c_0 are constants

$a = 4\,97$ Å
$b = 7\,478$ Å
$c = nc_0 + c_0$, with $c_0 = 2\,546$ Å $c_0 = 3\,75$ Å

(——) and one layer lower (– – –). The high and low molecules can be transformed into each other by the two-fold screw axes seen and one by the *c* glide planes seen end-on and other symmetry elements of the space group P_{bcm}. Molecules within one layer can be transformed into each other among others by the *b* glide plane perpendicular to the *a* axis. In fig. 1b, the high molecules

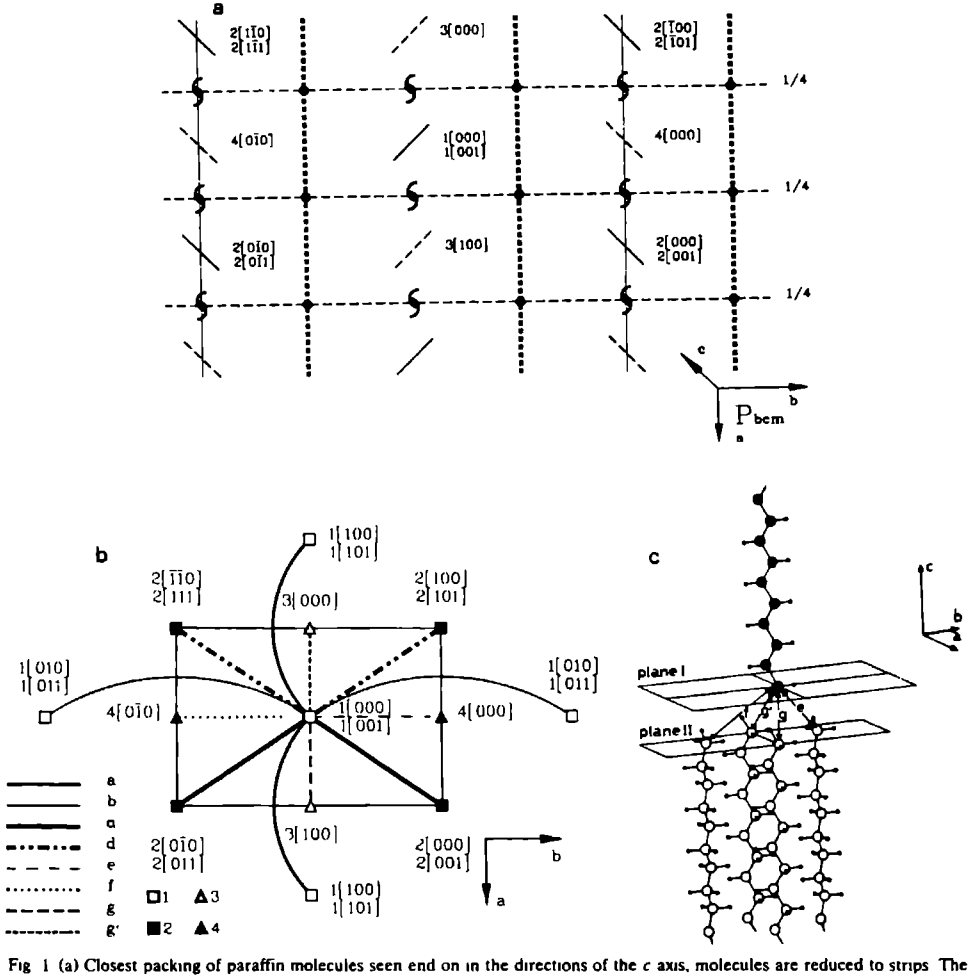

Fig 1 (a) Closest packing of paraffin molecules seen end on in the directions of the *c* axis, molecules are reduced to strips The *c* glide planes are indicated by dashed lines and the two-fold screw axes by the obvious signs, molecules lying one layer higher by solid slashes and those one layer lower as dashed slashes (b) Same as (a), but molecules are reduced to points The horizontal bonds d', d, a, b and the vertical bonds e, f, g, g' are indicated This figure represents the crystal graph of the odd orthorhombic crystal structure, seen in the direction of the *c* axis, *a* and *b* axes are indicated The different four molecules are indicated as 1, 2, 3 and 4 [*uLw*] *a*, *b* and *c* axes are indicated (c) One paraffin molecule in contact with four neighbouring molecules one layer lower The vertical head tail bonds e, f, g and g' are indicated.

Table 2
Extinction conditions of the space group P_{bcm} of the orthorhombic odd paraffin structure and the corrected interplanar distances

Crystal form	Extinction conditions	Thickness of connected net or slice
(hkl)	No conditions	$d_{(111)}$
$(0kl)$	$k = 2n$	$d_{(022)}$
$(h0l)$	$l = 2n$	$d_{(202)}$
$(hk0)$	No conditions	$d_{(110)}$
$(h00)$	No conditions	$d_{(100)}$
$(0k0)$	$k = 2n$	$d_{(020)}$
$(00l)$	$l = 2n$	$d_{(002)}$

are reduced to centres of gravity indicated with x and the lateral bonds between molecules, d, d', a and b are indicated (cf figs 1a and 1b) Next, the low molecules are reduced to centres of gravity indicated with · Now both in fig 1b and in the added special figure (fig 1c), the position of high molecules in reference to four first nearest neigbour low molecules, one layer lower, is presented In fig 1b this is seen in projection from above (as in figs 1a, 1b and 1c)

In fig 1c, part of the real paraffin structure is represented, seen from an oblique angle in perspective Four first nearest neighbour bonds, e, g, g' and f, can be distinguished The crystal graph consisting of points (centres of gravity of molecules) and relations between these points (bonds) of the orthorhombic paraffin structure is represented in fig 4 This corresponds to the projection of this crystal graph seen in the direction of the c axis (fig 1b) Looking at the crystal graph presented in figs 1b, 1c and 3, it can be seen how the bonds are transformed into each other by the symmetry operations of the space group

So we have identified four types of lateral "body–body' bonds, d, d', a and b, between molecules within a layer and four types of "vertical" "head–tail" bonds, e, g, g' and f, of one molecule in a certain layer and four molecules in an adjacent layer As will be shown below in section 2 2, all these bonds are overall bonds between molecules and consist in case of the lateral bonds of numerous atom–atom interaction potentials These overall lateral bond energies are much higher (i e much more negative)

Table 3
Energy parameters A B and C of the Buckingham potentials used in this paper (see eq (1)) in this paper the parameter sets 1b and 2b will be used because they yield enthalpies of evaporation in best agreement with measured data

Number of parameter set	Reference	Type of interaction	A (kcal mol^{-1} Å^6)	B (kcal mol^{-1})	C (Å^{-1})
1a	Williams [32]	CC	535	74460	3 6
		CH	139	9411	3 67
		HH	36	4000	3 74
1b	Williams [33]	CC	568	83630	3 6
		CH	125	8766	3 67
		HH	27 3	2654	3 74
1c	Williams [33]	CC	514	69600	3 6
		CH	141	9421	3 67
		HH	38 8	4000	3 74
2a	Kitaigorodsky [29a], p 170	CC	358	42000	3 58
		CH	154	42000	4 12
		HH	57	42000	4 86
2b	Kitaigorodsky [29b]	CC	421 53	30100	3 42
		CH	136 77	30100	4 13
		HH	43 25	30100	5 0

than the bond energies of the vertical bonds e, g, g' and f which in fact only consist of a few atom–atom interaction potentials. These weakest bonds, however, do play together with the lateral bonds an essential role in the crystal graph of paraffin. They determine the connectedness of the three-dimensional crystal graph and the connected nets.

2.2. Calculation of bond energies

We have calculated the corresponding overall bond energies of the bonds, d, d', b, a, e, g, g' and f, to be denoted as Φ_d, $\Phi_{d'}$, Φ_b, Φ_a, Φ_e, Φ_g, $\Phi_{g'}$ and Φ_f, respectively, for orthorhombic paraffin crystals with molecules with varying chain lengths of 15 to 41 C atoms.

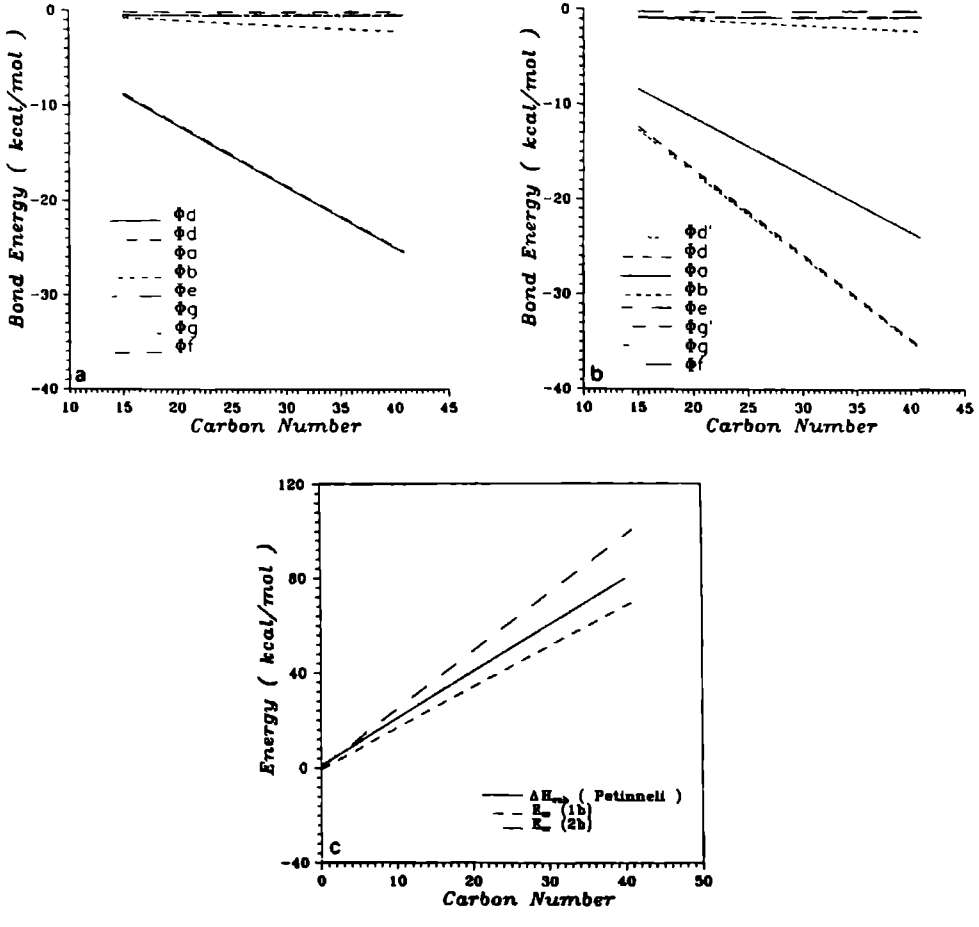

Fig. 2. (a) Bond energies of the bonds d', d, a, b and e, f, g, g' versus n for parameter set 1b. (b) Same as (a) but for parameter set 2b. (c) Upper curve sublimation energy versus n calculated for parameter set 2b. Lower curve is the same but for parameter set 1b. Middle curve is the measured sublimation curve versus n by Petinelli.

We selected for our calculations of bond energies those published interatomic potentials of CC, CH and NH interactions which gave the best agreement with measured enthalpies of sublimation (see below). In table 3, the constants A, B and C playing an essential role in the expression of the Buckingham potential $\Phi(r)$,

$$\Phi(r) = \frac{A}{r^6} + B \exp(-Cr), \tag{1}$$

are demonstrated. Here, r is the distance between two atoms. In this table, five different sets of values of A, B and C, which are used for the calculation of bond energies, together with the references, where these values of A, B and C come from are given (see refs. [29,32–33]). It follows from our calculations that set 1b and set 2b give much better results than other sets. Thereby, in the following, we just stick to those two parameters set (see section 3) Next, the corresponding bond energies have to be calculated using eq. (1). For the calculation of atom–atom bond energies, the crystallographic positions of the atoms must be known with high precision.

It follows from our calculations that for the lateral bond energies:

$$|\Phi_{d'}| \equiv |\Phi_d| > |\Phi_a| \gg |\Phi_b|. \tag{2}$$

For vertical bond energies

$$|\Phi_{g'}| \geq |\Phi_g| \geq |\Phi_e| > |\Phi_f|. \tag{3}$$

Table 4a
Lateral bond energies fulfilling the expression $\Phi_i(n) = \Phi_i^0 n + \Phi_i'$ (eq. (4)), the values of Φ_i^0 and Φ_i' are given for the overall bond energies (in kcal/mol)

Bond label	Parameter set 1b		Parameter set 2b	
	Φ_i^0	Φ_i'	Φ_i^0	Φ_i'
$\Phi_{d'}$	−0.6421	0.7351	−0.8893	0.6623
Φ_d	−0.6434	0.9000	−0.8950	1.0946
Φ_a	−0.3740	0.4718	−0.6021	0.6482
Φ_b	−0.0580	0.1082	−0.0758	0.0696
Φ_e	0	−0.48649	0	−0.78832
Φ_g	0	−0.49716	0	−0.84298
Φ_a	0	−0.56727	0	−0.84074
Φ_f	0	−0.18114	0	−0.21589

Table 4b
Values of ΔH^0 and $\Delta H'$ in the expression $\Delta H^{sub}(n) = \Delta H^0 n + \Delta H'$ for the experimental data of Petinelli [34], the calculated data of parameter sets 1b and 2b and the experimental data of Mnyukh [27]

Origin	ΔH^0	$\Phi H'$
Petinelli (exp)	1.971	0.983
Theoretical set 1b	1.71766	−0.48237
Theoretical set 2b	2.44467	0.17382
Mnyukh (exp)	1.84	1.03

In figs. 2a and 2b, we have plotted the calculated bond energies from Φ_a to Φ_g as a function of the number of C atoms in a paraffin chain n, for the bond energies calculated with the two parameter sets 1b and 2b respectively (table 3). It can be seen that the strong lateral bonds $\Phi_{d'}$, Φ_d, Φ_a and Φ_b depend linearly on n. This is not surprising because the number of CC, CH and HH contacts will increase proportionally with n. The four vertical bonds e to g′ are obviously primarily determined by the first nearest interactions between the end groups CH_3 of molecules, laying in two adjacent layers and these do not depend on the chain length. The overall bond energies can be fitted with the linear expression:

$$\Phi_i(n) = \Phi_i^0 n + \Phi_i', \tag{4}$$

where i stands for bonds a to g′. The vertical bond energies Φ_e to Φ_f do not depend on n. Hence $\Phi_i^0 = 0$.

In table 4a the values of slopes Φ_i^0 and Φ_i' of eq. (4) are presented.

3. Bond energies from a thermodynamic point of view

Looking at the crystal graph figs. 1b and 3, it can be seen that the total energy to remove a paraffin molecule from the bulk of the crystals is obtained by breaking the four lateral and the four vertical bonds. So the sublimation enthalpy ΔH^{sub} for one paraffin molecule is given by:

$$\Delta H^{sub} = \tfrac{1}{2}\Phi_{total} = \sum_{i=a}^{g'} |\Phi_i|. \tag{5}$$

$\frac{1}{2}\Phi_{total}$ can be considered as the energy to remove a paraffin molecule from the kink of a step at the surface of a Kossel-like crystal All energies are referenced to the absolute temperature 0 K.

The calculated values of $\Delta H^{sub}(n)$ are plotted in fig. 2c. The lowest curve corresponds to bond energies calculated with parameter set 1b, the highest curve from parameter set 2b. In fig. 2c also the experimentally determined $\Delta H^{sub}(n)$ curve for odd paraffins in dependence of n, measured by Petinelli (Petinelli thesis [34]), is plotted. It can be seen that the experimental $\Delta H^{sub}(n)$ curve is also linear and is situated in between the two theoretical curves. All $\Delta H^{sub}(n)$ curves can thus be fitted with the linear curve:

$$\Delta H^{sub}(n) = \Delta H^0 n + \Delta H'. \qquad (6)$$

The theoretically calculated values ΔH^0 and $\Delta H'$, obtained from a least squares fit of the theoretical curves and experimental values ΔH^0 and $\Delta H'$, also obtained from a least squares fit of the experimental data, are given in table 4b.

We have also added values of ΔH^0 and $\Delta H'$ determined by Mnyukh using a least squares method from an experimental $\Delta H^{sub}(n)$ curve These curves were calculated from melt enthalpies using a Born–Haber cycle [27]. It can be seen that the values of ΔH^0 and $\Delta H'$ of Petinelli and Mnyukh are very close to each other.

For even paraffin crystals growing from a petroleum ether same expressions were found as eq. (6), but ΔH^0 and ΔH^1 are more than two times lower (see also ref. [35]).

We note that from the point of view of the theory bond energies Φ_i have the shape [4–7]:

$$\Phi_i = \Phi_i^{sf} - \tfrac{1}{2}\left(\Phi_i^{ss} + \Phi_i^{ff}\right). \qquad (7)$$

The bond energies Φ_i^{ss}, Φ_i^{ff} and Φ_i^{sf} are negative numbers and due to the assumed relatively strong negative value of Φ_i^{ss}, Φ_i is always positive [4–12]. Here Φ_i^{ss} is a bond energy referenced to vacuum; this corresponds to the energy of breaking a bond. These are bonds and bond energies we were talking about so far. In eq. (7), Φ_i^{ss} corresponds to the bonds a to g'; Φ_i^{sf} is the energy to break a solid–fluid bond of type i and Φ_i^{ff} that of the corresponding fluid–fluid bond of type i. All bond energies are referenced to vacuum. As usual, if the morphology of crystals growing form the melt or solution is studied, the effective bond energies Φ_i (eq. (7)) of bonds occurring at the surface are not known. Therefore as usual the proportionality condition is introduced which implies:

$$\Phi_i : \Phi_j : \Phi_k : \ldots = |\Phi_i^{ss}| : |\Phi_j^{ss}| : |\Phi_k^{ss}| : \ldots. \qquad (8)$$

Eq. (8) can be justified because the more CC, CH and HH contacts in the solid state between paraffin molecules, the higher (the more negative) the bond energies Φ_i will be. If, in case of two adjacent molecules or cells, one molecule or cell is replaced by a fluid cell, the number of solid fluid CC, CH and HH contacts will be weaker but may be roughly the same. A similar argument holds for the overall interaction between two fluid cells.

4. Crystal graph and connected nets

In order to predict the morphology of paraffin crystals, we have according to theory to partition the crystal graph presented in figs. 1b and 3, in equal parallel connected nets Connected nets must have an overall thickness of the interplanar distance d_{hhkl}, corrected for the extinction con-

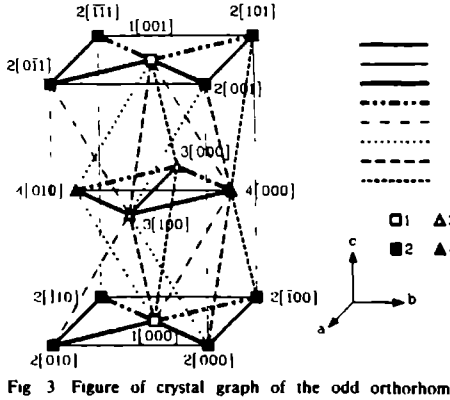

Fig 3 Figure of crystal graph of the odd orthorhombic structure This figure corresponds to fig 1b The four different molecules are again indicated as 1, 2, 3 and 4 [uvw]

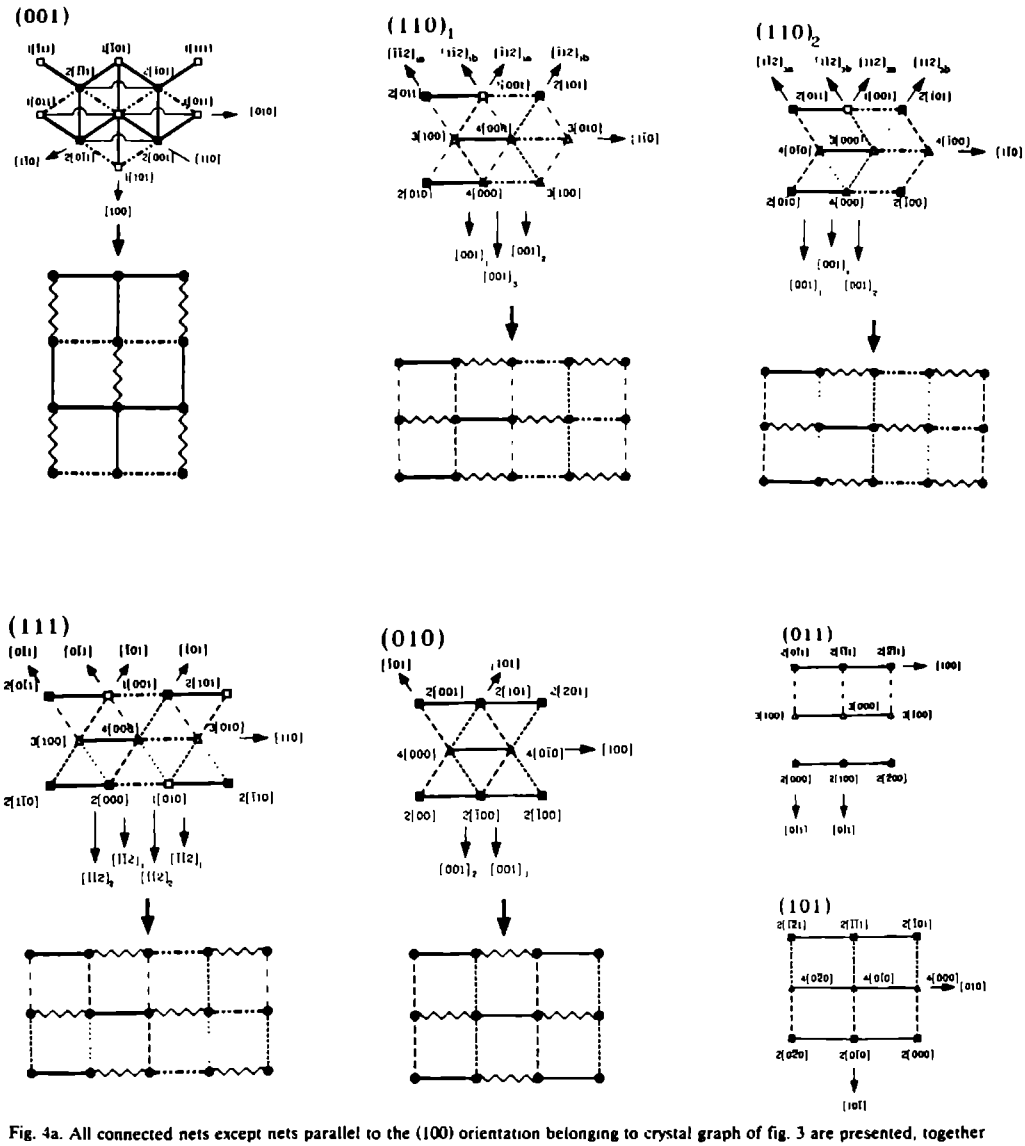

Fig. 4a. All connected nets except nets parallel to the (100) orientation belonging to crystal graph of fig. 3 are presented, together with their rectangularized versions.

ditions of the space group of the crystal graph given in table 2a [5,7 17,36–40]

The crystal graph presented in fig 3 can be considered as a pseudo F cell It is easy to derive all eight (or nine) connected nets from fig 3 as can be seen from figs 4a and 4b

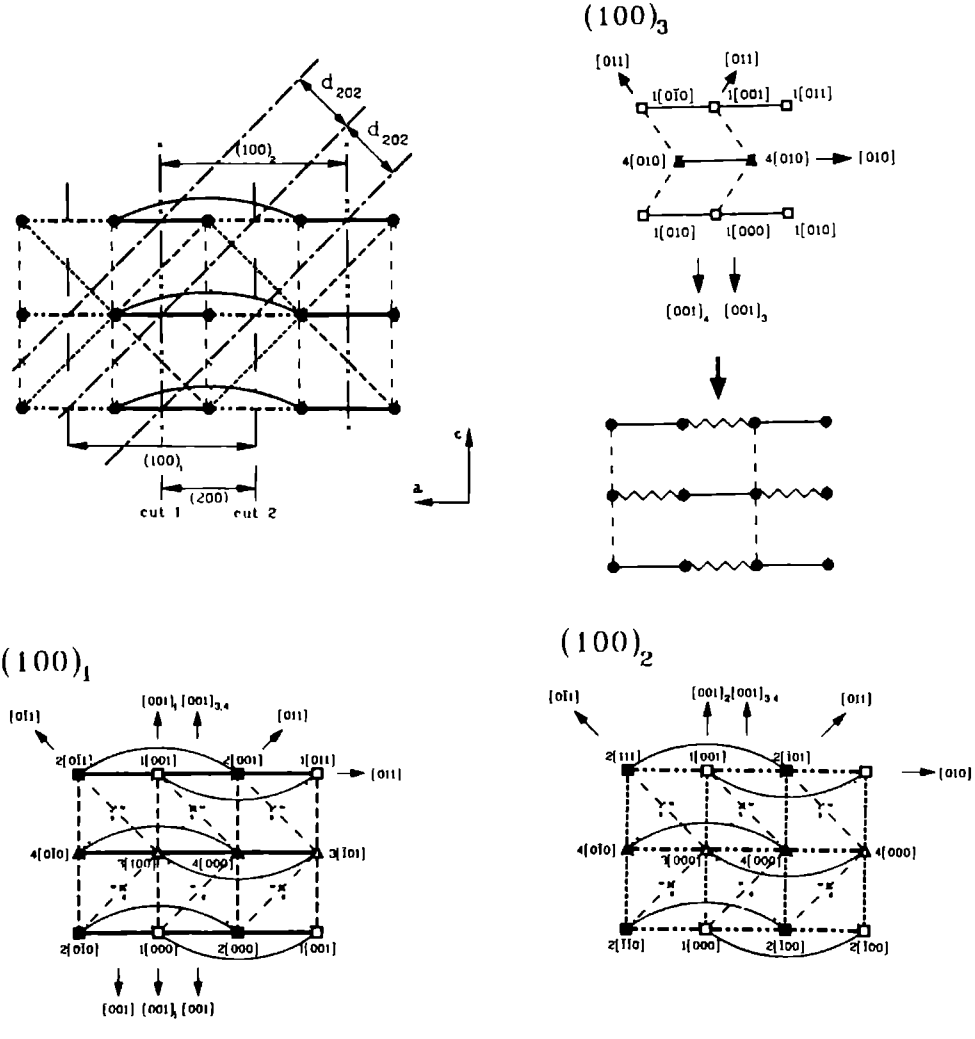

Fig 4b Upper left figure projection in [110] direction single connected net $(100)_3$ and double connected nets $(100)_{1,2}$ consisting of two single nets $(100)_1$ can be seen from aside The nets $(100)_{2,3}$ can be seen from above The rectangularized version of $(100)_1$ is presented

4 1 Determination of connected nets

The special figure of the crystal graph corresponding to figs 1b and 1c is again presented in fig 3 We have now labelled the centres of gravity of the crystal graph following the usual conventions We take four different reference points within the unit cell, which cannot be transformed into each other by translations as reference points These are labelled as 1[000], 2[000], 3[000] and 4[000] respectively All other points of the crystal graph are indicated with 1[uvw], 2[uvw], etc, according to the shifts ua, vb wc in reference to 1(000), etc Using the same labels of points in the graph as in connected nets, these nets can be identified from the crystal graph in fig 3, as shown in figs 4a and 4b In figs 4a and 4b, all the PBCs contained in the connected nets are indicated

In the connected net of (001) bonds b cross bonds a In order to calculate Ising temperatures the weak b bond is omitted and the remaining hexagonal net (i e a net where each centre of gravity is a source of six bonds) is "rectangularized" by splitting nodes into two nodes with a bond of infinite strength (indicated with a wiggled bond) connecting these two nodes As shown before [4–10], in this way a rectangular net is obtained, having the same partition function as the hexagonal net For a given ratio of bond energies, the dimensionless Ising temperature θ^c can then be calculated The neglect of the weak bond is necessary to obtain an unambiguous value of θ^c This neglect will only give a slight lowering of the real θ^c, which cannot be calculated exactly anyhow

There are two alternative connected nets, having the thickness $d_{(110)}$, which are parallel to the face $(110)_1$ Looking at fig 3, the net $(110)_1$ is zigzagging from 1[001] to 3[100] and 4[000] and back to 1[000] The alternative connected net $(110)_2$, is zigzagging from again 1[001], but then backwards to 4[0$\bar{1}$0] and 3[000], and forwards back to 1[000] (see fig 4a) In fig 4a the nets $(110)_1$ and $(110)_2$ are rectangularized In the same way other connected nets can be derived and rectangularized (see figs 3 and 4a)

We note that contrary to all connected nets corresponding to crystallographic directions (hkl), determined so far, some complication occurs for connected nets of the (100) orientations

In fig 4b a projection is made of the crystal graph of fig 3 seen in the [010] direction It can be seen that within the thickness $d_{(100)} = a$, given by table 2, two alternative slices of connected nets $(100)_1$ and $(100)_2$ can be made (see the slices $(100)_1$ and $(100)_2$ seen from the side in fig 4b) These slices $(100)_1$ and $(100)_2$ are projected in the [100] direction In slice $(100)_1$ g bonds are crossing b bonds and in slice $(100)_2$ f bonds cross b bonds respectively It follows from fig 4b that two types of cuts occur namely cut 1 and cut 2 For cut 1, d bonds and g bonds are cut for d' and g' bonds of cut 2 Using the bond energies of tables 4a and 4b, it can be concluded that the difference between Φ_d and Φ_g is just a few percent So, in practice, these two cuts will have almost the same surface energies We will assume in the following that both cuts have the same surface energies Then the whole crystal graph can be partitioned in equal connected nets $(100)_3$ Thus a halving of the thickness of (100) occurs (see also ref [41])

The nine (or eight or in total 10) connected nets presented in figs 4a and 4b are the only genuine connected nets occurring in the crystal graph of fig 3

4 2 Identification of PBCs connected nets and F faces (periodic bond chains)

It will be shown that an explicit use of PBCs [36–40] gives a powerful tool to check whether all possible connected nets are identified We recall that according to the Hartman–Perdok theory, PBCs (periodic bond chains) are uninterrupted chains of bonds having a periodicity [uvw] of the lattice (crystal graph) So in table 5 all different PBCs (indicated as [uvw]) are given The bonds occurring in each type of PBC are also given in this table It can be seen that in one direction more PBCs, containing different bonds, may occur

In table 6, connected nets containing certain PBCs are given At the same time the slice thickness of the nets, taking the extinction conditions

Table 5
List of all identified PBCs labelled as $[uvw]_x$, where $x = 1, 2, 3, 4$ (this indicates alternative PBCs), and of the bonds within the corresponding PBCs

PBC	Bonds
⟨110⟩	d, d′
[100]	a
$[010]_1$	b
$[010]_2$	d
$[010]_3$	d′
$[001]_1$	g
$[001]_2$	g′
$[001]_3$	e
$[001]_4$	f
⟨101⟩	g, g′
⟨011⟩	e, f
$\langle\bar{1}12\rangle_1$	e, g, e g′
$\langle\bar{1}12\rangle_2$	g, f, g′ f

of table 2, is given in table 6. In fig. 5, seven types of PBCs corresponding to the third column of table 6 are plotted in a schematic way as large circles in a stereogram. Where circles corresponding to PBC directions cut each other, potential F faces occur.

It can be seen that the potential F faces {311}, {131}, {201} and {021} show up It can be shown that these potential faces are no real F faces, because they are not parallel to connected nets All other faces are real F faces, parallel to one of the eight connected nets.

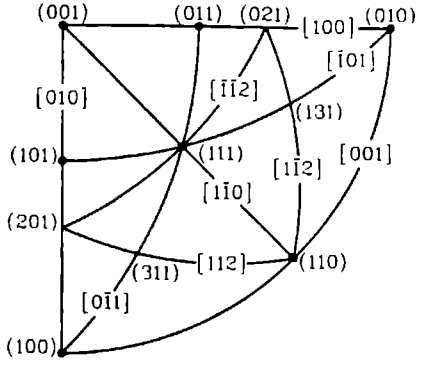

Fig 5 Stereogram where PBCs $[uvw]$, represented as large circles perpendicular to PBCs cut each other real connected nets (hkl) occur These are indicated as dots corresponding to normals to (hkl) Potential forms {021}, {201}, {311} and {131} do not correspond to F faces

5. Prediction of crystal growth forms and equilibrium forms

5.1 Alternative recipes to construct crystal forms

Contrary to equilibrium forms (see Kern [42]), there are no unambiguous logical recipes to construct crystal growth forms, each crystal has a unique form Average idealized crystal forms,

Table 6
List of connected nets (hkl), (if more connected nets parallel to the face (hkl) occur, $y = 1, 2, 3$), slice thicknesses (corrected for extinction conditions, see table 2), PBCs which can be identified in the connected nets of first column, and bonds occurring in the connected nets of first column

Connected net	Slice thickness	PBCs				Bonds
(001)	$d_{(002)} = \frac{1}{2}c$	⟨110⟩	[100]	$[0\bar{1}0]_{1\,4\,3}$		d, d′, a, b
$(110)_1$	$d_{(110)}$	$[11\bar{0}]$	$[001]_{1\,2\,3}$	$[\bar{1}12]_1$	$[1\bar{1}2]_1$	d, d′, g, g′, e
$(110)_2$	$d_{(110)}$	$[1\bar{1}0]$	$[001]_{1\,2\,3}$	$[\bar{1}12]$	$[1\bar{1}2]_2$	d, d′, g, g′, f
$(100)_1$	$d_{(100)} = a$	$[010]_1$	[011]	$[0\bar{1}1]$		d, b, g, e, f
$(100)_2$	$d_{(100)} = a$	$[010]_2$	[011]	$[0\bar{1}1]$		d, b, g′, e, f
$(100)_3$	$d_{(200)} = \frac{1}{2}a$	$[010]_3$	[011]	$[0\bar{1}1]$	$[001]_{3\,4}$	b, e, f
(101)	$d_{(202)}$	[010]	$[10\bar{1}]$			g, g′
(111)	$d_{(111)}$	$[1\bar{1}0]$	$[\bar{1}01]$	$[0\bar{1}1]$	$[\bar{1}\bar{1}2]_{1,2}$	d, d′, g, g′, e, f
(010)	$d_{(020)} = \frac{1}{2}b$	[100]	[101]	$[\bar{1}01]$	$[001]_{1\,2}$	a, g, g′
(011)	$d_{(022)}$	[100]	$[0\bar{1}1]$	$[\bar{1}01]$		a, e, f

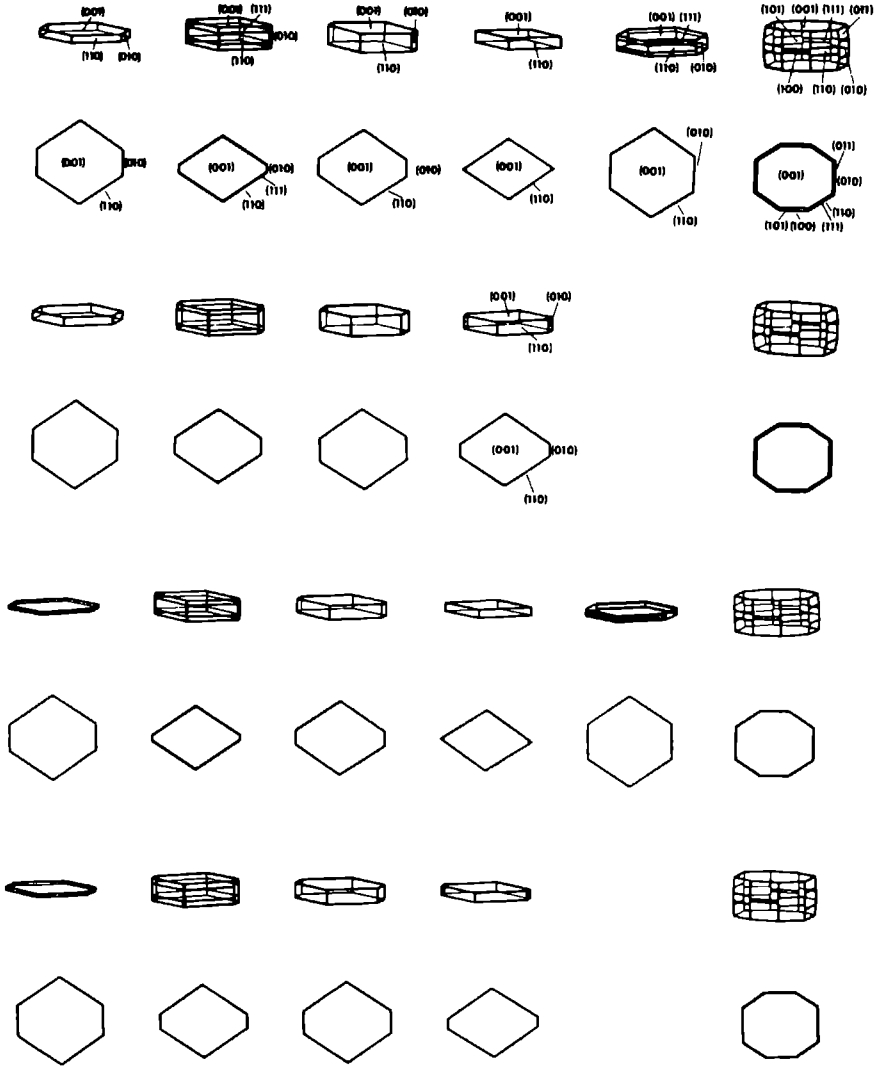

Fig 6 Lower half crystal forms of the odd paraffin structure for $n = 39$ Upper half, same crystal forms but for $n = 15$ The first two rows of upper and lower halves refer to calculations based on parameter set 1b and the next two rows below these to calculations with parameter set 2b (see table 3 and refs [29b 33]) The first, third, fifth and seventh rows correspond to crystals seen from a oblique angle the other rows to crystals seen in the direction of the c axis The crystal (growth) forms of column 1 correspond to eq (9), of column 2 to eq (10) of column 3 to eq 11), of column 4 to eq (12) of column 5 to eq (13) and of column 6 to eq (14) of section 2 1, respectively The Miller indices of the surviving faces are indicated in the two upper rows and also in one case in the two lower rows The Miller indices of the lower half are not indicated, but are the same

however, can be defined In the following we will try the logical recipes (i)–(vi), which will be used to construct idealized crystal growth forms

(i) the rate of growth of a face $R_{(hkl)}$ is taken to be proportional to $E^{att}_{(hkl)}$ [36–40]

$$R_{(hkl)} \sim E^{att}_{(hkl)} \tag{9}$$

(ii) In the same way $R_{(hkl)}$ is inversely proportional to $(E^{slice}_{(hkl)})$ [5,7,40]

$$R_{(hkl)} \sim \left(E^{slice}_{(hkl)}\right)^{-1} \tag{10}$$

(iii) $R_{(hkl)}$ is inversely proportional to the Ising temperature θ^c [5,7]

$$R_{(hkl)} \sim \left(\theta^c_{(hkl)}\right)^{-1} \tag{11}$$

(iv) An alternative for (iii) is to make an estimation of the actual dimensionless temperature θ and take

$$R_{(hkl)} \sim (\theta^c - \theta)^{-1} \tag{12}$$

If $\theta \geq \theta^c$ and $R_{(hkl)} \to \infty$, $R_{(hkl)}$ will be negative and we will assume that it will not occur on the growth form

(v) $R_{(hkl)}$ is inversely proportional to $d_{(hkl)}$, the interplanar distance [41]

$$R_{(hkl)} \sim \left(d_{(hkl)}\right)^{-1} \tag{13}$$

(vi) Construct equilibrium forms taking the distance of a face (hkl) to the origin $D_{(hkl)}$ proportional to the surface energy [42]

$$D_{(hkl)} \sim d_{(hkl)} E^{att}_{(hkl)} \tag{14}$$

Recipe (i) (eq (13)) is the traditional way to construct growth forms [36–40,43,44] For a justification of the other recipes we refer to a more extensive publication [45]

5 2 Derivation of crystal growth forms from set en connected nets

For the construction of growth forms according to recipe (ii) we need $E^{slice}_{(hkl)}$ The slice energy $E^{slice}_{(hkl)}$ (i e the energy per growth unit within a connected net) can immediately be calculated from the connected nets presented in figs 4a and 4b The expressions for $E^{slice}_{(hkl)}$ are summarized in table 7 In case two alternative nets occur (like $(110)_{1,2}$), the strongest net is chosen

Table 7
Expressions for $E^{slice}_{(hkl)}$ for 10 connected nets expressed in bond energies Φ_d to Φ_g

$E^{slice}_{(hkl)}$	Bond energies
$E^{slice}_{(100)}$	$\Phi_j + \Phi_d + \Phi_a + \Phi_h$
$E^{slice}_{(110)_1}$	$\frac{1}{2}(\Phi_j + \Phi_d) + \Phi_c + \frac{1}{2}(\Phi_g + \Phi_g)$
$E^{slice}_{(110)_2}$	$\frac{1}{2}(\Phi_d + \Phi_d) + \Phi_j + \frac{1}{2}(\Phi_g + \Phi_g)$
$E^{slice}_{(111)}$	$\frac{1}{2}(\Phi_d + \Phi_d + \Phi_c + \Phi_g + \Phi_g + \Phi_f)$
$E^{slice}_{(100)_1}$	$\Phi_d + \Phi_g + \Phi_h + \Phi_c + \Phi_f$
$E^{slice}_{(100)_2}$	$\Phi_d + \Phi_g + \Phi_h + \Phi_c + \Phi_j$
$E^{slice}_{(100)}$	$\Phi_h + \Phi_c + \Phi_f$
$E^{slice}_{(101)}$	$\Phi_h + \frac{1}{2}(\Phi_g + \Phi_g)$
$E^{slice}_{(010)}$	$\Phi_a + \Phi_g + \Phi_g$
$E^{slice}_{(011)}$	$\Phi_a + \frac{1}{2}(\Phi_c + \Phi_f)$

In fig 6, all kinds of constructed growth and equilibrium forms resulting from recipes (i) to (vi) of section 5 1 are presented We have chosen as two extremes of the paraffins $n = 15$ and $n = 39$ respectively The corresponding crystal forms for $n = 15$ and $n = 39$ are presented in the upper half and in the lower half of fig 6, respectively

The crystal forms of the first and the second rows correspond to forms calculated from parameter set 1b and the third and the fourth rows to parameter set 2b, respectively This holds for both the upper and the lower half of fig 6

The first column of fig 6 results from recipe (i), the second from recipe (ii), the third from recipe (iii), the fourth from recipe (iv) the fifth from recipe (v) and the sixth from recipe (vi), respectively In each pair of columns, the upper figure represents the crystal form seen from the same arbitrary angle and the lower represents a crystal form seen in the direction of the c axis These latter figures refer to crystals laying on the bottom of a crystallization vessel It can be seen that due to the higher anisotropy, paraffin crystals with a longer chain have a thinner habit The figures speak for themselves The "distance" be-

tween (001) and the side faces is better described by $(\theta^c)^{-1}$ than with $(E^{slice})^{-1}$ (figs. 9a and 9b) and even better with $(\theta^c - \theta)^{-1}$. This gives thinner crystals (fig. 6). For a further interpretation of fig. 6, we refer to ref. [45].

6. Comparison with experimental growth forms

6.1. Paraffin crystals crystallizing from diesel fuel

Paraffin crystals were obtained by cooling a sample of diesel fuel, which contains paraffins in the range from $n = 10$ to $n = 30$ with a cooling rate of 1°C/h. The crystals formed constitute approximately 2–4 wt% of the fuel. This fraction consists of the longest paraffin molecules. The crystals were filtered through silver filter paper, washed with kerosine and methyl ethyl ketone, at the same temperature and kept in a desiccator. The prepared sample together with the special holder is transferred to the liquid nitrogen cooled cold stage of the scanning electron microscope, after being coated with gold. In figs. 7a and 7b, two electron microscopic observations are presented. Notwithstanding the not well-defined growth conditions, it can be noted that the typical crystal forms agree with the predicted ones. It can be seen that crystals of higher paraffins are limited by large {001}, {110} faces and sometimes {010} faces in agreement with fig. 6. These crystals must be crystals with the odd orthorhombic structure, because it is well known that in mixtures, of even and odd paraffins, paraffin crystals, crystallize in this structure.

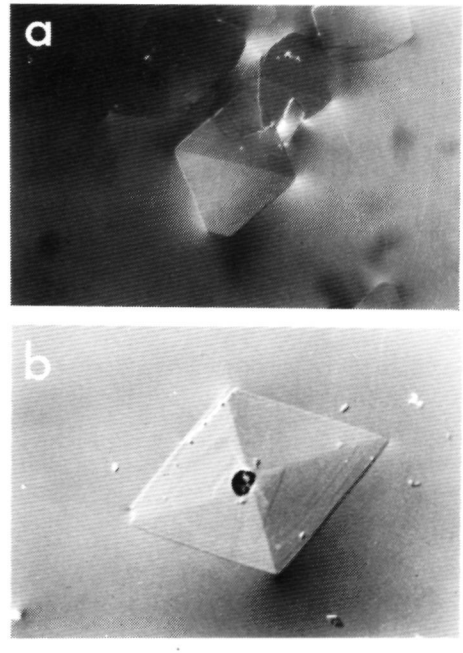

Fig. 7. (a) Electron-microscopic picture of paraffin crystals. Enlargement about 100 times. (b) Same as (a).

6.2. Influence of tailor made additives

In passing we just want to mention the influence of man-made tailor-made additives on the morphology. Searching for proper additives is very important for all companies producing fuels and has already been going on for quite some time [46,47]. Only for the last ten years have tailor-made additives showing a very specific interaction with particular side faces as faces of the forms {110} or {010} been developed. To apply specific tailor-made additives, a network analysis as presented above is necessary (see also refs. [48–51]).

Fig. 8a shows the effect of the addition of a small amount (10^{-3} wt%) of an additive type A. This additive is an ethylene–vinylacetate copolymer of 2×10^3 Mn and approximate 35% by weight vinylacetate. Now the crystal growth in the *ab* plane is inhibited and it can be seen from fig. 8a that the crystals are much thicker now. The {110} faces are roughened due to local blocking. The dramatic influence on the habit of an effective amount of additive of 5×10^{-3} wt% can be seen in fig. 8b. Instead of platy crystals now needle-like crystals limited by one half of the eight faces similar to the form {111} truncated by two small faces of the form {001} seem to develop. These crystals are smaller than the normally occurring platy crystals and no longer gel the fuel and block filters of pipes. Only one half

Fig. 8. (a) Same as fig. 7, but with tailor-made additive in a concentration of 10^{-5}%. (b) Same as (a), but with tailor-made additive concentration of 10^{-4}%.

of the faces which roughly correspond to four faces of the eight faces of the form {111} occur. We have no explanation for this observation.

6.3. Roughening side faces, from a theoretical point of view

In fig. 9a, θ^c is plotted as a function of n, the number of C atoms per chain. This results from computer calculations. It can be seen from fig. 9a that θ^c increases almost linearly with n for all connected nets. We have drawn an horizontal dimensionless equi-n line in fig. 9a. Now fig. 9a represents a kind of phase diagram. Looking at the $\theta^c_{(hkl)}(n)$ lines of the connected nets (hkl), it can be noted that if $\theta^c_{(hkl)}(n) - \theta > 0$, the connected nets grow at sufficiently low supersaturations as flat faces. But if $\theta^c_{(hkl)}(n) - \theta < 0$, they grow as rough faces.

We have to face the problem that we have no absolute scale, so that we cannot define the absolute position of an equi-n line, corresponding to growth from a certain solvent, in reference to the dimensionless $\theta^c_{(hkl)}(n)$ lines.

6.4. Observations of roughening temperature of {110} faces to paraffin crystals growing from an hexane solution

In fig. 10, a paraffin crystal for $n = 23$ is shown. This crystal results from growth of a supersaturated solution of hexane of less than 0.2% at a temperature of 6.14°C in a closed cell with a fixed compositon of paraffin and hexane. The supersaturation is very low and corresponds to $\Delta T = T_s - T(\text{actual}) = 0.01$°C. Since, as can be seen from the crystal, faces of the form {110} are straight, we may assume that the crystal grows below the roughening temperature of the $\{110\}_1$ connected net.

In fig. 10b, a paraffin crystal with $n = 23$ is shown which did grow under similar conditions as the crystal presented in fig. 10a. The growth temperature was about 19.36°C. Since the faces {110} (and {100}) are rounded off, even the supersaturation of $\Delta T = 0.01$°C corresponding to a few tenths of a percent, we may conclude that contrary to the crystal of fig. 10a, this crystal is growing above the roughening temperature of the connected net $\{110\}_1$. We have carried out precise experiments to determine the roughening temperature T^R, which gives

$$T^R \cong 10.65 \pm 0.50\text{°C}. \qquad (15)$$

The narrow margin of eq. (15) is obtained from observations under which temperatures {110} faces are just straight or just rounded (see ref. [51]). Taking this value $T^R_{(110)1}$, we can now draw a horizontal line in fig. 9a so that the horizontal line cuts the $\theta^c_{(110)1}(n)$ line at $n = 23$. Where the horizontal line cuts the vertical $\theta^c(n)$ axis, an

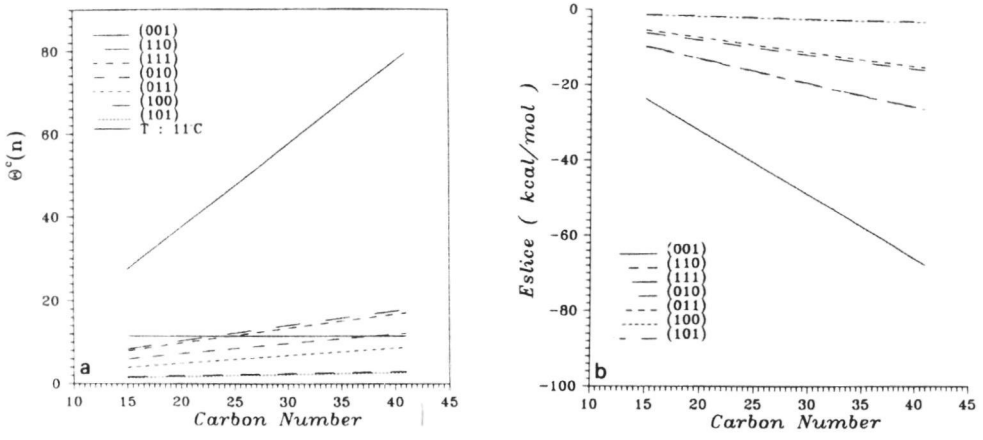

Fig. 9. (a) Dimensionless temperature $\theta^{c}_{(hkl)}(n)$ for the eight connected nets in dependence of n for parameter set 1b. Horizontal line is equi-n temperature line. (b) $E^{\text{slice}}_{(hkl)}$ in dependence of n for the eight connected nets for parameter set 1b.

absolute temperature of 284 K must occur. We limit ourselves to the values of parameter set 1b here and in the following.

Now all kinds of equi-n lines for all kinds of real temperatures can be drawn, and it can be predicted from the phase diagram fig. 9a whether a face (hkl) will be rough or flat for a given temperature. This holds for odd paraffin crystals growing from a hexane solution. Very recently, a similar phenomenon was found for faces on the

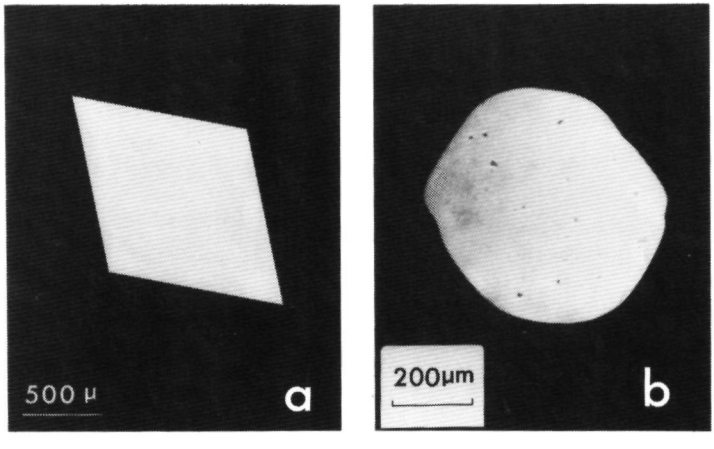

Fig. 10. (a) Paraffin crystal grown from an hexane solution below the roughening temperature of about 11°C at 6.14°C in a closed vessel at a supersaturation corresponding to 0.01°C. The faces {110} are straight. (b) Same as (a), but grown above the roughening temperature at a temperature of 19.36°C at a supersaturation of $\Delta T = 0.01$°C. Now the faces {110} are rounded off.

even triclinic paraffin structure [52] and the even monoclinic structure [53] Recently a special kind of kinetic roughening, namely a rough–flat–rough transition, was found [54] The theory presented above is also applied to fat crystals [55] It will be shown that the low roughening temperature (eq (15)) is due to an extra strong interaction between fluid molecules and solid molecules of hexane at the surface (work in progress) The reason is a good packing of fluid molecules on the solid surface This makes sf bonds strong and Φ energies low (eq (9))

6 5 *Summary and conclusions*

After an analysis of the orthorhombic paraffin structure for paraffin with an odd number of C atoms four lateral and four horizontal bonds were determined and calculated The crystal graph was defined and eight or nine connected nets derived

Crystal growth forms are constructed using six different recipes Predicted crystal growth forms are compared with observed growth forms of crystals crystallizing from diesel fuel In passing, the dramatic change in habit due to tailor-made additives is demonstrated In the last section the phenomenon of roughening is analysed and observed in reality It is shown that a phase diagram showing the flatness or roughness of faces in dependence on temperature and number of C atoms in the paraffin chain can be obtained

Acknowledgements

Two of us P Bennema and Xiang Yang Liu, want to thank Shell Netherlands B V for providing a donation which made it possible for Xiang Yang Liu to carry out a research program concerning growth and morphology of paraffin We also want to thank Dr B Vos and Drs M Reynhout of Shell for stimulating discussions and Mr J W M van Kessel for making the drawings

References

[1] K A Jackson in Liquid Metals and Solidification (Am Soc for Metals Metals Park OH 1958)
[2] W K Burton N Cabrera and F C Frank Phil Trans Roy Soc London A 243 (1951) 299
[3] L Onsager Phys Rev 65 (1944) 117
[4] J J M Rijpkema N J F Knops P Bennema and J P van der Eerden J Crystal Growth 61 (1983) 295
[5] P Bennema and J P van der Eerden in Morphology of Crystals Part A Ed I Sunagawa (Terra Tokyo and Reidel Dordrecht 1987) pp 1 75
[6] R Docherty G Clydesdale K J Roberts and P Bennema J Phys D 24 (1991) 89
[7] P Bennema in Morphology and Growth Units of Crystals Ed I Sunagawa (Terra Tokyo 1989) pp 219–245
[8] P Bennema E A Giess and J E Weidenborner J Crystal Growth 62 (1983) 41
[9] R A Terpstra J J M Rijpkema and P Bennema J Crystal Growth 76 (1986) 494
[10] F M Smet P Bennema J P van der Eerden and W J P van Enckevort J Crystal Growth 97 (1989) 430
[11] T A Cherepanova G T Didrihsons P Bennema and K Tsukamoto in Morphology and Growth Unit of Crystals Ed I Sunagawa (Terra Tokyo 1989) pp 163–199
[12] T A Cherepanova P Bennema Yu A Yanson and K Tsukamoto J Crystal Growth 121 (1992) 1
[13] H J Human J P van der Eerden L A M J Jetten and J G M Odekerken J Crystal Growth 51 (1981) 589
[14] L A M J Jetten H J Human P Bennema and J P van der Eerden J Crystal Growth 66 (1984) 503
[15] M Elwenspoek and J P van der Eerden J Phys A (Mathematics) 20 (1987) 669
[16] M Elwenspoek P Bennema and J P van der Eerden J Crystal Growth 83 (1987) 297
[17] R Docherty K J Roberts L A M J Jetten and P Bennema to be published
[18] B Simon A Grassi and R Boistelle J Crystal Growth 26 (1974) 77
[19] B Simon A Grassi and R Boistelle J Crystal Growth 26 (1974) 90
[20] R Boistelle and A Doussoulin J Crystal Growth 33 (1976) 335
[21] R Boistelle and H E Lundager Madsen J Crystal Growth 43 (1978) 141
[22] H E Lundager Madsen and R Boistelle J Crystal Growth 46 (1979) 681
[23] R Boistelle B Simon and G Pepe Acta Cryst B 32 (1976) 1240
[24] B Simon and R Boistelle J Crystal Growth 52 (1981) 779
[25] M G Broadhurst J Res Natl Bur Std (US) 66A (1962) 241
[26] S C Nyburg and J A Potworowski Acta Cryst Brag 347 (1973) 271
[27] Y V Mnyukh J Phys Chem Solids 24 (1963) 631
[28] A I Kitaigorodski in Molekul Kristalle (Akademie Verlag Berlin 1979)
[29] (a) A I Kitaigorodski Molecular Crystals and Molecules Engl Transl (Academic Press New York 1973) (cf German Transl ref [28])

(b) A I Kitaigorodski, Kristallografiya 9 (1964) 174 (set 2b)
[30] A E Smith, J Chem Phys 21 (1953) 2229
[31] International Tables for X Ray Crystallography, Vol I, Eds N F M Henry and K Londsdale (published for Intern Union of Crystallography by Kynoch Birmingham, 1969)
[32] D E Williams, J chem Phys 45 (1966) 3770 (set 1a)
[33] D E Williams, J Chem Phys 47 (1967) 3680 (sets 1b and 1c)
[34] J F C Petinelli, Thesis, Faculty of Science, University Aix-Marseille III (1977)
[35] I M Belny and J W Mullins, J Chem Ing Data 32 (1987)
[36] P Hartman and W G Perdok, Acta Cryst 8 (1955) 49
[37] P Hartman and W G Perdok, Acta Cryst 8 (1955) 521
[38] P Hartman and W G Perdok, Acta Cryst 8 (1955) 525
[39] P Hartman, in Crystal Growth An Introduction, Ed P Hartman (North-Holland, Amsterdam, 1973) pp 367–403
[40] P Hartman, in Modern PBC Theory in Morphology of Crystals, Part A, Ed I Sunagawa (Terra, Tokyo, and Reidel, Dordrecht, 1987) p 272
[41] J D H Donnay and G Donnay, Compt Rend (Paris) 252 (1961) 908
[42] R Kern, in Morphology of Crystals, Ed I Sunagawa (Terra, Tokyo and Reidel, Dordrecht, 1987) pp 79–206
[43] I Weissbuch, L Addadi Z Berkovitch-Yellin, E Gati, S Weinstein, M Lahav and L Leiserowitz, J Am. Chem Soc 105 (1983) 6615
[44] Z Berkovitch-Yellin, I Weissbuch and L Leiserowitz, in Morphology and Growth Units of Crystals, Ed I Sunagawa (Terra, Tokyo and Reidel, Dordrecht 1989) pp 247–278
[45] P Bennema, in Handbook on Crystal Growth, Ed D T J Hurle (North-Holland, Amsterdam, in press)
[46] G A Holder, J Macromol Sci Chem A4 (1970) 1049
[47] G A Holder and J Winkler, J Inst Petroleum 51 (1965) 499 228
[48] Z Berkovitch-Yellin J Am Chem Soc 107 (1985) 8239
[49] R A Visser and P Bennema, Neth Milk Dairy J 37 (1983) 109
[50] G M van Rosmalen and P Bennema, J Crystal Growth 99 (1990) 1053
[51] Xiang Yang Liu and P Bennema, to be published
[52] X Y Liu and P Bennema, J Crystal Growth to be published
[53] X Y Liu and P Bennema, to be published
[54] X Y Liu P Bennema and J P van der Eerden Nature 356 (1992) 778.
[55] P Bennema I J P Vogels and J de Jong, J Crystal Growth, in press

Chapter 3

ROUPHENING TRANSITION AND KINETIC ROUGHENING

Rough–flat–rough transition of crystal surfaces

Xiang-Yang Liu, P. Bennema & J. P. van der Eerden

RIM, Laboratory of Solid State Chemistry, Faculty of Science, University of Nijmegen, Toernooiveld, 6525 ED Nijmegen, The Netherlands

ABOVE a characteristic temperature, the free energy required to form a step on the surface of a growing crystal may fall to zero; the surface then undergoes a transition from smooth (faceted) to irregular (rough) growth. Here we describe studies of the growth of n-$C_{21}H_{44}$ crystals from n-hexane solutions close to the roughening transition. Beginning with equilibrium crystal growth at a temperature slightly above the roughening transition, we introduce progressively greater supersaturations by lowering the temperature. Observations of the growth morphology reveal a transition from rough to smooth growth, followed at greater supersaturations by a transition back to rough growth. To our knowledge, such a sequence of rough–smooth–rough crystal growth has not been reported before. Our measurements of the step free energy of the {110} faces indicate that it vanishes discontinuously at the equilibrium roughening transition temperature, in contrast to the continuous (critical) behaviour predicted by theoretical models[1–11].

Since Burton, Cabrera and Frank[1,2] first applied the results of the theory[3] of order-disorder phase transition in a two-dimensional Ising lattice to crystal surfaces, the roughening phase transition and kinetic roughening have been studied in great detail[4–28]. Monte Carlo simulations[12–16] led theoreticians to characterize the roughening transition as continuous transition of infinite order ('Kosterlitz-Thouless' roughening[8–11]). Roughening phenomena have also been observed experimentally on crystal faces[17–25]. According to the solid-on-solid (or SOS) lattice model[4,5] if the temperature approaches the roughening temperature T_r from below, the order parameter (the edge free energy per structural unit, γkT, where k is the Boltzmann constant and T the temperature) vanishes continuously as

$$\gamma \sim \exp\left[-\alpha(T_r - T)^{-1/2}\right], \qquad T \leq T_r \tag{1}$$

(α is a coefficient depending on the system). The implication of equation (1) is that at $T_s < T_r$ (T_s denotes equilibrium temperature) a two-dimensional nucleation barrier exists because $\gamma > 0$. Then we have a flat surface at equilibrium or at a small supersaturation σ ($\sigma = \Delta\mu / RT$, where $\Delta\mu$ is the chemical potential difference between the solid and the liquid phase and R the gas constant). In this case only two-dimensional nucleation or spiral growth is possible, and the growth rate R_g is a nonlinear function of σ for $\sigma < \sigma^c$ (σ^c is a critical supersaturation)[26,27]. When $\sigma \geq \sigma^c$, the nucleation barrier vanishes in the supersaturation enviornment, and 'kinetic roughening' occurs. The originally flat faces roughen kinetically, and the relation between R_g and σ becomes linear[27,28]. A relation between edge free energy and critical supersaturation for circular nuclei[28] can be expressed as

$$\sigma^c = \pi\gamma^2 \tag{2}$$

At $T_s \geq T_r$, $\gamma = 0$, and the interface therefore becomes rough on the molecular scale and macroscopically rounded; hence, the crystallographic orientation of the surface is lost. This corresponds to the (thermal) roughening transition. It follows that R_g is linearly dependent on the supersaturation σ.

Here we describe novel roughening phenomena occurring at the {110} surfaces of n-paraffin crystals in n-hexane solutions, from which we derive the behaviour of the order parameter γ of this system close to T_r. The n-paraffins used in our experiments are from analytically pure chemicals (Alfa, >99.0%) and

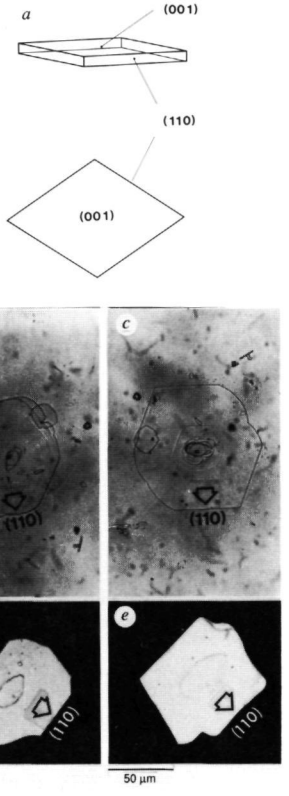

FIG. 1 *a*, Theoretical morphology of odd-numbered paraffins. *b–e*, Morphological transitions of a crystal of n-$C_{21}H_{44}$ growing from n-hexane solution ($X = 2.93 \times 10^{-2}$, where X is mole fraction of solute, $T_s \approx 0.14$ °C ($T_s \geq T^r_{\{110\}}$)). *b*, Rounded {110} faces at low supersaturation; $\sigma = 0.326$ %, $\sigma < \sigma^c_1$. *c*, *d*, Kinetic faceting of {110} faces; $\sigma = 0.761$ and 1.30 % respectively $\sigma^c_2 > \sigma > \sigma^c_1$. *e*, Kinetic roughening of {110} faces; $\sigma = 2.28$ %, $\sigma > \sigma^c_1 \approx 0.435$%, $\sigma^c_2 \approx 1.52$ %. *b*, *c*, Bright-field microscopy; *d*, *e*, cross-polarizing microscopy.

the n-hexane is spectroscopically pure (March, >98.0%). To obtain a well defined supersaturation in solutions of fixed composition, as usual we cool the solution from T_s to a certain value. From the definition of supersaturation, it follows that for a regular solution the supersaturation is linearly proportional to the supercooling ΔT

$$\sigma \approx \frac{\Delta h^{\text{diss}}}{RT_s^2}\Delta T \tag{3}$$

(Here Δh^{diss} is the molar dissolution enthalpy and $\Delta T = T_s - T$). For further details of experiments, see refs 29, 30.

Crystals of n-paraffin may exist in one of four forms[31]. Here we focus our attention on odd-numbered n-paraffins which are orthorhombic with space group P_{bcm} (ref. 32). Theoretical analysis[30,33] indicates that crystals of odd n-paraffins are lozenge-

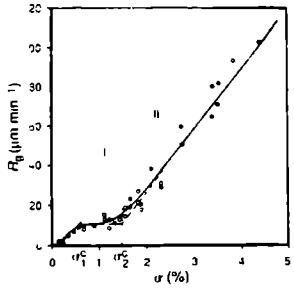

FIG 2 Growth rate R_g of the {110} faces of n-$C_{21}H_{44}$ growth from n hexane solutions $X = 2.939 \times 10^{-2}$ $T_s = 0.16$ °C $T_s > T_{110}$ $\sigma_1^c = 0.72\%$ $\sigma_2^c = 1.52\%$ The growth rate curve is divided into three areas (I II and III) corresponding to the two normal cases ($T > T$ area I $T < T$ areas II and III) In area I the linear part starts from the origin implying no nucleation barrier in the growth process In areas II and III the kinetics of growth show that at a critical value σ_1^c the original rough face changes into a flat face which will grow by a layer by-layer mechanism at $\sigma > \sigma_2^c$ the growth curve becomes linear again because of kinetic roughening

shaped (Fig 1*a*) We chose the {110} faces of crystals of n $C_{21}H_{44}$ for our investigations

We explore the situation where the equilibrium temperature is slightly higher than the roughening temperature ($0 < (T - T_r) < 0.1$ °C), and introduce supersaturations by lowering the temperature At equilibrium or a small supersaturation the interface is rough no facets in the {110} orientation develop on the growth form (Fig 1*b*) If the supersaturation exceeds a critical value σ_1^c, however {110} facets develop (Fig 1*c*) As the supersaturation increases further exceeding another critical value σ_2^c, the faceted faces roughen kinetically (Fig 1*d e*) The two transitions are completely reproducible In the reverse process exactly the same values σ^c and σ_1^c are obtained by lowering σ from above σ In this rough flat-rough sequence we consider rough to smooth transition occurring at σ_1 to be the most important because it occurs at a temperature very close to the thermal roughening transition temperature and to our knowledge has not been observed before This faceting, developing only in a supersaturated environment, may be called kinetic faceting It is different from the normal faceting which may occur at equilibrium

To clarify the rough-flat rough transition we determined the growth rates of {110} faces as a function of supersaturation σ Figure 2 shows a typical example of the process ($T \geq T_r$) The growth rate curve is divided into three areas which are a combination of the two typical normal cases $T > T_r$ (area I) and $T < T$ (areas II and III) The kinetic data clearly demonstrate that the development of facets on the rough faces is because the faces regain edge free energy ($\gamma > 0$) at a certain supersaturation This strongly supports our observations presented above The two critical values of σ_1^c and σ^c can be determined by extrapolating the linear parts of the curve to cut the horizontal line crossing the point of inflexion or independently by carefully observing the morphological transition[29,30] The results obtained by the two methods agree within experimental error In our experiments we mainly used the second method which offers an accuracy of $\Delta\sigma_1 < 0.1\%$

We know of no model that can directly explain our observations on this complicated organic system If we assume that the SOS Kossel model is valid to some extent for the n paraffin system we can combine equations (1) and (2) and plot the σ curve together with the trajectories (based on equation (3)) of the system in the phase space of (σ T) starting from different T values (see Fig 3) It can be seen from the schematic diagram that the phase space of (σ T) is divided into two regimes by the σ curve If crystal growth takes place under the σ curve faceted growth is expected above the σ_c curve rough growth is expected We now focus on dashed line c which starts from a temperature T slightly above T_r and cuts the σ^c curve at two points (σ_1^c and σ_2^c) At $\sigma_{system} < \sigma_1^c$ the growth of crystal faces

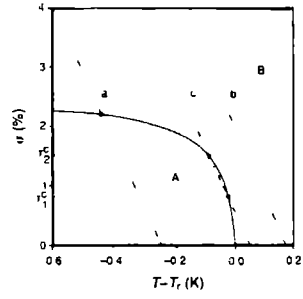

FIG 3 Schematic diagram of the phase space of (σ T) The solid line is the σ^c curve obtained from $\sigma^c - C \exp[\alpha/(T - T)^{1/2}]$ by combining equations (1) and (2) ($C = 2.55 \times 10^{-2}$ $\alpha = 0.150$) the dashed lines based on equation (3) ($\Delta h^{0\,\text{to}} = 6.411$ kcal mol) represent trajectories of the system starting from different values of T_s The phase space is divided by the σ^c curve into two regimes A flat interfaces B rough interfaces Lines a and b represent two normal cases ($T_s < T$ and $T_s > T$ respectively) Line c corresponds to the case of T_s slightly above T

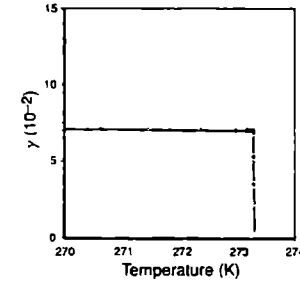

FIG 4 Edge free energy γ and temperature T for the {110} faces of n $C_{21}H_{44}$ crystals in n hexane solutions $T_{s110}(21) = 273.27 \pm 0.03$ K

is within the rough regime As soon as $\sigma_{system} \geq \sigma_1^c$, the growth re enters the flat regime At that point kinetic faceting occurs As σ_{system} continues to increase to above σ^c growth enters the rough regime again resulting in kinetic roughening of the faces

From equation (2) and the values of σ^c determined from our experiments we obtained a curve of γ against temperature for the {110} faces of n $C_{21}H_{44}$ crystals in n hexane solutions (Fig 4) Rather surprisingly the $\gamma(T)$ curve has the shape of a step function This result strongly suggests that the roughening transition in the n $C_{21}H_{44}$ n hexane system is much closer to a first order phase transition than to an infinite order or second order (the order disorder) phase transition The occurrence of this

kind of roughening transition may be due to a strong coupling of the thermal roughening with a structural surface phase transition related to a change in the rotation states of the molecules. Work is in progress to investigate this. □

Received 10 December 1991; accepted 17 March 1992

1 Burton, W. K. & Cabrera, N. *Discuss. Faraday Soc.* **5**, 33–40 (1949)
2 Burton, W. K., Cabrera, N. & Frank, F. C. *Phil. Trans. R. Soc.* **A243**, 299–358 (1951)
3 Onsager, L. *Phys. Rev.* **65**, 117–149 (1944)
4 van Beijeren, H. *Phys. Rev. Lett.* **38**, 993–996 (1977)
5 van der Eerden, J. P. & Knops, H. J. F. *Phys. Lett.* **A66**, 334–336 (1978)
6 Temkin, D. E. in *Crystallization Processes* (Consultants Bureau, New York, 1966)
7 Swendsen, R. H. *Phys. Rev.* **B15**, 5421–5431 (1977)
8 Kosterlitz, J. M. & Thouless, D. J. *J. Phys.* **C6**, 1181–1203 (1973)
9 Kosterlitz, J. M. *J. Phys.* **C7**, 1046–1060 (1974)
10 Wolf, P. E. *et al. J. Phys.* **46**, 1987–2007 (1985)
11 Nozieres, P. & Gallet, F. *J. Phys.* **48**, 353–367 (1987)
12 Gilmer, G. H. & Bennema, P. *J. Cryst. Growth* **13/14**, 148–153 (1972); *J. appl. Phys.* **43**, 1347–1360 (1972)
13 de Haan, S. W. H. *et al. J. Cryst. Growth* **24/25**, 491–494 (1974)
14 Durke, N. & Jaccucci, G. *Surf. Sci.* **144**, 92–95 (1984)
15 Ong, C. K., Tan, A. K. & Tan, H. S. *J. Phys.* **C21**, 3655–3661 (1988)
16 Weeks, J. D. & Gilmer, G. H. *Adv. chem. Phys.* **40**, 157–228 (1979)
17 Gallet, F., Balibar, S. & Rolley, E. *J. Phys.* **48**, 369–377 (1987)
18 Lipson, S. G. & Polturak, E. in *Progress in Low Temperature Physics* (ed. Brewer, D. F.) 128–188 (Elsevier, 1987)
19 Pavlovska, A. & Nenow, D. *J. Cryst. Growth* **39**, 346–352 (1977)
20 Pavlovska, A. *J. Cryst. Growth* **46**, 551–556 (1979)
21 Nenow, D. & Stoyanova, V. *J. Cryst. Growth* **46**, 779–782 (1979)
22 Avron, J. E. *et al. Phys. Rev. Lett.* **45**, 814–817 (1980)
23 Ohachi, T. & Taniguchi, I. *J. Cryst. Growth* **65**, 84–88 (1983)
24 Jackson, K. A. & Miller, C. E. *J. Cryst. Growth* **40**, 159–172 (1977)
25 Camel, D., Lesoult, G. & Eustathopoulos, N. *J. Cryst. Growth* **53**, 327–336 (1981)
26 Bennema, P. & Gilmer, G. H. in *Crystal Growth: an Introduction* (ed. Hartman, P.) 263–327 (North Holland, Amsterdam, 1973)
27 Bennema, P. & van der Eerden, J. P. in *Morphology of Crystals* (ed. Sunagawa, I.) 1–75 (Terra, Tokyo, 1987)
28 Elwenspoek, M. & van der Eerden, J. P. *J. Phys.* **A20**, 669–678 (1987)
29 Elwenspoek, M. & Boerhof, W. *Phys. Rev.* **B38**, 5326–5329 (1987)
30 Liu, X. Y. & Bennema, P. *J. Cryst. Growth* (submitted)
31 Broadhurst, M. G. *J. Res. natn. Bureau Standard* **A66**, 241–249 (1962)
32 Smith, A. E. *J. chem. Phys.* **21**, 2229–2231 (1953)
33 Bennema, P. *et al. J. Cryst. Growth* (in the press)

ACKNOWLEDGEMENTS. We thank B. Vos and M. J. Reynhout for discussions and Shell Netherlands BV for support.

Chapter 3.2

First order thermal roughening of normal alkane crystals

Xiang–Yang Liu

RIM, Laboratory of Solid State Chemistry, Faculty of Science, University of Nijmegen, Toernooiveld, 6525 ED Nijmegen, The Netherlands

ABSTRACT–In this paper a study of the critical behavior of the thermal roughening transition occurring at the {110} faces of odd–numbered n–paraffin crystals in n–hexane solution systems is presented It follows from our measurements that the edge free energy the order parameter of the roughening phase transition, remains constant when the temperature T is lower than the roughening temperature T_r, and abruptly vanishes at $T = T_1$ (T_r = 273.260 K) This critical behavior of order parameter shows the character of a first order phase transition, rather than the conventional infinite order phase transition of Kosterlitz–Thouless type To my knowledge, this is the first observation of this type of roughening transition on crystal surfaces An explanation of this observation is suggested in terms of the change of motional state of solid molecules in the interfacial phase

Phys. Rev. B48, (15 JULY 1993)

I. INTRODUCTION

The idea that at a critical temperature, a so–called thermal roughening could occur at a solid–fluid surface had been suggested long ago[1-3] However this phenomenon was well understood only when the relationship with the planar spin model (or the XY model)[4-10] and the coulomb gas model[11-12] had been established According to those models, the roughening transition is an infinite order phase transition The step edge free energy (per growth unit) γkT is the order parameter which vanishes at and above the roughening temperature T_r When the temperature T approaches T_r from below, then γ tends to zero showing a very weak singularity, as

$$\gamma \sim \exp[-C(T_r - T)^{\frac{1}{2}}] \qquad T \leq T_r \tag{1}$$

This is the so–called Kosterlitz–Thouless type of roughening transition[4,7]

The critical behavior of the roughening transition has been investigated by Monte Carlo computer simulations based on the solid on solid (SOS) Kossel model[12-15] It was also observed experimentally on some crystals composed of simple structural units, such as ^{4}He and ^{3}He crystals[16-18] It turned out that the roughening transitions occurring in those systems are truly of the Kosterlitz–Thouless type However, to our knowledge, no similar research has been carried out on crystals composed of complex structural units, such as n–paraffin molecules In this sense, it is worthwhile to check the critical behavior of the thermal roughening in those systems

Nevertheless, the problem with this order parameter is that it is very difficult to measure it directly But indirect measurement is possible One of the methods is to measure the critical supersaturation σ^c (= $\Delta\mu^c/kT$) at which kinetic roughening or kinetic faceting occurs[19] In the case of kinetic roughening (or kinetic faceting), the originally flat (or roughened) faces will become rounded (or faceted) In our previous paper[20], it was shown that for an interfacial system consisting of anisotropic structural units, the relation between the critical supersaturation σ^c and the step free energy can be expressed as

$$\sigma^c = [4\xi/(\zeta\eta)]\gamma_x\gamma_v = 4\gamma_y^2\xi/(\zeta^2\eta) \tag{2}$$

where the shape factor $\xi = (1+\eta)^2/(4\eta)$, the anisotropic factor of interactions $\zeta = \gamma_y/\gamma_x \simeq \phi_y/\phi_x$ (it is defined[20] that $\gamma_v \geq \gamma_x$, γ_y and γ_x are the dimensionless edge free energies, and φ_y and ϕ_x the edge energies in the y and the x orientations, respectively), and the geometric

factor of a growth unit $\eta = l_y/l_x$ (l_y and l_x are the dimensions of the growth units in the y and x directions, respectively) Note that these factors depend on the structure of solid surfaces. and for a given crystal surface they are fixed. It follows from Eq.(2) that for a given interfacial system σ^c is determined by γ On the other hand, the edge free energy γ can be derived from the measured critical supersaturation σ^c As mentioned a above. γ_x is associated with γ_y by the anisotropic factor ζ Then in the following discussions, we only concentrate on γ_y

It is the purpose of this work to investigate the critical behavior of γ in the neighborhood of the roughening transition temperature T_1 for the odd–numbered paraffin crystals in n–hexane solutions, and compare the results with existing theories. In Sec II, we will briefly introduce the experimental set up and procedures. In Sec III, first the relation between γ and T around the thermal roughening temperature and the characteristic of this roughening phase transition are discussed, then the cause of this particular roughening transition is given Finally summary and conclusions can be found in Sec IV

II. EXPERIMENTAL

In Sec. I, we notice that the measurement of the critical supersaturation of kinetic roughening is the key issue in our experiments. To obtain a well–defined supersaturation in a solutions of a fixed concentration, as usual we cool the solution from the equilibrium temperature T_s to a certain value T From the definition of supersaturation, it follows that for a regular solution the supersaturation is a function of the supercooling $\Delta T (= T_s - T)$ and the temperature T,

$$\sigma = [\Delta h^{diss}/(RT_sT)]\Delta T \tag{3}$$

(R is the gas constant.) In case that $T_s >> \Delta T$ (this holds for our experimental conditions), Eq.(3) can be rewritten as,

$$\sigma \simeq (\Delta h^{diss}/RT_s^2)\Delta T \tag{3'}$$

(Here Δh^{diss} is the molar dissolution enthalpy) Eq.(3') implies that σ is linearly proportional to ΔT. Therefore, to determine the critical supersaturation of kinetic roughening, we only need to determine the critical supercooling of the system $\Delta T^c (= T_s - T^c$, T^c is the temperature in which the kinetic roughening occurs).

Now the main experimental procedures are given as follows The n–paraffins used in our experiments are from analytically pure chemicals (Alfa, > 99 0%) and the n–hexane is

spectroscopically pure (Merck, > 98 0%) The chemicals were used without further purification

All our observations of the growth process and the morphology of crystals were carried out in a double walled thermostated glass cell system of cylindrical form, using a Leitz transmission microscope type Divert In order to record the growth processes of crystals, a video camera or a photographic camera were used

In preparing the samples, first, the materials, both n–paraffin and n–hexane, are exactly weighed into a cylindrical glass cell of about 60 mm diameter 4 mm height The filled cell is sealed at liquid N_2 temperature under vacuum It is necessary to leave a gas bubble in the cell to compensate for volume expansions Hence the solutions stand under their own vapor pressure The glass cell with the solutions is thermostated in a large cell The temperature is measured in this cell, outside the growth cell containing the solution It can be stabilized better than ± 0 003 K by the thermostat (Heto, Denmark) over several hours To begin the experiments the temperature of the solution must be lowered to a temperature well below the saturation temperature ($\Delta T \sim 1$ K) After nucleation, massive crystals are grown from the solution Then the temperature is raised to dissolve all the crystals except one, on which experiments are performed Since the volume of the remaining crystal is very small compared to the volume of the cell, the variation in concentration of the solution is negligible To measure the critical supercooling of kinetic roughening (or kinetic faceting), the morphological changes are observed by varying temperatures in very small intervals (in the neighborhood of critical points the intervals are about 0 005 ~ 0 01 K) Each temperature is kept constant for at least half an hour to ensure that the morphology of the crystal is stable At a certain temperature, due to the relative large driving force the originally flat crystal surfaces will microscopically roughen These surfaces lose their crystallographic orientations and become macroscopically rounded At that temperature the so–called kinetic roughening occurs and the supercooling is the critical supercooling for kinetic roughening Note that since the morphology of crystals is in a very subtle way influenced by kinetic roughening, the experimental error of measuring the critical supercooling of kinetic roughening can in principle be reduced to the accuracy limit of temperature control and the temperature measurement devices (in our case the accuracy may reach ± 0 003 K) This means that each datum of the critical supercooling is reproducible within the accuracy limit of our experimental set up Therefore this method, to my knowledge, is one of the most sensitive experimental methods to determine the edge free energy

III. RESULTS AND DISCUSSION

N–paraffin crystals have the space group symmetry P_{bcm} [21] From a theoretical analysis and observations [22], it is known that crystals of odd n–paraffins are plate–like, confined by large {001} faces and small narrow {110} faces In the following, we choose the {110} faces of n–$C_{21}H_{44}$ crystals for our investigations This is because the roughening transition of these faces can be observed under normal conditions Also other members of odd–numbered n–paraffins, such as n–$C_{23}H_{48}$ and n–$C_{25}H_{52}$, show the same behavior as n–$C_{21}H_{44}$

A. The edge free energy and the edge energy

We have already seen from Eq (2) that there is a direct link between the critical supersaturations of kinetic roughening (or kinetic faceting) and the edge free energy This means that by measuring those values of σ^c from a number of solution systems whose equilibrium temperatures are close to the thermal roughening temperature T_r, we can obtain γ as a function of temperature T according to Eq (2) In the case of n–$C_{21}H_{44}$ crystals grown from n–hexane solutions, for the {110} faces $\eta = 6\ 377$, $\zeta = 22\ 34$ The resulting $\gamma(T)$ function is shown in Fig 1

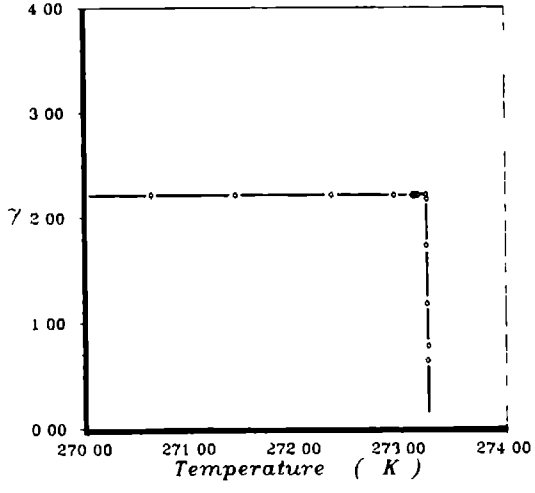

FIG 1 Phase diagram of the edge free energy γ and temperature T for the {110} faces of n–$C_{21}H_{44}$ crystals in n–hexane solutions $T_r = 273\ 260 \pm 0\ 005$ K

It is surprisingly found from Fig 1 that in this system the edge free energy γ is constant if $T < T_r$, and vanishes discontinuously at $T = T_r$ ($T_r = 273\ 260 \pm 0\ 005$ K) We notice that to due

to the accuracy of our experimental set up (see Sec. II), a rounded curve $\gamma(T)$ in the critical region could easily be determined if the roughening transition of the Kosterlitz–Thouless type occurred in n–paraffin/n–hexane systems. [In the case of the (0001) face of hcp ^{4}He crystals whose roughening temperature is 1.28 K, the critical region is larger than 0.2 K [17].) However, this is not the case, because no rounding of the curve $\gamma(T)$ is detectable. This implies that the change of γ is abrupt. It then follows that the curve $\gamma(T)$ can be expressed by the step function at T_r. Thus for the first derivative of γ with respect to T, we obtain that

$$\frac{d\gamma}{dT} = C'\delta(T_r - T) = \begin{cases} \infty, & T = T_r \\ 0, & T \neq T_r \end{cases}, \tag{4}$$

(here $C' \simeq 2.22\ K^{-1}$). According to thermodynamics,

$$\gamma = \phi/kT + T\frac{d\gamma}{dT}. \tag{5}$$

Here, the edge entropy s_{edge} is written as

$$s_{edge} = -\frac{d\gamma}{dT}. \tag{6}$$

From Eq.(4), it can be seen that the change of the edge entropy shows a singularity at the critical point $T = T_r$. This clearly demonstrates that the roughening transition occurring in n–paraffin/n–hexane solution systems is a first order phase transition up to our experimental accuracy. Without doubt this first order roughening transition is very different from the conventional Kosterlitz–Thouless type roughening.

Now let us compare this first order roughening transition and the conventional infinite order roughening transition. We may evaluate the edge energy independently by the thermal roughening transition and the kinetic roughening. It is shown from (4) and (6) that $s_{edge} = 0$ when $T < T_r$. Thus it follows from (5) that

$$\gamma \approx \phi/(kT). \tag{7}$$

Therefore the edge free energy (determined from kinetic roughening) is equal to the edge energy. For the {110} faces of n–$C_{21}H_{44}$/n–hexane systems, it turns out that for the strongest edge energy, $\phi_{str} = 1.21$ kcal/mol ($= \phi_y$).

Alternatively, the edge energy can also be deduced from T_r based on the SOS Kossel

model. According to this model, the roughening transition on the crystal surfaces {hkl} can be characterized by a dimensionless roughening temperature θ^{r}_{hkl}, as

$$\theta^{r}_{hkl} = 2kT_r/\phi_{str}. \tag{8}$$

As a specific property, a given crystal surface has a certain value of θ^{r}_{hkl}. It turns out that once T_r is determined, ϕ_{str} can be calculated from (8). According to our calculations[22], for the {110} faces of n–$C_{21}H_{44}$ crystal/n–hexane solution systems, $\theta^{r}_{110} \simeq 0.8997$. It then follows from (8) that $\phi_{str} \simeq 1.207$ kcal/mol. It is surprisingly found that this value is very close to the value derived from kinetic roughening. The coincidence of the two values implies that the actual roughening transition on the crystals takes place just in the neighborhood of the roughening transition of Kosterlitz–Thouless type.

B. The surface roughening coupling with the surface structural phase transition

From the discussion in Sec. III.B, we have found that a non–Kosterlitz–Thouless type of roughening transition occurs in the n–paraffin crystal system. The critical temperature of of this special roughening is very close to that of the Kosterlitz–Thouless type of roughening. In the following we will discuss the interfacial structure of our system and the reason of this first order roughening transition, based on the available knowledge.

First, the occurrence of this discontinuous phase transition strongly suggests that an abrupt change in the physical state of structural units occurs at the surface. It is most likely due to the sudden change of degrees of motional freedom of solid units. As we know, n–paraffin molecules have the zigzag chain structure. According to different crystalline modifications of n–paraffins[23-24], n–paraffin molecules mainly exist in two states in the bulk solid phases: rotational and non–rotational. When temperatures are relatively low, the rotation of n–paraffin molecules in those solid phases (called the β phase or low temperature phase) is seriously restricted. Therefore the molecules remain non–rotational. We call these non–rotational paraffin molecules β molecules. When the temperature is raised to a transition temperature T_{tr}, which is in the neighborhood of the melting point, this restriction disappears. Then it is supposed that n–paraffin molecules freely rotate around their molecular axes [23-24]. [It has to be noted that in fact the α molecules are not fully rotational. They are molecules with defects in their molecular chains[25-27].] At this moment the β solid phase changes into the α solid phase (or high temperature phase). We call these "rotational" n–paraffin molecules α molecules.

At crystal surfaces, an independent (but similar) process may occur. In our experiments, n–paraffin molecules crystallize in a β phase. Therefore at a low temperature, solid paraffin

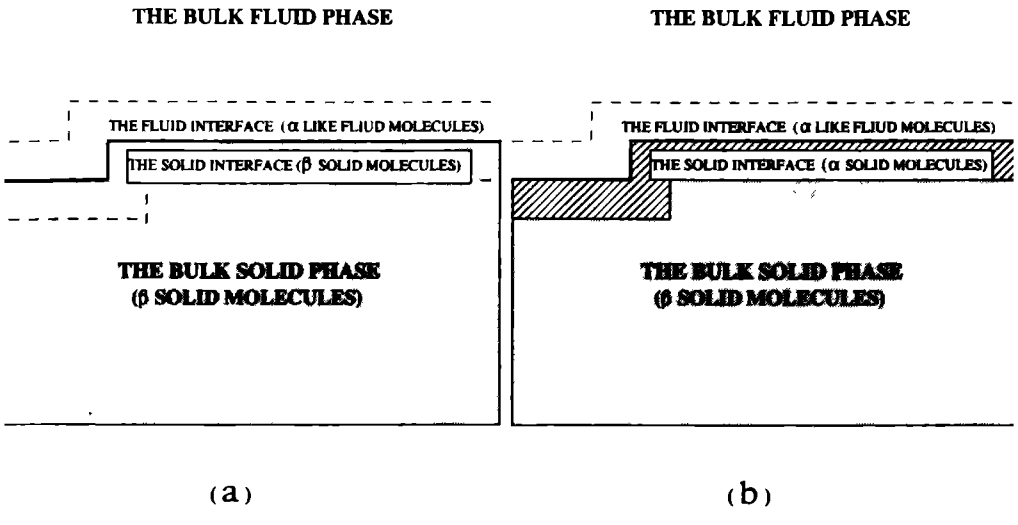

FIG.2. Schematic illustration of the solid–fluid interface between n–paraffin crystals and solutions. (a) $T < T_{tr}$(surf), fluid molecules in contact with β solid molecules at the interface. (b) $T > T_{tr}$(surf), fluid molecules in contact with α solid molecules at the interface.

ıolecules both at surfaces and in the bulk are the β molecules. (See Fig. 2a.) When the emperature increases to a certain value, T_{tr}^{surf}, which is still lower than the bulk α–β phase ransition temperature T_{tr}, due to some interfacial effects (including the thermal roughening ffect) and the influence of n–hexane molecules, the solid paraffin molecules at surfaces will tart to "rotate" prior to those in the bulk. This results in a *surface structural phase ransition* (β paraffin molecules turn to α paraffin molecules). Meanwhile n–paraffin ıolecules in the bulk solid phase still remain as β molecules. This is illustrated schematically n Fig. 2b.

One of the indirect evidences for the surface structural phase is from the Scanning unneling Microscopy (STM) images. It is shown from STM experiments[28-29] that under a ertain condition the monolayers of paraffin molecules adsorbed at the interface between rganic solutions and the basal plane of graphite reveal a high degree of ordering and rientation similar to the solid phases. Let us consider these adsorbed paraffin molecules as he analogous of solid paraffin molecules at crystal surfaces. It is found from our STM xperiments[29] that under a certain temperature, this ordered non–rotational structure of the

adsorbed molecules can be clearly imaged, while above this temperature the ordered structure disappears This can be attributed to the surface structural phase transition taking place in the adsorbed molecules at higher temperatures

Concerning the difference of energy level between various states, it is known that the potential energy of solid α paraffin molecules is higher than that of solid β paraffin molecules[23-27] It therefore follows that the energy difference between the solid α molecules and the fluid molecules is smaller As we know, the edge energy ϕ is mainly caused by the difference of energy levels between solid units and fluid units at the interface Hence, it turns out that the occurrence of the surface structural phase transition will cause a collapse of the edge energy from ϕ^{β} (for the β type solid surface) to ϕ^{α} (for the α type solid surface)

Now the picture of the surface roughening in n–paraffin/n–hexane systems seems to become much clearer The roughening temperature we determined for the paraffin system obviously is the surface structural phase transition temperature T_{tr}^{surf} This surface structural phase transition is strongly coupled with the surface roughening If we plot $\gamma kT/\phi$ against the dimensionless temperature kT/ϕ, a schematic phase diagram is obtained, as shown in Fig 3

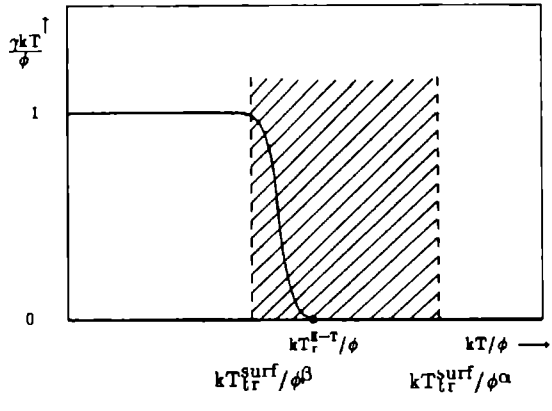

FIG 3 Schematic illustration of the temperature dependence of the edge free energy At $T = T_r^{KT}$ one shows the Kosterlitz–Thouless type roughening transition At $T = T_{tr}^{surf}$, the surface structural phase transition occurs, resulting in a sudden increase of dimensionless temperature from $kT_{tr}^{surf}/\phi^{\beta}$ to $kT_{tr}^{surf}/\phi^{\alpha}$

Provided that the surface structural phase transition did not occur, the roughening transition of Kosterlitz–Thouless type would take place at T_r^{KT} (or at a dimensionless temperature, kT_r^{KT}/ϕ) However, in practice when the temperature increases to the value $T = T_{tr}^{surf}$,

(probably) induced by the slight roughening, the surface structural phase transition occurs prior to the Kosterlitz–Thouless type of roughening This causes that the edge energy abruptly changes from ϕ^{β} to ϕ^{α} It follows that the dimensionless temperature of the system is enhanced from one value ($kT_{tr}^{surf}/\phi^{\beta}$) which is slightly lower than kT_r^{KT}/ϕ, to another value ($kT_{tr}^{surf}/\phi^{\alpha}$) which is much higher than kT_r^{KT}/ϕ (According to the SOS model, kT_r^{KT}/ϕ has a certain value for a given crystal surface) It is seen from Fig 3 that the shaded region between the two dashed lines in the diagram is missing Correspondingly, the step like $\gamma(T)$ curve is obtained

We notice that the possibility of first order roughening transition was discussed by Fisher and Weeks [30] According to them, as a consequence of the Kosterlitz–Thouless theory, the roughening transition temperature is related to the "surface stiffness" in the following way

$$T_{ro} = (2a^2/\pi)\,[\Gamma_x(T_{ro})\Gamma_y(T_{ro})]^{\frac{1}{2}} \tag{9}$$

Here a denotes the spacing of bulk crystalline phase normal to the interface, and the surface stiffness

$$\Gamma_x = \sigma^{s\text{-}t}(\hat{z}) + \partial^2\sigma^{s\text{-}t}/\partial\hat{n}_x\partial\hat{n}_x\,|_{\hat{n}=\hat{z}} \tag{10}$$

where $\sigma^{s\text{-}t}$ is the interface tension, $\hat{z}$ the normal of a crystalline plane with rational Miller indices, and $\hat{n}$ the interface normal (similarly Γ_y) It can be seen from (10) that this surface stiffness Γ can be related to the edge free energy γ Within this framework [30], a flat surface has infinite surface stiffness (the term $\partial^2\sigma^{s\text{-}t}/\partial\hat{n}_x\partial\hat{n}_x\,|_{\hat{n}=\hat{z}}$ diverges exponentially in case $T < T_r$) In contrast, for a rough surface ($T \geq T_r$), $\Gamma \simeq \sigma^{s\text{-}t} \simeq$ const due to the vanishing of γ

As predicted by Fisher and Weeks, it is in principle possible that some other (first order) mechanism causes the actual roughening temperature T_r' to be higher than T_{ro} In this case, the inequality occurs

$$T_r' \geq (2a^2/\pi)\,[\,\Gamma_x(T_r')\,\Gamma_y(T_r')\,]^{\frac{1}{2}} \tag{11}$$

This is similar to our aforementioned argument that $kT_{tr}^{surf}/\phi^{\alpha} \geq kT_r^{KT}/\phi$ Obviously, in our case the first order mechanism is the surface structural phase transition This surface structural phase transition causes the first order change in the surface stiffness that could drive the first order roughening transition

IV. CONCLUSION

I have discussed the roughening of surfaces on odd–numbered n–paraffin crystals. The roughening process is characterized by abruptly vanishing edge free energy when the temperature approaching the roughening temperature from below.

This roughening transition belongs to the first order phase transition, rather than the infinite order which we expect from theoretical models.

In my view the crucial difference between the practical system and those theoretical models is that the structural units in our system are much more complicated and anisotropic than those in the models. Once some degrees of freedom of interfacial molecules are changed, coupled with the surface roughening, the first order roughening transition may occur.

ACKNOWLEDGEMENTS

I would like to acknowledge helpful discussions with Prof. Dr. J.P. van der Eerden, and thank Prof. Dr. P. Bennema and Dr. H. Meekes for a critical reading of the manuscript and valuable suggestions for this work. I am also grateful to Shell Netherlands B V for supporting this work.

REFERENCES

1 D.E. Temkin, Sov. Phys. Cryst. **14**, 344 (1969).

2 W.K. Burton, N. Cabrera and F.C. Frank, Phil. Trans. Roy. Soc. A**243**, 299 (1951).

3 K.A. Jackson, in *Liquid Metals and Solidification*, 174 (ASM, Cleveland, OH, 1958).

4 J.M. Kosterlitz and D.J. Thouless, J. Phys. C**6**, 1181 (1973).

5 H.J.F. Knops, Phys. Res. Lett. **39**, 766 (1977).

6 J.V. José, L.P. Kadanoff, S. Kirkpatrick and D.R. Nelson, Phys. Rev. B**16**, 1217 (1977).

7 J.M. Kosterlitz, J. Phys. C**7**, 1046 (1974).

8 J.P. van der Eerden and H.J.F. Knops, Phys. Lett. **66A**, 334 (1978).

9 P. Nozières and F. Gallet, J. Physique **48**, 353 (1987).

10 R.H. Swendsen, Phys. Rev. B**17**, 3710 (1978).

11 S.T. Chui and J.D. Weeks, Phys. Rev. B**14**, 4978 (1976).

12 Y. Saito and H. Müller–Krumbhaar, Phys. Rev. B**23**, 308 (1981).

13 H. Müller–Krumbhaar, in *Curr. Top. in Materials Sci.*, edited by E. Kadis and H. J

Scheel, 1 (North Holland, Amsterdam, 1978)
14 J D Weeks and G H Gilmer, Adv Chem Phys **40**, 157 (1979)
15 C K Ong, A K Tan and H S Tan, J Phys C**21**, 3655 (1988)
16 S G Lipson and E Polturak, in *Progress in Low Temperature Physics*, edited by D F Brewer, 128 (Elsevier Sci , Amsterdam, 1987)
17 F Gallet, S Balibar and E Rolley, J Physique **48**, 369 (1987)
18 P E Wolf, F Gallet, S Balibar, E Rolley and P Nozières, J Physique **46**, 1987 (1985)
19 X Y Liu, P Bennema and J P van der Eerden, Nature **356**, 778 (1992)
20 X Y Liu and P Bennema, J Cryst Growth **128**, 69 (1993)
21 A E Smith, J Chem Phys **21**, 2229 (1953)
22 P Bennema, X Y Liu, K Lewtas, R D Tack, J J M Rijpkema and K J Roberts, J Cryst Growth **121**, 679 (1992)
23 M G Broadhurst, J Res Nat Bur Standards **66A**, 241 (1962)
24 Y V Mnyukh, J Phys Chem Solids **24**, 631 (1963)
25 S Blasenbrey and W Pechhold, Rhedogica Acta **6**, 74 (1967)
26 W Pechhold, W Dollhopf and A Engel, Acustica **17**, 61 (1966)
27 B G Sumpter, D W Noid and B Wunderlich, Macromolecules (in press)
28 J P Rake and S Buchholz, Makromol Chem, Macromol Symp **50**, 261 (1991)
29 M da Silva Couto, X Y Liu, H Meekes and P Bennema, J Appl Phys (submitted)
30 D S Fisher and J D Weeks, Phys Rev Lett **50**, 1077 (1983)

Chapter 3.3

VOLUME 71 NUMBER 1 PHYSICAL REVIEW LETTERS 5 JULY 1993

Surface Roughening of Normal Alkane Crystals: Solvent Dependent Critical Behavior

Xiang-Yang Liu, Peter van Hoof and Piet Bennema
Research Institute for Materials, Laboratory of Solid State Chemistry, Faculty of Science, University of Nijmegen, Toernooiveld 6525 ED Nijmegen, The Netherlands
(Received 5 March 1993)

The flat solid-fluid interface undergoes a roughening phase transition at the roughening temperature T^r. The step free energy γ vanishes at T^r if the temperature $T \to T^r$. For n-paraffin crystals the critical behavior of $\gamma(T)$ in the neighborhood of T^r is solvent dependent. If n-$C_{35}H_{52}$ crystals are grown from n-hexane solutions the step free energy $\gamma(T)$ of the {110} faces vanishes discontinuously at T^r. In contrast, for n-$C_{35}H_{52}$ crystals grown from toluene solutions $\gamma(T)$ vanishes continuously at T^r, showing a Kosterlitz-Thouless type of roughening transition.

PACS numbers: 68.45.−v, 61.50.Cj, 64.70.Dv, 68.35.Rh

The concept of a roughening transition (or thermal roughening) of planar surfaces was introduced long ago by Burton, Cabrera, and Frank [1] using the order-disorder phase transition of Onsager [2]. It is now well established that this transition is of the type described by Kosterlitz and Thouless [3–6] in a different context (it is called in the following the KT-type roughing transition). Generally speaking, the roughening transition is a phase transition which occurs on a crystal surface at the roughening temperature T^r. If the actual temperature T is equal to or larger than T^r, the free energy required to form a monostep (or the edge free energy per structure unit) γkT (where k is Boltzmann's constant) vanishes. If $T < T^r$, $\gamma kT > 0$. This implies that below T^r a surface will keep its overall flatness corresponding to the orientation (hkl). Above T^r the orientation is lost and the surface will become rough due to statistical fluctuations.

According to Kosterlitz and Thouless [2], the roughening transition is a phase transition of infinite order. This implies that the edge free energy γ vanishes continuously as

$$\gamma \sim \exp[-a(T^r - T)^{-1/2}], \quad T \le T^r \tag{1}$$

(a is a coefficient, depending on the system). This has been confirmed experimentally for simple crystals, such as ^{4}He and ^{3}He crystals [7–9]. It is worthwhile to investigate the nature of the roughening transition in complex molecular systems. Here we describe roughening phenomena occurring at the {110} surfaces of n-$C_{35}H_{52}$ crystals growing from two different types of solutions, n-hexane and toluene solutions, from which the critical behavior of the dimensionless edge free energy γ around T^r is derived.

In order to identify the character of the roughening transition, the critical behavior of $\gamma(T)$ around the roughening temperature T^r must be studied. It is very difficult to measure $\gamma(T)$ directly [10]. Nevertheless, indirect measurement is possible. For this purpose, there are some techniques available [10]. They are based on the determination of the facet size on a equilibrium form ($\sim\gamma$) [8,9] or growth rate data according to a 2D nucleation growth model [4,11]. However, for those techniques, well-defined experimental conditions and high-accuracy experimental results are not easy to achieve [10,12]. In this Letter, a technique based on an established relation between the critical supersaturation of kinetic roughening and the edge free energy is introduced to determine $\gamma(T)$.

Kinetic roughening is a transition occurring in a supersaturated environment in the case of $T < T^r$. In crystal growth, at a relatively small supersaturation $\sigma(\sigma = \Delta\mu/kT$, where $\Delta\mu$ is the difference in chemical potential between solid and fluid particles) a crystal face with $T_s < T^r$ (T_s is the equilibrium temperature of the crystal-solution system) will grow by a layer-by-layer mechanism (spiral growth or two-dimensional nucleation) because of the 2D nucleation barrier ($\gamma > 0$) and the overall orientation (hkl) is maintained. When $\sigma \ge \sigma^c$ (σ^c is the critical supersaturation), the critical size of 2D nuclei become so small that the 2D nucleation barrier vanishes due to thermal fluctuations. Then the originally flat surface becomes microscopically rough. The so-called kinetic roughening occurs. For crystal-solution systems with different T_s ($T_s < T^r$), kinetic roughening will occur at different temperatures. If σ^c is plotted versus T in the phase space of (σ T), a curve of $\sigma^c(T)$ is obtained (see the solid line in Fig. 1). This curve divides the phase space into two regimes. If crystal growth takes place under the σ^c curve, faceted growth is expected, above the σ^c curve, rough growth is expected.

Recent surveys on the issue of kinetic roughening [13,14] reveal that there is a direct link between σ^c and γ. According to our previous investigations [14], for surfaces with an anisotropic bond structure the critical supersaturation is directly correlated to the edge free energy for rectangular nuclei by

$$\sigma^c = [4\xi/(\delta^2\eta)]\gamma_y^2, \tag{2}$$

where the shape factor $\xi = (1+\eta)^2/4\eta$, the anisotropic factor of interactions $\delta = \gamma_y/\gamma_x$ (γ_y and γ_x are the specific edge free energy in x and y directions, respectively, and assume that $\gamma_y > \gamma_x$) and the geometric factor of a growth unit $\eta = l_y/l_x$ (l_x and l_y are the length of growth units in x and y directions, respectively). Those factors

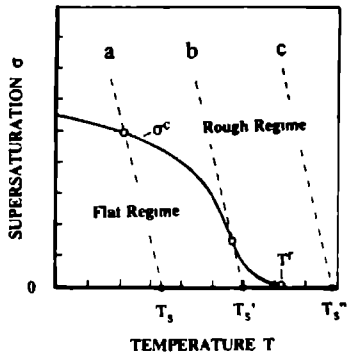

FIG 1 Schematic diagram of the phase space of (σ,T) Solid line the curve $\sigma^r(T)$, dashed lines trajectories $[\sigma_{system}(T)]$ of systems with different T_s

depend on the structure of solid surfaces It follows that since σ^r can be directly measured from experiments (the experimental procedures will be specified later) γ can then be determined according to Eq (2) In other words, the measured curve $\sigma^r(T)$ can be converted into $\gamma(T)$ We notice that if $T_s \geq T^r$, then $\gamma=0$, consequently $\sigma^r=0$ and the interface is macroscopically rounded off for all supersaturations From a macroscopic point of view, the phenomenon of kinetic roughening is similar to thermal roughening The cause, however, is different The former is a crossover whereas the latter is a real phase transition

In the experiments, we always start from solution systems with certain concentrations For a solution with a certain concentration, a well-defined relative supersaturation σ can be obtained by cooling the solution from T_s to a lower temperature T, according to the following relation

$$\sigma=\frac{\Delta h^{diss}}{RT_sT}\Delta T \qquad (3)$$

or

$$\sigma\simeq\frac{\Delta h^{diss}}{RT_s^2}\Delta T \quad (\text{if } T_s\gg\Delta T) \qquad (3')$$

(Here $\Delta T=T_s-T$, Δh^{diss} is the molar dissolution enthalpy) This implies that the supersaturation is linearly proportional to the supercooling ΔT In the phase space of (σ,T), trajectories of systems $\sigma_{system}(T)$ correspond to some straight lines (indicated by those dashed lines in Fig 1) For a solution system with $T_s\leq T^r$, the kinetic roughening occurs at a certain temperature $T^r\leq T_s$ where $\sigma_{system}(T)$ intercepts the σ^r curve in the phase space of (σ,T) $(\sigma_{system}=\sigma^r)$ Therefore, starting with solutions having different T_s (such as the systems indicated by lines a,b in Fig 1), a set of data $\sigma^r\sim T$ are obtained, from which the curve $\gamma(T)$ can be determined Note that as discussed above, starting with a solution with $T_s>T^r$ will normally cause no interception between $\sigma^r(T)$ and $\sigma_{system}(T)$ (see line c in Fig 1) Only when the curve σ^r (or γ) has a steep change around T^r and T_s is slightly above T^r, two interceptions at the σ^r curve by a $\sigma_{system}(T)$ are possible This then results in the so-called kinetic "rough-flat-rough" transition [15]

The n-paraffins and toluene used in our experiments are analytically pure chemicals (Alfa, >99 0%, and Merck, >99 9%, respectively) and the n-hexane is spectroscopically pure (Merck, >98 0%) All our observations of the growth process and the morphology of crystals were carried out in a double walled thermostated glass cell system of cylindric form, using a Leitz transmitted microscope type Divert In order to trace the growth of the crystals, a video camera or a microscope camera were employed In preparing the samples, first, the materials, both n-paraffin and the solvent, are exactly weighed into a cylindrical glass cell of about 60 mm diameter 4 mm height The filled cell is sealed at liquid N_2 temperature under vacuum It is necessary to leave a gas bubble in the cell to compensate for volume expansion Hence the solutions stand under their own vapor pressure The glass cell with the solutions is thermostated in a large cell of cylindrical form The temperature is measured in this cell, outside the growth cell containing the solution It can be stabilized to better than 0 005 K by the thermostat (Heto, Denmark) over several hours To begin the experiments, the temperature of the solution must be lowered to a temperature well below the saturation temperature ($\Delta T\sim 1$ K) After nucleation, massive crystals are grown from the solution. Then the temperature should be raised to dissolve all the crystals except one, on which experiments are performed Since the volume of the remaining crystal is very small compared to the volume of the cell, the variation in concentration of the solution is negligible To measure the critical supercooling of kinetic roughening ΔT^r $(=T_s-T^r)$, the morphological changes are observed by varying temperatures in very small intervals (in the neighborhood of critical points the intervals are about 0 005—0 01 K) Each temperature is kept constant for at least half an hour to ensure that the morphology of the crystal is stable At a certain temperature T^r, due to kinetic roughening, those originally smooth surfaces become macroscopically rounded if the temperature changes from $T>T^r$ to $T<T^r$ The transition is reversible at T^r if the temperature is enhanced from a lower value $(T<T^r)$ The supercooling ΔT^r is the critical supercooling of kinetic roughening A transition from the faceted growth to the kinetically rough growth in the orientations {110} is shown in Fig 2 Note that since the morphology of crystals is in a very subtle way influenced by kinetic roughening, the experimental error of measuring the critical supercooling of kinetic roughening can in principle be reduced to the accuracy limit of temperature control and the temperature measurement devices (in our case the accuracy may reach $\pm$0 005 K) This means that each datum of the critical supercooling is reproducible within the

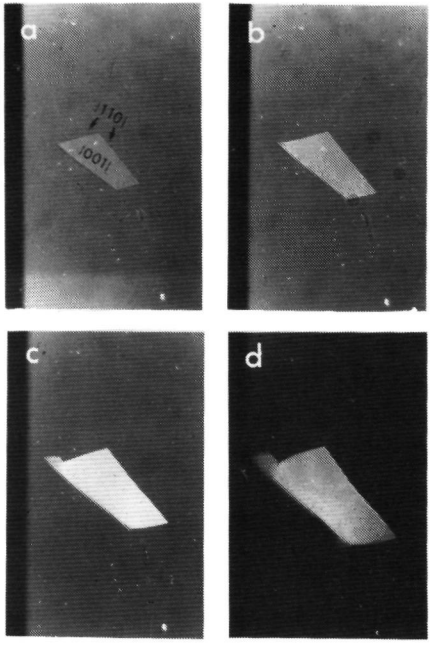

FIG. 2. The series of pictures [(a)–(d)] show the morphological change due to kinetic roughening for the {110} faces of an n-$C_{25}H_{52}$ crystal grown from an n-hexane solution: $T_s \simeq 285.665$ K, $T^c \simeq 285.555$ K. A crystal with the faceted {110} faces grows first at a temperature T' above T^c ($\sigma' < \sigma^c$) (a). Then the temperature is rapidly decreased to another value $T'' < T^c$ ($\sigma'' > \sigma^c$), and remains constant (b),(c),(d). Because of kinetic roughening, the {110} faces gradually become rounded. $T' = 285.560$ K, $T'' = 285.550$ K; from (a) to (d), $t = 0$, 10, 20, and 30 min, respectively.

accuracy limit of our experimental setup.

The low temperature phase of odd-numbered n-paraffins has the space group symmetry P_{bcm} [16]. Theoretical analysis [17] shows that crystals of odd n-paraffins are lozenge shaped, confined by the large {001} faces on the top and the bottom and the narrow side faces of {110}. In the following we will concentrate on the {110} faces.

First we will explore the case in which n-$C_{25}H_{52}$ crystals grow from n-hexane solutions. From Eq. (2) and the determined values of σ^c, a curve of γ versus temperature for this system is obtained (see Fig. 3). It is found that in this case the value of γ remains constant with increasing temperature. At $T = T^r$, γ vanishes abruptly. The first derivative of γ with respect to T shows a singularity at $T = T^r$. This indicates that a first-order roughening transition occurs, instead of an infinite-order phase transition as follows from Eq. (1). For other odd n-paraffin crystals, such as n-$C_{21}H_{44}$ and n-$C_{23}H_{48}$, grown from n-

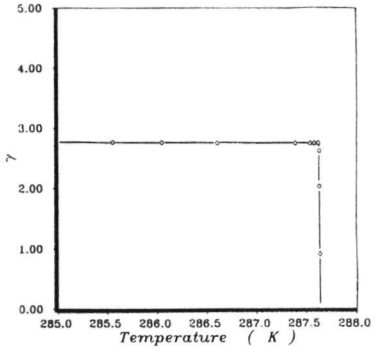

FIG. 3. The step free energy γ as a function of temperature T for the {110} faces of n-$C_{25}H_{52}$ crystals in n-hexane solutions. The $\gamma(T)$ curve has the shape of a step function, suggesting the first-order roughening transition of the system. $T^r_{110}(25) \simeq 287.635 \pm 0.005$ K. Note that the values of γ are derived from the experimental data σ^c, according to Eq. (2). For the surfaces of {110}, $\delta = 26.78$ and $\eta = 7.511$.

hexane solutions, the first-order roughening transition has also been observed (the results will be published elsewhere).

If an aromatic compound, toluene, is chosen as a solvent, a quite different behavior of the $\gamma(T)$ is observed. In this case, the experimental method which is the same as the first case is applied. It follows from experiments that the roughening temperature T^r is somehow higher than in the first case. Compared to the first case, it is found that the shape of the $\gamma(T)$ curve in the neighborhood of T^r is totally different. Figure 4 shows the edge free energy γ in dependence of the temperature T for the {110} faces of n-$C_{25}H_{52}$ crystals in toluene solutions. It is clearly shown in this figure that the edge free energy γ

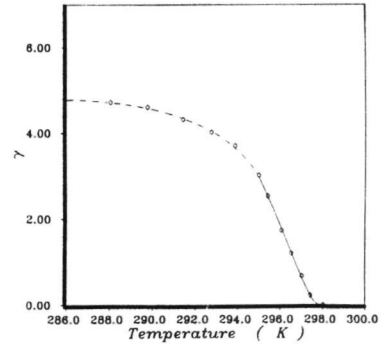

FIG. 4. The step free energy of the {110} faces plotted vs temperature for n-$C_{25}H_{52}$ crystals in toluene solutions. γ vanishes smoothly when T approaches $T^r \simeq 298.00$ K, which is consistent with the conventional XY model [2–6]. The full line corresponds to the least-squares fit of the experimental data, according to $\gamma = D\exp[-a(T^r - T)^{-1/2}]$ ($D \simeq 24.0$, $a = 3.62$).

vanishes continuously if T approaches T^r from below Actually this is in agreement with the KT-type of roughening transition Obviously, it shows from both cases that the critical behavior of the roughening transition of the faces {110} of n-$C_{25}H_{52}$ crystals is solvent dependent This implies that n-hexane and toluene molecules have a different influence on the solid surface. This influence determines the character of the roughening transition of the {110} surfaces of paraffin crystals. We note that if the first-order roughening transition was quite unexpected, then the observed solvent-dependent critical behavior of the roughening transition is more surprising and of great theoretical and practical interest. To the best of our knowledge this has never been observed before

The solvent-dependent critical behavior of surface roughening may be associated with a so-called surface structural phase transition It is well known that crystals of n-paraffin exhibit an α-β solid-solid phase transition [18,19] before melting (in fact, this corresponds to three successive solid-solid phase transitions [19]). In the low-temperature phase (β phase) n-paraffin molecules are perfectly situated in the structural sites. When the α-β phase transition occurs, motions of extended paraffin chains with a component in the chain direction become active. This then causes the change of the solid-solid interaction energies [19–23]. It is noted that the α-β phase transition temperature T^{tr} will be lowered considerably if a small amount of a homologue of n-paraffin is incorporated into the crystal structure [19–23]. This means that paraffinlike impurities can promote this phase transition. When n-paraffin crystals are grown from n-hexane solutions, n-hexane molecules cannot be incorporated into the crystal structure. However, those paraffinlike n-hexane molecules can definitely affect solid paraffin molecules on the surface. This may result in the occurrence of a surface structural phase transition (similar to the α-β phase transition in the bulk) at a temperature much lower than T^{tr}. The surface structural phase transition has been indirectly justified by scanning tunneling microscopy experiments in the n-paraffin solution system (work in progress) and the 1-dodecanol system [24]. We notice that the tendency of the KT type of roughening may also be one of the factors which induce the surface structural phase transition. (This can be seen from the fact that the actual roughening temperature is very close to the estimated roughening temperature of the KT type.) It follows that the coupling of the KT type of roughening with the surface structural phase transition results in the first-order roughening transition.

Toluene molecules are not paraffinlike. In this case solvent molecules have a negative influence on the solid surface [25]. When n-paraffin crystals are grown from toluene solutions, a similar structural phase transition on the surface as described above cannot be promoted. Therefore the conventional KT-type roughening phase transition results.

The first author would like to thank Shell Netherlands B.V. for the financial support of this work. We acknowledge Dr. H. Meekes for helpful discussions and a critical reading of the manuscript.

[1] W. K. Burton, N Cabrera, and F C. Frank, Philos. Trans. R. Soc. A 243, 299 (1951)
[2] L. Onsager, Phys Rev 65, 117 (1944)
[3] J. M. Kosterlitz and D. J. Thouless, J Phys. C 6, 1181 (1973); 7, 1046 (1974).
[4] P. E. Wolf, F Gallet, S Balibar, E. Rolley, and P Nozières, J. Phys. (Paris) 46, 1987 (1985); F Gallet, P Nozières, S. Balibar, and E. Rolleys, Europhys. Lett. 2, 701 (1986).
[5] H. J. F Knops, Phys. Rev. Lett. 39, 766 (1977)
[6] J. V. Jose, L. P. Kadanoff, S. Kirkpatrick, and D R. Nelson, Phys. Rev. B 16, 1217 (1977)
[7] F Gallet, S. Balibar, and E. Rolley, J Phys. (Paris) 48, 369 (1987).
[8] J. E. Avron, L. S. Balfour, C. G. Kuper, J. Landau, S G Lipson, and L. S. Schulman, Phys Rev Lett. 45, 814 (1980)
[9] S. G. Lipson and E. Poltural, in *Progress in Low Temperature Physics*, edited by D. F. Brewer (Elsevier, Amsterdam, 1987), p. 127.
[10] J. P van der Eerden, in *Morphology and Growth Unit of Crystals*, edited by I Sunagawa (Terra Sci., Tokyo, 1989), p. 37
[11] J P van der Eerden, P Bennema, and T A. Cherepanova, Prog Cryst Growth Charact. 1, 219 (1978)
[12] T. Ohachi, in *Morphology and Growth Unit of Crystals* (Ref. [10]), p. 17
[13] M. Elwenspoek and J. P. van der Eerden, J. Phys. A 20, 669 (1987).
[14] X Y Liu and P. Bennema, J. Cryst. Growth 128, 69 (1993).
[15] X. Y. Liu, P Bennema, and J. P van der Eerden, Nature (London) 356, 778 (1992).
[16] A. E. Smith, J. Chem. Phys. 21, 2229 (1953).
[17] P. Bennema, X Y Liu, K. Lewtas, R D Tack, J. J. M. Rijpkema, and K. J. Roberts, J. Cryst. Growth 121, 679 (1992).
[18] M. G. Broadhurst, J. Res. Natl. Bur. Stand. A 66, 241 (1962).
[19] B. Ewen, G. R. Strobl, and D. Riciter, Faraday Discuss. Chem. Soc. 69, 19 (1980).
[20] B. G. Sumpter, D W. Noid, and B. Wunderlich, J. Chem Phys. 93, 6875 (1990).
[21] B G. Sumpter, D. W Noid, and B. Wunderlich, Macromolecules (to be published)
[22] S. Blasenbrey and W Pechhold, Rheol. Acta 6, 174 (1967).
[23] W. Pechhold, W. Dollhopf, and A. Engel, Acustica 17, 61 (1966)
[24] Y. H. Yeo, G. C. McGonigal, and D. J. Thomson, Langmuir 9, 649 (1993)
[25] X. Y Liu and J. Faber (to be published)

Chapter 3.4

Surface roughening of n–paraffin crystals and the coupled Ising–SOS model

Xiang–Yang Liu [a], H J F Knops [b], P Bennema [a], P van Hoof [a] and J Faber [a]

[a] *RIM, Department of Solid State Chemistry, Faculty of Science, University of Nijmegen, Toernooiveld 1, 6525 ED Nijmegen, The Netherlands*

[b] *Department of Theoretical Physics, Faculty of Science, University of Nijmegen, Toernooiveld 1, 6525 ED Nijmegen, The Netherlands*

ABSTRACT–The equilibrium structure of the solid–fluid interface undergoes a phase transition from a flat mode to a rough mode if the temperature increases to a critical value (the so–called roughening temperature) At the roughening temperature T_r, the free energy γkT required to form a step on crystal surfaces vanishes Here we describe the solvent–dependent critical behavior of $\gamma(T)$ in the neighborhood of T_r, occurring in odd n–paraffin crystal systems Our experiments indicate that the step free energy of the {110} faces of the crystals grown from paraffin–like solutions vanishes discontinuously at T_r, implying the occurrence of a first–order roughening transition When some non paraffin–like solvents are chosen, the behavior of $\gamma(T)$ is like a "Kosterlitz–Thouless" type of roughening, showing a continuous phase transition at T_r These unusual phenomena may be related to a so–called surface structural phase transition, and can be interpreted based on a coupled Ising–SOS model

The roughening transition is a type of phase transition which takes place on the crystal surface at the roughening temperature T_r. This phase transition can be generally characterized by the step free energy (per structural unit) γkT (where k is the Boltzmann constant, T is the temperature). Below T_r, due to the existence of γkT (or two-dimensional nucleation barrier), the crystal surface will keep its overall flatness corresponding to the orientation (hkl). Above T_r, the step free energy vanishes and steps or kinks exist on the surface permanently even without screw dislocations. It follows that the surface will become rough microscopically and its crystallographic orientation is lost.

The roughening transition has been investigated in great deal by computer simulations [1-2], based on the so-called solid-on-solid (SOS) interfacial model [3]. This model is a generalization of the Ising model, where the crystal surface is considered as a collection of interacting columns. The Hamiltonian of this model system can be taken as

$$\mathcal{H} = J \sum_{<ij>} |h_i - h_j|^2 \tag{1}$$

(Here J is the step energy per unit length, and the column heights, h_i, are restricted to integer values.) This most simple model is well understood since the relationship with the planar XY model has been established [4-5]. It follows that the roughening transition described in this model is of the Kosterlitz-Thouless (KT) type (or a phase transition of infinite order)[6], which is characterized by the step free energy γ which vanishes continuously

$$\gamma \sim D\exp[-\alpha'(T_r - T)^{-1/2}], \quad \text{as } T \to T_r \ (T < T_r) \tag{2}$$

(D and α' are coefficients, depending on the system). This type of roughening transition has been confirmed experimentally for crystals consisting of simple molecules, such as ^{4}He and ^{3}He crystals [7-9]. Here the question which will be discussed is how a roughening transition occurs in more complex molecular systems such as n-paraffin crystals.

The key step to identify the character of the roughening transition is to study the critical behavior of $\gamma(T)$ around the roughening temperature T_r. In our investigations, $\gamma(T)$ is determined using a technique based on an established relation between the critical supersaturation of kinetic roughening and the step free energy γ [10-11].

Kinetic roughening is a cross-over transition which occurs in a supersaturated environment when $T < T_r$. At a relatively small supersaturation σ ($\sigma = \Delta\mu/kT$, where $\Delta\mu$ is the difference in chemical potential between solid and fluid particles), a faceted growth of a crystal face occurs due to a 2D nucleation barrier ($\gamma > 0$). In case $\sigma > \sigma^c$ (σ^c is a critical

supersaturation), the critical size of 2D nuclei become so small that the 2D nucleation barrier vanishes due to thermal fluctuation Then the originally flat surface becomes kinetically rough, and the so–called kinetic roughening occurs (Note that in contrast to kinetic roughening, the roughening transition takes place at equilibrium, and is a real phase transition) In connection with the step free energy, the critical supersaturation of kinetic roughening σ^c can be expressed as a function of γ [11], by

$$\sigma^c = f\gamma^2 \tag{3}$$

where f is a constant determined by the surface structure [11] This implies that γ can be determined by measuring σ^c

In the experiments, the supersaturation of a solution with a certain concentration can be obtained by cooling the solution from its equilibrium temperature T_s to a lower temperature T, according to the following relation [12]

$$\sigma \simeq (\Delta h^{diss}/RT_s^2)(T_s - T) \tag{4}$$

(Here Δh^{diss} is the molar dissolution enthalpy R is the gas constant) For a solution system with $T_s < T_r$, the kinetic roughening occurs at a certain temperature $T = T^c$ ($T^c \leq T_s$) where $\sigma = \sigma^c$ This means that σ^c can be obtained from measuring ΔT^c ($= T_s - T^c$) Starting with solutions having different T_s [a set of (σ^c, T) will be obtained from each solution], a curve $\sigma^c(T)$ is then obtained, which can be converted to $\gamma(T)$ according to Eq (3) Since the morphology of crystals is affected in a subtle way by kinetic roughening, ΔT^c (or σ^c) can be determined within the accuracy limit of the temperature measurements for our experimental system (the uncertainty is less than 0 005K) [13] For more details, see Refs 12–14

Crystals of odd–numbered n–paraffins which are in the low temperature phase are platy and lozenge–shaped (See Fig 1) In the following, our attention will be devoted to the side faces {110} of n–paraffin crystals, which are grown from various solutions

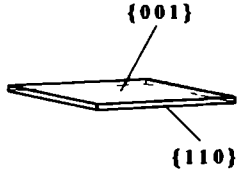

FIG 1 The morphology of odd–numbered n–paraffin crystals Crystals of the n–paraffins in the low temperature phase have the space group symmetry P_{bcm} [15] Theoretical analysis and observations [16] indicate that the crystals are platy and lozenge–shaped, confined by the large {001} faces on the top and the bottom and the narrow side faces of {110}

First we will explore the cases that n–$C_{25}H_{52}$ crystals grow from two different types of solution systems (see Fig 2) It is found that for n–$C_{25}H_{52}$ crystals growing from n–hexane solutions (indicated by curve 1), the value of γ remains constant with increasing temperature (meaning that the step entropy $s = -\mathrm{d}\gamma/\mathrm{d}T \simeq 0$) At $T = T_r$, γ vanishes abruptly The first derivative of γ with respect to T shows a singularity at $T = T_r$, implying the occurrence of a first–order roughening transition In case that toluene is chosen as the solvent, a completely different behavior of $\gamma(T)$ is observed (see curve 2 in Fig 2) In this case, the step free energy γ decreases with increasing T, and vanishes continuously as T approaches T_r from below Actually, this is in agreement with the KT–type of roughening transition (see the caption of Fig 2)

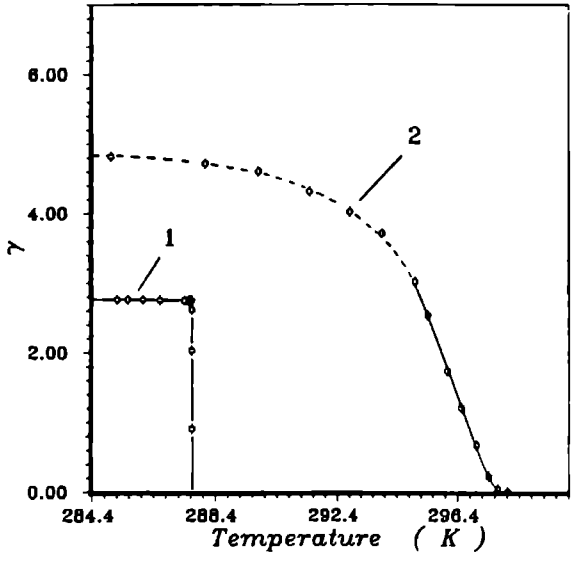

FIG 2 The step free energy γ as a function of temperature T for the {110} faces of n–$C_{25}H_{52}$ crystals in n–hexane and toluene solutions Curve 1 n–$C_{25}H_{52}$ crystals growing from n–hexane solutions The $\gamma(T)$ curve has the shape of a step function, suggesting the first ordering roughening transition of the system ($T_r \simeq 287\ 64$ K) Curve 2 n–$C_{25}H_{52}$ crystals growing from toluene solutions γ vanishes smoothly when T approaches $T_r \simeq 298\ 00$ K, which is consistent with the conventional XY model The full line in curve 2 corresponds to the least–square fit of the experimental data, according to Eq (2) ($D \simeq 24\ 0$, $\alpha' = 3\ 62$) Note that the values of γ are derived from the experimental data σ^c, according to Eq (3)

TABLE 1. The main characters of roughening transition for different odd n–paraffin crystals growing from various solutions

Systems	T_r (K)	Type of Roughening Transition
n–C_{21}/n–hexane	273 25	First order
n–C_{23}/n–hexane	283 80	First order
n–C_{25}/n–hexane	287 64	First order
n–C_{25}/iso–octane	292 77	First order
n–C_{25}/toluene	298 00	Infinite order
n–C_{25}/1–butanol	299 85	Infinite order

Note. these experimental data were measured using the same experimental technique

The above–mentioned results show that the critical behavior of the roughening transition for the faces {110} of n–$C_{25}H_{52}$ crystals is solvent dependent This behavior turns out to be typical for odd n–paraffin crystals growing from various solutions In Table 1, the main characters of roughening transitions for n–$C_{21}H_{44}$, n–$C_{23}H_{48}$ and n–$C_{25}H_{52}$ crystals growing from various solutions are summarized From these results, we can roughly classify the solvents in two types The solvents of type I include n–hexane and iso–octane These solvent molecules have an elementary molecular structure similar to solute n–paraffin molecules (such as the groups of CH_2 and CH_3) The solvents of type II include toluene and 1–butanol These solvent molecules have a special functional group (such as a hydroxyle group OH) or a large Π bond within the molecules, which makes them different from n–paraffin molecules Obviously, these two types of solvent molecules have a different influence on the crystal surface

The cross–over from a KT–type of transition to a first–order transition cannot be interpreted on the basis of the simple SOS model Virtually, a molecule is simplified into a structureless block in the SOS model When some internal motional freedom of molecules is active under certain conditions, the SOS model is not adequate any more It needs to be coupled with the internal motion of the molecules

We suppose that the first–order roughening transition is associated with a so–called surface structural phase transition, which is related to the activation of some internal

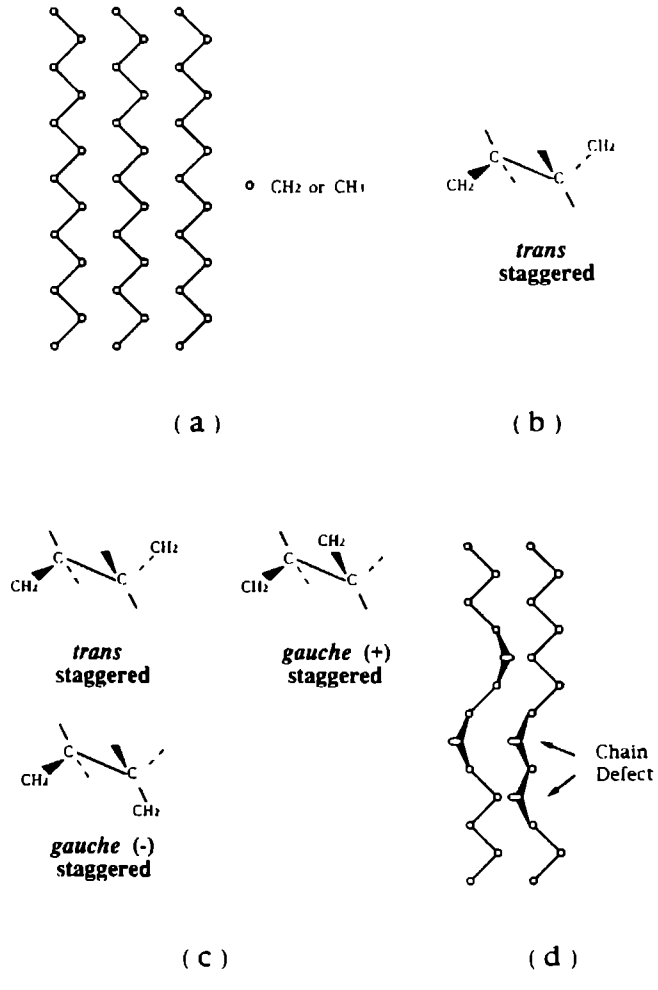

FIG.3. Illustration of the packing of n–paraffin molecules and different conformations of n–paraffin chains in different phases. (a) In the β phase, n–paraffin molecules are situated perfectly in the structure. (b) The *trans*–conformation is the only one in the β *phase. (c) All* the *trans*–, the *gauche*(+)– and the *gauche*(–)–conformation are possible in the α *phase (d)* In the α phase, interchain defects occurs in the n–paraffin molecules.

motional freedom of the interfacial solid molecules It is well known that bulk crystals of n–paraffins exhibit an α–β solid–solid phase transition at a temperature T^{tr} slightly below the melting temperature [17-18] In the low temperature (β or rigid phase) phase, n–paraffin molecules are perfectly situated on structural sites (see Fig 3a), having the most stable conformation the *trans*–conformation (see Fig 3b) When the α–β phase transition occurs, the rotation around C–C bonds in the paraffin chains becomes possible Then the less stable *gauche*–conformations together with the *trans*–conformation become occupied (see Fig 3c) This leads to the formation of interchain defects of the molecules in the high temperature (α or non–rigid) phase (see Fig 3d) Further, T^{tr} will be lowered considerably if a small amount of neighboring homologue of n–paraffins is incorporated into the crystal structure [20-21] This implies that paraffin–like impurities can promote this phase transition When n–paraffin crystals are grown from the solutions of type I, the solvent molecules cannot be incorporated in the crystal structure However, these paraffin–like solvent molecules can definitely affect solid paraffin molecules on the surface This may result in the occurrence of a *surface* structural phase transition (similar to the α–β phase transition in the bulk) at a temperature T^{tr}_{surf} much lower than T^{tr} This surface structural phase transition has been indirectly confirmed by our scanning tunneling microscopy (STM) experiments It is shown in our STM experiments that under a certain condition, the monolayers of paraffin molecules adsorbed at the interface between paraffin like organic solution and basal phase of graphite display a high degree of ordering and orientation similar to paraffins in the β crystal phase Consider these adsorbed paraffin molecules as analogous to solid paraffin molecules at the surface It is found that above a certain temperature T^{tr}_{surf} ($T^{tr}_{surf} < T^{tr}$) some changes in the molecular structure of the adsorbed paraffin molecules, which correspond to the α–β transition, can be imaged This evidently indicates the occurrence of the surface structural phase transition (work in progress)

Solvent molecules of type II are not paraffin–like According to our recent investigations based on the self–consistent field theory [22], those solvent molecules have a negative effect on the solid surface They are mutually associated at the solid–fluid interface These eventually hinder the occurrence of the surface structural phase transition Consequently, the conventional KT–type of roughening occurs

As explained above, a model that is able to capture the cross–over from KT–type of roughening to a first–order roughening should at least contain degrees of freedom connected to the possible α–β surface structural phase transition Let us introduce as an order parameter for this transition $t \equiv <t_1>$, where $t_1 \equiv 1$ for a "rigid" molecule and $t_1 \equiv 0$ for a molecule where one or more *gauche*–conformations are occupied We propose as (the most simple) model Hamiltonian

$$\mathcal{H} = u(T)\sum_{i} t_i - \sum_{<ij>} K t_i t_j + \sum_{<ij>} [J + L t_i \Theta(h_i - h_j) + L t_j \Theta(h_j - h_i)]\,|h_i - h_j|^2 \tag{5}$$

(details of our analysis will be published elsewhere [23]) In the first term $\exp[-u(T)/kT]$ designates the Boltzmann weight for finding a molecule in a rigid state When the activation energy for the transition from the *trans*– to the *gauche*–conformation is Δ', one finds [23] for a chain of length N

$$u(T) = kT \ln\{[1 + 2\exp(-\Delta'/kT)]^N - 1\} \tag{6}$$

The second term represents the decrease in rotational energy when two neighboring molecules are in the rigid state The last term finally represents the step energy which depends on the state of the molecule sitting at the edge, it is J for a non–rigid molecule but higher $J + L$ for a rigid molecule

A qualitative analysis of this model is simple For more details, see Ref 23 The transformation $t_i = 0\,5(1 + s_i)$ with $s_i = \pm 1$ transforms this model to a coupled Ising–SOS model in a field $\mathcal{H} = -0\,5u(T) + 0\,25qK$ (q is the coordinate number) A first order α–β transition is found at the temperature T^{tr} where $\mathcal{H}$ vanishes i e $u(T) = 0\,5qK$ [The location of this point can be shifted to some extent by field like terms from the third term in (5)] Let us now estimate the effective step energy J_{eff} from the excess free energy of an interface where a single, infinitely long, straight step is present At $T < T^{tr}_{surf}$ the bulk of the surface is in the $t = 1$ phase, molecules at the step experience however a negative field $\mathcal{H} - J$ and may therefore be either in the $t = 0$ or in the $t = 1$ phase In the first case the excess energy is the interface energy $I(K)$ between a surface with $t = 1$ and a boundary line at the step with $t = 0$, in the second case the excess is L Of course the lower of the two will prevail So one has

$$J_{eff} = J_1 \equiv J + \min\{L, I(K)\} \tag{7}$$

for $T < T^{tr}_{surf}$ For $T > T^{tr}_{surf}$ both the bulk and the edge will be in the $t \simeq 0$ phase and one has $J_{eff} = J$ Since T^{tr}_{surf} will depend via Δ' on the type of solvent used, this explains our experimental findings a KT–type transition when $T^{KT}_{r} = J_1/C \leq T^{tr}_{surf}$ (C is a constant, $C \simeq \pi/4$) but a first–order roughening transition at T^{tr}_{surf} when this inequality is reversed

ACKNOWLEDGEMENT

Two of us (X Y L & P B) would like to thank Shell Netherlands B V for supporting this work

REFERENCES

1 Jan der Eerden, J P , Bennema, P & Charepanova, T A *Prog Cryst Growth Charact* 1, 219–254 (1978)
2 Gilmer, G H & Jackson, K A in *Current Topics in Material Sci* (ed Kaldis, E) pp 80 –114 (North–Holland, Amsterdam, 1977)
3 Muller–Krumbhaar, H in *Current Topics in Material Sci* (ed Kaldis, E) pp 115–139 (North–Holland, Amsterdam, 1977)
4 Knops, H J F *Phys Rev Lett* **39**, 776–769 (1977)
5 Jose, J V *et al. Phys Rev* **B16**, 1217–1240 (1977)
6 Kosterlitz, J M & Thouless, D J *J Phys* **C6**, 1181–1203 (1973), *J Phys* **C7**, 1046–1060 (1974)
7 Gallet, F , Balibar, S & Rolley, E *J Physique* **48**, 369–377 (1987)
8 Avron, J E *et al Phys Rev Lett* **45**, 814–817 (1980)
9 Lipson, S G & Poltural, E in *Prog in Low Temp Phys* (ed Brewer, D F) pp 127–188 (Elsevier, Amsterdam, 1987)
10 Elwenspoek, M & van der Eerden, J P *J Phys* **A20**, 669–678 (1987)
11 Liu, X Y & Bennema, P *J Cryst Growth* **128**, 69–73 (1993)
12 Liu, X Y *Phys Rev* **B48**, (1993) (in press)
13 Liu, X Y , Van Hoof, P & Bennema, P *Phys Rev Lett* **71**, 109 (1993)
14 Liu, X Y , Bennema, P & van der Eerden, J P *Nature* **356**, 778–780 (1992)
15 Smith, A E *J Chem Phys* **21**, 2229–2231 (1953)
16 Bennema, P *et al J Cryst Growth* **121**, 679–696 (1992)
17 Broadhurst, M G *J Res Nat Bur Standards* **66A**, 241–249 (1962)
18 Ewen, B , Strobl, G R & Ricnter, D *Faraday Discuss Chem Soc* **69**, 19–31 (1980)
19 Sumpter, B G , Noid, D W & Wunderlich, B *J Chem Phys* **93**, 6875–6889 (1990)
20 Blasenbrey, S & Pechhold, W *Rheologica Acta* **6**, 174–185 (1967)
21 Pechhold, W , Dollhopf, W & Engel, A *Acustica* **17**, 61–72 (1966)
22 Liu, X Y & Faber J *Phys Rev* **E** (submitted)
23 Knops, H J F , Liu, X Y & Bennema, P , (to be submitted)

Chapter 3.5

JOURNAL OF CRYSTAL GROWTH

Kinetic roughening in relation to the roughening transition in odd-numbered alkane crystals

Xiang-Yang Liu and P. Bennema

RIM, Laboratory of Solid State Chemistry, Faculty of Science, University of Nijmegen, Toernooiveld, 6525 ED Nijmegen, Netherlands

In this paper kinetic roughening and thermal roughening are compared with each other in a quantitative way. First a non-equilibrium condition recipe is introduced to describe the shape of a 2D nucleus. After defining a proper criterion for the occurrence of kinetic roughening, a relation between critical supersaturations σ^c and the edge free energy γkT is derived. In comparison with the data of the roughening transition obtained from some n-paraffin–n-hexane solution systems, it is found that the relation between σ^c and the edge free energies γ_e and γ_v of a rectangular nucleus on surfaces is in very good agreement with experimental data.

1. Introduction

The roughening transition and kinetic roughening are two most important concepts in the theory of crystal surfaces and crystal growth. These concepts explain a lot of observed crystal growth phenomena [1]. First, the growth kinetics changes at the critical points of the roughening transition and kinetic roughening. Secondly, the roughening temperature T_r and the values of critical supersaturation σ^c reflect the physical state of a surface. Essential relation between the roughening transition and kinetic roughening can be derived on the basis of the order parameter: the edge free energy (per growth unit) γkT on crystal surfaces (k and T are the Boltzmann constant and the absolute temperature, respectively). According to the solid-on-solid (SOS) model or the XY model [1–7], γ will continuously vanish at T_r if T approaches T_r from below. When crystal growth occurs at $T < T_r$, a 2D nucleation barrier exists since $\gamma > 0$. Then we have a flat surface at equilibrium or a small supersaturation σ ($\sigma = \Delta\mu/kT$, $\Delta\mu$ is the chemical potential difference between the solid and the liquid phase). As soon as $\sigma > \sigma^c$, the nucleation barrier breaks down, and kinetic roughening occurs.

In a recent survey [8], Elwenspoek and Van der Eerden proposed a relation between σ^c and γ. Using this relation to locate T^r seems in satisfactory agreement with computer simulation results. However, for a system with highly anisotropic interactions between structural units, the estimated values of γ greatly deviate from real values of γ.

In this paper we attempt to derive a proper relation between σ^c and γ, taking the anisotropy of a surface and the shape of growth units into account. In section 2, we will try different approaches and criteria to derive the relation between σ^c and γ. In section 3, a comparison between theory and experiments is made, and finally conclusions can also be found in this section.

2. Two-dimensional nucleation models and kinetic roughening

We first define the normalized length of an edge in the direction i: $L_i' = L_i/l_i$. L_i represents the actual length in the direction and l_i the dimension of a structural unit in the corresponding direction. According to thermodynamics, the

formation of a 2D solid nucleus with a (normalized) perimeter $L'_n(n)$ and a surface area $S(n)$ in a solid–fluid interface will cause the change of Gibbs free enthalpy in the system

$$\Delta G = L'_n(n)\gamma kT - \Delta\mu\, S(n)/s_0, \qquad (1)$$

where s_0 is the surface area per structural unit and n the number of molecules per nucleus As a crystal, the external shape of a 2D nucleus may be determined by different physical factors Now we employ the following two recipes to describe the shape of a 2D nucleus

(i) The equilibrium condition

$$\frac{D_i}{\gamma_i/l_i} = \frac{D_j}{\gamma_j/l_j} = \frac{D_k}{\gamma_k/l_k} = \quad = \text{constant} \qquad (2)$$

The subscripts k, j, k, represent certain orientations of edges and D is the distance from an edge to the center of the nucleus This condition in fact is the expression of the well known Gibbs–Wulff theorem [9,10] in the 2D space

(ii) The non-equilibrium condition

$$D_i/\gamma_i = D_j/\gamma_j = D_k/\gamma_k = \quad = \text{constant} \qquad (3)$$

Note that this non-equilibrium condition recipe is an ad hoc presupposition, and for the first time introduced here in this paper It is in fact the 2D analogy of the ad hoc recipe used in the description of 3D growth forms according the Hartman–Perdok theory [11] In this theory it is assumed that $R_i \sim E_i^{att}$ In reality, many complex 2D lattices or connected nets can be simplified to rectangular lattices or connected nets, based on certain empirical regulations We will discuss this issue later in section 3 1 For a rectangular lattice, 2D nuclei have the rectangular shape at a low temperature, and gradually change to the elliptic shape with increasing T [12,13] In the following we will treat these two types of nuclei separately as two extreme cases

2 1 *The rectangular nucleus approach*

Now let us look at a solid surface with a rectangular lattice (see fig 1) A nucleus formed in this surface has the rectangular shape, and correspondingly eq (1) is expressed as

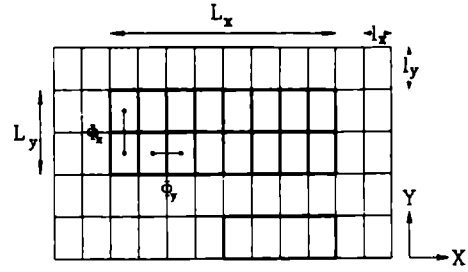

Fig 1 Schematic drawing of a solid surface with a rectangular lattice

$$\Delta G = 2kT(\gamma_x L'_x + \gamma_y L'_y) - L'_x L'_y \Delta\mu \qquad (1a)$$

Defining the anisotropic factor of interaction energies $\delta = \gamma_y/\gamma_x$ (assume that $\gamma_y > \gamma_x$) and the geometric factor of a molecule $\eta = l_y/l_x$, the equilibrium condition in this case can be written as

$$L'_x/L'_y = \gamma_y/\gamma_x = \delta, \qquad (2a)$$

and the non-equilibrium condition as

$$L'_x/L'_y = \eta\delta \qquad (3a)$$

Obviously, when we let $\eta = 1$, the non-equilibrium condition is converted into the equilibrium condition Therefore in this section and the following sections we will focus only on the non-equilibrium condition The corresponding consequences for the equilibrium condition can be obtained by setting $\eta = 1$ in the results obtained from the non-equilibrium condition

To maximize ΔG we now introduce a constraining relation $g = L'_x - \eta\delta L'_y = 0$, and a modified function $F = \Delta G + \lambda g$ Then solving the following simultaneous equations,

$$\partial F/\partial L'_x = 0, \quad \partial F/\partial L'_y = 0, \quad g = 0, \qquad (4)$$

we obtain the expressions for the critical size of the nucleus

$$L'^*_y = \gamma_x(1+\eta)/\eta\sigma, \quad L'^*_x = \gamma_y(1+\eta)/\sigma, \qquad (5)$$

and for the critical value of ΔG

$$\Delta G^* = (1+\eta)^2 \gamma_y \gamma_x kT/\eta\sigma, \tag{6a}$$

or

$$\Delta G^* = 4\tilde{\gamma}^2 \xi_{rec} kT/\sigma \tag{6b}$$

Here we define the shape factor ξ_{rec} as $\xi_{rec} = (1+\eta)^2/4\eta$, and the average edge free energy $\tilde{\gamma}$ as $\tilde{\gamma} = \sqrt{\gamma_x \gamma_y} = \gamma_x \sqrt{\delta}$ Explicitly for structural units with the square or circular shape, $\eta = 1$ and $\xi_{rec} = 1$

2 2 *The elliptic nucleus approach*

First we postulate that for an elliptic nucleus the two main axes $2a \sim L_x$ and $2b \sim L_y$ Then the normalized two main axes $2a' \sim L_x/l_x$ and $2b' \sim L_y/l_y$ In this case, eq (1) is expressed

$$\Delta G = L' kT\tilde{\gamma} - \pi a' b' \Delta\mu, \tag{1b}$$

where $L' \cong \pi[\frac{3}{2}(a'+b') - \sqrt{a'b'}]$ The non-equilibrium condition is given by

$$a'/b' = \eta\delta \tag{3b}$$

Based on eq (3b), maximizing ΔG with respect to a' yields the critical values

$$a'^* = \tilde{\gamma} E/2 \quad \sigma, \tag{7}$$

$$\Delta G^* = \pi \tilde{\gamma}^2 \xi_{ell} kT/\sigma, \tag{8}$$

where the shape factor $\xi_{ell} = \frac{1}{4}E^2/\eta\delta$ and $E = \frac{3}{2}(1+\eta\delta) - \sqrt{\eta\delta}$ For a circular nucleus $\eta = \delta = 1$, and then $\xi_{ell} = 1$

2 3 *Criteria for kinetic roughening*

To determine critical points where kinetic roughening occurs, Elwenspoek and Van der Eerden [8] introduced a demarcation criterion $\Delta G^*/kT = 1$ (which we call criterion 1 here) This criterion implies that when thermal energy kT is equal to or larger than the nucleation barrier, the crystal grows as if $\gamma = 0$, then the so-called kinetic roughening occurs Actually, this criterion is only valid for isotopic cases For anisotropic cases, referring to (3a) and (3b), this criterion should be modified as $\Delta G^*/kT = \eta\delta$ (which we call criterion 2) The isotropic case is involved in criterion 2 as a limiting case A qualitative discussion about criterion 2 will be given in section 3 2 In the following we will discuss the two criteria simultaneously Combining the expressions the eqs (6) and (8) with the two criteria, we consequently obtain the expressions of critical supersaturation for kinetic roughening, and summarize them in table 1

Table 1
The expressions of critical supersaturation σ^c for kinetic roughening

Models	Criterion 1	Criterion 2
The rectangular nucleus approach [a]	$\sigma^c_{rec\,1} = 4\tilde{\gamma}^2\xi_{rec}$	$\sigma^c_{rec\,2} = 4\tilde{\gamma}^2\xi_{rec}/\delta\eta$
The elliptic nucleus approach [a]	$\sigma^c_{ell\,1} = \pi\tilde{\gamma}^2\xi_{ell}$	$\sigma^d_{ell\,2} = \pi\gamma^2\xi_{ell}/\delta\eta$

[a] All the expressions listed here correspond to the non equilibrium condition Assuming $\eta = 1$ these formulas are automatically converted to those in the equilibrium condition

3. Surface structure and experimental verification

As analysed in the last section, we have already seen that the step free energy can be directly associated with the critical supersaturation of kinetic roughening In practice, one may ask which relation within the table 1 is the most realistic This will be discussed in this section

3 1 *Simplification of a complex net*

According to statistic mechanical models or interfacial Ising models, a flat face on a crystal corresponds to a connected net [1], where a two-dimensional array of nodes are connected to each other by important bonds This kind of net reflects the bond structure of the crystal surface, and determines the shape of a critical nucleus In many cases, however, connected nets are not rectangular In order to simplify a complex net to a rectangular net, we here introduce two empirical regulations

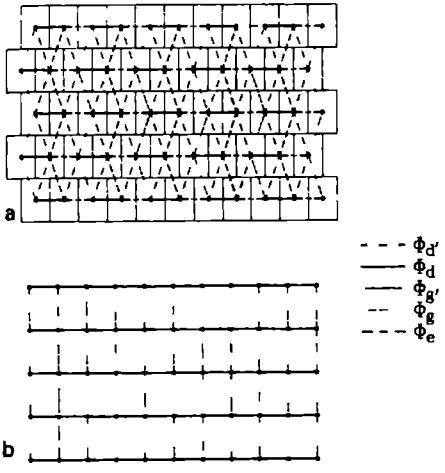

Fig 2 (a) The original bond structure of the {110} surfaces of odd numbered n paraffin crystals (b) The simplified bond structure of the surfaces

(1) Within an uninterrupted strong bond chain (or a PBC [11]), the weakest bond will decide the strength of the bond chain

(2) When a connected net contains more than two sets of PBC, the strongest two unparallel PBCs will decide the main character of the net

Now let us consider the {110} connected nets of n-paraffin crystals [14] (see fig 2a) This is hexagonal net containing five types of bonds The strength of these bonds are in the order of $\phi_d' > \phi_d \gg \phi_g > \phi_g > \phi_e$ Following the foregoing regulations, this net is simplified to a rectangular net consisting of only ϕ_d and ϕ_g (fig 2b) Comparing fig 1 with fig 2b it can be seen that $\phi_y = \phi_d$ and $\phi_x = \phi_g$

Table 2
The relevant factors and dimensionless edge energies for some n paraffin–n hexane solution systems

n Paraffins	δ	η	ϕ_y / kT [a]	ϕ_x / kT	$\phi = \sqrt{\phi_y \phi_x} / kT$
n-C_{11}	22 337	6 3765	2 2630	0 10176	0 47987
n-C_{23}	24 506	6 9439	2 3275	0 09497	0 45015
n-C_{25}	26 777	7 5114	2 3926	0 08934	0 46233

[a] Note that T is the actual temperature and under our experimental conditions is very close to the roughening temperature

3 2 Experimental comparison and discussion

The roughening transition of a flat crystal face can be characterized by a dimensionless temperature

$$\theta^r_{hkl} = 2kT^r/\phi_{str}, \tag{9}$$

where ϕ_{str} is the strongest bond energy at a surface Since for a given face, θ^r_{hkl} is fixed [1], then ϕ_{str} and the related edge energies can be measured by determining the roughening temperature Based on the calculated θ^r_{110} and the ratios of bond energies [14], and on the T^r data determined [15,16], we now list in table 2 the edge energies and factors δ and η for the {110} faces of n-$C_{21}H_{44}$, n-$C_{23}H_{48}$ and n $C_{25}H_{52}$ crystals in n-hexane solutions It has to be noted that due to the change of degrees of freedom of surface structure units, the roughening transition occurring in those n-paraffin systems belongs to the first order phase transition, other than the conventional infinite order phase transition [17,18] According to our results [18], this first order phase transition is in the neighbourhood of con-

Table 3
Comparison of the estimated critical values of kinetic roughening with experimental data (σ^c in %)

	Non equilibrium				Equilibrium				E_{exp} [a]
	$\sigma^c_{rec\,1}$	$\sigma^c_{rec\,2}$	$\sigma^c_{ell\,1}$	$\sigma^c_{ell\,2}$	$\sigma^c_{rec\,1}$	$\sigma^c_{rec\,2}$	$\sigma^c_{ell\,1}$	$\sigma^c_{ell\,2}$	σ^c
n C_{21}	197	1 39	5219	36 8	91 2	4 14	739	33 2	1 32
n C_{23}	201	1 18	6059	35 6	88 4	3 61	786	32 1	1 12
n C_{25}	206	1 03	6972	34 7	85.5	3 19	835	31 2	0 984

[a] These experimental data are corrected by considering the effect of resistances against volume transport For more details we refer to ref [16]

ventional infinite order roughening transition, then we can still use eq (9) to evaluate ϕ_{str}. In addition, we know that in this system $\gamma_i \simeq \phi_i/kT$, since the edge entropy does not play any role with increasing T [17]. Thus using the data in table 2, the values of σ^c estimated on the basis of the formulas in table 1 are given in table 3, together with the actual data determined from experiments [16]. It is found that $\sigma^c_{rec\,2}$ under non-equilibrium conditions is surprisingly close to experimental results. This is quite reasonable, because when kinetic roughening occurs, the system always diverges from equilibrium. Besides, it can be seen from table 3 that the rectangular shape is favoured for nuclei of critical sizes at points of kinetic roughening. Moreover, this result indicates that criterion 2 is the most realistic one for all cases. Looking at (6) (and (8)) and fig 1, we can easily see that causing kinetic roughening, critical sizes of anisotropic nuclei will be $\delta\eta$ times larger than those of isotopic nuclei. This may be because as soon as the shorter edges of critical anisotropic nuclei are of the same size as the edges of critical isotropic (cubic) nuclei, the thermal energy is already sufficient to cause the collapse of the 2D nucleation barrier of anisotropic surfaces. This results in the transition from flat faces to stepped faces (rough faces). Therefore the critical size of anisotropic nuclei is $\delta\eta$ times larger than isotropic ones. Assuming $\gamma_x\gamma_y$ = constant, for crystals with highly anisotropic interactions between building units (such as many organic crystals), σ^c will be $\delta\eta/\xi_{rec}$ times lower than in isotropic cases, and kinetic roughening is easily observed. We notice that a similar conclusion is drawn from the results of computer simulations [19].

Acknowledgements

We thank Mr J. van Kessel for making drawings and Shell Netherlands BV for financial support.

References

[1] P Bennema and J P van der Eerden, in Morphology of Crystals, Part A, Ed I Sunagawa (Terra, Tokyo 1987) p 1
[2] H van Beijeren, Phys Rev Letters 38 (1977) 993
[3] J P van der Eerden and H J F Knops Phys Letters A66 (1978) 334
[4] D E Temkin, in Crystallization Processes (Consultants Bureau, New York, 1966)
[5] J M Kosterlitz and D J Thouless, J Phys C 6 (1973) 1181
[6] J M Kosterlitz, J Phys C 7 (1974) 1046
[7] P Nozieres and F Gattet J Physique 48 (1987) 353
[8] M Elwenspoek and J P van der Eerden, J Phys A 20 (1987) 669
[9] S Toschev, in Crystal Growth An Introduction Ed P Hartman (North Holland Amsterdam 1973) p 328
[10] P Bennema, in Crystal Growth An Introduction Ed P Hartman (North Holland Amsterdam 1973) p 358
[11] P Hartman, in Morphology of Crystals Part A, Ed I Sunagawa (Terra, Tokyo 1987) p 271
[12] W K Burton, N Cabrera and F C Frank Nature 163 (1949) 398
[13] C van Leeuwen, PhD Thesis, Delft University of Technology (1977)
[14] P Bennema, X Y Liu K. Lewtas, R O Tack, J J M Rijpkema and K J Roberts, J Crystal Growth 121 (1992) 679
[15] X Y Liu and P Bennema, J Crystal Growth, submitted
[16] X Y Liu, G Arkenbout, P Bennema and P van Hoof J Crystal Growth to be published
[17] X Y Liu, P Bennema and J P van der Eerden Nature 356 (1992) 778
[18] X Y Liu, to be published
[19] J P van der Eerden, C van Leeuwen and P Bennema J Appl Phys 48 (1977) 2124

Chapter 3.6

Detailed observations on the roughening transition and the influence on morphology of crystals

Xiang–Yang Liu and P Bennema

RIM, Laboratory of Solid State Chemistry, Faculty of Science, University of Nijmegen, Toernooiveld, 6525 ED Nijmegen, The Netherlands

ABSTRACT–The theory of roughening transition is applied to crystals of odd numbered n–paraffins. Based on the fact that rough faces grow faster than flat faces, a criterion, taking the rate of growth of faces proportional to the reciprocal difference the roughening temperature and the actual temperature, is proposed to predict growth forms of n–paraffin crystals. The constructed crystal forms have a platy, lozenge shape, and are bounded by the large faces {001} and the small narrow faces {110} The predicted morphology agrees well with the observed morphology Experimentally, the roughening transition and kinetic roughening were observed for the faces {110} of crystals of n–paraffins with 21 C atoms and 23 C atoms Correspondingly, the actual roughening transition temperatures of 273 27 ± 0 02 K and 283 8 ± 0 5 K were measured for crystals of those two paraffins, respectively It follows that the influence of the roughening transition on the morphology of crystals was carefully studied As a consequence, a kinetic phenomenon, the so–called " kinetic faceting ", was observed in the neighborhood of the critical point

I. INTRODUCTION

One of the key parameters in studying the process of crystal growth is the growth rate of a face (hkl). The morphology of a crystal is determined by the relative growth rates of faces $\{hkl\}$, in which the crystal is bounded by the slowest growing faces. Both external conditions (e.g. solvents, temperature, impurities) and structural factors (e.g. bond structure and dislocation density) determine the normal growth rate of a face (hkl), and hence the external shape of the crystal. From a point of view of the internal structure or the bond structure of a crystal, the classical theories, such as the Bravais–Friedel–Donnay–Harker (BFDH) theory [1] and the Hartman–Perdok theory [2], are to some extent able to describe growth forms of crystals grown from the vapor. However, in many cases, the morphology of crystals predicted by the above-mentioned theories shows some discrepancy with real crystals grown from solutions and from the melt [3]. The main reason is that the external factors are not taken into account.

We note that the concept of roughening transition is a very important concept for the growth of crystals [4-7]. It follows from the theory that faces $\{hkl\}$ parallel to connected nets [7] show a roughening phase transition at the roughening temperature T^r. This implies that if the actual temperature $T < T^r$, the edge free energy of a step γ is larger than zero and the surface will keep its overall flatness corresponding to the orientation (hkl). If $T \geq T^r$, $\gamma = 0$, and the crystallographic orientation is lost. Correspondingly, the surface will become rough due to statistical fluctuations. In case of growth, a face with $T_s < T^r$ (T_s is the saturation temperature) will grow by a layer mechanism (spiral growth or two-dimensional nucleation) and the overall orientation (hkl) is maintained. In contrast, a face with $T_s \geq T^r$ will grow in a rough mode.

If the supersaturation increases, the critical size of two-dimensional nuclei becomes so small that the 2D nucleation barrier vanishes. Again the surface becomes microscopically rough and macroscopically rounded. This is the so-called kinetic roughening. The effect is the same as thermal roughening. The cause, however, is different. Note that the roughening temperature is determined by the physical state of the solid–fluid interface. A change of the roughening temperature will correspond to a change either in external factors or in internal factors. Also, the morphology of crystals can be affected. From the point of view of equilibrium forms, if a crystal is bounded by flat faces, the sizes of the facets shrink if the temperature of the crystal increases, and each facet disappears at its own roughening temperature. So, equilibrium forms depend on the actual temperature in reference to the the roughening transition of facets. For growth forms of crystals, a rough face grows much faster than a flat face [8-9]. In case that competing flat faces occur, rough faces sooner or later

disappear from the growth form.

Experimental studies on the roughening transition and kinetic roughening have been carried out on several molecular crystals, such as ^{3}He, ^{4}He, and some organic crystals [10-16] However detailed observations on n–paraffin crystals and precise roughening temperatures of the crystals have not been reported In our previous papers [17-18], the morphology of odd numbered n–paraffin crystals was studied mainly from a theoretical point of view We will in this paper focus our attention on the phenomena of the roughening transition and the influence on the morphology of odd n–paraffin crystals

This paper is arranged as follows. In Sec. 2, the theoretical morphology of crystals in relation to the roughening transition is analyzed, and the applicability of a recipe to be defined below is investigated In Sec 3, experimental procedures are introduced Section 4 reports experimental experimental observations in detail A comparison between theoretical predictions and observed growth forms is made, and discussions are presented in Sec 5 Finally, a summary and conclusions are given in Sec 6.

II. THE THEORETICAL GROWTH FORMS RELATED TO THE ROUGHENING TRANSITION

In order to characterize the roughening transition, the following dimensionless temperatures are used,

$$\theta^r = (2kT^r/\phi_{str}), \tag{1a}$$
$$\theta^c = (2kT^c/\phi_{str}) \tag{1b}$$

Here k is the Boltzmann constant and T the temperature, ϕ_{str} the strongest bond energy at interfaces, θ^r the dimensionless roughening temperature for a particular surface, and θ^c is the dimensionless order–disorder phase transition temperature of a connected net It was Onsager who for the first time showed that an order–disorder phase transition occur in a connected net [19] Recently a method was developed to calculate the θ^c of complex nets for a given set of relative bond energies [7,17-18] Although the character of the roughening transition and the order–disorder phase transition are different, it is assumed [7] that

$$\theta^r \simeq \theta^c \tag{2}$$

Therefore, θ^c is used as an estimation of θ^r

Within the framework of interfacial cell models, the bond energies of a crystal graph ϕ_1

are defined as

$$\phi_i = \phi_i^{sf} - \tfrac{1}{2}(\phi_i^{ss} + \phi_i^{ff}) \tag{3}$$

Here the subscript i refers to the i^{th} interaction energy between a structure unit and its neighbors, superscript ss refers to a solid–solid bond, ff to a fluid–fluid bond and sf to a solid–fluid bond.

We note that in expression (1), the strongest bond in the crystal structure is taken as a reference. For a paraffin series, this bond energy depends on the carbon number of paraffins. Therefore for different paraffins the reference varies. In order to compare the roughening temperature for the whole paraffin series, we need to fix the reference. Here we introduce a modified dimensionless critical temperature $\theta^c_{hkl}(n)$ and a actual dimensionless temperature θ:

$$\theta^c_{hkl}(n) = \theta^c_{hkl}\phi_{str}(n)/\rho, \qquad \theta = 2kT/\phi^i_{str} \tag{4}$$

where $\phi_{str}(n)$ is referred to as the strongest bond at the solid–fluid interface (n is the carbon number of paraffins), and ϕ^i_{str} is the reference of bond energies and is fixed for the whole paraffin series. The factor ρ is introduced to keep $\theta^c_{hkl}(n)$ as a dimensionless temperature, and depends on the unit used for $\phi_{str}(n)$ [for instance, in this paper $\phi_{str}(n)$ is expressed in kJ/mol, so ρ is chosen to be equal to 1 kJ/mol]. We note that $\phi_{str}(n)$ for a given crystal depends directly on the mother phase. Then $\theta^c_{hkl}(n)$ depends also on the environment around the crystal.

It is known [7,18] that flat faces with the roughening temperature close to the actual temperature {i.e. the value of $[\theta^c_{hkl}(n) - \theta]$ is small} have a small edge free energy Then the energy barrier for the 2–dimensional nucleation is relatively low. Consequently the resistance against crystal growth (or surface integration) for those faces is small, and the growth will be relatively fast. On the other hand, flat faces with very high roughening temperatures have large values of $[\theta^c_{hkl}(n) - \theta]$. The edge free energy and the resistance against growth for those faces are very high and the growth rate is relatively low. Henceforth they grow much slower and will be dominant on crystal forms. For those faces with a rough interfacial structure $[\theta^c_{hkl}(n) - \theta \leq 0]$, the resistance against surface integration disappears since the edge free energy vanishes. The growth is then controlled by volume diffusion. So normally they grow much faster than flat faces, and will sooner or later disappear from crystal forms. Based on this idea, we introduce a recipe,

$$R_{hkl} \sim [\theta_{hkl}(n) - \theta]^{-1}, \tag{5}$$

to predict growth forms of crystals. Here R_{hkl} is referred to as the normal growth rate of $\{hkl\}$ faces. That there will be a parallel relation between R_{hkl} and $[\theta_{hkl}(n) - \theta]^{-1}$ is obvious. However, that there will be a strict proportional relation is an *ad hoc* assumption. We notice that contrary to the equilibrium form which can be logically derived from thermodynamic principles and applied to tiny crystals in thermodynamic equilibrium, for crystal growth forms no unambiguous recipes exist. In reality, growth forms of crystals are unique. However, theoretical idealized crystals forms may be constructed using *ad hoc* recipes. Such constructed growth forms still have an heuristic value. The recipe given by (5) is based on essential ideas of growth mechanisms in relation to thermal roughening. In the following it will be shown that notwithstanding the *ad hoc* character of the recipe, it works reasonably well.

Note that in this recipe, a negative value of R_{hkl} corresponds to rough growth. If this occurs, we will neglect such a face. It can be seen from expression (5) that for this recipe, the choice of θ is an essential step to predict growth forms. The value of θ depends on external conditions of crystal growth. To make a choice of θ, the following approximation is introduced

$$\theta = [\theta^{F}_{h_1k_1l_1}(n) + \theta^{R}_{h_2k_2l_2}(n)]/2. \tag{6}$$

Here the face $(h_1k_1l_1)$ is a flat face whose roughening temperature T^r is just above the actual temperature T. The face $(h_2k_2l_2)$ is the rough face next to the face $(h_1k_1l_1)$. The flatness of $(h_1k_1l_1)$ and the roughness of $(h_2k_2l_2)$ follow from observations.

For odd–numbered n–paraffin crystals, seven F–forms (for the definition of F–forms or F faces, see Ref.2) were identified from the crystal structure [17]. They are {001}, {110}, {111}, {010}, {011}, {100} and {101}.

In our experiments, $\theta^{F}_{h_1k_1l_1}(n) \simeq \theta^{F}_{110}(21)$, $\theta^{R}_{h_2k_2l_2}(n) \simeq \theta^{R}_{111}(21)$, for odd n–paraffin crystals grown from n–hexane solutions. Assuming that the strongest bond energy and the carbon number of paraffins have a relation of

$$\phi_{str}(n) \simeq an \tag{7}$$

(a is a constant), we evaluated the relative growth rates, $\tilde{R}_{hkl}$ ($\tilde{R}_{hkl} = R_{hkl}/R_{001}$), of all F faces (flat faces [2]) on crystals from n–C_{15} to n–C_{41}. The results are presented in Table I, together with the morphological importance order (MI order). (A face with a lower growth

rate is dominant in growth forms, and of higher morphological importance) MI is a relative statistic measure for the relative size or relative frequency of occurrence on growth forms

Table I Relative growth rates of form {*hkl*} on orthorhombic odd n–paraffin crystals, and the relative morphological importance of those forms

Paraffins	$\tilde{R}_{hkl}$ †				
	{001}	{110}	{111}	{010}	{011}
n–$C_{15}H_{32}$	1	–11 391	–8 3066	–5 1666	–3 0607
n–$C_{17}H_{36}$	1	–26 561	–15 128	–7 4611	–4 0026
n–$C_{19}H_{40}$	1	–290 47	–34 412	–10 743	–5 073
n–$C_{21}H_{44}$	1	46 552	–602 62	–15 929	–6 3503
n–$C_{23}H_{48}$	1	24 981	53 278	–24 981	–7 8253
n–$C_{25}H_{52}$	1	18 229	28 918	–45 251	–9 5913
n–$C_{27}H_{56}$	1	15 122	21 190	–130 54	–11 778
n–$C_{29}H_{60}$	1	13 249	17 3599	249 57	–14 432
n–$C_{31}H_{64}$	1	12 009	15 086	72 439	–17 780
n–$C_{33}H_{68}$	1	11 150	13 608	45 582	–22 164
n–$C_{35}H_{72}$	1	10 499	12 573	34 467	–28 119
n–$C_{37}H_{76}$	1	10 023	11 810	28 634	–36 606
n–$C_{39}H_{80}$	1	9 6666	11 244	25 025	–49 974
n–$C_{41}H_{84}$	1	9 3480	10 780	22 446	–73 083
MI‡ Order	1	2	3	4	–

† $\tilde{R}_{hkl} = R_{hkl} / R_{001}$

‡ MI Morphological importance

In comparison, $\tilde{R}_{110}$ is plotted versus the carbon number in Fig 1 and the theoretical growth forms of n–C_{23}, n–C_{31} and n–C_{41} constructed by the Gibbs–Wulff plot according to this recipe are also presented in this figure

It can be seen from Fig 1 that crystals of orthorhombic odd n–paraffins are thin plate like, limited by the large faceted {001} faces and the small narrow {110} faces Apart from this, it can be seen that n–paraffin crystals become thicker with increasing carbon number This can be interpreted in the following way For a certain direction, absolute bond energies

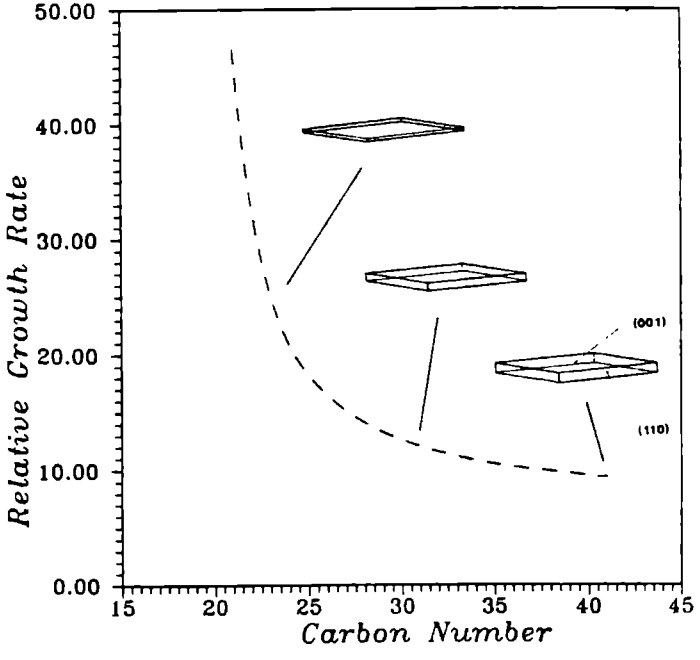

FIG.1. Relative growth rate $\tilde{R}_{hkl}$ of the {110} faces versus the carbon number of n–paraffins, ($\tilde{R}_{hkl} = R_{hkl}/R_{001}$), and Gibbs–Wulff constructions of growth forms of orthorhombic n–paraffin crystals based on the criterion $R_{hkl} \sim [\theta^c_{hkl}(n) - \theta]^{-1}$.

of paraffin crystals will increase with the carbon number. This will enhance the roughening temperature of $\{hkl\}$ faces, resulting in the hyperbolical decrease of $[\theta^c_{hkl}(n) - \theta]^{-1}$. It follows that for the {001} faces the value of $[\theta^c_{hkl}(n) - \theta]^{-1}$ doesn't change much because $\theta^c_{001}(n) >> \theta$. However for the most important side faces {110}, the roughening temperature is close to the actual temperature. Then a large influence on the value of $[\theta^c_{hkl}(n) - \theta]^{-1}$ and on the morphology due to the change of the carbon number occurs. Consequently, the relative difference of $[\theta^c_{hkl}(n) - \theta]^{-1}$ between side faces and the {001} faces becomes smaller with increasing n. It follows that habits of crystals become somewhat thicker.

III. EXPERIMENTS

Observations on growth forms and the growth processes of crystals were carried out in double–walled thermostated glass cells of cylindric form, using a Leitz inverted transmission

microscope type Diavert, in bright–field and with and without crossed polarizers

The process of crystal growth and the change of the morphology of crystals were recorded on a video camera or a microscope camera It is possible to control and to measure the temperature of the growth cell with an accuracy of ± 0 003 K This accuracy is necessary since it was found that the roughening depends in a very sensitive way on temperature

The solutions used in our experiments were prepared from analytical pure chemicals (n–paraffins Alfa, > 99 0%, n–hexane Merck, > 99 0%) The materials were weighed in a proper ratio according to various compositions of the solutions into a growth vessel After this, the vessel was sealed off

All experiments were performed in non–stirred solutions To start the experiments, first the temperature of the solution is lowered to a temperature much lower than the saturation temperature When crystals form in the growth cell, the temperature of the solution is raised to a temperature above the saturation temperature to dissolve most of the crystals The process was repeated several times until only one crystal survives in the solution Since the volume of the remaining crystal is very small compared to the volume of the cell, the change in the concentration during the experiments is negligible To measure the roughening temperature, the morphological change of a crystal at equilibrium must be observed very carefully The temperature of the solution in the cell must be slightly below, but as close as possible to the saturation temperature ($\Delta T < 0\ 01$ K) In order to determine the critical supersaturation of kinetic roughening σ^c, the temperature is changed in very small intervals (0 01–0 02 K) Each temperature must be kept constant for at least half an hour to ensure that the morphology of the crystal will not change anymore under the experimental condition

IV. OBSERVATIONS

In the following, detailed observations on the roughening transition and kinetic roughening, and its influence on the morphology were carried out for crystals of n–$C_{21}H_{44}$ and n–$C_{23}H_{48}$ grown from n–hexane solutions The results and are compared with theories Also, we will compare observed growth forms with the theoretical growth forms predicted according to (5) Since the roughening temperature of the {001} faces for paraffin crystals is much higher than room temperature, in the following we will focus our attention on the morphological changes of the {110} faces

A. Observations on n–$C_{23}H_{48}$ crystals

Crystals of n–$C_{23}H_{48}$ crystals were grown from solutions with saturation temperatures in the range of 278 15 K $\leq T_S \leq$ 298 15 K According to our experiments, the roughening

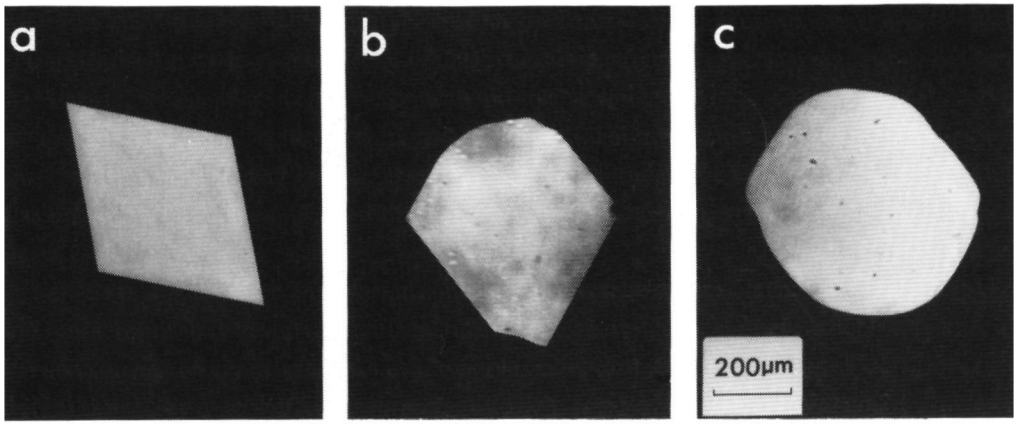

FIG.2. Morphologies of crystals of n–$C_{23}H_{48}$ growing from n–hexane solutions above and below the roughening temperature; (a) and (b): $T_s < T^r_{110}(23)$ platy crystal limited by faceted {110} faces, (c) $T_s > T^r_{110}(23)$ crystals limited by the rounded {110} faces. (a) $T_s = 279.29$ K, $\sigma = 0.1159$ %, (b) $T_s = 282.58$ K, $\sigma = 0.3395$ %, (c) $T_s = 292.48$ K, $\sigma = 0.2112$ %.

transition of the {110} faces for n–$C_{23}H_{48}$ crystals occurs at the temperature of $T^r_{110}(23) = 283.8 \pm 0.5$ K. The typical morphology of n–$C_{23}H_{48}$ crystals in n–hexane solutions with the saturation temperature below $T^r_{110}(23)$ and above $T^r_{110}(23)$ are illustrated in Fig.2. It can be seen from Figs. 2a,b that at a temperature below $T^r_{110}(23)$ the crystals have a platy and lozenge shape with the large flat {001} faces lying on the top and the bottom and the small narrow faceted side faces {110}. Sometimes crystals are truncated by the rounded off faces. (These faces disappear eventually). Above $T^r_{110}(23)$ crystals are still platy, but are bounded by rounded side faces {110} (Fig.2c). It is obvious that although the {110} faces roughen, a high anisotropy in growth rates of different orientations occur. The reason is that at $T_S > T^r$ a step of infinite length has no free energy, but a step of finite length has a positive free energy [20].

When a crystal grows from solutions with $T_S < T^r$, at relatively low supersaturations faceted growth of the {110} faces can be expected. The development of facets during growth from an initially rounded seed is illustrated in Fig.3. It is shown in Fig. 3 that rough faces grow faster than flat faces, and indeed disappear from the growth forms. At a relatively high supersaturation, $\sigma > \sigma^c$, the non–faceted growth of the {110} faces occurs again, due to kinetic roughening (Fig. 4). In all experiments, it was found that the region from kinetic

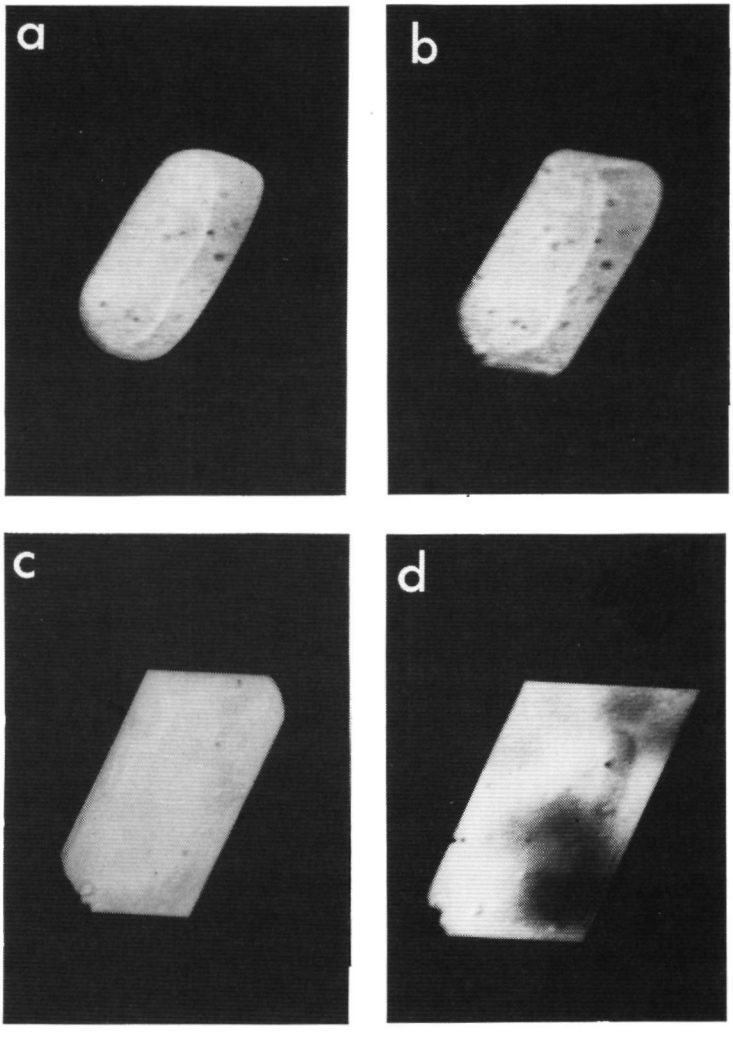

FIG.3. The faceting process of {110} faces on n–$C_{23}H_{48}$ crystals growing from n–hexane solution. $T_s = 279.29$ K, $\sigma = 0.8111$ %. (a)–(d) $\Delta t = 3$ min.

roughening to unstable growth (cellular growth or dendritic growth) is very narrow. In most cases, kinetic roughening and unstable growth occur on the {110} faces simultaneously. It can be seen from Fig.5. that growth fronts become unstable.

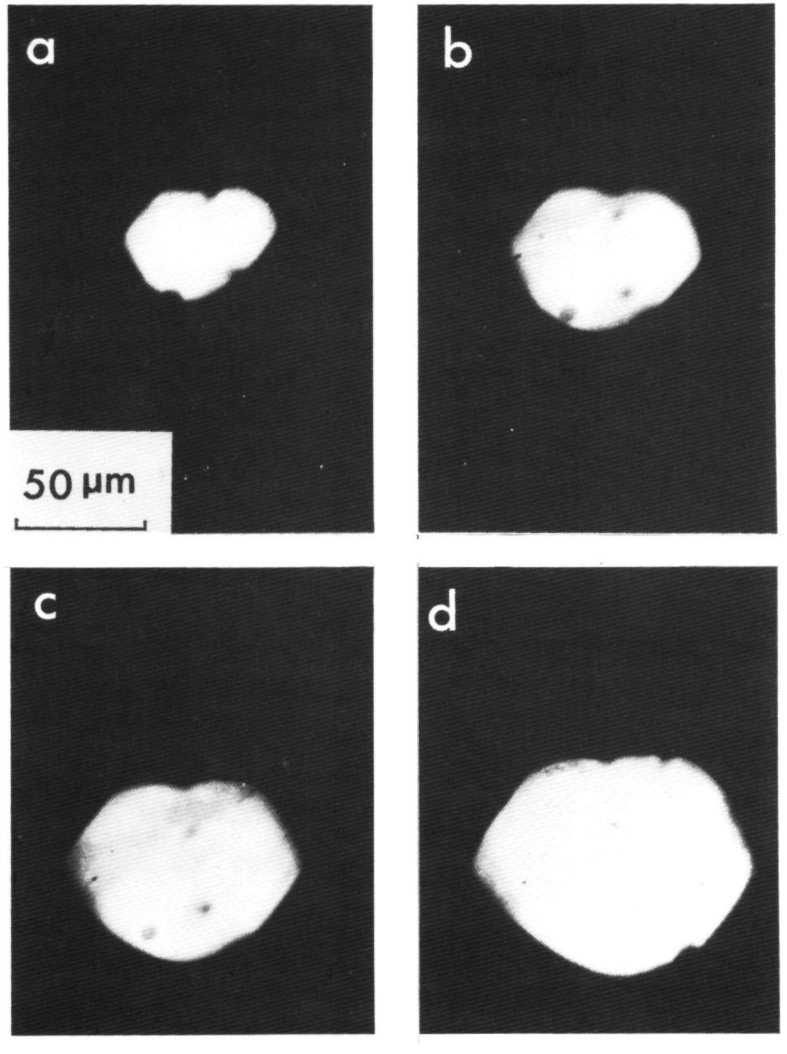

FIG.4. Kinetic roughening of {110} faces on n–$C_{23}H_{48}$ crystals growing from a n–hexane solution. $T_s = 282.58$ K, $\sigma = 1.585\%$, $T_s < T^r_{110}(23)$. (a)–(d) $\Delta t = 20$ sec.

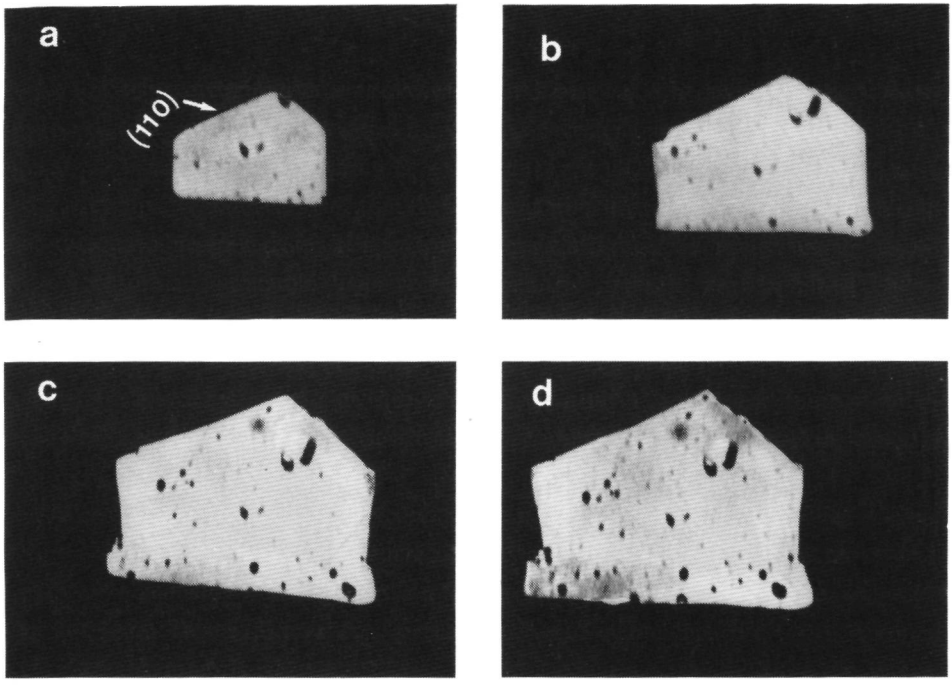

FIG.5. A crystal of n–$C_{23}H_{48}$ in n–hexane solutions. Growth fronts of side faces are getting unstable when {110} faces kinetically roughen; T_s = 282.58 K,σ = 1.585%, $T_s < T^r_{110}(23)$. (a)–(d), Δt = 1 min.

B. Observations on n–$C_{21}H_{44}$ crystals

Analogous experiments were carried out on crystals of n–$C_{21}H_{44}$ grown from n–hexane solutions within a range of 268.15 K–293.15 K. The {110} faces of n–$C_{21}H_{44}$ crystals show a similar behavior as those of the n–$C_{23}H_{48}$ crystals. Fig. 6 shows crystals growing below the roughening temperature of the {110} faces. At a low supersaturation, the crystals are platy, bounded by both the {001} faces and the {110} faces (see Fig. 6a). At a relatively high supersaturation kinetic roughening occurs on the {110} faces, accompanied by dendritic growth. The roughening temperature determined in our experiments if $T^r_{110}(21)$ = 273.27 ± 0.01 K.

In case crystals grow from solutions with saturation temperatures which are sufficiently higher than $T^r_{110}(21)$ the non–faceted growth of {110} is expected. At very low supersaturations, growth fronts remain stable (Fig.7a) With increasing the supersaturation,

stable growth gradually changes to unstable growth (Figs. 7a–c).

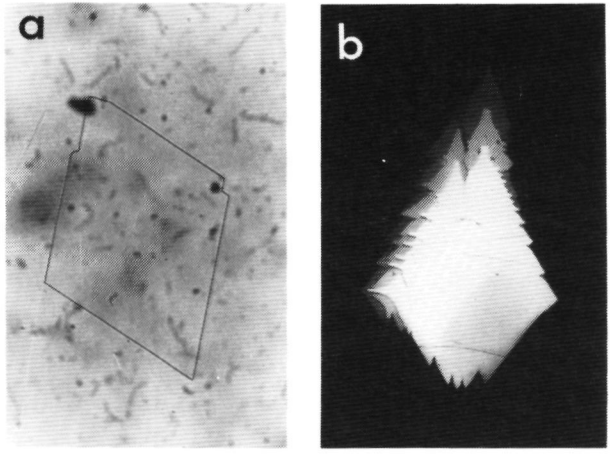

FIG.6. A crystal of n–$C_{21}H_{44}$ growing from a n–hexane solution with $T_s < T^r_{110}(21)$, T_s = 270.76 K. (a) The faceted {110} faces, σ = 1.463%. (b) Kinetic roughening and dendritic growth of the {110} faces, σ = 4.107%.

In this connection, we would like to report a kinetic phenomenon, the so–called " kinetic faceting ". In case that crystals grow from solutions with an equilibrium temperature slightly higher than T^r, first the {110} faces will grow in a rough mode at low supersaturations. When the supersaturation of the solution exceeds a certain value σ^* the {110} faces will show what will be called the kinetic faceting, and if the supersaturation increases further to another value σ^{**} ($\sigma^{**} > \sigma^*$), crystals will kinetically roughen again. This kinetic faceting is reversible. When the supersaturation decreases from $\sigma^{**} > \sigma > \sigma^*$ to $\sigma < \sigma^*$, the kinetically faceted faces will roughen again. A crystal showing kinetic faceting and the reversed process is given in Fig.8.

V. DISCUSSION

Comparing the observed morphology of odd n–paraffin crystals with theoretical predictions, it can be seen that by introducing the proper dimensionless actual temperature together with the Ising temperature, we can in a satisfactory way describe growth forms of crystals. Both theoretical and experimental growth forms, the crystals of n–$C_{21}H_{44}$ and

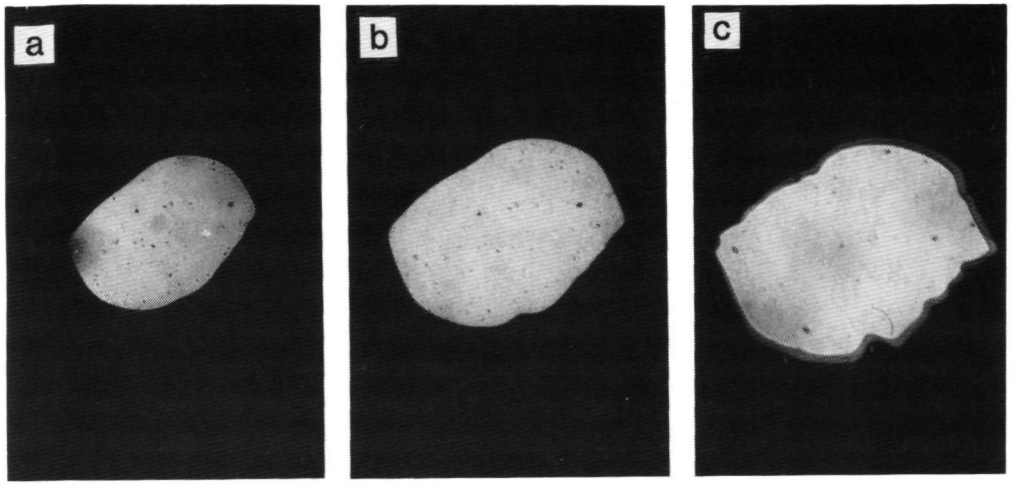

FIG.7. A n–$C_{21}H_{44}$ crystal in n–hexane solution with $T_s > T^r_{110}$, $T_s = 291.04$ K; With increasing supersaturation, the roughened up {110} faces getting unstable; a) $\sigma = 0.0729$ %, b) $\sigma = 0.2399$ %, c) $\sigma = 0.4317$ %.

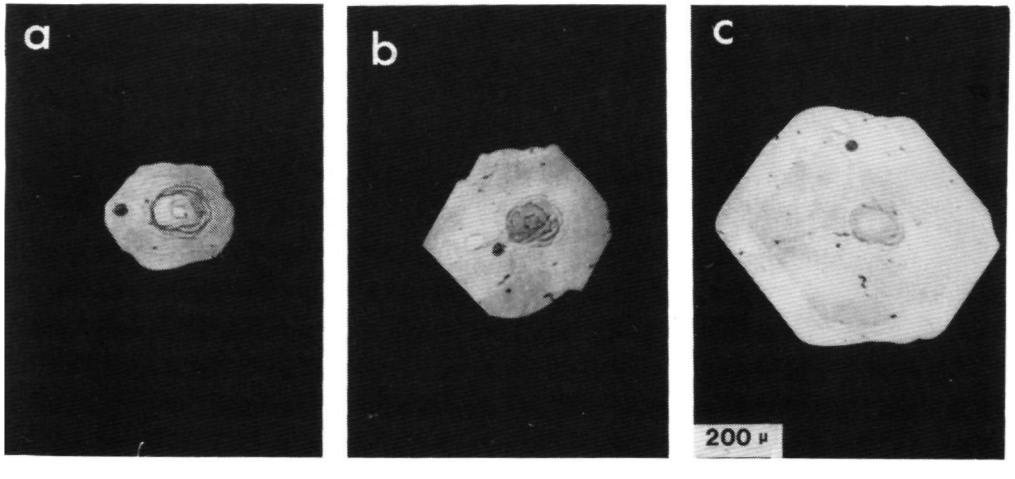

FIG.8. A crystal of n–$C_{21}H_{44}$ growing from a n–hexane solution with $T_s > T^r_{110}(21)$, $T_s = 273.29$ K. (a) A crystal with the roughened {110} faces, $\sigma = 0.1088\%$ ($\sigma < \sigma^*$); (b) The {110} faces are kinetically faceted, $\sigma = 0.8707$ % ($\sigma^* < \sigma < \sigma^{**}$); (c) The faceted {110} faces roughen again, $\sigma = 0.2176$ % ($\sigma < \sigma^*$).

n–$C_{23}H_{48}$ show a platy and lozenge shape of paraffin crystals, bounded only by the large {001} faces and the narrow {110} side faces

According to our previous paper [17], the morphology of odd n–paraffin crystals predicted on the basis of the Hartman–Perdok theory or the BFDH theory show thicker growth habits and too many side faces are present on crystals In most cases this is in conflict with the observations Secondly, the assumption, which the recipe is based on, that rough faces grow faster than flat faces is in most cases in agreement with our experimental observations (see Fig 3)

The reason for the successful application of the recipe introduced in this paper is obvious First, experimental conditions are included in this recipe by introducing θ Secondly the concept of roughening transition which gives the boundary between flat growth and rough growth is explicitly taken into account Both several internal and external factors which may affect the morphology of crystals are to a large extent considered in this approach In particular, experimental conditions concerning the character of the mother phase are included in this proposed recipe by introducing θ

VI. SUMMARY AND CONCLUSIONS

In this paper, a recipe used to predict growth forms of crystals was discussed, based on the concept of roughening transition Theoretical growth forms of odd n–paraffin crystals were constructed based on this recipe The agreement with observed and predicted growth forms is quite satisfactory Generally speaking, odd n–paraffin crystals have a lozenge shaped growth form, confined by the large {001} faces and the small {110} faces It follows from our experiments that the roughening transition temperatures of the faces {110} on crystals of n–$C_{21}H_{44}$ and n–$C_{23}H_{48}$ in n–hexane solutions are given by T^r = 273 27 ± 0 01 K and T^r = 283 8 ± 0 5 K, respectively In addition to normal kinetic phenomena, a so–called kinetic faceting was described This phenomenon is also related to the critical behavior of a special roughening transition occurring in the system[21]

ACKNOWLEDGEMENTS

We are much indebted to Shell Netherlands B V for providing a donation to support a research program on the growth and morphology of paraffins We also wish to acknowledge Dr B Vos and Drs M J Reynhout for stimulating discussions, and Mr Jan van Kessel for making some of the drawings

REFERENCES

1 J D H Donnay and D Harker, Am Mineralogist **22**, 446 (1937)

2 P Hartman and W G Perdok, Acta Cryst **8**, 49 (1955), **8**, 521 (1955), **8**, 525 (1955), P Hartman, in *Morphology of Crystals*, Part A, edited by I Sunagawa, (Terra Sci , Tokyo, 1987) pp 269

3 A A Chernov, in *Modern Crystallography III – Crystal Growth* (Springer–Verllag, Berlin, 1984) ch 5 p 208

4 W K Burton and N Cabrera, Disc Faraday Soc **5**, 40 (1949), W K Burton, N Cabrera and F C Frank, Phil Trans Roy Soc **A243**, 299 (1951)

5 G H Gilmer and K A Jackson, in *Crystal Growth and Materials*, edited by E Kaldis and H J Scheel (North – Holland, Amsterdam, 1977) p 79

6 H Muller – Krumbhaar, in *Crystal Growth and Materials*, edited by E Kaldis and H J Scheel (North – Holland, Amsterdam, 1977) p 116

7 P Bennema and J P van der Eerden, in *Morphology of Crystals*, Part A, edited by I Sunagawa (Terra Sci , Tokyo ,1987) p 1

8 P Bennema, J Crystal Growth **24/25**, 76 (1972)

9 P Bennema, J Boon, C van Leeuwen and G H Gilmer, Kristall Techik **8**, 659 (1973)

10 D Nenow and E D Dukova, J Cryst Growth **3/4**, 166 (1968)

11 A Pavloska, J Cryst Growth **46**, 551 (1979)

12 G A Alfintsev, G P Chemerinsky, O P Fedorov, Kristall Tech **15**, 643 (1980)

13 C E Miller, J Cryst , Growth **43**, 357 (1977)

14 V V Podolinski, J Cryst Growth **46**, 511 (1979)

15 V V Podolinski and V G Drykin, J Cryst Growth **62**, 532 (1983)

16 L A M J Jetten, H J Human, P Bennema and J P van der Eerden, J Cryst Growth **68**, 503 (1984)

17 P Bennema, X Y Liu, K Lewtas, R D Tack, J J M Rijpkema and K J Robert, J Cryst Growth **121**, 679 (1992)

18 P Bennema, in *The Handbook on Crystal Growth*, edited by D Hurle, (North–Holland, Elsevier, Amsterdam, 1993) (in press)

19 L Onsager, Phys Rev **45**, 117 (1944)

20 M Elwenspoek and W Boerhof, Phys Rev **B36**, 5326 (1987)

21 X Y Liu, Phys Rev **B48**, (1993) (in press)

Chapter 4

THERMODYNAMIC PROPERTIES AND THE STRUCTURE OF SOLID-FLUID INTERFACES

Chapter 4.1

The equilibrium state of solid–liquid interfaces of aliphatic compounds

Xiang-Yang Liu and P Bennema
RIM Laboratory of Solid State Chemistry, Faculty of Science, University of Nijmegen, Toernooiveld 6525 ED Nijmegen, The Netherlands

(Received 22 January 1992, accepted 18 May 1992)

The ordering and orientation of fluid units at interfaces of the aliphatic crystal solution system are the theme of this paper Based on the idea that the bulk phase and the interfacial phase are two different phases, appropriate relations between the interfacial bond energies and the bulk bond energies are developed by introducing a surface scaling factor C_f. As a description of the interfacial structure of aliphatic compounds, it is assumed that a high degree of ordering is stored in the interfacial fluid phase Then the so-called α molecule approach is used to estimate the values of bond energies in the interfacial phase This leads to the result of $C_f < 1$, meaning that the the interfaces of *n*-paraffin crystals and the solutions will be extra wetting This is consistent with the experimental data obtained from the roughening transitions occurring in several *n*-paraffin–*n*-hexane solution systems Finally, a roughening phase transition diagram of the n-$C_{23}H_{48}$–*n*-hexane system is presented, which indicates that the roughening temperature of a surface on a crystal is concentration dependent

I. INTRODUCTION

The structure of the solid–liquid interface is a central theme in crystal growth theories The interfacial structure determines the equilibrium form of a crystal (faceted or nonfaceted) and the growth mechanism (layer growth or continuous growth) It is well known that there is a critical temperature at which the phase transition, so-called roughening phase transition, occurs at the solid–fluid interface [1–6] The roughening temperature is defined as the temperature at which the edge free energy becomes zero [7] Subsequently, the dimensionless roughening temperature of a face (hkl) is written as

$$\theta^r_{hkl}=\frac{2kT^r}{\phi_{str}} \qquad (1)$$

Here T^r is the absolute roughening temperature of face (hkl), k the Boltzmann constant, and ϕ_{str} the strongest bond energy at the surface If the actual dimensionless temperature $\theta > \theta^r_{hkl}$ the surface grows as a rough nonfaceted face If $\theta < \theta^r_{hkl}$ the surface grows as a flat surface. As θ^r_{hkl} is the specific value for a given surface (hkl), the real roughening temperature T^r depends on the structure and effective bond energies of the interface The solvent (and impurities) in interaction with the interface also strongly influence T^r

In order to estimate bond energies at a surface, the so-called equivalent wetting condition[2,6–8] was used based on cell models, assuming that

$$\phi_i=\Phi_i, \qquad (2)$$

where subscript "i" refers to interactions of a unit in different directions, ϕ_i is the bond energy at the interface, Φ_i the corresponding bond energy in the bulk, which can be calculated from thermodynamic data of the solid–fluid system This implies that the fluid at the interface has the same structure as in the bulk By introducing this condition, bonds formed at the interface are directly brought into relation with the bonds formed in the bulk However, recent theoretical and experimental investigations show that in most cases the equivalent wetting condition leading to Eq (2) is not valid [7,9–11] It follows from a theoretical analysis of a lattice gas model (or cell model) applied to describe a solid–fluid interface that the bond strength is in a subtle way influenced by the fluid structure near the interface [9,20] The latest research based on density-functional theories (DFT) and computer simulations[9,11,20] show that at the solid–fluid interface, the fluid units adjacent to the surface become ordered, due to fitting with the structure of the solid surface On the other hand, the solid units get somewhat more "freedom" to deform themselves as in a "hot" solid In general, the fluid structure of the interface is different from that in the bulk, and this discrepancy will certainly affect bond energies at the surface

To describe the fluid structure adjacent to the solid surface, some models were put forward based on density-functional theory In these models, all differences between the interface and the bulk are due to variation of the density of fluid layers adjacent to the solid surface [9,11–20] This explains the discrepancy of behavior between the interfacial phase and the bulk phase to a quite large extent However, since most theories and models are based on simple systems (such as spheres or dumbbell), the conclusions drawn are only qualitative For sophisticated systems as organic crystals, we still need special methods to describe the interfacial structure and give a reasonable interpretation of experimentally found bond energies at the surface

In this paper we try to estimate the bond energies at the interfaces of aliphatic crystals by taking an ordered structure of the liquid near the crystal surface into account We will first develop a method on basis of regular solution theory to associate the interfacial structure and the bulk structure This, in principle, allows us to characterize the interfacial structure Our model for crystal–solution interfaces of aliphatic compounds is based on the principal conclusions drawn from statistical physics research on crystal surfaces This predicts the ordered structure in the liquid

layers adjacent to the surface of aliphatic crystals. The ordering compensates on the interaction energy differences between unlike units (such as solid–fluid units) and like units (such as solid–solid units or fluid–fluid units), resulting in a decrease of the step energy This paper consists of the following parts In Sec II, after distinguishing the bulk and the interface as two different phases, we derive expressions of bond energies in a multicomponent medium for both the interfacial phase and the bulk phase Introducing a surface scaling factor C_h, an essential concept, called more or less than equivalent wetting of solid–fluid interfaces, is presented Section III is devoted to estimations of the interfacial bond energies of aliphatic compounds and of the characteristic surface scaling factor, based on a so-called α molecules approach In Sec IV the theoretical expectation and experimental data are compared with each other The influence of solution concentrations on bond energies at the interface are also discussed in this section Finally in Sec V a summary and conclusion is presented

II. GENERAL MODEL

To begin with this section, we will first present a feature of our model Basically we consider the fluid phase as two different phases the bulk fluid phase and the interfacial fluid phase The interfacial fluid phase refers to the fluid layers adjacent to the solid surface, and the bulk fluid phase to the layers far from the solid surface Similarly, the interfacial solid phase and the bulk solid phase are defined Subsequently, we can reasonably infer that the bulk properties are different from the interfacial properties In order to discriminate the differences in bond energies, we use ϕ to stand for the bond energy in the interfacial phase, and Φ for that in the bulk phase In the following, we will treat the bulk phase and the interfacial phase separately, then use a certain scaling factor to associate the properties of the interfacial phase and those of the bulk phase.

A. Bond energies at the interface and in the bulk

It can be seen from expression (1) that the roughening temperature T^r depends on the bond energies at the interface We note that for the crystal–fluid interface, within the frame work of Ising models bond energies usually have the form

$$\phi_i=\phi_i^{sf}-\tfrac{1}{2}(\phi_i^{ss}+\phi_i^{ff}) \tag{3}$$

where superscripts s and f refer to solid and fluid, respectively, and corresponding bonds sf, ff, and ss to solid–fluid, fluid–fluid, and solid–fluid bonds, respectively, and ϕ's are the respective broken bond energies

In the case of a crystal in thermodynamic equilibrium with its melt, it is very clear that "solid" refers to the crystalline part of the interface and "fluid" to the fluid part For a crystal in thermodynamic equilibrium with its solution, the situation becomes more complicated In this case, the fluid consists of a mixture of different units A and B A represents the solute and B the solvent units The mole fractions of A and B particles are given by X_A and X_B, respectively We note that the term ϕ_i^{ff} consists of three different parts ϕ_i^{AA}, ϕ_i^{AB}, ϕ_i^{BB} and the term ϕ_i^{sf} is of two parts ϕ_i^{SA} and ϕ_i^{SB}

Using the well-known mean field or Bragg–Williams approximation,[21–24] it follows that the two constituents are distributed at random and the mixture behaves as a uniform liquid with average intermolecular potential

$$\langle\phi_i^{ff}\rangle=\sum_{\alpha=A\,B}\sum_{\beta=A\,B}X_\alpha X_\beta\phi_i^{\alpha\beta} \tag{4}$$

Solid units are treated as if they have their own type of equilibrium liquid with the average potential

$$\langle\phi_i^{sf}\rangle=\sum_{\beta=A\,B}X_\beta\phi_i^{SB} \tag{5}$$

We will first assume here that the units A and B are spherical and have a similar volume For rodlike units A and B expressions (4) and (5) are still valid This will be treated later in Sec III

Combining Eqs (3), (4), and (5) yields

$$\phi_i=\tfrac{1}{2}(\phi_i^{AA}-\phi_i^{SS})+X_B^2\,\phi_i^{\sigma}+X_A(\phi_i^{SA}-\phi_i^{AA})+X_B(\phi_i^{SB}-\phi_i^{AB}) \tag{6}$$

or

$$\phi_i=\tfrac{1}{2}(\phi_i^{AA}-\phi_i^{SS})+(1-X_A)^2\,\phi_i^{\sigma}+[1+(\alpha_i-1)X_A]\times(\phi_i^{SB}-\phi_i^{AB}), \tag{6'}$$

where

$$\phi_i^{\sigma}=\phi_i^{AB}-\tfrac{1}{2}(\phi_i^{AA}+\phi_i^{BB}) \tag{7}$$

and

$$\alpha_i=(\phi_i^{SA}-\phi_i^{AA})/(\phi_i^{SB}-\phi_i^{AB}) \tag{8}$$

In order to analyze the effective bond energies in the bulk, we continue to use the Bragg–Williams approach in our regular solution model As usual, we assume a pseudocrystalline state, where the whole space is partitioned in cells of equal size and shape Each cell contains either an A or B molecule If we now mix V_A molecules of a pure A "crystal" and N_B molecules of a pure B "crystal," the free energy of mixing ΔF^{mix} is

$$\langle\Delta F^{\text{mix}}_{(AB)}\rangle_{VT}=\frac{N_A\,N_B}{N_A+N_B}\sum_1^n\Phi_i^{\sigma}-kT\,\ln\frac{(N_A+N_B)!}{N_A!\,N_B!} \tag{9}$$

The energy change due to the mixing process is given by

$$\langle\Delta E^{\text{mix}}_{(AB)}\rangle=\frac{N_A\,N_B}{N_A+N_B}\sum_1^n\Phi_i^{\sigma}, \tag{10}$$

and the entropy change by

$$\langle\Delta S^{\text{mix}}_{(AB)}\rangle=k\,\ln\frac{(N_A+N_B)!}{N_A!\,N_B!}, \tag{10'}$$

where k is Boltzmann constant and, Φ_i^{σ} is exchange energy

$$\Phi_i^{\sigma}=\Phi_i^{AB}-\tfrac{1}{2}(\Phi_i^{AA}+\Phi_i^{BB}) \tag{7'}$$

Note that the cells are supposed to be incompressible blocks so that

$$\langle \Delta G^{\rm mix}_{(AB)} \rangle_{P,T} \cong \langle \Delta F^{\rm mix}_{(AB)} \rangle_{V,T} \tag{11}$$

and

$$\langle \Delta E^{\rm mix}_{AB} \rangle \cong \langle \Delta H^{\rm mix}_{AB} \rangle. \tag{12}$$

According to thermodynamics

$$F_{(A,B)} = F_A + F_B + \Delta F^{\rm mix}_{(A,B)}. \tag{13}$$

Here F_A and F_B are free energies of pure A and pure B liquids. Then the chemical potential of a solute unit in the mixture is

$$[\mu_A]_{(A,B)} \equiv \left(\frac{\partial F_{(A,B)}}{\partial N_A}\right)_{T,\Phi_{AA},\Phi_{BB},\Phi_{AB},N_A} = \left(\frac{\partial F_A}{\partial N_A}\right)_{\Phi_{AA},T} + \left(\frac{\partial \Delta F^{\rm mix}_{(A,B)}}{\partial N_A}\right)_{T,\Phi^{\sigma}}. \tag{14}$$

It follows from Eq. (14) after substituting $\langle \Delta F^{\rm mix}_{(AB)} \rangle$ given by Eq. (9) that

$$[\mu_A]_{(A,B)} = [\mu_A]_A + kT \cdot \ln X_A + (1-X_A)^2 \sum_1^n \Phi_i^{\sigma}. \tag{15}$$

Note that $[\mu_A]_A = [\partial F_A/\partial N_A]_{\Phi_{AA},T}$ is derived for the pure liquid state A, and the other part is due to the mixing process.

In the same way we found that for the enthalpy of the mixing process,

$$(\Delta h^{\rm mix}_A)_{(A,B)} \equiv \left(\frac{\partial \Delta H^{\rm mix}_{(A,B)}}{\partial N_A}\right)_{N_B,T,P} = (1-X_A)^2 \sum_1^n \Phi_i^{\sigma}. \tag{16}$$

We will now make the connection with thermodynamics of solution and phase equilibria. Along the solubility curve the component A in solid (we assume that B is not soluble in solid A) is in equilibrium with A in the liquid state mixture of A and B. Then the chemical potential of A in the solid $[\mu_A]_s$ is equal to that in the mixture $[\mu_A]_{(A,B)}$ for a given P and T. Therefore,

$$[\mu_A]_S = [\mu_A]_A + kT \cdot \ln X_A + (1-X_A)^2 \sum_1^n \Phi_i^{\sigma} \tag{17}$$

and

$$[\mu_A]_S - [\mu_A]_A = (h_A^s - h_A^m) - T(S_A^s - S_A^m) = \Delta h_A^f(T,P) - T \cdot \Delta S_A^f(T,P), \tag{18}$$

where h and S denote the molar enthalpy and entropy, respectively, and $\Delta h_A^f(T,P)$ and $\Delta S_A^f(T,P)$ are the enthalpy and entropy of fusion (per structural unit) of the solute, respectively. Finally, we obtain the usual expression for solubility

$$\ln X_A = -\frac{\Delta h_A^f(T,P)}{kT} + \frac{\Delta S_A^f(T,P)}{k} + (1-X_A)^2 \sum_1^n \frac{\Phi_i^{\sigma}}{kT}. \tag{19}$$

Generally $\Delta h_A^f(T,P)$ and $\Delta S_A^f(T,P)$ can be calculated from the enthalpy and entropy of fusion at the melting temperature, Δh_A^m and ΔS_A^m, by

$$\Delta h_A^f(T,P) = \int_T^{T_m} \Delta \tilde{C}_p \, dT + \Delta h_A^m \tag{20}$$

and

$$\Delta S_A^f(T,P) = \int_T^{T_m} \frac{\Delta \tilde{C}_p}{T} dT + \frac{\Delta h_A^m}{T_m}. \tag{21}$$

In case that solid–solid phase transition occurs, Eqs. (20) and (21) are rewritten as

$$\Delta h_A^f(T,P) = \int_{T_{\rm tr}}^{T_m} \Delta \tilde{C}_p^{\alpha-1} \, dT + \Delta h_A^m + \int_T^{T_{\rm tr}} \Delta \tilde{C}_p^{\alpha-\beta} \, dT + \Delta h_A^{\rm tr} \tag{22}$$

and

$$\Delta S_A^f(T,P) = \int_{T_{\rm tr}}^{T_m} \frac{\Delta \tilde{C}_p^{\alpha-1}}{T} dT + \frac{\Delta h_A^m}{T_m} + \int_T^{T_{\rm tr}} \frac{\Delta \tilde{C}_p^{\alpha-\beta}}{T} dT + \frac{\Delta h_A^{\rm tr}}{T_{\rm tr}}, \tag{23}$$

where superscripts l, α, and β denote the liquid state, high temperature crystalline state (α state) and low temperature crystalline state (β state), respectively, and T_m is melting temperature, $T_{\rm tr}$ α–β phase transition temperature, Δh_A^m and $\Delta h_A^{\rm tr}$ are the enthalpy of fusion and α–β phase transition enthalpy, respectively. It is noted that the α–β phase transition is quite common in both even and odd n-paraffin crystals.[24]

If $\Delta \tilde{C}_p \cong 0$, Eqs. (20), (21), (22), and (23) can be simplified as

$$\Delta h_A^f(T,P) \cong \Delta h_A^m, \tag{20'}$$

$$\Delta S_A^f(T,P) \cong \Delta h_A^m / T_m, \tag{21'}$$

$$\Delta h^f(T,P) \cong \Delta h_A^m + \Delta h_A^{\rm tr}, \tag{22'}$$

and

$$\Delta S^f(T,P) \cong \Delta h_A^m / T_m + \Delta h_A^{\rm tr} / T_{\rm tr}. \tag{23'}$$

In statistical thermodynamics, $\Delta h_A^f(T,P)$ has the form of

$$\Delta h_A^f(T,P) = \sum_1^n \tfrac{1}{2}(\Phi_i^{AA} - \Phi_i^{SS}). \tag{24}$$

Since

$$\Delta h_A^{\rm diss} = \Delta h_A^f + \Delta h_A^{\rm mix}, \tag{25}$$

combining Eqs. (16), (19), (24), and (25), we obtain another expression for the solubility of regular solutions

$$\ln X_A = -\frac{\Delta h_A^{\rm diss}(T,P,X_A)}{kT} + \frac{\Delta S_A^f(T,P)}{k}, \tag{19'}$$

where

$$\Delta h_A^{\text{diss}} = \sum_1^n \Phi_i \tag{26}$$

and

$$\Phi_i = \tfrac{1}{2}(\Phi_i^{AA} - \Phi_i^{SS}) + (1-X_A)^2\Phi_i^{\sigma} \tag{27}$$

In order to evaluate Φ_{str} from the enthalpy of dissolution of the ΔH^{diss}, we now introduce the assumption of the so-called proportionality condition It is stated that in going from one state to another, the absolute value of the potential is altered but the ratio between the value remains the same This implies that the form of the molecules is the same in the liquid state as in solid state The change in the potential is caused by a difference in energy levels and the altered structure which produces different effective potentials Then the proportionality condition can be written as

$$\begin{aligned}\Phi_i \Phi_j \Phi_k &= \Phi_i^{ss}\Phi_j^{ss}\Phi_k^{ss} \\ &= \Phi_i^{ff}\Phi_j^{ff}\Phi_k^{ff} \\ &= \Phi_i^{sf}\Phi_j^{sf}\Phi_k^{sf} \quad \cdot,\end{aligned} \tag{28}$$

where the subscripts i, j, k, represent directions in the cells, and corresponding bond energies In the following we define a relative enthalpy of a structure by summing the relative bond energies in reference to the strongest bond

$$\tilde{H} = \sum_1^n \tilde{\Phi}_i, \tag{29}$$

where $\tilde{\Phi}_i = \Phi_i^{ss}/\Phi_{str}^{ss}$ According to the proportional condition, $\tilde{H}$ is determined by structure, nature of bonds, and the shape of molecules, and is independent of the other external factors Consequently, the strongest bond strength in the liquid cell of the bulk phase can be evaluated by

$$\Phi_{str} = \Delta h^{\text{diss}}(T,P,X_A)/\tilde{H} \tag{30}$$

It is noted that in the foregoing discussions we did not distinguish concentrations of solute X_A in the interfacial phase and in the bulk phase because we assume that they are the same at equilibrium In fact this is an approximation

B. Scaling factor of interfaces

In the description of both the bulk phase and the interfacial phase, we are confronted with the fact that the interfacial phase is quite different from the bulk phase In order to link interfacial quantities to bulk quantities, a surface scaling factor is introduced,

$$C_I = \phi_i/\Phi_i \tag{31}$$

Here if we assume that the proportionality condition Eq (28) also holds for the interface, the factor C_I should be the same for a certain interface Similarly, two other relevant factors are defined as

$$C_I^0 = \frac{\phi_i^{AA} - \phi_i^{SS}}{\Phi_i^{AA} - \Phi_i^{SS}} \tag{32}$$

and

$$C_I^* = \frac{[\tfrac{1}{2}(\phi_i^{AA} - \phi_i^{SS}) + (1-X_A)^2\phi_i^{\sigma}]}{[\tfrac{1}{2}(\Phi_i^{AA} - \Phi_i^{SS}) + (1-X_A)^2\Phi_i^{\sigma}]} \tag{33}$$

According to Eqs (6'), (27), and (33), C_I can be divided into two parts,

$$C_I = C_I^* + C_I', \tag{34}$$

where

$$C_I' = \frac{\{[1+(\alpha_I-1)X_A](\phi_i^{SB} - \phi_i^{AB})\}}{[\tfrac{1}{2}(\Phi_i^{AA} - \Phi_i^{SS}) + (1-X_A)^2\Phi_i^{\sigma}]} \tag{35}$$

Since we only limit ourselves to strictly regular solutions, in expression (33) the terms $(1-X_A)^2\phi_i^{\sigma}$ and $(1-X_A)^2\Phi_i^{\sigma}$ are relatively small, compared with the terms $\frac{1}{2}(\phi_i^{AA} - \phi_i^{SS})$ and $\frac{1}{2}(\Phi_i^{AA} - \Phi_i^{SS})$, respectively So we may expect that $C_I^* \cong C_I^0$ It then follows that

$$C_I \cong C_I^0 + C_I' \tag{34'}$$

It can immediately be seen from expression (32) [or Eq (33)] that C_I^0 (or C_I^*) is (or almost) concentration independent and characterizes the bonding conditions in the two phases Therefore, it can be defined as a characteristic surface scaling factor In expression (35), C_I' involves surface bonds ϕ_i^{SA} and ϕ_i^{SB}, which have no corresponding bonds in the bulk, and this part is strongly influenced by the concentration of the solution and surface structure Nevertheless, in the paper we will call C_I^0 (or C_I^*), $(\phi_i^{SB} - \phi_i^{AB})$, $(\phi_i^{SA} - \phi_i^{AA})$ (or α_I), etc, surface parameters These parameters are subsequently used to characterize the interfacial phase in reference to the bulk phase

From the definition of C_I, we can distinguish three cases

$$C_I = 1 \tag{i}$$

On statistical average, the bonding condition in the interfacial phase is similar to that in the bulk phase, and the so-called equivalent wetting condition is fulfilled

$$C_I < 1 \tag{ii}$$

In this case the fluid molecules, both solute and solvents molecules, are quite ordered and are fitting quite well with the solid surface structure This compensates the bond energy difference between unlike units and like units The solid surface reveals a positive absorption effect to fluid units In this case the surface free energy and step free energy become small We classify this case the extra or more than equivalent wetting case

$$C_I > 1 \tag{iii}$$

In this case the difference of bond energies between unlike units and like units in the interfacial phase is much greater than in the bulk The value of bond energy expressed by Eq (3) is much more positive than the corresponding value in the bulk This case is known as the less than equivalent wetting We can expect that the two different kinds of units are much more separated from each other This is the so-called negative absorption effect,

caused by a repulsive effect between solid and fluid units or mismatch between unlike molecules in the interfaces [10,11] The density reduction of hard spheres at the hard sphere–hard wall interface, due to a fluid ordering is also one of these reasons [9,20]

For crystals growing from a normal solution C_l^0 (or C_l^* and C_l) may be roughly the same for all faces. It follows from expressions (34), (34'), and (35) that, in general, C_l and C_l' are concentration and temperature dependent If due to special shapes, confirmations of more or less complex molecules in subtle interactions with a crystal surface (hkl) having a specific structure occurs, C_l^0 (or C_l^*) and C_l may become strongly surface dependent Also tailor made additives and special solvents interacting with special surfaces can make C_l^0 (or C_l^*) and C_l strongly surface dependent

III. THE INTERFACIAL PHASE COMPOSED OF ALIPHATIC LIKE UNITS

In this section, we will deal with the systems consisting of aliphatiche or chainlike units In Sec II, we applied the regular solution theory to solutions of two types of molecules in our analysis For the time being these molecules are regarded as spheres of at least roughly the same size Any given configuration can be obtained from another distinct one by merely interchanging the position of a pair of unlike molecules This does not appreciably affect the configuration of remaining molecules The theory presented above has to be modified if the two types of molecules have a significantly different size and shape However, for the case of the arrangement of molecules in a linear chain, the number of distinguishable arrangement must be independent of the relative lengths of the two types of molecules, and the statistical results can be the same as the spherical molecules having the same size [17] If then a liquid is constructed out of large groups of such lines all parallel to one another it seems reasonable to expect the free enthalpy of mixing to be nearly the same as for a single linear array, or the same as for spherical molecules of the same size This must also be the case for a mixture of two paraffins having molecules of differing lengths, where, in principle, all molecules are arranged in parallel linear arrays Some experiments reported in Ref 25 and our solubility determinations showing regularly mixing behavior of n-paraffins and n hexane solutions strongly support the argument Therefore, all results derived from regular solution theory can also be applied to n paraffin solutions

A A highly ordered structure model

Before considering the interfacial phase and the bulk phase of n-paraffin solutions, we will review the solid phases and molecule behavior in the phases In the solid state, n paraffins may crystallize in several low temperature phases (β phases triclinic β_T, monoclinic β_m, and orthorhombic β_o) and a high temperature phase (hexagonal phase or α phase or rotatory phase),[24] depending on the parity of carbon number of n-paraffins and the external factors In β phases, rotation of a molecule around its axis is strongly restricted while in the α phase a molecule can

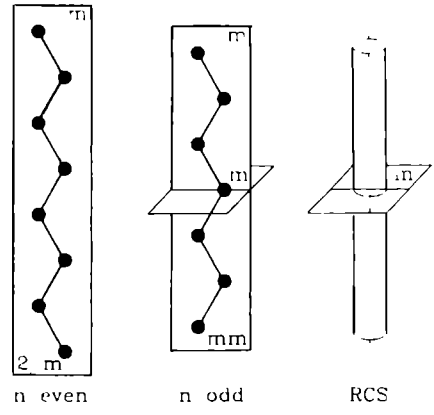

FIG 1 Symmetry of n paraffin molecules (Ref 26)

rotate freely around its axis It results in the dissimilarity of molecular symmetry for the β phase even paraffin molecules have a $2/m$ symmetry, while odd paraffin molecules have a mm symmetry With regard to the α phase, axial rotation of the molecules provides them with statistical mean cylindrical symmetry [26] The symmetry of molecules in different phases are presented in Fig 1 In the liquid state, n-paraffin molecules can rotate on their axes as in the α phase Hence from a statistical point of view, paraffin molecules in the α phase and liquid state are supposed to be similar the long rod shape with cylindrical symmetry

We now consider the interfaces of (β phase) paraffin crystals in thermodynamic equilibrium with their solutions As mentioned before, going from the bulk fluid phase to crystal surfaces configurations of the liquid state become much more ordered and oriented due to the influence of solid surfaces In this sense, we supposed that a kind of smectic order exists in the first few layers adjacent to the surfaces, as illustrated in Fig 2 Within the framework of cell models, each unit of both the fluid and the solid phase occupies one lattice point in the interfacial phase Accord-

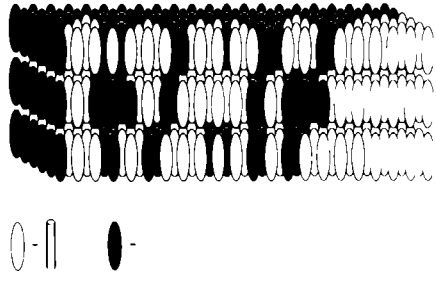

FIG 2 Schematic illustration of smectic order at the interfacial phase The black ellipsoidal blocks represent solid units the open ones fluid units

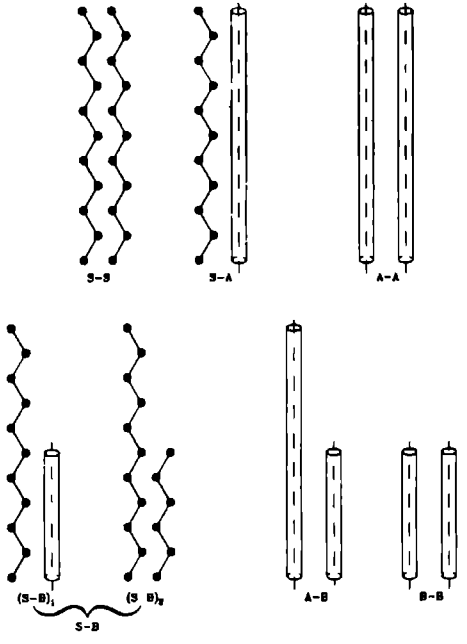

FIG 3 Different molecular interactions at the interfaces of *n* paraffin–*n* hexane solution system *A* and *B* referring to solid solute and solvent molecules, respectively

ing to the analysis of *n* paraffin molecular behavior in different states, we distinguish solid and fluid paraffin molecules by the symmetry resulting from statistically averaging over configurations Different molecular symmetry is caused by different states of motion, which strongly influences the interaction energy and the configurations In the following we limit ourselves to a regular solution system, where longer chain paraffins dissolve in shorter chain paraffins (such as *n*-hexane) It is supposed that no solid solution is formed in the solid state We assume that the solid paraffin molecules are the molecules with zigzag chains having *mm* or $2/m$ symmetry, and the solute molecules are those with the shape of cylinder having cylindrical symmetry Solvent molecules have different chain length from solute paraffin molecules Since they cannot enter the lattice points of paraffin crystals, they have both a zigzag chain symmetry and a cylindrical symmetry

As shown in Sec II A, six types of contacts are distinguished at the solid fluid interface, *S–S*, *S–A*, *S–B*, *A–A*, *A–B*, and *B–B*, which correspond to six types of interactions Combined with our classification of the molecules, these contacts at the surfaces of paraffin crystals (β phase) are illustrated in Fig 3 In this schematic illustration, *S–B* contacts are still indicated as $(S\text{–}B)_1$ and $(S\text{–}B)_2$

Now let us reconsider expression (35) In the expression, C_i' involves $(\phi_i^{SA}-\phi_i^{AA})$ and $(\phi_i^{SB}-\phi_i^{AB})$ terms Normally we take solid molecules as a reference, assuming that they are fixed Let us look at an individual contact of *S–A* If we change the reference to a solute molecule, the solid molecule in comparison with the reference solute molecule will rotate around its molecular axis In the sense, *S–A* and *A–A* contacts are not much different Hence we will assume that for *n*-paraffins–*n*-hexane solutions at solid–fluid interfaces the following approximation holds

$$\phi_i^{SA}\simeq\phi_i^{AA} \tag{36}$$

Concerning *S–B* interactions part we presume that $(S\text{–}B)_1$ is almost equal to *A–B* interactions, but $(S\text{–}B)_2$ is different It can be expected that

$$\phi_i^{SB}\neq\phi_i^{AB}, \tag{37}$$

and

$$\alpha_l\simeq 0 \tag{38}$$

Therefore, we can rewrite expression (35) as

$$C_i'=(1-X_A)(\phi_i^{SB}-\phi_i^{AB})\Big/\left[\frac{1}{2}(\Phi_i^{AA}-\Phi^{SS})+(1-X_A)^2\Phi_i^{\sigma}\right] \tag{35'}$$

B. Estimation of C_i: The α molecule approach

In order to calculate C_i, we need the data of C_i^0 and $(\phi_i^{SB}-\phi_i^{AB})$ It is impossible to calculate such data on purely theoretical grounds But for particular systems such as aliphatic solution systems, the data can be estimated from thermodynamic parameters In the following we will estimate C_i^0 and $(\phi_{str}^{SB}-\phi_{str}^{AB})$ for *n*-paraffin–*n*-hexane solution systems

As in the foregoing discussions, we know that *n*-paraffin molecules have cylindrical symmetry both in the liquid state and rotatory phase (α phase) It is very reasonable to presume that the solute molecules in the interfacial phase are similar to α molecules If a small change in cell parameters caused by phase transition is negligible (it is the case of the phase transition from the orthorhombic phase to the hexagonal phase), we can use α molecules to stand for solute molecules in the interface for our estimation This method is called *the α molecule approach* C_i^0 can be thus calculated from the enthalpy of the α–β phase transition and enthalpy of fusion Expression (32) has to be adjusted and gets the shape of

$$\begin{aligned}C_i^0&=\sum_1^n\frac{1}{2}(\Phi_i^{\alpha\alpha}-\Phi_i^{\beta\beta})\Big/\sum_1^n\frac{1}{2}(\Phi_i^{ll}-\Phi_i^{\beta\beta}),\\&=\Delta h_{tr}^{\alpha-\beta}/\Delta h_m^{\alpha-l},\\&=\Delta h_{tr}^{\alpha-\beta}/(\Delta h_{tr}^{\beta-\alpha}+\Delta h_m^{\alpha-l}),\end{aligned} \tag{32'}$$

where superscripts α, β, and l denote α state, β state, and liquid state, respectively In order to obtain Eq (32') we also assume $\Delta C_p\simeq 0$ The calculated results of thermodynamic parameters obtained from Ref 24 are given in Table I The uncertainty of C_i^0 for different *n*-paraffins may result

TABLE I The estimated values of C_l^0 for n-paraffins based on Eq (32')

n-Paraffin	C_l^0	$\overline{C_l^0}$
n-$C_{11}H_{24}$	0 236	
n-$C_{13}H_{28}$	0 212	
n-$C_{15}H_{32}$	0 209	
n $C_{17}H_{36}$	0 215	
n-$C_{19}H_{40}$	0 232	
n-$C_{21}H_{44}$	0 245	0 259
n-$C_{23}H_{48}$	0 248	
n-$C_{25}H_{52}$	0 311	
n-$C_{27}H_{56}$	0 323	
n-$C_{29}H_{60}$	0 323	
n-$C_{31}H_{64}$	0 266	
n-$C_{35}H_{72}$	0 258	

from experimental errors in the determination of the enthalpy of phase transitions

In comparison of the three cases mentioned earlier in Sec II B with the results listed in Table I, it can be seen that our system is the case of $C_l < 1$ (we suppose that C_l and C_l^0 have not much difference) This shows that surfaces of n-paraffin crystals in contact with their regular solutions will be extra wetting

The estimation of $(\phi_{str}^{SB} - \phi_{str}^{AB})$ is much more questionable In Sec III A we found that concerning in S–B interactions only $(S\text{–}B)_2$ are quite different from A–B interactions at the interfaces From a statistical thermodynamic point of view it can be said that the ratio between the number of rotating and fixed solvent molecules at the interface is temperature dependent In the following we will introduce the *ad hoc* assumption that the solvent molecules at the interface have an equal chance to be in a rotation state and a fixed state, hence

$$(\phi_{str}^{SB}-\phi_{str}^{AB}) \simeq \tfrac{1}{2}[\phi_{str}^{(SB)_1}-\phi_{str}^{AB}]+\tfrac{1}{2}[\phi_{str}^{(SB)_2}-\phi_{str}^{AB}],$$

$$=\tfrac{1}{2}[\phi_{str}^{(SB)_2}-\phi_{str}^{AB}]. \qquad (39)$$

We note that the interactions between n-paraffin molecules are van der Waals interactions, which are short range interactions It is reasonable to assume that $[\phi_{str}^{(SB)_2} - \phi_{str}^{AB}]$ is approximately equal to $[\phi_{str}^{(SS)_B} - \phi_{str}^{BB}]$ $(SS)_B$ denotes the solid–solid interaction in B-type crystals Combining expressions (30) and (32), we thus obtain

$$[\phi_{str}^{(SB)_2}-\phi_{str}^{AB}] \simeq [\phi_{str}^{(SS)_B}-\phi_{str}^{BB}]$$

$$= -2\Delta h_B^f\, C_l^0/\tilde{H}(\text{solvent}) \qquad (40)$$

(Δh_B^f is the enthalpy of fusion of pure solvent) Finally, the estimated values of $(\phi_{str}^{SB} - \phi_{str}^{AB})$, along with the necessary data for n-paraffin–n-hexane solution system, are listed in Table II

TABLE II Results of the estimation of $(\phi_{str}^{SB} - \phi_{str}^{AB})$ for n-paraffin–n-hexane solutions based on Eq (39) and along with necessary data

Δh_B^f[a] (cal/mol)	$\Delta\tilde{H}$ (n-hexane)	C_l^0[b]	$(\phi_{str}^{SB} - \phi_{str}^{AB})$ (cal/mol)
3114	2 676	0 259	−301

[a] Δh_B^f of n-hexane is quoted from Ref 24

[b] C_l^0 is $\overline{C_l^0}$ given in Table I

IV. EXPERIMENTAL VERIFICATION AND DISCUSSION

Recent observations of paraffin molecules within an adsorption layer on a solid substrate with scanning tunneling microscope (STM) technique strongly suggest how the interface of paraffin crystal solution may look We refer to the work of McGonigal and his colleagues[27,28] who have directly imaged n-paraffin layers adsorbed at the liquid/graphite interface using STM In their investigations, two types of adsorbed systems were explored One system exploited the preferential adsorption of n-$C_{32}H_{66}$ from two liquid solvents (iso-octane and n-decane) on a freshly cleaved substrate of highly oriented pyrolytic graphite The other system studied is the adsorption of pure n-$C_{17}H_{36}$ melt Their results exhibited an image of the adsorbed layer as a two dimensional array of n-$C_{32}H_{66}$ molecules, which is similar to the structure of solid n-$C_{32}H_{66}$ The results of the second system are similar We ourselves recently also carry out analogous experiments for the n-$C_{33}H_{48}$–n-hexane solution system, almost the same results are obtained (work in progress) All of these indicate that the adsorbed layers possess a high degree of two dimensional ordering Although here the adsorption occurs on a graphite substrate, it is very reasonably to infer from this that the same ordered structure exists at the liquid/n-paraffin interface where a n-paraffin crystal is the substrate Therefore, we can consider it as a strong experimental support to our ordering model of the interfacial structure schematically shown in Fig 2

In the following, we will use the roughening phase transition as a probe to determine the surface parameters, and subsequently to determine the bonding condition at the interfaces

A. Experimental determination of C_l

As we indicated in Sec I, the roughening temperature of face (hkl) is directly proportional to the bond energies at the interface, while the bond energies in the bulk are associated with dissolution enthalpy Basically we can rely on Eqs (1) and (30) to determine the bond energies at the interfaces and in the bulk experimentally, and the data for

TABLE III Experimental results of the determination of the interfacial bond energies and the bulk bond energies for three n-paraffin–n hexane solutions

	Δh^{dmm} (cal/mol)	$\Delta\tilde{H}^a$	Φ_{str} (cal/mol)	T_{hkl}^a (K)	σ_{hkl}^b	ϕ_{str} (cal/mol)
n-C_{33}/n-C_6	18 022	2 781	6483	283 80	0 8496	1327
n-C_{21}/n-C_6	16 411	2 791	5881	273 25	0 8741	1242
n-C_{16}/n-C_6	12 258	2 433	5049	284 80	0 9765	1160

[a] Δh^{dmm} and T_{hkl} are determined in our experiments (Refs 29–31) For n-$C_{33}H_{48}$ and n-$C_{21}H_{44}$, T_{hkl} corresponds to the roughening temperature of {110} faces for n $C_{16}H_{34}$ to {010} faces

[b] $\Delta\tilde{H}$ and σ_{hkl} are calculated data.

TABLE IV Results of surface parameters, C_l, C_l^0 and $(\phi_{str}^{SB} - \phi_{str}^{AB})$ resulting from experimental data

	C_l	C_l^0 (or C^0)	$(\phi_{str}^{SB} - \phi_{str}^{AB})$ (cal/mol)
n-C_{23}/n C_6	0 205	0 235	
n-C_{21}/n-C_6	0 211	0 244	−200
n-C_{16}/n C_6	0 230	0 244	

n-$C_{23}H_{48}$, n-$C_{21}H_{44}$, and n-$C_{16}H_{34}$ in n-hexane solutions have been determined systematically [29–31] The results are listed in Table III We note that the β phase of odd paraffins, n-$C_{23}H_{48}$, n-$C_{21}H_{44}$, differ from even ones (n-$C_{16}H_{34}$) Crystals of n-$C_{23}H_{48}$, and n-$C_{21}H_{44}$ belong to the orthorhombic phase, while crystals of n-$C_{16}H_{34}$ belong to the triclinic phase However, if we adapt the idea that C_l^0 is face independent, it can be inferred that C_l^0 is independent of the structures The implication is that the ordering and orientation process in the interfacial phase is similar for different β structures of n-paraffins

Using the data given in Table III the surface scaling factors and other surface parameters are calculated from expressions (32) [or Eq (33)], (34′), (35′), and presented in Table IV Since the term $(\phi_{str}^{SB} - \phi_{str}^{AB})$ is quite solvent and temperature dependent and T_{hkl}^r determined for the three n-paraffins is not very different (see Table III), in our calculation we assume that this term is constant

In comparison of experimental results with absolute values of C_l^0 presented in Table I, we have found that they agree quite well This suggests consequently that our interfacial model for aliphatic crystals in equilibrium with the solutions is a good model for this interface Looking at Table IV, it can be seen that C_l's for different n-paraffins with different structures are a bit different, but C_l^0's are almost constant, which is consistent with our expectation At this point, we conclude that upon using the scaling factor C_l^0 the discrepancy of bond situations between the interfacial phase and the bulk phase is explained adequately

The values of $(\phi_{str}^{SB} - \phi_{str}^{AB})$ presented both in Table II and Table IV are, in principle, comparative The difference results from our crude approximation in which we suppose that in the interface, rotating solvent molecules, and fixed ones share the same percentage In fact, the solvent molecules are fully rotating in the bulk phase The existence of fixed solvent molecules is because of the adsorption of solvent molecules at the interface and the restriction of other units on the rotation of solvent molecules in the interfacial phase Since our experimental temperature is higher than the melting point of the solvent (n-hexane), the number of fixed molecules should be less than the rotating ones Therefore, the result listed in Table II is overestimated

Taking a general view of n-paraffin–n-hexane solution system, the condition of more than equivalent wetting ($C_l < 1$) is indeed fulfilled As we have expected, it is because the smectic ordering and orientation of fluid units occur in the interfaces It makes the fluid units fit in well with the solid surface structures of paraffin crystals, so that step energies and step free energy caused by different arrangements and interactions between unlike units are considerably reduced

B. Dependence of roughening temperature on concentration of solutions

In Sec II B, we recall that C_l is concentration dependent Therefore, the interfacial bond energies are also concentration dependent Considering the direct relation between ϕ, and T^r, it will turn out that the roughening temperature varies with the change of concentration in solutions This is clearly indicated in Eq (41) or (41′)

$$T_{hkl}^r = \frac{2\theta_{hkl}^r}{R}\left|\left[\frac{1}{2}(\Phi_{str}^{AA} - \Phi_{str}^{SS}) + (1 - X_A)^2\,\Phi_{str}^{\sigma}\right] C_l^0 + [1 + (\alpha_l - 1)X_A](\phi_{str}^{SB} - \phi_{str}^{AB})\right| \tag{41}$$

or

$$T_{hkl}^r = \frac{2\theta_{hkl}^r}{R}\left|\frac{\Delta h^{diss}}{\tilde{H}} C_l^0 + [1 + (\alpha_l - 1)X_A](\phi_{str}^{SB} - \phi_{str}^{AB})\right| \tag{41}$$

Equations (41) and (41′) result from a combination of the Eqs (1), (6′) (30), (31), (33), (34), and (35) Now let us apply Eq (41) or (41′) to the n-$C_{23}H_{48}$ and n-hexane solution system The roughening temperature of face (110) vs mole fraction of solute is plotted in Fig 4(a), along with solubility curve of the system It should be noted that applying Eq (41) or (41′) we assume that $\theta_{hkl}^r \cong \theta_{hkl}^r$ as before[7] (θ_{hkl}^r denotes the dimensionless Ising temperature) It can be seen from Fig 4(a) that owing to the different shape, the two curves intercept each other at X_1^r and X_2^r According to the concept of roughening transition, we know that when the solubility curve is below the roughening transition curve, the equilibrium structure of (110) surface will be in flat mode, otherwise it will be in rough mode Therefore, in case

$$X_1^r < X < X_2^r \tag{42}$$

(110) faces are rough, while

$$X < X_1^r \quad \text{or} \quad X > X_2^r \tag{43}$$

(110) faces should be flat Theoretically, at X_1^r or X_2^r two kinds of roughening transitions will occur By lowering the liquidus temperature, a roughening phase transition from the rough to the flat structure occurs at X_1^r, while a roughening phase transition from the flat to the rough structure will happen at X_2^r $T^r(X_1^r)$ has been measured (see Table III), but it is impossible to determine $T^r(X_2^r)$ in our solution system The reason is that when $X > X_{tr}$, the phase transition from orthorhombic structure (or β_0 structure) to hexagonal structure (or α structure) will occur As α molecules are very similar to fluid molecules at the interface, $|\phi_{str}^{AA} - \phi_{str}^{SS}|$ becomes very small, and the value of ϕ_{str}, as well as T^r, will drop dramatically, which results in completely circular lateral faces [32] Since $X_2^r > X_{tr}$, roughening

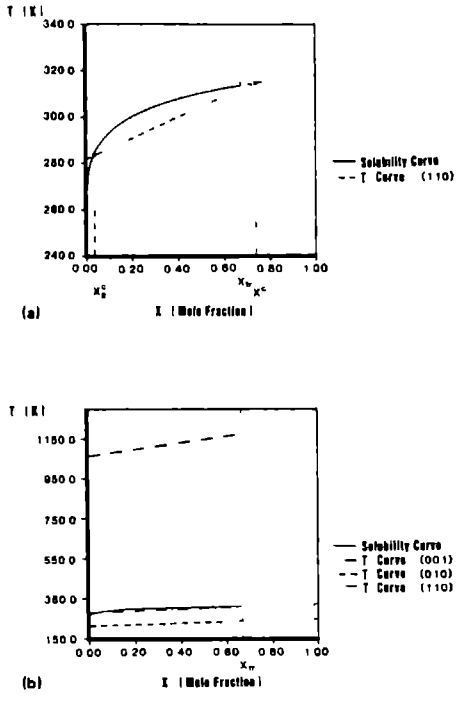

FIG 4 A roughening transition phase diagram of n-$C_{23}H_{48}$–n hexane system (a) Plots of roughening temperature T^r_{110} and equilibrium temperature T_e vs mole fraction of solute (X) (b) Plots of T^r_{001}, T^r_{110}, T^r_{010}, and T_e vs X

transition at $T^r(X_2^s)$ cannot be observed Anyway, a similar roughening transition from flat to rough mode, as we expect at $T^r(X_2^s)$, was observed in naphthalene–pyrene system [33]

In order to make a comparison, the roughening temperature of face (001) and face (010) against concentration is plotted in Fig 4(b), along with that of face (110) and liquidus curve In the whole range of concentration, T^r_{001} is much higher than the equilibrium temperature So the roughening transition never takes place on the (001) face On the other hand, T^r_{010} is much lower than the liquidus temperature under normal conditions unless the concentration of n-$C_{23}H_{48}$ is extremely low This is why in normal conditions a faceted (010) face cannot be observed

From Eq (41) we still can find that for n-paraffin–n-hexane systems, the variation of T^r_{hkl} is quite dependent on the value of $(\phi^{SB}_{str} - \phi^{AB}_{str})$ because ϕ^{σ}_{str} is very small When $(\phi^{SB}_{str} - \phi^{AB}_{str}) \sim 0$, T^r_{hkl} becomes concentration independent

In concluding this part, we may indicate that Fig 4 represent a kind of roughening phase transition diagram To determine the diagram, on one hand we must have precise roughening temperature data, on the other hand,

V. SUMMARY AND CONCLUSIONS

The interfacial bonding situation of crystals in contact with a saturated solution is in general different from that in the bulk, which can be described by the so-called surface scaling factors (C_l and C_l^0 or C_l^*) For the solution system formed by aliphatic crystals and similar solvent, a simple model is set up to estimate the interfacial parameters, such as C_l^0 (or C_l^*), $(\phi^{SA}_{str} - \phi^{AA}_{str})$ and $(\phi^{SB}_{str} - \phi^{AB}_{str})$ Experimentally, it turns out that for n-paraffin–n-hexane solution system,

$$C_l^0(\text{or } C_l^*) \sim 0\,244,$$

$$(\phi^{SA}_{str} - \phi^{AA}_{str}) \sim 0,$$

$$(\phi^{SB}_{str} - \phi^{AB}_{str}) \sim -200 \text{ cal/mol},$$

under normal conditions The agreement of estimated results with experimental ones confirms that the interfacial structures are in quasi crystalline state, the fluid units at the interfacial phase show a high degree of the ordering and orienting along the solid surface structure The similarity between solid and fluid units greatly compensates the interaction difference

Based on the relation between concentration and bond energy, a roughening phase transition diagram of n-$C_{23}H_{48}$ in n-hexane solvent system was presented It shows that the roughening temperature directly depends on the concentration of solutions

ACKNOWLEDGMENTS

Authors wish to appreciate Shell Netherlands B V providing a donation for the research program on growth and morphology of n-paraffins We also appreciate Mr Jan van Kessel's help to make some of the drawings

[1] W K Burton N Cabrera and F C Frank Philos Trans R Soc London Ser A 243 299 (1951)
[2] K A Jackson *Liquid Metals and Solidification* (Am Soc Metals Cleveland 1958)
[3] D E Temkin *Crystallization Process* (Consultants Bureau New York 1966)
[4] H J Leamy and K A Jackson J Appl Phys 42 2121 (1971)
[5] G H Gilmer and P Bennema J Appl Phys 43 1349 (1972)
[6] P Bennema and G H Gilmer in *Crystal Growth an Introduction* edited by P Hartman (North Holland Amsterdam 1972) p 263 P Bennema and J P van der Eerden in *Morphology of Crystals, Part A* edited by I Sunagawa (Terra Scientific Tokyo 1987) p 1
[8] L A M J Jetten H J Human P Bennema and J P van der Eerden J Cryst Growth 68 503 (1984)
[9] R D Groot M Elwenspoek and P Bennema, J Cryst Growth 79 817 (1986)
[10] M Elwenspoek Mol Phys 64 229 (1986)
[11] M Elwenspoek P Bennema, and J P van der Eerden J Cryst Growth 83 297 (1987)
[12] A D J Haymet and D W Oxtoby J Chem Phys 74 2559 (1981)
[13] M Baus and J L Colot Mol Phys 55 653 (1985)
[14] W A Curtin and N W Ashcroft Phys Rev A 32 2909 (1985)
[15] F F Abraham and J Q Broughton Phys Rev Lett 56 734 (1986)
[16] J Q Broughton and F F Abraham Chem Phys Lett 71 456 (1980)
[17] J Q Broughton and G H Gilmer J Chem Phys 79 5095 5105 5119 (1983) 84 5741 5749 5759 (1986)
[18] T A Cherepanova and A V Stekolnikov J Cryst Growth 99 88

[19] T A Cherepanova and A V Stekolnikov, in *Proc 11th Symposium on Industrial Crystallization*, edited by A Mersmann (Garmisch-Partenkirchen 1990), p 861
[20] R D Groot N M Faber, and J P van der Eerden, Mol Phys. 62, 861 (1987)
[21] M Plischke and B Bergensen, *Equilibrium Statistical Physics* (Prentice Hall International, New York, 1989)
[22] J M Ziman *Models of Disorder* (Cambridge University, London, 1979)
[23] S R Fowler and E. A Guggenheim, *Statistical Thermodynamics* (Cambridge University, London, 1960)
[24] M G Broadhurst, J Res Natl Bur Stand Sec A 66, 241 (1962)
[25] Hildebrand, J Am Chem Soc. 59, 794 (1937)
[26] Yu V Mnyukh, J Phys Chem Solids 24, 631 (1963)
[27] G C McGonigal R H Bernhardt, and D J Thomson. Appl Phys Lett 57, 28 (1990)
[28] G C McGonigal, R H Bernhardt, Y H Yeo and D J Thomson, J Vac Sci Techol B 9, 1107 (1991)
[29] P Bennema, X Y Liu, K Lewtas, R D Tack, J J M Rijpkema, and K J Roberts, J Cryst Growth (in press)
[30] X Y Liu and P Bennema, J Cryst Growth (submitted)
[31] X Y Liu and P Bennema, J Cryst Growth (submitted)
[32] A Toda, H Miyaji, Y Ogawa, and K Takamizawa. J Mat Sci 26. 2793 (1991)
[33] V V Podolinsky and V G Drykin, J Cryst Growth 62, 532 (1983)

Chapter 4.2

The relation between macroscopic quantities and the solid–fluid interfacial structure

Xiang-Yang Liu and P Bennema
RIM Laboratory of Solid State Chemistry, Faculty of Science, University of Nijmegen, Toernooiveld, 6525 ED Nijmegen, The Netherlands

(Received 19 June 1992, accepted 14 December 1992)

The relation between thermodynamic quantities and the interfacial structure is described on the basis of a layer model (or an inhomogeneous cell model) By introducing the surface characteristic scaling factor C_i^* (or C_i^0) and the surface concentration (or density) distribution constant K_i, thermodynamic quantities of the interfacial phase are correlated with the corresponding quantities of the bulk phase Relevant expressions are derived from basic principles of statistic thermodynamics In order to clarify the relevant consequences, two systems, the hard-sphere–hard-wall system and the crystal–solution system of aliphatic compounds, are discussed It is shown that within the framework of our model, experimental data are explained in a satisfactory way The character of solid–fluid interfaces is discussed, in terms of wetting conditions As a consequence of this approach, solid–fluid interfaces are classified into three typical cases the equivalent wetting case (C_i^* or $C_i^0=1$), the more than equivalent wetting case (C_i^* or $C_i^0<1$), and the less than equivalent wetting case (C_i^* or $C_i^0>1$) It turns out that except the equivalent wetting case, the concentration of solute (or the density of fluid units) in the interfacial phase will differ from that in the bulk fluid phase at equilibrium.

I. INTRODUCTION

In order to study crystal growth mechanisms and to predict the morphology of crystals, theoretical and experimental information must be available for the physical properties of the interface between the bulk of the crystal and the bulk of the fluid phase [1–3] Subtle changes at this interface may give a dramatic change in growth mechanisms Also, the relative growth rates of different crystallographic faces under the influence of a driving force for crystallization are determined in a subtle way by the differences in structures of interfaces. These relative growth rates of different faces determine the morphology of crystals In the study of crystal growth mechanisms and morphology of crystals, it is essential to predict and to understand whether a given surface (hkl) is growing above or below its roughening temperature [3] In the first case, a roughened rounded off surface occurs and in the second case a crystallographic face (hkl) grows by a layer by layer mechanism In case a surface growing below its roughening temperature is exposed to a supersaturation which is higher than a certain critical supersaturation, critical two-dimensional nuclei get the size of a few molecules, then the so-called kinetic roughening occurs In this case also a roughened rounded off surface results Both thermal roughening and kinetic roughening of a face (hkl) depend on the physical character of interface Expressed in the language of Ising or cell models, it can be stated that the physical state of the interface depends on the bond energies between solid and fluid units at the interface The dimensionless roughening temperature θ'_{hkl} which determines the roughening transition of a face is defined as[3]

$$\theta'_{hkl}=2kT'/\phi_{sir} \tag{1}$$

Here ϕ_{sir} represents the strongest bond energy at the interface, k is the Boltzmann constant, and T' is the actual roughening temperature In this paper, the convention is used that θ'_{hkl} is referenced to ϕ_{sir}. In cell models, where the whole space (both the bulk and the interface) is partitioned in solid and fluid cells of equal size and shape, the energy of the ith bond is defined as

$$\phi_i=\phi_i^{sf}-\frac{1}{2}(\phi_i^{ss}+\phi_i^{ff}) \tag{2}$$

In Eq (2), superscript sf refers to a solid–fluid bond energy, ss to a solid–solid, and ff to a fluid–fluid bond energy

In order to calculate the effective bond energies ϕ_i given by Eq (2) as they occur at the interface of a crystallographic face (hkl) in contact with the fluid phase, traditionally two *ad hoc* approximations[1–4] are introduced, which are (i) the proportionality assumption and (ii) the equivalent wetting assumption

The proportionality assumption states that for the bond energies ϕ_i occurring at the surface, the ratio of bond energies is the same as the ratio of the bond energies ϕ_i^{ss} referenced to vacuum If per structural unit has $i=1, 2, \ldots, n$ bonds in connection to neighboring units, the following relation holds,

$$\phi_1\phi_2 \quad \phi_i \quad \phi_n=\phi_1^{ss}\phi_2^{ss} \quad \phi_i^{ss} \quad \phi_n^{ss} \tag{3}$$

Then relative bond energies can in principle be calculated

The equivalent wetting assumption was first introduced by Jackson[4] according to a traditional cell model (here we call *the homogeneous cell model*) This assumption consists of two parts First, both the fluid and the solid are completely homogeneous from the bulk to the dividing surface (this will in the following be called *the homogeneous phase approximation*) This implies that various bond energies in the bulk (such as Φ_i^{ss}, Φ_i^{ff}, etc) are equiv-

 0021 9606/93/075863 10$06 00

alent to the corresponding bond energies in the interfacial phase (such as ϕ_i^{ss}, ϕ_i^{ff}, etc) Within this classical approach, it is assumed that the same types of cells are not distinguished by their positions Second, it is assumed that at the interface $\phi_i^{sf} \simeq \phi_i^{ff}$ [or for a mixture of A, B types of molecules, $\phi_i^{SA} \simeq \phi_i^{AA}$ and $\phi_i^{SB} \simeq \phi_i^{AB}$ (Ref 5)] Generally, it follows from this assumption that macroscopic quantities of the interface equal the corresponding quantities of the bulk This implies that

$$\sum_{i=1}^{n} \phi_i \simeq \Delta\tilde{H}_d \text{ or } \Delta\tilde{H}_m \tag{4}$$

Here $\Delta\tilde{H}_d$ and $\Delta\tilde{H}_m$ denote the enthalpy of dissolution and melting per structural unit, respectively Using Eqs (3) and (4), bond energies as they occur at the surface can be calculated

From research in the past on the growth and morphology of crystals, it was found that the equivalent wetting assumption leading to (4) is not fulfilled According to investigations on the roughening transition and 3D homogeneous nucleation, it was found that for metals and some inorganic crystals grown from their melt or solutions, the use of the equivalent wetting assumption underestimates ϕ_i by a factor of 2 5–6 [6–10] In contrast, for chain-like molecule systems, the wetting assumption overestimates ϕ_i by a factor of 2 5–6 [5] To remove the difficulties with the equivalent wetting assumption, some alternatives[11 12] have been developed In those attempts, people on one hand focused on the refinement of ϕ_i^{sf} in Eq (2) (or ϕ_i^{SA} and ϕ_i^{SB}, in the case of crystals in contact with solutions), people on the other hand accepted the very poor estimation of ϕ_i^{ss} and ϕ_i^{ff} based on the homogeneous phase approximation

Recently much progress concerning the structure of crystal–fluid interfaces has been made by computer simulations and density-functional theories [13–22] All results indicate that the structure and macroscopic quantities, such as the density (or concentration) and the potential energy in the regions adjacent to the surface are quite different from those of the bulk phase This can be seen from the fact that in solid–fluid interfacial systems, the interfacial profile showing oscillations of density on the solid side extends to the fluid side and gradually vanishes going from the solid surface to the bulk fluid Correspondingly, it follows that potential energies (or interaction energies) of fluid units in the interfacial phase differ from those in the bulk phase In addition to this, it was observed with the scanning tunneling microscope (STM) technique[23–25] that the structure of fluid n-paraffin and other organic molecules within adsorption layers on a graphite substrate also displays a high degree of two-dimensional ordering and orientation, which is similar to the structure of the solid phase This indicates explicitly that in the description of the solid–fluid interface, the equivalent wetting assumption, especially the homogeneous phase approximation, is invalid We notice that the failure of the equivalent wetting assumption is attributed to the relaxation or reconstruction of the solid layers and the ordering of the fluid layers at the interface Concerning Eq (2), ϕ_i^{ss} at the interface is different from the corresponding one in the bulk due to the relaxation or the reconstruction of interfacial solid layers Similarly, ϕ_i^{ff} at the interface is also different than that of the bulk due to the ordering of interfacial fluid layers Then ϕ_i^{sf} will be influenced and consequently ϕ_i at the interface differs from that in the bulk

In view of the above-mentioned facts, it is necessary to have a more precise model in place of the traditional homogeneous cell model to describe the interface In our previous paper,[5] we presented a first attempt to distinguish the interfacial bond energy (denoted by ϕ) from the bulk bond energy (denoted by Φ) Here we will systematically discuss this issue from the basis of statistic thermodynamic principles The purpose of this paper is to relate the structure of the interface with properties in a modified cell model This will provide a reliable method to deduce relevant interfacial quantities from theoretical results or from experimental data

This paper is organized as follows In Sec II, we develop an inhomogeneous cell model, the so-called layer model to describe the solid–fluid interface It can be seen later in our treatment that this model is much closer to reality than the traditional homogeneous cell model used by Jackson[4] and Temkin [2] In the model, a simplified interfacial system is defined using the two-step model, and relevant surface parameters are derived In Sec III, these results are applied to the hard-sphere–hard-wall system and the crystal-solution system of aliphatic compounds In Sec IV, three typical interfacial structures are discussed Finally, summary and conclusions are presented in Sec V

II. GENERAL MODEL AND INTERFACIAL QUANTITIES

In the following treatment, only solid–liquid systems are concerned The obtained results may straightforwardly be extended to other systems In order to simplify our treatment, in this section we will deal with normal (unassociated) liquids in contact with flat solid surfaces

A. The layer model and relevant surface parameters

Let us consider a solid–fluid system with a flat interface parallel to a face (hkl) of a crystal (see Fig 1) In this system, there is a sharp boundary (the horizontal solid line) between the solid phase and the fluid phase The space above the boundary belongs to the fluid phase and the space below to the solid phase Now we divide the whole space (for both the solid and the fluid), parallel to the orientation (hkl), into a set of layers Every layer has a thickness of the interplanar distance d_{hkl} (Actually, d_{hkl} corresponds to the periodicity of the density oscillation in the normal direction of the surface, according to density-functional theories and computer simulations [13–22]) Assume that each layer is a homogeneous and essential part of the system Then we may in principle use an independent set of state variables to characterize the thermodynamic equilibrium state of a layer On the other hand, for different layers, corresponding properties and structures can be different or the same, depending on the regions in which they are situated Here we define a single layer in the interfacial regions as an independent subphase because its

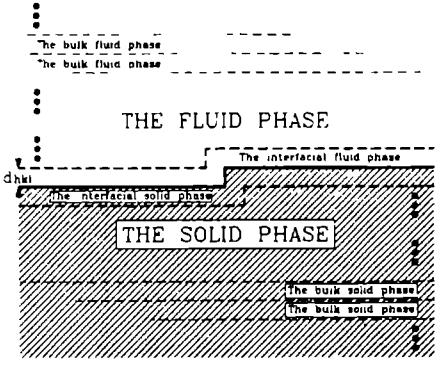

FIG 1 A schematic illustration for the slice model See the text for more details

structure is different from other layers Those layers which are in infinite distances from the dividing surface and have the same structure are considered as a single phase. Now the general picture of the solid–fluid interface according to the layer model can be described as follows· The structure of interfacial layers changes gradually from one to the other, as extending from the dividing surface to layers where the density gradients vanish. The same holds for the properties of structural units. Explicitly, we present here an inhomogeneous approach within the framework of a cell model for the interface. In this approach, all the same types of units are distinguished by the distance to the dividing plane of interfaces. Note that this local homogeneity within the thickness of a layer in the normal direction of the surface results from a cell model approximation. It looks somewhat different from those pictures presented by density-functional theories and computer simulations, in which the oscillation of the density occurs. Actually, in this layer model, we average the oscillation of the density (or other relative properties) over one period (d_{hkl}).

In comparison with conventional descriptions, it is found that our description is similar to Guggenheim's method,[26] where a new mediate phase, *the interfacial phase*, is defined in interfacial regions. However, ours is different from Gibbs' approach,[27] which is obtained from a geometrical construction In Gibbs' approach, somewhere in the interface a plane parallel to the surface is drawn. This is commonly referred to as Gibbs' equimolar dividing surface. From Gibbs' approach, interface excess functions, such as the interface excess free energy, etc, are defined.[27,28] In this connection, we notice that in the layer model, interface excess functions are distributed in the layers of interfacial regions and included in those functions of local layers. This can be seen from the fact that thermodynamic functions of those layers are different from the bulk. In order to calculate an interface excess function based on the layer model, one needs to integrate differences of the function between interfacial layers and the bulk. (A detailed description on this issue will be published elsewhere.)

Considering that many physical processes (such as the surface roughening) are directly related to the physical state and thermodynamic properties of the first solid and the first fluid layer adjacent to the dividing surface, we will focus our attention to the regions Now we simplify a solid–fluid interfacial system using a two-step interface model in the layer space First, we need to define our system. The fluid layer adjacent to the solid phase is defined as the interfacial fluid subphase Those fluid layers having infinite distances from the solid surface share the same corresponding physical properties. This implies that they are a homogeneous part of the system. The whole of those layers is therefore defined as the bulk fluid phase. Similarly, the interfacial solid subphase and the bulk solid phase are defined Basically, the bulk fluid (and the bulk solid) and the interfacial fluid (and the interfacial solid) are distinguished as different phases because they have different structure and macroscopic properties It has to be noted that once a solid surface with a certain area is given, the number of structural units in interfacial regions will also be fixed. In this sense, the interfacial phase is different from a normal bulk phase.

Secondly, it can be seen from earlier discussions that in the layer space, there are a number of intermediate layers between the bulk phase and the interfacial subphase In our consideration, structural units in all layers are supposed to be in thermodynamic equilibrium It thus follows that each bulk phase and interfacial subphase are in mutual thermodynamic equilibrium. We may then take two discontinuous steps in both the solid and the fluid sides to omit those intermediate layers and concentrate directly on the equilibrium between the bulk phase and the interfacial subphase According to thermodynamics, when thermal ($T^i = T^j$), hydrostatic ($P^i = P^j$), and chemical ($\mu_q^i = \mu_q^j$) equilibria occur, these four phases and subphases in the system can coexist in stable (thermostatic) equilibrium

$$\text{the fluid bulk phase} \rightleftharpoons \text{the fluid interfacial subphase} \rightleftharpoons \text{the solid interfacial subphase} \rightleftharpoons \text{the solid bulk phase}$$

Here superscript "i" denotes any one of the four phases, "j" one of the rest, and subscript "q" represents one of components coexisting in the four phases In this way, a solid–fluid interfacial system is simplified.

The coexistence of the four phases and subphases in this simplified interfacial system is also in agreement with Gibbs' phase rule For a single component system, normally one can have a maximum of three coexisting phases. In the case of the interface, Gibbs' phase rule must, however, be modified to include the extra surface tension variable For this layer model, when each extra subphase is defined in the system, an extra independent "subdividing surface" may be created simultaneously This follows that a new independent *sub*surface tension term is also introduced As a result, the degrees of freedom of this thermodynamic system remain unchanged

To connect macroscopic quantities between the two phases, as in our previous paper,[5] we again introduce the so-called surface characteristic scaling factor C_I^* (or C_I^0) to associate the enthalpy in the interfacial phase with that in the bulk phase For a crystal in contact with its melt or an ideal solution, this factor is expressed in the following way

$$C_I^0=\Delta\tilde{H}_m^I/\Delta\tilde{H}_m \tag{5}$$

When a crystal contacts a nonideal solution, this factor is rewritten as

$$C_I^*=\Delta\tilde{H}_d^I/\Delta\tilde{H}_d \tag{6}$$

Here superscript "I" distinguishes an interfacial quantity from the corresponding one in the bulk phase Since the concentration X (or density ρ) of interfacial fluid phase also differs from that of the bulk fluid phase, we define here the surface concentration (or density) distribution constant as the following

$$K_I=X_A^I/X_A, \tag{7}$$

or for crystals in equilibrium with the melt

$$K_I=(\rho_f^I/\rho_s)/(\rho_f/\rho_s) \tag{7a}$$

Here subscript "A" denotes the solute, "f" the fluid and "s" the solid state.

It will be seen in the following that C_I^* (or C_I^0) and K_I are the essential factors from which all other interfacial quantities can be derived

B. Thermodynamic derivation for K_I

In this section, we will derive the thermodynamic expression of K_I for crystal-solution systems In Sec II D, we will come back to crystal-melt systems

In the bulk phase, for a saturated solution in equilibrium with a solid at a given temperature, the chemical potential of the solute is identical with that of the pure solid solute at that temperature For a regular solution, the following relation holds[5 29]

$$\ln X_A=-\frac{\Delta\tilde{H}_d}{RT}+\frac{\Delta\tilde{S}_d}{R}, \tag{8}$$

where $\Delta\tilde{S}_d$ is the molar entropy of dissolution For the interfacial phase, the corresponding expression of Eq (8) is given by

$$\ln X_A^I=-\frac{\Delta\tilde{H}_d^I}{RT}+\frac{\Delta\tilde{S}_d^I}{R} \tag{8a}$$

On the other hand, for the simplified interfacial system, the chemical potential of solute (A) in the bulk fluid phase can be expressed as

$$(\mu_A)_{(A\ B)}=(\mu_A)_A^*+\ln X_A \tag{9}$$

$(\mu_A)_A^*$ is the chemical potential of component A at the reference state (where X_A is extrapolated to 1) and expressed as

$$(\mu_A)_A^*=(\mu_A)_A+(\mu_A)'_A, \tag{10}$$

where $(\mu_A)_A$ is the chemical potential of a solute molecule in the pure liquid state and $(\mu_A)'_A$ is the excess value of $(\mu_A)_A$ due to the mixing of two components in a regular solution For an ideal solution, $(\mu_A)_A^*=(\mu_A)_A$ because $(\mu_A)'_A=0$ If the exchange effect of mixing needs not be considered separately, Eq (10) is rewritten according to thermodynamics as

$$(\mu_A)_A^*=\tilde{H}_f-T\ \tilde{S}_f \tag{11}$$

Analogous functions hold for the interfacial fluid subphase

$$(\mu_A^I)_{(A\ B)}=(\mu_A^I)_A^*+\ln X_A^I, \tag{9a}$$

where

$$(\mu_A^I)_A^*=(\mu_A^I)_A+(\mu_A^I)'_A, \tag{10a}$$

or

$$(\mu_A^I)_A^*=\tilde{H}_f^I-T\ \tilde{S}_f^I \tag{11a}$$

In the bulk and the interface, the chemical potential of a solid unit can be expressed as

$$(\mu_A)_S=\tilde{H}_s-T\ \tilde{S}_s \tag{12}$$

and

$$(\mu_A^I)_S=\tilde{H}_s^I-T\ \tilde{S}_s^I, \tag{12a}$$

respectively As discussed in Sec II A, the four phases and subphases are supposed to be in thermodynamic equilibrium with each other Then the three independent relations hold

$$(\mu_A)_{(A\ B)}=(\mu_A^I)_{(A\ B)}, \tag{13}$$

$$(\mu_A^I)_{(A\ B)}=(\mu_A^I)_S, \tag{13a}$$

$$(\mu_A)_{(A\ B)}=(\mu_A)_S \tag{13b}$$

Combining Eqs. (9), (11), (9a), (11a), (12), and (12a) yields

$$\ln(X_A^I/X_A)=-\frac{\Delta\tilde{H}'}{RT}+\frac{\Delta\tilde{S}'}{R} \tag{14}$$

Here according to Eqs (8) and (8a),

$$\Delta\tilde{H}'=[(\tilde{H}_f^I-\tilde{H}_s^I)-(\tilde{H}_f-\tilde{H}_s)]=\Delta\tilde{H}_d^I-\Delta\tilde{H}_d, \tag{15}$$

and

$$\Delta\tilde{S}'=[(\tilde{S}_f^I-\tilde{S}_s^I)-(\tilde{S}_f-\tilde{S}_s)]=\Delta\tilde{S}_d^I-\Delta\tilde{S}_d \tag{16}$$

Thus the thermodynamic expression of K_I is given as

$$K_I=\exp\left(-\frac{\Delta\tilde{H}'}{RT}+\frac{\Delta\tilde{S}'}{R}\right) \tag{17}$$

C. Treatment based on cell models

In this section, the simplified interface model will be treated on the basis of cell models, regarding the differences between the interfacial phase and the bulk phase Now let us first start with the canonical partition function ψ of a condensed state system ψ of an ensemble of N molecules of mass m confined to a volume V has the form[29]

$$\ln \psi = \ln Q'(T) + \frac{1}{N} \ln \Omega(T) \tag{18}$$

The Helmholtz free energy is then given by

$$F = -NkT \ln \psi = -NkT \ln Q'(T) - kT \ln \Omega(T), \tag{19}$$

where $\Omega(T)$ is referred to as the partition function for the configurational potential energy and $Q'(T)$ is defined by

$$Q'(T) = [(2\pi mkT)^{3/2}/h^3]Q(T), \tag{20}$$

where $Q(T)$ denotes the partition function of a molecule for all the internal (including rotational, vibrational, electronic, and nuclear spin) degrees of freedom $\Omega(T)$ is approximately expressed as

$$\Omega(T) = \{v \exp[(-\epsilon + kT)/(kT)]\}^N, \tag{21}$$

where ϵ refers to the minimum potential energy of each liquid unit in the quasicrystalline liquid and can be expressed as

$$\epsilon = \sum_{i=1}^{n} \frac{1}{2} \Phi_i, \tag{22}$$

v is the so-called free volume of a unit defined in terms of the harmonic oscillator model[29] by

$$v = [kT/(2\pi m\nu^2)]^{3/2} \tag{23}$$

(ν is the vibration frequency of solid units in an Einstein crystal) At sufficiently high temperatures $kT \gg h\nu$, the vibrations will be effectively classical Then for the crystal state, a similar form for $\Omega(T)$ results

$$\Omega_S(T) = \{v_S \exp[-\epsilon_S/(kT)]\}^N \tag{21a}$$

Comparing this formula with the strictly analogous formula for the liquid, we notice that, apart from ϵ and ν having different values for the liquid and the crystal, there is a difference of an extra term $-kT$ in the free energy of the liquid. The corresponding extra term in the entropy is k This must be attributed to the fact that for given ϵ and ν the liquid is more disordered than the crystal

Let us now consider a mixture of two types A and B[29] For this system, the Helmholtz free energy $F_{(A,B)}$ is given by

$$F_{(A,B)} = -N_A kT \ln Q'_A(T) - N_B kT \ln Q'_B(T) - kT \cdot \ln \Omega_{(A,B)}(T), \tag{19a}$$

where $Q'(T)$ is defined for each species by Eq (20) and $\Omega(T)_{(A,B)}$ by

$$\Omega(T)_{(A,B)} = \{v_A \exp[(-\epsilon_A + kT)/(kT)]\}^{N_A} \times \{v_B \exp[(-\epsilon_B + kT)/(kT)]\}^{N_B} \times \frac{(N_A + N_B)!}{N_A!\, N_B!} \exp[-\bar{N}_{AB}\omega_{AB}/(kT)] \tag{21b}$$

Here ω_{AB} is the exchanging energy due to the formation of AB bonds and has the usual form

$$w_{AB} = \sum_{i=1}^{n} \Phi_i^o, \tag{24}$$

where

$$\Phi_i^o = \Phi_i^{AB} - \tfrac{1}{2}(\Phi_i^{AA} + \Phi_i^{BB}) \tag{24a}$$

$\bar{N}_{AB}$ is the high temperature limit of $\bar{N}_{AB}$. In reference to the pure state with corresponding free energies F_A and F_B, $F_{(AB)}$ is rewritten as

$$F_{(AB)} = F_A + F_B + \Delta F + F'' \tag{25}$$

The values of functions ΔF (and ΔH, ΔE, ΔS, etc) are due to ideal mixing F'' (and E'', H'', S'', etc) denote the excess values of the corresponding functions over the values given by the formulas for ideal solutions For ideal mixing, $\Delta H \cong \Delta E = 0$, and the usual expression is obtained

$$\Delta F = -T\Delta S = -kT \{N_A \ln[(N_A + N_B)/N_A] + N_B \ln[(N_A + N_B)/N_B]\} \tag{26}$$

Referring to Eqs (19a) and (21b), the following expressions hold

$$F'' = \bar{N}_{AB}\omega_{AB} \tag{27}$$

and

$$E'' = \bar{N}_{AB}\omega_{AB} - T \left(\frac{\partial(\bar{N}_{AB}\omega_{AB})}{\partial T}\right)_{V\,V}, \tag{28}$$

$$S'' = -\left(\frac{\partial(\bar{N}_{AB}\omega_{AB})}{\partial T}\right)_{V\,V} \tag{29}$$

$\bar{N}_{AB}$ can be expressed according to the Bragg–Williams approximation[29] as

$$\bar{N}_{AB} = N_A \, N_B/(N_A + N_B) \tag{30}$$

It follows from Eqs (27)–(30) that

$$S'' = 0 \tag{31}$$

and

$$F'' = E'' = [N_A \, N_B/(N_A + N_B)] \, w_{AB} \tag{32}$$

According to thermodynamics,

$$(\mu_A)_{(AB)} = \left(\frac{\partial F_{(AB)}}{\partial N_A}\right)_{T\,V\,N_B} = \left(\frac{\partial F_A}{\partial N_A}\right)_{T\,V\,N_B} - T \left(\frac{\partial \Delta S}{\partial N_A}\right)_{T\,V\,N_B} + \left[\left(\frac{\partial E''}{\partial N_A}\right)_{T\,V\,N_B} - T \left(\frac{\partial S''}{\partial N_A}\right)_{T\,V\,N_B}\right] \tag{33}$$

Substituting Eqs (19), (21), (26), (29), (30), (31), and (32) into Eq (33) yields

$$(\mu_A)_{(AB)}=(\mu_A)_A+kT\ln X_A+(1-X_A)^2\ w_{AB}, \tag{33a}$$

where

$$(\mu_A)_A=\left(\frac{\partial F_A}{\partial N_A}\right)_{T\,V\,N_B}$$

$$=-kT\ \ln Q'_A(T)-kT$$

$$[\ln v_A+(-\epsilon_A+kT)/(kT)] \tag{34}$$

Considering Eq (21a), a similar expression of the chemical potential can be written for a solid unit as

$$(\mu_A)_S=-kT\ln Q'_S(T)-kT\ \ [\ln v_S-\epsilon_S/(kT)] \tag{35}$$

If we take the equilibrium between the bulk solid phase and bulk fluid phase into account, we obtain from Eq (13b) that

$$\ln X_A=-\frac{1}{kT}\ \ [(\epsilon_A-\epsilon_S)+(1-X_A)^2 w_{AB}]$$

$$+\{\ln[Q_A(T)/Q_S(T)]+\ln(v_A/v_S)+1\}, \tag{36}$$

where

$$\Delta\tilde{H}_d=(\epsilon_A-\epsilon_S)+(1-X_A)^2\ w_{AB} \tag{37}$$

and

$$\Delta\tilde{H}_m=\epsilon_A-\epsilon_S, \tag{38}$$

or

$$\Delta\tilde{H}_d=\sum_{i=1}^{n}\left[\frac{1}{2}(\Phi_i^{AA}-\Phi_i^{SS})+(1-X_A)^2\ \Phi^\sigma\right] \tag{37a}$$

and

$$\Delta\tilde{H}_m=\sum_{i=1}^{n}\frac{1}{2}(\Phi_i^{AA}-\Phi_i^{SS}), \tag{38a}$$

$$\Delta\tilde{S}_d=\Delta\tilde{S}_m=k\ \{\ln[Q_A(T)/Q_S(T)]+\ln(v_A/v_S)+1\} \tag{39}$$

In the case of the interfacial phase, not only interactions between structural units within a layer, but also those in two adjacent layers are taken into account Therefore they can be treated in the same way as in a three-dimensional phase For the localized interfacial fluid phase, an expression similar to Eq (35) holds

$$(\mu_A^I)_A=-kT\ \ln Q'^I_A(T)-\mathrm{kT}\ \ [\ln v_A^I-\epsilon'^I_A/(kT)] \tag{35a}$$

For the mobile interfacial fluid subphase, $(\mu_A^I)_A$ is similar to Eq (34) Also the corresponding functions of the interfacial solid subphase have the expressions analogous to those of the bulk solid phase Then in case that the fluid interface is localized,

$$\ln X_A^I=-\frac{1}{kT}\ \ [(\epsilon_A^I-\epsilon_S^I)+(1-X_A^I)^2 w_{AB}^I]$$

$$+\{\ln[Q_A^I(T)/Q_S^I(T)]+\ln(v_A^I/v_S^I)\}, \tag{36a}$$

$$\Delta\tilde{S}_d^I=\Delta\tilde{S}_m^I=k\ \ \{\ln[Q_A^I(T)/Q_S^I(T)]+\ln(v_A^I/v_S^I)\} \tag{39b}$$

Otherwise for the system where the fluid interface is mobile, $\ln X_A^I$ and $\Delta\tilde{S}_d^I$ have the forms similar to Eqs (36) and (39), respectively

Based on Eqs (36), (36a), (37a), and (39), we can give the statistical mechanical expressions of Eqs (15) and (16) as

$$\Delta\tilde{H}'=\sum_{i=1}^{n}\left\{\left[\frac{1}{2}(\phi_i^{AA}-\phi_i^{SS})+(1-X_A^I)^2\ \phi_i^\sigma\right]\right.$$

$$\left.-\left[\frac{1}{2}(\Phi_i^{AA}-\Phi_i^{SS})+(1-X_A)^2\ \Phi_i^\sigma\right]\right\}, \tag{15a}$$

(ϕ_i^σ is the corresponding quantity of Φ_i^σ in the interfacial phase) for the systems consisting of the localized fluid interface

$$\Delta\tilde{S}'=k\ \ (\ln\{Q_A^I(T)\ \ Q_S(T)/[Q_S^I(T)\ \ Q_A(T)]\}$$

$$+\ln[v_A^I\ \ v_S/(v_S^I\ \ v_A)]-1), \tag{16a}$$

or for the mobile fluid interface

$$\Delta\tilde{S}'=k\ \ (\ln\{Q_A^I(T)\ \ Q_S(T)/[Q_S^I(T)\ \ Q_A(T)]\}$$

$$+\ln[v_A^I\ \ v_S/(v_S^I\ \ v_A)]) \tag{16b}$$

C_i^0 and C_i^* can also be rewritten as statistical mechanical expressions according to Eqs (37a) and (38a) as

$$C_i^0=\sum_{i=1}^{n}\frac{1}{2}(\phi_i^{AA}-\phi_i^{SS})\Big/\sum_{i=1}^{n}\frac{1}{2}(\Phi_i^{AA}-\Phi_i^{SS}), \tag{5a}$$

$$C_i^*=\sum_{i=1}^{n}\left[\frac{1}{2}(\phi_i^{AA}-\phi_i^{SS})+(1-X_A^I)^2\ \phi^\sigma\right]\Big/$$

$$\sum_{i=1}^{n}\left[\frac{1}{2}(\Phi_i^{AA}-\Phi_i^{SS})+(1-X_A)^2\ \Phi^\sigma\right] \tag{6a}$$

It can be seen from Eqs. (5a) and (6a) that in general C_i^0 is different from C_i^* if solutions are nonideal For regular solutions, the terms $(1-X_A^I)^2\ \phi^\sigma$ and $(1-X_A)^2\ \Phi^\sigma$ are relatively small compared to the terms $\frac{1}{2}(\Phi_i^{AA}-\Phi_i^{SS})$ and $\frac{1}{2}(\Phi_i^{AA}-\Phi_i^{SS})$, respectively In many cases, we can thus use C_i^0 as a good approximation of C_i^*

Note that the use of these corresponding statistical mechanical expressions is twofold First, it can be seen from the foregoing discussions that these formulas may be used to analyze the relations of different quantities between the bulk phase and the interfacial phase Second, these expressions can in some ways be used to estimate the corresponding functions in the interfacial phase This may help to understand the interfacial structure We will come back to these in Sec IV

D. The relations between C_i^* (or C_i^0) and other thermodynamic functions

In the equilibrium condition, Eq (8) must be satisfied Then combining and rearranging Eqs (6), (8), and (17) yields

$$K_I = f\ (X_A)^{(c_I^*-1)} \tag{40}$$

where

$$f = \exp[(\Delta\tilde{S}_d^I - C_I^*\Delta\tilde{S}_d)/R] \tag{41}$$

According to the definition of K_I given by Eq (7), we immediately obtain the expression

$$X_A^I = f\ (X_A)^{c_I^*} \tag{42}$$

Now we introduce here an empirical proportionality relation for a regular solution, which states that

$$\Delta\tilde{S}_d^I/\Delta\tilde{S}_d \simeq \Delta\tilde{H}_d^I/\Delta\tilde{H}_d = C_I^* \tag{43}$$

Looking back to Sec II B, this approximation can to some extent be justified For mobile fluid interfaces, the statistical mechanical expression of $\Delta\tilde{S}_d^I/\Delta\tilde{S}_d$ can be written according to Eq (39) as

$$\Delta\tilde{S}_d^I/\Delta\tilde{S}_d = \{\ln[Q_A^I(T)/Q_S^I(T)] + \ln(v_A^I/v_S^I) + 1\}/\{\ln[Q_A(T)/Q_S(T)] + \ln(v_A/v_S) + 1\} \tag{44}$$

Normally, the terms $\ln[Q_A(T)/Q_S(T)]$, $\ln[Q_A^I(T)/Q_S^I(T)]$, $\ln(v_A/v_S)$, and $\ln(v_A^I/v_S^I)$ are larger than zero When $\Delta\tilde{H}_d^I < \Delta\tilde{H}_d$ (or $C_I^* < 1$), the differences between the interfacial solid and the interfacial fluid will be smaller than those between the bulk fluid and the bulk solid phase It follows that $\ln[Q_A^I(T)/Q_S^I(T)]$ and $\ln(v_A^I/v_S^I)$ are also smaller than the corresponding terms of the bulk phases This means that $\Delta\tilde{S}_d^I < \Delta\tilde{S}_d$ Similarly, when $\Delta\tilde{H}_d^I > \Delta\tilde{H}_d$, it turns also out that $\Delta\tilde{S}_d^I > \Delta\tilde{S}_d$ On the other hand, Eq (43) can in an equivalent way be expressed as

$$\Delta\tilde{H}_d^I/\Delta\tilde{S}_d^I \simeq \Delta\tilde{H}_d/\Delta\tilde{S}_d \tag{43a}$$

This can be justified using available experimental data In Table I, we list the ratios of $\Delta\tilde{H}_d/\Delta\tilde{S}_d$ for several paraffins dissolved in various solvents It can be seen from the table that for a paraffin in different solutions, no matter how much the absolute $\Delta\tilde{H}_d$ (and $\Delta\tilde{S}_d$) differs, the ratio of $\Delta\tilde{H}_d/\Delta\tilde{S}_d$ is almost the same This means that the proportionality relation given in Eq (43a) [or Eq (43)] is a very good approximation

From Eq (43), we obtain that

$$f \simeq 1 \tag{41a}$$

It follows that

$$K_I \simeq (X_A)^{(c_I^*-1)} \tag{40a}$$

and

$$X_A^I \simeq (X_A)^{c_I^*} \tag{42a}$$

Relations (40a) and (42a) can be extended to crystal – melt systems approximately For normal liquids, under normal conditions $\rho_S > \rho_f$ This can be interpreted as the dissolution of "vacuum units" in melts Within the framework of cell models, melts can approximately be considered as a kind of "solutions" formed by liquid units and "vacuum units " These vacuum units have the same volume and shape as liquid units The dissolution of vacuum units makes $\rho_S > \rho_f$ From a statistical mechanical point of view, the existence of vacuum units is due to the difference of the free volume between solid units and fluid units Subsequently taking $X_A \simeq \rho_f/\rho_S$, for crystal-melt systems, Eqs (40a) and (42a) can be rewritten in the following way

$$K_I \simeq (\rho_f/\rho_S)^{(c_I^0-1)} \tag{40b}$$

and

$$(\rho_f^I/\rho_S^I) \simeq (\rho_f/\rho_S)^{c_I^0} \tag{45}$$

For crystals growing below their melting point, there will be only a little solid deformation at surfaces Hence we may assume that $\rho_S^I \simeq \rho_S$, and Eq (45) is rewritten as

$$(\rho_f^I/\rho_S) \simeq (\rho_f/\rho_S)^{c_I^0} \tag{45a}$$

It can be seen from the formulas derived in this section that if C_I^* (or C_I^0) can be determined, the values of K_I and X_A^I (or ρ_f^I) and other interfacial quantities are easily calculated In reverse, if the data of X_A^I (or ρ_f^I) are available, we may estimate C_I^* (or C_I^0) and other quantities, and subsequently infer the character of interfacial structure

TABLE I Solubility parameters and the ratios of $\Delta\tilde{H}_d/\Delta\tilde{S}_d$ for different paraffins in various solvents

n Paraffins	Solvents	ΔH_d^a (J mol^{-1} $\times 10^{-3}$)	ΔS_d^a (J mol^{-1} K^{-1})	$\Delta\tilde{H}_d/\Delta S_d$ (K $\times 10^{-3}$)
n $C_{18}H_{38}$	Heptane	97 4	295	3 30
	Pentane	99 5	302	3 29
	Pet ether	99 3	301	3 30
	m xylene	105 0	319	3 29
n $C_{12}H_{66}$	Heptane	109 7	324	3 38
	Pentane	111 0	329	3 37
	Pet ether	109 0	322	3 38
	m xylene	121 6	362	3 36
n-$C_{16}H_{72}$	Heptane	122 7	354	3 46
	Pentane	124 5	360	3 46
	Pet ether	128 5	374	3 44
	m xylene	146 7	430	3 41

[a]The data of ΔH_d and $\Delta\tilde{S}_d$ are selected from Ref 32

III. APPLICATIONS

In this section, we will apply the results derived in the last section to two different systems From these applications, we can obtain specific information of interfaces Also the practical uses of derived relevant formulas will be demonstrated

A. The hard-sphere–hard-wall system

The hard-sphere–hard-wall system is a simplified crystal–liquid system In this system, only the liquid phase consisting of hard spheres in contact with some artificially fixed flat wall is considered The special profile and the physical state of the solid surface are not taken into account Since this system is so simple, it has been investigated in more detail by computer simulations and density-functional theories [19–21 30 31]

TABLE II The values of C_l^0 for some metals

Metals	$(\rho_f/\rho_s)^a$	C_l^0
Pb	0 984	5 17
Sn	0 984	5 17
Na	0 976	3 87
Li	0 970	3 21
K	0 971	3 28
Rb	0 971	3 28
Cs	0 986	5 77

[a]The data of ρ_f and ρ_s are selected from Ref 33

Going back to Eq (45a), substituting (ρ_f^I/ρ_f) (ρ_f/ρ_s) for (ρ_f^I/ρ_s), this equation can be rewritten in the following way

$$C_l^0 \simeq 1+\ln(\rho_f^I/\rho_f)/\ln(\rho_f/\rho_s) \tag{46}$$

It is known from computer simulations interpreted with density-functional theories[19] that ρ_f^I/ρ_f depends weakly on ρ_f Then, within a small variation range of ρ_f/ρ_s, ρ_f^I/ρ_f can approximately be considered as a constant Hence it follows from Eq (46) that the value of C_l^0 will depend on (ρ_f/ρ_s) directly

In practice, the hard-sphere–hard-wall system may be considered as an approximation for metal systems Expression (46) may then be applied to this kind of systems From density-functional theories and computer simulations,[12,19] it was obtained that $\rho_f^I/\rho_f \simeq 0\,947$ for metals in contact with the melt The values of C_l^0 are therefore estimated from (ρ_f/ρ_s) for some metals, and listed in Table II As shown in Table II, for these metals C_l^0 is about 2 5–6 This explains the deviations between the results from the equivalent wetting condition and from experiments [6–10] We notice that in this approach, interaction energies between structural units are not taken into account Therefore the results obtained are not very relevant A more precise and detailed investigation on monomer systems is now carried out based on self-consistent field theories The results will be published soon

B. The solution–crystal system of aliphatic compounds

The equilibrium state of solid–liquid interfaces of aliphatic compounds have been studied to a large extent Looking back to (1) and (2), since θ_{hkl}' can be calculated for a crystallographic orientation (hkl)[3], ϕ_{str} can be obtained by measuring T' according to (1) Comparing ϕ_{str} with Φ_{str}, which is derived from ΔH_d, we concluded that for n-paraffins n-$C_{16}H_{34}$, n-$C_{21}H_{44}$, and n-$C_{23}H_{48}$ dissolved in the solvent of n-hexane,

$$C_l^* \simeq 0\,460 \sim 0\,410 \tag{47}$$

Therefore, for these systems,

$$X_A^I \simeq (X_A)^{0.435} \tag{48}$$

This implies that the concentration of solute at the interface is much higher than in the bulk To justify this result, we applied STM technique to image the adsorption layer of a very dilute n paraffin $\sim n$-hexane solution on a graphite substrate It is found that the graphite surface is to a large extent covered by n-paraffin molecules, not by n-hexane molecules which take a large percentage by volume in the bulk (to be published) This can be seen as independent experimental evidence of the positive adsorption of n-paraffin molecules at the surface

IV. DISCUSSION

In the foregoing sections, we have shown how interfacial quantities are related to bulk quantities by factors C_l^* (or C_l^0) and K_l Once some information about interfaces is available, the factors and the corresponding formulas may be used as a systematic procedure to withdraw interfacial quantities, such as effective bond energies, from available data This has been proven to be very successful in the description of many experimental results from surface roughening and 3D homogeneous nucleation (the results to be published elsewhere)

It has already been seen in Sec II that all relevant results derived are based on the inhomogeneous cell model (or layer model) We note that essential aspects of the interface resulting from recent theoretical and experimental progress[13–25] has been taken into account in this model We notice that it may not be always strictly correct to assume that the thickness of fluid layers in an orientation (hkl) is fixed It is shown in computer simulations[13,14] that in some orientations, the periodicity of the density oscillation in the fluid side changes slightly with the distance from the solid surface However, the first fluid layers adjacent to the solid surface, which are important from our point of view, always have almost the same periodicity as the solid phase with the orientation (hkl)

We will in the following focus our attention on the physical interpretation of C_l^* (or C_l^0) and K_l It can be seen from Eqs (38a), (38b), (40a), (41a), (42a), and (45a) that the surface characteristic scaling factor C_l^* (or C_l^0) is the most important factor All relevant interfacial properties are linked to the corresponding bulk properties by this factor The value of C_l^* (or C_l^0) determines the character of the interfacial phase Following previous discussion,[5] we now present the character of the interfacial phase for the three distinct cases by C_l^* (or C_l^0)

(1) The equivalent wetting condition

$$C_l^*(\text{or } C_l^0)=1 \tag{49}$$

(In addition, $\phi_l^{sf} \simeq \phi_l^{ff}$, or for a solution consisting of two types of molecules, $\phi_l^{SA} \simeq \phi_l^{AA}$ and $\phi_l^{SB} \simeq \phi_l^{AB}$) Then according to Eqs (42a) and (45a),

$$X_A^I = X_A, \quad \text{or} \quad \rho_f^I = \rho_f \tag{49a}$$

In this condition, both the solid and fluid from the bulk to the interface are completely homogeneous, which means that the interfacial phase has the same structure as the bulk phase Then interfacial properties can be described by macroscopic quantities of the bulk phase This is in fact a -very special case Strictly speaking, this condition is in most cases not valid It occurs only if in a system all opposite

effects are canceled mutually. Nevertheless, the equivalent wetting condition can be considered as the thermodynamic reference case, from which the following two cases are defined:

(2) Extra wetting or more than equivalent wetting

$$C_f^*(\text{or } C_f^0) < 1. \tag{50}$$

Since $0<X_A<1$, or $0<\rho_f/\rho_S<1$,

$$X_A^I > X_A, \quad \text{or } \rho_f^I > \rho_f. \tag{50a}$$

In this case, the solid surface shows a positive adsorption effect to solute units in the interfacial phase. Subsequently, solvent or other units will be repelled from the surface. Obviously the solution–crystal system of aliphatic compounds discussed in Sec. III B is subject to this case.

(3) Less than equivalent wetting

$$C_f^*(\text{or } C_f^0) > 1. \tag{51}$$

Then

$$X_A^I < X_A, \quad \rho_f^I < \rho_f. \tag{51a}$$

In this case, the negative adsorption effect between solid and solute units occurs in the interfacial phase. In contrast, solvent or impurity units are preferentially adsorbed on the solid surface. The hard sphere–hard wall system discussed in Sec. III A belongs to this case.

From the treatment discussed above, we can see that except in the equivalent wetting condition, at equilibrium, the concentration of solute (or density of pure fluid units) in the interfacial phase will differ from that in the bulk fluid phase. As we mentioned in Sec. II, there are some intermediate layers in between the bulk phase and the interfacial subphase. Therefore within the framework of the inhomogeneous cell model approach, the concentration (or density) of the fluid will gradually change from X_A (or ρ_f) to X_A^I (or ρ^I), instead of an abrupt change. The change in X_A (or ρ_f) is now illustrated schematically in Figs. 2(a)–2(c), for the three cases discussed above. A more precise description will be published elsewhere.

In case the fluid phase consists of almost spherical particles and the interactions between solid and fluid units in the interfacial phase are relatively weak, due to the relaxation or the reconstruction of the surface, the negative adsorption effect analogous to the hard sphere–hard wall system plays an essential role. Then the case of less than equivalent wetting (C_f^* or $C_f^0 > 1$) is expected to occur. This may explain the Nielsen–Söhnel plot for inorganic crystals.[10] If the fluid consists of chain-like particles, the fluid ordering involves molecular orientations as well. This may induce complicated long range and many point effective interactions, resulting in the case of more than equivalent wetting (C_f^* or $C_f^0 < 1$). This explains the anomalous roughening at low temperatures found on some organic chain-like molecule crystals.[5]

Concerning the actual value of C_f^* (or C_f^0), it can be calculated by density-functional methods, computer simulations, and the self-consistent field theory according to Eqs. (42a) and (45a), or by a special model for a certain system. It may also be determined from the roughening temperature or by x-ray scattering methods.

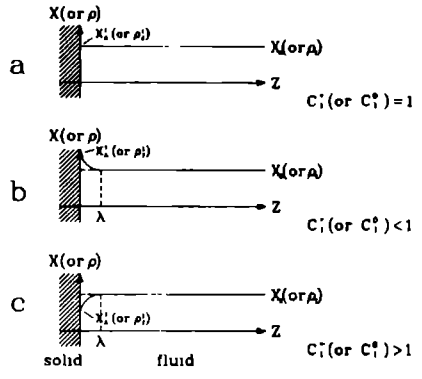

FIG 2 A schematic drawing showing the distribution of fluid concentration (or density) at different types of interfaces. λ is the distance from the interfacial fluid phase to the bulk fluid phase. (a) The equivalent wetting condition (or the homogeneous fluid approximation). C_f^* (or C_f^0) $=1$, $X_A^I = X_A$ (or $\rho_f^I = \rho_f$) (b) The more than equivalent wetting condition; C_f^* (or C_f^0) <1, $X_A^I > X_A$ (or $\rho_f^I > \rho_f$) (c) The less than equivalent wetting condition, C_f^* (or C_f^0) >1, $X_A^I < X_A$ (or $\rho_f^I < \rho_f$)

V. SUMMARY AND CONCLUSIONS

Macroscopic quantities of solid–fluid interfaces can be associated with those in the bulk by the surface characteristic scaling factors C_f^* (or C_f^0) and the surface concentration (or density) distribution constant K_h defined by Eqs. (5), (6), and (7), respectively. The expressions of these factors are derived for different situations from essential principles of statistic thermodynamics It concludes from our analyses that the character of solid–fluid interfaces is classified into three cases: the equivalent wetting, and more and less than equivalent wetting. Two typical systems, the hard-sphere–hard-wall system (correspondingly solid–melt systems of metals) and the aliphatic compound systems, are studied. They belong to the case of less than equivalent wetting [C_f^* (or C_f^0) >1 and $X_A^I < X_A$] and of more than equivalent wetting [C_f^* (or C_f^0) <1 and $X_A^I > X_A$], respectively.

ACKNOWLEDGMENTS

The authors wish to thank Shell Netherlands B. V. for supporting this work. We also appreciate Mr. Jan van Kessel's help to make some of the drawings.

APPENDIX: LIST OF SYMBOLS

d_{hkl} interplanar distance of a crystal structure in the orientation of (hkl).

C_f^0(or C_f^*), surface characteristic scaling factor defined by Eq. (5) [or Eq. (6)].

E, internal energy
F, helmholtz free energy
f, factor defined by Eq (41)
G, Gibbs' free enthalpy
h, Planck's constant
H, enthalpy
$\bar{H}$, enthalpy per structural unit (or per mole)
i, interaction of a structural unit in a certain direction
k, Boltzmann's constant.
n, coordinate number of a structural unit
N, number of a certain structural unit.
P, pressure.
R, gas constant.
S, entropy
$\bar{S}$, entropy per structural unit (or per mole)
T, temperature.
V, volume.
v, free volume of a structural unit, defined by Eq. (23)
Q', partition function of a structural unit, defined by Eq. (21)
Q, partition function of a structural unit for all the internal degrees of freedom.
w_{AB} exchanging energy defined by Eq (24)
X, mole fraction
ψ, canonical partition function of an assembly
σ, relative supersaturation
ϵ, minimum potential energy of a structural unit.
ν, frequency of lattice vibration
μ, chemical potential.
ϕ, bond energy in the interfacial phase.
Φ, bond energy in the bulk phase
θ'_{hkl} dimensionless roughening temperature of faces $\{hkl\}$
Ω, the partition for the configurational potential energy
K_i, surface concentration (or density) distribution constant, defined by Eqs (7) and (7a).
ρ, density

Subscripts

A, solute unit.
a, actual condition.
B, solvent unit.
d, dissolution.
f, fluid
i, interaction of a structural unit with its vicinal cells in a certain direction.
m, melting.
str, the strongest bond
s, solid or saturation.

Superscripts

A, solute unit.
AA, interaction between solute units
AB, interaction between solute and solvent units
B, solvent unit
f, fluid
ff, interaction between fluid units
I, interfacial phase
r, roughening transition
s, solid
SA, interaction between solid and solute units
SB, interaction between solid and solvent units.
sf, interaction between solid and fluid units

[1] P Bennema and G H Gilmer, in *Crystal Growth. an Introduction*, edited by P Hartman (North–Holland, Amsterdam, 1972), p 263
[2] D E Temkin, in *Crystallization Processes* (Consultants Bureau, New York, 1966), p 15
[3] P Bennema and J P van der Eerden, in *Morphology of Crystals, Part A*, edited by I Sunagawa (Terra Science, Tokyo, 1987), p 1
[4] K A Jackson, in *Liquid Metals and Solidification* (ASM, Cleveland, 1958), p 174
[5] X Y Liu and P Bennema, J Chem Phys 97, 3600 (1992)
[6] D Chatain, C Vahlas, and N Eustathopoulos, Acta Metallogr 32, 227 (1984)
[7] C Vahlas and N Eustathopoulos, J Chem Physique 6, 515 (1983)
[8] A Passerone and N Eustathopoulos, Acta Metallogr 30, 1349 (1982)
[9] W Tolksdorf and I Bartels, J Cryst. Growth 54, 417 (1981)
[10] A E. Nielsen and O Sohnel, J Cryst. Growth 11, 233 (1971)
[11] T Sawada, J Cryst Growth 60, 349 (1982)
[12] R D Groot, M Elwenspoek, and P Bennema, J Cryst Growth 79, 817 (1986)
[13] J Q Broughton and F F Abraham, Chem Phys. Lett 71, 456 (1980)
[14] J Q Broughyton and G H Gilmer, J Chem Phys 79, 5095 (1983), 79, 5105 (1983) 79, 5119 (1983) 84, 5741 (1986) 84, 5749 (1986), 84, 5759 (1986)
[15] M Baus and J L Colot, Mol Phys 55, 653 (1985)
[16] W A Curtin and N W Ashcroft, Phys Rev 32, 2909 (1985)
[17] F F Abraham and J Q Broughton, Phys Rev Lett. 56, 734 (1986)
[18] A D J Haymet and D W Oxtoby, J Chem Phys 74, 2559 (1981)
[19] R. D Groot, Mol. Phys 60, 45 (1987)
[20] R. D Groot and J P van der Eerden, Phys. Rev 36, 4356 (1987)
[21] R. D Groot, N M Faber, and J P van der Eerden, Mol Phys 60, (1987)
[22] T A Cherepanova and A V Stekolnikov, J Cryst Growth 99, 88 (1990)
[23] G C McGonigal, R H Bernhardt, and D J Thomson, Appl Phys. Lett. 57, 28 (1990)
[24] G C McGonigal, R H Bernhardt, Y H Yeo, and D J Thomson, J Vac. Sci Techol B 9, 1107 (1991)
[25] J P Rabe and S Buchholz, Makromol Chem., Macromol Symp. 50, 261 (1991)
[26] E A Guggenheim, Trans. Faraday Soc 36, 397 (1940)
[27] J W Gibbs, *The Scientific Papers of J Willard Gibbs*, (Longmans-Green, London, 1906), Vol 1, p 219
[28] F C Goodrich, in *Surface and Colloid Science*, edited by E. Matijevic (Wiley, New York, 1969), Vol 1, p 1
[29] S R Fowler and E. A Guggenhein, *Statistical Thermodynamics* (Cambridge University, London 1960)
[30] I K Snook and D Henderson, J Chem Phys. 68, 2134 (1978)
[31] V Y Antonchenko, V V Ilyin, N N Makovsky, A N Pavlov, and V P Sokhan, Mol Phys. 52, 345 (1984)
[32] D H M Being and J W Mullin, J Chem Eng Data 32, 9 (1987)
[33] R C Weast, M J Astle and W H Beyer, *CRC Handbook of Chemistry and Physics*, 67th ed (CRC, Boca Raton, FL, 1987)

Chapter 4.3

surface science

The solid–fluid interface: a comparison and further description using the layer model

Xiang-Yang Liu

RIM, Laboratory of Solid State Chemistry, Faculty of Science, University of Nijmegen, Toernooiveld, 6525 ED Nijmegen, Netherlands

Received 6 October 1992; accepted for publication 18 February 1993

The profiles of the concentration and the exchange enthalpy at the solid–fluid interface are investigated with the framework of a layer model (or inhomogeneous cell model). It is shown that for systems consisting of isotropic units, concentration distributions in the interfacial phase obey an exponential law. This is in agreement with results obtained from other theories or computer simulations. Subsequently, a characteristic thickness δ^* (or n^*d) is defined. This factor, together with the surface characteristic scaling factor C_f^* and the value of bulk concentrations, will determine the shape of distribution profiles of the concentration and the exchange energy in the interfacial phase. As a result, it is found that this factor δ^* is associated with C_f^*. This is employed to estimate C_f^* from δ^*. Finally, the connection between the attachment energy E^{att} and C_f^* is discussed for different faces of a crystal.

1. Introduction

The information on the interfacial structure is important to study the process of crystal growth. Recent theoretical and experimental progress in this field [1–13] makes us understand the solid–fluid interface better than before. In order to associate interfacial state functions with those in the bulk phase, we used in our previous papers [14,15] the so-called layer model to establish the relation between macroscopic quantities and the interfacial structures. In this model, the whole space is partitioned parallel to the surface into layers of the same thickness d. The relations are established by introducing the surface characteristic factor C_f^* (or C_f°, which is referred to the case that a crystal contacts its melt). The surface characteristic factor is defined as $C_f^* = \Delta h_d^i/\Delta h_d$ (or $C_f^\circ = \Delta h_m^i/\Delta h_m$). Here Δh_d (or Δh_m) is the dissolution (or melting) enthalpy per structural unit (or in the following called *the exchange enthalpy*), which is defined as the enthalpy changed due to bringing a structural unit from the solid state into the environment of solutions (or the melt). The superscript "i" indicates interfacial properties. This factor is used to scale the deviation of potential energies of interfacial structural units from those of bulk fluid units. In this sense it allows us to connect the surface properties with the bulk properties, and moreover to obtain some information on the interfacial structure. Based on this factor, three typical cases: the equivalent condition ($C_f^* = 1$, $X' = X$), the more than equivalent condition ($C_f^* < 1$, $X' > X$) and the less equivalent condition ($C_f^* > 1$, $X' < X$) are distinguished for the equilibrium structure of interfaces. The equivalent wetting corresponds to the case that the structure and properties are homogeneous from the bulk up to the dividing plane between the solid and the fluid phase. This is a reference state, and occurs only in some very special cases. The more than equivalent wetting (or the less than equivalent wetting) implies that an adsorption (or a depletion) of solute units occurs at the solid surface.

Since some surface phenomena, such as the roughening transition, are only concerned with the structure and properties of structural units in

the first solid and the first fluid layer, the relations between interfacial quantities and bulk quantities were derived from a simplified two-step interfacial system [15]. This simplified system is defined within the framework of the layer model. In this system, only four different "sub-phases" are concerned. They are the first solid layer at the surface, the first fluid layer adjacent to the solid surface, the fluid and the solid layers at an "infinite distance" from the surface. From such a simplified system, relevant conclusions can easily be drawn. However, to describe the whole structure of an interface, obviously this is not sufficient. In fact particular properties of the first layers are associated with the structure in the intermediate layers. Those intermediate layers are the layers which extend from the first layer at the interface to the bulk phase. Therefore, when we consider the interface, all the intermediate layers must be involved. In this paper, we will pay special attention to the interface including all the intermediate layers.

It has to be noted that the layer model is employed to describe the inhomogeneity of interfacial regions. Although it is unable to give direct images of the local atomic structure or arrangement of interfaces (especially in the directions normal to the surface), this model can be used to investigate the average of interfacial properties, and the interfacial structure in the direction normal to the surface. In the following we will use this model to describe the concentration (or density) and the potential energy distribution as functions of z, the normal distance from the surface, for different types of interfaces. Actually the results obtained with this model reveal the average of distribution profiles in the interface, instead of oscillatory profiles in the density, resulting from computer simulations or density-functional theories.

This paper is arranged as follows. In section 2, the profiles of the concentration and the exchange enthalpy are derived within the framework of the layer model. The results are compared with those from other theories. In section 3, estimations and general expectations are made for different types of interfaces. The main results of our investigations are summarized in section 4.

2. The solid–fluid interfacial structure and the layer model

2.1. The profile of concentration and enthalpy distribution at the interface

We first choose a Cartesian coordinate system as follows: the x, y axes are in the plane of the solid surface, the z axis is normal to the surface and the origin is in the center of the first fluid layer adjacent to the solid surface. From the first fluid layer to the bulk fluid phase, the concentration of solute will change gradually from X' to X. In between X' and X, the concentration $X^m(z)$ is a function of z, independent of x and y. In case that $z = 0$ and ∞, $X^m(z) = X'$ and X, respectively. According to the layer model, $z = nd$ ($n \geq 0$). If we take the bulk concentration as a reference, then the concentration difference between the interfacial phase and the bulk phase $\Delta X^m(z)$ is given by

$$\Delta X^m(z) = X^m(z) - X. \tag{1}$$

Assume that for interfacial systems consisting of isotropic structural units, the ordered structure in the layer z has a constant influence by a certain factor on the successive layer $z + 1$, then the rate of $X^m(z)$ approaching X is proportional to $\Delta X^m(z)$. It follows that the derivative equation can be written as

$$\frac{d\Delta X^m(z)}{dz} = -\alpha\, \Delta X^m(z), \tag{2}$$

(α is a constant, and we will discuss its physical meaning later in this section). This assumption is based on the fact resulting from computer simulations [3,4,8,9] that *average* profiles of the density of fluid units approach smoothly (or exponentially) the density of the bulk away from the solid surface. (We will come back to this in section 2.2.) For this equation, the boundary condition is given by

$$z \to \infty, \quad \Delta X^m(z) \to 0; \quad z = 0,$$

$$\Delta X^m(0) = X' - X. \tag{3}$$

Consequently, the solution of eq. (2) is

$$\Delta X^m(z) = X^m(z) - X = (X' - X)\exp(-\alpha z). \tag{4}$$

If the liquid phase in the system behaves as a regular solution, we have the relation [15]

$$X' \approx X^{\eta}, \tag{5}$$

and here the exponent $\eta = C_f^*$. Then eq. (4) can be rewritten in the following way

$$X^m(z) = X\left[1 + (X^{C_f^*-1} - 1)\exp(-\alpha z)\right] \tag{6}$$

For those systems where crystals are in contact with the melt, we can substitute ρ_f/ρ_s for X and $\rho_f^m(z)/\rho_s$ for $X^m(z)$. Then the expression similar to (6) can be obtained as

$$\rho_f^m(z) = \rho_f\left\{1 + \left[(\rho_f/\rho_s)^{C_f^*-1} - 1\right]\exp(-\alpha z)\right\}. \tag{7}$$

For simplicity, in the following discussions, we only concentrate on those cases of crystals in contact with solutions (or mixtures). The obtained results can straightforwardly be applied to the cases of crystals contacting the melt by the same substitution as done in eq. (7).

Now we define the characteristic thickness of interfaces δ^* (or n^*d) as the following, at $z = \delta^*$ (or n^*d),

$$\Delta X'(\delta^*)/\Delta X'(0) = e^{-1} \tag{8}$$

Combining (4) and (8) yields

$$\delta^* = 1/\alpha, \quad \text{or } n^*d = 1/\alpha. \tag{9}$$

It follows that the expression (6) can be rewritten in the following way

$$X^m(z) = X\left\{1 + [X^{C_f^*-1} - 1]\exp(-z/\delta^*)\right\} \tag{6a}$$

Here we can see the physical meaning of the coefficient α. The slope of the $X^m(z)$ curve is obtained by differentiating (6) with respect to z,

$$\frac{dX^m(z)}{dz} = -\Delta X^m(0)\exp(-z/\delta^*)/\delta^* \tag{10}$$

It can be seen from (10) that for $z = 0$,

$$\frac{dX^m(0)}{dz} = -\Delta X^m(0)/\delta^* = X(1 - X^{C_f^*-1})/\delta^* \tag{11a}$$

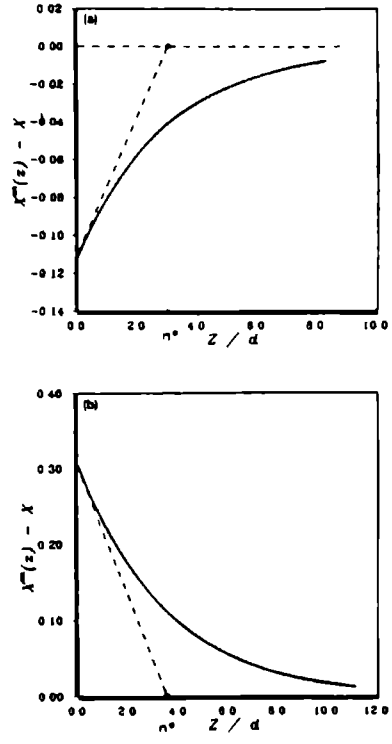

Fig. 1. The concentration (or density) distribution profile and the corresponding characteristic thickness $n^*(=\delta^*/d)$ for different types of interfaces (a) $C_f^* = 5$ (the less than equivalent wetting case), $X = 0.970$ and $n^* = 3$; (b) $C_f^* = 0.25$ (the more than equivalent wetting case), $X = 1 \times 10^{-2}$, $n^* = 3.5$.

and for $z \to \infty$,

$$\frac{dX^m(z)}{dz} = 0. \tag{11b}$$

When the concentration distribution profile of an interface is available, the tangent line of the curve at $z = 0$ will intercept the horizontal line $X^m(z) = X$ at $z = \delta^*$ (or n^*d). Therefore, by drawing the two lines in the graph the characteristic thickness can be estimated. In fig. 1 two typical examples corresponding to the more than equivalent wetting case and the less than equivalent wetting case are given. We can see that in

the case of less than equivalent wetting, $X' < X$ (or $\rho_f' < \rho_f$), and the concentration (or density) of solute increases exponentially with the distance away from the surface. Correspondingly, the concentration of solvent in the interfacial phase decreases from $(1-X')$ to $(1-X)$. Profiles of the concentration (or density) for the interface of more than equivalent wetting will be the reverse. The concentration of solute in the interfacial phase decreases from X' to X, while that of solvent increases from $(1-X')$ to $(1-X)$ exponentially.

The profile of enthalpy (or potential energy) can be derived from the previous results, based on the relations between the concentration and the exchange enthalpy. The relation between the concentration and the exchange enthalpy of solute in the intermediate layers and the bulk fluid is expressed for systems consisting of regular solutions, by

$$\Delta h_d^m(z)/\Delta h_d \simeq \ln X^m(z)/\ln X. \tag{12}$$

(See Appendix). Subsequently the enthalpy distribution profile in the intermediate layers with respect to the bulk fluid can be obtained from (6) and (12), as

$$\Delta h_d^m(z)/\Delta h_d = 1 + \frac{1}{\ln X}\ln\left[1 + (X^{C_f^*-1} - 1) \times \exp(-z/\delta^*)\right]. \tag{13}$$

It has to be noted that since the volume difference between the solid and the liquid state is negligible, the exchange energy is almost equal to the exchange enthalpy. Therefore, the exchange enthalpy distribution discussed above in fact is the exchange energy distribution. It can be seen from (6), (7) and (13) that profiles of the concentration and the exchange energy are determined by the factors C_f^* and δ^* and the bulk concentration X. In figs. 2 and 3, the samples of distributions of the concentration, $[X^m(z)-X]/X$, and of the relative enthalpy or potential, $[\Delta h^m(z) - \Delta h]/\Delta h$, with the reduced distance from the surface (z/d) are given for the interface in the case of less than equivalent wetting $(C_f^* > 1)$ and that of more than equivalent wetting $(C_f^* < 1)$,

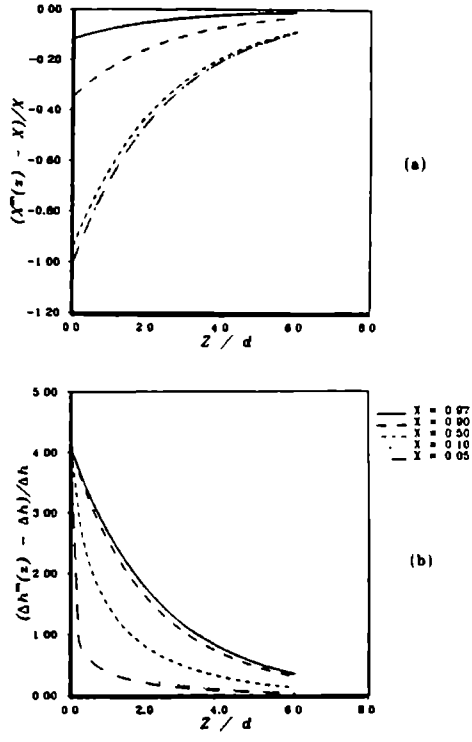

Fig. 2. The distributions of the relative concentration $[X^m(z) - X]/X$ and of the relative enthalpy $[\Delta h^m(z) - \Delta h]/\Delta h$, as the function of z/d for the interfaces with less than equivalent wetting ($C_f^* = 5$, $n^* = 2.5$), and the influence of bulk concentrations on the profiles. (a) The concentration distribution profiles. (b) The potential distribution profiles.

respectively. In the two graphs, the influence of the concentration on distribution profiles is shown. Explicitly, for a given interfacial system (it is supposed that C_f^* and n^* are fixed), profiles of the concentration and of the exchange energy are different. In the case of more (or less) than equivalent wetting, a lower bulk concentration corresponds to a drastic change of the concentration in the interfacial phase. This implies that at low concentrations, the solid surface has a strong influence on the interfacial structure. We note that for the interfacial system shown in fig. 2a ($C_f^* = 5$, $n^* = 2.5$), when $X < 0.1$, the concentra-

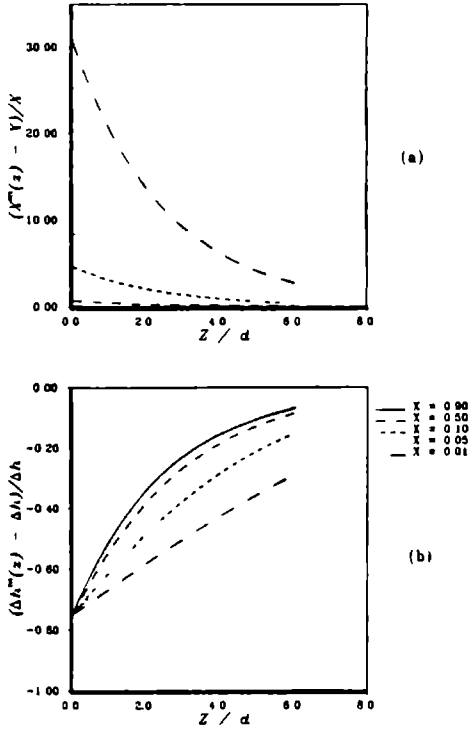

Fig. 3. The similar graph as fig. 2 for an interface with more than equivalent wetting ($C_f^* = 0.25$, $n^* = 2.5$). For the captions of (a) and (b), see figs. 2a and 2b.

tion of solute in the first fluid layer becomes zero (or $\Delta X^m(0)/X = -1$), meaning that "the complete dewetting" of solute occurs on the solid surface. On the other hand, the influence of the concentration on the exchange energy distribution is case dependent. In the case of less than equivalent wetting, a low bulk concentration will cause a sharp increase of the exchange energy within only a few layers adjacent to the solid surface. In contrast, in the more than equivalent wetting case, a lower bulk concentration corresponds to a very smooth decay of the enthalpy within the interfacial phase. This implies that the surface excess energy caused by the lateral pressure will be distributed in only a few layers in case the less than equivalent wetting occurs, or in a number of layers in case the more than equivalent wetting occurs.

Since for a given system X is always known, in this sense, C_f^* and δ^* are the most important factors to decide the character of profiles. To my knowledge, only a limited number of techniques are available, which can be used to determine those two factors. Therefore most relevant consequences concerning the solid–fluid structure result from theoretical analyses and computer simulations [1–13]. From our recent investigations it follows that a so-called self-consistent field lattice model theory (or the SF theory [16]) can easily be used to calculate the factors.

2.2. Comparison with other theories

The relevant information about the interface which we know from theoretical methods, such as density-functional theories and correlation-function theories, and computer simulations, consists of profiles of the density for a certain type of interface. This can be seen as an oscillation of the distribution profile gradually vanishing at the fluid side of interface [3,4,8,9]. The variation of amplitude of the oscillation or in some cases the average of the density profile indeed shows the exponential change with increasing the distance away from the surface. This in fact is the physical basis to establish eq. (2).

Another similar result is obtained from the SF theory [16], which also gives the average distribution profile at the interface. For the system consisting of a mixture of polymers (with completely flexible C–C bonds) and monomers, the distribution profile similar to the one in fig. 1b is obtained from the theory. Using least square regression of the calculated data [16], it is shown in fig. 4 that for a given polymer system $\ln[X^m(z) - X]$ depends linearly on z/d. This is in agreement with (6) and (6a). (We notice that for a mixture of polymers and monomers, the concentration of the system is expressed as a volume fraction φ. In our case, $X \ll 1$, and thus $\varphi \approx MX$. Therefore using φ instead of X leads to the same conclusion). Recently, our calculated results based on the SF

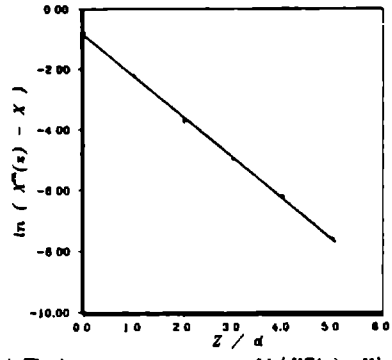

Fig. 4. The least-squares regression of $\ln[X^m(z)-X]$ versus the vertical distance from the surface (z/d), for the interfacial system of a flat face in contact with the mixture of polymer (1000 segments) and monomer. The bulk concentration of polymer (expressed by the volume fraction φ) $\varphi = 0.1$. The data (indicated by black dots) are calculated by the self-consistent field theory and selected from ref. [16]. It can be seen that $\ln[X^m(z)-X]$ is linearly related to z/d. This is in agreement with the expectation in expression (9).

theory indicate that for monomer systems, the linear relation between $\ln[X^m(z)-X]$ and z/d is also obtained.

It is worthwhile to mention that the surface free energy of the solid–fluid interface for metal systems has been derived on the basis of eqs. (6a) and (13). It turns out [22] that the calculated values are surprisingly close to the experimental data. This can be seen as a successful application of our model.

3. Estimation of the interfacial structure of different systems

In this section, we will first discuss the relation between the characteristic thickness and relevant interfacial thermodynamic properties. Then the relation is applied to estimate C_f^* of solid–fluid interfacial systems, and qualitatively analyze C_f^* in relation to different flat faces on the same crystal.

From $z = nd$ to $z = (n+1)d$, the ratio of concentration difference between the layers, according to expression (9), are constant for a system, as

$$\Delta X^m((n+1)d)/\Delta X^m(nd) = e^{-1/n^*} = K, \tag{14}$$

($n^* = \delta^*/d$). Obviously, K is constant, independent of z. This is consistent with our basic assumption given in the beginning of section 2.1. Within this framework, we postulate that the structure of the first fluid layer ($z = 0$) is also adapted from an (*artificial*) previous layer. Then

$$X^1 = X\{1 + [X^s(0)/X - 1]K\}, \tag{15}$$

and

$$C_f^* = \ln X^1/\ln X = 1 + \frac{1}{\ln X}\ln\{1 + [X^s(0)/X - 1]K\}, \tag{16}$$

where $X^s(0)$ is the concentration of the (artificial) layer preceding the first fluid layer. It can be shown below that the choice of $X^s(0)$ depends on the wetting condition of the interface.

In practice, n^* is weakly dependent on the concentration of the system. As an estimation we assume that n^* (and consequently K) is fixed, in case the concentration difference is not large. By the way, we can see from (16) that C_f^* is still concentration dependent.

In the following we will analyze the two different wetting conditions, mainly for crystals in contact with the melt. We assume that in the pure liquid state $X = \rho_l/\rho_s \to 1$.

(i) The more than equivalent wetting condition: C_f^* (or C_f°) < 1 and $X^1 > X$.

In this case, the concentration (or density) distribution at the fluid interface can be regarded as that extending from the solid interface. When $X \to 1$, $X^s(0)$ can be considered as the concentration (or density) at the solid interface, and almost equals unity. Then $X^s(0)/X \to 1$, and $0 < |[X^s(0)/X - 1]K| \ll 1$. Consequently eq. (16) is rewritten in the following way

$$C_f^* = 1 + \frac{1}{\ln X}[X^s(0)/X - 1]K, \quad (X \to 1). \tag{17a}$$

Taking the limit of C_f^* and assuming that $X^1(0)/X \simeq 1.1$, we therefore obtain the expression of C_f°

$$C_f^\circ = \lim_{x \to 1} C_f^* = 1 - [X^1(0)/X]K \simeq 1 - 1.1K. \tag{17b}$$

For the polymer system we discussed in section 2.2, it is obtained from fig. 4 that $n^* \simeq 0.78$. It follows from (17b) that in case $X \to 1$, $C_f^\circ \sim 0.72$. According to eq. (5), it was estimated from the calculated profiles of the concentration [16] that $C_f^* \sim 0.734$. It is known from our previous paper [15] that for a regular solution, $C_f^\circ \simeq C_f^*$. Indeed, those two results are very close to each other.

(ii) The less than equivalent wetting condition: $C_f^* > 1$, and $X^1 < X$.

Explicitly, in this situation, $X^1(0) < X$. We can not derive $X^1(0)$ from the solid phase. This makes our estimation more difficult. As an approximation, we estimate from the result of the hard wall–hard sphere system that for a crystal in equilibrium with its melt, $X^1(0)/X \sim 0.80$ and $n^* \simeq 1.5 \sim 2$. It follows from (17a) that

$$C_f^\circ \simeq 1 - 0.20K/\ln X, \quad (X \to 1). \tag{17c}$$

For some metal systems, $X = \rho_l/\rho_s \sim 0.97$ [17]. Based on (17c), this results in $C_f^\circ \sim 4.4$, which is in good agreement with experimental results $C_f^\circ \simeq 2.5 \sim 6$ [18–20]

Although we know from the assumption given above that C_f^* (or C_f°) can be obtained by other methods, the relation (5) shows the direct link between the interfacial structure and C_f^*. As aforementioned, the structuring and ordering in the interfacial fluid phase is to a large extent induced by the excess potential field (or the lateral pressure) of the solid surface. It is very reasonable to infer that in the case of $C_f^* < 1$ or $C_f^* > 1$ the larger the excess energies of solid surfaces, the larger $|\Delta X^\infty(0)|$, and then C_f^* is much smaller or much larger than unity, respectively. This conclusion is very useful to analyze the wetting condition of different faces on a crystal. According to the Hartman–Perdok theory [21], we know that each flat solid surface has a certain attachment energy E_{hkl}^{att}. This is the energy released per structural unit when a new crystal slice attaches to the crystal surface. In relation to the crystallization energy E^{cr} (per structural unit), the attachment energy [21] is expressed as

$$E^{cr} = E_{hkl}^{att} + E_{hkl}^{slice}, \tag{18}$$

where E_{hkl}^{slice} is the slice energy of crystal faces $\{hkl\}$ [21], and defined as the two-dimensional crystallization energy of a crystal slice with a thickness d_{hkl} in the orientations of $\{hkl\}$. It is explicit that E_{hkl}^{att} is proportional to the surface excess energy. Therefore, in case that no special adsorption occurs on crystal surfaces, the surface excess energy will promote the non-equivalent wetting effect. It follows that the wetting condition of those flat faces with higher attachment energy E_{hkl}^{att} will differ much more from the equivalent wetting condition. In other words, it can be concluded that C_f^* is face dependent.

4. Summary and conclusion

The concentration (or density) profile and the exchange energy profile for the solid–fluid interface are derived within the framework of the layer model. They show an exponential variation with the distance from the surface, as expressed by eqs. (6a) and (13). Basically, the profiles are determined by three essential factors. the surface characteristic scaling factor C_f^*, the characteristic thickness δ^*, and the bulk concentration of fluid phase in the system. In the case of a crystal in contact with its melt, an approximate relation between C_f^* and δ^* is given by (16) This relation is used to estimate C_f^* for different types of interfaces. Finally, it follows from the qualitative analysis that for different surfaces on a crystal the surface with the higher attachment energy E^{att} corresponds to a C_f^* which differs much more from unity.

Acknowledgements

The author wishes to thank Professor Dr. P. Bennema and Dr. H. Meekes for stimulating discussions and a critical reading of the manuscript.

He would also like to acknowledge Shell Netherlands for providing financial support for this research program.

Appendix

Eq. (12) can be derived using statistical thermodynamics. In the following we start with the grand canonical partition function of the solid–fluid interfacial system.

For an open system (fixed μ, V, T), the grand canonical partition function Ξ is defined as [23]

$$\Xi(\mu, V, T) = \sum_N \psi(N, V, T) \exp[N\mu/(kT)], \tag{A.1}$$

where $\phi(N, V, T)$ is the canonical partition function for a closed system (fixed N, V, T). For a multi-component system,

$$N = \sum_i N_i, \quad \mu N = \sum_i N_i \mu_i,$$

and

$$\psi(N, V, T) = \psi(\{N_i\}, V, T). \tag{A.2}$$

Here the subscript i represents different species. We notice that in the layer model, each slice which is identified by the z coordinate may be considered as an independent subphase. The corresponding functions and quantities must be a function of z. Then expression (A.1) is written as

$$\Xi(\mu, V, T) = \sum_{\substack{\text{all} \\ \{N_i(z)\}}} \prod_z \psi(\{N_i(z)\}, z, V(z), T) \times \exp\Big[\sum_i N_i(z)\mu_i(z)/(kT)\Big]. \tag{A.3}$$

In the following treatment the condition of fixed V (also $V(z)$) and T is always satisfied, for simplicity, the notation of fixed V, T will be omitted.

Since many distributions $\{N_i(z)\}$ are possible, the sum in (A.3) contains many terms. It is known that in equilibrium Ξ should be at its maximum. Therefore a standard approximation (exact for very large N) is to take only the maximum terms, corresponding to the equilibrium distribution $\{N_i(z)\}$. It thus follows that

$$\ln \Xi = \sum_z \Big[\ln \psi(\{N_i(z)\}, z) + \sum_i N_i(z)\mu_i(z)/(kT)\Big]. \tag{A.4}$$

The latter is found for the following total differential

$$\sum_i \sum_z \left\{\frac{\partial \ln \Xi}{\partial N_i(z)}\right\}_{V,T} \mathrm{d}N_i(z) = 0. \tag{A.5}$$

If the variable $N_i(z)$, $N_j(z)$,... were independent, each independent term in (A.5) would be zero. However, it is not the case of the multi component system. Within the framework of cell models, for a given surface, the number of cells for each layer, N°, is constant. Then for each layer in the system, there is a constraining relation which must be satisfied

$$\sum_i N_i(z) - N^\circ = 0, \quad z = 0, \pm 1, \pm 2, \ldots . \tag{A.6}$$

To find the maximum of the constrained function, the method of undetermined multipliers, due to Lagrange, is applied. Subsequently, a new function is defined

$$\ln \Xi + \sum_z \beta(z)\Big[\sum_i N_i(z) - N^\circ\Big], \tag{A.7}$$

which is equal to $\ln \Xi$ on account of (A.6). By differentiating this new function, we obtain

$$\frac{\partial \ln \Xi}{\partial N_i(z)} + \beta(z) = 0. \tag{A.8}$$

Combining (A.4) and (A.8) yields

$$\frac{\partial \ln \psi(\{N_i(z)\}, z)}{\partial N_i(z)} + \mu_i(z)/(kT) + \beta(z) = 0. \tag{A.9a}$$

In our case, normally the system consists of a crystal in contact with a two-component solution (solute A and solvent B). According to the choice of coordinate system, the regions of $z \geq 0$ correspond to the fluid, and $\psi(\{N_i(z)\}, z) = \psi_{A,B}(z) = \psi_A(z)\psi_B(z)\psi_M(z)$. The regions of $z < 0$ corre-

spond to the solid, and $\psi([N_i(z)], z) = \psi_S(z)$. Then for solid and solute units, according to (A.9a), we have

$$\frac{\partial \ln \psi_S(-z)}{\partial N_S(-z)} + \mu_S(-z)/(kT) + \beta(-z) = 0, \tag{A.9b}$$

$$\frac{\partial \ln \psi_A(z)}{\partial N_A(z)} + \frac{\partial \ln \psi_M(z)}{\partial N_A(z)} + \mu^A_{A,B}(z)/(kT) + \beta(z) = 0. \tag{A.9c}$$

In equilibrium, each component has the same chemical potential in the different phases. This means that $\mu_S(-z) = \mu^A_{A,B}(z)$. Here we consider the system on the basis of regular solution theories. So each species has approximately the same size. Then $\beta(z)$ for each slice must be almost the same. Subtracting (A.9b) and (A.9c) yields

$$\frac{\partial \ln \psi_A(z)}{\partial N_A(z)} - \frac{\partial \ln \psi_S(-z)}{\partial N_S(-z)} + \frac{\partial \ln \psi_M(z)}{\partial N_A(z)} = 0. \tag{A.10}$$

According to statistical thermodynamics [15,23], the following expression can be derived from (A.10),

$$kT \ln X^m(z) = -\Delta h^m(z) + T\Delta S^m(z), \tag{A.11}$$

where

$$\Delta h^m(z) = [\epsilon_A(z) - \epsilon_S(-z)] + [1 - X^m(z)]^2 w_{AB}(z), \tag{A.12}$$

$$\Delta S^m(z) = k\{\ln[Q_A(T, z)/Q_S(T, -z)] + \ln[v_A(z)/v_S(-z)] + 1\} \tag{A.13}$$

and

$$X^m(z) = N_A(z)/[N_A(z) + N_B(z)]. \tag{A.14}$$

When $z \to \infty$, (A.11) is converted to the corresponding expression of the bulk phase, which is given by

$$kT \ln X = -\Delta h_d + T\Delta S_d. \tag{A.15}$$

Following (A.12) and (A.13), it can be seen that for a regular solution, the expression of $\Delta S^m(z)/\Delta S_d$ is given by

$$\Delta S^m(z)/\Delta S_d = \{\ln[Q_A(T, z)/Q_S(T, -z)] + \ln[v_A(z)/v_S(-z)] + 1\} \times \{\ln[Q_A(T, \infty)/Q_S(T, -\infty)] + \ln[v_A(\infty)/v_S(-\infty)] + 1\}^{-1}. \tag{A.16}$$

Normally, the terms $\ln[Q_A(T, z)/Q_S(T, -z)]$, $\ln[v_A(z)/v_S(-z)]$, $\ln[Q_A(T, \infty)/Q_S(T, -\infty)]$ and $\ln[v_A(\infty)/v_S(-\infty)]$ are larger than unity. In case $\Delta h^m(z)/\Delta h_d \geq 1$ (or $\Delta h^m(z) \geq \Delta h_d$), $\ln[Q_A(T, z)/Q_S(T, -z)] \geq \ln[Q_A(T, \infty)/Q_S(T, -\infty)]$ and $\ln[v_A(z)/v_S(-z)] \geq \ln[v_A(\infty)/v_S(-\infty)]$. Consequently, $\Delta S^m(z)/\Delta S_d \geq 1$. Similarly, if $\Delta h^m(z)/\Delta h_d < 1$ (or $\Delta h^m(z) < \Delta h_d$), $\Delta S^m(z)/\Delta S_d < 1$. Then the following relation holds for regular solutions

$$\Delta h^m(z)/\Delta h_d = \Delta S^m(z)/\Delta S_d \tag{A.17}$$

We notice that a relation similar to (A.17) has been experimentally justified in ref. [15]. Now it can be seen that relation (12) can be obtained from dividing (A.11) by (A.15).

List of symbols

C_i^* (or C_i°)	Surface characteristic scaling factor.
d	Interplanar distance of a crystal structure in the surface orientation.
Δh	Enthalpy per structural unit.
k	Boltzmann constant.
M	The number of monomer segments of a polymer molecule
N	The number of certain species
P	Pressure
Q	The partition function of a molecule for all the internal degrees of freedom.
ΔS	Entropy per structural unit.

T	Temperature.
V	Volume
X	Molar fraction of solute.
$X^s(0)$	Molar fraction of solute in the artificial layer preceding the first fluid layer.
v	The free volume per structural unit [23].
μ	Chemical potential.
α	Coefficient introduced in eq. (5).
δ^* (or n^*d)	Characteristic thickness of interfaces.
ρ	Density.
φ	Volume fraction of solute.
ϵ_i	Lattice energy per structural unit, which is equal to $\sum_{k=1}^{n} \frac{1}{2}\phi_k^{ii}$.
w_{AB}	The change energy, defined by $w_{AB} = \sum_{k=1}^{n}[\phi_k^{AB} - \frac{1}{2}(\phi_k^{AA} + \phi_k^{BB})]$

Subscripts

d	Dissolution
f	Fluid.
m	Melting.
M	Mixing.
s	Solid.

Superscripts

1	The first fluid layer in the interfacial phase.
m	The intermediate layers in the interfacial phase.

References

[1] M Baus, J Phys C 23 (1990) 211
[2] A D J Haymet and M Annu, Rev Phys Chem 28 (1987) 89
[3] J Q Broughton and F F. Abraham, Chem. Phys. Lett 71 (1980) 456
[4] J Q Broughton and G H Gilmer, J Chem Phys 79 (1983) 5095, 5105, 5119; 84 (1986) 5741, 5749, 5759
[5] M Baus and J.L. Colot, Mol Phys 55 (1985) 653
[6] W A Curtin and N W Ashcroft, Phys Rev 32 (1985) 2909
[7] F F Abraham and J Q Broughton, Phys. Rev Lett 56 (1986) 734
[8] A.D.J Haymet and D W Oxtoby, J Chem Phys 74 (1981) 2559
[9] R D Groot, Mol Phys 60 (1987) 45
[10] R D Groot, J P van der Eerden and N M Faber, J Chem Phys 87 (1987) 2263
[11] R D Groot, N M Faber and J P van der Eerden, Mol Phys 60 (1987)
[12] R D Groot and J P van der Eerden, Phys. Rev A 36 (1987) 4356
[13] I K. Snook and D Henderson, J Chem Phys 68 (1978) 2134
[14] X Y Lu and P Bennema, J Chem Phys 97 (1992) 3600
[15] X Y Lu and P Bennema, J Chem Phys. 98 (1993), in press
[16] J M H M Scheutjens, in Macromolecules (lecture note), J.M H M Scheutjens and G.J. Flees, J Phys Chem 83 (1979) 1619
[17] R C. Weast, M J Astle and W H Beyer, CRC Handbook of Chemistry and Physics, 67th ed. (CRC Press, Florida, 1987)
[18] D Chatain, C. Vahlas and N Eustathopoulos, Acta Met 32 (1984) 227
[19] R D Groot, M Elwenspoek and P Bennema, J Cryst Growth 79 (1986) 817
[20] T Sawada, J Cryst Growth 60 (1982) 349
[21] P Hartman, in: Morphology of Crystals, Part A, Ed. I Sunagawa (Terra, Tokyo, 1987) p 271
[22] X.Y Lu, J Chem Phys 98 (1993), in press.
[23] S R Fowler and E.A Guggenheim, Statistical Thermodynics (Cambrdige University, London, 1960)

Chapter 4.4

The surface free energy of solid–fluid interfaces: An inhomogeneous cell model description

Xiang-Yang Liu
RIM, Laboratory of Solid State Chemistry, Faculty of Science, University of Nijmegen, Toernooiveld 6525 ED Nijmegen, The Netherlands

(Received 7 October 1992, accepted 11 February 1993)

Many important issues in the field of crystal growth and surface science can be interpreted satisfactorily on the basis of the surface free energy of solid–fluid interfaces However, the values of energies are not always available either from theory or from experiment In this paper, starting from the grand canonical partition function, a general expression of the surface free energy is derived within the framework of an inhomogeneous cell model The results are applied to estimate surface free energies of metal-melt systems, which are compared with the experimental results of Turnbull. Our estimated results agree well in almost every case with Turnbull's results Based on our model, various factors which may affect the surface free energy are discussed

I. INTRODUCTION

The concept of surface free energy plays an important role in surface science. Many important issues, such as equilibrium forms of crystals and 3D nucleation, are directly related to its value. However, for most solid–fluid systems, this value is very difficult to predict accurately It is even more difficult to obtain reliable values from experiments. Conventionally, it is suggested that the surface free energy σ is proportional to the enthalpy of melting for a crystal-melt system or the enthalpy of dissolution for a crystal-solution system[1–3] as

$$\sigma s=\xi\Delta h, \tag{1}$$

where Δh is the molar enthalpy, s is the area per surface site, and ξ is a proportionality constant This is understandable It is known that the enthalpy of melting (or dissolution) results mainly from the change of bond energies in the process of the phase transition [4] Note that the energy difference due to the change of densities between the solid and the liquid phase is negligible compared to that due to the change in bonds [4]

To determine the value of ξ, an *ad hoc* assumption (the so-called equivalent wetting condition) was first introduced by Jackson [5] This assumption implies that the changes of bond energies of a solid unit dissolved in a saturated solution or in the melt are the same as the corresponding values of solid–mother phase interactions of a solid unit at the surface. Based on this assumption, it is expected that for faces with the minimal surface energy $\xi\simeq 0.2$ (± 0.05). However, the classical 3D homogeneous nucleation experiments of Turnbull yield $\xi\simeq 0.45$ for a large number of metal-melt systems and $\xi\simeq 0.32$ for some other metals This shows explicitly a discrepancy as compared to the equivalent wetting assumption These experimental results cannot be predicted from present theories

Recent progress in experiments and theories[6–20] indicates that properties of solid and fluid units in the interfacial regions are different from those in the bulk Results of computer simulations and various theories[6–15] reveal that concentrations (or densities) and potential energies of structural units in the interface are a function of the distance from the surface In our previous papers,[16–18] the relation between interfacial quantities and bulk quantities, as well as the distribution profiles of these quantities, are derived from the layer model which is an inhomogeneous cell model In this paper, we attempt to apply those results to derive an expression for the surface free energy σ using basic principles of statistical thermodynamics The implications are applied to metal-melt systems

This paper is arranged as follows In Sec II, the general expression of surface free energy is first derived from the grand canonical partition function of a solid–fluid interfacial system Next, analytical expressions are discussed under the equivalent wetting condition and the nonequivalent wetting condition separately Section III is devoted to an estimation of ξ for metal-melt systems based on our model The results are compared with experimental results Finally discussions and conclusions are given in Sec IV

II. GENERAL MODEL

To describe the solid–fluid interface within the framework of a layer model, we first define a Cartesian coordinate system in the following way the X and Y axes are in the plane of the solid surface, the Z axis is normal to the surface, and the origin is in the dividing plane of the surface. The dividing surface is chosen to follow the edges of the unit cells of the crystal structure and all points in the plane have a similar environment in the boundary region between the two phases For simplicity, we here take the dividing surface as a flat plane parallel to (hkl) In fact, this is the low temperature limit According to the layer model,[16–18] macroscopic quantities such as the density (or concentration) and the enthalpy of a system are functions of z and independent of x and y

We notice that according to Gibbs,[21] the division must be chosen in such a way that both the interface excess volume ΔV_{excess} and the interface excess particles ΔN_{excess} should be equal to zero Within the framework of cell mod-

 0021-9606/93/108154-06$06.00

els, this condition is automatically fulfilled using the aforementioned convention This is because for a solid–fluid interface with a given area, according to the convention the number of cells for each layer N^0 is constant It follows then that $\Delta V_{excess}=\Delta N_{excess}=0$ This consequently leads to a constraining condition

$$\sum_i N_i(z)-N^0=0, \quad z=0,\pm 1,\pm 2,\pm 3,\ldots, \tag{2}$$

where subscript i denotes a certain species and $N_i(z)$ is the corresponding number of particles of this species in the layer z

For a solid–fluid interface, we first start with the grand canonical partition function of the system. According to our analysis,[18] in this slice model, the grand canonical partition function Ξ for a multicomponent system is defined as

$$\Xi(\mu,V,T)=\sum_{\substack{\text{all}\\ \{N_i(z)\}}}\prod_z \psi\{[N_i(z)],z,V(z),T\} \times\exp\left[\sum_z N_i(z)\mu_i(z)/(kT)\right], \tag{3}$$

where $\psi\{[N_i(z)],z,V(z),T\}$ is the canonical partition function for a closed subsystem at z {fixed $[N_i(z)],V(z),T$}, k is the Boltzmann constant, μ is the chemical potential, V is the volume, and T is the temperature In the following, we omit the notation of fixed V,T because this condition is supposed to be always satisfied.

In expression (3), all distributions $[N_i(z)]$ are possible However, we only consider the maximum terms, since at equilibrium, Ξ should be at its maximum Corresponding to the equilibrium distribution $[N_i(z)]$, Eq (3) can be rewritten as

$$\ln \Xi_{eq}=\sum_z\left(\ln\psi\{[N_i(z)],z\}+\sum_i N_i(z)\mu_i(z)/(kT)\right) \tag{4}$$

Before discussing the surface free energy, we need to define a reference state (labeled with *) for the solid–fluid interface. The homogeneous bulk state (where $|z|\to\infty$) is chosen as the reference state. In this reference state, any surface effect is not taken into account. Therefore the grand canonical partition function for this state is given by

$$\ln \Xi^*_{eq}=\sum_z\left[\ln\psi[N_i]+\sum_i N\mu_i/(kT)\right] \tag{5}$$

We notice that in the reference state all quantities are independent of z

According to standard statistical thermodynamics, it is known that the Helmholtz free energy of the system is expressed as

$$F=-kT\ln\Xi_{eq}+\sum_z\sum_i[N_i(z)\mu_i(z)] \tag{6}$$

(Since the solid and liquid phases are incompressible,[4] any change of the Helmholtz free energy between the two phases is equal to that of the Gibbs free enthalpy) Thus the total surface free energy (σA) of the interface, defined as the excess free energy relative to the homogeneous bulk phase (the reference state), is expressed as

$$\sigma A=-kT\ln(\Xi_{eq}/\Xi^*_{eq})+\sum_z\sum_i[N_i(z)\mu_i(z)-N\mu_i], \tag{7}$$

where $A=N^0s$ Substituting Eqs. (4) and (5) into Eq (7) yields

$$\begin{aligned}\sigma s&=-\frac{kT}{N^0}\sum_z\left[\ln(\psi\{[N_i(z)],z\}/\psi[N_i])+\sum_i[N_i(z)\mu_i(z)-N\mu_i]/(kT)\right]\\&\quad+\frac{1}{N^0}\sum_z\sum_i[N_i(z)\mu_i(z)-N\mu_i]\\&=-\frac{kT}{N^0}\sum_z\ln(\psi\{[N_i(z)],z\}/\psi[N_i])\end{aligned} \tag{8}$$

Now consider the system which consists of a crystal (indicated by subscript s) in contact with a two-component solution (solute A and solvent B) It is assumed in this system that solvent B cannot be incorporated into the crystal According to the choice of the coordinate system, the region where $z\geq 0$ belongs to the fluid and that of $z<0$ to the solid Then

$$\psi[N_i(z)],z]=\begin{cases}\psi_{A,B}(z)=\psi_A(z)\psi_B(z)\psi_M(z), & z\geq 0\\ \psi_i^A(z), & z<0,\end{cases} \tag{9}$$

where ψ_i ($i=A$, B, and S, denoting component A, B, and the crystal state) represents the canonical partition function of a certain species in the pure state, and ψ_M results from mixing A and B Based on cell models,[4,17] the canonical partition function ψ for a certain species has the form

$$\ln\psi=N\ln Q'(T)+\ln\Omega \tag{10}$$

$Q'(T)$ is defined by

$$Q'(T)=[(2\pi mkT)^{3/2}/h^3]Q(T), \tag{11}$$

where $Q(T)$ denotes the partition function of a molecule for all internal degrees of freedom, m is the mass of a structural unit, and h is Planck's constant Ω is referred to as the partition function for the configuration potential energy and for the fluid state is defined as

$$\Omega=\{v\exp[(-\epsilon+kT)/(kT)]\}^N. \tag{12}$$

Here ϵ refers to the minimum potential energy per unit and is given by

$$\epsilon=\tfrac{1}{2}\sum_k\phi_k, \tag{13}$$

ϕ is the interaction energy in a certain direction (the subscript k indicates interaction energies in different directions), v is the so-called free volume of a structural unit and in terms of the harmonic oscillator model[4] can be expressed as

$$\upsilon=[kT/(2\pi m\nu^2)]^{1/2}, \tag{14}$$

where ν is the frequency of vibration For the crystal state, at a sufficiently high temperature ($kT\gg h\nu$),

$$\Omega=\{\upsilon_i\exp[-\epsilon_i/(kT)]\}^{\lambda} \tag{12a}$$

In addition, ψ_M can be written according to the Bragg–Williams approximation[4] as

$$\ln\psi_M=N_A\ln[(N_A+N_B)/N_A]+N_B\ln[(N_A+N_B)/N_B]$$
$$-N_AN_B/(N_A+N_B)w_{AB}/kT, \tag{15}$$

where

$$w_{AB}=\sum_k\phi_k^{\sigma} \tag{15a}$$

and

$$\phi_k^{\sigma}=\phi_k^{AB}-\tfrac{1}{2}(\phi_k^{AA}+\phi_k^{BB}) \tag{15b}$$

After substituting Eqs (10) and (15) into Eq (8), we obtain that

$$\sigma s\simeq(\sigma_1+\sigma_2)s, \tag{16}$$

where

$$\sigma_1 s=\sum_j\phi_j \tag{16a}$$

(the subscript j represents all interactions crossing the dividing surface) and

$$\sigma_2 s\simeq\frac{1}{d}\int_0^{+\infty}\{[X_A(z)\Delta h_d^A(z)-X_A\Delta h_d^A]$$
$$+[X_B(z)\Delta h_d^B(z)-X_B\Delta h_d^B]$$
$$-kT\Delta X_A(z)\ln(X_A/X_B)\}dz \tag{16b}$$

Here $\Delta X_A(z)=X_A(z)-X_A$, d is the thickness of a layer and Δh_d^i ($i=A$ or B) is the exchange energy per structural unit of a certain species defined as

$$\Delta h_d^i(z)=[\epsilon_j^{i'}(z)-\epsilon_i^{i'}(-z)]+X_n(z)^2w_{i,n}(z) \tag{17}$$

(i and $i'=A$ or B, and $i\neq i'$) This corresponds to the energy change due to bringing a structural unit i ($i=A$ or B) from an environment of the pure crystal state into the solution state Obviously, for solute units ($i=A$) Δh_d^A is the dissolution enthalpy (per structural unit) For Eq (16a),

$$\phi_j=\{\tfrac{1}{2}[\phi_j^{AA}(0)-\phi_j^{SS}(0)]+X_B^2(0)\phi_j^{\sigma}(0)\}+X_A(0)$$
$$\times[\phi_j^{SA}(0)-\phi_j^{AA}(0)]+X_B(0)[\phi_j^{SB}(0)-\phi_j^{BB}(0)] \tag{18}$$

To derive expressions (16), (16a), and (16b), we need the constraining condition (2) and the following assumptions

(i) On the solid side, the difference in the density and the energy between the interface and the bulk is not large In fact, this condition is almost satisfied when the temperature is below the melting point

(ii) Some terms resulting from solute A may approximately cancel out those from solvent B such as

$$\ln\left|\frac{[\upsilon_A(z)\,Q_A(z)]^{X_A(z)}}{(\upsilon_A\,Q_A)^{X_A}}\right|\simeq-\ln\left|\frac{[\upsilon_B(z)\,Q_B(z)]^{X_B(z)}}{(\upsilon_B\,Q_B)^{X_B}}\right| \tag{19}$$

and

$$[X_A(z)\epsilon_S^A(-z)-X_A\epsilon_S^A]\simeq-[X_B(z)\epsilon_S^B(-z)-X_B\epsilon_S^B] \tag{20}$$

Looking at the constraining condition (2), it can be seen that if the surface adsorbs one component, it should repel the other Therefore those effects caused by A and B should be opposite

It can be seen from Eq (16b) that when both the solid and the fluid are homogeneous up to the dividing surface, $\sigma_2=0$ This is *the so-called homogeneous phase approximation* Normally, the real structure of the solid–fluid interface will differ from the homogeneous phase approximation Then $\sigma_2\neq0$ In the following, we will treat those two distinct cases separately

A. The equivalent wetting condition

As mentioned in Sec I, the equivalent wetting condition is introduced to estimate bond energies at solid–fluid interfaces The condition can be considered as two parts The first is the homogeneous phase approximation [17] It follows that for a certain interaction, the effective interfacial bond energy is equal to the corresponding bond energy in the bulk $\phi_k(z)\simeq\phi_k$ According to Eq (16a), $\sigma_2=0$ Then Eq (16) can be written in the following way

$$\sigma\simeq\sigma_1 \tag{21}$$

The second part of the equivalent wetting condition can be expressed as $\phi_j^{SA}\simeq\phi_j^{AA}$ and $\phi_j^{SB}\simeq\phi_j^{AB}$ Equation (18) can thus be rewritten as

$$\phi_j\simeq\tfrac{1}{2}(\phi_j^{AA}-\phi_j^{SS})+X_B^2\phi_j^{\sigma} \tag{18a}$$

With this expression, ϕ_j can be brought into direct relation with the dissolution enthalpy Δh_d^A according to Eqs (13), (15a), and (17) This allows us to evaluate $\Sigma_j\phi_j$ by introducing the proportionality assumption,[22] which states that

$$\phi_j\ \phi_{j'}\ \phi_{j''}\quad=\phi_j^{ss}\,\phi_{j'}^{ss}\,\phi_{j''}^{ss} \tag{22}$$

The implication of this assumption is that in any case the ratio of bond energies in different directions will be constant, although the absolute bond energy in a certain direction will alter in different states From this proportionality assumption, we may then define a crystallographic factor

$$\eta_{hkl}=E_{hkl}^{att}/(2E^{cr}), \tag{23}$$

where E_{hkl}^{att} is the so-called attachment energy of face (hkl) (defined as the energy released per structural unit when a crystal layer is moved from an infinite distance to attach to the crystal surface) and E^{cr} is the lattice energy (or sublimation enthalpy) of a crystal (see Refs 23 and 24) As a result of the homogeneous phase approximation, the surface free energy can simply be written

$$\sigma s \simeq \sigma_1 s \simeq \eta_{hkl} \Delta h_d^A, \tag{24}$$

or in comparison with Eq (1) ξ is expressed as

$$\xi = \eta_{hkl} \tag{25}$$

B. The inhomogeneous fluid phase approach

As mentioned earlier, the equivalent wetting condition is a very rough assumption, which in most cases causes a large deviation of predicted values from experimental data. We notice that the main drawback of the equivalent wetting assumption is the homogeneous phase approximation Actually this approximation comes from the traditional homogeneous cell models, where the same type of cells are equal in all positions

In our inhomogeneous cell model (or the layer model), the same type of cells are distinguished by z Hence to deal with problems concerning the interface, this model does not have those difficulties which the homogeneous cell models always encounter Note that earlier in this section, it was assumed that the solid phase is almost homogeneous So we only consider here the inhomogeneity of the fluid phase

Within the framework of the layer model, for the profile of concentrations (or densities) and enthalpies in the interfacial phase, it was obtained[18] that

$$X_A(z) = X_A\{1 + D \exp[-z/(n^* d)]\} \tag{26}$$

and

$$\Delta h_d^A(z)/\Delta h_d^A = 1 + \frac{1}{\ln X_A} \ln\{1 + D \exp[-z/(n^* d)]\}, \tag{27}$$

where

$$D = X_A^A - 1 \text{ and } \lambda = C_f^* - 1 \tag{28}$$

($X_A D$ is the difference between the concentration of the first interfacial fluid layer and that of the bulk phase), C_f^* is the surface characteristic scaling factor,[17] defined by

$$C_f^* = \Delta h_d^A(0)/\Delta h_d^A, \tag{29}$$

and n^* is the normalized characteristic thickness of the interface defined in such a way that at $z = n^* d$, $[X_A(z) - X_A]/(X_A D) = 1/e$

Obviously σ_1 will now be expressed differently from expression (24), which is based on the homogeneous phase approximation From the definition of C_f^*, it is easily derived according to this inhomogeneous fluid phase approach that

$$\sigma_1 s \simeq \eta_{hkl} C_f^* \Delta h_d^A \tag{24a}$$

Without doubt, according to Eq (16a), σ_1 is expressed more precisely by Eq (24a) than by Eq (24) because the differences of corresponding interaction energies between solid and fluid units are modified from the bulk phase to the interfacial phase by C_f^* We notice that in Eq (24a) since $\Sigma_j \phi_j$ has mainly been modified by C_f^*, the second part of the equivalent wetting assumption may be regarded as a reasonable approximation and is adopted in expression (24a)

Second, in this approach, $\sigma_2 \neq 0$ According to Eqs (16b), (26), and (27),

$$\sigma_2 s \simeq n^* X_A D\{-kT \ln(X_A/X_B) + \Delta h_d^A[D/(2 \ln X_A) + 1] + \Delta h_d^B[(X_A D/2 - X_B)/(X_B \ln X_B) - 1]\} \tag{30}$$

Finally, combining Eqs (24a) and (30) yields

$$\sigma s \simeq \eta_{hkl} C_f^* \Delta h_d^A + n^* X_A D\{-kT_s \ln(X_A/X_B) + \Delta h_d^A[D/(2 \ln X_A) + 1] + \Delta h_d^B[(X_A D/2 - X_B)/(X_B \ln X_B) - 1]\} \tag{31}$$

It can be seen that Eq (24) can be included in Eq (31) as a limit case [When $C_f^* \to 1$, Eq (31) automatically reduces to Eq (24)] Similarly, ξ has the general form

$$\xi \simeq \eta_{hkl} C_f^* + n^* X_A D\{-kT_s/\Delta h_d^A \ln(X_A/X_B) + [D/(2 \ln X_A) + 1] + \Delta h_d^B/\Delta h_d^A[(X_A D/2 - X_B)/(X_B \ln X_B) - 1]\} \tag{25a}$$

III. APPLICATION TO SOME METAL-MELT SYSTEMS

Relations (31) and (25a) can be justified using available experimental data In this section, we will apply them to metal-melt systems and then compare them with the data from 3D homogeneous nucleation experiments

Before applying Eqs (31) and (25a) to a crystal-melt system, form (25a) must first be modified As was done in our previous paper,[17] for a crystal-melt system, we assume that $X_A \simeq \rho_f/\rho_s$ and also $\Delta h_d^B \simeq -\Delta h_d^A$ Then Eq (25a) is rewritten as

$$\xi \simeq \eta_{hkl} C_f^* + n^* \frac{\rho_f}{\rho_s} D\left\{-kT_m/\Delta h_m^A \ln\left[\left(\frac{\rho_f}{\rho_s}\right)\Big/\left(1-\frac{\rho_f}{\rho_s}\right)\right] + \left(\frac{D}{2}\right)\Big/\ln\left(\frac{\rho_f}{\rho_s}\right) - \left[\left(\frac{\rho_f}{\rho_s}\right)\frac{D}{2} - \left(1-\frac{\rho_f}{\rho_s}\right)\right]\Big/\left[\left(1-\frac{\rho_f}{\rho_s}\right)\ln\left(1-\frac{\rho_f}{\rho_s}\right)\right] + 2\right\}, \tag{25b}$$

where ρ_f and ρ_s denote the density of the fluid and the solid, respectively

Explicitly, the crystallographic factor depends on the structure of the crystal face For faces with minimal surface energy, it is expected that the lowest limit is $\eta_{hkl} \sim 0.15$ (Ref 9) (we will come back on this in the next section) On the other hand, those results from the experiments of surface roughening and homogeneous nucleation reveal that for different faces of inorganic and metal crystals $C_f^* \simeq 2.5$–6 Here, for the homogeneous nucleation, we take the lowest value $C_f^* \simeq 2.5$ The choice of this value is made for various reasons First, this is because the crystal faces with the lower surface energies are of greater morphological importance Those faces normally have smaller C_f^* [16] Second, the experimental data of Turnbull, which we will

TABLE I Relevant thermodynamic data and the ratio of interfacial energies to the molar enthalpy of fusion for various metal melt systems

Metal	$kT_m/\Delta h_m$[a]	ξ[b]	ξ[c]
Mercury	0 835	0 476	0 53
Tin	0 583	0 393	0 418
Silver	0 907	0 465	0 457
Gold	0 875	0 456	0 436
Copper	0 868	0 454	0 439
Iron	1 0	0 440	0 445
Manganese	0 860	0 452	0 480
Cobalt	0 955	0 479	0 490
Palladium	0 883	0 458	0.450
Nickel	0 877	0 457	0 444
Platinum	0 864	0 453	0 455
Bismuth	0 432	0 330	0.33
Antimony	0 376	0 314	0 302
Germanium	0 402	0 321	0 348

[a]Reference 1
[b]The data are theoretically estimated based on Eq (25a)
[c]The observed data are selected from Ref 1

compare with our results in the following, represent lower bounds on the surface free energy (we will come back to this in Sec IV) For many metals in the neighborhood of the melting temperature, $\rho_f/\rho_s \simeq 0\,97$–$0\,99$ (Ref 24) According to theoretical results,[13] for these systems $n^* \simeq 2$

Now we substitute the data of $kT_m/\Delta h_m^A$ into Eq (25b) and then ξ for various metal systems is obtained These values are listed in Table I, together with those from 3D homogeneous nucleation experiments [1] Very surprisingly, our model predicts not only the value ξ for most metals that $\xi \sim 0\,45$, but also for some metals such as bismuth, antimony, germanium, etc $\xi \sim 0\,32$ If the experimental error [$\pm 5\%$ in the measurement of the maximum supercooling $(\Delta T)_{max}$ (Ref 1)] is taken into account, our estimations agree very well with the experimental data

IV. DISCUSSION AND CONCLUSIONS

In the last section, we have mentioned that the crystallographic factor η_{hkl} depends both on the structure of a crystal and on the orientation of crystal faces According to Eq (23), it is obtained that for a simple cubic (sc) (100) face $\eta_{hkl} \simeq 0\,167$, and for a face centered cubic (fcc) (111) face $\eta_{hkl} \simeq 0\,25$ It seems that those values, especially for a fcc (111) face, are a bit larger than the value $\eta_{hkl} \simeq 0\,15$, which we chose in our estimation However, in most cases, the surface relaxation or the surface reconstruction may occur This will to a large extent reduce the value of η_{hkl} According to a modified model,[26] it is estimated that for a sc (100) and a fcc (111) face, η_{hkl} is about 0 125 and 0 187, respectively These values are roughly around our value 0 15 This is why this value is suitable for most metals.

Looking at expression (25b), other effects may also influence the value of ξ Assume that for most metals in contact with the melt, at the melting point, the profile of the density distribution in the interfacial phase differs not much Then C_f^* and n^* for different metals are close to each other In case the value ρ_f/ρ_s is almost the same, the main effect on ξ for those metals can be regarded as the difference in the melting entropy $(\Delta h_m/T_m)$ Otherwise, the value ρ_f/ρ_s will also have some influence on ξ This can be seen from the data listed in Table I

Concerning the case of a crystal in contact with a solution, it can be seen from Eq (25a) that the concentration of solution and the ratio of dissolution enthalpy between solute and solvent will also influence the value of σ This may explain the experimental relation between σ and the concentration of a solution [27]

We notice that Turnbull's calculation for the solid–fluid interfacial surface free energy of various metals was based on the assumption that, at the lowest solidification temperature recorded, homogeneous nucleation kinetics were operative Then this parameter was estimated by measuring the maximum supercooling of a variety of molten metal droplets Some authors cast doubts on Turnbull's assumption that homogeneous nucleation occurred in his droplets [28–31] Some later experiments have suggested that much lower supercoolings are possible than those observed by Turnbull, making Turnbull's values for σ too low by a factor of $\frac{1}{3} \sim 2$ [28–33] In addition, if the thickness of the solid–fluid interface has the same order as the critical nucleus size, then some corrections must be applied to the homogeneous nucleation results This will also enhance the actual values for σ (or ξ) [34] In this sense, Turnbull's results only represent the lower bounds of the surface free energy for a variety of metals This is one of the reasons that we chose a lower C_f^* in our estimations (see Sec III) To calculate more accurate σ (or ξ) in a particular case, a more precise C_f^* and n^* are needed These can be done by computer simulations, density-functional theory calculations, and self-consistent field calculations, or measured by some experimental techniques

In summary, the surface free energy of solids in contact with saturated solutions is proportional to their dissolution enthalpy as suggested by Eq (1) The expression of this proportionality constant is derived within the framework of a layer model, as in Eq (25a) The results are successfully applied to estimate the surface tension of metal-melt systems

In the case of a crystal in contact with its melt, factors which may affect the value of the surface tension are mainly the surface structure and the interfacial wetting condition (determined by C_f^* and n^*) In addition, the entropy of melting also plays an important role

ACKNOWLEDGMENTS

The author wishes to thank Professor P Bennema and Dr H Meekes for stimulating discussions and a critical reading of the manuscript He also acknowledges Shell Netherlands B V for providing financial support for this research

[1] J Turnbull, J Appl Phys 21, 1022 (1950)
[2] M Kahlweit Z Phys Chem (NK) 28 245 (1960)
[3] B Lewis and J C Anderson *Nucleation and Growth of Thin Films* (Academic New York 1979) Chap 2
[4] S R Fowler and E A Guggenheim *Statistical Thermodynamics* (Cambridge University London, 1960)

[3] K. A. Jackson, in *Liquid Metals and Solidification* (ASM, Cleveland, 1958), p. 174.
[4] D. Chatain, C. Vahlas, and N. Eustathopoulos, Acta Metall. 32, 227 (1984).
C. Vahlas and N. Eustathopoulos, J. Chem. Physique 6, 515 (1983).
[6] A. Passerone and N. Eustathopoulos, Acta Metall. 30, 1349 (1982).
[7] R. D. Groot, M. Elwenspoek, and P. Bennema, J. Cryst. Growth 79, 817 (1986).
[10] J. Q. Broughton and F. F. Abraham, Chem. Phys. Lett. 71, 456 (1980).
[11] J. Q. Broughyton and G. H. Gilmer, J. Chem. Phys. 79, 5095 (1983), 79, 5105 (1983); 79, 5119 (1983); 84, 5741 (1986); 84, 5749 (1986); 84, 5759 (1986).
[12] M. Baus and J. L. Colot, Mol. Phys. 55, 653 (1985).
[13] W. A. Curtin and N. W. Ashcroft, Phys. Rev. 32, 2909 (1985).
[14] A. D. J. Haymet and D. W. Oxtoby, J. Chem. Phys. 74, 2559 (1981).
[15] R. D. Groot, Mol. Phys. 60, 45 (1987).
[16] X. Y. Liu and P. Bennema, J. Chem. Phys. 97, 3600 (1992).
[17] X. Y. Liu and P. Bennema, J. Chem. Phys. 98, 5863 (1993).
[18] X. Y. Liu, Surf. Sci. (in press).
[19] G. C. McGonigal, R. H. Bernhardt, Y. H. Yeo, and D. J. Thomson, J. Vac. Sci. Technol. B 9, 1107 (1991).
[20] J. P. Rabe and S. Buchholz, Makromol. Chem., Macromol. Symp. 50, 261 (1991).
[21] J. W. Gibbs, *The Scientific Papers of J. W. Gibbs* (Longmans–Green, London, 1906), Vol. 1, p. 219.
[22] P. Bennema and J. P. van der Eerden, in *Morphology of Crystals, Part I*, edited by I. Sunagawa (Terra Scientific, Tokyo, 1987), p. 1.
[23] P. Hartman, in *Morphology of Crystals, Part A*, edited by I. Sunagawa (Terra Scientific, Tokyo, 1987), p. 269.
[24] R. Kern, in *Morphology of Crystals, Part A*, edited by I. Sunagawa (Terra Scientific, Tokyo, 1987), p. 77.
[25] R. C. Weast, M. J. Astle, and W. H. Beyer, *CRC Handbook of Chemistry and Physics*, 67th ed. (CRC, Boca Raton, FL, 1987).
[26] J. P. van der Eerden, R. D. Groot, M. Elwenspoek, and P. Bennema, Ph.D. thesis of R. D. Groot, Nijmegen University, 1988.
[27] P. Bennema and O. Sohnel, J. Cryst. Growth 102, 547 (1990).
[28] T. Takahashi and W. A. Tiller, Acta Metall. 17, 643 (1969).
[29] G. A. Colligan, W. T. Loomis, and V. A. Surprenant, J. Aust. Inst. Metals 10, 89 (1965).
[30] D. W. Gomersall, S. Y. Shiraishi, and R. G. Ward, J. Aust. Inst. Metals 10, 220 (1965).
[31] G. L. F. Powell, J. Aust. Inst. Metals 10, 223 (1965).
[32] W. A. Miller and G. A. Chadwick, Acta Metall. 15, 607 (1967).
[33] M. J. Stowell, Philos. Mag. 22, 1 (1970).
[34] J. E. Hilliard and J. W. Cahn, Acta Metall. 6, 772 (1958).

Chapter 4.5

Self–consistent field calculation of structure of static properties of the solid–fluid interface: monomer systems

Xiang–Yang Liu

RIM, Laboratory of Solid State Chemistry, Faculty of Science, University of Nijmegen, Toernooiveld, 6525 ED Nijmegen, The Netherlands

ABSTRACT–A study of the interface between the crystal and the fluid phase has been carried out, using self–consistent field (SCF) theory calculations The results are expressed in terms of two interfacial factors the surface characteristic scaling factor C_l^* and the characteristic thickness of the interface n^* The interfacial structure and interfacial properties can be described employing those two factors The influence of various parameters, such as the bulk concentration and energy parameters, on the structure and properties of interfaces are discussed in terms of C_l^* and n^* As a consequence, the surface free energies of some metal systems are estimated from the calculated results They are compared with experimental values, and turn out to be in good agreement with them Finally, the interfacial bond energies for some inorganic and metal crystals are analyzed based on the calculated results in the context of the wetting condition

I INTRODUCTION

Information on the structure of crystal surfaces can improve our understanding of a number of important physical processes Crystal growth is one of the processes that take place primarily at the crystal–fluid interface, and hence is strongly influenced by the atomic arrangements in this region To study the interface of crystals, monomer fluid systems are a good starting point Many inorganic and metal systems can be treated as monomer systems In other words, monomer systems represent a large number of real crystal systems Because these systems are relatively simple, detailed investigations on them have been carried out, using Monte Carlo (MC), Molecular Dynamics (MD) computer simulations [1-3] and density–functional theories [4-7] The results obtained from those methods reveal important information at the interface concerning the ordering of the fluid units in the regions adjacent to the solid surface, surface melting etc However, it is not always easy to interpret those results and to associate them with measurable properties (such as the step energy at the surface) Also, MD and MC involve a large number of need many parameters and sometimes require a large computer capacity

The same purpose may also be achieved by statistical mechanical calculations based on a Self–Consistent Field (SCF) theory [8-10], which provides insight into the behavior of structural units in interfacial regions SCF calculations rely comparatively less on computer capacity than MD or MC techniques do The quality of the outcome of such calculations depends on how rigorously the partition function is derived In addition, the results can easily be interpreted within the framework of an inhomogeneous cell model developed recently [11-14]

In the field of crystal growth, the interfacial bond energies ϕ_1 are one of the most crucial parameters The values of ϕ_1 at the surfaces $\{hkl\}$ determine the growth mechanism of the surfaces and e g the critical temperature of surface roughening (The subscript 1 denotes the interaction between a structural unit and its neighbors in direction 1) Due to the inhomogeneity of the interfacial regions, the interfacial bond energy is in most cases different from the bond energy in the bulk [11-12] In the language of cell models [11], ϕ_1 can be expressed for a two–component (A, B) solution system as

$$\phi_1 = \tfrac{1}{2}(\phi_1^{AA} - \phi_1^{SS}) + [1 - X_A(0)]^2 \phi_1^q + \Delta_1, \tag{1}$$

$$\phi_1^q = \phi_1^{AB} - \tfrac{1}{2}(\phi_1^{AA} + \phi_1^{BB}) \tag{2}$$

and

$$\Delta_1 = X_A(0)(\phi_1^{SA} - \phi_1^{AA}) + [1 - X_A(0)](\phi_1^{SB} - \phi_1^{AB}) \tag{3}$$

(the superscripts AA, BB, SS, AB, SA and SB represent solute–solute, solvent–solvent,

solid–solid, solute–solvent, solid–solute and solid–solvent interactions, respectively, $X_A(0)$ is the concentration of the solute in the first fluid layer adjacent to the crystal phase). As an approximation [12], it is assumed that $\phi_i^{SA} \simeq \phi_i^{AA}$ and $\phi_i^{SB} \simeq \phi_i^{AB}$. It then follows that $\Delta_i \simeq 0$.

To associate ϕ_i with the corresponding bond energy in the bulk Φ_i [Φ_i has a form similar to (1), with $\Delta_i = 0$], a so–called surface characteristic scaling factor C_ℓ^* is introduced [12]. This factor is defined as

$$C_\ell^* = \Delta h_{diss}^I / \Delta h_{diss} \simeq \phi_i / \Phi_i \tag{4}$$

Here $\Delta h_{diss}^I = \sum_{i=1}^{m} \phi_i$ and $\Delta h_{diss} = \sum_{i=1}^{m} \Phi_i$. According to the inhomogeneous cell model [11-12], C_ℓ^* is directly correlated with the concentration in the following way

$$C_\ell^* \simeq \ln X_A(0) / \ln X_A, \tag{5}$$

where X_A is the concentration of the solute in the bulk. Based on this surface characteristic scaling factor C_ℓ^*, three distinct cases can be recognized for the solid surface [12]: (i) the equivalent wetting [$C_\ell^* = 1$, or $X_A(0) = X_A$]; (ii) the less than equivalent wetting [$C_\ell^* > 1$, or $X_A(0) < X_A$]; (iii) the more than equivalent wetting [$C_\ell^* < 1$, or $X_A(0) > X_A$]. The equivalent wetting case is an artificial reference state, which happens only in some very special situations. Normally, the other two cases occur. The more than equivalent wetting case implies that the solid surface shows an adsorption of solute units. Considering the boundary condition of cell models, $X_A(z) + X_B(z) = 1$ [13-14], this equivalently corresponds to a repulsion between the surface and solvent units. In contrast, the less than equivalent wetting case means that the solid surface shows a repulsion to solute units (or an adsorption to solvent units).

To gain sufficient information about the structure of the crystal–fluid interface, in addition to C_ℓ^*, another factor, the so–called characteristic thickness of the interface n^*, is introduced [13]. This factor is defined as

$$[X_A(n^*) - X_A] / [X_A(0) - X_A] = e^{-1} \tag{6}$$

at $z = n^*$. (z is the distance away from the solid surface, and normalized by the interplanar spacing d_{hkl} of the crystal phase in the orientation of the surface). Within this framework, profiles of the concentration of solute units at the interface can be described by an exponential law [13] as

$$X_A(z) = X_A[1 + D\exp(-z/n^*)] \tag{7}$$

where $$D = X_A^{\zeta} - 1 \quad \text{and} \quad \zeta = C_l^* - 1 \tag{7a}$$

Obviously, C_l^* and n^* are the two key factors which determine the interfacial structure of monomer systems The roughening temperature T^r and the surface free energy of faces $\{hkl\}$ may in principle be estimated if these two factors are available[11-14] We notice that the interfacial structure is commonly determined by the internal structure of crystals and the mother phase Any change in these regions may in a subtle way affect the morphology of crystals Therefore, the values of C_l^* and n^* are also relevant for the description of the morphology of crystals[15]

To calculate the values of C_l^* and n^* in certain crystallographic orientations $\{hkl\}$, the SCF calculation is an appropriate technique This technique allows all molecules to be freely distributed throughout the system In this way, the equilibrium between the interface and the bulk solution is automatically guaranteed It follows from the calculations that profiles of the density for monomer systems obey the exponential law given by (7) (This result will explicitly be shown in Sec III) Then C_l^* and n^* can easily be extracted from the calculated results

In this study, I use the SCF method to calculate the factors C_l^* and n^* in various conditions for monomer interfacial systems The paper is arranged as follows In Sec II, principles of the SCF calculation are briefly explained Section III is devoted to the calculations of various monomer systems An estimate of the surface free energies for some metals is made based on the calculated results Finally, some discussions are given in Sec IV

II. INHOMOGENEOUS CELL MODELS AND SCF CALCULATIONS

Within the framework of cell models, both the solid and the fluid are divided into cells of equal shape and size Assume that the fluid phase consists of $M + 1$ layers of cells parallel to the surface (see Fig 1) The layer number, z, is counted from the surface and runs from 0 (the first fluid layer adjacent to the solid surface) to M (in the bulk solution) Every layer has L cells Each cell has m nearest neighbors, a fraction λ_0 of these are found in the same layer and a fraction λ_1 in each of the adjacent layers (Explicitly, $\lambda_0 + 2\lambda_1 = 1$)

For a two–component fluid system (A, B), each cell in the fluid phase is considered to be occupied by a molecule (or a monomer) of type i (i = A or B) (This is the so–called full occupancy constraint) Within the framework of regular solution theories, different monomers are supposed to have approximately the same volume

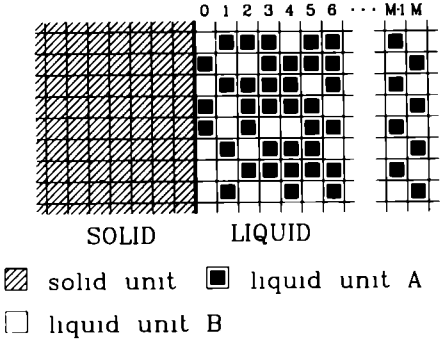

FIG.1. Illustration of the solid—fluid interface. The fluid phase having M layers of cells parallel to the surface, consists of two components A and B. Each cell is filled with either A or B. Cells in the solid phase are only filled with solid units.

In a mixture near a surface, a concentration gradient for every type of molecules is found due to spatial restrictions and mutual interactions between molecules and between molecules and the surface. Every individual molecule is subjected to a local potential which depends on the distance from the solid surface and on its chemical nature.

In inhomogeneous cell models [12-13], the chemical potential μ_i is expressed for species i as

$$\mu_i = \mu_i^\circ(z) + kT\ln X_i(z) = \mu_i^\circ + kT\ln X_i \tag{8}$$

where $\mu_i^\circ(z)$ and μ_i° denote the standard chemical potential of species i in layer z and in the bulk, and $X_i(z)$ and X_i the concentration of species i (expressed in mole fraction) in layer z and in the bulk, respectively, k is the Boltzmann constant, and T is the temperature. It then follows that

$$X_i(z) = X_i G_i(z) \tag{9}$$

and

$$G_i(z) = \exp[-u_i(z)/kT] \tag{9a}$$

Here $G_i(z)$ is known as the weighting factor [8], and $u_i(z)$ is the (relative chemical) potential and is expressed according to (8) as

$$u_i(z) = \mu_i^\circ(z) - \mu_i^\circ. \tag{10}$$

Explicitly, in the bulk phase ($z = M$), $u_i(M) = 0$. It can be seen that in case the potential profiles $u_A(z)$, $u_B(z)$, ··· are known, the molecular density (or concentration) profiles $X_A(z)$, $X_B(z)$, ··· can be calculated for every type of molecules. In turn, if the molecular density profiles are known, the potential profiles can be directly calculated.

The SCF theory [8-10] is based on a mean – field approximation within a layer This implies that fluctuations of the potential within the layer are neglected From this point of view, the potentials are assumed for solute molecules to be a linear function of the concentrations

$$u_A(z) = u'(z) + u_A^{int}(z) \tag{11}$$

and

$$u_A^{int}(z) = kT \sum_B \chi_{AB} [<X_B(z)> - X_B] \tag{11a}$$

The parameter $u'(z)$ may be interpreted as a "hard core potential", which guarantees the surface region to be filled by structural units Actually, it is of both enthalpic and entropic nature χ_{AB} is the Flory–Huggins interaction parameter, defined as the energy change (in units of kT) associated with the transfer of a molecule of type A from a liquid of pure A into a liquid of pure B For monomers of equal size, $u'(z)$ is approximately the same for different types of monomers According to the definition of χ_{AB}, it can be seen that $\chi_{AB} = \Sigma_{i=1}^{m} \Phi_i^q / kT$ [Φ_i^q has an expression analogous to ϕ_i^q in Eq (2)] Explicitly, $\chi_{AB} = \chi_{BA}$ and $\chi_{AA} = \chi_{BB} = 0$ $<X_B(z)>$ is the average concentration of B in layer z, and is given by

$$<X_B(z)> = \lambda_1 X_B(z-1) + \lambda_0 X_B(z) + \lambda_1 X_B(z+1) \tag{12}$$

To include the adsorption energy, Eq (11a) is rewritten for the first fluid layer as

$$u_A^{int}(0) = kT \chi_{AS} \lambda_1 + kT \sum_B \chi_{AB} [<X_B(0)> - X_B] \tag{11b}$$

where χ_{AS} is the Flory–Huggins parameter for the interaction of an A–monomer with surface sites of the adsorbent For molecules of type B, similar formulas hold In addition to Eqs (9)–(12), for the computation in a self–consistent manner, the boundary condition,

$$\sum_i X_i(z) = 1 \text{ (for any } z) \tag{13}$$

should be fulfilled This is obviously due to the full occupancy constraint

To obtain the density (or the concentration) profiles of monomer interfacial systems, the SCF method is to numerically solve the nonlinear equations (9), (9a), (11) and (13) For more details concerning the calculations, see Refs 8–10

III RESULTS

In this section, attention will be focused on two–component systems According to cell models [12], even for crystals in contact with the melt, the fluid (and the solid) can also be considered as a two–component system The system consists of structural units and vacuum units The existence of those vacuum units is due to the free volume in the crystal and the fluid phase Therefore, in interfacial regions the density of structural units changes Eq (5) can be rewritten in this case as,

$$C_{\ell}^{*} \simeq \ln [\rho_f(0)/\rho_s(-1)]/\ln(\rho_f/\rho_s) \qquad (5a)$$

(See appendix) Here ρ_f and ρ_s are the density of the fluid and the solid phase, respectively, $\rho_f(0)$ is the density of fluid units in the first fluid layer adjacent to the solid phase, and $\rho_s(-1)$ is the density of solid units in the first solid layer adjacent to the fluid phase

A. Influence of macroscopic properties on the interfacial structure

As mentioned in Sec I, the structure of solid–fluid interfaces can be characterized by two

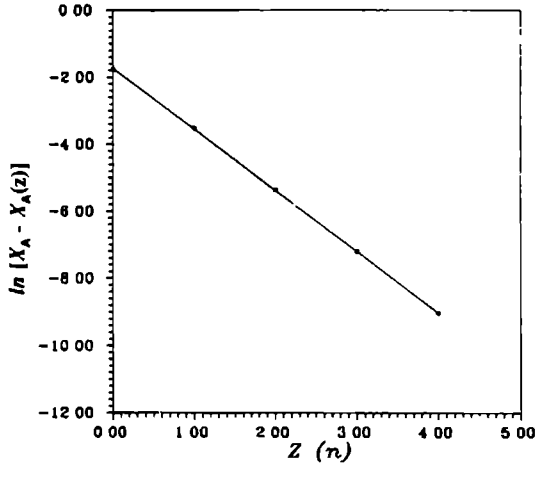

FIG 2 The linear relation between $\ln[X_A - X_A(z)]$ and the distance z for a monomer system This relation indicates that the exponential law is valid for monomer systems, $X_A = 0\ 80$, $\chi_{AS} = 1\ 47$, $\chi_{BS} = 0$ and $\chi_{AB} = 1\ 47$

key factors: C_ℓ^* and n^*. On the other hand, once profiles of the density $X_A(z)$ are available, C_ℓ^* and n^* can be easily calculated. Plotting $\ln [X_A - X_A(z)]$ versus z, a linear relation is obtained due to the exponential law expressed by (7) and (7a). Then C_ℓ^* and n^* can be directly calculated from the linear relation. An example of calculated data is shown in Fig.2.

Note that using the SCF method to calculate $X_A(z)$, some parameters, such as X_A, χ_{AS}, χ_{BS} and χ_{AB}, are needed, This implies that both C_ℓ^* and n^* are functions of those parameters. Assuming that those parameters are related to bulk properties of interfacial systems, the dependence of C_ℓ^* and n^* on those parameters will be investigated in the following.

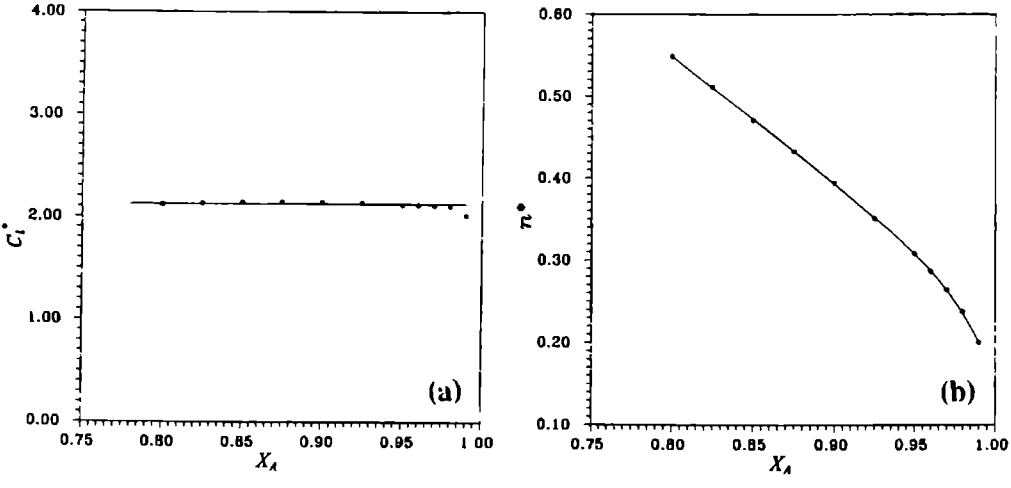

FIG 3. The relations between the two interfacial factors C_ℓ^*, n^* and the bulk concentration of solute X_A $\chi_{AS} = \chi_{AB} = 1.47$, $\chi_{BS} = 0$. (a) The surface characteristic scaling factor C_ℓ^* plotted versus X_A C_ℓ^* is almost constant for different concentrations (b) The characteristic thickness of interfaces n^* plotted versus X_A n^* linearly decreases with increasing X_A

Let us first consider the influence of the concentration X_A, under the condition that these energy parameters remain constant. In Fig 3, C_ℓ^* and n^* are plotted as a function of X_A for systems with $\chi_{AS} = \chi_{AB} = 1.47$, $\chi_{BS} = 0$. In this case C_ℓ^* remains constant for various concentrations. Only when $X_A \to 1$, does C_ℓ^* decrease slightly (see Fig.3a). A somewhat different relation can be found between n^* and X_A. It can be seen from Fig.3b that the (characteristic) thickness of the interface decreases almost linearly with X_A. The nonlinearity of the curve occurs when X_A is very close to unity, leading to $n^* = 0$. These results indicate that in almost the whole range of X_A (0–1), the thickness of the interface is influenced by the

concentration, but C_ℓ^* is not. In case $X_A \to 1$, both C_ℓ^* and n^* have a tendency to approach zero, which causes the nonlinearity of the curves. From the point of view of cell models, this particular behavior of C_ℓ^* and n^* at $X_A \to 1$ is understandable. As mentioned earlier, even in the case of crystals in contact with the melt, X_A is smaller than unity ($\simeq \rho_f/\rho_s$). Therefore, the fact that $X_A = 1$ implies that differences between the solid and the fluid phase disappear, and the two phases become one phase. It follows that the interface vanishes, resulting in $C_\ell^* = n^* = 0$. Profiles of the density $[X_A(z) - X_A]$ plotted versus distance z away from the solid surface for systems with various bulk concentrations are given in Fig.4. This figure in fact shows the dependence of the interfacial profiles of the density on n^*.

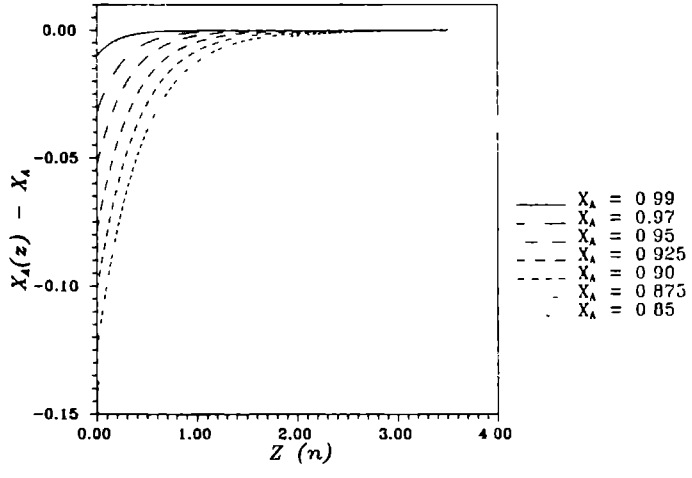

FIG 4 Profiles of the density $[X_A(z) - X_A]$ plotted versus distance z away from the solid surface for systems with different bulk concentrations

In contrast to the concentration, the influence of the energy parameters, χ_{AS}, χ_{BS} and χ_{AB}, on the interfacial structure are quite complex It can be seen from Fig 5 that in case that X_A and χ_{AB} remain constant, varying χ_{AS} or χ_{BS} independently will cause non–linear changes in C_ℓ^* (see Fig 5a). n^*, however, remains almost constant (see Fig.5b). It is shown in Fig.5a that with increasing χ_{BS}, C_ℓ^* is monotonically decreasing. On the other hand, an increase in χ_{AS} will cause an increase in C_ℓ^*. We notice that for most cases discussed in Fig. 5, the less than equivalent wetting occurs ($C_\ell^* \geq 1$). An increase in χ_{BS} corresponds to a weaker adsorption (or a stronger repulsion) between the solid surface and solvent units. Subsequently, the density of solute in the first fluid layer will become higher According to

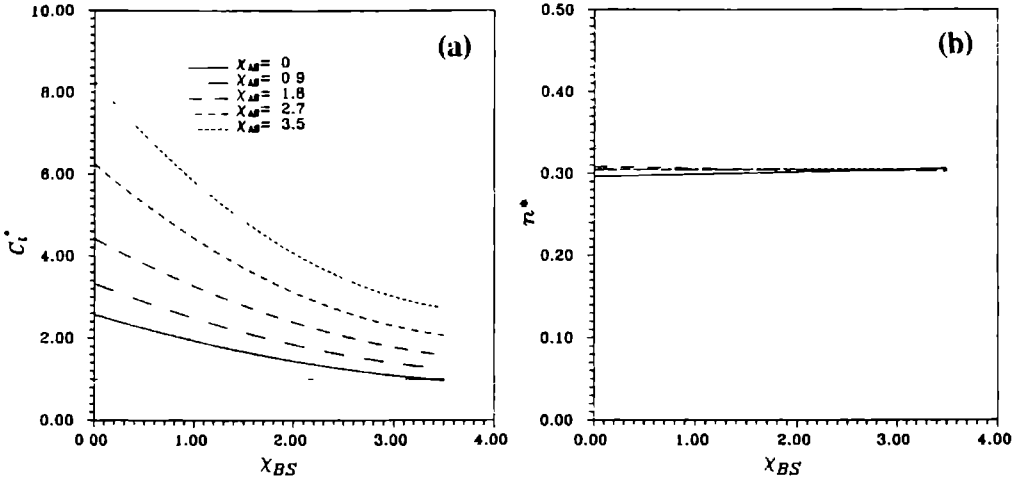

FIG.5 Dependence of the two interfacial factors n^* and C_1^* on χ_{AS} and χ_{DS} for systems with constant X_A and χ_{AD} ($X_A = 0.98$, $\chi_{AD} = 3.5$). (a) C_1^* plotted as a function of χ_{DS} (or χ_{AS}). In contrast, C_1^* will increase if χ_{AS} increases (b) n^* plotted as a function of χ_{DS} (or χ_{AS}) n^* is almost constant for different χ_{AS} and χ_{DS}

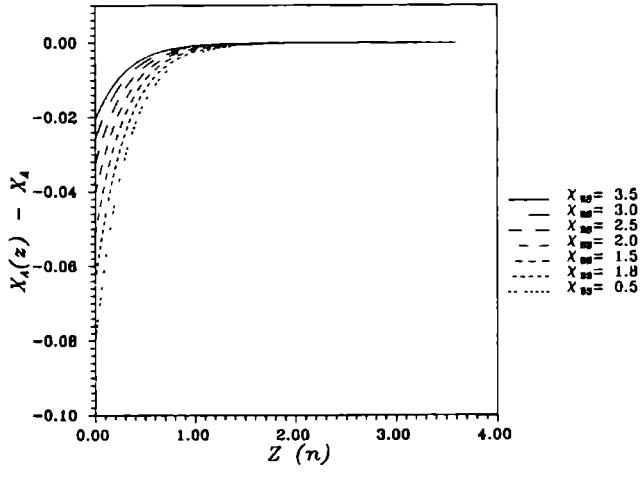

FIG.6. Profiles of the density $[X_A(z) - X_A]$ plotted versus distance z away from the surface for systems with different χ_{BS} $X_A = 0.98$, $\chi_{AB} = 3.5$, $\chi_{BS} = 2.7$.

Eq.(5), this corresponds to the increase of C_ℓ^*. Alternatively, an increase in χ_{AS} corresponds to a weaker adsorption between the solid surface and solute units In the competition with solvent units, $X_A(0)$ decreases accordingly This is followed by an increase in C_ℓ^* In Fig 6, profiles of the density $[X_A(z) - X_A]$ are plotted versus distance z away from the surface for systems with different χ_{BS}. Differently from Fig.4, Fig 6 (combined with Fig 5a) shows the influence on the solid–fluid interfacial structure of monomer systems due to the change of C_ℓ^*

Keeping X_A constant, simultaneously changing χ_{AS}, χ_{BS} and χ_{AB} will cause changes in both C_ℓ^* and n^* (see Fig.7). For simplicity, assume that $\chi_{AS} \cdot \chi_{BS}$ $\chi_{AB} = a \cdot b$ c (a, b, c are independent constants, respectively) Then C_ℓ^* and n^* can be described as a function of χ_{AB} Obviously, n^* depends linearly on χ_{AB} (Fig.7a), while C_ℓ^* turns out to be a non–linear function of χ_{AB} (Fig.7b) It is interesting to see that in case the $\chi_{AB} \to \chi_{AB}'$ (curve 1), C_ℓ^* approaches infinity. Referring to Eq (7), this implies a phase separation It follows that the solid surface and the solution can probably be separated by pure B layers In the case of crystals grown

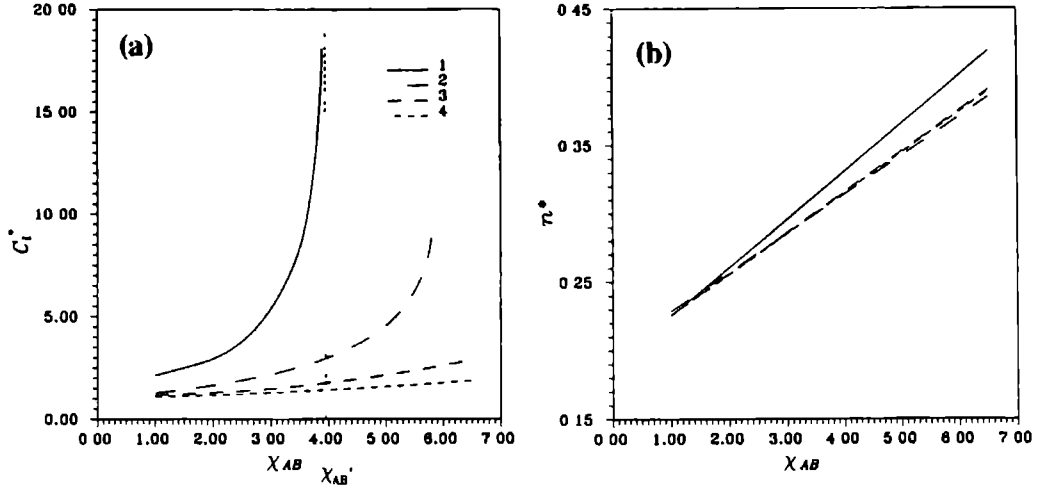

FIG 7 The influences on C_ℓ^* and n^* due to simultaneously changing χ_{AB}, χ_{AS} and χ_{BS} Assume that χ_{AS} χ_{BS} $\chi_{AB} = a$ b c If follows that C_ℓ^* and n^* can be expressed as functions of χ_{AB} (a) C_ℓ^* plotted versus χ_{AB}, C_ℓ^* depends nonlinearly on χ_{AB} (b) n^* plotted versus χ_{AB}, n^* is a linear function of χ_{AB} Curve 1· $a = c = 1$, $b = 0$, Curve 2. $a = b = 0$, $c \neq 0$, Curve 3. $a = 0.076$, $b = 0\ 52$ and $c = 1$, Curve 4. $a = 0\ 057$, $b = 0\ 70$ and $c = 1$

from the melt, gas (or vacuum) is considered as the B component (this corresponds to a larger χ_{AB}). This then implies that bubbles can be easily formed on the solid surface This has

indeed been observed in many crystal–melt systems[16-17]

Note that in Fig 7, the simple case with $\chi_{AS} = \chi_{BS} = 0$, $\chi_{AB} \neq 0$, is shown by curve 2 This case is comparable to the hard–sphere/hard–wall system [1,18] However, in the system χ_{AB} is a variable which determines the character (or properties) of the systems In case that surface reconstruction or similar surface phenomena occur, the surface becomes additionally flat, and the interactions between solid and fluid units become relatively weak This can then be seen as an approximation (We will discuss this in detail later in Sec IV)

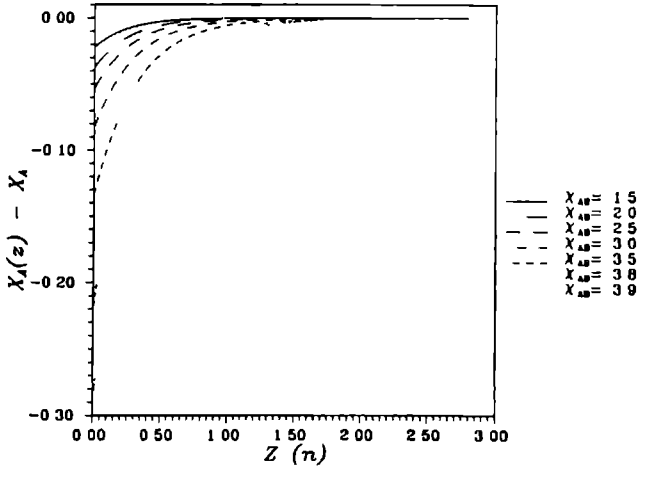

FIG 8 Profiles of the density $[X_A(z) - X_A]$ plotted versus distance z for systems with different χ_{AB} $X_A = 0\ 98$, $\chi_{AS} = \chi_{AB}$, $\chi_{BS} = 0$

In comparison with Fig 4 and Fig 6, the influence on the interfacial profiles of the density $[X_A(z) - X_A]$ due to simultaneously changing C_l^* and n^* (via a change in χ_{AB}) are shown in Fig 8 Because in this case, the two factors C_l^* and n^* change simultaneously, changes in the interfacial structure are more pronounced than in the former two cases

In spite of these effects mentioned above, the lattice structure also influences C_l^* and n^* The reason is that different lattice structures have different λ_1 or λ_0 For different structures, C_l^* and n^* are listed in Table I together with λ_1 It can be seen from Table I that a larger λ_1 corresponds to a large C_l^* The interpretation can be given as follows According to the definition of λ_1, the surface excess energy or the adsorption energy of a surface is proportional to λ_1 This implies that the enhancement of λ_1 will lead to an increase in the number of adsorbed solvent units (or B units) in the first fluid layer (We note that in this case the less

TABLE I. Influence of different crystal structures on the surface scaling factor C_ℓ^* and the characteristic thickness n^*

Cryst. Structure	{*hkl*}	$\lambda_{1(hkl)}$	C_ℓ^*	n^*
FC Cubic	{100}	0 333	1.88	0 303
Hexagonal	{001}	0.250	1.63	0 302
BC Cubic	{110}	0 250	1 63	0 302
SC	{100}	0 125	1 40	0 303

Note. For this system, $X_A = 0\ 98$, $\chi_{AS} = 0\ 267$, $\chi_{BS} = 1\ 83$ and $\chi_{AD} = 3\ 50$

that equivalent wetting occurs) As a result, solute units will decrease in this region [see Eq.(13)], resulting in an increase of C_ℓ^* λ_1 (or λ_0) is also different for different orientations of the crystal structure Therefore, analogous results can be expected.

B. Estimation of the surface free energy of metals

The concept of surface free energy is relevant for crystal growth Some important issues in this field are related to its value However, for most solid–fluid systems, this value is not always available either from experiment or from theory Therefore, it is important if the surface free energy can be estimated

Conventionally, it is suggested that the surface free energy σ is proportional to the enthalpy of dissolution for a crystal–solution system [19-21], as

$$\sigma s = \xi \Delta h_{diss} \tag{14}$$

where s is the area per surface and ξ a proportionality constant In case that crystals are in contact with the melt, Δh_{diss} should be replaced by the molar enthalpy of melting Δh_m

According to our inhomogeneous cell model [14], the coefficient ξ is expressed for crystals in contact with the melt, as

$$\xi \simeq \lambda_1 C_\ell^* + n^* \frac{\rho_f}{\rho_s} D\{-kT_m/\Delta h_m \ln[(\frac{\rho_f}{\rho_s})/(1-\frac{\rho_f}{\rho_s})] + (\frac{D}{2})/\ln(\frac{\rho_f}{\rho_s}) - [(\frac{\rho_f}{\rho_s})\frac{D}{2} + (\frac{\rho_f}{\rho_s}) - 1]/[(1-\frac{\rho_f}{\rho_s})\ln(1-\frac{\rho_f}{\rho_s})] + 2\} \tag{15}$$

where T_m is the melting temperature. Note that ρ_f, ρ_s and $\Delta h_m/kT_m$ are bulk properties, and are assumed to be available. If the interfacial factors C_ℓ^* and n^* can be calculated and measured, ξ can be estimated from (15). Then σ may be directly obtained from (14). In this sense, ξ is a key factor to obtain σ.

For metal–melt systems, surface relaxation or surface reconstruction occurs quite often. Therefore, accurately estimating the influence of the solid phase on the interfacial fluid structure is difficult. This leads to some difficulties in accurately calculating C_ℓ^* and n^* by the SCF method. (Note that in SCF calculations, the solid phase is to a large extent excluded from direct consideration. Therefore, it is implicitly assumed in the calculations that properties of solid units at the surface should not differ too much from those of solid units in the bulk). However, we can still use simplified models to estimate the values of C_ℓ^* and n^* for metal systems. For this purpose, it is assumed that in a simplified system, $\chi_{AS} = \chi_{BS} = 0$ and $\chi_{AB} \neq 0$. This is the case described by curve 2 in Fig.7. This corresponds to the system where the fluid is in contact with a very flat and neutral solid surface. In fact, it is a reasonable approximation when the solid surface is very flat due to surface reconstruction or surface relaxation.

For this kind of simplified systems, χ_{AB} must be known. As mentioned earlier, in a melt system, fluid units are considered as component A, and vacuum units as component B. Then χ_{AB} is directly related to the evaporation enthalpy Δh_{ev}, as

TABLE II. The proportionality constant ξ and some other relevant parameters for three different metal systems.

Metals[a]	$\frac{\Delta h_{ev}}{kT_m}$ [b]	$kT_m/\Delta h_m$ [c]	C_ℓ^*	n^*	ξ(est.)	ξ(exp.)
Pd	40.0	0.974	3.00	0.314	0.762	0.800[d]
Ag	24.2	0.907	1.87	0.270	0.473	0.457[e]
Cu	27.7	0.868	2.06	0.281	0.520	0.436[e]

[a] Those metals have the fcc structure [19]. Then $\lambda_1 = 0.25$. $\rho_f/\rho_s \simeq 0.98$ [31].

[b] Reference 32. [c] Reference 19.

[d] The experimental value of ξ(exp.) for Pd was determined by Stowell [22].

[e] The experimental values of ξ(exp.) for Ag and Cu were determined by Turnbull [19].

$$\chi_{AD} \simeq \nu \Delta h_{ev}/kT_m \tag{16}$$

Here ν is a coefficient It is found empirically that $\nu \simeq 0\ 1$ It follows that C_l^* and n^* can be estimated from curve 2 in Fig 7a and b Consequently, the estimated values of the proportionality constant ξ(est) for three metals Pd, Ag and Cu are listed in Table II, together with other relevant parameters In order to make a comparison, the observed values of ξ(exp) determined from 3–dimensional homogeneous nucleation experiments by Stowell [22] and Turnbull [19], are also listed in this table

It can be seen from Table II that the estimated values of ξ are in good agreement with the observed values, especially for the value determined by Stowell In connection with Turnbull's results, there are reports and comments [22 27] indicating that for various reasons, Turnbull's values are a bit too low (This can also be seen from my estimates) In this sense, Turnbull's values represent the lowest bound of σ Considering this fact, my results are quite reasonable

IV DISCUSSION AND CONCLUSIONS

It can be seen from the calculated results given in the last section that if solid–fluid interactions at the surface are relatively weak, the so–called less than equivalent wetting case will occur This has been confirmed by some experimental facts

According to recent statistical mechanisms[28], a crystal surface undergoes a roughening phase transition at the roughening temperature T^r If the actual temperature T is lower than the roughening temperature T^r, the surface is flat on a molecular scale Otherwise, the surface will be rough The roughening temperature T^r for a given crystal face is directly related to interfacial bond energies ϕ_i, expressed in terms of the dimensionless roughening temperature θ^r, by

$$\theta^r = \frac{2kT^r}{\phi_{str}} \tag{17}$$

Here ϕ_{str} is the strongest bond energy at the surface Note that θ^r is a dimensionless quantity and has a certain value for a given surface Obviously, T^r is linearly proportional to ϕ_{str}

Previously, the roughening temperature sometimes has usually been estimated based on the equivalent wetting condition[11,12,28] This condition implies that in Eq (17) ϕ_{str} is equal to Φ_{str} However, for many inorganic and metal systems, it turns out that the roughening temperature is underestimated by the equivalent wetting assumption For instance,

Abbaschiam and Eslamloo [29] indicated that faceted faces occur on Sn crystals when they grow from the melt This is in conflict with the obtained estimate that the roughening temperature of the strongest faces on Sn crystals is much lower that the melting point The growth of garnets from a PbO flux [30] revealed that the bond energies at the (332) faces are almost four times higher than those estimated by the equivalent wetting assumption Obviously for those systems, $\phi_j > \Phi_j$, meaning that the less than equivalent wetting case occurs

The presence of the less than equivalent wetting in those systems is to some extent attributed to surface relaxation or surface reconstruction Because of those surface effects, the interactions between fluid units and the solid surface become weaker Alternatively, due to the restriction of the solid surface, fluid units will lose some amount of entropy at interfacial regions The loss of entropy cannot be fully compensated by those very weak solid–fluid interactions at the surface It then follows that the free energy per fluid unit at the interface will increase, causing a decrease of the density of fluid units at interfacial regions This finally results in the less than equivalent wetting

In summary, the dependence of the structure and some thermodynamic properties of monomer interfacial systems on various parameters was studied using SCF theory calculations As expected, the exponential law can be applied to this kind of systems As an application, the surface free energies of three metal systems were estimated, which turn out to be in good agreement with the experimental results

ACKNOWLEDGEMENTS

Helpful discussions with Dr F A M Leermakers and Prof Dr G J Fleer are acknowledged I would like to thank Dr H Meekes, Dr C S Strom and Professor Dr P Bennema for a critical reading of this manuscript I also thank Shell Nederland B V for supporting this project

APPENDIX

According to principles of statistical thermodynamics [12], the chemical potential of structural units is expressed for the fluid and the solid as

$$\mu_f = -kT\ln Q_f'(T) - kT\{\ln v_f + [-\epsilon_f + kT]/kT\} \quad \text{(A1)}$$

and

$$\mu_s = -kT\ln Q_s'(T) - kT[\ln v_s - \epsilon_s/kT], \quad \text{(A2)}$$

$$Q'(T) = [(2\pi m^* kT)^{3/2}/h^3]Q(T) \quad \text{(A3)}$$

where $Q(T)$ denotes the partition function of a molecule for all the internal degrees of freedom, v is the free volume of a molecule, ϵ is the minimal potential energy per structural unit, m^* is the mass of a structural unit, h is Planck's constant, and subscripts f and s represent the fluid and the solid phase. At equilibrium, $\mu_f = \mu_s$. It follows that

$$\ln(v_s/v_f) = -\Delta h_m/kT + \Delta S'/k \tag{A4}$$

where the melting enthalpy (per structural unit) $\Delta h_m = \epsilon_f - \epsilon_s$, and $\Delta S' = k[\ln(Q_f'/Q_s') + 1]$. Since $\ln(v_s/v_f) \simeq \ln(\rho_f/\rho_s)$, (A4) can be rewritten as

$$\ln(\rho_f/\rho_s) \simeq -\Delta h_m/kT + \Delta S'/k, \tag{A5}$$

where ρ_f and ρ_s denote the density of the fluid and of the solid phase, respectively If we define $X_A \simeq \rho_f/\rho_s$, then Eq. (A5) assumes an expression similar to the Van't Hoff equation. Referring to Eq.(5), X_A can therefore be replaced by ρ_f/ρ_s and $X_A(0)$ by $\rho_f(0)/\rho_s(-1)$. It then follows that Eq.(5) can be rewritten as Eq.(5a).

REFERENCE

1 R.D. Groot, N.M. Faber and J P. van der Eerden, Mol. Phys. **60**, (1987).

2 J.Q. Broughton and G.H. Gilmer, J. Chem. Phys. **79**, 5095, 5105, 5119 (1983); **84**, 5741, 5749, 5759 (1986).

3 J.Q. Broughton and F.F. Abraham, Chem. Phys. Lett. **56**, 734 (1986).

4 T.A. Cherepanova and A.V. Stekolnikov, J. Cryst. Growth **99**, 88 (1990).

5 A.D.J. Haymet and D.W. Oxtoby, J.Chem Phys. **74**, 2559 (1981)

6 M. Baus and J.L. Colot, Mol. Phys. **55**, 653 (1985).

7 W.A. Curtin and N.W. Ashcroft, Phys. Rev. A**32**, 2909 (1985).

8 J.M.H.M. Scheutjens and G.J. Fleer, J. Phys. Chem. **83**, 1619 (1979); **84**, 178 (1979).

9 J.M.H.M. Scheutjens and G.J. Fleer, Macromolecules **18**, 1882 (1985).

10 F.A.M. Leermakers and J.M.H.M. Scheutjens, J. Chem. Phys. **89**, 3264, 6912 (1988); J. Phys. Chem. **93**, 7417 (1989).

11 X.Y. Liu and P. Bennema, J. Chem. Phys. **97**, 3600 (1992).

12 X.Y. Liu and P. Bennema, J. Chem. Phys. **98**, 5863 (1993).

13 X.Y. Liu, Surf. Sci. **290**, 403 (1993).

14 X.Y. Liu, J. Chem. Phys. **98**, 8154 (1993).

15 X.Y. Liu and P. Bennema, Phys. Rev. E, (1993) (in press).

16 L M Williams, H Z Cummins, L O Ladeira and O N Mesquita, Phys Rev A45, 3880 (1992)

17 J P Vesenka and Y Yeh, J Cryst Growth **108**, 19 (1991)

18 R D Groot, Mol Phys **60**, 45 (1987)

19 J Turnbull, J Appl Phys **21**, 1022 (1950)

20 M Kahlweit, Z Phys Chem (NK) **28**, 245 (1960)

21 B Lewis and J C Anderson, *Nucleation and Growth of Thin Films* (Academic, New York, 1979), Chap 2

22 M J Stowell, Phil Mag **22**, 1 (1970)

23 D W Gomersall, S Y Shiraishi and R G Ward, J Aust Inst Metals **10**, 220 (1965)

24 G L F Powell, J Aust Inst Metals **10**, 223 (1965)

25 W A Miller and G A Chadwick, Acta Metall **15**, 607 (1967)

26 G A Colligan, W T Loomis and V A Surprenant, J Aust Inst Metals **10**, 89 (1965)

27 D P Woodruff, *The Solid - Liquid Interface* (Cambridge University Press, London, 1973)

28 P Bennema and J P van der Eerden, in *Morphology of Crystals*, Part A, edited by I Sunagawa (Terra Scientific, Tokyo, 1987), p1

29 G J Abbaschian and M Eslamloo, J Cryst Growth **28**, 372 (1975)

30 W Tolksdorf and I Bartels, J Cryst Growth **54**, 417 (1981)

31 *CRC Handbook of Chemistry and Physics*, edited by R C Weast (Chemical Rubber, Boca Raton, 1980)

32 T Sawada, J Cryst Growth **13/14**, 148 (1972)

Chapter 4.6

Self–consistent field calculation of structures and static properties of the solid–fluid interface: paraffin–like molecule systems

Xiang–Yang Liu and P Bennema

RIM, Laboratory of Solid State Chemistry, Faculty of Science, University of Nijmegen, Toernooiveld, 6525 ED Nijmegen, The Netherlands

ABSTRACT–The interfacial structure and interfacial properties of solid–fluid systems were investigated within the framework of an inhomogeneous cell model, using self–consistent field (SCF) calculations For interfacial systems consisting of completely flexible chain molecules, profiles of the segment density of fluid molecules always vanish exponential versus distance z from the solid surface It can be shown that the structure of the solid–fluid interface can be characterized by two key factors the surface scaling factor C_1^* and the characteristic thickness of the interface n^* In contrast, the exponential law cannot be applied to interfacial systems consisting of molecules with somewhat rigid chains For those systems, the ordering and the layering of chain molecules occur at the solid–fluid interface, due to the energy and the entropy effect In addition to the factor C_1^*, the structure of the solid–fluid interface of the system may qualitatively be related to half of the chain length of solute molecules and of solvent molecules Finally, the calculated values of C_1^* are compared with the experimental ones for a variety of n–paraffin systems The results are very satisfactory

---

Phys Rev E, (1993) *(in press)*

I. INTRODUCTION

In this study, the description of the solid–fluid interface is within the framework of our inhomogeneous cell model developed recently[1-4]. The results which are obtained from calculations of self–consistent field (SCF) theories can be seen as applications and extensions of our model. The subject of the solid–fluid interface has important implications for different fields, such as polymer and colloid science, catalysis, crystal growth etc.. However, in this paper we only concentrate on those issues which may be related to the growth of crystals. In these cases, crystal surfaces are in contact with a solution or the melt. Following from recent investigations, more attention is paid to problems of the morphology and growth of n–paraffin crystals in solutions (or the melt)[5-8]. First, the study of the morphology of normal paraffin crystals has practical implications. Many of the products derived from crude petroleum contain n–paraffins and these waxes can cause severe problems if they are allowed to crystallize. Crude oil, heavy fuel, diesel fuel, heating oil etc. all contain significant proportions of higher n–paraffins. If the temperature drops abruptly during the winter, these paraffins crystallize as thin, flat plates. Those platy paraffin crystals can gel the fuel or block pipes and filters, which are present in every system. To solve this problem, additives are developed, which change the habit of these crystals and significantly decrease their sizes so that they no longer suffer from the drawbacks mentioned above. Certainly, the additives must have a significant influence on the structure of the solid–fluid interface, and hence on the morphology of crystals. In this sense, to understand the influence of additives on the interfacial structure will be a key step for the molecular design of tailor–made additives. Secondly, it was found[7-8] that a first–order roughening transition occurs on surfaces of paraffin crystals when they are grown from n–hexane solutions. In case aromatic solvents are chosen, the order of surface roughening may be changed from the first order to the infinite order[9]. These novel phenomena are of theoretical and practical importance, and are also directly related to the structure and properties of the solid–fluid interface.

Paraffin systems are also considered as intermediate systems which bridge the gap between small molecule systems (i.e. monomer systems) and macromolecule systems (i.e. polymer systems). Therefore, a better understanding of crystal interfaces of paraffins is of particular practical and scientific interest for both small molecular and macromolecular crystals.

Early theoretical studies on the structure and static properties of the solid–fluid interface treated mostly simple fluids[10-16], while more recently increased attention has been focused on molecularly complex systems[17-19]. However, for complex molecule systems, such as polymers, molecules with flexible chain are the major subject. There are not many reports on paraffin

systems.

In this study, interfacial systems of paraffin–like molecules, especially crystals in contact with solutions or the melt, are treated. Within the framework of the inhomogeneous cell model, the structure of the interface is calculated by the SCF theory of Scheutjens and Fleer *et al.* [20-23]. This approach, similar to our formalisms of the solid–fluid interface[1-4], is based on the principles of cell models. So the results obtained can easily be interpreted by our interfacial model. This paper will be organized as follows. We will in Sec. II briefly introduce the interfacial model and the principles of the SCF calculations. The results of the interfacial structure and detailed interpretations will be given in Sec. III. This is to gain physical insight of the interface of paraffin systems. Finally, some conclusions are presented in Sec. IV.

II. THE INTERFACIAL MODEL AND THE SCF CALCULATION

A. The interfacial inhomogeneous cell model

In our previous papers[2-4], a so–called inhomogeneous cell model was developed to describe the solid–fluid interface. Within the framework of this model, the Cartesian coordinate system is defined in the following way: the x, y axes are in the plane of the solid surface, the z axis is normal to the surface and the origin is in the center of the first fluid layer. According to cell models[24], the whole space is divided into cells of the same shape and size. In addition to this, in our inhomogeneous cell model the same type of cells (or units) are characterized by the distance (z) from the solid surface. This implies that the same types of cells will be in different environments if the distance z is different. It follows that physical properties of cells also depend on the distance z. Since the equilibrium state is taken into account, most or all cells are in mutual equilibrium and their chemical potentials are constant. Suppose that each structural unit is connected by the bonds i = 1,2,..., m to neighboring units. Using the language of regular solution theories[3,24], the exchange bond energy ϕ_i (per mole) in the direction i is expressed for crystals in contact with a two–component solution, as

$$\phi_i(z) \simeq \tfrac{1}{2}[\phi_i^{AA}(z) - \phi_i^{SS}(-z)] + [1 - X_A(z)]^2\, \phi_i^{\sigma}(z) \tag{1}$$

and

$$\phi_i^{\sigma}(z) = \phi_i^{AB}(z) - \tfrac{1}{2}[\phi_i^{AA}(z) + \phi_i^{BB}(z)] \tag{1a}$$

where superscripts A, B and S denote solute, solvent and solid, and AA, BB, AB and SS denote solute–solute, solvent–solvent, solute–solvent and solid–solid interactions, respectively, $X_A(z)$ is the concentration of solute in layer z. The molar enthalpy of dissolution

in layer z is given by

$$\Delta h_d(z) = \sum_{i=1}^{m} \phi_i(z) \tag{2}$$

Note that $\phi_1(0)$ and $\Delta h_d(0)$ correspond to $\phi_1(z)$ and $\Delta h_d(z)$ in the first interfacial layer, and ϕ_1 and Δh_d to those in the bulk, i e $z \to \infty$.

In order to calculate the bond energies $\phi_i(z)$ from experimental data, the traditional proportionality assumption[6,25] is introduced This implies that for a structural unit in a layer at a distance z away from the solid surface, the following relation is supposed to hold

$$\phi_1(z) \ \phi_2(z) \cdots \phi_i(z) \cdots \phi_m(z) =$$
$$\phi_1^{ss} \ \phi_2^{ss} \cdots \phi_i^{ss} \cdots \phi_m^{ss} \tag{3}$$

(Here ϕ_i^{ss} represents the solid–solid bond energies of the bulk phase in the direction i) In other words, for the bond energies $\phi_i(z)$ occurring in any environment, the ratio of bond energies is the same as the ratio of the bond energies ϕ_i^{ss} ϕ_i^{ss} can in principle be calculated from a given crystal structure Then $\phi_i(z)$ may also be calculated if $\Delta h_d(z)$ is available (Normally, only Δh_d is available from solubility data)

As mentioned earlier, the exchange bond energy in the first interfacial fluid layer is important for physical processes occurring on the crystal surface In connection of $\phi_1(0)$ with ϕ_1, a so–called surface characteristic scaling factor C_ℓ^* was introduced[1-2]

$$C_\ell^* = \Delta h_d(0)/\Delta h_d \simeq \phi_1(0)/\phi_1 \tag{4}$$

This factor can be related to the concentration of solute for regular solutions as [2]

$$C_\ell^* \simeq \ln X_A(0)/\ln X_A \tag{4a}$$

(X_A is the concentration of solute in the bulk, $X_A(0)$ is that in the first fluid layer adjacent to the solid phase) Actually, the factor C_ℓ^* is used to characterize the solid–fluid interface [1-2] If $C_\ell^* = 1$ [$X_A(0) = X_A$], the so–called equivalent wetting occurs on the solid surface Otherwise, if $C_\ell^* < 1$ [$X_A(0) > X_A$], or $C_\ell^* > 1$ [$X_A(0) < X_A$], the so–called more than equivalent wetting case or the less than equivalent wetting case occurs, respectively The equivalent wetting corresponds to the case that the structure and properties of a phase are homogeneous from the

bulk up to the dividing plane between the solid and the fluid phase We consider this as a reference state, and it will occur only in some very particular cases The more than equivalent wetting (or the less than equivalent wetting) implies that the crystal surface shows a positive adsorption (or a negative adsorption) to solute units In normal cases, the non–equivalent wetting will occur in solid–fluid interfacial systems

Experimentally, the factor C_l^* can also be determined First, ϕ_1 may be calculated based on (2) and (3) $\phi_1(0)$ can be determined from experiments of roughening transitions of crystal surfaces[5-7] The roughening transition is a phase transition occurring at a crystal surface at the roughening temperature T^r If the temperature T is lower than T^r, at equilibrium the crystal surface is flat on a molecular scale If $T \geq T^r$, the crystal surface roughens on a molecular scale[5-7] According to the definition of the dimensionless roughening temperature,

$$\theta^r_{hkl} = 2kT^r/\phi_1(0) \tag{5}$$

the roughening temperature T^r is directly related to the interfacial bond energy $\phi_1(0)$ Here θ^r_{hkl} is the dimensionless roughening temperature of crystal faces $\{hkl\}$, and the value of which can be calculated by a computer program [6], k is the Boltzmann constant Therefore, $\phi_1(0)$ can be determined by measuring the roughening temperature of the crystal surface T^r Alternatively, assuming that the step free energy is approximately equal to the step energy, $\phi_1(0)$ can also be measured by fitting the data of growth rate R versus the supersaturation β, according to a 2D nucleation growth mechanism (a Birth and Spread mechanism[25]), by

$$R = A'\beta^{5/6}\exp(B'/\beta) \quad (A' \text{ kinetic constant}) \tag{6}$$

and

$$B' \simeq f[\phi_1(0)]^2 \tag{6a}$$

Here f is a factor depending on the shape of nuclei, the temperature and structural parameters of crystal surfaces, and can be calculated for a given crystal and surface structure As soon as B' is obtained from experiments, $\phi_1(0)$ can be calculated according to (6a) On the other hand, in case the concentration at the interface can be calculated or measured, C_l^* can also be obtained using (4a) In the following, it will be shown that C_l^* can be calculated according to (4a) for various systems, using SCF calculations

Concerning the structure of the solid–fluid interface, profiles of the concentration, in systems consisting of isotropic structural units, obey an exponential law[3] This implies that

$$X_A(z) = X_A\{1 + D\exp[-z/(n^*d)]\}, \tag{7}$$

$$D = X_A^{\zeta} - 1 \quad \text{and} \quad \zeta = C_\ell^* - 1. \tag{7a}$$

Here d is the interplanar thickness of the solid in the orientations $\{hkl\}$ n^* is the normalized characteristic thickness of the interface, which is defined in such a way that at $z = n^* d$, $[X_A(z) - X_A]/(X_A D) = \exp(-1)$. Note that in this approach[3], the mean–field approximation is applied. This means that fluctuations of the density within a layer are neglected. It follows that Eq.(7) represents an average profile of the density at the interface. It can be seen from (7) that interfacial profiles of the density will be fixed if X_A, C_ℓ^* and n^* are given. Obviously, since X_A is always available, C_ℓ^* and n^* are the most important ones in question.

B. The self–consistent field theory calculation

The SCF theory developed by Scheutjens, Fleer *et al.*[20] is also based on a cell model. Similar to the above–mentioned inhomogeneous model, the space is divided in lattice layers parallel to the solid surface. A molecule of type i has a volume fraction $\varphi_i(z)$ in layer z and φ_i in the bulk solution. Only inhomogeneities perpendicular to the surface are considered. Since the mean field approximation is applied in the calculation, fluctuations with the lattice layers are also neglected. A chain molecule consists of r segments, and fills r lattice sites. In the case of paraffin solutions, it is assumed that chain molecules are homogeneous (all segments of a molecule are of the same type), and molecules with longer chains are solute molecules (denoted by A) and molecules with shorter chains are solvent molecules (denoted by B).

For n–paraffin crystals in contact with paraffin solutions, the exchange energy per segment between n–paraffin A and n–paraffin B is supposed to be zero. The interaction between a segment i (i = A or B) and a surface site is expressed by the Flory–Huggin parameter χ_{si} (i = A or B). This parameter is expressed in units of kT and corresponds to the energy changed (per segment) due to bringing a segment i from the pure liquid state i into an environment of the pure solid state s. In the case of growth of paraffin crystals, substrates are the solid paraffins. Then, for n–paraffin crystals with the orthorhombic structure, $\chi_{si} \simeq -1.54 + 6.0/r$ and for the triclinic structure $\chi_{si} \simeq -1.63 + 4.69/r$ (the values of χ_{si} are obtained from the enthalpy of melting[26]). If it is not specified, χ_{si} is referenced to $T = 298.15$ K.

Due to the energy difference between the trans conformation and the gauche conformation of molecular chains, there are some torsional energies ϵ^{tor} in carbon chains of n–paraffin molecules. In the calculations, this can also be considered. For the formalisms and other calculation details, see Refs.20–23.

III. RESULTS AND DISCUSSION

A. Molecules with completely flexible chains

Polymer molecules are in many cases treated as flexible molecules However, under conditions of crystal growth, paraffin molecules are considered as somewhat rigid molecules In connection with polymer systems, we will first consider paraffin molecules to be flexible

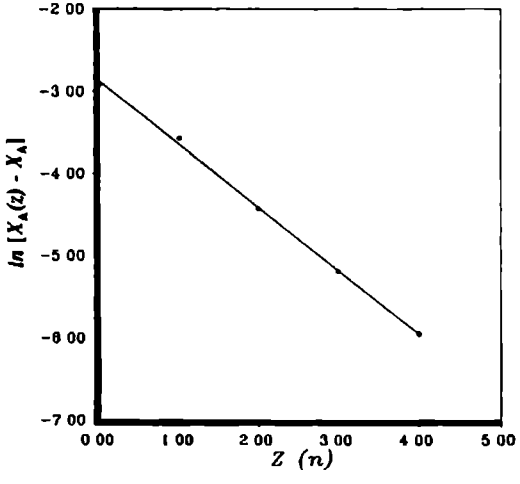

FIG 1 The linear relation between $\ln[X_A(z) - X_A]$ and the distance z for systems of C_{36}/C_6^1 solution X_A the mole fraction of solute, The lattice structure hexagonal, $\varphi_A = 0\ 1$

Solute and solvent molecules are denoted by C_r and C_r^1, respectively Since in this case chain molecules are fully flexible, they can be considered as isotropic structural units Therefore, profiles of the concentration will obey the exponential law In Fig 1, a linear relation between $\ln[X_A(z) - X_A]$ and z for systems of C_{36} in C_6^1 solutions is presented [Note that the calculated volume fractions $\varphi(z)$ are converted into molar fractions $X_A(z)$] It is known from last section that in this case the structure of the solid–fluid interface can be characterized by the two factors C_ℓ^* and n^* Hence, we will in the following discuss the influence of the chain length and the concentration of solute molecules on those two factors

In Fig.2, the dependence of C_ℓ^* and n^* on the chain length of solute molecules for C_6^1 solution systems are shown, respectively It can be seen from Fig 2a that $C_\ell^* < 1$ This means that the more than equivalent wetting case occurs in chain molecule systems It can also be seen that C_ℓ^* decreases further from unity with the segment number of solute molecules In contrast, n^* is increasing with the segment number This suggests that with increasing

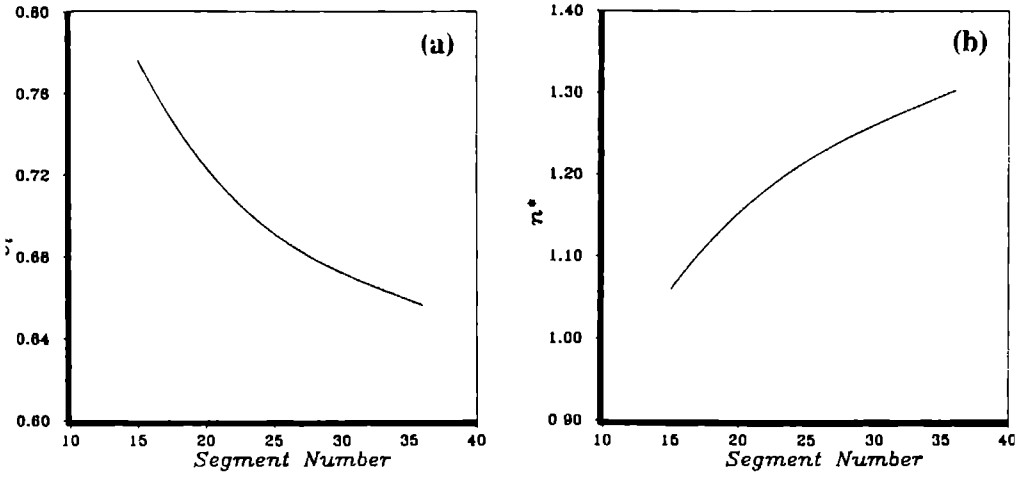

FIG 2. The influence of the chain length of solute molecules on the interfacial structure (a) The relation between the factor C_l^1 and the chain length (b) The relation between the characteristic thickness of interfaces and the chain length. Solvent. C_6^1, $\varphi_A = 0.1$, The lattice structure: hexagonal

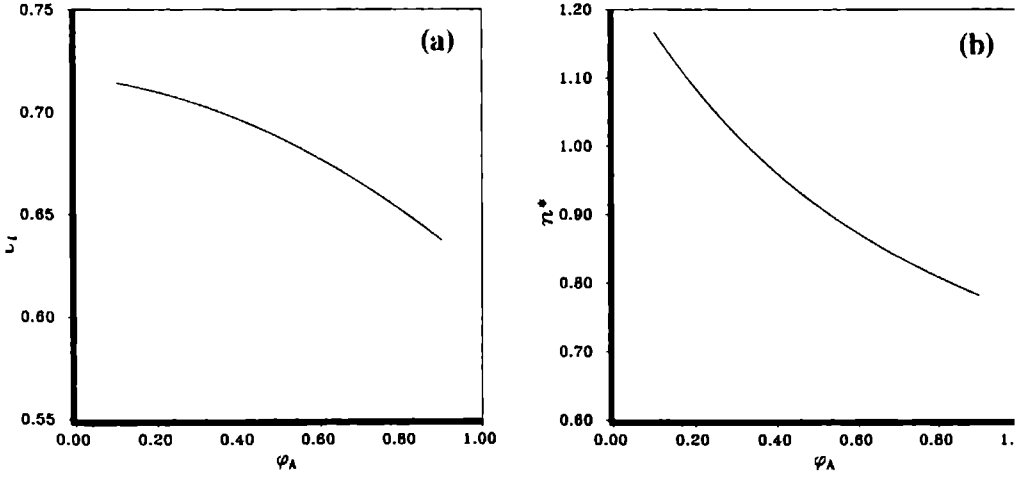

FIG.3. The influence of the bulk concentration of solute on the interfacial structure (a) The dependence of C_l^1 on the concentration (b) The dependence of n^* on the concentration System . $C_{21} + C_6^1$, The lattice structure: hexagonal

segment number, solute molecules are more strongly adsorbed on the solid surface, and that the solid–fluid interface will become somewhat thicker

For a system with given solute and given solvent, the structure of the solid–fluid interface can also be influenced by the bulk concentration of the solution An example of this influence is displayed in Fig 3 As shown in Figs 3a,b, both C_ℓ^* and n^* decrease with the concentration of solute These parallel changes of C_ℓ^* and n^* are different from those shown in Figs 2a,b The results of Fig 3 mean that when the concentration increases, solute molecules show stronger tendencies to be adsorbed at the solid surface However, the solid–fluid interface become thinner We notice that for monomer systems, only n^* is influenced by the concentration C_ℓ^* is independent of X_A (This result will be published elsewhere)

In addition to Fig 3, segmental profiles of the concentration of solute [expressed by the volume fraction $\varphi_A(z)$] are plotted versus the distance away from the solid surface for various concentrations, and presented in Fig 4

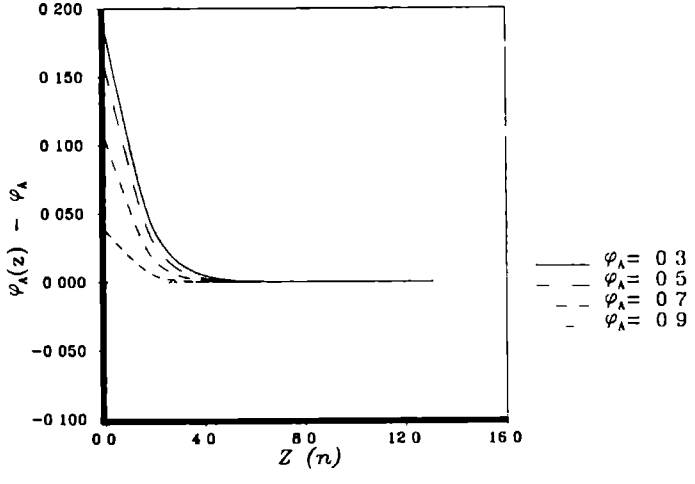

FIG 4 Exponential profiles of the relative segment density $[\varphi_A(z) - \varphi_A]$, plotted as a function of the distance z, for various bulk concentrations Relevant parameters the same as Fig 3

B Molecules with rigid chains

In the case of paraffin molecules, molecular chains are not completely flexible It follows that the torsional energy of C–C chains should be taken into consideration in the calculations

This will lead to some particular results. In the following, we will first concentrate on the problems of the ordering and the structuring of the interface due to the rigidity of molecular chains. Then discussions on the wetting condition and the influence on interfacial properties are given later

1. Ordering of molecules at the interface

The torsional energy ϵ^{tor} of C–C chains is due to the energy difference between the *trans*– and the *gauche*– conformation of molecules. This energy for normal paraffin molecules is about $2kT_0$ [27]. In comparison with Fig.4, the profile of the concentration of n–C_{21} $\varphi_A(z)$ in a n–C_6 solution ($\varphi_A = 0.1$, $\epsilon^{tor} = 2\ kT_0$) is plotted versus distance z from the first fluid layer ($z = 0$). (See Fig.5). It can be seen from Fig 5 that for rigid chain molecules, since the anisotropy occurs in the molecular structure, the exponential law can not be applied to the system. Instead, $\varphi_A(z)$ shows an oscillatory decrease (c.f. Figs.6 and 7). This leads to the concentration depletion of the solute between the first fluid layer and the layer $z = \lambda_0$ where $\varphi_A(\lambda_0) \simeq \varphi_A$.

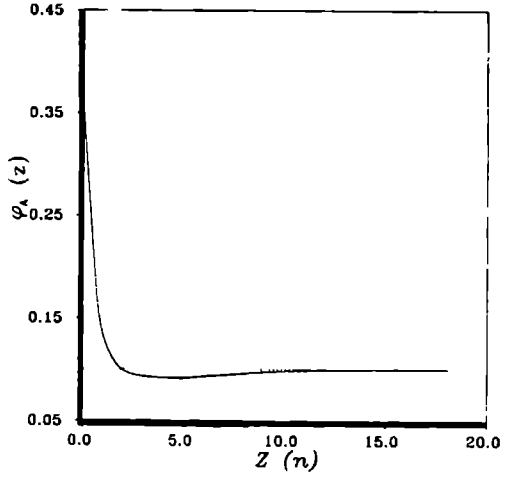

FIG.5. Segment density profile $\varphi_A(z)$ of n–C_{21} molecules in a n–C_6 solution plotted versus distance z from the solid surface, with the origin at the center of the first fluid layer adjacent to the solid substrate. The segment density in the bulk $\varphi_A = 0.1$, $\epsilon^{tor} = 2kT_0$, $T = T_0 = 298.15$ K. The lattice structure: fcc.

It is interesting to see from our calculations that for rigid chain molecular systems, the position of λ_0 (or λ_{max}) and the position of the first minimum of $\varphi_A(z)$ (at $z = \lambda_{min}$) are directly associated with the structure of solute molecules and of solvent molecules For completely rigid molecular solution systems, a maximum of $\varphi_A(z)$ occurs in the layer $z = \lambda_{max}$ after the first fluid layer, and λ_{max} corresponds to half of the change length of solute molecules λ_A whereas λ_{min} corresponds to half of the chain length of solvent molecules In the case of normal alkane molecules, molecular chain are not completely rigid ($\epsilon^{tor} \simeq 2\,kT_0$), then λ_{max} is replaced by λ_0 Due to the lagging of $\varphi_A(z)$, it turns out for the n–paraffin solution system that $\lambda_{min} \simeq \lambda'_B \simeq \lambda_B + 3$ and $\lambda_0 \simeq \lambda'_A \simeq \lambda_A + 3$ These results are explicitly shown in Fig 6 From this point of view, the structure of the solid–fluid interface explicitly depends on the structure of paraffin–like molecules

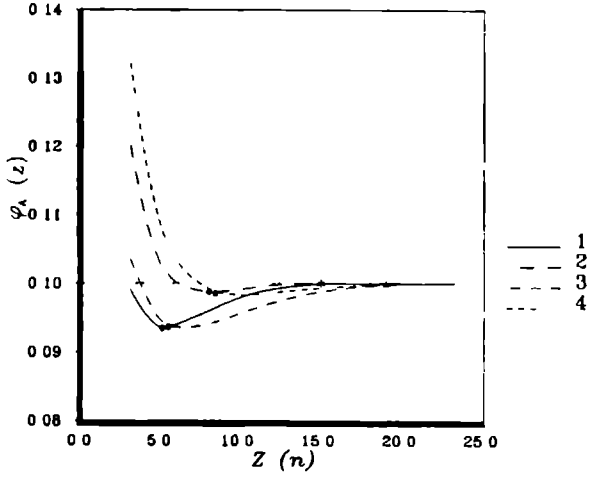

FIG 6 Segment density profiles in dependence of the structure of chain molecules The structure of substrates hexagonal, $\varphi_A = 0\,1$, $\epsilon^{tor} = 2kT_0$ Curve 1 n–C_{23} + n–C_6, Curve 2 n–C_{23} + n–C_{12}, Curve 3 n–C_{33} + n–C_6, Curve 3 n–C_{33} + n–C_{12} The positions of λ_{min} (•) and those of λ_0 (*) are associated with the chain length of solute molecules and of solvent molecules, respectively

For crystals in contact with the melt (assuming $\varphi_A \simeq \rho_f/\rho_s$, ρ_f and ρ_s are the density of the melt and the solid[2]), the oscillation also does occur in profiles of the segmental density However, the profiles are characterized by $z = \lambda_{max} \simeq \lambda_A$ since molecules of one kind exist in

the system. It follows that the profiles will be smoothed if the temperature increases (see Fig.7)

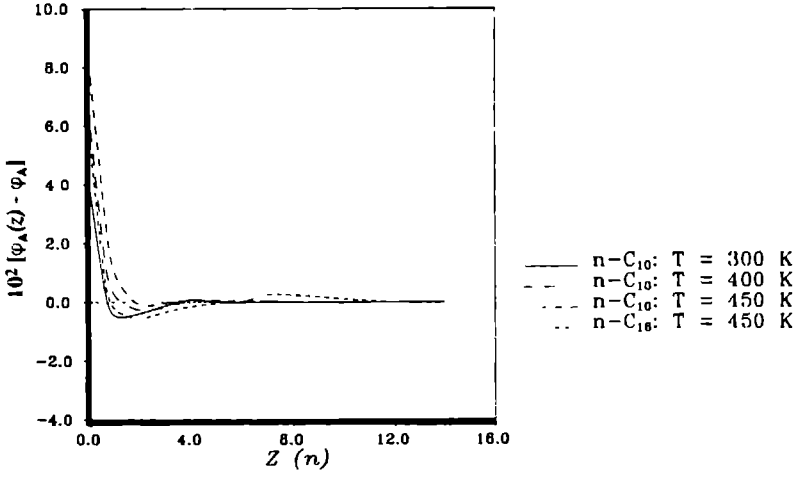

FIG.7. Profiles of the relative segment density $[(\varphi_A(z) - \varphi_A),\ \varphi_A \simeq \rho_f/\rho_s]$ for different paraffin melt (n–C_{10}, n–C_{16}) systems, and the dependence of the profiles for n–C_{10} system on the temperature: $\epsilon^{tor} \simeq 1$ kcal/mol. For n–C_{16} systems, $T = 450$ K, $\rho_f/\rho_s \simeq 0.80$. For n–$C_{10}$, $T =$ 300 K, 400 K, 450 K, then $\rho_f/\rho_s \simeq 0.900, 0.798, 0.738$ respectively. Note that the profiles are characterized by $z = \lambda_{max} \simeq \lambda_A$, and the ascillations are smoothed with increasing the temperature. The lattice structure fcc.

In order to characterize the ordering of chain molecules, a segment order parameter[23] is defined as

$$s = (3\langle\cos^2\alpha\rangle - 1)/2, \tag{8}$$

where α is the angle between the axis of an unit and a given direction. Here, the orientation of segments occurs with respect to the normal to the solid surface. For a certain species, the order parameter $s(z)$ is a function of z. In the case of a chain molecule, we use $\bar{s}(z)$, which is the ensemble average over all segments of the molecule, to characterize the ordering of this molecule. It is explicit that in case that all bonds of the molecule are completely parallel to the surface, the order parameter is -0.5. If all of the bonds are perpendicular to the surface, $s(z) = 1$. On the other hand, a random distribution of bonds will result in the order parameter $s(z) = 0$ [23]. It follows that at the solid surface, the order parameter should be very close to –

0 5 if molecules are highly ordered (parallel to the surface) In Fig 8, the values of $\bar{s}(z)$ are given as a function of z, for a C_{16}/C_6 solution system with different torsional energies of molecular chains ϵ^{tor} It can be seen first that in any case, both solute and solvent molecules are preferentially adsorbed parallel to the solid surface in the first fluid layer After the first fluid layer, the order parameter is increasing considerably, meaning that the degree of ordering is drastically reduced In spite of this, chains with various torsional energies show a different behavior Comparing with rigid chain molecules ($\epsilon^{tor} > 0$), molecules with completely flexible chains ($\epsilon^{tor} = 0$) are less ordered, and in this case there is almost no difference between long chain molecules and short chain molecules (see Fig 8a) As a result, loops occur in those adsorbed flexible molecular chains This can be seen from Fig 8a that a positive peak occurs in the second fluid layer With increasing torsional energy ϵ^{tor}, chain molecules are more preferentially adsorbed parallel to the solid surface Also, longer chain molecules are more ordered than short chain molecules These results can be seen from Figs 8b–d, which correspond to $\epsilon^{tor} = 1$, 2 and 3, respectively The negative $s(z)$ in the successive interfacial fluid layers after the first fluid layer, suggests that a low degree of ordering, which may be related to the oblique packing of molecules, still occurs in these regions It is noted that in case that $\epsilon^{tor} \geq 2kT_0$, the ordering parameter $\bar{s}(z)$ becomes almost zero at $z \simeq \lambda_i^1 \simeq \lambda_1 + 3$ (i = A or B), for both solute and solvent molecules This implies that the parallel ordering of molecules almost completely vanishes in the layer

The ordering of rigid chain molecules and the oscillation of the segmental density are attributed to the energy and the (negative) entropy effect For the arrangement of rigid molecules, in the solid–fluid interface two opposite trends compete with each other To achieve the maximum adsorption energy, chain molecules are strongly adsorbed and ordered on the solid surface On the other hand, to gain the maximum conformational entropy, molecules tend to be oriented randomly In the regions near the surface [$z < \lambda_i^1$ (or λ_1 for completely rigid chain molecules)], the number of orientations is restricted This will cause the loss of the conformational entropy for chain molecules Then chain molecules would rather avoid the solid surface Obviously, those two effects become more pronounced when molecules become longer In the first fluid layer, the adsorption is the dominant effect, and solute (or longer) molecules are adsorbed strongly on the solid surface for energic reasons In order to release the maximum adsorption energy per molecule, most fluid molecules are oriented in directions parallel to the surface In the successive liquid layers, the adsorption energy decreases considerably The entropy effect then becomes relatively important As a consequence, solute (or longer chain) molecules are repelled from these regions Instead, those layers are preferentially filled with solvent (or shorter chain) molecules At $z = \lambda_{min} \simeq \lambda_B^1$ (or

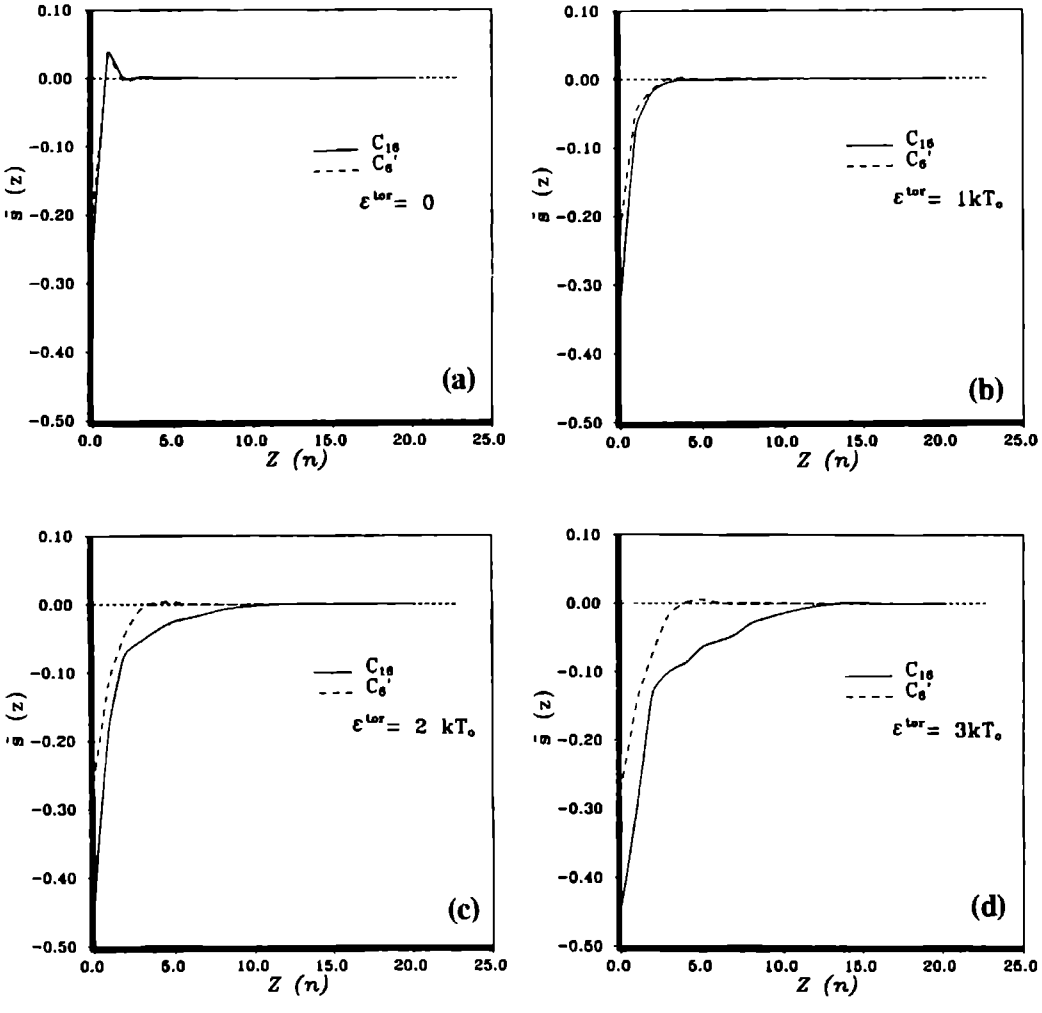

FIG.8. The average order parameter $\bar{s}(z)$ of molecules as a function of z for crystals in contact with a n–C_{16}/n–C_6 solution. $\varphi_{\perp} = 0.1$. Molecules in the first fluid layer ($z = 0$) are highly ordered in case that $\epsilon^{tor} > 0$. It follows that degree of the ordering drops drastically in the successive layers after the first fluid layers. (a)–(d) correspond to different ϵ^{tor}, respectively

λ_B) the entropy effect of solvent molecules vanishes, and all conformations all possible Then the space can be filled the best with solvent molecules This causes a substantial depletion of solute molecules. Similarly, the entropy effect of solute molecules vanishes at $z = \lambda_0$ (or λ_{max}) $\simeq \lambda_A'$ (or λ_A), resulting in an increase of $\varphi_A(z)$ Chain conformations in interfacial regions and the relation to the energy and the entropy effect for the completely rigid chain molecular system are illustrated in Fig 9

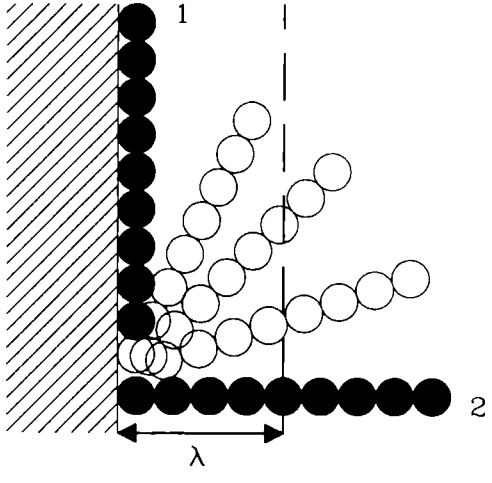

FIG 9. Schematic illustration of chain conformations and in relation to the energy and the entropy effect at the surface In the first fluid layer, the energy effect is dominant Between the first fluid layer and the layer $z = \lambda$, the entropy effect becomes important In the layer $z \geq \lambda$, the entropy effect almost vanishes For more explanations, see the text λ: half of the chain length of molecules

2 Influences of various factors on the interfacial structure and properties

As was shown in last section, the exponential law is not valid for the description of the interfacial structure of rigid chain molecule systems However, $C_{\tilde{\ell}}$ is still a key factor for understanding the solid–fluid interface, because the wetting condition and interfacial properties can in principle be described by this factor

It can be seen from in Fig.10 that the change of the surface scaling factor $C_{\tilde{\ell}}$ as a function of the segment number of chain molecules (or the carbon number of n–paraffin molecules) is shown, in the case that the solvent is given. (n–C_6 is chosen as the solvent in this case) In

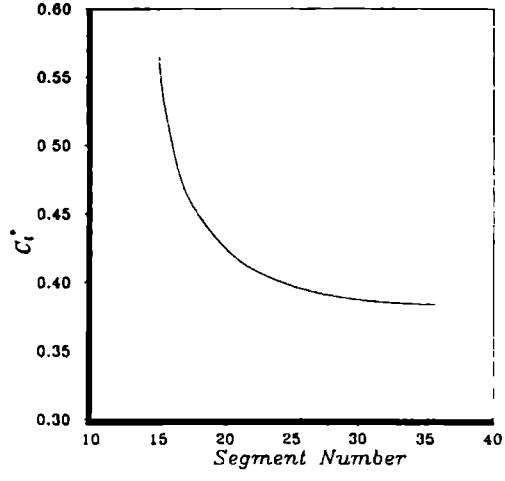

FIG 10 The relation between the surface characteristic scaling factor C_l^* and the carbon number of paraffin molecules This lattice structure: hexagonal For the given solvent (n–C_6), the dependence of C_l^* on the chain length of solute molecules

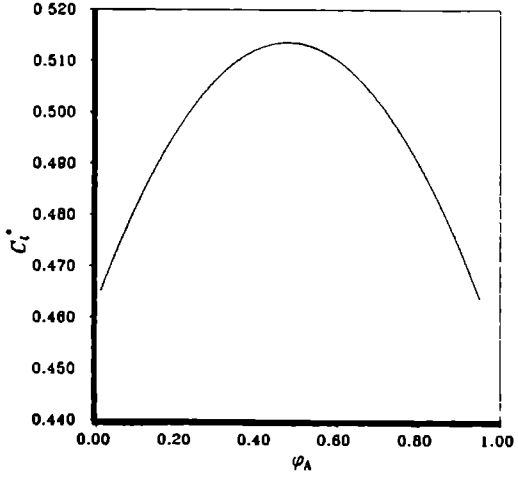

FIG.11. The dependence of the surface scaling factor C_l^* on the bulk concentration of solutions φ_A The lattice structure. hexagonal. The curve of C_l^* has a parabolic shape with the maximum at $\varphi_A \approx 0\,5$.

general, the value of C_ℓ^* decreases as the segment number increases When the segment number becomes relatively large, C_ℓ^* changes slowly This is because with increasing carbon number, the difference between neighboring homologous of paraffin become smaller

In spite of the segment number of molecules, the bulk concentration will also influence C_ℓ^* Fig.11 displays a relation between C_ℓ^* and the concentration of solute. As can be seen, the dependence of C_ℓ^* on the concentration is very weak Unlike flexible chain molecular systems presented in Fig 3, the calculated $C_\ell^*(\varphi_A)$ curve for somewhat rigid chain molecular systems can be fitted perfectly well with a parabolic curve with the maximum at $\varphi_A \simeq 0\ 5$.

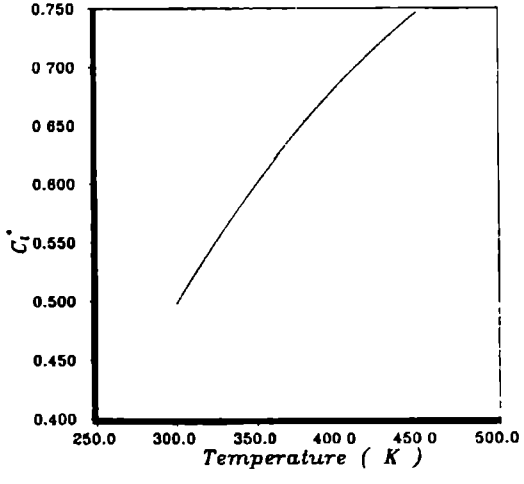

FIG 12 The dependence of the surface scaling factor C_ℓ^* on the temperature for the system of n–C_{25}/n–C_{12} solutions The lattice structure. fcc

The influence of the temperature on C_ℓ^* is similar to the energy For a given interfacial system, raising the temperature corresponds to increasing the influence of the entropy This will reduce the effect of adsorption energy Also, molecular chains become more flexible at a higher temperature because in this case the thermal energy may compensate the torsional energy. It follows that the adsorption of solute molecules on the solid surface becomes less pronounced. It can be seen from Fig.12 that with increasing temperature, C_ℓ^* increases correspondingly As expected, at higher temperatures profiles of the segment density of paraffins molecules have a character similar to that of flexible chain molecules

In addition to other effects, crystal structures also influence C_ℓ^* In order to make a comparison between different structures, we will first define an orientation factor of crystal

surfaces ξ_{hkl}

According to the Hartman–Perdok theory [6,25], we know that each flat crystal surface has a certain attachment energy E^{att}_{hkl}. This is the energy released per structural unit when a new crystal slice is attached to the crystal surface. In relation to the crystallization energy (per structural unit), the attachment energy is expressed as

$$E^{cr} = E^{att}_{hkl} + E^{slice}_{hkl} \tag{9}$$

where E^{slice}_{hkl} is the slice energy of crystal surfaces $\{hkl\}$ [6,25]. It can also be defined as the 2D crystallization energy of a crystal slice with a thickness d_{hkl} for orientations $\{hkl\}$. Within this framework, the orientation factor of crystal surfaces $\{hkl\}$ ξ_{hkl} is defined as

$$\xi_{hkl} = E^{att}_{hkl}/(2E^{cr}) \tag{10}$$

ξ_{hkl} is approximately proportional to the surface excess energy or the adsorption energy for a given system, and used to characterize the anisotropy of bond energies of crystal structures. For different crystal structures, ξ_{hkl} will be different. It follows that for a given set of energy parameters and the bulk concentration, C^*_ℓ will also be different. Table I shows that different structures affect C^*_ℓ in the case of n–C_{21} crystals in n–C_6 solutions ($\varphi_A = 0.1$). It is explicit that for those crystal structures, ξ_{hkl} plays a key role in determination of the value of C^*_ℓ. For a given crystal structure, different crystal surfaces may also have different ξ_{hkl}. Then a

TABLE I. Influence of different crystal structures on the surface scaling factor C^*_ℓ for the system of n–C_{21} crystal in n–C_6 solutions

Cryst. Structure	$\{hkl\}$	ξ_{hkl} †	C^*_ℓ
FC Cubic	{100}	0.333	0.416
Hexagonal	{001}	0.250	0.485
BC Cubic	{110}	0.250	0.485
Simple Cubic	{100}	0.125	0.573

Note. For this system, $\varphi_A = 0.1$, $\epsilon^{to} \simeq 2\,kT_o$, $\chi_{SA} = -1.269$ and $\chi_{SB} = -0.594$.
† The orientation factor ξ_{hkl} is referred to crystals consisting of monomer units.

similar influence can be expected It can be seen from Table I that a larger ξ_{hkl} (or a larger E^{a}_{hkl}) corresponds to a lower C^{*}_{ℓ} This can be interpreted as follows As mentioned above, the surface excess energy or the adsorption energy of a crystal surface is proportional to E^{a}_{hkl} or ξ_{hkl} Henceforth, the enhancement of ξ_{hkl} (or E^{a}_{hkl}) will lead to the increase of the number of preferentially adsorbed molecules in the first fluid layer adjacent to the solid phase Since for paraffin systems the more than equivalent wetting occurs ($C^{*}_{\ell} < 1$), solute molecules are the preferentially adsorbed molecules It therefore follows from Eq (4) that C^{*}_{ℓ} will decreases further from unity

C. Comparison with experimental data

We know from the foregoing discussions that C^{*}_{ℓ} can be evaluated from the calculated $\varphi_{A}(0)$ and the φ_{A} However, from an experimental point of view, C^{*}_{ℓ} can also be determined As was mentioned in Sec II A For the bulk phase the exchange energy in direction 1 for the bulk phase ϕ_{1} can be calculated from the dissolution enthalpy Δh_{diss}, based on Eqs (2) and (3) On the other hand, the corresponding value at the interface $\phi_{1}(0)$ can precisely be measured from surface roughening experiments according to Eq (5) or obtained from the kinetic data of crystals growth kinetics according to Eqs (6) and (6a) C^{*}_{ℓ} is then obtained from Eq (4) As a comparison, we list in Table II the calculated and experimental values of C^{*}_{ℓ} for various paraffin systems, together with other relevant data

TABLE II Calculated and experimental values of the surface scaling factor C^{*}_{ℓ} for various paraffin solution systems

Solutions	φ_{A}*	$\varphi_{A}(0)$	C^{*}_{ℓ}(cal)	C^{*}_{ℓ}(exp)
n–C_{21}/n–C_{6}	0 100	0 519	0 406	0 414‡
n–C_{25}/n–C_{6}	0 100	0 579	0 382	0 373‡
n–C_{16}/n–C_{6}	0 820	0 911	0 457	0 460‡
n–C_{36}/Pet eth†	0 100	~ 0 489	~ 0 440	0 457††

* φ_{A} is the bulk concentration in which C^{*}_{ℓ}(exp) was determined

† Pet eth (petroleum ether) is a mixture of different components In our calculations, an average is made for several n–paraffin solution systems

‡ C^{*}_{ℓ}(exp) determined according to Eqs (4) and (5)

†† C^{*}_{ℓ}(exp) calculated according to Eqs (4), (6) and (6a), based on the data quoted from Ref 29

It is interesting to see that although different experimental methods are used to measure C_ℓ^* for various systems, the calculated values of C_ℓ^* agree well in every case with the experimental ones It can also be seen from the above mentioned discussions that C_ℓ^* is directly associated with the whole interfacial structure Any change of C_ℓ^* corresponds to a certain change in the interfacial structure Therefore, as a key factor, C_ℓ^* plays an important role to characterize the interfacial structure From this point of view our results are quite convincing

Another important issue described earlier is the ordering of paraffin molecules in the first fluid layer This has also been justified by experiments It is known from recent scanning tunneling microscopic (STM) experiments[28] that once paraffin solutions are applied to a graphite substrate, highly ordered mono–molecular layers occur at the graphite surface This is consistent with our calculated results (see Fig 8c) We notice that investigations on the ordered structure of paraffins at the solid–fluid interface can offer physical insight to the molecule behavior at the interface This will help us to understand the influence of solvents and impurities on the morphology of crystals, which leads to the molecular design of tailor–made additives Without doubt, further investigations from theoretical and experimental points of views are needed We expect that more significant progress can be made in the near future

IV SUMMARY AND CONCLUSIONS

The structure and some thermodynamic properties of the solid–fluid interface were investigated using the SCF calculations For systems of completely flexible chain molecules, the exponential law is valid, and the structure of the interface can be characterized by two key factors C_ℓ^* and n^* For somewhat rigid chain molecule systems, the ordering and the layering of molecules at the interface become a crucial issue The oscillation of segmental density profiles has the one–to–one relation with the chain length of molecules In addition to C_ℓ^*, the interfacial structure of rigid molecule systems is determined in a qualitative way by λ_A' and λ_B' C_ℓ^* determines the wetting condition at the solid surface, while λ_A' and λ_B' may characterize the oscillation of profiles of the segmental density When the structure of molecules in interfacial systems are changed, the oscillation in densities and the values of C_ℓ^* will be altered accordingly Moreover, C_ℓ^* depends directly on bulk properties, such as the bulk concentration and χ_{si}, and also on the crystal structure or orientations of crystal surfaces

ACKNOWLEDGEMENTS

We are very much indebted to Dr F A M Leermakers, Prof Dr G J Fleer and Drs C Meijer for fruitful discussions and providing the SCF computer program for our calculations We would also like to thank Drs R Geertman for technical support and Dr H Meekes for a critical reading of the manuscript This research was supported by Shell Netherlands B V

REFERENCES

1 X Y Liu, and P Bennema, J Chem Phys **97**, 3600 (1992)
2 X Y Liu, and P Bennema, J Chem Phys **98**, 5863 (1993)
3 X Y Liu, Surf Sci **209**, 403 (1993)
4 X Y Liu, J Chem Phys **98**, 8154 (1993)
5 P Bennema, X Y Liu, K Lewtas, R D Tack, J J M Rijpkema, and K J Roberts, J Cryst Growth **121**, 679 (1992)
6 P Bennema, in *Handbook on Cryst Growth*, edited by D T J Hurle (North–Holland, Amsterdam, 1993) (in press)
7 X Y Liu, P Bennema, and J P van der Eerden, Nature **356**, 778 (1992)
8 X Y Liu, Phys Rev **B48**, (1993) (in press)
9 X Y Liu, P van Hoof, and P Bennema, Phys Rev Lett **71**, 109 (1993)
10 J Q Broughton, and F F Abraham, Chem Phys Lett **71**, 456 (1980)
11 J Q Broughton, and G H Gilmer, J Chem Phys **79**, 5095, 5105, 5119 (1983), **84**, 5741, 5749, 5759 (1986)
12 A Bonissent, in *Interfacial Aspects of Phase Transformation,* edited by B Mutaftschiev (Reidel, Dodrecht, 1982)
13 U Landman, C S Brown, and C L Cleveland, Phys Rev Lett **45**, 2032 (1980)
14 E T Chen, R N Barnett, and U Landman, Phys Rev B40, 924 (1989)
15 J D Weeks, J Chem Phys **67**, 3106 (1977)
16 O Guiselin, L T Lee, B Farnoux, and A Lapp, J Chem Phys **95**, 4632 (1991)
17 H K Christenson, W R Gruen, R G Horn, and J N Israelachvili, J Chem Phys **87**, 1834 (1987)
18 (a) T Pakula, J Chem Phys **95**, 4685 (1991),
(b) T Pakula, and E B Zhulina, J Chem Phys **95**, 4691 (1991)
19 T K Xia, Jia Ouyang, M W Ribarsky, and U Landman, Phys Rev lett **69**, 1967 (1992)
20 J M H M Scheutjens, and G J Fleer, J Phys Chem **83**, 1619 (1979), **84**, 178

(1979).

21 O.A. Evers, J.M.H.M. Scheutjens, and G.J. Fleer, Macromolecules **23**, 5221 91990); **24**, 5558 (1991).

22 J.M.H.M. Scheutjens, and G.J. Fleer, Macromolecules **18**, 1882 (1985).

23 F.A.M. Leermakers, and J.M.H.M. Scheutjens, J. Chem. Phys. **89**, 3264, 6912 (1988); J. Phys. Chem. **93**, 7417 (1989).

24 S.R. Fowler and E.A. Guggenheim, *Statistical Thermodynamics* (Cambridge University, London, 1960).

25 P. Bennema, and J.P. van der Eerden, in *Morphology of Crystals, Part A*, edited by I. Sunagawa (Terra Scientific, Tokyo, 1987), p.1.

26 M.G. Broadhurst, J. Res. Nat. Bur. Stand. A**66**, 241 (1962).

27 A.S. Wingrove, and R.L. Caret, *Organic Chemistry* (Harper & Row, New York, 1981).

28 M. Couto, X.Y. Liu, H. Meekes, and P Bennema, J. Appl. Phys. (submitted).

29 B. Simon, A. Grassi, and R. Boistelle, J. Cryst. Growth **26**, 77 (1974).

Chapter 4.7

Ordering of paraffin–like molecules at the solid–fluid interface

Xiang–Yang Liu[a], P Bennema[a], C Meijer[b] and M S Couto[a]

[a] *RIM, Laboratory of Solid State Chemistry, Faculty of Science, University of Nijmegen, Toernooiveld, 6525 ED Nijmegen, The Netherlands*

[b] *Department of Physical and Colloid Chemistry, Wageningen Agricultural University, Dreijenplein 6, 6703 HB Wageningen, the Netherlands*

ABSTRACT–Structures of the liquid molecules at the solid–fluid interface for paraffin–like molecule solution systems are studied via calculations of self–consistent field lattice models Periodic oscillations of the segmental density are directly associated with the length of molecular chains Molecules in the first and sometimes the second liquid layers lie preferentially parallel to the surface, due to interfacial effects Comparisons between the calculated data and the results obtained from surface roughening experiments are made for several n–paraffin systems

The structure and physical properties of solid–fluid interfaces are of both fundamental and technological interest in different areas This subject has been studied from experimental and theoretical points of view [1-8] Early theoretical studies of interfacial systems were mainly concentrated on solid substrates in contact with simple fluids [1-4] Recently attention is focused on solid–fluid systems of complex molecules [5-8]

In this study, we will use self–consistent field lattice model calculations [9-13] to investigate the ordering trends of fluid units at the solid–fluid interface In addition, the influence on some interfacial properties of chain–like molecule systems will be investigated In this paper, we will mainly focus on paraffin molecule systems The results obtained are compared with images of interfaces by scanning tunneling microscopy (STM) and with especially experimental data of the roughening phase transition

In the calculations of lattice models, paraffin molecules are described as chain–like molecules formed by segments of the same size, which are connected to each other (Each segment represents a CH_2 or a terminal CH_3 group) The system is homogeneous on a segmental scale, meaning that the Bragg–Williams (or mean field) approximation is applied in the calculations This implies that regularly spaced oscillations (or fluctuations) in the dimension of one segment[7] were neglected Instead, the average of oscillatory profiles are obtained in our calculations Moreover, the system consists of paraffin solutions in contact with paraffin solid substrates If not specified, the orientations of static substrates are set in the orientation of (001) of the hexagonal lattice [The reason is that the {110} surfaces of odd n–paraffin crystals have a pseudo–hexagonal structure, and the graphite substrates used later in our experiments have also this structure] Since in the system van der Waals interactions are dominant, only the nearest neighbor interactions need to be considered For solutions consisting of two different n–paraffins, those with a longer carbon chain are regarded as the solute (denoted by A), and those with a shorter carbon chain as the solvent (denoted by B) The exchange energy per segment between n–paraffin A and n–paraffin B is supposed to be zero (This is the so–called good solution approximation) The interaction energy between a segment of a molecule i (i = A or B) and a surface site is expressed by the Flory–Huggins parameter χ_{si} (i = A or B) This corresponds to the energy change (per segment) (in units of kT k is the Boltzmann constant, T is the temperature) due to bringing a segment of molecule i from the pure liquid state i into an environment of the pure solid state s In the case of crystal growth, the substrates are solid paraffins For orthorhombic n–paraffin crystals, $\chi_{si} \simeq -1\,54 + 6\,0/n$ [14] Here n is the carbon number of a paraffin molecule, and χ_{si} is referred to $T =$ 298 15 K

The calculations were carried out on the basis of formalisms first developed by Scheutjens, Fleer *et al* (the so–called SF theory [9-12]) This theory is based on an

nhomogeneous cell model, where the same type of units (or cells) are characterized by the listance (z) to the solid surface Within the framework of this theory, all cells in each layer should be filled with either solute units or solvents units It then follows that the interfacial structure and profiles of the density in the direction perpendicular to the solid surface can in principle be calculated on the basis of the SF theory For further details, see Refs 9–12,15

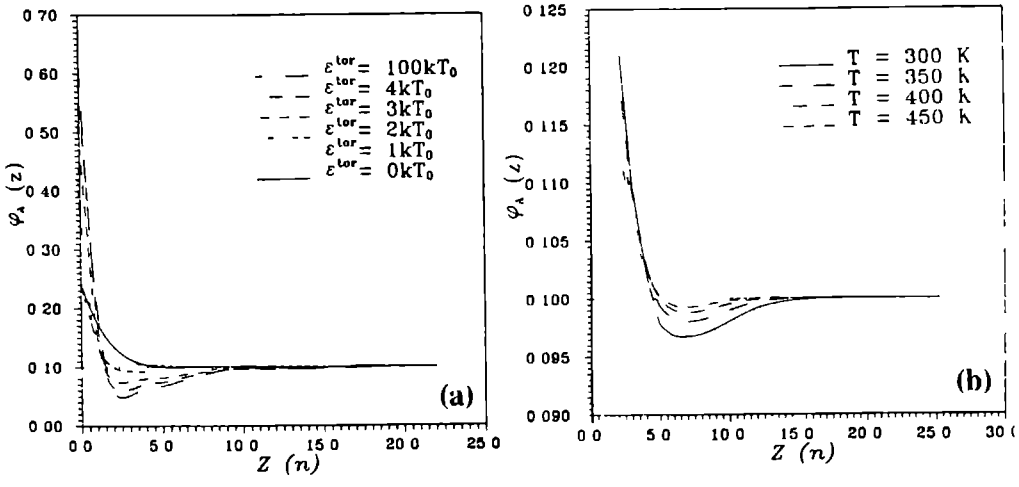

FIG 1 (a) Segment density profiles $\varphi_A(z)$ of n–C_{21} molecules in n–C_6 solutions for different torsional energies of molecular chains ϵ^{to}, plotted versus distance z from the solid surface, with the origin at the center of the first fluid layer adjacent to the solid substrate The segment density in the bulk $\varphi_A = 0\ 1$, $T = T_0 = 298\ 15$ K (b) Segment density profiles of n–C_{23} in n–C_{12} solutions for different temperatures $\epsilon^{tor} = 2kT_0$, $\varphi_A = 0\ 1$

Segmental density profiles [expressed by the volume fraction $\varphi_A(z)$] of n–C_{21} in n–C_6 solutions, for different torsional energies of molecular chains ϵ^{tor}, plotted versus distance z (z is normalized by the interplanar distance d_{hkl}) from the first fluid layer ($z = 0$) adjacent to the solid surface, are displayed in Fig 1a Two different profiles of the segmental density can easily be distinguished, according to two torsional energies $\epsilon^{tor} = 0$ and $\epsilon^{tor} = 100\ kT_0$ ($T_0 =$ 298 15 K) Those two energies correspond to two extreme cases molecules with completely flexible chains and molecules with completely rigid chains It can be seen that for completely flexible chains the segmental density profile of the solute shows an exponential decay with distance z away from the solid surface However, for molecules with completely rigid chains, an oscillatory decreasing behavior is shown The density of segments of solute molecules drops drastically after the first fluid layer It follows that a depletion of solute occurs between

roughly the second fluid layer and the first maximum of the profile (c.f. Fig.2) When the torsional energy ϵ^{tor} is reduced from $\epsilon^{tor} = 100kT_0$ to $\epsilon^{tor} = 0$, the oscillatory profile of the segmental density is gradually replaced by the exponential profile. In case $\epsilon^{tor} \lesssim 1kT_0$, the oscillation can hardly be identified from the profiles. In the case of normal alkanes, the torsional energy due to the energy difference between the *trans* conformation and the *gauche* conformation is about $2\,kT_0$ [18]. Therefore the oscillation profile could be recognized according to Fig.1a. On the other hand, for a system having all energy parameters fixed, the oscillatory profiles will change into exponential profiles if the temperature increases. (See Fig, 1b). Nevertheless, the profiles show a characteristic behavior. For a system consisting of completely rigid chain molecules, if the solute or the solvent is given, the position of the first minimum ($z = \lambda_{min}$) or the first maximum ($z = \lambda_{max}$) of curve $\varphi_A(z)$ remains almost constant. When the chain length of solute (or solvent) molecules is changed, λ_{max} (or λ_{min}) will be changed correspondingly This is explicitly shown in Fig 2.

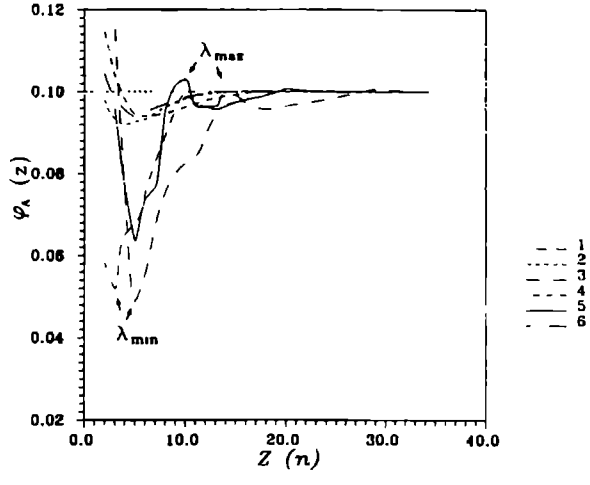

FIG 2. Segment density profiles in dependence of the structure of chain molecules The structure of substrates: hexagonal; $\varphi_A = 0.1$ Curves 1,2: n–C_{21} + n–C_6, Curves 3,4: n–C_{30} + n–C_{12}; Curves 5,6: n–C_{21} + n–C_{12}, Curves 1,3,5: $\epsilon^{tor} = 100\,kT_0$, Curves 2,4,6 $\epsilon^{tor} = 2kT_0$ For completely rigid chain molecule systems ($\epsilon^{tor} = 100\,kT_0$), the positions of the first minimum and the first maximum of the profiles correspond to half of the chain length of solvent molecules and of solute molecules, respectively.

In the case of normal alkane molecules, the molecular chains are not completely rigid ($\epsilon^{tor} \simeq 2kT_0$). Then the maximum and the minimum at curve $\varphi_A(z)$ are smoothed. However,

eminent change in the segment density can still be recognized at $z \simeq \lambda_{max}$ and $z \simeq \lambda_{min}$ although some lag occurs We can see from both Fig 1 and Fig 2 that λ_{min} corresponds to half of the chain length of solvent molecules, and λ_{max} to half of the chain length of solute molecules Thus implies that the profiles depend on the structure of the chain–like molecules at the solid–fluid interface

The reason for the oscillation of segmental density can be interpreted as follows In the solid–fluid interface, rigid molecules show two opposite trends which are competing with each other To achieve the maximum adsorption energy, chain molecules show a strong tendency to be adsorbed and ordered on the solid surface (We call this *the energy effect.*) On the other hand, to gain a maximum entropy, chain molecules tend to be oriented randomly In the regions near the surface ($z < \lambda_1$, λ_1 is half of the length of chain molecule 1, 1 = A or B), the number of orientations is restricted This will cause the loss of entropies of interfacial fluid molecules (such as the conformational, the rotational, the translational entropy etc)

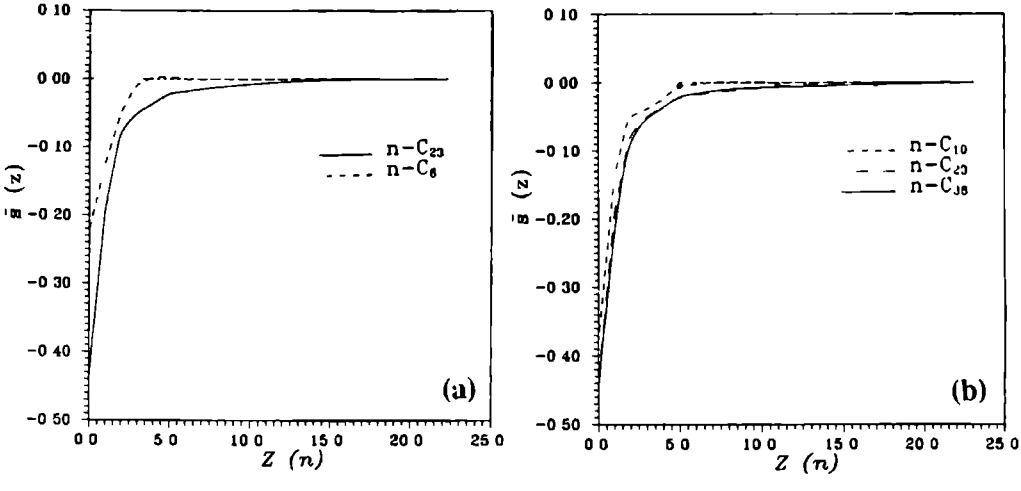

FIG 3 The average order parameter $\bar{s}(z)$ of molecules as a function of z for crystals in contact with paraffin solutions $\epsilon^{tor} = 2\ kT_0$, $\varphi_A = 0\ 1$ (a) The order parameter $\bar{s}(z)$ of solute and solvent molecules for a n–C_{23}/n–C_6 solution, (b) The order parameter $\bar{s}(z)$ of solute molecules for paraffins n–C_{10}, n–C_{23} and n–C_{36} in n–C_6 solutions Molecules in the first fluid layer ($z = 0$) are highly ordered The degree of the ordering drops drastically in the successive layers after the first fluid layers In case $z \simeq \lambda_1$ (1 = A or B), $\bar{s}(z) \simeq 0$, corresponding to the vanishing of the ordering

Henceforth, from the entropy point of view, chain–like molecules would rather avoid the solid surface. (We call this *the entropy effect*, and this effect vanishes at $z = \lambda_i$) Obviously, these two effects become more pronounced with increasing the length of molecules. In the first fluid layer the adsorption is the dominant effect, and solute (or longer chain) molecules adsorb strongly on the solid surface for energy reasons. In order to release the maximum adsorption energy per molecule, most fluid molecules are oriented in the directions parallel to the surface.(We will in later discussions come back to this issue). In the successive liquid layers, the entropy effect becomes more important. Consequently, solute (or longer chain) molecules are repelled from these regions. Instead, those layers are preferentially filled with solvent (or shorter chain) molecules whose entropy effect is less pronounced. At $z = \lambda_{min} = \lambda_B$, the entropy effect for solvent molecules vanishes, and the space will be filled very well with solvent molecules. Then the density of solute molecules is substantially decreased. Similarly, at $z = \lambda_{max} = \lambda_A$ due to the vanishing of the entropy effect of the solute molecules, $\varphi_A(z)$ increases remarkably after the first fluid layer.

As is known [6], the order parameter, $s = (3\langle\cos^2\theta\rangle - 1)/2$, can be used to characterize the orientation of polymers or chain–like molecules with respect to a given direction; θ is the angle between the longitudinal axis of a segmental unit and a given direction. In our cases, the orientation of segmental units occurs with respect to the normal to the solid surface. Here the order parameter $s(z)$ is a function of z for a certain species. Obviously, in case that molecules are completely parallel to the surface, $s(z) = -1/2$. A random bond distribution will result for an order parameter $s(z) = 0$ [12]. To compare the ordering occurring in different interfacial layers, we use the value of $\bar{s}(z)$ to characterize the molecule in the layer z. $\bar{s}(z)$ is the ensemble average of $s(z)$ over the segments of molecule i (i = A or B). Now, the order parameter of solute and solvent molecules for a system of n–C_{23}/n–C_6 solutions is calculated [15] and plotted as a function of z, in Fig.3a. As was expected, it can be seen that first, both solute and solvent molecules are adsorbed parallel to the surface. After the first interfacial fluid layer, the value of $\bar{s}(z)$ increases considerably, indicating that the degree of ordering decreases drastically. This result can also be seen in both Fig.1 and Fig.2 where $\varphi_A(z)$ drops sharply after the first fluid layer. The implication is that in spite of the parallel "compact" structure of the first interfacial layer, molecules tend to be obliquely packed in other interfacial layers. A similar result was obtained by molecular dynamics simulations [7]. In general, the solute molecules are more ordered than the solvent molecules.

We note that this ordered structure of the first interfacial layer appears to be a general phenomenon of chain–like molecules, and is justified both from computer simulations[7] and experiments[17-18]. As a demonstration, we present in Fig.4 a picture of highly ordered mono–molecular layers of n–C_{23} molecules adsorbed on a graphite substrate, imaged by

STM. It is interesting to note that these ordered adsorbed paraffin molecules are limited to the first and sometimes the second mono–molecular layers[19]. This is consistent with the results given in Fig.3. (Note that for the time being, the ordering of n–paraffins in the plane parallel to the surface can not be taken into account in our calculations.)

In addition, it is shown in Fig.3b that in case that the chain length of solute molecules increases from n–C_{10} to n–C_{36}, the distance from the solid surface to the fluid layer where paraffin chains distribute randomly $[\overline{s}(z) \simeq 0]$ increases correspondingly. Compared with Fig.3a, it is explicit that at $z \simeq \lambda_i$ (i = A or B) paraffin molecules show a random packing. Obviously, this is due to the vanishing of the entropy effect. These results are consistent with Fig.2.

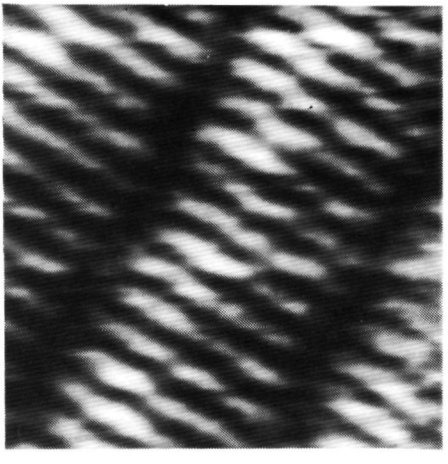

FIG.4. STM image of mono–layers of n–$C_{23}H_{48}$ molecules adsorbed on a graphite substrate from a n–$C_{12}H_{26}$ solution, showing that those n–$C_{23}H_{48}$ molecules form highly ordered arrays within molecular layers parallel to the graphite surface. $T \simeq 294$ K, the scan area is 6.3nm × 5.5 nm.

In the context of interfacial properties, it is of interest to see how bond energies are influenced by the interfacial structure. This can be characterized by a so–called surface scaling factor $C_{\ell}^{*}\,(= \phi_j/\Phi_j)$ [8,20]. In the language of Ising models [8,17], the interfacial exchange bond energy ϕ (per molecule) in direction j is expressed for a two–component system, as

$$\phi_j \simeq \tfrac{1}{2}(\phi_j^{AA} - \phi_j^{SS}) + [1 - X_A(0)]^2\,\phi_j^{\sigma} \qquad (1)$$

and

$$\phi_j^{\sigma} = \phi_j^{AB} - \tfrac{1}{2}(\phi_j^{AA} + \phi_j^{BB}), \qquad (1a)$$

where superscripts AA, BB, AB and ss denote solute–solute, solvent–solvent, solute–solvent and solid–solid interactions, respectively, $X_A(0)$ denotes the mole fraction of solute molecules in the first fluid layer. The value of ϕ_j can be determined by measuring the roughening temperature T^r of a crystal surface [20-21], according to the relation

$$\theta^r = 2kT^r/\phi_j \,. \tag{2}$$

(θ^r is the dimensionless roughening temperature, and can be calculated for a given crystal surface[20-21].) Alternatively, the corresponding value in the bulk phase (denoted by Φ_j) can be evaluated from the data of the dissolution enthalpy Δh_{diss} ($= \Sigma_{j=1}^{m} \Phi_j$, m in the coordinate number) [17,21]. Then the ratio of $C_\ell^s = \phi_j/\Phi_j$ can be determined from experiments[22-24]. For n–C_{21}, n–C_{23} and n–C_{25} paraffin crystals grown from n–hexane solutions, the results of C_ℓ^s (exp.) are given in Table I.

On the other hand, this ratio is directly related to the segment density profiles of the solute[20]. Therefore, it can also be obtained from the SF theory calculations, based on the following relation[20],

$$C_\ell^s = \phi_j/\Phi_j \simeq \ln X_A(0)/\ln X_A. \tag{3}$$

Here X_A is the corresponding value in the bulk. The corresponding calculated values of C_ℓ^s(cal.) for those three paraffin systems are also listed in Table I.

TABLE I. Calculated and experimental values of the surface scaling factor C_ℓ^s for various paraffin solution systems.

Solutions	φ_A †	$\varphi_A(0)$	C_ℓ^s(cal.)	C_ℓ^s(exp.)‡
n–C_{21}/n–C_6	0.100	0.519	0.406	0.414
n–C_{23}/n–C_6	0.100	0.543	0.392	0.401
n–C_{25}/n–C_6	0.100	0.579	0.382	0.372

† φ_A is the bulk concentration under experimental conditions [22-24].

‡ References 8, 19, 22–24.

It can be seen that the experimental and calculated results agree in a quantitative way with each other. We notice from the aforementioned discussions that the density of paraffin

Errata

Page 183 and page 206:

The orientation factor (λ_{hkl} or ξ_{hkl}) of the {100} faces for sc structure listed in Table I should be ***0.167***, not *0.125*.

molecules in the first fluid layer are associated with the interfacial structure of systems (see Fig 1) Therefore, it can be concluded from Table I that our calculations are quite convincing

The results presented above reveal the ordered structure of alkanes at the solid–fluid interface This gives physical insight to the molecular behavior at the interface, and offers a better understanding of the influence of solvents on the morphology of crystals Some progress has been made in this respect, and the results will be published elsewhere It is noted that the molecule–dependent oscillatory profiles for chain–like molecular systems is, to the best of our knowledge, identified for the first time by our calculations This result is relevant for the interpretation of the phenomena concerning a first order roughening transition and the solvent dependent critical behavior of surface roughening, which occur on alkane crystals[25-27] Without doubt, further investigations are needed We hope that our results will attract more attention to this issue both from the experimental and theoretical points of views

ACKNOWLEDGEMENTS

Helpful conversations with Dr F A M Leermakers and Prof Dr G J Fleer are gratefully acknowledged We are much indebted to Drs R Geertman for technical support, Dr C S Strom and Dr H Meekes for a critical reading of the manuscript This research was supported by Shell Netherlands B V

REFERENCES

1 J Q Broughton, and F F Abraham, Chem Phys Lett **71**, 4560 (1980)

2 J Q Broughton, and G H Gilmer, J Chem Phys **79**, 5095, 5105, 5119 (1983), **84**, 5741, 5749, 5759 (1986)

3 (a) A Bonissent, in *Interfacial Aspects of Phase Transformations*, edited by B Mutaftschiev (Reidel, Dodrecht, 1982), (b) U Landman, C S Brown, and C L Cleveland, Phys Rev Lett **45**, 2032 (1980), (c) E T Chen, R N Barnett, and U landman, Phys Rev **B40**, 924 (1989), (d) J D Weeks, J Chem Phys **67**, 3106 (1977)

4 O Guiselin, L T Lee, B Farnoux, and A Lapp, J Chem Phys **95**, 4632 (1991)

5 H K Christenson, D W R Gruen, R G Horn, and J N Israelachvili, J Chem Phys **87**, 1834 (1987)

6 (a) T Pakula, J Chem Phys **95**, 4685 (1991), (b) T Pakula, and E B Zhulina, J Chem Phys **95**, 4691 (1991)

7 T K Xia, Jian Ouyang, M W Ribarsky, and U Landman, Phys Rev Lett **69**,

1967 (1992).

8 X.Y. Liu, P. Bennema, J. Chem. Phys. **97**, 3600 (1992).

9 J.M.H.M. Scheutjens, and G. J. Fleer, J. Phys. Chem. **83**, 1619 (1979); **84**, 178 (1979).

10 O.A. Evers, J.M.H.M. Scheutjens, and G. J. Fleer, Macromolecules **23**, 5221 (1990).

11 J.M.H.M. Scheutjens, and G. J. Fleer, Macromolecules **18**, 1882 (1985).

12 F.A.M. Leermakers, and J.M.H.M. Scheutjens, J. Chem. Phys. **89**, 3264 (1988); **89**, 6912 (1988); J. Phys. Chem. **93**, 7417 (1989).

13 (a) J. Marqusee, and K. Dill, J. Chem. Phys. **85**, 434 (1986); (b) K. M. Hong, and J. Noolandi, Macromolecules **14**, 1229 (1981); (c) I. Szleifer, A. Ben–Shaul, and W.M. Gelbart, J. Phys. Chem. **94**, 5081 (1990).

14 M.G. Broadhurst, J. Res. Nat. Bur. Stand. **A66**, 241 (1962).

15 The calculations of the SF theory can be carried out using the computer program called "Goliath", which has recently been developed by the Department of Physics and Colloid Chemistry of Wageningen University.

16 A.S. Wingrove, and R.L. Caret, *Organic Chemistry*, (Harper & Row, New York, 1981).

17 G.C. McGonigal, R.H. Bernhardt, and D.J. Thomson, Appl. Phys Lett. **57**, 28 (1990).

18 G.C. McGonigal, R.H. Bernhardt, Y.H. Yeo, and D.J. Thomson, J. Vac. Sci. Tech. **B9**, 1109 (1991).

19 F. Thibaudau, G. Watel and J. Cousty, Surf. Sci. Lett. **281**, L303 (1993).

20 X.Y. Liu and P. Bennema, J. Chem. Phys. **98**, 5863 (1993).

21 P. Bennema, and J.P. van der Eerden, in *Morphology of Crystals*, edited by I. Sunagawa,(Terra, Tokyo, 1987) p.1.

22 P. Bennema, X.Y. Liu, K. Lentas, R.D. Tack, J.J.M. Rijpkema, and K.J. Roberts, J. Cryst. Growth **121**, 679 (1992).

23 X.Y. Liu, and P. Bennema, J. Cryst. Growth (to be published).

24 X.Y. Liu, and P Bennema, J. Appl. Cryst. **26**, 229 (1993).

25 X.Y. Liu, P. Bennema, and J.P. van der Eerden, Nature **356**, 779 (1992).

26 X.Y. Liu, Phy. Rev. **B48**, (1993).

27 X.Y. Liu, P. van Hoof, and P. Bennema, Phy. Rev. Lett. **71**, 109 (1993).

Chapter 4.8

Scanning tunneling microscopy studies on n–alkane molecules adsorbed on graphite

M. Couto, X.Y. Liu, H. Meekes, and P. Bennema

RIM, Laboratory of Solid State Chemistry, Faculty of Science, University of Nijmegen, Toernooiveld, 6525 ED Nijmegen, The Netherlands.

ABSTRACT–The adsorption of n–alkanes on graphite has been studied by scanning tunneling microscopy. These molecules can form very well ordered layers on the graphite surface. It was observed that the degree of ordering is dependent on the sample temperature. A model for the structure of the adsorbed layer and a possible explanation for the temperature effects are given.

Studies of odd–numbered n–alkane crystals in n–hexane solution have shown a first order roughening transition occurring at the {110} faces of these crystals[1,2]. It was suggested that the unusual first order character of this transition is due to changes in the motional state of the crystal molecules at the crystal–solution interface. Above a critical temperature the surface molecules of the crystal start to rotate around their molecular axes. This makes the energy difference between the surface molecules of the crystal and the solution molecules very small, which causes the collapse of the edge free energy, leading to the roughening of the crystal faces.

Recently there have been reports on scanning tunneling microscopy (STM) studies of n–alkane molecules absorbed on the surface of highly oriented pyrolytic graphite (HOPG)[3-6], showing that these molecules can form ordered arrays with the molecules parallel to the surface of the HOPG.

In this letter we report on the use of the technique of STM to give some evidence of the effect of temperature on n–alkanes adsorbed on a HOPG surface. The systems studied were the n–alkanes ranging from 17 to 27 carbon atoms.

The samples were prepared taking advantage of the fact that in a solution of different n–alkanes in contact with graphite, the n–alkanes with a higher number of carbon atoms are adsorbed more preferentially than those with a lower number of carbon atomes[7], The solution consisted of the n–alkane of interest dissolved in n–dodecane as a saturated solution at room temperature. A small amount of this solution was then applied to a freshly cleaved HOPG surface. The measurements were carried out at a temperature of 21°C, unless specified differently.

The STM was home–built and is similar to that described by Hottenhuis *et al.*[8]. For our experiments the electrochemical cell on the lower part of the STM was replaced by a small teflon cell containing the HOPG and the solution. The tips used were mechanically sharpened Pt–Ir wires with a diameter of 0.5 mm. The tunneling voltage was 0.5 V (sample positive) and the tunneling current was 200 pA. Lower voltages resulted in a decrease of resolution for the molecules, bringing the HOPG atoms into resolution. Higher voltages resulted in an increase in noise level. All the images were taken in constant current mode.

Normally several attempts were necessary before we could observe the ordered layers. This can be explained by the fact that the ordered n–alkane molecules do not cover the HOPG surface entirely but form islands separated by a distance larger than the scan range of out STM (1 μm), making it difficult to locate them.

With our STM it was impossible to find the exact location of the C–atoms with respect to the graphite lattice, due to drift. It nevertheless was relatively easy to observe that the molecules are aligned along the crystallographic axes of the graphite unit cell.

For the solutions of n–alkanes ranging form 17 to 22 carbon atoms we could not observe any ordered layer on the HOPG surface. An explanation for this is that at the temperature of 21° C the molecules are too mobile on the surface. This either makes an ordering of the molecules impossible or makes it easier for the tip to push the molecules away during the scan, disturbing the ordered layer.

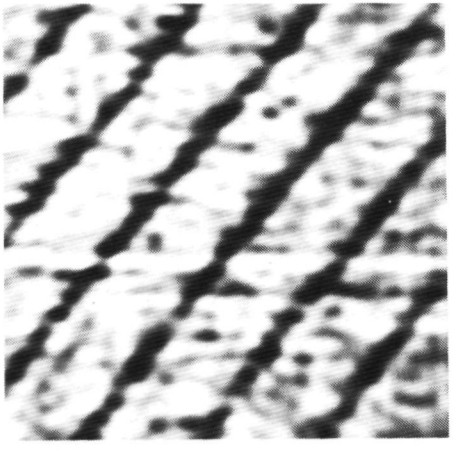

FIG.1. STM atmospheric image of n–$C_{19}H_{40}$ molecules adsorbed on HOPG. The molecules are adsorbed parallel to the HOPG surface. The scan area is 12.5 nm x 12.4 nm.

Experiments with n–$C_{19}H_{40}$, however, showed that after leaving the solution in contact with the HOPG for one moth an ordered layer could be imaged after removing the solution and cleaving the HOPG. During this time some n–$C_{19}H_{40}$ could diffuse in between the graphite layers and adsorb in some areas. Fig.1 shows an STM image obtained for this material. The molecules are very well ordered in rows, with their long axis perpendicular to the direction of these rows and parallel to the HOPG surface. These ordered layers extended without defects for more than 50 nm x 50 nm. The measured distance between two molecules in a row is 0.42 nm and the distance between two rows is 2.24 nm.

Fig.2 shows a STM image of adsorbed n–$C_{23}H_{48}$ obtained in solution. This n–alkane presents the same degree of ordering as observed for n–$C_{19}H_{40}$. It can be seen that across the rows the molecules are shifted vertically by half of the distance between two molecules in a row. The distance between two molecules is 0.40 nm and the width of the rows is 2.57 nm. Fig.3 shows another region of the same sample were we can see the boundary between an ordered region and a region were no molecular ordering could be imaged. For this region either there are no adsorbed molecules or the molecules are adsorbed perpendicular to the

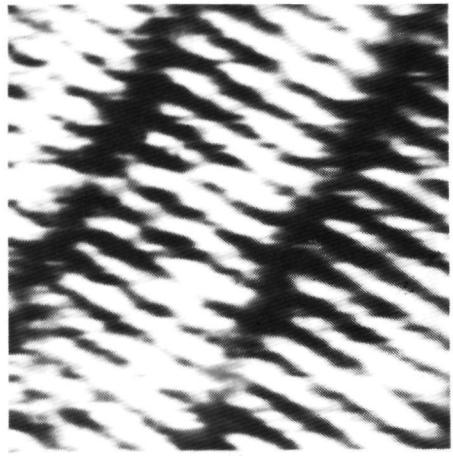

FIG.2. STM solution image of n—$C_{23}H_{48}$ molecules. The shift of the molecules across the rows can be seen. The scan area is 6.3 nm x 5.5 nm.

surface, making the imaging process more difficult.

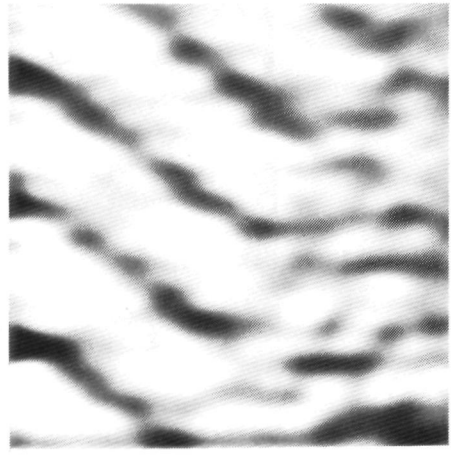

FIG.3. n—$C_{23}H_{48}$ solution at a domain boundary. No resolution was achieved in the right side of this area. The image size is 12.5 nm x 11.1 nm.

n—$C_{27}H_{56}$ also showed the same ordering as observed for the materials above. For this material it was found that in a region of a step on the HOPG surface the direction of the rows of molecules on the lower terrace is rotated 120° in relation to the direction of the rows on the

upper terrace. The measured molecular distance is 0.38 nm and the width of the rows is 3.27 nm. Fig.4 shows a high magnification of some n–$C_{27}H_{56}$ molecules. For this material it was possible to achieve resolution of the individual CH_2 groups.

FIG.4. STM solution image of n–$C_{27}H_{56}$ molecules. The zigzag of dots along the molecules are the individuals CH_2 groups. The scan size is 0.8 nm x 0.8 nm.

Fig.5 shows two proposed models for the adsorbed layer. In Fig.5(a) the plane of the carbon atoms in the molecule is perpendicular to the HOPG surface and in Fig.5(b) it is parallel. Both structures are different from the crystallographic planes of the bulk of the n–alkane crystal. For the molecules adsorbed in the way shown in Fig.5(a) the higher CH_2 groups will be imaged differently and the molecule will appear as a series of clearest dots which number is half of that of the carbon atoms in the molecule. For both orientations the molecules should be compressed by a small amount along their long axis to let the length of 0.251 nm of the C–C–C zigzag match with the length of 0.246 nm between the center of two adjacent hexagons on the HOPG surface[7]. For n–$C_{23}H_{48}$ all the measurements showed the molecules oriented in the way shown in Fig.5(a). This can be seen on the video screen but unfortunately is difficult to observe in Fig.2. For n–$C_{19}H_{40}$ and n–$C_{27}H_{56}$ both orientations were found in different areas of the same sample. The measured intermolecular distances of n–$C_{19}H_{40}$ and n–$C_{27}H_{56}$ agree very well with the expected molecular length of 2.26 nm and 3.26 nm respectively. The length of n–$C_{23}H_{48}$ was measured as being 0.19 nm shorter than expected. We attribute this to a temperature effect. At the temperature at which the measurements were realized the formation of defects, like kinks, in n–alkane molecules can be favoured[9], shortening the molecules. An indication for this can be found in Fig.2, where the

molecules in a row seem to have slightly different lengths

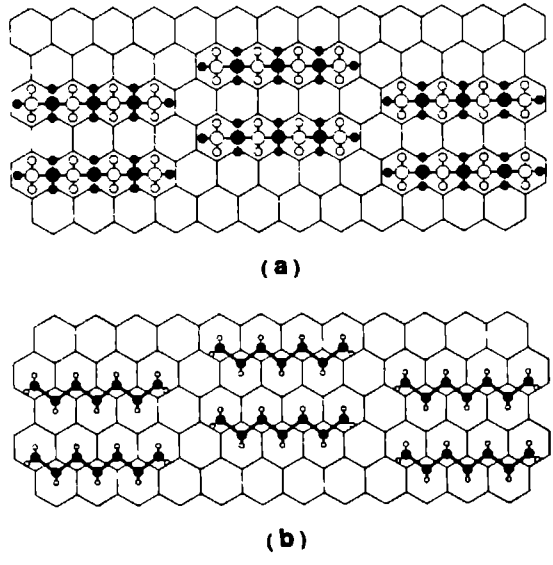

FIG 5 Proposed models for the adsorbed layer (a) The molecules are perpendicular to the HOPG surface (b) The molecules are parallel to the HOPG surface In both cases the spacing between to molecules in a row is 0 425 nm

Another attempt was make to image n–$C_{23}H_{48}$ and n–$c_{24}H_{50}$ at a temperature of 28° C None of these compounds could be imaged at this temperature This suggests that at some temperature between 21° C and 28° C the molecules become too mobile on the HOPG surface, making it impossible to image them with the STM This can be attributed, again, to the formation of defects on the molecules If the number of these defects increases very much, the number of carbon atoms in contact with the HOPG surface decreases Two effects can then occur First, the molecules can still be adsorbed to the HOPG surface making an ordered array but the adsorption is so weak that during the scan the STM tip pushes the molecules away and no resolution is achieved Second, the adsorption can be so weak that n–alkane molecules will mix with solvent molecules no longer making an ordered array and we have a disordered layer

New experiments are being prepared to study the effect of temperature in a specific n–alkane and to find a transition from an ordered to disordered arrangement Controlling the temperature of the solution during the measurements will make it possible to find at which temperature the molecules can no longer be imaged

In conclusion, we could see that temperature effects play an important role in the adsorption and ordering of n–alkane molecules on the HOPG surfaces, leading from a complete ordering of the molecules to a complete disordering

One of the authors, M Couto, is indebted to CAPES (Coordenação de Aperfeiçoamento de Pessoal de Nível Superior), Brazil, for a scholarship making this research possible They want to thank Shell Netherlands B V for providing the n–alkanes used in the research program

REFERENCES

1 X Y Liu and P Bennema, J Chem Phys **97** 3600 (1992)

2 X Y Liu, Phys Rev B**48**, (1993) (in press)

3 G C McGonigal, R H Bernhardt, and D J Thomson, Appl Phys Lett **57**, 28 (1990)

4 G C McGonigal, R H Bernhardt, Y H Yeo, and D J Thomson, J Vac Sci Technol B**9** 1107 (1991)

5 J P Rabe and S Buchholz, Science **253**, 424 (1991)

6 J P Rabe and S Buchholz, Makromol Chem , Macromol Symp **50**, 261 (1991)

7 A J Groszek, Proc Roy Soc Lond A **314**, 473 (1970)

8 M H J Hottenhuis, M A H Mickers, J W Gerritsen and J P van der Eerden, Surf Sci **206**, 259 (1988)

9 B G Sumpter, D W Noid and B Wunderlich, Macromolecules (to be published)

Chapter 4.9

Influence of solvents on properties and the structure of crystal–solution interfaces of normal alkanes

Xiang–Yang Liu and J Faber

RIM, Laboratory of Solid State Chemistry, Faculty of Science, University of Nijmegen, Toernooiveld, 6525 ED Nijmegen, The Netherlands

ABSTRACT–The step energy and the interfacial structure of the {110} faces of n–paraffin crystals growing from various solutions are studied, using experimental and Self–Consistent Field (SCF) calculation techniques The step energy is determined mutually by the interfacial structure and the bulk properties of the solution Its value can be measured from thermal roughening experiments or theoretically calculated by SCF techniques in terms of the surface scaling factor C_l^* The results obtained from the two techniques turn out to be in good agreement The interfacial fluid structure of the n–paraffin crystals in different solutions is identified by means of SCF calculations The ordering and structuring occurring in the interfacial region change explicitly, depending on the molecular structures and properties of the solvent Subsequently, a ternary system, i e the n–$C_{25}H_{52}$/butanol/n–hexane solution, is studied It turns out that, when the segmental density of the solute is kept constant, mixing a small amount of one solvent with the other will lead to an increase in the step energy Finally, the influence of the solvent molecules on the interfacial parameters and on the roughening transition is discussed

I INTRODUCTION

The kinetic mechanism of crystal growth depends directly on interfacial properties, such as the step energy ϕ and the step free energy $\gamma k_b T$ (k_b is the Boltzmann constant, T the temperature) Changes in those properties drastically affect the kinetic mechanism of crystal growth For a flat face, if the temperature T is lower than a critical temperature, so–called roughening temperature T^r, the step free energy $\gamma > 0$ A face becomes flat as a consequence of the two–dimensional nucleation barrier, at relatively low supersaturation σ ($\sigma = \Delta\mu/k_b T$, $\Delta\mu$ denotes the difference of the chemical potential between the solid and the fluid phase) The crystal face grows in a layer–by–layer mechanism and the growth rate is a nonlinear function of σ In case that the supersaturation σ is larger than a critical supersaturation σ^c), the nucleation barrier which controls the growth of flat crystal faces can be overwhelmed by the chemical potential difference Growth units can be directly incorporated into the crystal face Thus the so–called kinetic roughening occurs, and the surface becomes kinetically rough Then the growth rate depends linearly on the supersaturation σ If $T \geq T^r$, the so–called roughening transition occurs The step free energy vanishes This implies that the reversible work to create a step is zero, and so thermal fluctuations produce a large number of steps on the crystal face Then each position at the surface is a kink position The surface is rough at equilibrium, and the growth rate follows the Wilson–Frenkel law[1]

Without doubt, the value of γ and the critical behavior of $\gamma(T)$ near the roughening transition temperature are directly related to the structure of the solid–fluid interface According to the XY model [2-4], the roughening transition is of infinite order This is the so–called Kosterlitz–Thouless type of roughening transition The existence of this type of roughening transition has been confirmed by computer simulations [1,5-6], and by experiments carried out on some simple crystal systems [7-9] However, this model seems inadequate for some complex crystal systems like the n–paraffin crystal systems In the case of odd n–paraffin crystals growing from toluene solutions, it is found [10-12] that $\gamma(T)$ vanishes continuously at T^r, indicating the onset of infinite order phase transition However, when the n–paraffin crystals grow from n–hexane solutions, $\gamma(T)$ vanishes discontinuously at T^r, indicating the occurrence of a first order roughening transition rather than the Kosterlitz–Thouless type of roughening transition Obviously, different solvents can exert a significantly different influence on the solid–fluid structure, hence on the critical behavior of the roughening transition

The roughening temperature T^r for a given crystal face is directly related to the interfacial bond energies ϕ_i, expressed in terms of the dimensionless temperature θ^r, as

$$\theta^r = 2k_b T^r / \phi_{str}. \tag{1}$$

Here ϕ_{str} is the strongest bond energy (or the edge energy) at the surface. We notice that θ^r is a specific property and has a certain value for a given surface. Therefore, T^r depends directly on the value of ϕ_{str}. In the language of cell models [13-15], the interfacial bond energy ϕ_i in direction i is expressed for a two–component (A,B) solution system as

$$\phi_i = \tfrac{1}{2}(\phi_i^{AA} - \phi_i^{SS}) + [1 - X_A(0)]^2 \phi_i^{\sigma} + \Delta_i, \tag{2}$$

$$\phi_i^{\sigma} = \phi_i^{AB} - \tfrac{1}{2}(\phi_i^{AA} + \phi_i^{BB}) \tag{3}$$

and

$$\Delta_i = X_A(0)(\phi_i^{SA} - \phi_i^{AA}) + [1 - X_A(0)](\phi_i^{SB} - \phi_i^{AB}) \tag{4}$$

(Here superscripts AA, BB, SS, AB, SA and SB represent solute–solute, solvent–solvent, solid–solid, solute–solvent, solid–solute and solid–solvent interactions, respectively, $X_A(0)$ is the concentration of the solute in the first fluid layer adjacent to the crystal phase.)

In the framework of theories of regular solutions [13], and models of the solid–fluid interface [14], the value of ϕ_i is determined by (i) the enthalpy of dissolution (or of melting) of systems; (ii) interfacial structures. In the case of crystals growing from solution, the enthalpy of dissolution characterizes the bulk properties of the solution and the mixing between solute and solvent molecules. If the exchange energy W_{AB} [$= \Sigma_{i=1}^{m} \Phi_i^{\sigma}$; Φ_i^{σ} having an expression similar to Eq.(3)] is very small (or equal to zero), solute molecules can mix very well with solvent molecules. As a consequence, that the molar enthalpy of dissolution Δh_{diss} is very close to the molar enthalpy of melting Δh_m. ($\Delta h_{diss} = \Sigma_{i=1}^{m} \Phi_i$; Φ_i is expressed similarly to Eq.(2), presuming that $\Delta_i = 0$ and $X_A(0) = X_A$, where X_A is the concentration in the bulk.) In contrast, if Δh_{diss} is much larger than Δh_m (meaning that W_{AB} is larger), the mixing between solute and solvent molecules is poor. Then the solubility of the crystal has a very low value. Generally speaking, the interfacial bond energy ϕ_i is a function of Δh_{diss}.

In spite of this, the structure of the interface will certainly affect the value of ϕ_i. According to recent progress based on density–functional theories, computer simulations and experiments [16-23], the fluid units in interfacial regions possess a certain degree of ordering. The solid units near the surface undergo a certain degree of deformation resulting in surface reconstruction or surface relaxation. In general, the interfacial structure is different from that of the bulk. It then follows that interfacial properties, such as $X_A(0)$, ϕ_i^{SS}, ϕ_i^{AA}, ϕ_i^{BB}, etc. are different from those in the bulk (X_A, Φ_i^{SS}, Φ_i^{AA}, Φ_i^{BB}, etc.). (Note that here ϕ represents the

bond energy at the interface, Φ the bond energy in the bulk) In order to associate interfacial properties with those of the bulk phase, a so–called surface scaling factor C_ℓ^s is introduced [14-15]

$$C_\ell^s = \sum_{i=1}^{m} \phi_i \left[\sum_{i=1}^{m} \Phi_i \right]^{-1} \simeq \phi_i / \Phi_i \tag{5a}$$

(Here we assume that $\Delta_i \simeq 0$) This factor can be associated with the concentration (or the density) of solute in different regions [14] in the following way

$$C_\ell^s \simeq \ln X_A(0) / \ln X_A \tag{5b}$$

Based on this factor, three distinct cases can be identified for crystal surfaces [14-15]
(i) equivalent wetting, $C_\ell^s = 1$, or $X_A(0) = X_A$, (ii) less than equivalent wetting, $C_\ell^s > 1$, or $X_A(0) < X_A$, (iii) more than equivalent wetting, $C_\ell^s < 1$, or $X_A(0) > X_A$ The equivalent wetting case is an artificial reference state It is realized in some very special situations Normally, the other two cases occur The more than equivalent wetting case implies that the crystal surface shows a preferred adsorption of solute units Due to the boundary condition of cell models which implies that $X_A(z) + X_B(z) = 1$, this condition corresponds to a repulsion of solvent units at the surface On the other hand, the less than equivalent wetting case means that the crystal surface shows a preferred adsorption of solvent units (and a depletion of solute units)

Looking at Eq (5a) Φ_i can be directly related to Δh_{diss} by means of the proportionality condition [5] This condition implies that from one state to another, the absolute value of the bond energy is altered, but the ratio between the values remains the same It then follows that

$$\Phi_i = (\Phi_i^{SS} / 2E^{cr})\, \Delta h_{diss}, \quad E^{cr} = \sum_{i=1}^{m} \tfrac{1}{2} \Phi_i^{SS} \tag{6}$$

It can be seen from Eqs (5a) and (6) that

$$\phi_i = (\Phi_i^{SS} / 2E^{cr})\, C_\ell^s \Delta h_{diss} \tag{7}$$

Obviously, $\Phi_i^{SS} / 2E^{cr}$ is constant for a given crystal structure, and can easily be calculated As anticipated previously, ϕ_i is determined by C_ℓ^s and Δh_{diss} Here C_ℓ^s characterizes the wetting condition of the solid–surface, and is determined by the interfacial structure

Now, the influence of the enthalpy of dissolution and interfacial structure on ϕ_i is clearly demonstrated in Eq (7) We notice that both Δh_{diss} and C_ℓ^s are associated with the

properties and the shape of the solvent molecules It can be said that solvents have a decisive influence on the interfacial bond energy ϕ_1, and thus on some important physical processes, such as the roughening transition [see Eq (1)]

In this paper, we will investigate the influence of solvents on the structure of solid–fluid interfaces, with special attention on the step (free) energy for n–paraffin crystal systems The problem will be dealt with from both experimental and theoretical points of view The fluid interfacial structure is calculated based on self–consistent field (SCF) theories [24-27], thus some calculated results will be compared with experimental results Note that concerning the solvent influence on the surface structure and the surface roughening, a number of investigations on other organic crystals have been carried out Two interesting examples are naphthalene crystals and biphenyl crystals growing from various solutions [28-29] Therefore, it is worthwhile to include those systems in our discussions

II. EXPERIMENTS AND RESULTS

It has already been seen from Eq (7) that if C_l^* is available, then this factor for a given crystal structure, together with Δh_{diss} and structural parameters, can be used to estimate ϕ_1 Vice verse, if ϕ_1 is available, C_l^* can be calculated Thus some information concerning the interface can be obtained In this section, we will first determine ϕ_1 and Δh_{diss} experimentally Then ϕ_1 and Δh_{diss} will be compared with each other for different solvents These results will be further discussed in the next section, together with the calculated results from the self–consistent field theories

A Experiments

Odd n–paraffins crystallize in the space group P_{bcm} with four molecules in an unit cell The structural parameters are $a = 4\ 96$, $b = 7\ 478$, $c = 2\ 546n + 3\ 75$ Å (n is the carbon number) [30] Theoretical analysis [31] indicates that crystals of odd n–paraffins are lozenge shaped, bounded by the large {001} faces on the top and the bottom and the narrow side faces of {110} Our concentrations are focused on the {110} faces

In our experiments, n–paraffins, such as n–$C_{21}H_{44}$, n–$C_{23}H_{48}$, n–$C_{25}H_{52}$ etc , and various solvents, such as, n–hexane, cyclo–hexane, iso–octane, toluene, butanol, etc , were used The n–paraffins used in our experiments were from analytically pure chemicals (Alfa, > 99 %) and the n–hexane was spectroscopically pure (Merck, > 98 0%) The other solvents used in our experiments were analytically pure and purchased from Merck Materials were used without further purification

In our experiments, observations of the growth forms and the morphological transitions

of crystals were made at various supersaturations in different solutions These observations were carried out in a system of double–walled glass cells of cylindrical form, using a Leitz transmission microscope type Divert The temperature of the system could be stabilized within ± 0 003° C by the thermostat (Heto, Denmark) over several hours After dissolving the solid material, high supersaturations were imposed and the crystals nucleated Subsequently all but one of the crystals were dissolved, and the remaining one was used for carrying out experiments by observing this crystal The volume of this crystal was always very small compared to that of the cell, so that changes of concentration in the solution were negligible during the experiment

In the experiments, two types of data were measured the saturation temperature, and the critical supercooling of kinetic roughening $\Delta T^c = T_s - T^c$ (T^c is the temperature where kinetic roughening occurs) During the measurements, the morphological changes are observed by varying the temperature in very small intervals (in the neighborhood of critical points or of the equilibrium temperature, the intervals are about 0 005–0 01° C) Each temperature is kept constant for at least half an hour to ensure that the morphology of the crystal is stable Suppose that the growth and dissolution of the crystal are not affected by impurities At equilibrium, the crystal neither grows nor dissolves If the shape and size of the crystal won't change with time, the temperature is the saturation temperature T_s To determine ΔT^c, we lower the temperature from T_s At the temperature T^c where kinetic roughening occurs, the flat crystal faces will lose their original crystallographic orientations and become macroscopically rounded off ΔT^c is then obtained from T_s and T^c

According to the definition of supersaturation, it follows that for a regular solution the supersaturation is linearly proportional to the supercooling ΔT

$$\sigma \simeq \frac{\Delta h_{\text{diss}}}{RT_s^2} \Delta T, \quad \Delta T = T_s - T \tag{8}$$

Therefore, the critical supersaturation σ^c of kinetic roughening can be obtained from ΔT^c Note that the experimental error of our measurements of ΔT^c can in principle be reduced to the accuracy limit of temperature control (and the temperature measurement device) This implies that each determination of ΔT^c is reproducible within the accuracy limit of our experimental set up (± 0 003° C)

B. Thermodynamic properties of the solutions

It is known that bulk properties of the solutions can be characterized by the solubility In the case of n–paraffin solutions, the solubilities can be fitted well by the van Hoff equation [32]

$$\ln X_A = -\frac{\Delta h_{diss}}{RT_s} + \frac{\Delta S^\circ_{diss}}{R} \quad (9)$$

(R is the gas constant) For a given solution system, it follows that a linear relation between $\ln X_A$ and $1/T_s$ can be obtained by fitting the experimental data Then Δh_{diss} and ΔS°_{diss} can be obtained from the slope and the y–intercept The parameters Δh_{diss} for different n–paraffin solution systems are given in Table I

TABLE I Experimental data thermodynamic properties of the bulk phase and of the interface

Solutions	Δh_{diss} [kcal/mol]	ΔS°_{diss} [cal/(K·mol)]	T^r_{110} [K]	ϕ_{str} [kcal/mol]	Φ_{str} ‡ [kcal/mol]
nC_{21}*/nC_6	16 411	52 925	273 25	1 218	2 939
nC_{23}*/nC_6	18 022	56 880	283 80	1 301	3 240
nC_{25}*/nC_6	20 106	62 429	287 64	1 351	3 627
nC_{25}/nC_{12}	19 453	59 771	< 263 55†	< 1 238	3 509
nC_{25}/cyc–C_6	20 436	64 319	≤ 278 15	≤ 1 307	3 687
nC_{25}/i–C_8	21 642	67 170	292 77	1 376	3 904
nC_{25}/butanol	23 132	64 225	299 7	1 406	4 173
nC_{25}/toluene	23 532	73 600	298 00	1 400	4 245

* For crystal of n–C_{21}, n–C_{23}, n–C_{25}, $\Phi^{SS}_{str}/2E^{cr}$ = 0 1791, 0 1798 and 0 1804, respectively, θ^r_{110} = 0 8916, 0 8666 and 0 8458 respectively

† For those n–paraffin solutions, the roughening temperature T^r of the {110} faces is lower than the melting point of solvents

‡ Φ_{str} is calculated from Δh_{diss} according to Eq (6)

Additionally, the interfacial properties are characterized by the roughening transition temperature It is explicitly shown in Eq (1) that for a given crystal surface, the interfacial bond energies are directly proportional to the roughening temperature T^r Experimentally, T^r can be obtained by determining σ^c as a function of temperature According to recent investigations [33], the critical supersaturation is directly correlated to the step free energy by

$$\sigma^c = f\gamma^2 \tag{10}$$

where the factor f depends on the shape of the 2D nuclei [33] and the bond structure of the surfaces, and is constant for a given surface structure In particular, at $T = T^r$, σ^c is equal to zero since γ vanishes The resulting T^r and ϕ_{str} of the {110} faces are listed in Table I for various paraffin crystal–solution systems

Now, it can be seen that for a given crystal structure, the bulk property Δh_{diss} has an influence on the interfacial bond energy ϕ_{str} Table I roughly indicates that as Δh_{diss} increases, ϕ_{str} is somewhat enhanced This can be interpreted as follows In the language of regular solution theories [13-15], Δh_{diss} is approximately expressed as

$$\Delta h_{diss} \simeq \Delta h_m + (1 - X_A)^2 W_{AB} \tag{11}$$

(For ideal solutions, $W_{AB} = 0$, and $\Delta h_{diss} = \Delta h_m$) It then follows that W_{AB} can be estimated from the data of Δh_m and Δh_{diss} listed in Table I [Note that in our case, $X_A << 1$ Then $(1 - X_A)^2 W_{AB} \simeq W_{AB}$] For n–$C_{25}H_{52}$ crystals, Δh_m is about 20 kcal/mol [34] It can be seen that when n–$C_{25}H_{52}$ crystals are dissolved in an alkane solvent, Δh_{diss} is very close to Δh_m, indicating that $W_{AB} \simeq 0$ This is because solvent and solute molecules have similar linear structures and similar intermolecular bonds Therefore, the mixing between solute and solvent molecules is very good On the contrary, if solvent molecules are not linear (such as cyclo–hexane, iso–octane, toluene etc) or if the molecular structure and intermolecular bonds are quite different from the n–alkane molecules (such as butanol, toluene etc), the value of Δh_{diss} (or W_{AB}) of the solution increases, indicating that the mixing between solute and solvent molecules is poor We notice that in the case of butanol, a hydroxyl group OH is attached to an alkane chain It follows that in the solutions, hydrogen bonds occur between butanol molecules, resulting in an association structure between the molecules [35] This association causes an independent solvent unit in the solutions to have a structure much different from that of an independent solute unit (consisting of a linear carbon chain molecule) In this sense, the shape of butanol molecules differs considerably from that of alkane molecules, when these molecules are considered as the solvent Therefore Δh_{diss} (or W_{AB}) is much larger than Δh_m

The cyclo–hexane and iso–octane molecules, considered as a whole taken in their entirety are not like normal alkane molecules However, the basic structures of those molecules, such as the chain form of the ring of the cyclo–hexane and all the branches of the iso–octane molecule, are very similar to the basic structure of normal alkane (the zigzag bond chain) Hence the degree of fitting between solvent and solute molecules in solutions is reasonable,

resulting in a modest increase in Δh_{diss} (or W_{AB}) On the other hand, the toluene molecules are have a flat shape This turns out to be very different from the molecular structure of alkane, so that the fitting between solute and solvent molecules is poor As shown in Table I, this results in a significant increase in Δh_{diss} (or W_{AB}) Regardless degree of the fitting between solute and solvent molecules, the interfacial structure has a significant influence on the value of ϕ_1 It can be seen from Table I that first ϕ_{str} is much smaller than Φ_{str}, due to the more than equivalent wetting Secondly, ϕ_{str} is not linearly proportional to Φ_{str} A typical example is n–$C_{25}H_{52}$ crystals grown from cyclo–hexane solutions Compared with the case of n–$C_{25}H_{52}$ crystals grown from n–hexane solutions, the n–$C_{25}H_{52}$/cyclo–hexane system has a larger Δh_{diss} (or Φ_{str}), but a smaller ϕ_{str} Evidently, the character and the structure of the interface play a key role in those issues As mentioned in Sec I, we use the surface characteristic scaling factor C_ℓ^* to characterize the interface According to Eq (5a), this factor

TABLE II

The experimental and the calculated data of the surface characteristic scaling factor C_ℓ^* for various paraffin solution systems

Solutions *	C_ℓ^*(exp)	C_ℓ^*(cal)	Order of RT ††
nC_{21}/nC_6	0 4144	0 41	First order
nC_{23}/nC_6	0 4015	0 39	First order
nC_{25}/nC_6	0 3735	0 38	First order
nC_{25}/nC_{12}	< 0 353	0 32	–
nC_{25}/cyc–C_6	≤ 0 355	– †	–
nC_{25}/i–C_8	0 3523	0 35	First order
nC_{25}/butanol	0 3369	0 33 ‡	Infinite order
nC_{25}/toluene	0 3298	– †	Infinite order

* The fcc lattice is chosen as the basic structure of systems

† For the time being, SCF calculations could not be applied to systems consisting of molecules with a ring structure

‡ For butanol molecules, it is estimated according to Table I that $\chi_{CB} = \chi_{CA} \simeq 5$, $\chi_{CS} \simeq 3$ (the subscript c denotes OH segments)

†† Order of RT represents the order of roughening transition, which is determined by the critical behavior of the edge free energy γ at $T^{T\ 10\text{-}12}$

can be calculated from the experimental data listed in Table I. The results denoted by C_2^*(exp.) are given in Table II. These results will be compared with the results calculated according to self–consistent field (SCF) theories described in the next section. A detailed discussion on the influence of solvents on the interfacial structure will also be given in next the section.

In addition to the thermodynamic properties mentioned above, it is also interesting to compare the character of the roughening transition occurring in different paraffin solution systems. As discussed in Sec. I, the character of the roughening transition can be identified from the critical behavior of γ (or σ^c) at the roughening transition temperature [10-12]. It is found from our experiments that when n–paraffin crystals grow from alkane solutions (including iso–octane solutions), the roughening transition turns out to be a first order phase transition. When non–alkane solvents are chosen, such as the toluene and the butanol, the roughening transition occurs as the conventional infinite order phase transition. (These results are summarized in Table II). Obviously, solvents have a significant influence on the nature of the roughening transition. We will discuss this issue later in Sec. IV.

III. SCF CALCULATION AND THE STRUCTURE OF INTERFACES

A. SCF theory calculation

Calculations employing the SCF theory are based on lattice models; that theory was first developed by Scheutjens and Fleer [24-27], and is based on an inhomogeneous cell model, where the same type of units (or cells) are characterized by the distance (z) to the solid surface. (Here z is normalized by the interplanar distance of the solid surface d_{hkl}.) Within the framework of this theory, paraffin molecules are regarded as chain–like molecules formed by segments of the same size, which are connected to each other. (Each segment represents a CH_2 or a terminal CH_3 group). Systems are homogeneous on a segmental scale, meaning that the Bragg–Williams (or mean field approximation is applied in the calculations. This implies that fluctuations on a monomer scale are negligible. Since in paraffin systems van der Waals interactions are dominant, only the nearest neighbor interactions need to be taken into account. In SCF theories the modeling and the calculation of various units in systems are carried out at monomer levels. Therefore, the concentration of solutions is expressed by the volume fraction φ_k (k = A, B, C, etc.; A denotes segments of solute molecules, and B, C, etc. denote various segments of solvents, respectively). To carry out SCF calculations, some parameters, such as the exchange energy between different segments and the bulk concentration, are needed. The bulk concentration can be determined from experiments, and in the following we assume that $\varphi_A = 0.1$. It can be seen that energy parameters must be

estimated. The exchange energy between segment k and segment l can be expressed in terms of the Flory–Huggins interaction parameter χ_{kl} (k and l = A, B, C, etc.), defined as the energy change (in units of k_bT) associated with the transfer of a segment of type k from a solution of pure k to a solution of pure l. For segments of equal size, the same energy effect occurs upon the transfer of a segment l from pure l to a solution of pure k, so that $\chi_{kl} = \chi_{lk}$ and $\chi_{kk} = 0$. Actually, for paraffin solutions $\chi_{AB} = W_{AB}/k_bT$, $\chi_{AC} = W_{AC}/k_bT$, etc.. It follows that the χ_{AB}, χ_{AC}, etc. can be estimated from the difference between the enthalpy of dissolution and the enthalpy of melting according to Eq. (11). (For paraffin–butanol solutions, the exchange energy between paraffin segments and the segment OH can be estimated in this way.) Obviously, if paraffin segments in solute molecules are denoted by A and those in solvent molecules by B, due to the very good mixing we have $\chi_{AB} \simeq 0$. Another important energy parameter is the adsorption energy between the solid surface and various fluid segments. This can also be defined by a Flory–Huggins parameters χ_{ks} (k = A, B, C, etc.). This energy (in units of k_bT, if not specified, $T = T_0 = 298.15$ K) corresponds to the interaction between a segment k and a surface site, resulting from bringing a segment from pure k into an environment of pure s (s: solid). Based on this definition, χ_{AS} can in principle be estimated for the case of paraffin molecules from the enthalpy of melting. For n–$C_{25}H_{52}$, on average $\chi_{AS} \simeq 1.30$ [34]. Those segments of CH_2 (or CH_3) in solvent molecules (denoted by B) which are on the crystal surface will behave in a similar way to rotatory paraffin solid segments in the hexagonal phase [15,34]. Then $\chi_{BS} \simeq -0.901 + 2.1/n$. Here n is the carbon number of the solvent paraffin chain. Note that χ_{BS}, as given above, is averaged over the CH_2 and CH_3 segments. Due to this averaging, χ_{BS} becomes dependent of the carbon number of the paraffin molecules.

In spite of those energy parameters, the torsional energy of molecular chains ϵ^{tor} can also be taken into account in SCF calculations. This is the energy difference between the *trans*– and the *gauche* conformation of the paraffin chains, and is about $2k_bT_0$ [35]. For more details concerning SCF calculations, we refer to Refs. 24–27.

B. Thermodynamic properties of the solid–fluid interface

It follows from the foregoing sections that in order to obtain the values of the interfacial bond energies and information about the interfacial structure, the surface scaling factor C_ℓ^* is relevant and must be available. Using SCF techniques, the distribution of the density of fluid units at the interface can easily be calculated. Therefore, C_ℓ^* may be estimated according to Eq.(5a). For the above–mentioned systems of paraffin solutions, the calculated values of C_ℓ^*, C_ℓ^*(cal.), are listed in Table II, and compared with experimental data. It can be seen from

Table II that C_{ℓ}^{*}(exp) and C_{ℓ}^{*} (cal) are very close to each other This implies that our calculated results are quite convincing

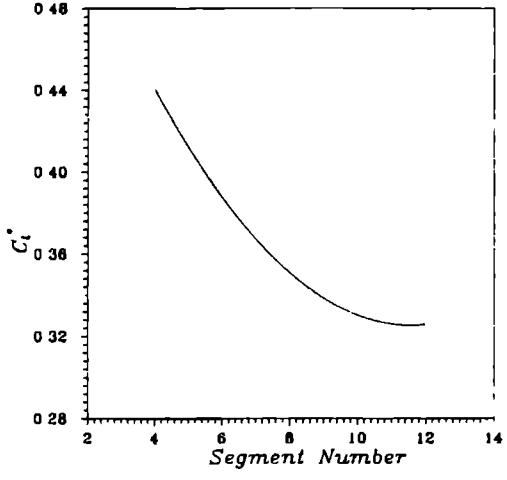

FIG 1 The surface characteristic scaling factor C_{ℓ}^{*} plotted versus the carbon number of solvent chain molecules for n–$C_{25}H_{52}$ in various alkane solutions $\varphi_{A} = 0\ 1$

Concerning crystals of a certain paraffin grown from n–alkane solutions, within a certain range C_{ℓ}^{*} decreases with increasing the chain length of the solvent alkane molecules This can be seen from Fig 1, where C_{ℓ}^{*} is plotted versus the carbon number of solvent alkane molecules This result can be interpreted as follows The value of C_{ℓ}^{*} depends on the concentration of solute (or solvent) at the surface in comparison with that in the bulk This depends on the competition between solute molecules and solvent molecules Since the more than equivalent wetting case occurs on paraffin crystal surfaces, this implies that solute molecules are preferentially adsorbed on solid surfaces For a given solute system C_{ℓ}^{*} is directly dependent on the structure of the solvent molecules Suppose that in all cases the bulk concentration is constant If the solvent molecules of one type fit on the surface much better than of others, the interfacial concentration of the solvent will be higher than other types of solvents It follows that $X_{A}(0)$ may then decrease $[X_{A}(z) + X_{B}(z) = 1]$ It turns out that C_{ℓ}^{*} increases

For a molecule in interfacial regions, two effects occurs On one hand, the molecule can be adsorbed at the surface, releasing adsorption energy (This is called *the energy effect*) On the other hand, the solid surface will impose some restrictions on the "freedom" of the fluid molecules, resulting in loss of the conformational and other entropy of the fluid molecules

(This is called *the entropy effect*) In the context of the free energy, whether a fluid molecule is adsorbed on the surface or is repelled from the surface depends on the competition between those two opposite effects If the entropy effect can be completely overcome by the energy effect, the molecule will be adsorbed onto the crystal surface Otherwise, it will be repelled from the surface

For alkane solvent molecules, the increase of the chain length of the molecules will at the same time increase both the entropy effect and the energy effect However, it is obvious that in a certain range of chain lengths the increase of the entropy effect is much larger than the increase of the energy effect This causes more solvent molecules to be repelled from the surface Then C_l^* decreases It is evident that the entropy effect of solvent alkane molecules with branches (such as iso–octane) or with a ring structure (such as cyclo–hexane) will certainly be larger than that of linear molecules, because branched structures and ring structures cannot fit on the solid structure of the surface as well as linear structures can Therefore, C_l^* will be smaller than linear solvent molecule solutions This can be seen from both the calculated and the experimental results given in Table I

For solvent molecules with a geometrical structure or intermolecular bond structure quite different from that of solute molecules, the fitting between solvent molecules and solid molecules at the surface may be very poor This implies that the entropy effect of the solvent molecules may become very pronounced Subsequently, the energy effect can be relatively weak Toluene and butanol belong to those solvents Toluene molecules are flat because of an aromatic ring This shape of the molecules cannot match the surface structure of solid paraffin molecules, which possess a zigzag chain structure On the other hand, butanol molecules have a geometric structure similar to alkane molecules However, because of the existence of the hydroxyl group, OH, those molecules are linked by intermolecular hydrogen bonds This association structure may in some way be broken near the solid surface, which causes a negative energy effect In addition, the association also causes poor matching between solvent molecules and the paraffin crystal surface As a consequence, the solid surface strongly repels those solvents It follows that the density of the solute at the solid surface will be enhanced, resulting in a further decrease of C_l^* These results can be seen from Table II

C. The interfacial structure

Normally, the structure of solid–fluid surfaces includes both the solid and the fluid part In this paper, we only concentrate on the fluid part of the interface

For paraffin crystals dissolving in various solutions, the interfacial structure of the the fluid phase depends directly on the structure of both solvent and solute molecules Within

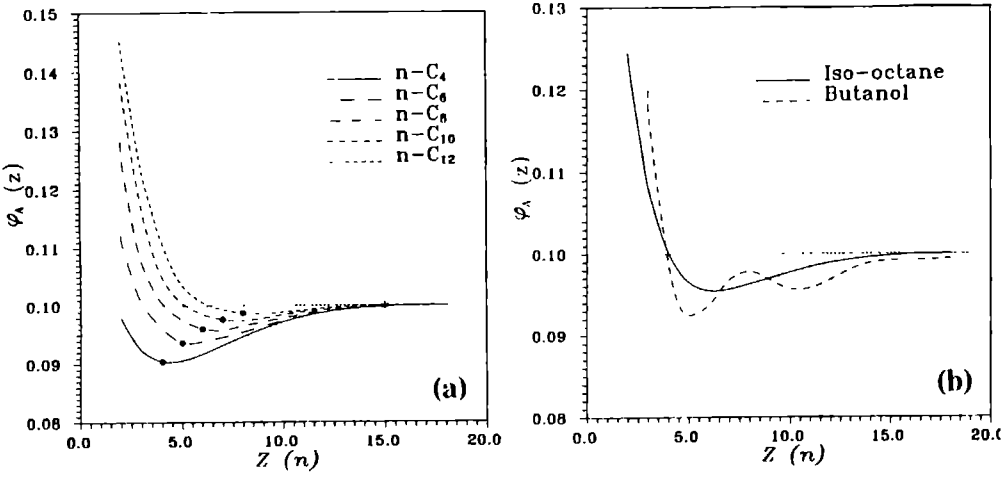

FIG.2. Profiles of the segmental density of n–$C_{25}H_{52}$ in various solutions, plotted versus distance z away from the solid surface. $\varphi_A = 0.1$ (a) n–$C_{25}H_{52}$ in various alkane solutions. The minimum positions (•) of the profiles $z = \lambda_{min}$ are related to the chain length of solvent molecules B ($\lambda_{min} \simeq \lambda_B^{half} + 3$), the position where the depletion of the solute almost vanishes $z = \lambda_{max}$ (*) is related to the chain length of the solute ($\lambda_{max} \simeq \lambda_A^{half} + 3$), λ_{min} and λ_{max} correspond to the position where the entropy effects of the solvent and solute vanish, respectively. (b) n–$C_{25}H_{52}$ in iso–octane and in butanol solutions. The former has a shape similar to the n–$C_{25}H_{52}$/n–C_5H_{12} system; the latter shows oscillations with the distance z.

much higher than that of the bulk fluid phase, due to the more than equivalent wetting. In the fluid layers following the first fluid layer, depletion of the solute occurs, and (at least) one minimum can be found in the $\varphi_A(z)$ curve at $z = \lambda_{min}$ Profiles of the solute density $\varphi_A(z)$ for n–$C_{25}H_{52}$ crystals grown in various alkane solutions are shown in Fig.2a. For those alkane solvents λ_{min} is directly correlated with the chain length of solvent molecules. Assuming that λ_k^{half} denotes half the chain length of the paraffin molecule k (k = A or B; A represents solute and B solvent), it can be seen from Fig.2a that in every case, $\lambda_{min} \simeq \lambda_B \simeq \lambda_B^{half} + 3$. Obviously, the depletion occurs in these interfacial layers where the entropy effect of the solute plays a major role. Those layers are then mainly filled with solvent molecules which have a smaller entropy effect. When $z = \lambda_B$, the entropy effect of the solvent molecules vanishes. Then the fluid is best filled with the solvent molecules, and $\varphi_A(z)$ reaches its

minimum. Moreover, When $z \geq \lambda_A \simeq \lambda_A^{half} + 3$, the entropy effect of the solute vanishes. This implies that the depletion disappears and $\varphi_A(z) \simeq \varphi_A$. This is clearly demonstrated in Fig.2a. (The variation of λ_A with respect to different solutes is discussed in Ref.36.)

For n–$C_{25}H_{52}$ crystals grown from other solutions, a specific structure of the solvents molecules may significantly influence the interfacial structure. It is shown in Fig.2b how $\varphi_A(z)$ is affected by the structure of the iso–octane and butanol molecules. Compared with Fig. 2a, it can be seen that the λ_B of iso–octane is shorter than that of n–C_8, and very close to n–C_5 (or n–C_6). We notice that the iso–octane we used is 2, 2, 4 –trimethyl pentane. Then those molecules have a molecular length similar to n–C_5. This molecular structure will cause a similar disturbance on the interfacial structure as the n–C_5 molecules.

For butanol molecules, the hydroxyl group, OH, is attached to a alkane chain. As we mentioned earlier, those hydroxyl groups will repel paraffin segments and tend to become mutually associated by intermolecular hydrogen bonding. This tendency will cause a remarkable disturbance on the interfacial structure. It can be seen from Fig. 2b that oscillations of $\varphi_A(z)$ occur in butanol solutions. If the density (or the volume fraction) of the hydroxyl group is plotted versus the distance from the solid surface, a profile of the density of the OH group in the interfacial regions is obtained (see Fig.3), showing oscillations in the $\varphi_{OH}(z)$ curve . This indicates that some specific ordering and structuring take place in the interfacial regions.

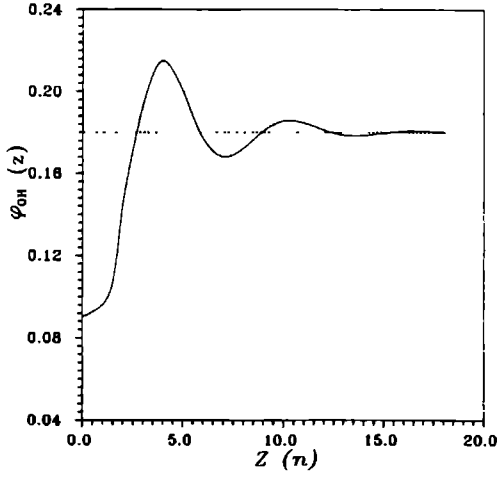

FIG.3. Profiles of the OH group in butanol molecules, plotted vs distance z. The oscillations indicate the specific ordering and the structuring occurring in the interfacial regions.

In order to clarify the ordering and the structuring, a segment order parameter can be calculated for both n–$C_{25}H_{52}$ molecules and butanol molecules. The segment order parameters is defined as

$$s = (3<\cos^2\alpha> - 1) / 2, \tag{12}$$

where α is the angle between the axis of a unit and a given direction. Here, the orientations of the segments refers to the normal to the solid surface. For a certain species, the order parameter $s(z)$ is a function of z. In the case of a chain molecule, we use $<s(z)>$, which is the ensemble average over all segments of the molecule, to characterize the ordering of this molecule. According to the definition of the order parameter, if $<s(z)> = -0.5$, all bonds of the molecule are completely parallel to the solid surface. If all bonds of the molecule are perpendicular to the surface, $<s(z)> = 1$. On the other hand, a random distribution of bonds leads to $<s(z)> = 0$ [26]. In Fig.4, the calculated values of the order parameter $<s(z)>$ of the solute and solvent molecules are plotted as a function of the distance z, for an n–$C_{25}H_{52}$/

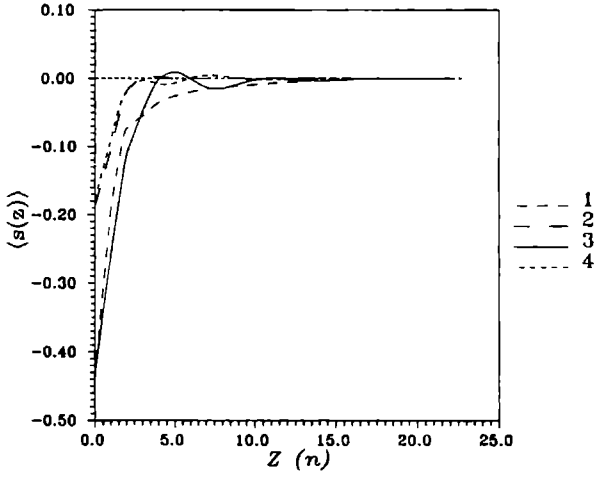

FIG.4. The order parameter $<s(z)>$ of solute and of solvent, plotted against distance z for the n–$C_{25}H_{52}$/n–C_5H_{12} system and the n–$C_{25}H_{52}$/butanol system. $\varphi_A = 0.1$, curve 1. the order parameter of n–$C_{25}H_{52}$ in the first system; Curve 2: that of n–C_5H_{12} in the first system, Curve 3: that of n–$C_{25}H_{52}$ in the second system; Curve 4; that of butanol in the second system.

butanol solution system In order to make a comparison, the parameter $<s(z)>$ for a n–$C_{25}H_{52}$/n–pentane solution system is also plotted in Fig 4.

First of all, it can be seen that in two cases, solute molecules are preferentially adsorbed parallel to the solid surface in the first fluid layer adjacent to the solid phase This kind of ordering also happens to a large extent to solvent molecules in the first fluid layer. For n–$C_{25}H_{52}$/n–C_5 solutions, this ordering disappears at $z = \lambda_k$ (k = A and B) due to the vanishing of the entropy effect. For the n–$C_{25}H_{52}$/butanol solution, two tendencies exist simultaneously· the ordering as n–$C_{25}H_{52}$/n–C_5 solutions and the additional ordering due to the OH group of butanol molecules. The latter can be considered as the perturbation of the OH group in the interfacial structure which causes the oscillations.

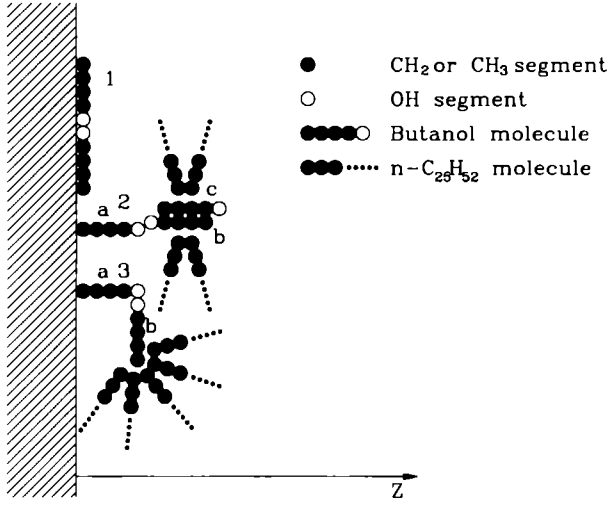

FIG.5. Illustration of the ordering and the structuring in the interfacial regions of the n–$C_{25}H_{52}$/butanol system. See the text for more details.

Based on the above–mentioned results, the specific ordering at the interface due to butanol molecules is illustrated Fig 5. This can be explained as a major character of this system. It can be seen from Fig.4 that some butanol molecules are ordered in the first fluid layer ($z = 0$) (indicated by 1 in Fig. 5), while many other butanol molecules are adsorbed perpendicular to the solid surface as a molecules in conformations 2 and 3. Due to the repulsion between the OH groups and the solid surface, the ends of the butanol molecules containing the OH group are oriented toward the fluid bulk, away from the surface. A

consequence of this is the fact that OH groups are very rich at $z = 4$ It can be seen in Fig 3 that a peak occurs in $\varphi_{OH}(z)$ at $z = 4$ The OH groups of those "perpendicular" butanol molecules will be associated with OH groups of other butanol molecules Typically, the OH groups of butanol molecules can be associated in two ways, denoted by z and 3, as shown in Fig 5 In the conformation 2, butanol molecule b is associated in parallel with a molecule a This association may be easily extended by a solvent molecule c attached to molecule b In this way the association structure may continue over some distances away from the surface This continuous association results in the second and the third peaks of $\varphi_{OH}(z)$ found in Fig 3 Correspondingly, this causes the ordering of solvent molecules perpendicular to the solid surface As can be seen in Fig 4, the resulting order parameter of the butanol molecules (curve 4) shows positive peaks in the layers corresponding to the middle positions of molecules a and molecules b in conformation 2 For conformation 3, a butanol molecules a is associated with a butanol molecule b which is parallel to the solid surface This conformation will explicitly result in the parallel ordering of solvent molecules at $z = 4$–5 This corresponds to a negative peak on curve 4 of Fig 4

Undoubtedly, this ordering and the structuring considerably influences distribution profiles of the density of the solute Because of the repulsion between CH_2 (or CH_3) groups and OH groups (which are abundant in the layer $z = 4$), the packing of the solute molecules parallel to the solid surface becomes almost untenable in the layer $z = 5$ Instead, the packing vertical to the solid surface becomes a favored conformation It then follows that the segmental density of the solute reaches a minimum in the layer $z = 5$ (see Fig 2b), and at the same time a positive peak appears on curve 3 of Fig 4 In the layer $z \simeq 10$, a similar behavior is observed For the aforementioned reason, conformation 2 will result in packing of solute molecules parallel to the surface in the layers $z \simeq 7$–8 This can be identified from the order parameter curve of solute molecules $<s(z)>$ which shows a negative peak at $z \simeq 7\ 5$ (see curve 3 in Fig 4) It can also be seen from profiles of the segmental density of the solute $\varphi_A(z)$ that a density peak occurs at $z \simeq 7\ 5$ (see Fig 2), implying that the segmental density of the solute increases due to parallel packing

The particular structuring and ordering due to the associations between butanol molecules is expected to form a certain network structure at the interface, which will affect the kinetic condition of crystal growth A direct influence is the enhancement of the diffusion resistance This network will obviously hinder the diffusion of paraffin molecules from the bulk to the crystal surface To transport a certain number of growth units to the crystal surface, an extra driving force is needed This implies that for a given system the supersaturation at the crystal surface is much smaller than the bulk supersaturation if $\sigma >> 0$ Our experimental results for $n\text{–}C_{25}H_{52}$ crystals show that although the edge energy ϕ_{str} (or

the roughening temperature T^r) increases by only about 2% from n–hexane solutions to butanol solutions, the critical supersaturation of kinetic roughening σ^c in the bulk phase increases by about a factor 10. Moreover, at the same bulk supersaturation, n–$C_{25}H_{52}$ crystals grow much more slowly in butanol solutions than in n–hexane solutions.

D. Mixture of solvents: thermodynamic properties and the interfacial structure

In the light of the results presented in the foregoing sections, it may be interesting to examine systems of paraffin crystals in contact with a two–solvent mixture solution. We notice that the relevant equations presented above were derived on the basis of binary solution systems. However, it can be seen from the discussions in the Appendix that the principles may straightforwardly be applied to multi–component solution systems, giving rise

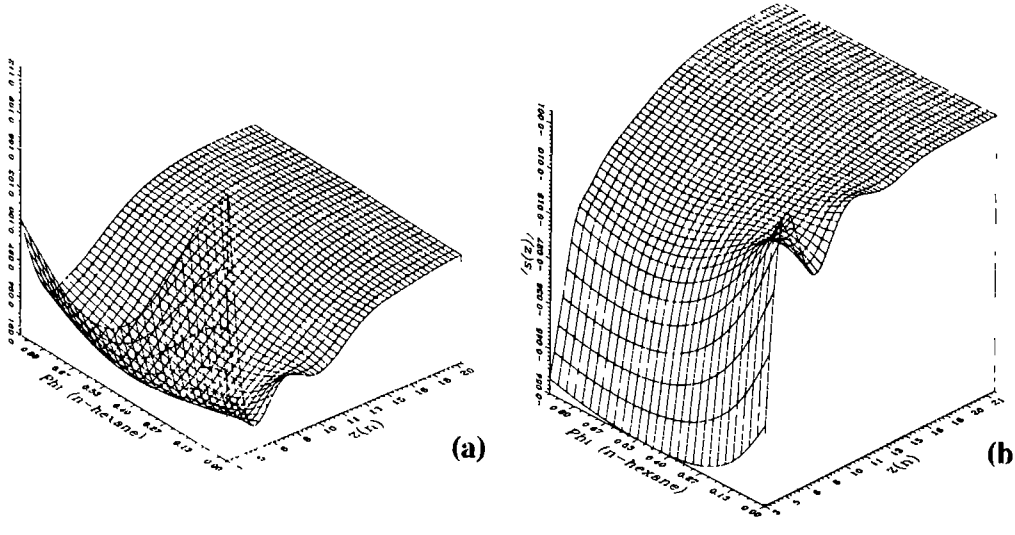

FIG.6. (a) Profiles of the segmental density $\varphi_A(z)$ [expressed by $Phi(z)$ (solute) in the figure] of n–$C_{25}H_{52}$ in the n–$C_{25}H_{52}$/butanol/n–hexane ternary system, plotted versus distance z and the bulk concentration of n–hexane φ_B [expressed by Phi(n–hexane) in the figure] φ_A = 0.1, $\varphi_B + \varphi_C = 0.9$ (φ_C: the bulk concentration of butanol). (b) The order parameter of n–$C_{25}H_{52}$ in the ternary system, plotted as functions of z and φ_B, the bulk concentrations are the same as (a). In the ternary solution system, that $\varphi_B = 0$ corresponds to the n–$C_{25}H_{52}$/n–hexane binary system. The specific character of the ordering in the n–$C_{25}H_{52}$/butanol disappears when an amount of n–hexane ($\varphi_B \geq 0.3$) is present in the system.

to analogous equations (see Appendix).

In the following, we will treat ternary interfacial systems consisting of n–$C_{25}H_{52}$, (denoted by A), butanol (denoted by C) and n–hexane (denoted by B), by self–consistent field calculations. In our discussions, we first start with a n–$C_{25}H_{52}$/butanol binary solution system. The n–hexane is gradually added into the system, in order to enable observation of the changes of the interfacial structure and thermodynamic properties of the system. Finally, we end up with the n–$C_{25}H_{52}$/n–hexane system. During the entire process, the bulk concentration of n–$C_{25}H_{52}$ is maintained at $\varphi_A = 0.1$. This implies that $\varphi_B + \varphi_C = 0.9$.

Figure 6a shows how the profiles of the segmental density of the solute $\varphi_A(z)$ change with increasing concentration of n–hexane φ_B. In comparison, the variation of the order parameter $<s(z)>$ of the solute due to the change of φ_B is given in Fig. 6b. Obviously, the oscillations of the profiles of n–$C_{25}H_{52}$/butanol systems due to the particular structuring and ordering will gradually disappear with increasing φ_B. The specific behavior of the n–$C_{25}H_{52}$/butanol system is hardly observed in Fig.6 when $\varphi_B/\varphi_C \geq 2/7$ (or $\varphi_B \geq 0.2$). This can be attributed to the stronger interaction of the n–hexane molecules with the crystal surface than the butanol molecules. We notice that this is consistent with the result relating the corresponding scaling factors that C_ℓ^*(n–hexane) > C_ℓ^*(butanol) (see Table II).

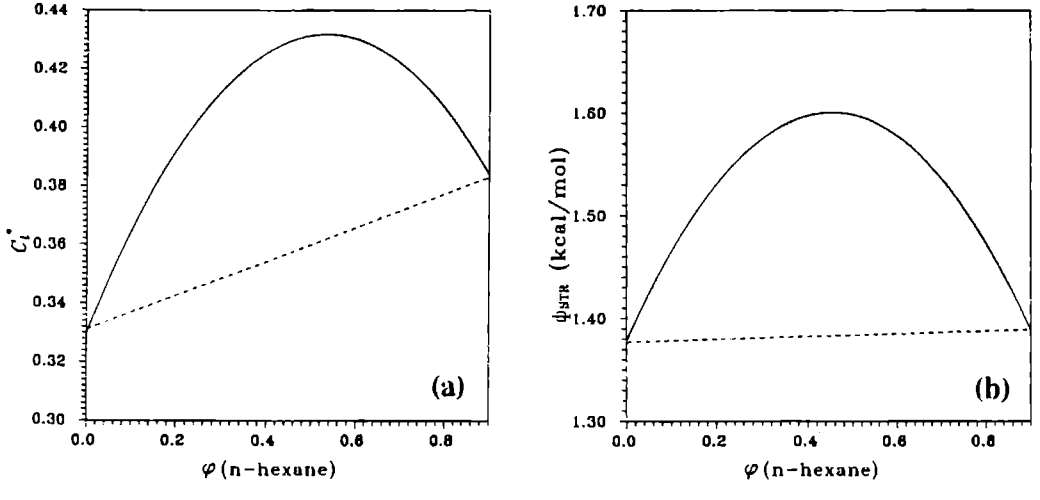

FIG.7. (a) The surface characteristic scaling factor C_ℓ^* of the ternary system (see the caption of Fig.6) plotted versus the concentration of n–hexane. (b) The step energy plotted as a function of the concentration of n–hexane.

The surface characteristic scaling factor C_ℓ^* shows an unexpected behavior in the ternary solution system when the concentration of n–hexane increases (see Fig 7a) The change of C_ℓ^* is not linear (indicated by the broken line) with increasing φ_B, but approximately parabolic This implies that a maximum of C_ℓ^* occurs at a certain concentration of solvents (in this system $\varphi_B \simeq 0\,5$), and C_ℓ^* (max) > C_ℓ^* (n–hexane) A consequence of Fig 7a is that in any case, when a small amount of the second solvent (or impurity) is added to a binary solution system, C_ℓ^* always increases

As a consequence of Fig 7a, it may also be interesting to see the change of the edge energy ϕ_{str} with increasing φ_B This can be obtained from Eq (7) and the experimental and calculated data presented earlier According to Eq (7), for a given crystal structure, ϕ_{str} depends on C_ℓ^* and Δh_{diss} Since C_ℓ^* has been calculated and presented in Fig 7a, the main problem now is to estimate for the various φ_B, the value of Δh_{diss} of the ternary system Based on Eqs (A 13b) and (A 14b), Δh_{diss} can be expressed for this ternary regular solution system as

$$\Delta h_{diss} = \Delta h_m + X_B^2\, W_{AB} + X_C^2\, W_{AC} \tag{13}$$

Now, the key point is to estimate Δh_m It is however difficult to find accurate data in the literature We assume that for the n–$C_{25}H_{52}$/n–$C_{12}H_{26}$ binary solution system, the solvent molecules n–$C_{12}H_{26}$ have a similar structure and thermodynamic behavior as the solute molecules n–$C_{25}H_{52}$ in the liquid phase This implies that the mixing between the two components is ideal Then the enthalpy of dissolution of this system can be used to estimate the enthalpy of melting ($\Delta h_{diss} \simeq \Delta h_m$) Subsequently, W_{AB} and W_{AC} may therefore be estimated from the difference between the quantity Δh_{diss} of n–$C_{25}H_{52}$/n–hexane and the quantity Δh_m together with the difference between Δh_{diss} of n–$C_{25}H_{52}$/n–butanol system and Δh_m, respectively From the data listed in Table I, it turns out that $W_{AB} \simeq 688$ cal/mol and $W_{AC} \simeq 3768$ cal/mol Based on those results, ϕ_{str} is plotted as a function of φ_B in Fig 7b It can be seen that the shape of the ϕ_{str} curve is somewhat similar to the shape of C_ℓ^*

The results of this section are relevant for understanding the influence of impurities on the edge energy or the free energy For crystals in contact with a binary solution, the addition of a small amount of the third component (or impurity) usually results in an increase of the edge energy of the crystal surface

IV DISCUSSION AND CONCLUSION

In Sections II and III, the influence of solvents on the interfacial structure and interfacial

properties of n–paraffin solution systems have been discussed from both the theoretical and experimental points of view. In general, it can be said that the interfacial properties, such as the edge energy and the edge free energy, depend, first, on the bulk properties, (such as the enthalpy of dissolution), and second on the ordering and the structuring of interfaces. The former is correlated to the degree of matching between the solute and the solvent molecules in the liquid bulk phase. The latter is to a large extent determined by the geometrical and the bonding structure of the fluid units. Different types of solvents may result in completely different interfacial structures at the crystal surface, which then significantly affect the interfacial properties. In this sense, the properties of the solvent may in many cases exert a stronger influence on the interfacial regime than the bulk properties.

We note that similar investigations on the edge free energy in relation to ordering in crystal–solution interfaces for the naphthalene crystal system have been carried our by Elwenspoek et al [28-29]. In their studies, a non–equivalent wetting case has been identified ($\phi_i \neq \Phi_i$, meaning that $C_\ell^* \neq 1$). To interpret their observations, they suggested that a certain–smectic–like ordering of fluid naphthalene molecules occurs near the crystal surface. This ordering of solute molecules could be optimized or disturbed by different types of solvents, which might lead to a reduction or an increase of the step free energy in the presence of solutions. In fact, the idea of ordering of the interfacial fluid units is very much in line with the modern concepts of the solid–fluid interfaces [16-23]. However, the main interpretations of the influence of different solvents (such toluene and n–hexane) on the edge free energy of the crystal surface are inaccurate both experimentally and theoretically.

First, the edge free energies of the crystal surfaces were measured by determining the critical supersaturation of kinetic roughening σ^c. Since σ^c is related to kinetic processes, volume transport resistances play a certain role under experimental conditions. These resistances consume a certain amount of driving force. This has the consequence that the bulk value of σ^c(bulk) is larger than the corresponding value σ^c(interface) at the interface. This implies that to derive directly the absolute value of the surface free energy from the data of σ^c(bulk), the resistance effect needs to be taken into account [37]. {Only when the actual temperature is slightly lower than T^r and σ^c is very close to zero, may the volume resistances be neglected [σ^c(bulk) $\simeq$ σ^c(surface)]. Then the edge free energy can directly be derived from σ^c(bulk).} In the case of naphthalene crystals, the actual temperature is far from T^r of the crystal faces in various systems. Obviously, if the volume transport resistances are not taken into account, the comparison of the edge free energy between different solution systems will be misleading.

Secondly, the picture of the ordering of the interface and the influence on the edge free energy (or the edge energy) proposed by Elwenspoek *et al* [28-29] is rather vague. In his model,

Elwenspoek on one hand realized the failure of the equivalent wetting condition in the prediction of the edge energy of the crystal surface, but on the other hand limited his investigation to the trivial terms $\phi_1^{Sk} - \phi_1^{Ak}$ [see (A 18) and (A 19a)], without abandoning the homogeneous phase approximation Since as is known [14], the main drawback of the equivalent wetting is the homogeneous phase approximation, it is not surprising that his analysis based on cell models led to a contradictory conclusion [28-29]

It can be seen from our recent investigations [14-15] and the discussions given in the foregoing sections that, for the purpose of describing the interface, the inhomogeneous cell model should replace the homogeneous cell models employed in the past Moreover, not only solute molecules but also solvent molecules in the interfacial regions are ordered Generally speaking, the ordering is due to the energy and the entropy effect Therefore, the solid–fluid interaction, the fluid–fluid interaction and the molecular conformations of the fluid units can directly affect the ordering, and consequently the interfacial structure profiles of the density of fluid units (Note that the fluid includes both the solute and the solvent, so that the interfacial structure is commonly determined by solute and solvent units) Regardingless of the value of the enthalpy of dissolution, the edge energy and edge free energy, as indicated by (5b), are determined directly by the concentration of solute at the surface This depends on the competition between the solute and the solvent molecules at the surface If due to a certain interfacial structure solute molecules are preferentially adsorbed on the surface, $X_A(0)$ will be enhanced Then the edge energy will in principle decrease If solvent molecules are strongly adsorbed onto the surface $X_A(0)$ will decrease This results in an increase of ϕ_{str}, otherwise it results in a decrease

Concerning the influence of solvent molecules on the character of the roughening transition, it can be seen from Table II that, in the case of n–paraffin crystals growing from alkane solutions (including iso–octane solutions), the roughening transition is first order According to our investigations[11-12], this special type of roughening transition is due to the coupling of the conventional Kosterlitz–Thouless roughening transition [2-3] and a surface structural phase transition, in the neighborhood of the roughening temperature The results from our experiments indicate that solvent molecules having a basic intermolecular bond structure similar to that of the solute paraffin molecules may stimulate the surface to undergo a structural phase transition, a subsequently a first–order roughening transition Solvent molecules having a different functional group (such as the OH group) within the molecular structure or having a different intermolecular bond structure (such as toluene) may result in a particular interfacial structure That particular interfacial structure may substantially reduce the influence of fluid units on solid units at the surface This will prevent the

occurrence of the surface structural phase transition, and thus the first order phase transition

ACKNOWLEDGEMENTS

We acknowledge Professor Dr Bennema and Dr C Strom for stimulating discussions and a critical reading of this manuscript We would like to thank Shell Nederland B V for supporting this research

APPENDIX

The thermodynamic properties of the multi–component systems can be expressed in a similar way to those of binary systems, within the framework of the mean field or Bragg–Williams approximation [13] The essential assumptions of this approximation are that the free enthalpy of mixing (per mole) is expressed as

$$<\Delta g^{mix}> = <\Delta h^{mix}> + <\Delta S^{\circ}{}^{mix}> \qquad (A\ 1)$$

where the molar enthalpy of mixing is given by

$$<\Delta h^{mix}> = \sum_{k,l} \tfrac{1}{2} X_k X_l W_{kl} \qquad (A\ 2)$$

The molar entropy of mixing is ideal and is given by

$$<\Delta S^{\circ}{}^{mix}> = -R \sum_{k} X_k \ln X_k \quad (R \text{ the gas constant}) \qquad (A\ 3)$$

W_{kl} is the exchange energy between molecules of type k and l, and is written as

$$W_{kl} = \sum_{i=1}^{m} \Phi_i^{\sigma}(kl), \quad \Phi_i^{\sigma}(kl) = \Phi_i^{kl} - \tfrac{1}{2}(\Phi_i^{kk} + \Phi_i^{ll}) \qquad (A\ 4a,b)$$

Obviously, $W_{kk} = 0$ and $W_{kl} = W_{lk}$ [This is the reason that a factor $\frac{1}{2}$ appears in Eq (A 2)]

From thermodynamics, the free enthalpy of a multicomponent solution is

$$G_{solution} = \sum_{k} G_k + \Delta G^{mix} \qquad (A\ 5)$$

Here G_k is the free enthalpy of pure liquid k Assuming that A denotes the solute of the solution, then the chemical potential of a solute unit in the solution is

$$[\mu_A]_{\text{solution}} = \left[\frac{\partial \Delta G^{\text{mix}}}{\partial N_A}\right]_{T,P,\{N_k\}} = \left[\frac{\partial G_A}{\partial N_A}\right]_{T,P} + \left[\frac{\partial \Delta G^{\text{mix}}}{\partial N_A}\right]_{T,P,\{N_k\}} \tag{A 6}$$

Here N_A is the number of solute units and N_k is the number of k type of units (Note that in Eq (A 6) $N_A \notin \{N_k\}$) It follows from Eq (A 6) after substituting ΔG^{mix} $(= \Sigma N_k \Delta g^{\text{mix}})$ given by (A 1) that

$$[\mu_A]_{\text{solution}} = [\mu_A]_A + RT \ln X_A + \sum_{k \neq A} X_k^2 W_{Ak} \tag{A 7}$$

Note that $[\mu_A]_A = [\partial G_A / \partial N_A]_{T,P}$ is derived for the pure liquid state A, and the molar enthalpy of mixing A with solvents is given by

$$<\Delta h_A^{\text{mix}}>_{\text{solution}} = \left[\frac{\partial \Delta H^{\text{mix}}}{\partial N_A}\right]_{T,P,\{N_k\}} = \sum_{k \neq A} X_k^2 W_{Ak} \tag{A 8}$$

$(\Delta H^{\text{mix}} = \Sigma N_k \Delta h^{\text{mix}})$ Assume that solvent units can not be incorporated into the crystals In the case of thermodynamic equilibrium, the chemical potential of A in the crystal is equal to $[\mu_A]_{\text{solution}}$ for a given P and T It follows from (A 7) that

$$[\mu_A]_S = [\mu_A]_A + RT \ln X_A + <\Delta h_A^{\text{mix}}>_{\text{solution}} \tag{A 9}$$

$$[\mu_A]_S - [\mu_A]_A = \Delta h_m(T,P) - T \Delta S^{\circ}{}_m(T,P) \tag{A 10}$$

According to statistical thermodynamics, $\Delta h_m(T,P)$ has the form

$$\Delta h_m(T,P) = \sum_{i=1}^{m} \tfrac{1}{2}(\Phi_i^{AA} - \Phi_i^{SS}), \tag{A 11}$$

$$\Delta h_{\text{diss}} = \Delta h_m + <\Delta h_A^{\text{mix}}>_{\text{solution}} \tag{A 12}$$

Finally, the usual expression for the solubility of regular solutions is obtained,

$$\ln X_A = -\frac{\Delta h_{diss}}{RT} + \frac{\Delta S^\circ_{diss}}{R}, \quad \Delta h_{diss} = \sum_{i=1}^{m} \Phi_i, \tag{A 13a,b}$$

$$\Phi_i = \tfrac{1}{2}(\Phi_i^{AA} - \Phi_i^{SS}) + \sum_{k \neq A} X_k^2 \Phi_i^q(kl), \Delta S^\circ_{diss} \simeq \Delta S^\circ_m \tag{A 14a,b}$$

The bond energy of the interface ϕ_i is generally expressed within the framework of cell models as

$$\phi_i = \phi_i^{sf} - \tfrac{1}{2}(\phi_i^{SS} + \phi_i^{ff}) \tag{A 15}$$

According to the mean field approximation, the multicomponents are distributed at random and the mixture behaves as a uniform liquid with average intermolecular potential

$$<\phi_i^{ff}> = \sum_{k,l} X_k X_l \phi_i^{kl} \tag{A 16}$$

Similarly, the solid units are treated as if they have their own type of equilibrium liquid with average intermolecular potential

$$<\phi_i^{sf}> = \Sigma X_k \phi_i^{\gamma k} \tag{A 17}$$

Combining (A 15)–(A 17) yields

$$\phi_i = \tfrac{1}{2}(\phi_i^{AA} - \phi_i^{SS}) + \sum_{k \neq A} X_k^2 \phi_i^{\sigma}(Ak) + \Delta_i' \tag{A 18}$$

$$\Delta_i' = \sum_k X_k (\phi_i^{Sk} - \phi_i^{Ak}), \phi_i^{\sigma}(AK) = \phi_i^{Ak} - \tfrac{1}{2}(\phi_i^{AA} + \phi_i^{kk}) \tag{A 19a,b}$$

It can be seen that Eq (A 18) is similar to Eq (2) Based on Eqs (A 14a) and (A 18), the surface scaling factor C_ℓ and the surface characteristic scaling factor C_ℓ^γ can also be given for crystals in contact with multicomponent solutions According to the definition [14-15], the surface scaling factor is expressed as

$$C_\ell = \sum_{i=1}^{m} \phi_i / \sum_{i=1}^{m} \Phi_i = C_\ell^\gamma + C_\ell \tag{A 20}$$

$$C_{\ell}^{*} = \Delta h_{\mathrm{diss}}^{\mathrm{I}} / \Delta h_{\mathrm{diss}} = \frac{\sum_{i=1}^{m} [-\tfrac{1}{2}(\phi_i^{AA} - \phi_i^{SS}) + \Sigma_{k \neq A} X_k^2(0)\ \phi_i^{\sigma}(Ak)]}{\sum_{i=1}^{m} [-\tfrac{1}{2}(\Phi_i^{AA} - \Phi_i^{SS}) + \Sigma_{k \neq A} X_k^2\ \Phi_i^{\sigma}(Ak)]}, \tag{A 21}$$

and

$$C_{\ell} = \sum_{i=1}^{m} \Delta_i' / \Delta h_{\mathrm{diss}} \tag{A 22}$$

In the case of regular solutions, the term $\phi_i^{Sk} - \phi_i^{Ak}$ is normally a very small number, compared to Δh_{diss}. It then follows that $C_{\ell}^{*} \simeq 0$ and $C_{\ell} \simeq C_{\ell}^{*}$ In connection with the concentration (or the density) of solute in different regions, C_{ℓ}^{*} can be derived in the same way as shown in Ref 14, so that Eq (5b) still holds

REFERENCES

1 J D Weeks and G H. Gilmer, in *Advances in Chemical Physics*, Vol 40, edited by I. Prigogine and S.A. Rice, (Wiley, New York, 2979) p 157.

2 J M. Kosterlitz and D J Thouless, J Phys C6, 1181 (1973).

3 J M. Kosterlitz, J Phys C7, 1046 (1974)

4 H F.J Knops, Phy Rev Lett **39**, 766 (1977)

5 P Bennema and J P van der Eerden, in *Morphology of Crystals*, edited by I Sunagawa, (Terra, Tokyo, 1987)

6 G H. Gilmer and K.A. Jackson, in *Current Topics in Materials Science*, Vol 2, edited by E. Kaldis, (North–Holland, Amsterdam, 1977)

7 S G. Lipson and E. Polturak, in *Progress in Low Temperature Physics*, edited by D F Brewer, (Elsevier, Amsterdam, 1987)

8 A Pavlovska and D Nenow, J Cryst Growth **39**, 346 (1977)

9 A. Pavlovska, J Cryst. Growth **46**, 551 (1979)

10 X.Y. Liu, P Bennema and J P van der Eerden, Nature **356**, 778 (1992)

11 X.Y. Liu, P van Hoof and P Bennema, Phys Rev Lett **71**, 109 (1993)

12 X.Y. Liu, Phys. Rev B**48**, (1993) (in press)

13 S.R. Fowler and E.A. Guggenheim, *Statistical Thermodynamics* (Cambridge Univ Press, London, 1960).

14 X.Y. Liu and P Bennema, J. Chem. Phys. **98**, 5863 (1993).

15 X.Y. Liu and P Bennema, J Chem. Phys **97**, 3600 (1992)

16 J.A. Cherepanova and A.V. Stekolnikov, in *Proc 11th Symposium on Industrial Crystallization*, edited by A Mersmann (Garmish–Partenkirchen, 1990), p 861

17 A D J Haymet and D W Oxtoby, J Chem Phys **74**, 2559 (1981)

18 A Bonissent, in *Interfacial Aspects of Phase Transformations*, edited by B Mutaftschiev (Reidel, Dodrecht, 1982)

19 U Landman, C S Brown and C L Cleveland, Phys Rev Lett **45**, 2032 (1980)

20 J D Weeks, J Chem Phys **67**, 3106 (1977)

21 M Baus and J L Colot, Mol Phys **55**, 653 (1985)

22 J Q Broughton and G H Gilmer, J Chem Phys **79**, 5095, 5105, 5119 (1983), **84**, 5741, 5749, 5759 (1986)

23 G C McGonigal, R H Bernhardt, Y H Yeo and D J Thomson, J Vac Sci Tech B**9**, 1109 (1991)

24 J M H M Scheutjens and G J Fleer, J, Phys Chem **83**, 1619 (1979), **84**, 178 (1979)

25 J M H M Scheutjens and G J Fleer, Macromolecules **18**, 1882 (1985)

26 F A M Leermakers and J M H M Scheutjens, J Chem Phys **89**, 3264 (1988), **89**, 6912 (1988), J Phys Chem **93**, 7417 (1989)

27 The calculations of SCF theories can be carried out using the computer program called "Goliath", which has recently been developed by the Department of Physics and Colloid Chemistry of Wageningen University

28 M Elwenspoek, Mol Phys **64**, 229 (1988)

29 M Elwenspoek, P Bennema and J P van der Eerden, J Cryst Growth **83**, 297 (1987)

30 S C Nyburg and J A Potworowski, Acta Cryst B**29**, 347 (1973)

31 P Bennema, X Y Liu, K Lewtas, R D Tack, J J M Rijpkema and K J Roberts, J Cryst Growth **121**, 679 (1992)

32 D H M Beiny and J W Millin, J Chem Eng Data **32**, 9 (1987)

33 X Y Liu and P Bennema, J Cryst Growth **128**, 69 (1993)

34 M G Broadhurst, J Res Nat Bur Std (US) 66A, 241 (1962)

35 A S Wingrove and R L Caret, *Organic Chemistry*, (Harper & Row, New York, 1981)

36 X Y Liu and P Bennema, Phys Rev **E** (in press)

37 X Y Liu, G Arkenbout, P Bennema, P van Hoof, J Cryst Growth (in press)

Chapter 5

MORPHOLOGY OF CRYSTALS: INTERNAL AND EXTERNAL CONTROLLING FACTORS

The morphology of crystals: internal and external controlling factors

Xiang–Yang Liu and P. Bennema

RIM, Laboratory of Solid State Chemistry, Faculty of Science, University of Nijmegen, Toernooiveld, 6525 ED Nijmegen, The Netherlands.

ABSTRACT–Internal and external factors which influence the morphology of crystals are studied based on an inhomogeneous cell model. After discussing the reason of the failure of two basic assumptions: the equivalent wetting condition and the proportionality condition, the influence of the ambient phase is explicitly taken into account in terms of the surface characteristic scaling factor C_l^{γ}. In connection with the solid–fluid interfacial structure which is commonly determined by the crystal and the ambient phase, C_l^{γ} will provide the essential information concerning how the morphology of crystals is affected. Within the framework of our formalism, internal and external factors controlling both equilibrium forms and growth forms of crystals are described separately. This offers a guideline for the modification of the habit of crystals. To describe the morphology of crystals, the Periodic Bond Chain (PBC) analysis can be used to determine the internal controlling factors, and the Interfacial Structure (IS) analysis, which is developed in this paper, can be used to determine the external controlling factors. These analyses are applied to predict the growth forms of orthorhombic n–paraffin crystals.

I. INTRODUCTION

As a historical subject, the morphology of crystals has drawn attention for centuries Initial problems were related to why a particular crystal possesses a certain shape when it grows from a certain environment With the development of theories in crystal growth mechanisms and in the structure of the solid–fluid interface [1-2], knowledge of this subject has been improving Recently, research on the influence of tailor–made additives on the morphology of crystals has been carried out for various practical reasons It is known that the morphology of crystals is controlled both by the structure of crystals and the growth parameters [1-2] As was realized nearly three hundred years ago [3], the anisotropy of the growth rates determines the morphology of crystals This anisotropy is partly determined by the crystal structure, but can be drastically influenced by the growth parameters Therefore, as a key step for the molecular design of tailor–made additives, understanding the internal and external factors affecting the morphology of crystals is necessary

To predict the growth morphology of crystals, theories like the Hartman–Perdok theory [4-8], have been developed According to the principles of the Hartman–Perdok theory, the relative growth rate of faces $\{hkl\}$ on crystals is assumed to be proportional to the attachment energy of faces $\{hkl\}$ E^{a}_{hkl} This is the energy released per structural unit when a slice of crystal (with the thickness d_{hkl}) is attached to the crystal surface [8] This relationship between the relative growth rate and E^{a}_{hkl} has been justified by Hartman and Bennema,[7] based on the theories of growth kinetics and certain conditions like the proportionality condition (this condition will be discuss in the next section) This theory is successful to some extent, especially in the case that crystals are grown from the vapor phase However, in many cases discrepancies between the theoretical morphology and the observed morphology occur especially when crystals are grown from solutions or the melt To remove this difficulty, some prescriptions based on statistical mechanical Ising models have been developed to predict the growth forms of crystals [2,9-10] In the context of these prescriptions, the concept of roughening phase transition is introduced This implies that the influence of the ambient phase is to some extent taken into account Indeed, compared with various theories, the results obtained from the approach of roughening transition theories are much closer to reality [9-10] Nevertheless, some deviations still remain

We notice that the crystal surfaces are boundaries between the crystal phase and the ambient phase (including solute, solvents and impurities) Therefore, in the growth process or when crystals are in equilibrium with their mother phase, the structures of both the crystal and the ambient phase will influence the shape and the size of the surfaces of the crystals, and the morphology of the crystals Since the growth of crystals is determined by thermodynamic

driving forces, parameters, such as temperature and supersaturation, will also affect the morphology of crystals In the cases of the Hartman–Perdok theory and Ising models, although the influence of the mother phase can be taken into account in a limited way, they are still based on the assumption that the structure and molecular behavior of solid and solute molecules is similar (This is one of the basic assumptions of cell models The proportionality condition results from this similarity) Hence those theories are still mainly based on the structure and properties of crystal phases This is the main cause of the discrepancies between predicted and observed growth forms.

Contrary to growth forms, the equilibrium form of a crystal can unambiguously be described using the surface free energy of the faces $\{hkl\}$, according to the Gibbs–Wulff theorem [11] However, calculations of the surface free energy for crystallographic orientations $\{hkl\}$ remain problematic due to lack of knowledge of the structure of the solid–fluid interface

This paper describes a study on the morphology of crystals from both points of view of the internal structure of crystals and the external effects of the ambient phase We will start from the interfacial region to analyze the mutual influence of both the solid and the ambient phase on the morphology of crystals The basic idea is that we first analyze the influence of the solid structure (this can be done by the conventional PBC analysis or the network analysis [1-2,8]) The results of the PBC analysis are coupled with the influence of the ambient phase (or fluid phase). Since the interactions between the solid and the fluid phase occur at the solid–fluid interface, this coupling is related to the interfacial structure In order to characterize this coupling, a so–called surface characteristic scaling factor $C_{\hat{l}}$ is introduced The following discussions will be primarily devoted to investigating this factor Note that other growth parameters, such as the supersaturation, which may also affect the growth morphology of crystals, will be left out of consideration for the time being

II TWO BASIC ASSUMPTIONS AND THE RELATION TO AN INHOMOGENEOUS CELL MODEL

In the world of crystal growth, cell models or Ising models are commonly used, both implicitly and explicitly In cell models, both the crystal and the ambient phase are divided into cells of the same shape and size When each cell has m bonds connecting to neighboring cells, the dissolution enthalpy (per structural unit) for a solution system consisting of the solute A and the solvent B is given by

$$\Delta \bar{H}_{\mathrm{diss}} = \sum_{j=1}^{m} \Phi_j \qquad (1)$$

Here Φ_j is the exchange bond energy between cells in the two bulk phases in the j^{th} direction, and is expressed as [12-14]

$$\Phi_j \simeq \tfrac{1}{2}(\Phi_j^{AA} - \Phi_j^{SS}) + (1 - X_A)^2 \Phi_j^{\sigma} \tag{2a}$$

and

$$\Phi_j^{\sigma} = \Phi_j^{AB} - \tfrac{1}{2}(\Phi_j^{AA} - \Phi_j^{BB}) \tag{2b}$$

where X_A is the mole fraction of solute A, the superscripts AA, BB, AB, SS represent the interaction of solute–solute units, solvent–solvent units, solute–solvent units and solid–solid units respectively.

We notice that we still cannot use expressions (1) and (2a) to calculate Φ_j directly from experimental data The values of Φ_j^{SS} in Eqs (2a) and (2b) may often be calculated from general physical chemical consideration or quantum chemical considerations However, the values of Φ_j^{AA}, Φ_j^{BB} and Φ_j^{AB} are normally unknown In order to overcome this difficulty *the proportionality condition* was introduced [1-2] This condition implies that in this case the bond energies Φ_j^{AA}, Φ_j^{BB} and Φ_j^{AB} are supposed to be proportional to Φ_j^{SS}. In other words for bonds in all directions, we may write

$$\Phi_1\ \Phi_2\ \cdots \Phi_j\ \cdots \Phi_m = \Phi_1^{AA}\ \Phi_2^{AA}\ \cdots\ \Phi_j^{AA} \cdot \cdots\ \Phi_m^{AA} = \cdots$$
$$= \Phi_1^{AB}\ \Phi_2^{AB} \cdot \cdots\ \Phi_j^{AA}\ \cdots\ \Phi_m^{AD} = \Phi_1^{SS}\ \Phi_2^{SS}\ \cdots\ \Phi_j^{SS}\ \cdots\ \Phi_m^{SS} \tag{3}$$

From Eq (3) we find

$$\Phi_j \Big/ \sum_{k=1}^{m} \Phi_k = \Phi_j^{SS} \Big/ \sum_{k=1}^{m} \Phi_k^{SS}. \tag{4}$$

It then follows from Eq.(4) that, after substituting Eq (1),

$$\Phi_j = (\Phi_k^{SS} / E_{ss}^{cr}) \Delta \tilde{H}_{diss}, \tag{5}$$

$$E_{ss}^{cr} = \sum_{k=1}^{m} \Phi_k^{SS} \tag{6}$$

which is the crystallization energy if a molecule crystallizes from a very dilute vapor, in the absence of interaction between molecules. It has to be noted that normally the proportionality condition introduced in (3) is associated with the equivalent wetting condition when morphological issues are discussed It follows that Eq (3) is equally applicable to different faces on a crystal. This implies that the anisotropy of the interaction energies of a

solid–fluid system is the same as that of the crystal structure In other words, the morphology referenced to vacuum is supposed to be the same as that referenced to the fluid phase

The exchange bond energy between the first interfacial fluid layer adjacent the the solid phase and the first interfacial solid layer adjacent to the fluid phase, is expressed by [12,14]

$$\phi_j = \tfrac{1}{2}(\phi_j^{AA} - \phi_j^{SS}) + [1 - X_A(0)]^2\,\phi_j^{\sigma} + X_A(0)(\phi_j^{SA} - \phi_j^{AA}) + [1 - X_A(0)](\phi_j^{SB} - \phi_j^{AB}) \tag{7}$$

$X_A(0)$ is the concentration of the solute in the first fluid layer, the expression for ϕ_j^{σ} is similar to (2b), and the superscripts SA and SB denote the solid–solute, solid –solvent interactions, respectively The value of ϕ_j is directly related to physical processes occurring at the solid–fluid interface, such as the roughening transition, 2–dimensional nucleation etc [1-2,12,14] The bond energies and the structure of the interface determine the growth kinetics and the growth rate of a crystal surface

To estimate the bond energy at the surface, *the so–called equivalent wetting condition* was for the first time introduced by Jackson [15] Although there are various expressions for the equivalent wetting condition depending on the case, in general this condition implies

$$\phi_j \simeq \Phi_j \tag{8}$$

As a consequence of Eq (8), various bond energies in the bulk phase (such as Φ_j^{SS}, Φ_j^{AA}, Φ_j^{AB} etc) are equal to the corresponding bond energies at the interface (such as ϕ_j^{SS}, ϕ_j^{AA}, ϕ_j^{AB} etc) It thus follows that the concentration of solute (or solvent) in the bulk phase X_A (or X_B) is equal to that at the interface This implies that both the fluid and the solid are completely homogeneous throughout the bulk up to the dividing surface [12,14] This is the so–called homogeneous phase approximation or the first approximation of the equivalent wetting On the other hand, it can be seen from Eq (7) that to fulfill Eq (8), we must have $\phi_j^{SA} \simeq \phi_j^{AA}$ and $\phi_j^{SB} \simeq \phi_j^{AB}$ [12] We call this the second approximation of the equivalent wetting condition

From past research on the growth and morphology of crystals, the equivalent wetting condition leading to (8) has turned out to be invalid in most cases For crystals grown from systems consisting of simple structural units, the use of the equivalent wetting condition underestimates ϕ_j, while for systems consisting of chain like molecules, the equivalent wetting overestimates ϕ_j According to our recent investigations [14], the main reason for the failure of

the equivalent wetting is the application of the homogeneous phase approximation Progress concerning the structure of crystal–fluid interfaces has been made recently by computer simulations and density–functional theories [16 20] The results show that due to the ordering of fluid layers and the relaxation or reconstruction of solid layers in the interfacial regions, the structure of the solid–fluid interface is different from that of the bulk This explicitly indicates that the homogeneous phase approximation and hence the equivalent wetting condition are invalid (Note that the second approximation of the equivalent wetting condition is somehow considered to be reasonable if the homogeneous phase approximation is modified) In addition, the interfacial structure in one crystallographic orientation is different from the others Therefore the proportionality condition is also questionable

To describe the solid–fluid interface of a crystal–solution system, the so–called inhomogeneous cell model has recently been developed [12,14,21] According to this model, the surface characteristic scaling factor is defined in the following way

$$C_{\ell}^{*} = \sum_{j=1}^{m} \phi_j / \sum_{j=1}^{m} \Phi_j = \Delta \tilde{H}_{diss}^{I} / \Delta \tilde{H}_{diss}, \tag{9a}$$

$$\Delta \tilde{H}_{diss}^{I} = \sum_{j=1}^{m} \phi_j \tag{9b}$$

This factor depends on the orientations of the crystal faces [21] In terms of the concentration or the density of the structural units, this factor can be written as [14]

$$C_{\ell}^{*} \simeq \ln X_A(0) / \ln X_A \tag{10a}$$

or in the case of crystals in contact with the melt, as

$$C_{\ell}^{*} \simeq \ln (\rho_f^{I} / \rho_s^{I}) / \ln (\rho_f / \rho_s), \tag{10'}$$

where ρ_f and ρ_s denote the density of structural units in the fluid and in the solid phase respectively, and the superscript "I" indicates the corresponding properties in the regions adjacent to the dividing plane between the solid and the fluid

Based on this factor, the character of solid–fluid interfaces can be classified in three different cases (i) equivalent wetting [$C_{\ell}^{*} = 1$, $X_A(0) = X_A$, this is the same expression as Eq (9a)], (ii) more than equivalent wetting case [$C_{\ell}^{*} < 1$, $X_A(0) > X_A$], and (iii) less than equivalent wetting case [$C_{\ell}^{*} > 1$, $X_A(0) < X_A$] The equivalent wetting case is an artificial reference state, which seldom occurs In contrast to this, the other two cases occur in most

systems. The more than equivalent wetting case implies that crystal surfaces show an adsorption effect to solute units, and the less than equivalent wetting indicates that the reverse effect occurs.

For an interfacial system consisting of isotropic structural units, profiles of the concentration of fluid units at the interface can be described by an exponential law [21] as

$$X_A(z) = X_A\,[1 + (X_A^{\zeta} - 1)\exp(-z/n^*)] \tag{11}$$

where z is the distance away from the solid surface (normalized by the interplanar distance of the crystal face d_{nhnknl}), the exponent $\zeta = C_{\ell}^* - 1$, n^* is the normalized characteristic thickness of the interface, and defined in such a way that at $z = n^*$, $[X_A(n^*) - X_A]/[X_A(0) - X_A] = e^{-1}$. Using Eqs. (9a) and (11), the surface free energy may in principle be calculated for interfacial systems of isotropic units if the factors C_{ℓ}^* and n^* are known [22].

We notice that within the framework of cell models the proportionality condition given by Eq.(3) is in principle valid for the bulk phase. However, directly extending Eq.(3) to all crystallographic orientations is invalid. Here we assume that the principle of the constancy of the ratio in of Eq.(3) can be independently applied to different crystallographic orientations. This means for crystal face $(h_i k_i l_i)$

$$\begin{aligned}&\phi_1^{(i)} : \phi_2^{(i)} : \cdots : \phi_j^{(i)} : \cdots : \phi_m^{(i)} = \Phi_1 : \Phi_2 : \cdots : \Phi_j : \cdots : \Phi_m \\ &= \Phi_1^{SS} : \Phi_2^{SS} : \cdots : \Phi_m^{SS}\end{aligned} \tag{12}$$

It follows from Eq.(9a) that for a particular orientation,

$$\begin{aligned}&\phi_1^{(i)}/\Phi_1 \simeq \phi_2^{(i)}/\Phi_2 \simeq \cdots \simeq \phi_j^{(i)}/\Phi_j \simeq \cdots \simeq \phi_m^{(i)}/\Phi_m \simeq \Delta\tilde{H}_{diss}^{I(i)}/\Delta\tilde{H}_{diss} = C_{\ell(i)}^* \\ &\text{or} \\ &\phi_1^{(i)}/\Phi_1^{ss} \simeq \phi_2^{(i)}/\Phi_2^{ss} \simeq \cdots \simeq \phi_j^{(i)}/\Phi_j^{ss} \simeq \cdots \simeq \phi_m^{(i)}/\Phi_m^{ss} \simeq C_{\ell(i)}^*\,\Delta\tilde{H}_{diss}/E_{ss}^{cr}.\end{aligned} \tag{13}$$

Equation (12) therefore holds for each crystallographic orientation i, provided the ratio C_{ℓ}^* depends on i. The surface characteristic scaling factor is explicitly used to scale the bond energy difference between the bulk phase and the interfacial phase in a certain crystallographic orientation. In order to get reasonable results, it is necessary to apply both (12) and (13). In contrast to the proportionally condition given by (3), Eqs. (12) and (13) are called ***the generalized proportionality condition***, and form the basis for the following

treatment. The following discussions are based on Eqs.(12) and (13). It can be seen that the proportionality condition is a special case of the generalized proportionality condition. Under the assumption that C_i^* is independent of the surface orientation, Eqs (12) and (13) reduce to Eq.(3).

Note that if Eq.(3) expresses to a large extent the basic factor determining the morphology of crystals due to the bond energy structure of crystals, Eq. (13) shows the modification in the morphology of crystals due to surface specific influence of the fluid phase (or the ambient phase) at equilibrium. This influence of the fluid phase includes mainly the conformation entropy effects of the fluid molecules. (In the case of crystal growth, kinematic factors, such as surface integration kinetics and mass and heat transport also play an important role. However, we will not discuss those kinematic factors in this paper.)

III. EQUILIBRIUM FORMS AND GROWTH FORMS OF CRYSTALS

A. Equilibrium forms

As mentioned in Sec.I, equilibrium forms of crystals can be described on the basis of the Gibbs–Wulff theorem. Within the framework of this theorem, equilibrium forms of crystals depend on the surface free energy in different orientations and can be constructed by Wulff plots. In Wulff plots, sharp cusps occur corresponding to all orientations of flat (or F) faces. In case the temperature is relatively low [1,11,24], the equilibrium form has a polygonal shape due to the occurrence of those sharp cusps in different directions, and is bounded by F faces. In this case, the equilibrium form can be determined by a complete set of F faces and their radius vectors[11]. On the other hand, according to Herring [23], the surface free energies of rough faces, such as stepped (S) or kinked (K) faces, are linearly related to the surface free energies of flat (or F) faces. Therefore, F faces play an essential role in the determination of the equilibrium forms of crystals. In the following the equilibrium form will be discussed from this point of view.

Suppose that in total n F faces are identified from a given crystal structure under certain conditions[1]. The radius vector D_i indicates the orientation of F face $(h_i h_i k_i)$ $(i = 1, 2, \cdots, n)$, and the distance from the face to the origin($|D_i|$). The set of mutual ratios of the radius vectors is well defined and represent the main characters of the Wulff plot[1,10,24]. Therefore, the shape of crystals can be fully determined by that set. This implies that the equilibrium form of crystals E.F. can be described by a set of radius vectors

$$\text{E.F.} = D = \{D_1, D_2, \ldots, D_n\}. \tag{14}$$

Presume that the crystallographic orientations of those F faces are set in a certain order from 1 to n. Then the equilibrium form of crystals E.F. can be simply expressed as an ordered set of elements by

$$\text{E.F.} = D = \{D_1, D_2, \ldots, D_n\}. \tag{15}$$

(We will define the order of the crystallographic orientations 1, 2, ... , n in later discussions.) Here D_i denotes the length of D_i, and is proportional to a certain physical property (such as the surface free energy). From a physical point of view, the values for different orientations are independent.

According to the character of the Wulff plot, D_i is indistinguishable from CD_i, where C is any constant independent of i. It follows that the set D is indistinguishable from the set $C\{D_i\}$ (i = 1, 2, ... , n). The shape–determining factor is the set of n–1 ratios ($\neq 1$) among the $\{D_i\}$. That set of ratios can be expressed by setting $C = (D_{min})^{-1}$ and writing the set D as

$$D = \{\tilde{D}_1, \tilde{D}_2, \ldots, \tilde{D}_n\}, \tag{16}$$

$$\tilde{D}_i = D_i / D_{min}. \tag{17}$$

Based on this convention, if two ordered sets are equal to each other, the the same morphology of crystals is defined.

According to the Gibbs–Wulff theorem, the following proportionality relation holds

$$D_i = K \sigma_i \quad (K\text{: const.}), \tag{18}$$

where σ_i denotes the surface free energy of face $(h_i k_i l_i)$. It follows from Eqs.(16) and (17) that,

$$D = \sigma, \tag{19}$$

$$\sigma = \{\tilde{\sigma}_i\} \quad \text{and} \quad \tilde{\sigma}_i = \sigma_i / \sigma_{min}. \tag{20}$$

(Here the subscript i = 1, 2, ... , n). In this sense, the ordered set σ is the key factor to determine the equilibrium shape of crystals.

It is known from our previous research [22] that for a crystal in contact with two–component solutions, the surface free energy can be expressed for crystal surface $(h_i k_i l_i)$ as

$$\sigma_i M_i = \sigma_i^{\circ} C_{\ell(i)}^{\circ} + \sigma_i' \tag{21}$$

where M_i is the mesh area of the face,

$$\sigma_i^{\circ} = \eta_i \Delta h_d^A \tag{22}$$

and

$$\sigma_i' = n_i^s X_A W_i \{ -kT_s \ln (X_A/X_B) + [W_i/(2 \ln X_A) + 1] + \Delta h_d^B [(X_A W_i/2 - X_B)/(X_B \ln X_B) - 1]\} \tag{23}$$

($W_i = X_A^{\zeta} - 1$) Δh_d^q (q = A or B) corresponds to the (bulk) exchange energy due to bringing a structural unit q from an environment of the pure solid state into the solution state For the solute units (q = A), it can be seen that $\Delta h_d^A \simeq \Delta \bar{H}_{diss}$ η_i is the orientation factor of crystal face $(h_i k_i l_i)$ Presuming that only the first or somewhat the second nearest–neighbor interactions need to be taken into account, this factor can be defined according to the Hartman–Perdok theory [8] as

$$\eta_i = E_{ss}^{att}{}_{(i)} / (2E_{ss}^{cr}) \simeq E_{(i)}^{att} / \Delta \bar{H}_{diss} \tag{24}$$

where $E_{(i)}^{att}$ is the attachment energy of crystal face i in the environment of solutions, $E_{ss}^{att}{}_{(i)}$ is the attachment energy in reference to the vacuum

From Eqs (21), (22), (23) and (24), it is clear that each element σ_i in the set σ is a function of the parameters M_i, $C_{\ell(i)}^{\circ}$, η_i and σ_i' This implies that in relation to σ, the other four ordered sets of parameters can be defined in the following way

$$M = \{M_i\}, \tag{25}$$

$$\eta = \{\eta_i\}, \tag{26}$$

$$C_{\ell}^{\circ} = \{C_{\ell(i)}^{\circ}\} \tag{27}$$

and

$$\sigma' = \{\sigma_i'\} \tag{28}$$

($i = 1, 2, \ldots, n$) The relation between σ and those parameter sets is defined by Eqs (21) and (22) In other words, the set is determined by those parameter sets element by element

Obviously, η and M are determined by the bond structure of crystals Therefore they represent the influence of the internal structural factor on σ (or the morphology of crystals)

On the other hand, C_{ℓ}° and σ' are determined by the structure of the solid–fluid interface and thermodynamic properties of both the solid and the fluid bulk phase Therefore, in spite of the crystal structure, various spatial conformations of fluid units (including impurities), and interactions between those units and the solid surface will affect the parameter sets C_{ℓ}°

and σ'. In this sense, both sets incorporate the symmetry and properties which the crystal and the mother phase have in common.

Let us now define the crystallographic order of elements in D. In the description of the morphology of crystals, the ordering of the face orientations which follows from the structure should be invariant with respect to the mother phase and independent of the external factors. The elements of η possess that character. Therefore, we define that the order of crystallographic orientation i is set in such a way to be $\eta_1 < \eta_2 < \ldots < \eta_n$. This order of crystallographic orientations from 1 to n is maintained in the elements of D and other parameter sets, disregarding the magnitude of each element in those sets.

B. Growth forms

In analogy with equilibrium forms, growth forms of crystals may also be constructed by the Wulff plot. Instead of D_i, we use R_i, the relative growth rate of the face i, to describe growth form of crystals. Then analogous to (15), the growth form of a crystal G.F. can be described in the following way

$$\text{G.F.} = R = \{R_1, R_2, \ldots, R_n\}, \tag{29}$$

where R_i is the normalized growth rate of face $(h_i k_i l_i)$, and the crystallographic order of elements in R is followed according to the aforementioned convention. Similarly to the equilibrium form, the growth forms of crystals having a given structure are determined by set R. The elements of set R depend on the growth rates in different orientations. Therefore, R is related to the growth kinetics. Obviously, the growth kinetics will be influenced by the structure of different crystal surfaces, kinetic factors, and conformations and configurations of fluid molecules. Again, these factors can be classified as internal and external factors, i.e., can be attributed to the structure and properties of the crystal, and of the ambient phase, respectively.

As mentioned in Sec.I, up to now there is no unambiguous theory to describe growth forms of crystals. The *ad hoc* theories developed so far, which to some extent work reasonably well, are the Hartman–Perdok theory and the approach of the roughening transition theory. Similar to the former theory[7], the latter may also be qualitatively justified [25]. In this section, we will discuss these two approaches in the context of the inhomogeneous cell model.

According to the approach of the roughening transition theory [2,9,25], the growth rate of flat faces $(h_i k_i l_i)$ may be expressed as

$$R_1 = \bar{K}_{RT}/\Delta\theta_1^r \quad (\bar{K}_{RT} \text{ the normalizing constant}) \tag{30a}$$

where $\Delta\theta_1^r = \theta_1^r - \theta$,

$$\theta_1^r = 2kT_1^r/\phi_1^{str}, \quad \theta = 2kT/\phi^{str} \tag{31}$$

[Eq (30a) is valid in the domain $\Delta\theta_1^r > 0$] Here θ_1^r is the dimensionless roughening temperature of face $(h_1k_1l_1)$, T_1^r is the actual roughening temperature, ϕ_1^{str} is the strongest bond energy in the structure, and θ is the dimensionless temperature The expression (30a) is inspired by the fact that the larger the difference between θ and θ_1^r (for a flat face, $\theta < \theta_1^r$) the higher the resistance against growth (or surface integration), and hence the lower the growth rate

In this approach, it is assumed that if a surface has $\Delta\theta^c \leq 0$, it is a rough face Rough faces grow faster than flat faces, and ultimately disappear from the growth form Therefore those rough faces ($\Delta\theta^c \leq 0$) are crystallographically irrelevant, and are not taken into account in this approach

There are various approximate versions of the principle of the Hartman–Perdok theory[1,8] Here we would express this approach in the following way,

$$R_1 = \bar{K}_{HP}(E_1^{att}/\Delta\bar{H}_{diss}) \quad (\bar{K}_{HP} \text{ the normalizing constant}) \tag{32a}$$

We note that Eqs (30a) and (32a) are introduced on the basis of the proportionality condition and the equivalent wetting condition Since the growth of crystals is directly correlated to the interfacial structure and interfacial bond energies, Eqs (30a) and (32a) should be modified within the framework of the inhomogeneous cell model According to the definition of the surface characteristic scaling factor C_{ℓ}^* given by (9a), (30a) can be rewritten as

$$R_1 = \bar{K}_{RT}\,(C^*_{\ell(1)}\,\Theta_1^r - \Theta)^{-1}, \tag{30b}$$

$$\Theta_1^r = 2kT_1^r/\Phi^{str}, \quad \Theta = 2kT/\Phi^{str} \tag{33}$$

When $C^*_{\ell(1)}\,\Theta_1^r >> \Theta$, Eq (30b) can be simplified as

$$R_1 \simeq \bar{K}_{RT}\,(C^*_{\ell(1)}\,\Theta_1^r)^{-1} \tag{30c}$$

In Eq.(32a), the proportionality condition given by (3) is implied. If it is assumed that in a certain direction, interfacial solid units have bond energies close to those of bulk solid units, then it follows that E_i^{att} in Eq.(32a) is independent of the interfacial fluid structure, and this value remains almost constant. However, $\Delta \bar{H}_{diss}$ in Eq. (32a) is correlated to the exchange energy at the surface. For this reason, it must be replaced by its value at the interface, $\Delta \bar{H}^{I}_{diss}$. Then Eq.(32a) upon substitution of (9a) becomes

$$R_i = \bar{K}_{HP} \eta_i / C^*_{\ell(i)} \tag{32b}$$

Following (30b) and (30c), a new ordered set of parameters is defined as

$$\Theta^r = \{\Theta^r_i\} \quad (i = 1, 2, \ldots, n). \tag{34}$$

Similar to η, this set is also determined by the structure of crystals.

In the case of the proportionality condition, expressions (30b) and (32b) are converted to

$$R_i = \bar{K}_{RT}'(\Theta^r_i - \Theta')^{-1} \tag{30d}$$

and

$$R_i = \bar{K}_{HP}' \eta \tag{32c}$$

where $\bar{K}_{RT}' = \bar{K}_{RT}/C^*_\ell$, $\Theta' = \Theta/C^*_\ell$ and $\bar{K}_{HP}' = \bar{K}_{HP}/C^*_\ell$. As expected in Sec. III A, this implies that the growth form of crystals is almost only determined by internal factors of crystals Θ^r or η.

Similarly to D, the set R is also dependent on the parameter sets η, Θ^r and C^*_ℓ. Those parameters will influence R in such a way as expressed in Eqs.(30b) and (32b). It is clear that η and Θ^r represent internal factors which influence growth forms, while C^*_ℓ represents the influence of the ambient phase on the morphology of crystals.

It has to be noted that for complicated molecular systems, conformations and configurations of growth units are very relevant in considering the structure and properties at the surface. In relation to the solid surface structure, configurations and conformations of interfacial fluid units vary for different crystallographic orientations. Some of those growth units adjacent to the solid surface are in such favorable conformations, that they can be directly in equilibrium with solid units at the surface. (We call them the "effective growth units" in what follows). Others may be in unfavorable conformations, which cannot come directly in equilibrium with the solid units at the surface. Therefore, in the calculation of C^*_ℓ

mainly the effective growth units are taken into account. Concerning the effect of molecular conformations, it can in principle be estimated by means of C_l^*. We will come back to this issue in Sec. IV.

C. Principles of prediction and modification of the morphology of crystals

It can be seen from the foregoing discussion that the internal and external factors controlling the morphology of crystals can easily be separated within the framework of our formalism as η, Θ^r, C_l^* and σ'. It can be seen that factors expressed in terms of η and Θ^r are subject to the bond structure of crystals, and cannot be changed. They in principle determine the characteristic habit of crystals. From this point of view, they belong to the internal controlling factors. As mentioned earlier, these factors can be determined by the network analysis or PBC (Periodic Bond Chain) analysis[1,2,9,10].

On the other hand, changes in the external factors affect C_l^* and σ' and consequently the shape of crystals. In this sense, C_l^* and σ' represent the external controlling factors. Since C_l^* and σ' are directly related to the interfacial structure of crystals, they can in principle be determined by an Interfacial Structure (IS) analysis. (We will practically describe this analysis in Sec IV). As soon as η, Θ^r, C_l^* and σ' are available, the morphology of crystals can finally be predicted on the basis of Eqs.(21), (30a) and (30b).

We notice that the habit of crystals with a given structure can be modified by changing C_l^* (as well as σ'). This can in principle be done by introducing tailor–made additives to the system, or changing the concentration and other growth conditions. Using tailor–made additives is obviously one of the most efficient ways, because C_l^* can be directly affected in the way as shown in (10a) or (10a). Suppose that some impurity or solvent molecules are preferentially adsorbed on crystal faces $\{h_i k_i l_i\}$. Then, in competition with those impurity or solvent molecules, growth units are repelled from the surfaces. According to Eq.(10a), the value of $C_{l(i)}^*$ will be enhanced resulting in the modification of C_l^*. From the point of view of growth kinetics, it follows that the roughening temperature of those faces will increase, and the growth of the faces becomes relatively slower. Therefore, the growth habit of crystals is modified.

Based on this principle, the molecular design of tailor–made additives becomes possible. Let us consider the way to modify the shape of crystals by inhibiting the growth of crystals in some directions. (This is relatively easy to achieve.) We may design additives which can preferentially adsorb onto the surface, leaving other important surfaces unaffected. Then, for the aforementioned reasons, the growth habit of crystals will be changed. The efficiency of specific tailor–made additives and the influence on the morphology of crystals can be estimated by calculating C_l^* for different crystal faces. The value of C_l^* can be calculated by

computer simulations, density–functional theories etc.. At present, the calculations can easily be carried out by self–consistent field formalisms [26-29]. In the near future, we expect significant progress to be made in the field of molecular design for tailor–made additives.

IV. THE MORPHOLOGY OF N–PARAFFIN CRYSTALS

As mentioned in Sec.III.C, the morphology of crystal can be predicted by carrying out the PBC analysis and the IS analysis. In this section, we will apply this principle to predict growth forms of n–paraffin crystals. We will pay more attention to the IS analysis since the concept is for the first time put forwards in this paper. In the following, growth forms of crystals of n–$C_{21}H_{44}$ and n–$C_{36}H_{74}$ are described independently according to Eq.(32a) (only the PBC analysis is performed) and the modified approach given by (32b) (both the PBC analysis and the IS analysis need to be carried out). The theoretic growth forms will be compared with observed growth forms.

Normal paraffins crystallize in four modifications: triclinic, monoclinic, orthorhombic and hexagonal, depending on the number and parity of the number of carbon atoms in paraffin molecules, and on the temperature, impurities and other factors [30]. Recently the morphology of n–paraffin crystals with different structures has been investigated in great detail [9-10]. In the following, we focus our concentration only on normal paraffin crystals having orthorhombic structure, in the space group P_{bcm} for odd numbered paraffins [31-32] and P_{ca2_1} for even numbered paraffins [31,33]. According to (32a), the elements of η must be calculated. This can be done on the basis of the Hartman–Perdok (or PBC) theory [1,2,8]. First, important bonds in a given crystal structure should be first calculated. It follows that PBCs can then be identified from the crystal structure. A PBC is defined as an uninterrupted chain of bonds which has the periodicity $[uvw]$ of the lattice. From the obtained PBCs, F faces (or flat faces) can be found. For those faces we can carry out further calculations. (An F face is a crystallographic face having two non–parallel sets of PBCs, both parallel to the surface). For more details concerning the PBC analysis of paraffin crystals, we refer to Refs.9–10. Note that under certain conditions, some roughened F faces whose roughening temperatures are much lower than the actual temperature. In most cases, such faces are very unlikely to occur on crystals. Therefore, they can be excluded from our considerations. In the following discussions, only those faces whose roughening temperatures are above or slightly below the actual temperature under current growth conditions are relevant and are taken into account. Following the ordering convention mentioned above, the elements of those sets are ordered as: the faces $\{001\}$, $\{110\}$ for n–$C_{21}H_{44}$ crystals, the faces $\{001\}$, $\{00\bar{1}\}$, $\{110\}$, $\{111\}$ and $\{11\bar{1}\}$ for n–$C_{36}H_{74}$ crystals. According to our results [9-10], the growth forms of n–$C_{21}H_{44}$ and

n–$C_{36}H_{74}$ are defined according to (32a) in the following sets,

$$R = \eta = \{1, 12.6\} \qquad (\text{for n–}C_{21}H_{48}) \tag{35}$$

and

$$R = \eta = \{1, 1, 23.8, 23.9. 23.9\} \quad (\text{for n–}C_{36}H_{74}). \tag{36}$$

Constructed according to the Wulff plot, n–$C_{21}H_{44}$ and n–$C_{36}H_{74}$ crystals have a lozenge shape, bounded by the large {001} faces and the narrow {110} side faces. The growth forms of crystals of n–$C_{21}H_{44}$ and n–$C_{36}H_{74}$ according to (35) and (36) are shown in Figs.1a and 1b, respectively.

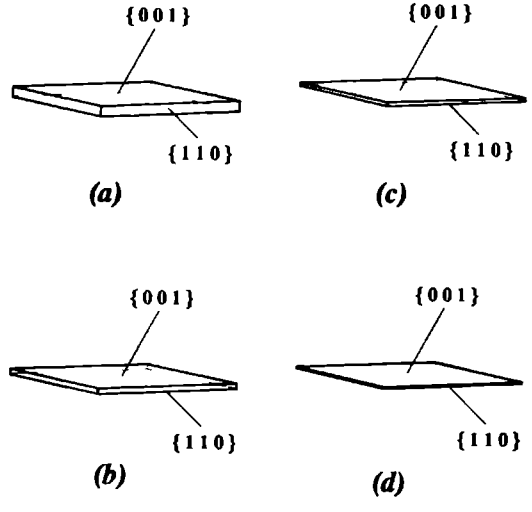

FIG.1. (a) and (c) : theoretical growth forms of n–$C_{21}H_{44}$ crystals; (b) and (d): theoretical growth forms of n–$C_{36}H_{74}$ crystals. The growth forms of (a) and (b) correspond to Eq.(33a) and (c) and (d) to Eq.(33b). The growth forms of n–paraffin crystals are platy, bounded by the large {001} faces (and the $\{00\bar{1}\}$ faces for n–$C_{36}H_{74}$ crystals) and the narrow side faces {110}. After considering the influence of the ambient phase, the growth habits given by (c) and (b) are much thinner.

For the purpose of comparison, the theoretical and observed growth forms of n–$C_{21}H_{44}$ crystals (grown from a n–hexane solution) and of n–$C_{36}H_{74}$ crystals (grown from a m–xylene solution) are shown in Fig. 2. It can be seen that orthorhombic paraffin crystals indeed have a lozenge shape. Nevertheless, some discrepancies between predicted growth forms and observed growth forms remain. The predicted growth forms show too thick a growth habit for

the n–paraffin crystals. From the discussions given in Sec. III, we can see that those contradictions result from the application of the proportionality condition given by Eq. (3). In the morphological analysis, C_{ℓ}^{*} was implicitly considered to be independent of crystallographic orientations and the carbon number of n–paraffin molecules. According to our recent studies [21,29], C_{ℓ}^{*} depends not only on orientations of surfaces, but also on the chain length of paraffin molecules. Undoubtedly, to improve our predictions, Eq.(32b) is a better alternative.

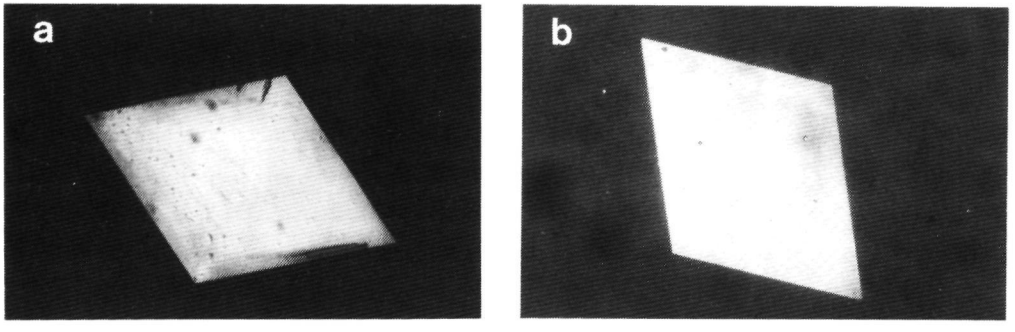

FIG.2. (a) A crystals of n–$C_{21}H_{44}$ grown from a n–hexane solution; the equilibrium temperature $T_S \simeq -3.23^{\circ}$ C and the supercooling $\Delta T \simeq 0.03^{\circ}$ C. (b) A crystal of n–$C_{36}H_{74}$ grown from a m–xylene solution; $T_S = 33.08^{\circ}$ C, $\Delta T = 0.16^{\circ}$ C.

Now the problem is how to calculate C_{ℓ}^{*} for different surfaces. This is the question of the IS analysis. The calculation is carried out using Eqs. (10a) or (10b). In the equations, the term $X_A(0)$ can be evaluated according to various theories. Here a self–consistent field theory [26-28] is used to calculate $X_A(0)$. (This formalism was first developed by Scheutjens and Fleer to investigate solid–fluid interfacial systems of polymers. Now a computer program has been developed to calculate profiles of density at the interface according to this theory. For more details, see Refs.26–29). As discussed in Sec. IV B, we notice that the fraction of effective growth units at the surface is in a subtle way related to the interfacial structure, and hence influences the morphology of crystals. In order to predict the morphology, an analysis of effective conformations and configurations of n–paraffin molecules at different surfaces becomes necessary.

According to the results obtained from self–consistent field calculations [29], at equilibrium, most fluid paraffin molecules in the first fluid layer adjacent to the solid phase are preferentially lying parallel to the solid surface, while only a very small number of fluid n–paraffin molecules are transverse. As regards the surface structure of n–paraffin crystals, at the side faces (including the {110} faces) solid paraffin molecules are packed lying parallel

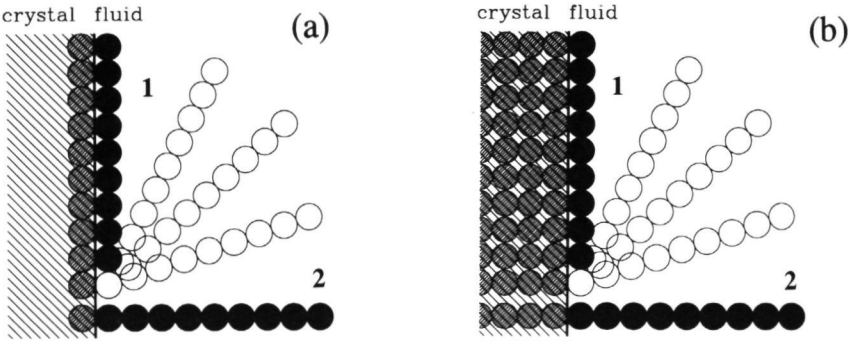

FIG.3. Illustration of the structure of the crystal surfaces and the conformations of n–paraffin molecules at the interface. (a) The {110} faces of orthorhombic n–paraffin crystals. (b) The {001} faces of n–paraffin crystals. Conformation "1" indicating the molecules lying parallel to the surface; conformation "2" indicating the molecules "standing" on the surface.

to the surface having a similar alignment as molecules in the crystal structure (see Fig.3a). Note that among those parallel fluid paraffin molecules, different orientations of molecular chains within the XY plane and different chain conformations of molecules still occur. However, they can easily be converted from one state to another by thermal fluctuations, and for that reason, we will not distinguish between them. Non–parallel fluid paraffin molecules have higher energy levels than molecules lying parallel to the surface. They tend to transfer spontaneously to parallel conformations, provided the available space is sufficient. Therefore all fluid paraffin molecules are considered to be effective with respect to the solid surface structure of the {110} faces. For the {001} faces, the surface structure of the crystal phase is different Solid n–paraffin molecules are positional with their chain axis transverse to the surface. Therefore, for fluid n–paraffin molecules to be incorporated in the structure, their molecular chains must also be aligned transversely to the surface; thus, only those molecules which "stand" on the surface will become effective. (See Fig.3b). Because this transverse orientation of the fluid molecular chain axis does not correspond to the ground state, an extra driving force is necessary to activate the parallel–lying molecules causing them to "stand" on the surface; the longer the molecular chains, the larger the driving force. Ultimately, the "standing" molecules are effective, the parallel–lying molecules are ineffective. In the calculation of $X_A(0)$ at the {001} faces, only the portion of "standing" n–paraffin molecules is taken into account.

In addition to the effect of molecular conformations, the excess energy (per structural unit), has a direct influence on C_ℓ^*. In this case, the excess energy is proportional to E_1^{att}. This

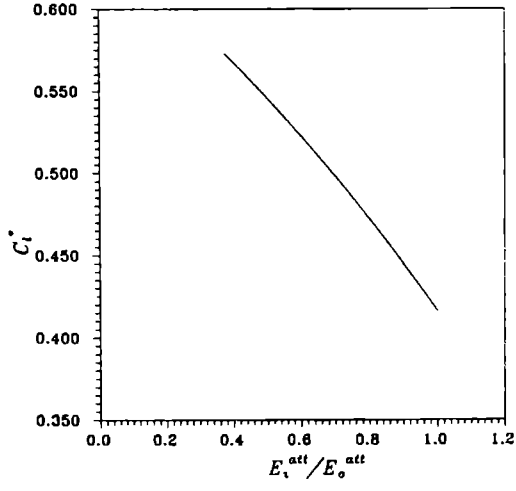

FIG.4. The surface characteristic factor C_l^* plotted versus the relative attachment energy E_1^{att}/E_0^{att} for n–$C_{21}H_{44}$ crystals. Here the influence of chain conformations is not taken into account. $E_0^{att} = E_{110}^{att}$

implies that $C_{l(i)}^*$ depends monotonically on E_1^{att}. Fig.4 shows the value of $C_{l(i)}^*$, calculated by the self–consistent field theory, as a function of E_1^{att}/E_0^{att} (here $E_0^{att} = E_{110}^{att}$). It is clearly indicated in this figure that as the relative attachment energy E_1^{att}/E_0^{att} decreases, $C_{l(i)}^*$ increases almost linearly.

From the results of the self–consistent field theory calculations [26-29], the values of the elements of C_l^* for both n–$C_{21}H_{44}$ and n–$C_{36}H_{74}$ crystals are now given by

$$C_l^* = \{3.1, 1\} \quad (\text{for n–}C_{21}H_{44}) \tag{37}$$

and

$$C_l^* = \{3.32, 3.32, 1\,003, 1, 1\} \ (\text{for n–}C_{36}H_{74}) \tag{38}$$

According to (32b), (35) and (36) should be modified according to

$$R = \{1, 39.6\} \quad (\text{for n–}C_{21}H_{44}) \tag{39}$$

$$R = \{1, 1, 78.6, 79.1, 79.1\} \quad (\text{for n–}C_{36}H_{44}) \tag{40}$$

Based on Eqs.(39) and (40), the modified growth forms of n–$C_{21}H_{44}$ and n–$C_{36}H_{74}$ crystals are constructed by the Wulff plot, and shown in Figs 1c and 1d. It can be seen that the

modified theoretical growth forms are now much closer to the observed growth forms

The simple example discussed in this section demonstrates the relevant formalisms discussed in Sec III In this case, only a small number of different crystal faces are in competition The influence of the ambient phase causes the change in the thickness of the crystals If the influence of the ambient phase is very strong, the shape of the crystals can change drastically For example, when some tailor–made additives are added to the system for that purpose, the paraffin crystal shape is modified from plate–like to needle–like [9] On the other hand, when many different crystal faces are in competition, small changes in R, brought about by the influence of the ambient phase, may cause the disappearance of some crystal faces Then a considerable change in the crystal shape can be observed

V. CONCLUSIONS

Internal and external factors controlling the morphology of crystals are given by M, η, Θ^r, C^*_{ℓ} σ' etc If we define the behavior of fluid units and other external factors as the "symmetry" of the ambient phase, it follows from (21), (30b) and (32b) that the shape and external symmetry of crystals is a composite result brought about by the macroscopic symmetry of crystals and the "symmetry" of the ambient phase In the case of crystals in contact with an isotropic medium, the highest external symmetry of crystals, which is determined by the macroscopic symmetry of crystals, occurs (In fact, crystals consisting of isotropic building units growing from vapor come very close to this situation) Otherwise, the actual external symmetry of crystals may be lower than the highest external symmetry We may in principle influence the shape and external symmetry of crystals by changing the "symmetry" of the ambient phase

ACKNOWLEDGEMENTS

We are much indebted to Dr H Meekes and Dr C S Strom for valuable discussions and a critical reading of this manuscript We also acknowledge Shell Nederland B V for providing financial support

REFERENCES

[1] P Bennema and J P van der Eerden, in *Morphology of Crystals, Part A*, edited by I Sunagawa (Terra, Sci , Tokyo, 1987) p 1

[2] P Bennema, in *Handbook on Cryst Growth*, edited by D T J Hurle,

(North–Holland, Amsterdam, 1993) (in press)

3 N Steno, *De Solido Intra Solidum Naturaliter Contento Dissertationis Prodromus*, (Florence, 1669)

4 P Hartman and W G Perdok, Acta Cryst **8**, 49 (1955)

5 P Hartman and W G Perdok, Acta Cryst **8**, 521 (1955)

6 P Hartman and W G Perdok, Acta Cryst **8**, 145 (1955)

7 P Hartman and P Bennema, J Cryst Growth **49**, 145 (1980)

8 P Hartman, in *Morphology of Crystals, Part A*, edited by I Sunagawa, (Terra Sci , Tokyo, 1987) p 271

9 P Bennema, X Y Liu, K Lewtas, R D Tack, J J M Rijpkema and K J Roberts, J Cryst Growth **121**, 679 (1992)

10 X Y Liu and P Bennema, J Appl Cryst **26**, 229 (1993)

11 R Kern, in *Morphology of Crystals, Part A*, edited by I Sunagawa, (Terra Sci , Tokyo, 1987) p 79

12 X Y Liu and P Bennema, J Chem Phys **97**, 3600 (1992)

13 S R Fowler and E A Guggenheim, *Statistical Thermodynamics* (Cambridge University, London, 1960)

14 X Y Liu and P Bennema, J Chem Phys **98**, 5863 (1993)

15 K A Jackson, in *Liquid Metals and Solidification* (Am Soc for Metals, Metal Park, OH, 1958)

16 J Q Broughton and F F Abraham, Chem Phys Lett **71**, 456 (1980)

17 J Q Broughton and G H Gilmer, J Chem Phys **79**, 5090, 5105, 5119 (1983), **84**, 5741, 5749, 5759 (1986)

18 A Bonissent, in *Interfacial Aspects of Phase Transformation*, edited by B Mutaftschiev (Reidel, Dodrecht, 1982)

19 A D J Haymet and D W Oxtoby, J Chem Phys **74**, 2559 (1981)

20 W A Curtin and N W Ascroft, Phys Rev A**32**, 2909 (1985)

21 X Y Liu, Surf Sci **290**, 403 (1993)

22 X Y Liu, J Chem Phys **98**, 8154 (1993)

23 C Herring, Phys Rev **82**, 87 (1951)

24 C Rottman and M Wortis, Phys Reports **103**, 59 (1984)

25 X Y Liu and P Bennema, J Cryst Growth (to be published)

26 J M H M Scheutjens and G J Fleer, J Phys Chem **83**, 1619 (1979), **84**, 178 (1979)

27 J M H M Scheutjens and G J Fleer, Macromolecules **18**, 1882 (1985)

28 F A M Leermakers and J M H M Scheutjens, J Chem Phys **89**, 3264, 6912 (1988), J Phys Chem **93**, 7417 (1989)

29 X Y Liu and P Bennema, Phys Rev E, (1993) (in press)
30 A A Chenov, *Modern Crystallography III– Crystal Growth* (Springer–Verllog, Berlin, 1984)
31 S C Nyburg and J A Potworowski, Acta Cryst B**29**, 347 (1973)
32 A E Smith, J Chem Phys **21**, 2229 (1953)
33 P W Teare, Acta Cryst **12**, 294 (1959)

Chapter 6

RELATION BETWEEN ROUGH AND FLAT GROWTH OF CRYSTAL FACES: AN EFFECTIVE APPROACH TO VOLUME TRANSPORT RESISTANCES

The relation between rough and flat growth of crystal faces: an effective approach to volume transport resistances

Xiang–Yang Liu, G Arkenbout, P Bennema and P van Hoof

RIM, Laboratory of Solid State Chemistry, Faculty of Science, University of Nijmegen, Toernooiveld, 6525 ED Nijmegen, The Netherlands

ABSTRACT–In this paper, a simple approach has been presented to describe and to estimate the resistances against volume transport during crystal growth Following from a simple model, it is obtained that the resistances against volume diffusion can be estimated, using the relation between the kinetics of rough growth and that of flat growth Within the framework of this approach, a so–called auxiliary straight line method is developed for the faceted growth to extract the faction of the total driving force remaining at the surface As applications and an experimental verification, the kinetic data of different n–paraffin and naphthalene crystal–solution systems are analyzed by the aforementioned method For the n–paraffin systems, the data obtained from kinetic roughening experiments are compared with those obtained from thermal roughening experiments The results turn out to be in excellent agreement with each other

J Cryst Growth *(in press)*

I. INTRODUCTION

Crystal growth is usually described in terms of surface integration kinetics depending non–linearly or linearly on the driving force according to different mechanisms, and a first–order relationship for transport of the solidifying materials from the bulk to the crystal surface. According to thermodynamics and the definition, the driving force for crystallization in reference to the bulk phase is expressed as the difference of the chemical potentials of the crystallizing component $\Delta\mu$ between the actual state and the equilibrium state:

$$\beta = \Delta\mu/kT = \ln(x_b/x_b^*) \tag{1}$$

where x_b is the bulk concentration of the solute, k is Boltzmann's constant, the asterisk denotes the equilibrium value at temperature T and pressure P. In the case of a relatively low deviation from equilibrium,Eq. (1) becomes equal to the the relative supersaturation. By expanding the logarithmic term in a Taylor series and truncation after the first term it can be seen that

$$\beta \approx (x_b - x_b^*)/x_b^*. \tag{2}$$

In the process of crystal growth, growth units must be first transported through boundary layers to the surface. In boundary layers resistances against mass and heat transport occur. Consequently, the resistances will more or less result in a reduction of the original supersaturation at the interface. To describe this decrease of supersaturation, the fraction of the total driving force remaining active at the solid–liquid interface is introduced by the factor m, defined as

$$m = \beta_i/\beta \tag{3}$$

where β_i is referred to as the effective interfacial supersaturation, and has the form

$$\beta_i \approx (x_i - x_i^*)/x_i^*, \tag{4}$$

To determine the value of β_i is a very important step in the research of crystal growth kinetics.

To describe volume transport processes and surface integration kinetics, Goede *et al.* [1] developed a simple model, assuming that the growth of crystals is analogous to the electric current in the series of electric resistances. The same subject was treated theoretically by

other authors [2-3]. Moreover, surface supersaturations were measured precisely by Onuma *et al.* [4], using an optical method. In this paper, we will attempt to find a simple and effective way to estimate the effective supersaturation at the surface by considering volume transport resistances, based on Goede's results.

II. MODIFIED APPROACH

In a crystal growth process, the resistances against volume transport are mainly concentrated in a thermal and diffusion layer, respectively. The mass flux and heat flux can be expressed as follows:

$$J_m = \frac{k_d}{1-x_b}(x_b - x_i)\frac{\rho_l}{M_l} = R\frac{\rho_s}{M_s} \tag{5}$$

and

$$J_h = \alpha(T_i - T_b) = R\frac{\rho_s}{M_s}\Delta H. \tag{6}$$

Here J_m denotes the mass flux, J_h the heat flux, k_d is the mass transfer coefficient, α is the heat transfer coefficient, ρ is the density, M is the molecular weight of structural units, R is the growth rate of a crystal face, ΔH is the enthalpy of dissolution (or melting), and the subscripts i, b, l, and s are referred to as the interface, the bulk, the liquid and the solid, respectively.

On the other hand, surface integration kinetics can be expressed as

$$R = k_G(\beta_i)^n \tag{7}$$

where k_G is the growth kinetic coefficient at the surface, the superscript n is the kinetic order of surface integration. In case that the condition

$$[\Delta H_m^2/(kT_b)^2][\rho_s/(M_s\alpha)]R \tag{8}$$

is fulfilled, (in fact it is the case for n–paraffin/n–hexane solution systems, e.g. for n–$C_{21}H_{44}$/n–hexane solutions $[\Delta H_m^2/(kT_b)^2][\rho_s/(M_s\alpha)]R \sim 3.4 \times 10^{-2} << 1$), then it can be derived from (1), (2), (4), (5) and (6) [1] that

$$\beta_i = \beta - \frac{R}{k_d'} \tag{9}$$

where k_d' is a total resistance to transport phenomena, and depends on k_d, α, π_b, ρ_s, ρ_l, the enthalpy of melting ΔH_m, the melting point T_m, etc [1]

For $n = 1$, substituting (9) into (7) and rearranging yields

$$R = \frac{1}{1/k_G + 1/k_d'}\beta \tag{10}$$

Goede *et al* [1] suggested that for the dissolution of a crystal, $n = 1$, and the disintegration process at the crystal surface proceeds without any resistance, so $k_G \to \infty$ It follows that k_d' can be measured by determining the dissolution rate R_{diss} versus β However, it is known that dissolution is a kind of "unstable growth" for many organic crystals, and all results obtained above is only valid for stable growth Therefore, using R_{diss} to estimate k_d' is improper Also, in many cases the data of R_{diss} versus β are very difficult to determine with sufficient accuracy due to the instability of dissolving crystal surfaces

For a face which roughens on a molecular scale, every site on the surface can be seen as a kink site Thus the growth units can be incorporated directly into the crystal, although in this case surface integration still needs some relaxation time This implies that if the anisotropy of rough faces does not play an important role, the surface integration can be regarded as a very fast event in comparison with the volume diffusion ($k_G >> k_d'$) The growth rate is then controlled by transport of the growth units across the diffusion layers Subsequently (10) is rewritten

$$R_{rough} \approx k_d' \beta \tag{10'}$$

and compared with (9) it follows that

$$m \approx 1 - R/R_{rough} \tag{11}$$

Explicitly, for a given crystal face, once we know the ratio of R/R_{rough} at a certain supersaturation, m may be evaluated The key issue now is how to derive R_{rough} at a supersaturation where a smooth growth occurs In case that the growth of a flat surface takes place in the neighborhood of the roughening transition temperature T_r, the data $R_{rough}(\beta)$ may be determined from a referent system with T_s slightly above T_r In this case the temperature of systems is only slightly different from the referent system Then k_d' can be seen as a constant However, when the experimental temperature is quite below the

roughening temperature, this method is inapplicable For many organic crystals, phenomena of kinetic roughening are frequently observed on some flat surfaces In the following, we will show how to derive the relevant data from kinetic roughening data

III ROUGH GROWTH DUE TO THERMAL ROUGHENING AND KINETIC ROUGHENING

As mentioned before, rough growth will take place at the temperature above the roughening temperature for the whole range of supersaturations In this case the growth rate is linearly related to the supersaturation

$$R_{\text{rough}} = A\beta \tag{12}$$

where A is a kinetic coefficient

When the temperature is lower than the roughening temperature and the supersaturation is relatively small, the faceted growth of the crystal face occurs, and k_G is relatively small It follows that the surface integration is a very important step in a growth process In this case, the growth rate is a non–linear function of supersaturation [5 7]

When β is sufficiently large, the originally flat face will kinetically roughen According to a recent survey [8] based on computer simulations and experimental data, in this case, the relation between R and β is given by

$$R_{\text{kr}} = A'(\beta - \beta^{\text{c}}) \qquad (\beta > \beta^{\text{c}}) \tag{13}$$

where β^{c} is the critical supersaturation of kinetic roughening, A' a kinetic coefficient and the subscript kr denotes kinetic roughening In our experiments it is found that for some systems, such as n–paraffin/n–hexane solution systems, the expression (13) also holds According to the Wilson–Frenkel model [9], assuming that the surface integration is a very fast event, the coefficient A in (12) A' in (13) can approximately be expressed as

$$A \simeq A' \sim \frac{h\nu}{kT} x_{\text{b}} \exp(-Q_{\text{f}}/kT) \tag{14}$$

(h is Planck's constant, ν the frequency of lattice vibration and Q_{f} the activation energy to transport growth units trough boundary layers) Here A and A' are in fact comparable with k_{d}^{i} The implication is that for a thermal rough growth or a kinetically rough growth of a face,

the linear parts of $R(\beta)$ expressed either in (12) or in (13) have the same slope In practice, when the faceted growth occurs at a crystal face, the real rough growth does not always occur in the neighborhood of the experimental temperature However, in the case of organic crystals, kinetic roughening may often be observed Then the above–mentioned principle can be applied to estimate the relation between "R_{rough}" and β for a flat face This implies that in this case

$$R_{rough} \simeq A'\beta \tag{15}$$

It comes that once curve $R(\beta)$ of this face is measured both in the flat and the kinetically rough regime, an auxiliary straight line can be drawn through the origin in parallel to the linear part of the curve $R(\beta)$ This straight line corresponds to the curve "R_{rough}"(β), which may be employed to evaluate m based on (11) This method is known as *the auxiliary straight line method* hereafter

IV. EXPERIMENTAL VERIFICATION AND DISCUSSION

A. Experimental

Crystal–solution systems investigated in this paper are the n–paraffin/n–hexane solution system. The solutions which are used in our experiments are prepared from analytical grade n–paraffins (Alfa, > 99 0%) and spectrum grade n–hexane (Merck, > 98 0%)

The experiments were carried out in a double–walled thermostated glass cell system of cylindric form, using a Leitz transmission microscope–type Divert The growth cell is a cylindric glass cell of about 60 mm in diameter and 4 mm in height During experiments, the solutions in the growth cell were non–stirred In order to trace the growth of crystals, a video camera was employed to record the growth process To determine the growth rate of a crystal face, the growth process was recorded on a video tape by means of a video camera, which was directly adapted to the microscope The recorded video image was processed later in a digital image processing computer system, to improve the quality and to measure the displacement of the growth front at a certain time interval (For more details about the experimental set up and the experimental procedures, see Refs 8,10 & 11)

The experiments of n–paraffin crystals growing from n–hexane solutions were performed with a crystal growing on the bottom of the cell at constant β. According to our investigation [12], the growth habit of odd–numbered n–paraffin crystals is platy The external shape of these crystals is lozenge, with the large faces {001} and the narrow side faces {110} In our

experiments, we only concentrate on the growth kinetics of the {110} faces

B. Results and discussion

1. Some organic crystals growing from solutions

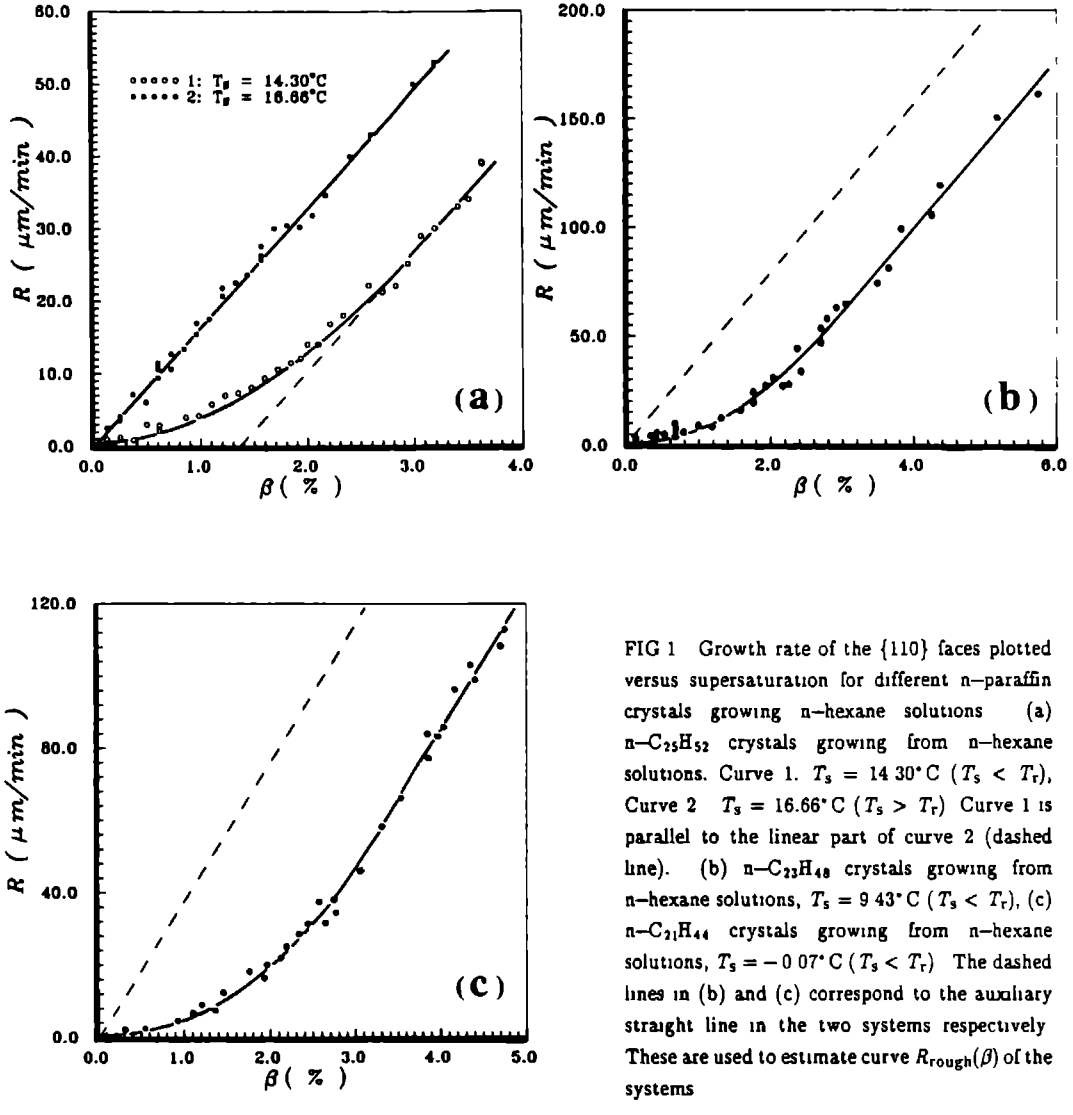

FIG 1 Growth rate of the {110} faces plotted versus supersaturation for different n–paraffin crystals growing n–hexane solutions (a) n–$C_{25}H_{52}$ crystals growing from n–hexane solutions. Curve 1. T_s = 14 30°C ($T_s < T_r$), Curve 2 T_s = 16.66°C ($T_s > T_r$) Curve 1 is parallel to the linear part of curve 2 (dashed line). (b) n–$C_{23}H_{48}$ crystals growing from n–hexane solutions, T_s = 9 43°C ($T_s < T_r$), (c) n–$C_{21}H_{44}$ crystals growing from n–hexane solutions, $T_s = -0\ 07$°C ($T_s < T_r$) The dashed lines in (b) and (c) correspond to the auxiliary straight line in the two systems respectively These are used to estimate curve $R_{rough}(\beta)$ of the systems

As shown in Fig 1a, the growth rate is plotted versus supersaturation for n–$C_{25}H_{52}$ crystals growing from n–hexane solutions with an equilibrium temperature T_s below and above T_r (corresponding to Curve 1 and Curve 2, respectively) The difference of T_s between the two systems is less than 2 5 °C So we can consider k_d^1 as a constant It can be seen that for the solution with $T_s < T_r$, at $\beta \leq \beta^c$ the growth rate R is a nonlinear function of β, as expected from theories [2-4] As soon as $\beta > \beta^c$, the $R(\beta)$ curve turns to linear due to kinetic roughening Obviously, in this situation relation (13) is satisfied Comparing with the case that $T_s > T_r$, it is found that the slope of the linear part of Curve 1 is truly equal to that of Curve 2 This indicates that the auxiliary straight line method is an effective method to derive the relation between R_{rough} and β for a flat face Based on the kinetic data $R(\beta)$ of the flat {110} faces, $R_{rough}(\beta)$ of the faces is estimated in figs 1b and 1c for of n–$C_{23}H_{48}$ and n–$C_{21}H_{44}$ crystals growing from n–hexane solutions, respectively

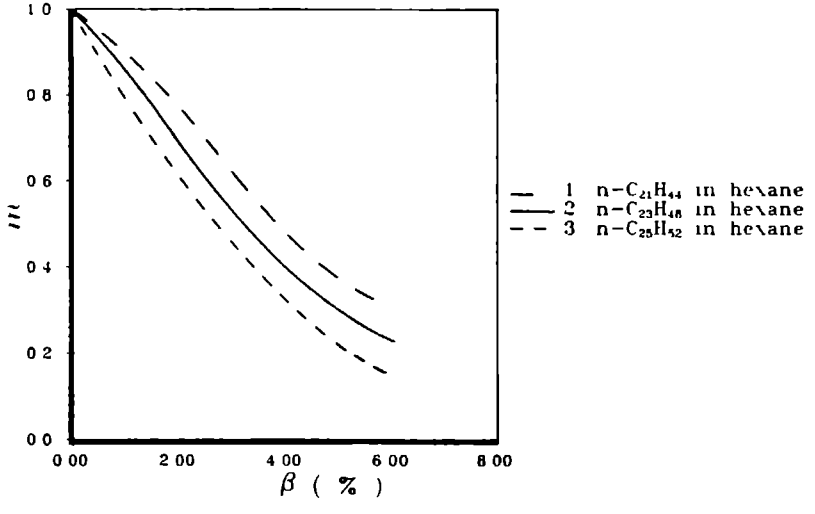

FIG 2 The fraction of the total driving force remaining effective at the solid–liquid interface, m, as a function of the supersaturation β (1) n–$C_{21}H_{44}$ crystal/n–hexane solution system, $T_S = -0\,07$° C, (2) n–$C_{23}H_{48}$ crystal/n–hexane solution system, $T_s = 9\,43$° C, (3) n–$C_{25}H_{52}$ crystal/n–hexane solution system, $T_s = 14\,30$° C

It follows from Fig 1 that m as a function of β for the systems of n–$C_{21}H_{44}$, n–$C_{23}H_{48}$ and n–$C_{25}H_{52}$ crystals grown from n–hexane solutions in the neighboring temperature of T_r are obtained and plotted in Fig 2 The equilibrium temperatures for the three systems are –0 07° C, 9 43° C and 14 30° C, respectively It can be seen that at a low supersaturation, m is

very close to unity With increasing β, the value of m will progressively decrease This means that the rate limited step of crystal growth is the surface integration at a low supersaturation, then gradually changes to the transport of heat and mass with increasing supersaturations It is also shown in Fig 2 that at the same supersaturation, the resistances against volume diffusion become greater when the chain lengths of n–paraffins become larger This is more pronounced at higher supersaturations, where the transport of heat and mass is much more important We notice that the experimental temperatures for the three systems are not much different Therefore, the decrease in diffusion coefficient due to the increase of the chain length will have a dominant influence on volume transport This will substantially enhance the resistances against mass transport, resulting in the decrease of effective supersaturation at the interface

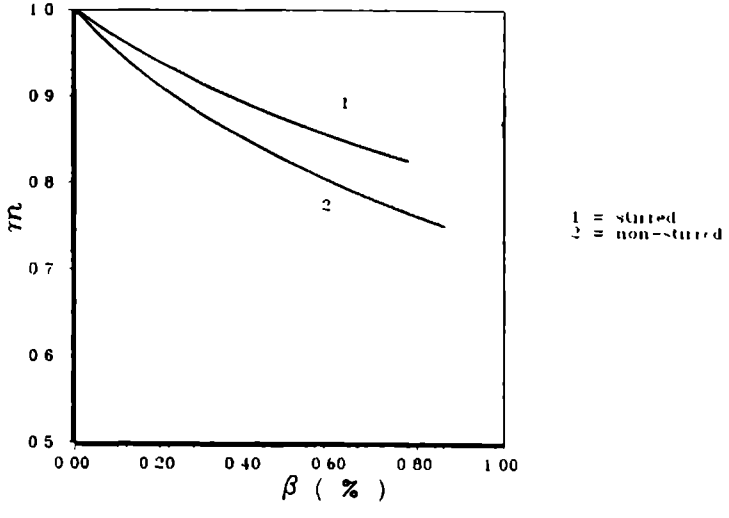

FIG 3 m versus β for systems of naphthalene crystals grown from a mixture of biphenyl and toluene (9 1) under different hydrodynamics conditions x_b = 0 36, 1 = stirred, 2 = non–stirred

In order to investigate the influence of different hydrodynamic conditions on the effective interfacial supersaturation, the $R(\beta)$ data of naphthalene crystals grown from a mixture solvent system (biphenyl toluene = 9 1) under an uncontrolled stirring and a non–stirring condition are selected from Ref 13 Again the auxiliary straight line method is applied The results of $m(\beta)$ are given in Fig 3 Stirring in solution will improve the volume diffusion condition In that case, growth units are more easily transported through the diffusion layer

It follows that the effective supersaturation at the interface and the growth rate increase evidentially, especially at a higher supersaturation Note that here we just demonstrate the influence of hydrodynamic conditions on m (or β_1)

2 Comparison of kinetic roughening with the thermal roughening

The thermal roughening and kinetic roughening are two very important concepts in the theory of crystal growth Many phenomena related to crystal growth can be explained based on the two concepts Actually, these two kinds of phenomena can be associated with each other by the edge free energy, γkT, at crystal surfaces So we can compare the results obtained from thermal roughening and kinetic roughening experiments It is noted that since the thermal roughening occurs only at equilibrium, volume transport does not influence the results Therefore, the experimental data of the thermal roughening directly reflects the physical state of interfaces We use the dimensionless roughening temperature θ^r to characterize the thermal roughening at a surface, which is defined as

$$\theta^r_{hkl} = \frac{2kT_r}{\phi_{str}} \tag{16}$$

Since for a given face, θ^r_{hkl} is fixed [14], then ϕ_{str} and the related edge energies can be determined by measuring T_r On the other hand, according to a recent paper [15], the relation between critical supersaturation of kinetic roughening and the edge free γkT energy is

TABLE I Anisotropy of interaction energies δ, geometric factor of growth units and the calculated dimensionless roughening temperatures θ^r_{110} for the {110} faces of the three n–paraffins, and the actual roughening temperatures T_r of those n–paraffin crystals growing from n–hexane solutions

n–Paraffins	δ	η	θ^r_{110}	T_r (K)
n–$C_{21}H_{44}$	22 34	6 377	0 8916	273 27
n–$C_{23}H_{48}$	24 51	6 944	0 8635	283 95
n–$C_{25}H_{52}$	26 78	7 511	0 8458	287 58

expressed by

$$\beta_i^c = 4\gamma_x\gamma_y\xi/(\delta\eta) \tag{17}$$

where the shape factor $\xi = (1+\eta)^2/(4\eta)$, the anisotropic factor of interaction $\delta = \gamma_y/\gamma_x$, and the geometric factor of growth unit $\eta = l_y/l_x$ These factors are fixed for a given crystal structure

For n–paraffin/n–hexane solution systems, it is found [16] that up to T_r, ϕ is equal to γkT, because in this case the edge entropy does not play any role This implies that β_i^c can be derived by substituting the determined ϕ/kT for γ For the n–paraffins, the determined roughening temperatures of the {110} faces, and the relevant factors δ, η and θ_{hkl}^r are given in Table I Based on these data and eqs (16) and (17), we can derive critical supersaturations of kinetic roughening β_i^c(deri) which are listed in Table II

TABLE II Comparison between experimental data of critical supersaturation of kinetic roughening and those derived from the thermal roughening transition

n–Paraffins	β^c (%)	m	β_i^c (%)	β^c(deri) (%)
n–$C_{21}H_{44}$	1 55 ± 0 02	0 845 [a]	1 31	1 33
n–$C_{23}H_{48}$	1 43 ± 0 02	0 791 [a]	1 13	1 10
n–$C_{25}H_{52}$	1 35 ± 0 02	0 734 [a]	0 99	0 99

[a] The relative error is about ± 5%

In comparison, the determined data β^c and the corresponding data β_i^c resulted from modification according to Eq (3) and Fig 2, are also given in Table II It is shown in Table II that without considering the resistances against volume transport, the data β^c show about 15%–30% deviations from the data β_i^c(deri) derived from the thermal roughening experiments In contrast, after considering the resistances, β_i^c is surprisingly close to β_i^c(deri) (The difference is less than 4% This is within the range of experimental error)

V. CONCLUSIONS

As a conclusion of this paper, it can be stated that starting from the Goede's result, the kinetic data of rough growth, $R_{rough}(\beta)$, can be used to estimate the resistances to the

transport of growth units through the diffusion layer. Correspondingly, the interfacial effective supersaturation remaining for surface integration can be deduced from a simple relation [Eq.(11)]. For the faceted growth, the so–called auxiliary straight line method is developed suggested to derive the relevant data R_{rough}–β and m. This method turns out to be a reliable and convenient method for the estimation of the resistance against volume transport.

ACKNOWLEDGEMENT

The first author (X.Y. Liu) would like to thank Shell Netherlands BV for financial support.

REFERENCES

1 R. de Goede and G.M. van Rosmalen, J. Cryst. Growth **104**, (1990) 392.

2 P.H. Karpinski, Chem. Eng. Sci. **35**, 2321 (1980).

3 J. Garside, Chem. Eng. Sci. **40**, 3 (1985).

4 K. Onuma, K. Tsukamoto and I. Sunagawa, J. Cryst. Growth **98**, 377 (1989).

5 W.K. Burton, N. Cabrera and F.C. Frank, Phil. Trans. Roy. Soc. London **A234**, 299 (1951).

6 P. Bennema and G.H. Gilmer, in *Cryst. Growth: An Introduction*, edited by P. Hartman, (North–Holland, Amsterdam, 1973) p.263.

7 M. Ohara and R.C. Reid, *Modeling Crystal Growth Rates from Solution*, (Prentice Hall, Englewood Cliffs, N.J., 1973).

8 M. Elwenspoek and J.P. van der Eerden, J. Phys. A20, 669 (1987).

9 N.B. Ming, *Physical Fundamentals of Crystal Growth*, (Shanghai Sci. and Tech., Shanghai, 1982).

10 X.Y. Liu and P. Bennema, J. Cryst. Growth (submitted).

11 J.P. Vogels, Ph.D. Thesis (University of Nijmegen, 1991).

12 P. Bennema, X.Y. Liu, K. Lewtas, R.O. Tack, J.J.M. Rijpkema and K.J. Roberts, J. Cryst. Growth **121**, 679 (1992).

13 L.A.M.J. Jetten, Ph.D. Thesis (University of Nijmegen, 1983).

14 P. Bennema and J.P. van der Eerden, in *Morphology of Crystals, Part A*, edited by I. Sunagawa (Terra Sci., Tokyo, 1987) p.1.

15 X.Y. Liu and P. Bennema, J. Cryst. Growth **128**, 69 (1993).

16 X.Y. Liu, P. Bennema and J.P. van der Eerden, Nature **356**, 778 (1992).

摘　要

自从我于1989年9月加入奈梅亨大学固体化学实验室以来，人们已将注意力充分地集中到了固液界面这一专题上来．有关固液界面的知识对于基础表面科学，工业生产及高科技材料等领域具有极大的价值．晶体生长科学家们正致力于晶相与母相之间的界面的结构与性质的研究．其主要原因是由于界面的结构与晶体生长科学的中心议题:粗糙化转变，晶体生长机制,晶体生长动力学及晶体形态直接相关．此外，从事工业结晶的科学家们对特制的用于改变晶体生长习性的添加剂很感兴趣，因为晶体的形态在质量控制及一些重要的工业生产过程中起着重要的作用．为了理解添加剂对晶体形态的影响并对添加剂进行分子设计，有必要对界面结构进行较入的研究．因此，这些因素就成了我将界面这一专题作为串通该论文的中心议题的动机．

本论文的第2章对三斜，单斜和正交这三种不同结构的石蜡晶体的形态进行了研究．统一的Hartman-Perdok粗糙化转变理论和 Bravais-Friedel-Donnay-Harker (BFDH) 理论被系统地应用于预计这三种不同结构的石蜡晶体的形态． 为了比较所预计的与观测到的形态的异同，本章描述了晶体在不同条件下进行生长所得到的形态．这方面的研究着重了粗糙化转变对晶体形态的影响．此外，在考虑晶体结构影响的前提下，本章分析了石蜡晶体的形貌和无量纲粗糙化温度与石蜡分子碳原子数之间的依赖关系．在某种意义上,该章主要体现晶体内部结构对晶体形态的影响程度．

第3章主要描述发生于奇数石蜡晶体{110}晶面上的粗糙化转变．石蜡晶体的粗糙化相变临界现象及属性是该章的关键议题．第3.1章报导了正己烷溶液体系的粗糙化转变温度附近的一种奇特的称之为"平坦-粗糙-平坦" 的动力学转变．该动力学转变是首次被观察到并被识别出来．该现象能够被应用于测定棱边能在粗糙化温度附近依赖于温度的特殊的临界行为．第3.2章从理论和实验上描述了一个新发现:一级粗糙化相变．做为该研究的继续，第3.3章报导了一个重要的发现:石蜡晶体粗糙化转变的溶剂依赖性临界特性．该章叙述了石蜡晶体{110}面的粗糙化相变在将正己烷溶剂换成甲苯溶剂之后，由一级相变转化为无限级相变．该研究表明，烷烃状溶剂分子能促进一种与常规的KT粗糙化相变相耦合的表面结构相变的产生．正如第3.4章所指出的，这种表面结构相变以及上述的耦合很明显地导致了石蜡晶体体系的非常规粗糙化相变．这一重要而非同寻常的表面现象可以在文中所提出的耦合的Ising-SOS模型的原理的基础上得到合理解释．第3.5章推导了不同晶体表面结构的棱边自由能与动力学粗糙化临界过饱和度的关系．为了确证该关系，由动力学粗糙化实验测定的棱边自由能与由粗糙化相变实验得到的棱边能进行了比较．第3.6章从实验上研究粗糙化及动力学粗糙化对石蜡晶体形貌的影响．

有关界面结构与界面键能是第4章的主题．为了描述界面的结构与性质，本章提出了非均一囚胞模型，用以描述界面的结构与性质．该模型保持了传统囚胞模型的优点，又克服了传统模型在描述固液体系时所遇到的困难．第4.1章提出了该模型的基本原理与主要轮廓．为了将整体键能与所对应的界面键能相联系，该模型引入了表面特征比率因子C_γ．基于该因子，系统的表面性质能够与固体表面的润湿条件直接关联起来．第4.3章进一步深入地研究了密度

及键能在界面的分布．该章也定性地研究了界面键能与一晶面(hkl)的附着能的关系．第4.4章依据热力学统计物理和非均一囚胞模型的原理分析和研究了由各向同性构筑单元组成的晶体的表面自由能．该体系表面自由能可定量地表示为界面因子与整体性质的函数．在第4章的后一部分，自洽场(SCF)理论(或 Scheutjens-Fleer 理论)被应用于计算和研究界面性质(如界面键能)和液相界面结构.第4.5和4.6章初次应用了该计算方法对两种不同类型的界面体系:单体体系与聚合物体系分别进行了详细的研究．第4.7章尤其对靠近固体界面的链状液体分子的有序化从理论和实验上进行了深入的探讨．随后，第4.8章用遂道扫描显微镜对吸附在石墨表面上的奇数及偶数石蜡分子的结构进行了观测．毫无疑问，SCF方法将成为一种崭新的研究晶体界面的手段．第4.9章从理论与实验上系统地分析了各种溶剂对石蜡晶体体系界面结构及棱边能的影响．这一分析的结果充分地改善与加深了人们对固液界面这一区域基本结构的认识．根据理论计算结果，在一定浓度范围内使用两种混合溶剂可导致体系棱边能的增加．

母相对晶体形态的影响是第5章的重点．这一方面的研究可通过本章新发展起来的界面结构(IS)分析来进行．本章在预计石蜡晶体形态时阐述了IS分析的原理．在该分析中，求算界面上具有适配构型的"有效"生长基元的浓度是其关键所在．该分析能应用于研究特制添加剂对晶体生长习性及结晶过程的影响,并对添加剂的分子设计提供指导．

体输运对晶体生长速度的影响是晶体生长的另一个重要问题．在晶体生长过程中溶质与热输运的阻力将降低固体表面晶体生长的有效驱动力．该阻力能从"粗糙生长"与"平坦生长"的关系中估计出来．基于该原理，第6章提出了称之为辅助直线法的方法．该方法被应用于石蜡晶体体系中{110}晶面的有效驱动力的测定．

SAMENVATTING

Sedert september 1989 ben ik werkzaam op het laboratorium van Vaste Stof Chemie aan de KUN. In de afgelopen tijd is veel aandacht besteed aan problemen rondom vast–vloeibare grensvlakken. Kennis van vast–vloeibare grensvlakken is van groot belang voor fundamentele oppervlakte wetenschappen, industrie en andere wetenschapsgebieden. Wetenschappers werkzaam op het gebied van kristalgroei bestuderen de structuur en eigenschappen van het grensvlak tussen kristal en moederfase. Dit vanwege het feit dat de eigenschappen van het grensvlak rechtstreeks gekoppeld zijn aan fundamentele thema's van de wetenschap van de kristalgroei, als verruwingsovergang, groeimechanismen, groeikinetiek en morfologie van kristallen. Bovendien zijn wetenschappers die werkzaam zijn op het gebied van industriële kristallisatie geïnteresseerd in zogenaamde tailor made additieven, die speciaal ontworpen zijn om de habitus van kristallen planmatig te veranderen. Dit vanwege het feit, dat de efficiency van scheiding van vaste en vloeibare fase in de kristallisator afhangt van grootte en habitus van kristallen. Om de invloed van additieven op de vorm van kristallen te begrijpen is een beter begrip van interfaces noodzakelijk. Dit is voor mij een belangrijk motief om het thema "interfaces" tot een centraal integrerend thema van mijn proefschrift te maken.

In hoofdstuk 2 wordt de morfologie van drie verschillende paraffine structuren namelijk: trikliene, monokliene en orthorhombische structuren bestudeerd. De geïntegreerde Hartman–Perdok theorie, verruwingsovergangtheorie en Bravais–Friedel–Donnay–Harker theorie wordt daarbij toegepast om de morfologie behorende bij deze drie structuren te voorspellen. tegelijkertijd werden kristallen van deze paraffines gegroeid in de verschillende groeicondities om voorspelde en waargenomen morfologieën te vergelijken. In deze studies werd speciale aandacht besteed aan de invloed van de verruwingsovergang op de morfologie van kristallen. Bovendien werd de afhankelijkheid van de morfologie van de dimensieloze verruwingstemperatuur. die weer afhangt van het aantal C atomen, geanalyseerd, voor de drie paraffine structuren. Uit dit hoofdstuk volgt hoe de inwendige kristalstructuur tot op grote hoogte de morfologie van kristallen bepaalt.

Hoofdstuk 3 handelt over het fenomeen verruwingsovergang en de verschillende mogelijke typen van verruwingsovergang, die voorkomen op de {110} oppervlakken van de oneven orthorhombische paraffine kristallen. kritische verschijnselen in relatie tot de aard van de verruwingsovergang vormen de kernproblemen van dit hoofdstuk. In hoofdstuk 3.1 wordt een geheel nieuw type kinetische fasenovergang, de zogenaamde ruw–glad–ruw overgang beschreven. Deze fasenovergang is voor de eerste keer waargenomen en geïdentificeerd. Deze fasenovergang kan worden toegepast om het speciale gedrag van vrije randenergie γ in

afhankelijkheid van de temperatuur T en om de verruwingstemperatuur T^r experimenteel te bestuderen In hoofdstuk 3 2 wordt een eerste orde verruwingsfasenovergang beschreven zowel vanuit een experimenteel als vanuit een theoretisch standpunt Dit wordt gevolgd in hoofdstuk 3 3 door de beschrijving van een ander nieuw verschijnsel de aard van de verruwingsovergang in afhankelijkheid van het oplosmiddel In dit hoofdstuk wordt beschreven dat de verruwingsovergang op de {110} vlakken van n–paraffine veranderen van een eerste orde fasenovergang naar een fasenovergang van oneindige orde als de oplossing van n–hexaan vervangen wordt door tolueen

Er wordt gesuggereerd dat paraffine–achtige oplosmoleculen een fasenovergang op het oppervlak stimuleren, die gekoppeld is aan een KT type verruwing Blijkbaar resulteert deze koppeling in een onconventionele verruwingsovergang van het n–paraffine systeem De koppeling wordt op een voorlopige wijze geinterpreteerd binnen het kader van de gekoppelde Ising–SOS model In hoofdstuk 3 5 wordt de relatie tussen stepvrije energie en de kritische oververzadiging voor kinetische verruwing afgeleid voor verschillende structuren Om de relaties te bevestigen, worden vrije energieen van steps verkregen uit kinetische verruwing vergeleken met vrije energie van steps verkregen uit verruwingstemperaturen De morfologie van n–paraffine kristallen onder de invloed van de verruwingsovergang en kinetische verruwing wordt zorgvuldig bestudeerd met behulp van experimenten beschreven in hoofdstuk 3 6

De structuur van het interface en de bindingsenergieen van het interface zijn het onderwerp van hoofdstuk 4 Studies van dit hoofdstuk zijn gebasseerd op een zogenaamd inhomogeen cellenmodel Dit model werd ontwikkeld om de structuur en eigenschappen van het interface te beschrijven De basisprincipes en het framewerk van het model worden eerst gepresenteerd in hoofdstukken 4 1 en 4 2 Om een relatie te leggen tussen de bindingsenergieen tussen bulk van kristal en moederfase en de overeenkomende bindingen van het interface wordt de zogenaamde karakteristieke schaalfactor C_l^* geintroduceerd Met behulp van deze factor kunnen de eigenschappen van de interface direct in relatie gebracht worden met de zogenaamde bevochtigingscondities van het vaste oppervvlak Een vervolgstudie betreffende dichtheidsverdelingen en distributie van bindingsenergieen aan het interface wordt gegeven in hoofdstuk 4 3 Een relatie tussen de bindingsenergie van het interface en attachment energie van een kristalvlak (hkl) vanuit een kwalitatief standpunt wordt bestudeerd in hoofdstuk 4 3 In hoofdstuk 4 4 wordt de oppervlakte vrije energie van kristallen die uit isotrope bouweenheden bestaan bestudeerd volgens de principes van statistische thermodynamica en het inhomogene celmodel De oppervlakte energie wordt op een kwantitatieve manier

uitgedrukt als een functie van factoren van het interface en bulkeigenschappen Om eigenschappen van het interface te berekenen (zoals bindingsenergieen van het interface) en om de structuur van vloeibare deel van het interface te bestuderen wordt de zogenaamde zelf consistente veldtheorie (de Scheutjens–Fleer theorie) toegepast Met behulp van deze berekeningstechniek worden verschillende typen systemen monomeer en polymeer systemen respectievelijk tot in details onderzocht In het bijzonder wordt in hoofdstuk 4 7 de ordening van ketenachtige fluide moleculen vlakbij het oppervlak zorgvuldig bestudeerd vanuit theoretisch en experimenteel gezichtspunt Daarna wordt in hoofdstuk 4 8 de structuur van oneven en even n–paraffine moleculen geabsorbeerd op een grafiet substraat en waargenomen met behulp van een scanning tunneling microscoop bestudeerd In hoofdstuk 4 9 wordt een systematische studie gepresenteerd betreffende de invloed van verschillende oplosmiddelen op de structuur van het interface en de trede energie van een n–paraffine systeem Uit de verkregen resultaten volgt dat binnen een zeker gebied van concentraties het gebruik van mengsels kan leiden tot een toename van de stepenergie van het systeem

De invloed van de moederfase op de morfologie is het onderwerp van hoofdstuk 5 Studies over dit onderwerp worden uitgevoerd door een analyse van de interface structuur (IS) De principes van de IS analyse wordt besproken in verband met de voorspelling van de morfologie van n–paraffine kristallen In deze analyse speelt de concentratie van effectieve moleculen met de juiste conformatie in het interface een centrale rol Deze analyse kan toegepast worden om het effect van tailor made additieven op de groei habitus en kristallisatie van n–paraffine kristallen te onderzoeken

De invloed van volume transport op de groeisnelheid is een belangrijk probleem voor kristalgroei De weerstand veroorzaakt door volume diffusie en warmte transport tijdens kristalgroei zal de effectieve drijvende kracht voor kristalgroei aan het oppervlak van het groeiend kristal reduceren Weerstanden kunnen geschat worden uit de relatie tussen ruwe groei en gladde groei Binnen dit kader wordt een zogenaamde rechte lijn methode als hulp methode geintroduceerd in hoofdstuk 6 Deze methode wordt toegepast op het n–paraffine systeem

LIST OF PUBLICATIONS

1. X.Y. Liu, M.H. Jiang and Y G. Liu: "An investigation on crystallizing processes in high temperature solution by optical method (I)". *Journal of Shandong University* **21** Suppl., 81 (1986).
2. X.Y. Liu and M.H. Jiang: "An investigation on crystallizing processes in high temperature solution by optical method (II)". *Journal of Shandong University* **21** Suppl., 87 (1986).
3. Y.G. Liu, B. Xu, J.R. Han, X.Y. Liu and M.H. Jiang: "The growth of KT_iOPO_4 crystals for high efficiency SHG devices and its main properties", *Chinese Journal of Lasers* **13** [7], 439 (1986).
4. X.Y. Liu and M.H. Jiang: "An investigation on the physico–chemical processes of KTP crystals grown from phosphate flux (I)", *Chinese Journal of Lasers* **15** [8], 482 (1988), or *Chinese Physics Lasers* (in English) **15** [8], 596 (1988).
5. X.Y. Liu and M.H. Jiang: "An investigation on the physico–chemical processes of KTP crystals grown from phosphate flux (II)", *Journal of the Chinese Silicate Society* **16** [2], 163 (1988).
6. X.Y. Liu, M.H. Jiang and Z.S. Shao: "A study on the theoretical habits of KTP crystals", *Acta Physica Sinica* **37** [2], 274 (1988).
7. X.Y. Liu and M.H. Jiang: "The growth mechanism and crystalline habits of KTP crystals in phosphate flux", *Journal of the Chinese Silicate Society* **16** [4], 345 (1988)
8. Y.S. Wang, M.N. Zheng, P. Bennema, R. Zhu, G.F. Ye, X.Y Liu and W.J P. van Enckevort: "The occurrence of scattering centers and dislocations in KDP crystals", *J. Cryst. Growth* **108**, 821 (1991).
9. P. Bennema, X.Y. Liu, K. Lewtas, R.D. Tack, J.J.M. Rijpkema and K J. Roberts: "Morphology of orthorhombic long chain normal alkanes: theory and observation", *J. Cryst. Growth* **121**, 679 (1992).
10. X.Y. Liu and P. Bennema: "On the morphology of normal alkane crystals with triclinic structure: theory and observation", *J. Cryst. Growth* (to be published).
11. X.Y. Liu and P. Bennema: "On the morphology of normal alkane crystals with monoclinic structure: theory and observation", *J. Appl. Cryst.* **26**, 229 (1993).
12. X.Y. Liu and P. Bennema: "Detailed observations on the roughening transition and the influence on morphology of crystals", *J. Cryst. Growth* (to be published).
13. X.Y. Liu, P. Bennema and J.P. van der Eerden: "The rough–flat–rough transition at crystal surfaces", *Nature* **356**, 778 (1992).

14 X Y Liu and P Bennema "The equilibrium state of solid–liquid interfaces of aliphatic compounds", *J Chem Phys* **97**, 3600 (1992)

15 X Y Liu and P Bennema "The relation between macroscopic quantities and the solid–fluid interfacial structure", *J Chem Phys* **98**, 5863 (1993)

16 X Y Liu and P Bennema "Kinetic roughening in relation to the roughening transition and on odd–numbered alkane crystals", *J Cryst Growth* **128**, 69 (1993)

17 X Y Liu, G Arkenbout, P Bennema and P van Hoof "The relation between rough and flat growth of crystal faces an effective approach to volume transport resistances", *J Cryst Growth* (in press)

18 M da Silva Couto, X Y Liu, H Meekes and P Bennema "Scanning tunneling microscopy studies on odd and even n–paraffin molecules adsorbed on graphite", *J Appl Phys* (submitted)

19 X Y Liu "First order surface roughening of crystals", *Phys Rev* B**48**, (1993) (in press)

20 X Y Liu and P Bennema "The growth and morphology of paraffin crystals with different structures", in *Crystallization of Polymers Theoretical and experimental aspects* (ed M Dosère), NATO ASI–C Series "**Mathematical and Physical Science**", (Kluwer Academic Publishers, 1993)

21 X Y Liu and P Bennema, *Cryst Properties and Preparation* **36–38**, 273 (1991)

22 X Y Liu "The solid–fluid interface a comparison and further description using the layer model", *Surf Sci* **290**, 403 (1993)

23 X Y Liu "The surface free energy of solid–fluid interfaces an inhomogeneous cell model description", *J Chem Phys* **98**, 8154 (1993)

24 X Y Liu, P van Hoof and P Bennema "Surface roughening of n–alkane crystals solvent dependent critical behavior", *Phys Rev Lett* **71**, 109 (1993)

25 X Y Liu, P Bennema, C Meijer and M Couto "Ordering of chain–like molecules at the solid–fluid interface", *J Chem Phys* (submitted)

26 X Y Liu and P Bennema "Self–consistent field calculation of structure and static properties of the solid–fluid interface paraffin–like molecule systems", *Phys Rev* E (in press)

27 X Y Liu "Self–consistent field calculation of structure and static properties of the solid–fluid interface monomer systems", *Surf Sci* (submitted)

28 X Y Liu and P Bennema "The morphology of crystals internal and external controlling factors", *J Phys* D (submitted)

29 X Y Liu and J Faber "Influence of solvents on properties and the structure of crystal–solution interfaces of normal alkanes", *Phys Rev* E (submitted)

30. X.Y. Liu, H.F.J. Knops, P. Bennema, P. van hoof and J. Faber: "Surface roughening of n–paraffin crystals and the coupled Ising–SOS model", *Phys. Rev. Lett.* (submitted).

CURRICULUM VITAE

Xiang–Yang LIU

Date of birth : November 25, 1960
Place of birth : Fuzhou, Fujian, CHINA.

EDUCATION

Graduate Study

Oct.1978–July 1982 : Analytical Chemistry at the Dept. of Chemistry, Shandong University, Jinan, Shandong, China.

July 1982 : Degree–**Bachelor of Science.**

Postgraduate Study

Sept.1982–Oct.1985 : Solid State Physics at the Institute of Crystal Materials (Shandong University), with particular emphasis on: Crystal Growth and Kinetics of Crystal Growth.

Field of research:

Δ *On the development of optical methods for high temperature solution investigation.*

Δ *On the physico–chemical processes and the growth mechanism of KTP crystals grown from phosphate flux.*

Δ *On theoretical habits of ionic crystals.*

Δ *Engaged in the growth of crystals from flux.*

Oct.1985 : Degree–**Master of Science.**

Sept.1989–Sept.1993 : *Ph.D.* research at Laboratory of Solid State Chemistry, Faculty of Science, University of Nijmegen, The Netherlands.

Field of research:

Δ *On the morphology and growth of n–alkanes crystals.*

Δ *On the surface roughening of crystals.*

Δ *The Modeling of the solid–fluid interface.*

RESEARCH

Oct.1985–Sept.1989 · Fujian Institute of Research on the Structure of Matter, Chinese Academy of Sciences, Fuzhou, Fujian, (***Research assistant; Research associate***).

Field of research:

Δ *On the growth mechanism of enlargement of the cross section of KDP crystals by splicing technique.*

Δ *Engaged in the growth of crystals from aqueous solutions.*